

VOLUME 80

FEBRUARY 26, 1976

NUMBER 5

JPCA X

---

THE JOURNAL OF  
PHYSICAL  
CHEMISTRY

---



PUBLISHED BIWEEKLY BY THE AMERICAN CHEMICAL SOCIETY

# THE JOURNAL OF PHYSICAL CHEMISTRY

**BRYCE CRAWFORD, Jr.**, *Editor*  
**STEPHEN PRAGER**, *Associate Editor*  
**ROBERT W. CARR, Jr.**, **FREDERIC A. VAN-CATLEDGE**, *Assistant Editors*

**EDITORIAL BOARD:** C. A. ANGELL (1973-1977), F. C. ANSON (1974-1978), V. A. BLOOMFIELD (1974-1978), J. R. BOLTON (1976-1980), L. M. DORFMAN (1974-1978), H. L. FRIEDMAN (1975-1979), H. L. FRISCH (1976-1980), W. A. GODDARD (1976-1980), E. J. HART (1975-1979), W. J. KAUFMANN (1974-1978), R. L. KAY (1972-1976), D. W. McCLURE (1974-1978), R. M. NOYES (1973-1977), W. B. PERSON (1976-1980), J. C. POLANYI (1976-1980), S. A. RICE (1976-1980), F. S. ROWLAND (1973-1977), R. L. SCOTT (1973-1977), W. A. STEELE (1976-1980), J. B. STOTHERS (1974-1978), W. A. ZISMAN (1972-1976)

Published by the  
**AMERICAN CHEMICAL SOCIETY  
BOOKS AND JOURNALS DIVISION**  
D. H. Michael Bowen, Director

Editorial Department: Charles R. Bertsch,  
Head; Marianne C. Brogan, Associate  
Head; Celia B. McFarland, Joseph E.  
Yurvati, Assistant Editors

Graphics and Production Department:  
Bacil Guiley, Head

Research and Development Department:  
Seldon W. Terrant, Head

Advertising Office: Centcom, Ltd., 50 W.  
State St., Westport, Conn. 06880.

© Copyright, 1976, by the American  
Chemical Society. No part of this publica-  
tion may be reproduced in any form with-  
out permission in writing from the Ameri-  
can Chemical Society.

Published biweekly by the American  
Chemical Society at 20th and Northampton  
Sts., Easton, Pennsylvania 18042. Sec-  
ond class postage paid at Washington, D.C.  
and at additional mailing offices.

## Editorial Information

**Instructions for authors** are printed in  
the first issue of each volume. Please con-  
form to these instructions when submitting  
manuscripts.

**Manuscripts for publication** should be  
submitted to *The Journal of Physical  
Chemistry*, Department of Chemistry, Uni-  
versity of Minnesota, Minneapolis, Minn.  
55455. Correspondence regarding **accepted  
papers and proofs** should be directed to  
the Editorial Department at the ACS East-  
on address.

**Page charges** of \$60.00 per page are as-  
sessed for papers published in this journal.  
Ability to pay does not affect acceptance or  
scheduling of papers.

**Bulk reprints or photocopies** of indi-  
vidual articles are available. For informa-  
tion write to Business Operations, Books  
and Journals Division at the ACS Wash-  
ington address.

Requests for **permission to reprint**  
should be directed to Permissions, Books  
and Journals Division at the ACS Wash-  
ington address. The American Chemical  
Society and its Editors assume no responsi-  
bility for the statements and opinions ad-  
vanced by contributors.

## Subscription and Business Information

1976 Subscription rates—including sur-  
face postage

	U.S.	PUAS	Canada, Foreign
Member	\$24.00	\$29.75	\$30.25
Nonmember	96.00	101.75	102.25
Supplementary material	15.00	19.00	20.00

**Air mail and air freight** rates are avail-  
able from Membership & Subscription Ser-  
vices, at the ACS Columbus address.

**New and renewal subscriptions**  
should be sent with payment to the Office  
of the Controller at the ACS Washington  
address. **Changes of address** must include  
both old and new addresses with ZIP code  
and a recent mailing label. Send all address  
changes to the ACS Columbus address. Please  
allow six weeks for change to become  
effective. **Claims** for missing num-  
bers will not be allowed if loss was due to  
failure of notice of change of address to be  
received in the time specified; if claim is

dated (a) North America—more than 90  
days beyond issue date, (b) all other for-  
eign—more than 1 year beyond issue date;  
or if the reason given is "missing from  
files". Hard copy claims are handled at the  
ACS Columbus address.

**Microfiche subscriptions** are available  
at the same rates but are mailed first class  
to U.S. subscribers, air mail to the rest of  
the world. Direct all inquiries to Business  
Operations, Books and Journals Division,  
at the ACS Washington address or call  
(202) 872-4444. **Single issues** in hard copy  
and/or microfiche are available from Spe-  
cial Issues Sales at the ACS Washington  
address. Current year \$4.75. Back issue  
rates available from Special Issues Sales.  
**Back volumes** are available in hard copy  
and/or microform. Write to Special Issues  
Sales at the ACS Washington address for  
further information. **Microfilm** editions of  
ACS periodical publications are available  
from volume 1 to the present. For further  
information, contact Special Issues Sales at  
the ACS Washington address. **Supplemen-  
tary material** must be ordered directly  
from Business Operations, Books and Jour-  
nals Division, at the ACS Washington ad-  
dress.

	U.S.	PUAS, Canada	Other Foreign
Microfiche			
Photocopy	\$2.50	\$3.00	\$3.50
1-7 pages	4.00	5.50	7.00
8-20 pages	5.00	6.50	8.00

Orders over 20 pages are available only on  
microfiche, 4 × 6 in., 24X, negative, silver  
halide. Orders must state photocopy or mi-  
crofiche if both are available. Full bibli-  
ographic citation including names of all au-  
thors and prepayment are required. Prices  
are subject to change.

American Chemical Society  
1155 16th Street, N.W.  
Washington, D.C. 20036  
(202) 872-4600

Member & Subscription Services  
American Chemical Society  
P.O. Box 3337  
Columbus, Ohio 43210  
(614) 421-7230

Editorial Department  
American Chemical Society  
20th and Northampton Sts.  
Easton, Pennsylvania 18042  
(215) 258-9111



Substituent Effects on Nitroaromatic Radical Anions in Aqueous Solution . . . P. Neta and Dan Meisel*	519
Mass Spectrometric Observation of Large Sulfur Molecules from Condensed Sulfur . . . D. L. Cocke, G. Abend, and J. H. Block*	524
Stabilization of the Daughter Species Following the Auger Event in Some Cobalt(III) Chelates in Different Matrices . . . . . T. S. Srivastava and Amar Nath*	529
An Investigation of the Fluorescence Properties of Carboxyl Substituted Anthracenes . . . T. C. Werner,* Thomas Matthews, and Babs Soller	533
Electron Spin Resonance Line Width Studies of Vanadium(IV) in Acidic and Basic Aqueous Solutions . . . . . Melanie M. Iannuzzi, Clifford P. Kubiak, and Philip H. Rieger*	541
Very Low-Pressure Pyrolysis of Alkyl Cyanides. III. <i>tert</i> -Butyl Cyanide. Effect of the Cyano Group on Bond Dissociation Energies and Reactivity . . . Keith D. King* and Richard D. Goddard	546
Fourier Transform Magnesium-25 Nuclear Magnetic Resonance Study of Aqueous Magnesium(II) Electrolytes . . . . . Larry Simeral and Gary E. Maciel*	552

### COMMUNICATIONS TO THE EDITOR

Arrhenius Parameters for the Reaction of Oxygen Atoms with Dicyanoacetylene . . . Clifford W. Hand* and Richard M. Myers	557
---	-----

■ Supplementary material for this paper is available separately (consult the masthead page for ordering information); it will also appear following the paper in the microfilm edition of this journal.

\* In papers with more than one author, the asterisk indicates the name of the author to whom inquiries about the paper should be addressed.

### AUTHOR INDEX

Abend, G., 524	Goddard, R. D., 546	Maciel, G. E., 552	Schoonheydt, R. A., 511
Ache, H. J., 451	Granoth, I., 508	Madia, W. J., 451	Seely, G. R., 441, 447
Armishaw, R. F., 501	Hand, C. W., 557	Matthews, T., 533	Sharafi-Ozeri, Sh., 454
Bard, A. J., 459	Heicklen, J., 433	Meisel, D., 519	Simeral, L., 552
Block, J. H., 524	Hentzschel, P., 494	Miller, J. R., 457	Simonaitis, R., 433
Boileau, J., 466	Hines, J. J., 457	Morimoto, T., 471	Soller, B., 533
Bowman, M. K., 482	Iannuzzi, M. M., 541	Muszkat, K. A., 454	Srivastava, T. S., 529
Brown, C. W., 480	James, D. W., 501	Myers, R. M., 557	Steen, H. B., 482
Cliff, B. E., 457	Jayanty, R. K. M., 433	Nagao, M., 471	Takenaka, T., 475
Cocke, D. L., 524	Johnson, K. W., 457	Nakanaga, T., 475	Velghe, F., 511
Daly, F. P., 480	Jolicoeur, C., 466	Nath, A., 529	Watkins, A. R., 494
De Wilde, W., 511	Kevan, L., 482	Neta, P., 519	Wen, W.-Y., 466
Donohue, T., 437	King, K. D., 546	Poupko, R., 454	Werner, T. C., 533
Eftink, M. R., 486	Kubiak, C. P., 541	Pownall, H. J., 508	Wiesenfeld, J. R., 437
Ghiron, C. A., 486	Laser, D., 459	Rieger, P. H., 541	Yanai, H., 471
	LoSurdo, A., 466	Rosenthal, I., 454	
		Runowski, R. F., 457	

# THE JOURNAL OF PHYSICAL CHEMISTRY

Registered in U. S. Patent Office © Copyright, 1976, by the American Chemical Society

VOLUME 80, NUMBER 5 FEBRUARY 26, 1976

## Reaction of $\text{NH}_2$ with $\text{NO}$ and $\text{O}_2$

R. K. M. Jayanty, R. Simonaitis, and Julian Heicklen\*

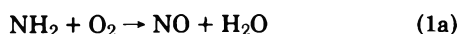
Department of Chemistry and Ionosphere Research Laboratory, The Pennsylvania State University, University Park, Pennsylvania 16802  
(Received August 18, 1975)

$\text{NH}_3$  was photolyzed with 213.9-nm light at 25 °C in the presence of  $\text{NO}$  or  $\text{O}_2$ . With  $\text{NO}$  present the products measured were  $\text{N}_2$ ,  $\text{H}_2$ , and  $\text{N}_2\text{O}$ , and for  $[\text{NH}_3] = 5.6\text{--}7.2$  Torr, their respective quantum yields were  $1.05 \pm 0.05$ ,  $0.33 \pm 0.03$ , and  $0.09 \pm 0.02$ . At  $[\text{NH}_3] = 11$  Torr pressure, the yields are somewhat smaller. The mechanism of reaction is:  $\text{NH}_3 + h\nu \rightarrow \text{NH}_2 + \text{H}$ ;  $\text{NH}_2 + \text{NO} \rightarrow \text{N}_2 + \text{H}_2\text{O}$  (2);  $\text{H} + \text{NO} + \text{M} \rightarrow \text{HNO} + \text{M}$  (3);  $\text{H} + \text{HNO} \rightarrow \text{H}_2 + \text{NO}$  (4);  $2\text{HNO} \rightarrow \text{N}_2\text{O} + \text{H}_2\text{O}$  (5); with  $k_3k_5^{1/2}/k_4 = (1.6 \pm 0.6) \times 10^{-28} \text{ cm}^9/2 \text{ s}^{-1/2}$ . With  $\text{O}_2$  present,  $\text{N}_2$  and  $\text{N}_2\text{O}$  were produced with quantum yields of  $\Phi(\text{N}_2) = 0.23 \pm 0.02$  independent of  $\text{O}_2$  pressure, and  $\Phi(\text{N}_2\text{O}) = 0.06 \pm 0.01$  for  $[\text{O}_2] < 2$  Torr and  $0.09 \pm 0.01$  for  $[\text{O}_2] > 20$  Torr. The quantum yield of  $\text{NH}_3$  removal was  $0.49 \pm 0.03$ . The oxidation of the  $\text{NH}_2$  radical proceeds mainly, if not exclusively (>98%), by addition:  $\text{NH}_2 + \text{O}_2 + \text{M} \rightarrow \text{NH}_2\text{O}_2 + \text{M}$  (1c). The products observed are then explained in terms of the sequence of reactions:  $2\text{NH}_2\text{O}_2 \rightarrow 2\text{NH}_2\text{O} + \text{O}_2$  (13);  $\text{NH}_2\text{O}_2 + \text{NH}_2\text{O} \rightarrow \text{N}_2\text{O} + 2\text{H}_2\text{O}$  (14);  $2\text{NH}_2\text{O} \rightarrow \text{N}_2 + 2\text{H}_2\text{O}$  (15);  $\text{NH}_2\text{O}_2 + \text{HO}_2 \rightarrow \text{NH}_3 + 2\text{O}_2$  (16).

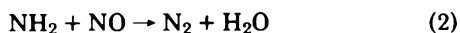
### Introduction

Ammonia is an important atmospheric constituent; therefore our understanding of the oxidation processes of this gas is very important. To date few studies of the room temperature photooxidation of  $\text{NH}_3$  have been carried out and there is very little known about the elementary reactions involved. The available literature up to 1971 has been recently reviewed.<sup>1</sup> We know of no additional oxidation studies of this system since that time, except for a study of the  $\text{O}_3\text{--NH}_3$  system.<sup>2</sup>

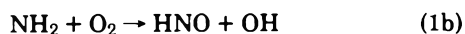
The major products of the room temperature photooxidation which have been reported are  $\text{N}_2$ ,  $\text{H}_2\text{O}$ ,  $\text{H}_2$  and  $\text{NH}_4\text{NO}_3$ .<sup>1</sup> Gesser<sup>3</sup> suggested that the  $\text{N}_2$  is produced via



followed by



Two paths have been suggested for the room temperature reaction of  $\text{NH}_2$  with  $\text{O}_2$ :<sup>1</sup> reaction 1a and



However, there is little compelling evidence for these reactions at room temperature. Dalby<sup>4</sup> has reported that the flash photolysis of  $\text{NH}_3\text{--O}_2$  mixtures does not give rise to

the HNO spectrum. The addition reaction



is also possible and must be considered in any analysis of the  $\text{NH}_3\text{--O}_2$  system. As far as we know no absolute measurements of rate coefficients for  $\text{NH}_2 + \text{O}_2$  have been reported, but it has been suggested that reaction 1 is slow compared to reaction 2 if the  $\text{N}_2$  production in the photolysis of  $\text{NH}_3\text{--O}_2$  system can be explained by reaction 1a followed by reaction 2.<sup>3</sup>

The reaction between  $\text{NH}_2$  and  $\text{NO}$  has been studied more extensively. Bamford<sup>5</sup> found  $\text{N}_2$  as a major product in the photolysis of  $\text{NH}_3\text{--NO}$  mixtures and suggested reaction 2 as the exclusive reaction between  $\text{NH}_2$  and  $\text{NO}$ . Later Serewicz and Noyes<sup>6</sup> and Srinivasan<sup>7</sup> also photolyzed  $\text{NH}_3\text{--NO}$  mixtures and confirmed the above reaction. More recently absolute rate coefficients for reaction 2 have been determined to be  $2.7 \times 10^{-11} \text{ cm}^3 \text{ s}^{-1}$  by pulse radiolysis of  $\text{NH}_3\text{--NO}$  mixtures,<sup>8</sup>  $0.8 \times 10^{-11} \text{ cm}^3 \text{ s}^{-1}$  by flash photolysis of  $\text{NH}_3\text{--NO}$  mixtures in a discharge flow reactor,<sup>9</sup> and  $2.1 \times 10^{-11} \text{ cm}^3 \text{ s}^{-1}$  by the laser fluorescence technique.<sup>10</sup>

In this paper we report on our study of the photooxidation of  $\text{NH}_3$  at room temperature and the photolysis of  $\text{NH}_3\text{--NO}$  mixtures. The primary objective was to determine the reaction paths of  $\text{NH}_2$  with  $\text{O}_2$ .

## Experimental Section

A conventional high vacuum line utilizing Teflon stopcocks with Viton O rings was used. Pressures were measured with a dibutylphthalate manometer and a Wallace and Tiernan gauge. The reaction vessel was a cylindrical quartz cell 10 cm long and 5 cm in diameter.

The  $N_2O$ ,  $O_2$ ,  $NO$ , and  $NH_3$  were Matheson CP grade. The  $N_2O$  was degassed at  $-196^\circ C$  and distilled in vacuo from a dry ice-acetone bath. The  $NH_3$  was degassed at liquid nitrogen temperature and purified by distillation from  $-96$  to  $-130^\circ C$ .  $O_2$  was purified by passage over traps at  $-186^\circ C$ . The  $NO$  was degassed at  $-196^\circ C$  and distilled in vacuo from  $-186^\circ C$ .

Irradiation was from a Phillips Zn resonance lamp TYP 93106E. The effective radiation was at 213.9 nm. After irradiation the gases noncondensable at  $-196^\circ C$  were expanded into a calibrated volume and analyzed for  $N_2$  by gas chromatography using a 10 ft. long, 0.25 in. o.d. copper column packed with 5 Å molecular sieves. The condensables were then analyzed for  $N_2O$  using a 24 ft. long, 0.25 in. o.d. copper column packed with Porapak Q. These columns were operated at room temperature. The carrier gas in all cases was helium. There was always some  $N_2$  ( $\leq 5\%$ ) and  $N_2O$  ( $\leq 10\%$ ) found in the dark runs and therefore these corrections were applied to all the experimental results.

$NO$  production in the  $NH_3-O_2$  system was determined using a chemiluminescent detector described earlier.<sup>11</sup> The lower limit of the detector sensitivity was about 10 ppb, but the system always gave a background signal corresponding to about 150 ppb of  $NO$  at atmospheric pressure. Therefore concentrations of  $NO$  could be measured only above 150 ppb. Ammonia removal rates were determined by uv and/or infrared absorption measurements using a Cary 14 and a Perkin-Elmer 521 spectrometer, respectively.

$NO_2$  analyses were done by visible absorption spectroscopy. The limit of detection was 15 mTorr.

Actinometry was done by photolysis of an optically equivalent amount of  $N_2O$ . The quantum yield of  $N_2$ ,  $\Phi\{N_2\}$ , for this system is known to be 1.41<sup>12</sup> at 213.9 nm. The relative absorption coefficient for  $N_2O$  and  $NH_3$  was determined for the 213.9-nm Zn resonance line using a wheatstone bridge arrangement to cancel the other unabsorbed wavelengths from the lamp. It was found that  $\epsilon\{NH_3\}/\epsilon\{N_2O\} = 50 \pm 5$ .

## Results

*Photolysis of  $NH_3$  in the Presence of  $O_2$ .* The photolysis of  $NH_3$  in the presence of  $O_2$  ( $\geq 0.6$  Torr) at 213.9 nm and  $25^\circ C$  leads to the production of  $N_2$  and  $N_2O$ . Attempts to measure  $H_2$ ,  $NO$ , and  $NO_2$  production were also made in the presence of  $O_2$  ( $>1$  Torr), but none of these gases were found. Their quantum yields were  $<0.01$ . At very low  $[O_2]$  (0.16 Torr)  $H_2$  production was observed. The  $NO$  concentration after 30-min photolysis was  $\leq 0.15$  mTorr independent of the  $O_2$  pressure from 1 to 45 Torr. Thus if  $NO$  is in the steady state the upper limit to  $[NO]_{ss}$  is 0.15 mTorr up to  $[O_2] = 45$  Torr. The experimental results for the  $NH_3-O_2$  system are given in Table I. From Table I it is apparent that the results are nearly independent of variation of conditions. There is no dependence on the time of irradiation or on the absorbed light intensity,  $I_a$ . In spite of large variation in  $[NH_3]$  (factor of 11) and  $[O_2]$  (factor of nearly 800)  $\Phi\{N_2\}$  is nearly constant. The average value of  $\Phi\{N_2\}$  is  $0.23 \pm 0.02$ . Similarly,  $\Phi\{N_2O\}$  is independent of  $[NH_3]$  variation (factor of 4) and nearly independent of changes in  $[O_2]$

TABLE I: Photolysis of  $NH_3-O_2$  Mixtures at 213.9 nm and  $25^\circ C$

$[O_2],^a$ Torr	$I_a,^b$ mTorr/ min	Irradiation time, min	$\Phi\{N_2\}$	$\Phi\{N_2O\}$	$-\Phi\{NH_3\}$
$[NH_3]^a = 1.6 \pm 0.3$ Torr					
0.62	8.30	30	0.25		
1.05	9.29	30	0.23		
1.09	8.27	30	0.23		
1.45	8.40	40	0.26		
1.55	8.40	30		0.05	
1.56	8.04	60		0.05	
22.20	8.14	40		0.11	
35.70	8.24	50	0.27		
$[NH_3] = 7.1 \pm 0.4$ Torr					
	25.0	30	0.093 <sup>c</sup>		
1.17	24.6	60		0.07	0.54
1.30 <sup>d</sup>	25.3	30	0.20		
1.36	25.7	10	0.21		
1.36	23.1	120	0.24		0.50
1.36	25.3	30	0.20		
1.40	25.5	25		0.06	
1.44	23.9	90		0.07	
1.44	25.7	10		0.05	
1.56	24.8	60	0.20		0.43
1.63	25.4	20	0.19		
1.63	25.0	40	0.26		
1.70	25.3	30	0.20		0.50
2.10	24.3	30		0.06	
6.92	25.5	10		0.08	
32.0	25.7	10		0.09	
33.2	23.7	90		0.11	0.54
47.0	25.7	30	0.26		
65.0	24.1	40		0.08	
80.0	24.6	30		0.11	
108.0	24.3	30		0.08	
124.0	25.3	30		0.06	
126.0	25.3	30	0.26		
$[NH_3] = 15.5 \pm 0.1$ Torr					
0.16	51.6	10.0	0.23		
1.17	51.6	10.0	0.23		

<sup>a</sup> Initial pressure. <sup>b</sup>  $I_a$  is corrected for  $NH_3$  consumed by using the average concentration of the  $NH_3$  during the course of the experiment. <sup>c</sup>  $H_2$  also produced,  $\Phi\{H_2\} = 0.23$ . <sup>d</sup> 285 Torr of helium also present.

(factor of 100). The average value of  $\Phi\{N_2O\}$  at low  $[O_2]$  ( $<2$  Torr) is  $0.06 \pm 0.01$ , and  $0.09 \pm 0.01$  at high  $[O_2]$  ( $>20$  Torr). Thus there may be a slight increase in  $\Phi\{N_2O\}$  with increasing  $[O_2]$ .

In a few experiments the ammonia loss quantum yield was also determined. The last column in Table I gives  $-\Phi\{NH_3\}$ . The average value of  $-\Phi\{NH_3\} = 0.49 \pm 0.03$  independent of the  $O_2$  pressure. The sum  $2\Phi\{N_2\} + 2\Phi\{N_2O\}$  is  $0.59 \pm 0.04$ . This is very nearly equal to  $-\Phi\{NH_3\}$  indicating that no other major products containing nitrogen could have been produced.

Several experiments were done in the absence of  $O_2$ . The products measured were  $N_2$  and  $H_2$ . The results for one experiment are also given in Table I. It is apparent that in the absence of  $O_2$ ,  $\Phi\{N_2\}$ , is significantly lower than in the presence of  $O_2$ .

Two experiments were done with 1.6 Torr of  $O_2$  and 6.9 Torr of  $NH_3$  in the presence of either 46 or 100 Torr of  $CO$  with  $I_a = 25$  mTorr/min. The quantum yield of  $CO_2$  was measured and found to be 0.08 and 0.11, respectively, for the two runs.

*Photolysis of  $NH_3$  in the Presence of  $NO$  and  $NO-O_2$  Mixtures.* In the photolysis of  $NO-NH_3$  and  $NO-O_2-NH_3$

TABLE II: Photolysis of NH<sub>3</sub>-NO Mixtures at 213.9 nm and 25 °C

[NH <sub>3</sub> ], Torr	[NO], Torr	[O <sub>2</sub> ], Torr	I <sub>a</sub> , mTorr/min	Irradiation time, min	Φ{N <sub>2</sub> }	Φ{H <sub>2</sub> }	Φ{N <sub>2</sub> O}	10 <sup>28</sup> k <sub>3</sub> k <sub>5</sub> <sup>1/2</sup> /k <sub>4</sub> , cm <sup>9/2</sup> s <sup>-1/2</sup>
5.64	1.59		20	30.0	1.00		0.08	1.0
6.90	1.63	0.07	25	10.0	1.10	0.31		
7.00	1.50	0.11	25	20.0	1.03	0.28		
7.00	1.60		25	15.0	1.04	0.36	0.11	1.5
7.20	1.79		25	31.0			0.09	0.92
7.20	1.40		26	5.0	1.08	0.35		2.1
11.8	1.59		42	5.0	0.87	0.22		
11.9 <sup>a</sup>	1.44		43	5.0	0.69			
13.3	1.63		47	6.0	0.76	0.23		2.5

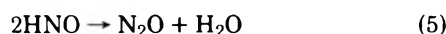
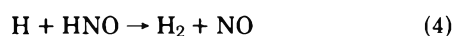
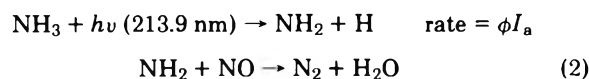
<sup>a</sup> 285 Torr of helium also present.

mixtures the products identified were N<sub>2</sub>, H<sub>2</sub>, and N<sub>2</sub>O. We did not look for any other products. In this system -Φ{NH<sub>3</sub>} was not determined. The results are presented in Table II. In the absence of O<sub>2</sub> the NH<sub>3</sub> pressure was varied from 5.64 to 13.3 Torr, but the NO pressure was constant at 1.6 ± 0.2 Torr. Φ{N<sub>2</sub>} = 1.0 ± 0.1 at [NH<sub>3</sub>] ~ 7 Torr, but is below one at higher total pressures. Φ{H<sub>2</sub>} also decreases as the total pressure increases. The effect of total pressure on Φ{N<sub>2</sub>O} was not determined.

Two experiments were done in which a small amount (0.11 and 0.066 Torr) of O<sub>2</sub> was added to the NH<sub>3</sub>-NO mixtures. The results show that Φ{N<sub>2</sub>} was not affected by these small quantities of O<sub>2</sub>. Φ{H<sub>2</sub>} may have decreased slightly, but this decrease is probably within experimental error.

## Discussion

*Photolysis of NH<sub>3</sub>-NO and NH<sub>3</sub>-NO-O<sub>2</sub> Mixtures.* Mixtures of NH<sub>3</sub>-NO and NH<sub>3</sub>-NO-O<sub>2</sub> were photolyzed in order to determine the quantum efficiency of NH<sub>3</sub> photolysis at 213.9 nm. The reaction scheme in the absence of O<sub>2</sub> is the following:<sup>6</sup>



Φ{N<sub>2</sub>} = φ, since NH<sub>2</sub> radicals can react only with NO. Table II shows Φ{N<sub>2</sub>} = 1.0 ± 0.1 for the experiments at [NH<sub>3</sub>] ~ 7 Torr. At higher [NH<sub>3</sub>], and for the run in which 285 Torr of He is present, Φ{N<sub>2</sub>} is somewhat below one indicating that at higher pressures some deactivation of excited NH<sub>3</sub> may be occurring. At low pressures where any deactivation of excited NH<sub>3</sub> is not important φ = 1, and the mechanism leads to the relations:

$$(\Phi\{\text{H}_2\}^{-1} - 1)\Phi\{\text{N}_2\text{O}\}^{1/2}I_a^{1/2} = \frac{k_3k_5^{1/2}}{k_4}[\text{NO}][\text{M}] \quad (a)$$

and

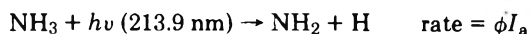
$$\Phi\{\text{N}_2\} = 2\Phi\{\text{N}_2\text{O}\} + 2\Phi\{\text{H}_2\} \quad (b)$$

From the measured values of Φ{N<sub>2</sub>}, Φ{H<sub>2</sub>}, or/and Φ{N<sub>2</sub>O} the ratio k<sub>3</sub>k<sub>5</sub><sup>1/2</sup>/k<sub>4</sub> may be computed. The results are given in Table II. The average value is (1.6 ± 0.6) × 10<sup>-28</sup> cm<sup>9/2</sup> s<sup>-1/2</sup>, if we assume equal efficiencies for NO and NH<sub>3</sub> in reaction 3. This value can be compared to (6.7 ± 0.5) × 10<sup>-28</sup> cm<sup>9/2</sup> s<sup>-1/2</sup> obtained by Serewicz and Noyes at 31 °C by a similar technique<sup>6</sup> and to 7.2 × 10<sup>-27</sup> cm<sup>9/2</sup> s<sup>-1/2</sup> computed

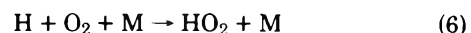
from the recommended values for the individual rate coefficients.<sup>13</sup> In the latter computation the relative efficiencies of H<sub>2</sub>:NH<sub>3</sub> = 0.5 was estimated for reaction 3, and the upper limit of 1 × 10<sup>-12</sup> cm<sup>3</sup> s<sup>-1</sup> for k<sub>4</sub> was used. A lower value of k<sub>4</sub>, or a greater value for the efficiency of NH<sub>3</sub> in promoting reaction 3, would make the disagreement worse. Therefore it is likely that either the recommended value for k<sub>5</sub><sup>13</sup> is significantly too high or the value for k<sub>4</sub> is >10<sup>-12</sup> cm<sup>3</sup> s<sup>-1</sup>.

Two experiments were done in the presence of a small amount of O<sub>2</sub> (~100 mTorr) to see if oxygen might be an efficient deactivator of an excited state of NH<sub>3</sub>, since in the NH<sub>3</sub>-O<sub>2</sub> mixtures (see Table I and discussion below) -Φ{NH<sub>3</sub>} or 2Φ{N<sub>2</sub>} ~ 0.5 even at very low O<sub>2</sub> pressures. The [O<sub>2</sub>]/[NO] ratio was adjusted such that the reaction of O<sub>2</sub> with NH<sub>2</sub>, H, and HNO would be minimal. The results in Table II show that 113 mTorr of O<sub>2</sub> had no effect on Φ{N<sub>2</sub>} or on Φ{H<sub>2</sub>}. Thus it appears that 113 mTorr of O<sub>2</sub> does not deactivate electronically excited NH<sub>3</sub>.

*Photolysis of NH<sub>3</sub>-O<sub>2</sub> Mixtures.* The number of possible reactions for this system is large. However, the invariance of Φ{N<sub>2</sub>} and Φ{N<sub>2</sub>O} with reaction conditions presented in Table I imposes a great number of constraints reducing the number of possible reactions significantly. The primary act in the photolysis is



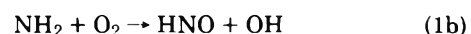
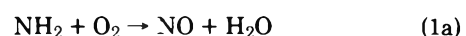
The H atoms produced in the primary process can only react with O<sub>2</sub>, since the results are independent of the O<sub>2</sub> pressure.



Any OH radicals in this system can only react with NH<sub>3</sub>.

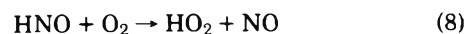


There are three possible reactions between NH<sub>2</sub> and O<sub>2</sub>:

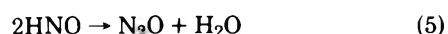


In order to decide the relative importance of the above three reactions it is convenient to first assume that reaction 1c is not important and that the products, i.e., N<sub>2</sub> and N<sub>2</sub>O, arise from reactions 1a and 1b.

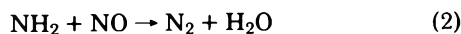
According to this mechanism the HNO produced in reaction 1b will react via<sup>14</sup>



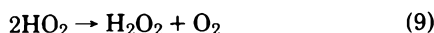
or



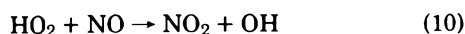
leading to  $N_2O$ . The  $N_2$  is produced from



where the NO is produced by reactions 1a and 8. The  $HO_2$  radical produced in reaction 6 will react with itself.



The reaction of  $HO_2$  with NO



is not important compared to reaction 9, since  $NO_2$  is not an important product. This is confirmed by calculation with the known rate coefficients for reactions 9 and 10. A reaction of  $HO_2$  with HNO is unknown, but even if it occurs to some extent this is not important to the present argument.

The mechanism outlined above predicts that  $\Phi\{N_2O\}$  should be independent of  $[O_2]$  at low  $O_2$  pressures ( $<2$  Torr),<sup>14</sup> but decrease as  $[O_2]^2$  at high  $[O_2]$ . The measured  $\Phi\{N_2O\}$  is nearly independent of  $[O_2]$  (it may increase slightly as the  $O_2$  increases) over a range of 1–120 Torr. Thus reaction 1b cannot be the source of  $N_2O$ , and it must all originate from  $NH_2O_2$  produced in reaction 1c. Not only is reaction 1b not the principal source of  $N_2O$  production, but it cannot be an important process at all for three reasons: (1) Dalby<sup>4</sup> could not find HNO as a product of the reaction; (2) we find that no NO or  $NO_2$  are formed ( $\Phi < 0.01$ ); and (3) the experiments with added CO indicated that HO is not a major species since it would react with CO to give  $CO_2$

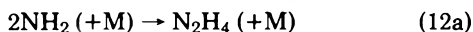


Since  $\Phi\{CO_2\} = 0.09 \pm 0.02$ , this gives the upper limit ( $CO_2$  could be produced from other reactions) to the efficiency of the reaction channel 1b (assuming  $\phi = 1.0$ ). The source of  $N_2$  may still be reaction 1a followed by reaction 2, as the mechanism predicts that  $\Phi\{N_2\}$  is independent of conditions if reaction 1b is minor. However, as the following argument shows, reaction 1a cannot be important.

The above mechanism leads to the following equation for the steady state of NO (neglecting reaction 1b):

$$[NO]_{ss} = k_{1a}[O_2]/k_2 \quad (c)$$

Therefore since  $[NO]_{ss} \leq 0.15$  mTorr,  $k_{1a}/k_2 \leq 3 \times 10^{-6}$ , and since  $k_2 \sim 2 \times 10^{-11} \text{ cm}^3 \text{ s}^{-1}$ ,<sup>8-10</sup>  $k_{1a} \leq 6 \times 10^{-17} \text{ cm}^3 \text{ s}^{-1}$ . Also  $NH_2$  could react with itself via<sup>15,16</sup>



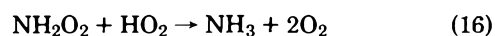
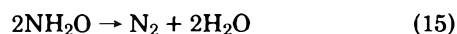
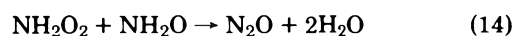
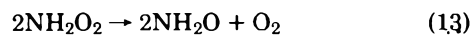
The relative importance of reactions 12 and 1 are

$$R\{12\}/R\{1\} = k_{12}\phi I_a/k_1(2k_{1a} + k_{1c})[O_2]^2 \quad (d)$$

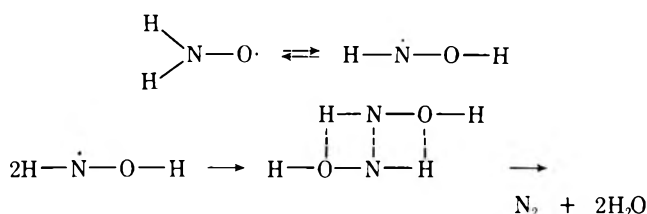
where  $R\{X\}$  is the rate of reaction X. If reaction 12 were important at low  $O_2$  pressures,  $\Phi\{N_2\}$  should have declined to  $\leq 0.09$  obtained for the photolysis of pure  $NH_3$  (see Table I). Furthermore  $\Phi\{N_2O\}$  should have been reduced to nearly zero, since it is not produced in the pure  $NH_3$  system. However the data in Table I show that this is not the case and that reaction 12 is negligible even at 0.16 Torr of  $O_2$  pressure. Since  $k_{12} \simeq 5 \times 10^{-12} \text{ cm}^3 \text{ s}^{-1}$  at  $[NH_3] = 5-10$  Torr,<sup>15</sup> then  $k_1 > 4 \times 10^{-15} \text{ cm}^3 \text{ s}^{-1}$ .

We conclude that reaction 1a followed by 2 cannot be the source of the  $N_2$ , and that the  $N_2$  must be produced from the  $NH_2O_2$  radical. From the measured upper limit to

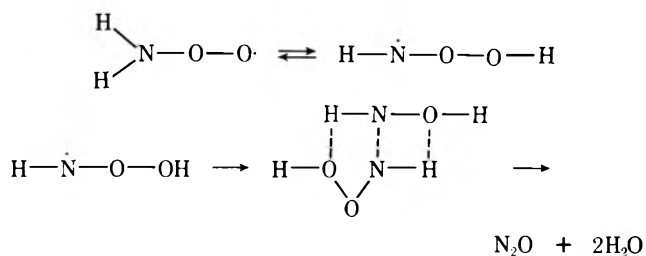
$\Phi\{NO\} \leq 0.01$ , and since  $N_2$  is not produced from reaction 1a it may be concluded that  $(k_{1a} + k_{1b})/k_{1c} \leq 0.02$ . The reactions we propose to account for the results subsequent to the formation of  $NH_2O_2$  by reaction 1c are the following:



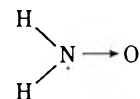
The proposed mechanism consisting of the primary process and reactions 6, 9, and 13–16 predict that  $\Phi\{N_2\}$ ,  $\Phi\{N_2O\}$ , and  $-\Phi\{NH_3\}$  are independent of variation in all reaction conditions, since reactions 9 and 13–16 are all radical-radical reactions. Reaction 15 has been proposed before to account for  $N_2$  formation in the  $NH_3-O_3$  system.<sup>2</sup> One way reaction 15 could proceed is as follows



Similarly reaction 14 could proceed via



An alternative possibility is that the free-radical site is on the nitrogen atom even when it is bonded to two H atoms.



This can occur because O is more electronegative than N, and N has a lone pair of electrons which can be donated. Such a tautomerization occurs when the H is removed from HONO; even though the H–O bond is broken, the free radical site is on the nitrogen in  $NO_2$ . Reaction 15 would then proceed by dimerization of  $H_2\dot{N}-O$  followed by ejection of  $H_2O$ . Reaction 14 would proceed in an analogous manner.

The second possibility is the one we favor as a general route in nitrogen-oxygen radicals because  $(C_2H_5)_2NO$  reacts with NO in the presence of  $O_2$  to give  $N_2O$  and  $CH_3CHO$ .<sup>17</sup> Clearly the free-radical site in  $(C_2H_5)_2NO$  is on the nitrogen atom, but it is difficult to believe that any isomerization could have occurred. Reaction 16 is introduced to account for the fact that  $-\Phi\{NH_3\} = 0.49$ , since we have shown above that it is unlikely that the low  $NH_3$  removal quantum yield is due to deactivation of an excited state of  $NH_3$  by  $O_2$ , but this possibility cannot be entirely ruled out from the present data.

We have shown that the reaction between  $NH_2$  and  $O_2$  at room temperature produces  $NH_2O_2$  predominantly. The subsequent reactions leading to  $N_2$  and  $N_2O$  are specula-



tive. However the reaction sequence 13–16 is consistent with all of the data. Proofs of reactions 13–16 will have to await the observation of  $\text{NH}_2\text{O}_2$  and  $\text{NH}_2\text{O}$  by direct means.

*Acknowledgment.* This work was supported by the Atmospheric Sciences Section of the National Science Foundation through Grant No. GA-42856 and the National Aeronautics and Space Administration through Grant No. NGL-39-009-003 for which we are grateful.

## References and Notes

- (1) N. Cohen and J. Heicklen, "Comprehensive Chemical Kinetics", C. H. Bamford and C. F. H. Tipper, Ed., Elsevier, Amsterdam, 1972, p 1.
- (2) K. J. Olszyna and J. Heicklen, *Adv. Chem. Ser.*, **No. 113**, 191 (1972).
- (3) H. Gesser, *J. Am. Chem. Soc.*, **77**, 2626 (1955).
- (4) F. W. Dalby, *Can. J. Phys.*, **36**, 1336 (1958).
- (5) C. H. Bamford, *Trans. Faraday Soc.*, **35**, 568 (1939).
- (6) A. Serewicz and W. A. Noyes, Jr., *J. Phys. Chem.*, **63**, 843 (1959).
- (7) R. Srinivasan, *J. Phys. Chem.*, **64**, 679 (1960).
- (8) S. Gordon, W. Mulac, and P. Nangia, *J. Phys. Chem.*, **75**, 2087 (1971).
- (9) M. Gehring, K. Hoyermann, H. Schacke and J. Wolfrum, *Symp. (Int.) Combust., [Proc.]*, **14**, 1972, 99 (1973).
- (10) G. Hancock, W. Lange, M. Lenzi, and K. H. Welge, *Chem. Phys. Lett.*, **33**, 168 (1975).
- (11) R. Simonaitis and J. Heicklen, *J. Phys. Chem.*, **80**, 1 (1976).
- (12) R. Simonaitis, R. I. Greenberg, and J. Heicklen, *Int. J. Chem. Kinet.*, **4**, 497 (1972).
- (13) D. Garvin and R. F. Hampson, National Bureau of Standards Report NBSIR 74-430 (1974).
- (14) H. A. Wiebe, A. Villa, T. M. Hellman, and J. Heicklen, *J. Am. Chem. Soc.*, **95**, 7 (1973).
- (15) J. D. Salzman and E. J. Bair, *J. Chem. Phys.*, **41**, 3654 (1964).
- (16) R. A. Back and T. Yokata, *Int. J. Chem. Kinet.*, **5**, 1039 (1973).
- (17) L. Stockburger, III, B. K. T. Sie, and J. Heicklen, Center for Air Environment Studies Report No. 407-75, Penn State University, 1975, *Sci. Total Environ.*, in press.

## Photochemistry of Alkyl Iodides

T. Donohue and J. R. Wiesenfeld\*

Department of Chemistry, Cornell University, Ithaca, New York 14853 (Received June 9, 1975)

Publication costs assisted by the Office of Naval Research

The chemical kinetics of ground state ( $5p^5 \ ^2P_{3/2}$ ) and electronically excited ( $5p^5 \ ^2P_{1/2}$ ) iodine atoms following the flash photolysis of RI ( $R = \text{H}, \text{C}_n\text{H}_{2n+1}$ , and  $\text{C}_n\text{F}_{2n+1}$ ) has been monitored using time-resolved attenuation of atomic resonance radiation. The deactivation efficiencies of  $\text{I}(^2P_{1/2})$  by RI have been determined and are discussed in terms of formation of a short-lived collision complex. In addition, the role of the photolytically generated R group in the chemistry of  $\text{I}(^2P_{1/2})$  and  $\text{I}(^2P_{3/2})$  has also been investigated and rates of a number of recombination and deactivation processes are estimated using modeling techniques. Of special significance to development of the iodine photochemical laser are the rate constants for deactivation of  $\text{I}(^2P_{1/2})$  by alkyl radicals and hydrogen atoms.

### 1. Introduction

There have been numerous studies on the photochemistry of alkyl iodides.<sup>1-6</sup> The earliest of these were concerned with the determination of the energy content and reactivity of the dissociated alkyl radical which receives considerable excess vibrational and translational energy in the initial photolysis.<sup>1,4,5</sup> The electronic state of the corresponding iodine atom remained a matter of conjecture until the iodine photodissociation laser was reported.<sup>7</sup> The observation of laser action following the photolysis of some of the simpler alkyl iodides<sup>6,7</sup> indicates that a substantial amount of electronically excited iodine,  $\text{I}(5^2P_{1/2})$ , is formed in the photodissociative process. As the iodine laser is currently being considered as a candidate for laser fusion experiments due to its potential for high output power,<sup>8</sup> interest has been renewed in the role of radicals in the photochemistry of alkyl iodides.

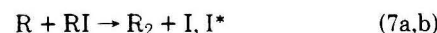
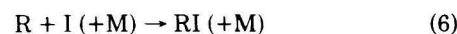
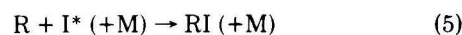
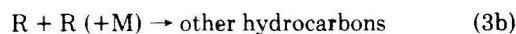
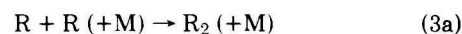
There are several important chemical and physical processes in the kinetics of the iodine photodissociation laser. The extent of population inversion is related to the initial photolytic branching ratio,  $\Phi$ , where

$$\Phi = [\text{I}(5^2P_{1/2})]_0 / [\text{I}(5^2P_{3/2})]_0$$

This parameter has recently been investigated in some detail.<sup>9</sup> The inversion can be depleted in a number of different processes. Most important is physical quenching of  $\text{I}(5^2P_{1/2})$  (hereafter,  $\text{I}^*$ ) by the source gas to produce ground state iodine atoms, I



which is presumably accompanied by some internal excitation of the RI. Also, the following reactions involving R,  $\text{I}^*$ , and I must be considered:



Note that reaction 7b could actually increase the inversion

following photolysis; indeed, this effect has been invoked to account for an apparent "late-time gain" observed in some laser experiments.<sup>10,11</sup> There are a number of other reactions possible, particularly if vibrationally and translationally "hot" radicals are included, but they are not considered, as a large excess of inert buffer gas was used in these experiments to ensure thermal equilibration of the radicals.

## 2. Experimental Section

The apparatus used in these experiments has been described previously.<sup>9,12</sup> Briefly, alkyl iodides (at 1–50  $\mu$  pressure) in 20 Torr of argon buffer gas were photolyzed by a 100-J Kr flash with absorption occurring in the region 240–280 nm. The resulting I and I\* products were monitored using time-resolved absorption spectroscopy. Here, a microwave powered electrodeless discharge lamp, containing a small amount of I<sub>2</sub> in Ar, was used to produce an atomic iodine emission spectrum. Appropriate resonance transitions [178.3 nm ( $6^2P_{3/2} \leftarrow 5^2P_{3/2}$ ) and 206.2 nm ( $6^2P_{3/2} \leftarrow 5^2P_{1/2}$ )] were selected using a vacuum monochromator. Transient absorption signals were digitized and the signal-to-noise ratio enhanced by addition of successive runs in a signal averager. The volume of the photolysis vessel was swept out between flashes to prevent accumulation of photolysis products.

A modified form of Beer's law was used to relate the observed absorption signal to the concentration of the atomic state being monitored, where

$$\ln(I_0/I_t) = \epsilon(lc)\gamma \quad (8)$$

and the symbols have their usual meaning. This relationship and the determination of  $\gamma$  are discussed in detail elsewhere.<sup>9,13</sup>

## 3. Results and Discussion

**A. Deactivation of I\* by RI.** The two processes that lead to an observed first-order decay of I\* in the presence of RI are (1) physical quenching and (2) chemical reaction. Figure 1 shows typical data at various concentrations of CH<sub>3</sub>I. The linear plots of  $\ln[I^*]$  vs.  $t$  obtained under conditions where  $[RI] \gg [I^*]$  indicate negligible contribution from processes 4, 5, and 7b, which would not display overall first-order kinetics. However, the branched iodides (isopropyl, *sec*-butyl, and *tert*-butyl), along with HI, display a pronounced curvature in their  $\ln[I^*]$  vs. time plots (Figure 2), indicating the importance of other processes. Therefore, a modeling technique (discussed below) was necessary to estimate the deactivation rates given by (1) and (2) for these four compounds. Table I lists the deactivation rates determined here. While several perfluoro compounds were studied, their deactivation rates were too slow to be observed at the low RI pressures used in these experiments.<sup>14</sup>

The correlation between deactivation rates and alkyl group size is interesting. The rates increase with radical size, in an almost linear fashion, so that the collision number (number of collisions required for deactivation) remains almost constant, except for HI, which gives a much lower collision efficiency. There does, however, appear to be a tendency for the collision efficiency to increase slightly as the alkyl group becomes larger. These effects can qualitatively be explained in terms of a short-lived collision complex, I-RI<sup>†</sup>, where the extent to which this entity can be formed is determined by the magnitude of the attractive forces between RI and I.<sup>15–18</sup> Alternatively, the larger number of hydrogen atoms or multitude of vibrational modes in

TABLE I

Source	$k_1 + k_2, 10^{-13} \text{ cm}^3 \text{ molecule}^{-1} \text{ s}^{-1}$		Collision no.
	Selected lit. values	This work	
CH <sub>3</sub> I	2.6 ± 0.6 <sup>a</sup>	5.7 ± 0.6	295
C <sub>2</sub> H <sub>5</sub> I	1.9 ± 0.2 <sup>b</sup>	6.1 ± 0.3	305
<i>n</i> -C <sub>3</sub> H <sub>7</sub> I	2.0 ± 0.2 <sup>b</sup>	8.0 ± 0.7	270
<i>i</i> -C <sub>3</sub> H <sub>7</sub> I	2.0 ± 0.2 <sup>b</sup>	6.3 ± 1.9	335
<i>n</i> -C <sub>4</sub> H <sub>9</sub> I	2.9 ± 0.2 <sup>b</sup>	9.3 ± 0.3	225
<i>s</i> -C <sub>4</sub> H <sub>9</sub> I		12.0 ± 2.4	185
<i>i</i> -C <sub>4</sub> H <sub>9</sub> I	2.9 ± 0.2 <sup>b</sup>	11.1 ± 0.7	205
<i>t</i> -C <sub>4</sub> H <sub>9</sub> I	3.8 ± 1.3 <sup>b</sup>	> 5.2 <sup>d</sup>	< 430 <sup>d</sup>
HI	1.5 ± 0.4 <sup>c</sup>	1.5 ± 0.2	1130
CD <sub>3</sub> I	0.046 ± 0.008 <sup>a</sup>	0.18 ± 0.01	9250

<sup>a</sup> Reference 21. <sup>b</sup> R. J. Donovan, F. G. M. Hathorn, and D. Husain, *Trans. Faraday Soc.*, **64**, 3192 (1968). <sup>c</sup> Reference 30. <sup>d</sup> Only limits can be given here due to rapid decomposition of the source gas.

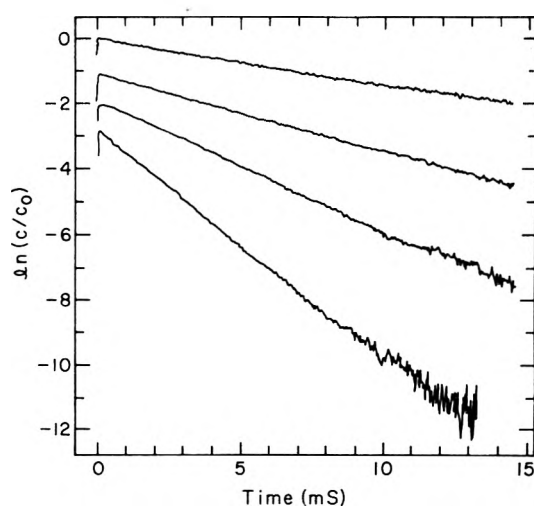


Figure 1. Deactivation of I\* in the presence of increasing partial pressures of CH<sub>3</sub>I:  $p_{Ar} = 20$  Torr;  $p_{CH_3I} = 1.4, 7.9, 21.2, 44.1 \mu$  (top to bottom). Traces are shifted by 1.0 ln unit for clarity.

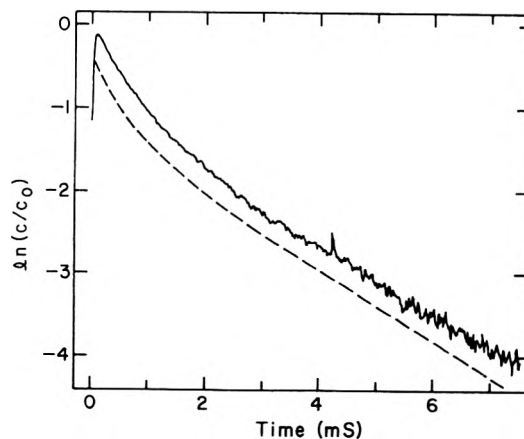


Figure 2. Deactivation of I\* in the presence of 9.9  $\mu$  of *sec*-butyl iodide and 20 Torr of Ar. Dashed line represents calculated fit (shifted downward by 0.3 ln unit for clarity) to the data, using rate constants given in Tables I and II. Initial concentrations used:  $[I^*]_0 = 8.9 \text{ m}\mu$ ;  $[I]_0 = 78 \text{ m}\mu$ ;  $[R]_0 = [I^*]_0 + [I]_0 = 87 \text{ m}\mu$ .

the heavier radicals might also be invoked to account for the observed enhancement of deactivation by these molecules.

The extent of chemical reaction 2 with respect to physical quenching (1) in the deactivation of  $I^*$  by alkyl iodides has been vigorously debated.<sup>3,19,20</sup> The importance of these processes in laser kinetics is clear. While (1) produces a ground state iodine atom, (2) results in an iodine molecule which has a large cross section for quenching of  $I^*$ , and a radical, which can further participate in reactions 3–7. Experiments performed by Meyer and others<sup>20</sup> using  $CH_3I$  indicate that the rate of process 2 could be quite large compared to that of (1). On the other hand, there is extensive evidence to indicate that deactivation is completely dominated by (1), at least for the normal, perhydro species.<sup>3,19,21,22</sup> As has been previously suggested,<sup>21</sup> one would expect the reactive channel, (2), to have equal probability for  $CH_3I$  and  $CD_3I$ . Since the measured deactivation rate is several orders of magnitude smaller for  $CD_3I$ ,<sup>21</sup> the dominant channel leading to deactivation of  $I^*$  by  $CH_3I$  must be quenching.

An upper bound for  $k_2/(k_1 + k_2)$  of 20% may be set for all of the normal, perhydro alkyl iodides examined here.<sup>23</sup> Unfortunately, a more detailed comparison between these compounds is precluded due to limitations imposed by the signal-to-noise ratio for the ground state line, as well as by limited accuracy of the numerical analysis. However, our results extend earlier work on  $CH_3I$  to higher members in the homologous series and confirm that quenching of  $I^*$  by RI proceeds with a much higher efficiency than reaction.

**B. Kinetics of Processes Involving Free Radicals.** While free radicals cannot be directly detected using the methods discussed here, their role may be deduced by observation of the temporal profiles of  $I^*$  and I following photolysis. The coupled, nonlinear differential kinetic equations describing reactions 1–7 may be integrated numerically by the standard Runge–Kutta method in order to obtain estimates of the kinetic parameters associated with processes 4–7. The relative importance of these processes following photolysis allows the iodides discussed here to be conveniently divided into three groups: primary iodides, branched iodides, and HI.

**Primary Iodides.** The kinetics for removal of  $I^*$  following the photolysis of primary iodides (Figure 1) are sensibly first order with respect to reactant concentrations. The removal of I is also a first-order process, since it is governed by diffusion through Ar to the walls, where heterogeneous recombination takes place.<sup>12</sup> These facts imply that processes 4–7 are slow compared to (1) + (2), particularly if (3) is fast. The rate of the radical recombination step (3a) has been measured for  $CH_3$  by a variety of methods<sup>24</sup> and has been found to be rapid, occurring in every 5–10 collisions. Reaction 3b is a disproportionation step, where  $R + R \rightarrow RH + R(-H)$ ; it is slow compared to (3a) for primary alkyls ( $k_{3b}/k_{3a} < 0.2$ ).<sup>25</sup> As the observed kinetic profiles would permit detection of a 2% nonlinearity in the  $I^*$  decay rate, a limit of  $\leq 5 \times 10^{-12} \text{ cm}^3 \text{ molecule}^{-1} \text{ s}^{-1}$  can be set on  $k_4 + k_5$  for the primary species. This parameter has recently been estimated<sup>22</sup> (for  $R = CH_3$ ) by modeling of laser amplifier gain measurements to be  $5.5 \times 10^{-12} \text{ cm}^3 \text{ molecule}^{-1} \text{ s}^{-1}$ , in agreement with the limits suggested here.

Deviations from first order would be difficult to observe in the case of I atom decay, especially since processes 4, 6, and 7a could combine in such a fashion as to yield no perceivable effect. However, since processes 4 + 5 and 6 are less important for primary radicals (due to rapid radical–radical recombination) than the corresponding ones involving branched radicals (see below), it would be expected

that the rates for reactions 4, 6, and 7a would be similarly unimportant.

**Branched Iodides.** In contrast to the primary compounds, the branched iodides all display curvature in both the plots of  $\ln [I^*]/[I^*]_0$  vs.  $t$  (Figure 2) and  $\ln [I]/[I]_0$  vs.  $t$  (Figure 3). As  $k_1 + k_2$  is similar for all of the hydrogenic iodides, this curvature suggests that the rates of processes 4 + 5 and 6 are much larger for the branched alkyls than for the primary isomers. Clearly, the enhanced contribution to  $I^*$  and I removal by processes 4 + 5 and 6 must be due to higher concentrations of alkyl radicals at times on the order of the kinetic observations (ca. 5–10 ms). This is reasonable in view of the relatively slow recombination of the branched radicals with respect to the unbranched species<sup>26</sup> (Table II). By fixing the measured values of  $k_1$  and  $k_3$ , as well as the known branching ratio of the initial photolysis ( $\Phi = 0.10$ ), it is possible to obtain estimates of the rate constants for processes 4 + 5 and 6 as well as overall photolysis yields. Process 2 is deemed to be of negligible importance. The value of  $\Phi$  does not affect  $k_5$  or  $k_6$  so long as  $\Phi \ll 1$ . As  $k_3$  has not been reported for  $s\text{-}C_4H_9$  it was estimated by assuming that the photolysis yield of  $s\text{-}C_4H_9I$  was the average of the yields of  $i\text{-}C_3H_7I$  and  $t\text{-}C_4H_9I$ . Examples of typical fits to  $I^*$  and I data are displayed in Figures 2 and 3, respectively, using values of the rate constants and photolysis yields given in Table II.

The deactivation of  $I^*$  by the perhydrogenated alkyl radicals  $i\text{-}C_3H_7$ ,  $s\text{-}C_4H_9$ , and  $t\text{-}C_4H_9$  is seen to proceed with a rate constant of ca.  $5 \times 10^{-12} \text{ cm}^3 \text{ molecule}^{-1} \text{ s}^{-1}$ . These rates are consistent both among themselves and with the suggested upper limit for  $I^* + CH_3$  quenching derived above. In addition, they are in good agreement with the value of  $5.5 \times 10^{-12} \text{ cm}^3 \text{ molecule}^{-1} \text{ s}^{-1}$  obtained in laser gain measurements.<sup>22</sup> It is interesting to note that the rate constants for radical deactivation of  $I^*$  are 5–10 times larger than those for deactivation by the corresponding alkyl iodides, thus necessitating inclusion of processes 4 + 5 in any attempt to model iodine laser systems where the fraction of photolysis is greater than ca. 5%. The rate constant for deactivation of  $I^*$  by the perfluorinated radicals<sup>27</sup> lies around  $2 \times 10^{-12} \text{ cm}^3 \text{ molecule}^{-1} \text{ s}^{-1}$ ; the ratio  $(k_4 + k_5)/k_1$  is much larger for the perfluorinated than for the perhydro species.

To the best of our knowledge, no values of  $k_6$  for perhydrogenated radicals have previously been reported. In view of its large value, about  $7 \times 10^{-12} \text{ cm}^3 \text{ molecule}^{-1} \text{ s}^{-1}$ , this recombination must be in the second-order pressure region. The only other reported measurement of  $I + R$  is that for the perfluorinated radicals<sup>27</sup> where  $k_6 \sim 3 \times 10^{-11} \text{ cm}^3 \text{ molecule}^{-1} \text{ s}^{-1}$ . This process would only be expected to play a significant role for lasers or amplifiers operating near threshold, as the use of photolytic sources with  $\Phi \gg 1$ , would result in very low concentrations of I. However, lasers based on the use of inefficient photolytic sources or electric discharge initiation<sup>28</sup> might depend on significant depletion of I by (6) before laser threshold is achieved.

**HI.** HI displays curvature in its plots of  $\ln [I^*]/[I^*]_0$  vs.  $t$  in a manner similar to those of the branched iodides (Figure 2), but in this case, it is clear that this deviation is caused by process 4 and not 5 as the latter is not probable; the  $HI^*$  "complex" could exist for only about one vibrational period, leaving little possibility for collisional stabilization. This argument also applies to processes 3 and 6. Modeling of  $I^*$  decay data demonstrates that the quenching process 4 occurs with a surprisingly large probability, with

TABLE II: Radical Reaction Rates and Photolysis Yields

	$k, 10^{-12} \text{ cm}^3 \text{ molecule}^{-1} \text{ s}^{-1}$			Photolysis yield, % per flash
	$k_3$	$k_4 + k_5$	$k_6$	
<i>i</i> -C <sub>3</sub> H <sub>7</sub>	9 <sup>a</sup>	5	9	3.0
<i>s</i> -C <sub>4</sub> H <sub>9</sub>	2 <sup>b</sup>	7	10	3.5
<i>t</i> -C <sub>4</sub> H <sub>9</sub>	1 <sup>a</sup>	5	5	4.0

<sup>a</sup> Reference 26. <sup>b</sup> See text.

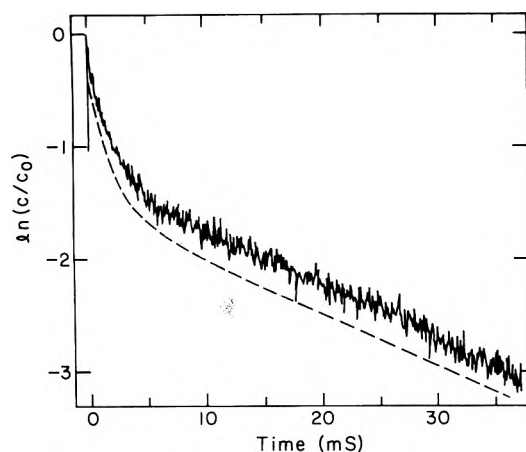


Figure 3. Decay of I in the presence of 3.3  $\mu$  of sec-butyl iodide and 20 Torr of Ar. Dashed line represents calculated fit (shifted down by 0.2 ln unit) to the data, using rate constants given in Table II. Initial concentrations used:  $[I^*]_0 = 3.0 \text{ m}\mu$ ;  $[I]_0 = 26 \text{ m}\mu$ ;  $[R]_0 = 29 \text{ m}\mu$ . The long-time decay ( $t > 10 \text{ ms}$ ) is due to diffusion by I to the walls ( $k_{\text{diff}} = 45 \text{ s}^{-1}$ ).

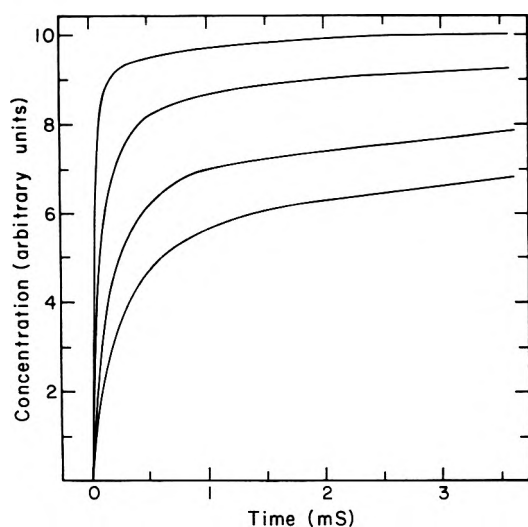


Figure 4. Initial rise of I in the presence of increasing partial pressures of HI.  $p_{\text{Ar}} = 20 \text{ Torr}$ ;  $p_{\text{H}_2} = 90 \mu$ ;  $p_{\text{HI}} = 1.0, 2.3, 4.2, 16.8 \mu$  (bottom to top). Data have been smoothed by hand and traces are not normalized to one another.  $\text{H}_2$  ( $k_{\text{H}_2} = 1.2 \times 10^{-14} \text{ cm}^3 \text{ molecule}^{-1} \text{ s}^{-1}$ , for  $I^* + \text{H}_2 \rightarrow I + \text{H}_2$ ) is used to control the rate at which  $I^* \rightarrow I$ ; this feature can aid in data interpretation.

a rate constant of  $\sim 5 \times 10^{-11} \text{ cm}^3 \text{ molecule}^{-1} \text{ s}^{-1}$ . All of the energy released in this quenching process ( $21.7 \text{ kcal mol}^{-1}$ ) must go into translation; the hydrogen atom is produced extremely "hot" following such a quenching collision, as it acquires over 99% of the available kinetic energy. Process 4 has also been observed in the H atom quenching of  $\text{Cl}^*(^3\text{P}_{1/2})$  atoms, which proceeds at an even faster rate,<sup>29</sup>  $\sim 7 \times 10^{-10} \text{ cm}^3 \text{ molecule}^{-1} \text{ s}^{-1}$ , about the gas kinetic value.

Figure 4 demonstrates the rise in [I] for varying HI concentrations. The rate of increase is clearly a function of [HI], and results from processes 4 and 7a. Modeling of the concentration profile of the I atoms, using the value determined above for  $k_4$ , yields a rate constant,  $k_{7a}$ , of  $2.0 \pm 1.0 \times 10^{-11} \text{ cm}^3 \text{ molecule}^{-1} \text{ s}^{-1}$ . Cadman et al.,<sup>30</sup> in calculations on some earlier experimental data of Sullivan,<sup>31</sup> obtained  $3.3 \times 10^{-11} \text{ cm}^3 \text{ molecule}^{-1} \text{ s}^{-1}$ . As had been suggested earlier,<sup>32</sup> no evidence of reaction 7b could be found in our results.

#### 4. Conclusions

Rate constants have been determined for a variety of processes involving alkyl iodides and related photofragments. Deactivation rate constants for  $I^*$  by RI measured here appear  $\sim 2$ – $4$  times faster than those reported earlier. No systematic cause for these discrepancies (i.e., impurities, such as  $\text{O}_2$ , in the samples used were found to be negligible) have been found. Alternatively, a systematic error in the determination of  $\gamma$  for the transition ( $6^2\text{P}_{3/2} \leftarrow 5^2\text{P}_{1/2}$ ) at 206.2 nm could result in  $k_{\text{CH}_3\text{I}}$  being as much as 1.75 times too large if  $\gamma$  were 1.0 instead of our measured value, 0.57. However, the rates for HI and  $\text{H}_2$ <sup>12</sup> determined in the same apparatus agree, within error limits, with recent literature values.<sup>30,32</sup> Processes involving alkyl radicals have been found to be rapid, and of potential significance to practical laser systems. Of course, the estimates of the rate constants associated with these processes depend upon the absolute values of the radical-radical recombination rates, and so can be no more accurate than these parameters.<sup>26</sup>

*Acknowledgment.* We are indebted to the Office of Naval Research for their generous support of this research.

#### References and Notes

- J. R. Majer and J. P. Simons, *Adv. Photochem.*, **2**, 137 (1964), and references cited therein.
- M. R. Levy and J. P. Simons, *J. Chem. Soc., Faraday Trans. 2*, **71**, 561 (1975), and references cited therein.
- D. Husain and R. J. Donovan, *Adv. Photochem.*, **8**, 1 (1971), and references cited therein.
- S. J. Riley and K. R. Wilson, *Faraday Discuss. Chem. Soc.*, **53**, 132 (1972).
- G. M. Harris and J. E. Willard, *J. Am. Chem. Soc.*, **76**, 4678 (1954).
- J. V. V. Kasper, J. H. Parker, and G. C. Pimentel, *J. Chem. Phys.*, **43**, 1827 (1965).
- J. V. V. Kasper and G. C. Pimentel, *Appl. Phys. Lett.*, **5**, 231 (1964).
- K. Hohla and K. L. Kompa, *Appl. Phys. Lett.*, **22**, 77 (1973).
- T. Donohue and J. R. Wiesenfeld, *J. Chem. Phys.*, **63**, 3130 (1975).
- T. L. Andreeva, V. I. Malyshev, A. I. Maslov, I. I. Sobel'man, and V. N. Sorokin, *JETP Lett.*, **10**, 271 (1969).
- K. Hohla and K. L. Kompa, *Chem. Phys. Lett.*, **14**, 445 (1972); *Z. Naturforsch. A*, **27**, 938 (1972).
- T. Donohue and J. R. Wiesenfeld, *Chem. Phys. Lett.*, **33**, 176 (1975).
- R. J. Donovan, D. Husain, and L. J. Kirsch, *Trans. Faraday Soc.*, **66**, 2551 (1970).
- D. Husain and J. R. Wiesenfeld, *Trans. Faraday Soc.*, **63**, 1349 (1967).
- A more detailed treatment of collision complex dynamics can be found in S. J. Riley and D. R. Herschbach, *J. Chem. Phys.*, **58**, 27 (1973), and references cited therein.
- P. J. Robinson and K. A. Holbrook, "Unimolecular Reactions", Wiley-Interscience, New York, N.Y., 1972.
- W. Forst, "Theory of Unimolecular Reactions", Academic Press, New York, N.Y., 1973.
- The theory of unimolecular decay is now well understood; see ref 16 and 17. However, the effect of electronically excited levels in energy partitioning among the modes of a complex has now just begun to be treated. See D. W. Setser, *MTP Int. Rev. Sci., Phys. Chem.*, **Ser. One**, **9**, 1 (1972); J. C. Tully, *J. Chem. Phys.*, **62**, 1893 (1975).
- S. Aditya and J. E. Willard, *J. Chem. Phys.*, **44**, 418 (1966).
- R. T. Meyer, *J. Chem. Phys.*, **46**, 4146 (1967); *J. Phys. Chem.*, **72**, 1583 (1968); D. M. Haaland and R. T. Meyer, *Int. J. Chem. Kinet.*, **6**, 297 (1974).
- R. J. Donovan and C. Fotakis, *J. Chem. Phys.*, **61**, 2159 (1974).
- T. D. Padrick, private communication.
- A recent study<sup>22</sup> using  $\text{CH}_3\text{I}$  gives 2% for this ratio.

- (24) F. C. James and J. P. Simons, *Int. J. Chem. Kinet.*, **6**, 887 (1974), and references cited therein.
- (25) E. Whittle, *MTP Int. Rev. Sci., Phys. Chem., Ser. One*, **9**, 75 (1972).
- (26) D. M. Golden, G. N. Spokes, and S. W. Benson, *Angew. Chem.*, **12**, 534 (1973).
- (27) S. V. Kuznetsova and A. I. Maslov, *Sov. J. Quantum Electron. (Engl. Trans.)*, **3**, 468 (1974).
- (28) L. D. Pleasance and L. A. Weaver, *Appl. Phys. Lett.*, **27**, 407 (1975).
- (29) R. J. Donovan, D. Husain, A. M. Bass, W. Braun, and D. D. Davis, *J. Chem. Phys.*, **50**, 4115 (1969).
- (30) P. Cadman, J. C. Polanyi, and I. W. M. Smith, *J. Chim. Phys.*, **64**, 111 (1967).
- (31) J. H. Sullivan, *J. Chem. Phys.*, **36**, 1925 (1962).
- (32) R. J. Donovan and D. Husain, *Trans. Faraday Soc.*, **62**, 1050 (1966).

## Chlorophyll-Poly(vinylpyridine) Complexes. V. Energy Transfer from Chlorophyll to Bacteriochlorophyll<sup>1</sup>

G. R. Seely

Charles F. Kettering Research Laboratory, Yellow Springs, Ohio 45387 (Received June 20, 1975)

Publication costs assisted by the Charles F. Kettering Laboratory

The transfer of singlet excitation energy from chlorophyll a to bacteriochlorophyll on poly(4-vinylpyridine) in nitromethane solution has been measured by quenching and sensitization of fluorescence. The directly excited fluorescence of both chlorophyll a and bacteriochlorophyll is strongly quenched by transfer to weakly interacting, weakly fluorescent pairs of pigment molecules. The dominant quencher is apparently a bacteriochlorophyll-chlorophyll a pair. The fluorescence of bacteriochlorophyll is correlated with the presumed density of quenching pairs, but the quenching of chlorophyll a fluorescence has also a component due to transfer to bacteriochlorophyll. The quenching of chlorophyll a fluorescence is described mathematically by Förster's equation for transfer from a donor to randomly distributed acceptors, provided that the effective critical transfer distance  $R_0$  is proportional to the sixth root of the donor/acceptor ratio. In this way energy trapping can be described, when there is extensive transfer among randomly distributed donor molecules. The equations pertaining to the model system can be extrapolated to pigment systems typical of photosynthetic units, and maximum sizes of the units can be estimated, which depend on pairwise transfer parameters and attainable pigment concentrations. The estimated sizes approximate those of the presumed natural ones.

### Introduction

Chlorophyll or its derivatives bound to the randomly coiled macromolecule poly(4-vinylpyridine) in nitromethane solution constitutes a three-dimensional aggregate of variable pigment density, useful as a model for studying energy transfer and trapping processes like those of the photosynthetic unit of green plants.<sup>2-5</sup> In a previous paper we demonstrated energy transfer in this system by depolarization of fluorescence, and have related the probability of it to the configurational properties of the polymer.<sup>3</sup> The other "classical" way of demonstrating energy transfer is by sensitization of the fluorescence of one kind of molecule through excitation of another.<sup>6</sup> While depolarization of fluorescence detects whether energy transfer occurs at all, sensitization of fluorescence detects only energy transferred from donor to acceptor, and therefore can be studied at pigment concentrations at which many transfers among donor molecules occur. Sensitization of fluorescence is therefore an appropriate means by which to study energy transfer in dense pigment aggregates, including the photosynthetic unit itself.

We have measured energy transfer from chlorophyll b to chlorophyll a, and from chlorophyll a to bacteriochlorophyll, in mixed pigment aggregates on poly(4-vinylpyridine). Because of unexpected complications in the former

system, we confine ourselves here to the latter, more straightforward system.

The essential question to be examined is how multiple transfer among donor molecules (chl) affects the probability of transfer to acceptor (bchl), as a function of the ratio of acceptor to donor,  $\beta = (\text{bchl})/(\text{chl})$ , and of the pigment density in the polymeric aggregate, expressed as the ratio of bound chlorophyll a or bacteriochlorophyll to polymer pyridine units. It will be found possible to include the effect of multiple transfer within the conceptual framework of energy trapping developed by Duysens<sup>7</sup> and Förster.<sup>8</sup>

The pigments of the present system resemble those of the green sulfur bacteria, where transfer occurs from an antenna array of chlorobium chlorophyll to a core array and reaction center of bacteriochlorophyll.

### Experimental Section

**Materials.** Chlorophyll a was extracted from spinach and purified chromatographically. Bacteriochlorophyll was extracted from species of photosynthetic bacteria with acetone and chromatographed twice on sugar with toluene +0.5% 1-propanol eluent. The poly(4-vinylpyridine) used was a fraction of molecular weight 320 000 (fraction A3 of ref 3). The purification of nitromethane has been described.<sup>3</sup>

**Procedure.** Portions of stock solutions of chlorophyll a and of bacteriochlorophyll in acetone and 0.005 ml of  $\alpha$ -methyl-naphthalene were evaporated nearly to dryness in the cuvette, and diluted with 3.5 ml of nitromethane. The  $\alpha$ -methyl-naphthalene helps keep chlorophyll in suspension when nitromethane is added.<sup>2</sup> Portions of a stock solution of poly(4-vinylpyridine) were added, and the spectrum was recorded in the red and near-infrared band regions on a Cary Model 14 spectrophotometer. Operations were conducted under cover of N<sub>2</sub>.

Fluorescence was measured with the apparatus used for depolarization,<sup>3</sup> with interference filters instead of polarizers to select fluorescence excitation and observation wavelengths. The direct fluorescence of bacteriochlorophyll was excited at 760 nm and measured at 800 nm. Chlorophyll a was excited at 660 nm; its fluorescence was read at 680 nm, and the sensitized fluorescence of bacteriochlorophyll at 800 nm. Drift in the intensity of the source lamp was followed by light scattered by a solution of colloidal silica (Ludox), and correction for it made.

The relative spectral sensitivity of the EMI 9558B photomultiplier had been determined to 700 nm with rhodamine B and methylene blue quantum counters;<sup>3</sup> the manufacturer's curve for sensitivity of the S-20 surface was used to extend the relative sensitivity to 800 nm.

The ratio of bacteriochlorophyll to chlorophyll a was determined from absorbances at the band peaks near 781 and 666 nm, observed with large excess of polymer. Molar absorptivities  $\epsilon$  were  $7.0 \times 10^4 \text{ M}^{-1} \text{ cm}^{-1}$  for chlorophyll a (666 nm) and  $9.0 \times 10^4 \text{ M}^{-1} \text{ cm}^{-1}$  for bacteriochlorophyll (781 nm). The latter was calculated from Clayton's values for ether and acetone-methanol solutions<sup>9</sup> and the approximation  $\epsilon\delta = 1.35 \times 10^7$ , where  $\delta$  is the difference (in Å) between the peak wavelength and the wavelength at which the absorbance is half the peak absorbance, on the long-wave side of the band.

**Quantum Yields.** As in the previous work, but without the complications of polarization, quantum yields were calculated from observed fluorescence intensities by relations such as

$$\phi_{680}^{660} = I_{680}^{660} / \Omega I_0 (F_{680} S_{680} a(\rho) D (1 - R) (1 + R \phi_{680}^{660})) \quad (1)$$

in which  $\phi_{680}^{660}$  is the quantum yield of chlorophyll a fluorescence excited by 660-nm radiation,  $I_{680}^{660}$  is the observed fluorescence intensity, normalized to a standard light source intensity by  $I_0$ ,  $\Omega$  is an instrument constant which includes a refractive index correction,  $F_{680}$  is the fraction of chlorophyll a fluorescence passed by the 680-nm interference filter,  $S_{680}$  is the sensitivity of the photomultiplier in quantum units,  $a(\rho)$  is the fraction of incident light absorbed, expressed as a function of the optical density,  $\rho$ , at the chlorophyll band peak,  $D$  is a dissymmetry factor,  $R$  is the fraction of fluorescence reabsorbed, and the last parentheses is a correction for secondary fluorescence.<sup>3</sup>

Rigorous application of the corrections for reabsorption and secondary fluorescence is impracticable because both chlorophyll and bacteriochlorophyll absorb and reemit light. Certain simplifications made the calculation tractable by the procedures described in part II of this series.<sup>3</sup> The fluorescence of chlorophyll a in the presence of excess polymer, observed over a range of pigment concentration, with and without a 680-nm interference filter, gave  $F_{680}$  and curves for  $D(1 - R)$  as functions of  $\rho$ . Comparison with light scattered from Ludox gave the quantum yield of chlorophyll a fluorescence,  $\phi_{680}^{660} = 0.206$ , and the lumped con-

stant  $\Omega I_0 S_{680}$ . The correction for secondary chlorophyll a fluorescence was neglected; its value was judged not to exceed about 2% at most, and is difficult to estimate when bacteriochlorophyll is present.

The quantum yield,  $\phi_{800}^{760} = 0.086$ , filter factor  $F_{800}$ , and reabsorption curve were determined similarly for bacteriochlorophyll. As chlorophyll a does not reabsorb bacteriochlorophyll fluorescence, its presence does not affect this calculation.

In the calculation of the yield of sensitized fluorescence,  $a(\rho)$  and  $D$  were taken from curves for chlorophyll a, and  $(1 - R)$  from the reabsorption curve for bacteriochlorophyll.

Transfer of energy from chlorophyll a to bacteriochlorophyll by reabsorption of fluorescence is by no means insignificant in these systems, but its value is limited by that of  $\phi_{800}^{660}$  as the ratio of polymer pyridine units to chlorophyll a, (py)/(chl), becomes very large. Also included in this limit is the yield of bacteriochlorophyll fluorescence directly excited by absorption of 660-nm light.

## Results

Series of fluorescence yield measurements over increasing polymer concentrations were made with (chl)/(bchl) ratios of 14.1, 7.2, 3.0, 2.55, and 0.73. Binding of bacteriochlorophyll was indicated by the same sort of spectral changes that characterize binding of other chlorophyll derivatives.<sup>2</sup> In dense aggregates, the infrared band peak is displaced from its position in nitromethane solution (7760–7780 Å) to a position in the range 7815–7830 Å. In the presence of large excess of polymer the band peak moves into the range 7811–7817 Å and becomes narrower. The exact position of the peak is affected by the presence of traces of water or other polar impurities in the solvent.

Quantum yields measured in the system in which (chl)/(bchl) = 7.2 are typical, and are plotted as functions of polymer concentration in Figure 1. It is evident that at low ratios of polymer to pigment, the fluorescence of both chlorophyll a and bacteriochlorophyll is substantially quenched. At (py)/(chl) = 30 and below, the fluorescence of chlorophyll a increases somewhat because of incomplete binding to the polymer. Quenching at low (py)/(chl) ratios is commonly observed in systems like these and has been attributed to transfer of singlet state excitation energy from bound monomeric pigment molecules, which are fluorescent, to weakly interacting pairs of pigment molecules, which act as quenching centers.<sup>2-5</sup> Absorption spectral changes support this interpretation, and the energy of interaction has even been estimated, using an appropriate site model of the polymer chain.<sup>2</sup>

Although the self-excited fluorescence of both pigments is quenched at low (py)/(chl) ratios, that of bacteriochlorophyll is restored before (i.e., at lower (py)/(chl) ratios) than that of chlorophyll a. When measured in the absence of chlorophyll a, the fluorescence of bacteriochlorophyll is restored to half maximal value at (py)/(bchl) = 180. In Figure 1, half maximal value is attained at (py)/(chl) = 68, which corresponds to (py)/(bchl) = 490. In the absence of bacteriochlorophyll, the fluorescence of chlorophyll a,  $\phi_{680}^{660}$ , was completely restored at (py)/(chl) = .200, but in Figure 1, restoration is deferred until (py)/(chl) > 1000.

In contrast to these, the fluorescence of bacteriochlorophyll, sensitized by chlorophyll a, rises to a maximum at (py)/(chl) = 100, then falls to a much lower value as (py)/(chl) increases. The declining part of the curve for  $\phi_{800}^{660}$  is virtually a mirror image of the curve for  $\phi_{680}^{660}$ . This is clear

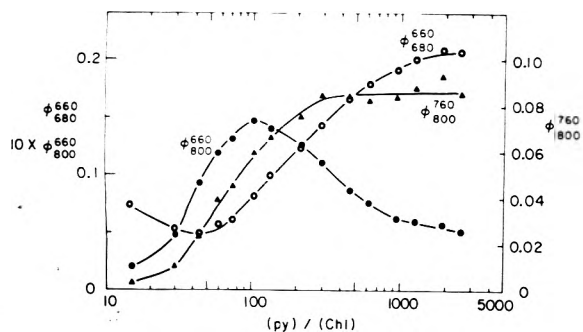


**Figure 1.** Quantum yields of directly excited fluorescence of bacteriochlorophyll ( $\phi_{660}^{760}$  and  $\phi_{680}^{760}$ ) and chlorophyll a ( $\phi_{660}^{660}$  and  $\phi_{680}^{660}$ ), and of sensitized fluorescence of bacteriochlorophyll ( $\phi_{660}^{680}$  and  $\phi_{680}^{680}$ ), as functions of (py)/(chl) for the series in which (chl)/(bchl) = 7.2.

evidence of transfer of light energy absorbed by chlorophyll a to bacteriochlorophyll.

Further insight into the fate of energy absorbed by chlorophyll a is obtained from a plot of the probabilities that the excitation energy remains on bound monomeric chlorophyll a molecules ( $\phi_{chl}$ ) or is transferred to monomeric bacteriochlorophyll ( $\phi_{bchl}$ ), i.e., bacteriochlorophyll not in quenching centers: The former is the observed fluorescence quantum yield divided by its maximum value,  $\phi_{chl} = \phi_{660}^{660}/0.206$ ; the latter is the sensitized fluorescence yield divided by the directly excited fluorescence yield,  $\phi_{bchl} = \phi_{660}^{680}/\phi_{660}^{660}$ . The latter assumes that the quantum yield of fluorescence of bacteriochlorophyll, excited by transfer from chlorophyll, is the same as that of directly excited bacteriochlorophyll. Singlet excitation energy not accounted for by  $\phi_{chl}$  and  $\phi_{bchl}$  is considered to have been trapped in quenching centers:  $\phi_{trap} = 1 - \phi_{chl} - \phi_{bchl}$ . These quantities are plotted for the data of Figure 1 in Figure 2.

Plots such as Figure 2 for the several series show a steady decline in energy transferred to monomeric bacteriochlorophyll when (py)/(chl) increases above 100, and a more rapid decline in energy transferred to traps. The two curves cross between (py)/(chl) = 600 and 900, usually closer to the latter. In all series a surprisingly large fraction of energy must be allotted to  $\phi_{trap}$ .

When (py)/(chl) decreases below 70, the curve for  $\phi_{bchl}$  does not always continue upward as it does in Figure 2, but as often levels off. Since  $\phi_{bchl}$  is the ratio of two small numbers in this region, it is not clear what the trend of the curves should be, and we shall not be further concerned with data in this region.

**Quenching of Bacteriochlorophyll Fluorescence.** The curve for  $\phi_{680}^{760}$  in Figure 1 shows that directly excited bacteriochlorophyll fluorescence is partially quenched up to (py)/(chl) = 300. This corresponds to (py)/(bchl) = 2160. Fluorescence is also quenched in a system containing bacteriochlorophyll only, but is fully restored at a (py)/(bchl) ratio of about 1000. If it is accepted that quenching in pure bacteriochlorophyll systems is due to interacting pairs of bacteriochlorophyll molecules, then the additional quenching when chlorophyll a is present, as in Figure 1, must be due to interacting bacteriochlorophyll and chlorophyll a molecules. If trapping by (bchl)<sub>2</sub> pairs and by (bchl-chl) pairs is equally effective, and trapping by (chl)<sub>2</sub> pairs is excluded on energetic grounds, the fluorescence yield should be a function of the density of traps, which is then proportional to (bchl)<sup>2</sup> + (bchl)(chl).

A plot of all data for  $\phi_{680}^{760}$  against (py)<sup>2</sup>/(bchl)[(bchl) + (chl)] shows that these data are quite well correlated by the

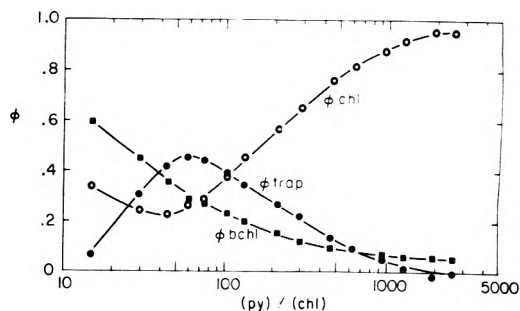


**Figure 2.** Probabilities that excitation energy, absorbed by chlorophyll a, remains on (monomeric) chlorophyll a ( $\phi_{chl}$ ), is transferred to monomeric bacteriochlorophyll ( $\phi_{bchl}$ ), or is captured by quenching centers ( $\phi_{trap}$ ), which are probably mostly (bchl-chl). From data of Figure 1, (chl)/(bchl) = 7.2.

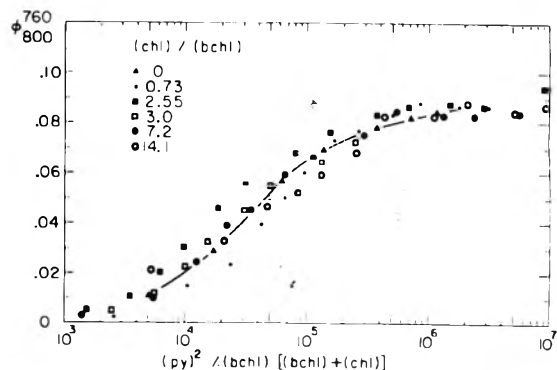


**Figure 3.** Correlation of bacteriochlorophyll fluorescence yield with density of quenching centers, estimated by (bchl)[(bchl) + (chl)]/(py)<sup>2</sup>. Curve through points for bacteriochlorophyll alone on poly(vinylpyridine).

curve for the system of bacteriochlorophyll alone on polymer (Figure 3). Plots against other functions of pigment density show a distinctly wider divergence of the sets of points.

The presence of interacting pairs of pigment molecules in dense aggregates is marked by a displacement of absorption bands to the red, and their dissociation on increasing the polymer/pigment ratio by a shift to the blue.<sup>2</sup> The position of the red band peak of chlorophyll a, and of the infrared band peak of bacteriochlorophyll, plotted in Figure 4 for the case in which (chl)/(bchl) = 0.73, undergo a blue shift with midpoint near (py)/(chl) = 400. The directly excited fluorescence of bacteriochlorophyll is restored in the same region, consistently with the dissolution of quenching dimers. The fluorescence of chlorophyll a is restored more slowly, because transfer to monomeric bacteriochlorophyll persists after the disappearance of quenching dimers. The shift of the chlorophyll a band occurs at larger (py)/(chl) ratios than it does in systems without bacteriochlorophyll, which further shows that the predominant quenching centers are interacting chlorophyll a-bacteriochlorophyll pairs.

**Quenching of Chlorophyll a Fluorescence.** If bacteriochlorophyll fluorescence is quenched by transfer to (bchl-chl) and (bchl)<sub>2</sub> pairs, it is to be expected that chlorophyll a fluorescence would be quenched primarily by transfer to (chl)<sub>2</sub> and (bchl-chl) pairs, the concentration of (bchl)<sub>2</sub> being relatively low. In the absence of transfer to monomeric bacteriochlorophyll, a plot of  $\phi_{chl}$  against (py)<sup>2</sup>/(chl)[(chl) + (bchl)] would correlate the data uniformly, as the plot of Figure 3 does for bacteriochlorophyll. What is

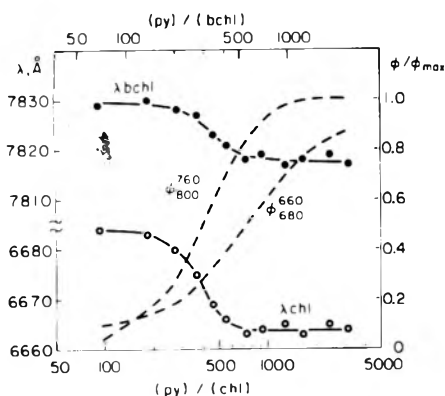


**Figure 4.** Evidence for interaction of chlorophyll a and bacteriochlorophyll on poly(vinylpyridine): solid curves, left ordinate scales, positions of peaks of chlorophyll a red band and of bacteriochlorophyll infrared band, for series with  $(chl)/(bchl) = 0.73$ ; dashed curves, right ordinates, relative quantum yields of directly excited fluorescence of chlorophyll a ( $\phi_{660}^{chl}$ ) and bacteriochlorophyll ( $\phi_{760}^{bchl}$ ).

observed in such a plot is that restoration of chlorophyll a fluorescence is retarded by an amount which is directly related to the proportion of bacteriochlorophyll in the system (Figure 5). This plot displays the effect of transfer to monomeric bacteriochlorophyll dissected from transfer to quenching centers.

### Discussion

Interest in multiple transfer of energy in artificial systems is inspired by efforts to account for the behavior of photosynthetic systems, in which trapping excitation energy out of a large array of pigment molecules is an essential step in their function. Although the theory of pairwise transfer of energy according to Förster has been verified rigorously and in detail in recent years, extension to transfer in systems of many molecules encounters conceptual difficulties which have baffled attempts to estimate the probability of trapping energy out of an arbitrary array of molecules in a rigorous and satisfying way.<sup>10</sup> Our use of a model system is an attempt to study this probability in a system in which pigment density can be varied in a way not possible in natural photosynthetic systems.

Duysens has discussed the problem of trapping probability in terms of an equation of the Stern-Volmer type, in which that probability is  $nT/(1 + nT)$ , where  $n$  is the number of "different" transfers per excited state lifetime, and  $T$  is the ratio of traps to antenna molecules.<sup>7</sup> In our terms,  $n$  is proportional to the square of the chlorophyll a concentration, or equivalently to  $[(chl)/(py)]^2$ , and  $T = (bchl)/(chl) = \beta$ . An equation for  $\phi_{chl}$  may then be written in the form

$$\phi_{chl} = 1/(1 + K\beta[(chl)/(py)]^2) = 1/(1 + K(bchl)(chl)/(py)^2) \quad (2)$$

A plot of  $\phi_{chl}$  against  $(py)^2/(chl)(bchl)$ , (Figure 6) shows a uniform and satisfactory correlation with this variable. However, the recovery of fluorescence is slower than predicted by the function of eq 2. The deviation is in the direction expected if a statistical distribution of pigment arrays must be taken into account.

For energy transfer from a donor to acceptors Förster derived an equation which we may express as

$$\phi_{chl} = 1 - 2qe^{q^2} \int_q^\infty e^{-x^2} dx \quad (3)$$

where  $q$  is the ratio of acceptor concentration to a "critical concentration" defined by the rate of pairwise transfer from donor to acceptor.<sup>8</sup> Derivation of the equation assumed a random distribution of acceptors about a donor, but also assumed no transfer between donor molecules. However, we shall adapt this equation to the case where transfer among donor molecules is prevalent.

In the presence of the acceptors monomeric bacteriochlorophyll,  $(chl)_2$ , and  $(bchl-chl)$ ,  $q$  may be expressed as

$$q = \frac{\left(\frac{(chl)_2}{py}\right)}{\left(\frac{(chl)_2}{py}\right)_0} + \frac{\left(\frac{(bchl-chl)}{py}\right)}{\left(\frac{(bchl-chl)}{py}\right)_0} + \frac{\left(\frac{(bchl)}{py}\right)_m}{\left(\frac{(bchl)}{py}\right)_0} \quad (4)$$

where the subscripts  $m$  and  $0$  refer to monomeric pigment and to "critical concentrations" for transfer from chlorophyll a to the acceptors.<sup>8</sup> Since, at low trap density

$$\left(\frac{(chl)_2}{py}\right) \approx K_c \left(\frac{(chl)}{py}\right)_m^2$$

and

$$\left(\frac{(bchl-chl)}{py}\right) \approx K_b \left(\frac{(chl)}{py}\right)_m \left(\frac{(bchl)}{py}\right)_m$$

$$q \approx K_c \frac{\left(\frac{(chl)}{py}\right)_m^2}{\left(\frac{(chl)_2}{py}\right)_0} + K_b \left(\frac{(chl)}{py}\right)_m \left(\frac{(bchl)}{py}\right)_m \times$$

$$\left\{ \frac{1}{\left(\frac{(bchl-chl)}{py}\right)_0} - \frac{1}{\left(\frac{(bchl)}{py}\right)_0} \right\} + \frac{\left(\frac{(bchl)}{py}\right)_t}{\left(\frac{(bchl)}{py}\right)_0} \quad (5)$$

where the subscript  $t$  refers to total concentration. At low concentrations of quenching pairs, the subscripts  $m$  and  $t$  may be suppressed in eq 5 and  $q$  becomes an expression quadratic in  $(chl)/(py)$ :

$$q = \frac{\beta \left(\frac{(chl)}{py}\right)}{\left(\frac{(bchl)}{py}\right)_0} + \left[ \frac{K_c}{\left(\frac{(chl)_2}{py}\right)_0} + K_b \beta \left\{ \frac{1}{\left(\frac{(bchl-chl)}{py}\right)_0} - \frac{1}{\left(\frac{(bchl)}{py}\right)_0} \right\} \right] \left(\frac{(chl)}{py}\right)^2 \quad (6)$$

Values of  $q$  corresponding to  $\phi_{chl}$  in the range 0.3 to 0.9 were determined from a curve of the function of eq 3, and the corresponding values of  $(chl)/(py)$  were read from the experimental curves of Figure 5. In the plot of  $q$  against  $(chl)/(py)$ , Figure 7, data over much of the quenching range are represented by straight lines passing near the origin, for series containing bacteriochlorophyll. For the series with chlorophyll a only, the points do not approach the origin linearly.

The slopes of the lines,  $q/[(chl)/(py)]$ , are equal to  $\beta/[(bchl)/(py)]_0$ , and since  $\beta$  is known, provide values of  $[(bchl)/(py)]_0$ . These values are listed in Table I. Equation 6 would be compatible with either upward or downward deviation of the data from straight lines; the absence of a definite trend either way indicates that the second term in eq 6 is rather small, and that therefore the parameter for



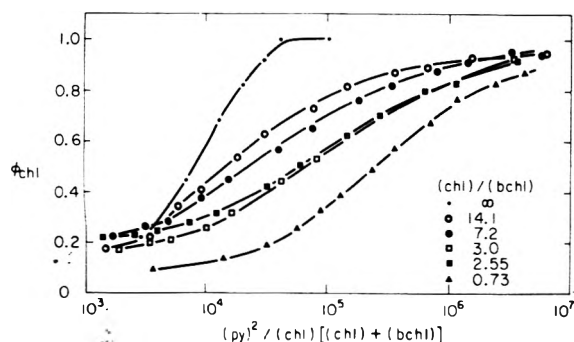


**Figure 5.** Correlation of fraction of light absorbed by chlorophyll a, not transferred to bacteriochlorophyll or quenching centers, with the density of the latter estimated by  $(chl)[(chl) + (bchl)]/(py)^2$ . Curve for chlorophyll a only (---) represents quenching by  $(chl)_2$  pairs only. Spread of remaining curves reveals transfer to bacteriochlorophyll not in quenching centers.

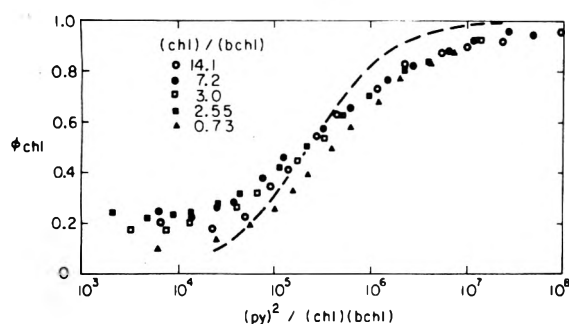


**Figure 6.** Correlation of the relative fluorescence of chlorophyll a with the density function  $(bchl)(chl)/(py)^2$  suggested by modified Duysens eq 2. The dashed line is a function of the form of eq 2 drawn through midpoint of plot.

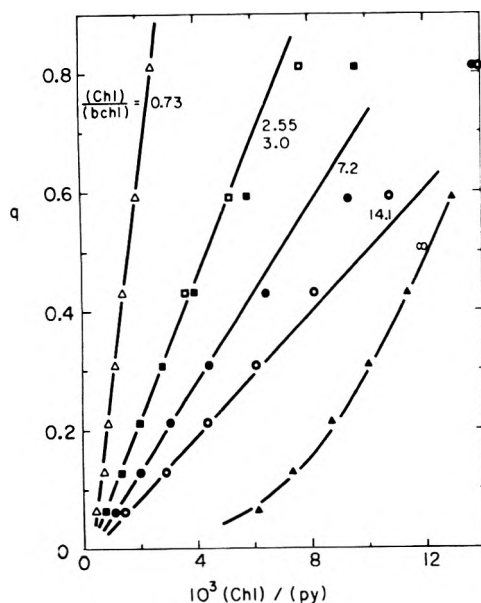


**Figure 7.** Plots of independent variable  $q$  of eq 3 against  $(chl)/(py)$ , for evaluation of slopes  $\beta/[(bchl)/(py)]_0$  in eq 6.

transfer from chlorophyll a to  $(bchl-chl)$  is about the same as that for transfer to monomeric bacteriochlorophyll.

It is seen in Table I that the value of  $[(bchl)/(py)]_0$  decreases as  $(chl)/(bchl)$  increases. A logarithmic plot of these (Figure 8) implies a correlation of these quantities according to

**TABLE I: Critical Ratios  $[(bchl)/(py)]_0$  and Effective Radii for Transfer of Energy from Chlorophyll a to Bacteriochlorophyll at Different Ratios of the Two Pigments**

$(chl)/(bchl)$	$10^3 [(bchl)/(py)]_0$	$\frac{1}{4} R_0, \text{ \AA}$	$R_0, \text{ \AA}^b$
Pyrochlorophyll <sup>a</sup>	4.09	42	58
0.73	3.7	43	59
2.55	3.34	43.5	60
3.0	2.83	45	62
7.2	1.88	54	75
14.1	1.38	60	83
Extrapolated Values			
50	0.71	75	104
100	0.50	85	118
200	0.355	95	131
300	0.29	102	141

<sup>a</sup> Values from ref 3. <sup>b</sup>  $R_0$  calculated for chlorophyll a in ether, from ref 10.

$$[(bchl)/(py)]_0 = 0.0050[(chl)/(bchl)]^{-1/2} \quad (7)$$

when  $(chl)/(bchl) > 2$ . If this is inserted into what is left of eq 6 we obtain

$$q = 200\beta^{1/2}(chl)/(py) = 200[(bchl)(chl)/(py)^2]^{1/2} \quad (8)$$

which through eq 3 reproduces the functional dependence of  $\phi_{chl}$  on  $(bchl)(chl)/(py)^2$  predicted by eq 2 and found in Figure 6.

A critical pigment/polymer ratio such as  $[(bchl)/(py)]_0$  is proportional to  $1/R_0^3$ , where  $R_0$  is Förster's parameter for pairwise energy transfer, the separation at which transfer is as probable as other modes of deactivation of the excited donor molecule. In our study of depolarization of fluorescence of pyrochlorophyll,<sup>3</sup> a critical transfer ratio  $[(pyrochl)/(py)]_0 = 0.00409$  was found to correspond to a critical distance  $R_0 = 42 \text{ \AA}$ . This enables us to calculate effective  $R_0$ 's corresponding to the values of  $[(bchl)/(py)]_0$  by the relation

$$R_0^3(\text{\AA}) = (42)^3(0.00409)/[(bchl)/(py)]_0 \quad (9)$$

These values are included in Table I.

The situation can be summarized as follows. Förster's eq 3 correctly describes the dependence of donor fluorescence on pigment concentration when there is transfer of energy among donor molecules, provided that the effective value of the critical distance  $R_0$  for transfer to acceptor is proportional to the sixth root of the ratio of donor to acceptor concentration. The same provision largely reconciles the Förster and Duysens expressions, eq 2 and 3.

We are now in a position to estimate an upper limit to the size of a photosynthetic unit. Since the critical concentration parameters for pyrochlorophyll and  $[(bchl)/(py)]_0$  are very similar, and since pyrochlorophyll closely resembles chlorophyll a, the following calculation is fortuitously better applicable to green plant systems than to bacterial.

First, the foregoing arguments make it reasonable to extrapolate the line of Figure 8 into the range of donor-to-trap ratios more representative of photosynthetic units, and calculate the corresponding  $R_0$ 's for use in eq 3. This is done in the lower part of Table I.

The meaning of  $R_0$  is that if a photon is captured within a sphere of that radius about an acceptor, it has a better-than-even chance of being transferred to that acceptor. There is, however, an upper limit to the density at which

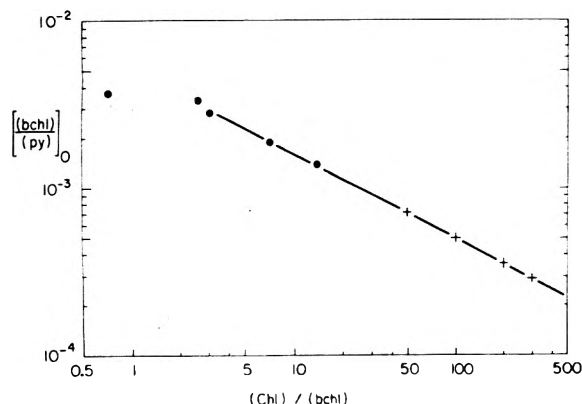


**Figure 8.** Correlation of critical ratio  $[(bchl)/(py)]_0$  for transfer of energy from chlorophyll a to bacteriochlorophyll with  $(chl)/(bchl)$ . Data of Table I; crosses indicate tabulated extrapolated values.

donors may be packed; in natural photosynthetic units this appears to be between 0.1 and 0.2 M. This limits the number of donors that can be accommodated within the sphere of radius  $R_0$ , and therefore the size of a photosynthetic unit, if it is to capture energy efficiently. If the lower value is chosen, the number of chlorophyll molecules within a radius  $R_0$  about the acceptor is

$$(chl)/(bchl) = 6(4/3)\pi R_0^3 10^{19} \quad (10)$$

Equation 10, together with eq 7 and 9, gives the maximum values of  $R_0$  and  $(chl)/(bchl)$  that can be realized in the present construction of a photosynthetic unit. With a critical distance of 42 Å for pyrochlorophyll, the maximum  $R_0$  and  $(chl)/(bchl)$  are 126 Å and 507.

In his recent review of energy transfer, Knox concludes that a higher value of  $R_0$  may be more appropriate for chlorophyll a.<sup>10</sup> If 42 Å is indeed too low, it is probably because of failure of polymer configuration theory to describe segment distributions accurately at short range.<sup>3,10</sup> If the value calculated for chlorophyll in ether, 58 Å, is used in eq 9, the values of  $R_0$  in the last column of Table I are obtained, and the maximum size of a photosynthetic unit expands to  $R_0 = 279$  Å and  $(chl)/(bchl) = 5490$ .

About these numbers, certain points should be kept in mind. They refer to a spherically symmetrical distribution

of chlorophylls, whereas the natural distribution is usually laminar; they assume a photosynthetic unit operating with about 50% efficiency, whereas actual units must be much more efficient and therefore smaller; they are critically dependent not only on the concentration of pigment, but also on the orientation and distribution of spectral varieties of the molecules.<sup>11,12</sup>

Still, the lower set of values does approximate the size and population of chloroplast lamella particles which are thought to correspond to photosynthetic units.<sup>13</sup> The population of the larger units of green bacteria, in which a more nearly spherical distribution of pigment may exist, lies between the calculated values.<sup>14</sup> What is more significant is that from this study of a model system, it has been possible to deduce a rational basis for calculating the size of a photosynthetic unit.

*Acknowledgments.* The experimental work was supported in part by a grant from the National Science Foundation, and was performed with the skilled technical assistance of Mr. T. H. Meyer.

## References and Notes

- (1) Contribution No. 548 from the Charles F. Kettering Research Laboratory.
- (2) G. R. Seely, *J. Phys. Chem.*, **71**, 2091 (1967).
- (3) G. R. Seely, *J. Phys. Chem.*, **74**, 219 (1970).
- (4) G. R. Seely, *J. Phys. Chem.*, **75**, 1667 (1971).
- (5) G. R. Seely, *J. Phys. Chem.*, **76**, 172 (1972).
- (6) T. Förster, *Discuss. Faraday Soc.*, No. 27, 7 (1959).
- (7) L. N. M. Duysens, *Prog. Biophys. Mol. Biol.*, **14**, 1 (1964).
- (8) T. Förster, *Z. Naturforsch. A*, **4**, 321 (1949). The form of eq 4 for  $q$  in the presence of more than one kind of acceptor results from a reexamination of the original derivation of this quantity, in particular of the transformation represented by eq 14 of this reference.
- (9) R. K. Clayton, *Photochem. Photobiol.*, **5**, 669 (1966).
- (10) R. S. Knox in "Bioenergetics of Photosynthesis", Govindjee, Ed., Academic Press, New York, N.Y., 1975, Chapter 4, has reviewed theories of energy transfer, particularly those based on lattices, where the problem is, in principle at least, soluble in specialized cases. However, this approach is difficult to apply to systems with statistical distributions of transferring molecules.
- (11) G. R. Seely, *J. Theor. Biol.*, **40**, 173, 189 (1973).
- (12) A. Yu. Borisov and Z. G. Fetisova, *Mol. Biol. (Moscow)*, **5**, 509 (1971).
- (13) R. B. Park in "The Chlorophylls", L. P. Vernon and G. R. Seely, Ed., Academic Press, New York, N.Y., 1966, Chapter 9.
- (14) C. F. Fowler, N. A. Nugent, and R. C. Fuller, *Proc. Proc. Natl. Acad. Sci. U.S.A.*, **68**, 2278 (1971).



TABLE I: Spectral Properties of Chlorophyll b in Solution

Solvent:	$\lambda_r, \text{\AA}$	$\delta_r, \text{\AA}$	$\epsilon_r, \text{M}^{-1} \text{cm}^{-1}$	$\lambda_s, \text{\AA}$
Acetone	6459	106	44 800 <sup>b</sup>	4543
Nitromethane + 3% acetone	6460	106	42 000	4572
Nitromethane	6462-6465	101-104	43 000	4576-4580
Nitromethane, very dry	6459	120		4673
Nitromethane + pvp, (py)/(chl b) = 35	6511	136		4660
Nitromethane + pvp... (py)/(chl b) = 1000	6501	131	33 200	4634
Nitromethane + $\epsilon$ -ethyl- pyridine, (py)/(chl b) = 1500	6465	102		

<sup>a</sup> Peak wavelengths  $\lambda_r$  and  $\lambda_s$  of red and Soret bands, molar absorptivity  $\epsilon_r$ , and half-width  $\delta_r$  at half-height of red band. <sup>b</sup> Reference value from A. S. Holt and E. E. Jacobs, *Am. J. Botany*, 41, 710 (1954).

decisively in variation of fluorescence activation and emission spectra.

**Absorption Spectra.** Some spectral properties of chlorophyll b in various solvent mixtures are compiled in Table I. As chlorophyll b tends to be more soluble in nitromethane than chlorophyll a, more thorough drying of the solvent is necessary to induce aggregation before polymer is added. The clearest indication in Table I of two species in the presence of excess polymer is that the half-width,  $\delta_r$ , does not return to the smaller value characteristic of monomeric solutions. The spectral bands, however, are broadened and shaped in such a way as to suggest the presence of two close, overlapping bands. The red displacements reported here are not as large as those presented before,<sup>4</sup> which suggests that the purity of the solvent has much to do with the appearance of the spectrum even in the presence of excess polymer.

**Fluorescence.** Changes in fluorescence intensity, excited at 460 nm and measured at 650 and 680 nm, ( $I_{650}^{460}$  and  $I_{680}^{460}$ ), and the position of the Soret peak, are plotted against the equivalent ratio of polymer pyridine units to pigment, (py)/(chl b), in Figure 1. At low polymer concentration, fluorescence is partially quenched, but not as strongly as with chlorophyll a and bacteriochlorophyll.<sup>2,3</sup> The curves for restoration of fluorescence intensity at 650 and 680 nm have different shapes, and the difference between them, corrected for photomultiplier sensitivity, passes through a maximum at (py)/(chl b) = 60, just beyond the maximum red shift of the Soret band near (py)/(chl b) = 40. The change in relative fluorescence intensity at 650 and 680 nm continues well beyond the point where weak associations between bound pigment molecules have been broken up, as indicated by return of the Soret band to its normal position, in a manner which suggests transfer of energy from the shorter-wave to the longer-wave emitting species.

In Figure 2, the relative intensities of fluorescence at 650 and 680 nm, excited in the Soret band at 460, 470, and 480 nm, are compared. If there were only one emitting species, the curves would all be proportional to each other, differing only in intensity, but this is not the case. As in Figure 1, 680-nm fluorescence rises before 650 nm, however excited. Fluorescence at 650 nm is excited most strongly at 460 nm, followed by 470 and 480 nm. Fluorescence at 680 nm is excited most strongly at 470 nm, followed by 480 and 460 nm. This difference persists at large (py)/(chl b) ratios. The ratio of total fluorescence emitted at 680 nm to that at 650 nm maximizes at about (py)/(chl b) = 60, as in Figure 1. This ratio reflects the extent to which energy is transferred from the predominantly 650-nm species to the longer-wave species.

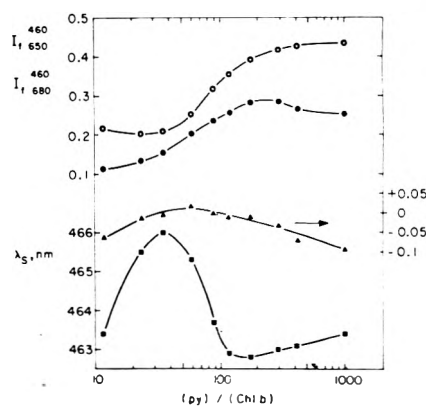


Figure 1. Spectral and fluorescence intensity changes as functions of chlorophyll b-polyvinylpyridine composition. From top: fluorescence intensities, excited at 460 nm and read at 650 nm and at 680 nm, not corrected for photomultiplier sensitivity; the difference between them,  $I_{680}^{460} S_{650} / S_{680} - I_{650}^{460}$ , corrected for photomultiplier sensitivity (right ordinate scale); position of Soret band peak. Gradual rise in  $\lambda_s$  between (py)/(chl b) = 200 and 1000 is unusual and probably indicates minor change in solvation of bound pigment by impurities.

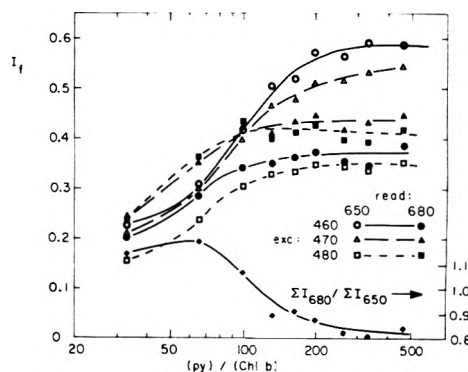


Figure 2. Comparison of fluorescence intensities, excited at 460, 470, and 480 nm in the Soret band, and measured at 650 and 680 nm. Fluorescence intensities on a relative scale. Lower curve: ratio of total fluorescence emitted at 680 and 650 nm, i.e.,  $(I_{680}^{460} + I_{680}^{470} + I_{680}^{480}) / (I_{650}^{460} + I_{650}^{470} + I_{650}^{480})$ .

In another experiment, the fluorescence spectrum was traced with an Aminco-Bowman spectrophotofluorometer for three (py)/(chl b) ratios, with excitation at 450, 460, 470, and 480 nm. The positions of the fluorescence peaks are compared in Table II. When no polymer is present, the fluorescence peak is at 650 nm, irrespective of excitation wavelength. When polymer is present, the fluorescence

TABLE II: Variation of Fluorescence Peak Wavelength with Excitation Wavelength and (py)/(chl b)

(py)/(chl b)	0	33	165	428
Excitation wavelength, nm				
450	650	651	654	652
460	650	654	654	653
470	650	655	657	656
480	650	658	658	658

peak wavelength changes by 4–7 nm as excitation passes through the Soret band.

It was considered that part of the chlorophyll b might have undergone a chemical reaction in solution with the polymer, perhaps similar to the oxidation reported earlier for chlorophyll a,<sup>4</sup> which could account for the displacement of the band to longer wavelengths. After the above experiment, the nitromethane was evaporated and the pigment extracted from the residues with acetone. Only the spectrum of chlorophyll b was found, with no sign of a longer wave compound. Evidently only one chemical species is responsible for the two spectrally distinct forms.

**Chlorophyll b-Chlorophyll a Systems.** When chlorophyll a is present together with chlorophyll b, transfer to the former is shown by increased fluorescence intensity at 680 nm, though at 460 nm only chlorophyll b is excited. Series of fluorescence intensity measurements were made at (chl b)/(chl a) ratios of 36, 14, 9.4, 4.9, 2.6, and 2.5. Fluorescence intensities for the series with (chl b)/(chl a) = 4.9 are typical and are shown in Figure 3. In comparison with the series without chlorophyll a (Figure 1), the fluorescence at 680 nm is stronger and peaks at a smaller (py)/(chl b) ratio. The difference between  $I_{680}^{460}$  and  $I_{650}^{460}$  is peaked more sharply and at a larger (py)/(chl b) ratio than the corresponding difference in Figure 1. The difference between these two curves reflects the transfer of energy to chlorophyll a, in addition to that transferred to the long wavelength form of bound chlorophyll b.

Quenching of fluorescence by associated pigment pairs becomes prominent at (py)/(chl b) < 100. The fluorescence of chlorophyll b as measured by  $I_{650}^{460}$  is reduced by this process as well as by transfer to chlorophyll a. In the chlorophyll a-bacteriochlorophyll system, these processes were separated by plotting the chlorophyll a fluorescence against  $(py)^2/[(chl a) + (chl b)]$ , which quantity was supposed to be inversely proportional to the density of quenching pairs along the polymer chain. The corresponding plot for the present system is presented in Figure 4, in which  $I_{650}^{460}$ , relative to its limiting value at large polymer concentration, is plotted against the reciprocal of the total pigment density on the polymer. In the absence of better information, it was assumed that all pigment pairs, (chl a)<sub>2</sub>, (chl a-chl b), and (chl b)<sub>2</sub>, occur in statistical proportions and quench fluorescence equally; the abscissa then is inversely proportional to the square root of quenching center density.

In Figure 4, the recovery of chlorophyll b fluorescence is delayed in the presence of chlorophyll a, but not by nearly as much as in the chlorophyll a-bacteriochlorophyll system. There is also less regularity in the displacement of the curves as a function of (chl b)/(chl a). Perhaps the strongest effect is decreased fluorescence intensity at small (py)/[(chl b) + (chl a)] values. These results become understandable if we consider that chlorophyll a, at the ratios used, makes a relatively small addition to the long wave-

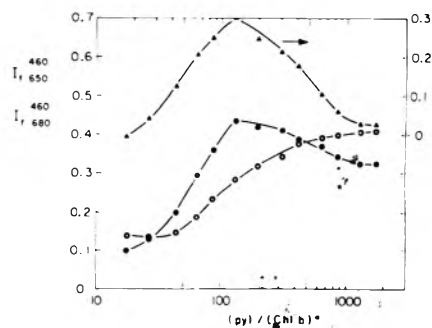


Figure 3. Fluorescence intensities as functions of (py)/(chl b) for series with (chl b)/(chl a) = 4.9: open circles,  $I_{650}^{460}$ ; solid circles,  $I_{680}^{460}$ ; triangles,  $I_{680}^{460}S_{650}/S_{680} - I_{650}^{460}$  (right ordinate scale).

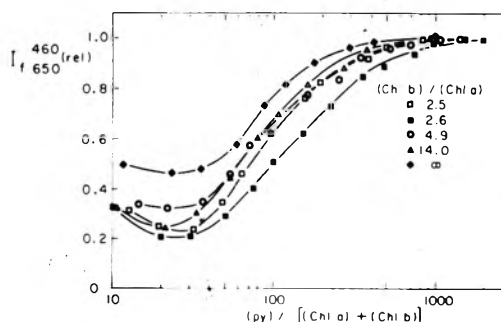


Figure 4. Plot of chlorophyll b fluorescence, as measured by  $I_{650}^{460}$  relative to its value at high polymer concentration, against reciprocal pigment density on the polymer, assumed proportional to the square root of the quenching pair density. Curves for (chl b)/(chl a) = 36 and 9.6 are omitted to reduce crowding.

length form of chlorophyll b, which already serves as acceptor of the fluorescence measured by  $I_{650}^{460}$ . The long wavelength form also functions as an intermediate trap for energy, which has the effect of retarding its transfer to the deeper traps of chlorophyll a.

The fraction  $\phi_t$  of absorbed quanta transferred from chlorophyll b to chlorophyll a was estimated by<sup>5</sup>

$$\frac{\phi_t}{1 - \phi_t} = \frac{\phi_b}{\phi_a} \left[ \frac{F_{650}^b I_{680}^{460} S_{650} - F_{680}^b I_{650}^{460} S_{680}}{F_{680}^a I_{650}^{460} S_{680} - F_{650}^a I_{680}^{460} S_{650}} \right] \quad (1)$$

In eq 1,  $S_{650}$  and  $S_{680}$  are the sensitivities of the photomultiplier at the two wavelengths, and the factors  $F_{650}^b$ ,  $F_{650}^a$ ,  $F_{680}^b$ , and  $F_{680}^a$  are the fractions of total fluorescence of chlorophylls b and a passed by the 650- and 680-nm interference filters. The chlorophyll b and chlorophyll a fluorescence quantum yields,  $\phi_b$  and  $\phi_a$ , were taken from curves for the pure pigment systems; the ratio  $\phi_b/\phi_a$  ranged from 2.39 at small (py)/[(chl a) + (chl b)] to 0.78 at large. The ratio  $F_{680}^b/F_{650}^b$  is identified with the value of  $I_{680}^{460}S_{650}/I_{650}^{460}S_{680}$  for pure chlorophyll b, and varies with (py)/(chl b) (Figure 1).

Equation 1 does not correct for reabsorption and reemission of fluorescence; calculated values of  $\phi_t$  may therefore be high by something on the order of 5–10%.

Values of  $\phi_t$  for the several series are plotted against (py)/[(chl a) + (chl b)] in Figure 5. In this plot, the curves through the points for each series are strongly peaked near (py)/[(chl a) + (chl b)] = 50. It appears that if quenching or failure of chlorophyll b to bind entirely did not prevail, the transfer to chlorophyll a would be essentially complete at smaller values of the abscissa.

**Chlorophyll b-Chlorophyll a-Bacteriochlorophyll System.** We made one series of fluorescence measurements

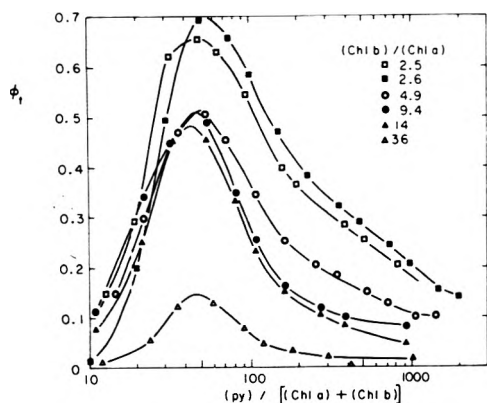


Figure 5. Fraction  $\phi_t$  of excitation energy quanta, absorbed by chlorophyll b and transferred to chlorophyll a, as function of reciprocal pigment density on polymer;  $\phi_t$  calculated by eq 1.

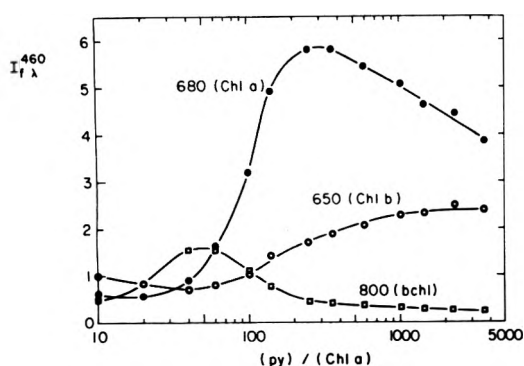


Figure 6. Intensity of fluorescence at characteristic wavelengths in ternary system of chlorophyll b, chlorophyll a, and bacteriochlorophyll in the ratio 14.25:28.5:1. Fluorescence intensities in relative units but corrected for photomultiplier sensitivity.

with a three pigment system which was set up to operate somewhat like a natural photosynthetic unit. The pigment concentration ratios were set at chl b:chl a:bchl = 14.25:28.5:1. At these ratios and with excitation at 460 nm, nearly all the light was absorbed by chlorophyll b, and transferred to chlorophyll a within one or two jumps. Chlorophyll a then acted as the principal energy transfer pigment and bacteriochlorophyll as the trap.

Fluorescence intensities, corrected for photomultiplier sensitivity, are plotted in Figure 6 for the representative wavelengths. The fluorescence of the trapping pigment,  $I_{f800}^{460}$ , peaks at  $(py)/(chl a) = 50$ , then declines as the fluorescence of chlorophyll a,  $I_{f680}^{460}$ , rapidly rises. At larger  $(py)/(chl a)$  values, the fluorescence of chlorophyll b increases at the expense of that of chlorophyll a, just as it does in the series with those two pigments alone (Figure 3).

If the peak fluorescence intensity of bacteriochlorophyll is compared with that of chlorophyll b at large  $(py)/(chl a)$ , and account is taken of the quantum yields (0.086 and 0.160) and filter factors ( $F_{800}^{bchl} = 0.293$ ,  $F_{650}^b = 0.101$ ), it is estimated that at least 35% of absorbed quanta are transferred to bacteriochlorophyll at  $(py)/(chl a) = 50$ . Since bacteriochlorophyll constitutes only 2.3% of the pigment molecule population, trapping of the energy would appear to be rather efficient in this system. Maximum sensitization of bacteriochlorophyll fluorescence is found at pigment densities at which most of the fluorescence of chlorophylls a and b would be quenched by interacting pigment

pairs; this suggests that transfer to quenching centers may not be irreversible, and that further transfer to deeper traps is still possible.

## Discussion

The presence of two spectrally distinct and fluorescent forms of chlorophyll b on poly(vinylpyridine) was unexpected, and an explanation for it is not obvious. The two forms are the same chemical species, because only chlorophyll b can be recovered from the complex. The forms are monomeric, because they persist at large polymer concentrations, and are distinct from the pair interactions that give rise to fluorescence quenching.

The presence of traces of water and other impurities in solution probably modifies the spectra of bound chlorophyll b somewhat, but this alone cannot account for two forms, because they are not found with chlorophyll a. In an experiment in which the total chlorophyll b plus polymer concentration was varied at fixed large and small  $(py)/(chl b)$  ratios, the spectrum of the dense aggregate was broadened and reddened with increasing concentration, but the spectrum of the sparse aggregate was unaffected. This is interpreted as the expected effect of traces of impurities on the extent of pigment association in dense aggregates, and as the lack of an effect on the relative amounts of the two forms in sparse aggregates.

Chlorophyll b differs structurally from chlorophyll a only in having a formyl group at the 3 position instead of a methyl. Conjugation of the formyl group with the chlorin ring system produces a hypsochromic displacement of the red band from its position for chlorophyll a. Construction of a model shows that if chlorophyll b is bound to syndiotactic poly(4-vinylpyridine) by a dative bond from pyridine to Mg, the next pyridine but one along the polymer chain is able to come in contact with the C atom of the formyl carbonyl group. Nucleophilic approach by pyridine at this position would tend to reduce the interaction between the formyl group and the rest of the molecule, and produce the bathochromic shift, with respect to chlorophyll b, that characterizes the long wavelength form. We have, however, no independent support for the conjecture that this manner of binding is responsible for the longer wavelength form.

There is convincing evidence that chlorophyll a in algae exists in distinct spectral species, differing in the positions of their red bands by about 8 nm.<sup>6</sup> A possible role of these species in accelerating the transfer of energy to the trap has been discussed.<sup>7</sup> There is also evidence for two spectral species of chlorophyll b in algae, with bands at 640 and 649.5 nm. There has been much speculation as to what kind of interactions between chlorophylls and their environment produce these spectrally distinct forms; the prevailing opinion is probably that they arise from exciton interaction of closely associated chlorophyll molecules in dimers and higher aggregates.<sup>8,9</sup> Displacement of the spectra can also arise in monomeric pigments by association with other polar or polarizable molecules in their vicinity.<sup>10,11</sup> It is interesting, though not necessarily relevant to the photosynthetic unit structure, that in our model system, two monomeric forms of a chlorophyll coexist and transfer energy one to the other.

*Acknowledgment.* The experimental work was supported in part by a grant from the National Science Foundation,

and performed with the technical assistance of Mr. T. H. Meyer.

## References and Notes

- (1) Contribution No. 549 from the Charles F. Kettering Research Laboratory.
- (2) G. R. Seely, *J. Phys. Chem.*, preceding paper in this issue.
- (3) G. R. Seely, *J. Phys. Chem.*, **74**, 219 (1970).
- (4) G. R. Seely, *J. Phys. Chem.*, **71**, 2091 (1967).
- (5) To derive eq 1, note first that if both chlorophylls a and b are present, the measured fluorescences excited by 460-nm irradiation are each composed of two parts, and in the absence of reabsorption and secondary fluorescence, can be expressed as the sum of two components, viz.  $I_{460} = I_{460}^{a+b} + I_{460}^{b+a}$  and  $I_{680} = I_{680}^{a+b} + I_{680}^{b+a}$ . Application of eq 1 of the previous paper<sup>2</sup> to each fluorescence component separately, with neglect of reabsorption and dissymmetry ( $R = 0$ ,  $D = 1$ ), gives the following:

$$\begin{aligned}\phi_a &= I_{680}^{a+b} / \Omega(\phi_1 I_0) F_{680}^a S_{680} \alpha(\rho) \\ &= I_{680}^{a+b} / \Omega(\phi_1 I_0) F_{680}^b S_{680} \alpha(\rho) \\ \phi_b &= I_{460}^{a+b} / \Omega(1 - \phi_1) I_0 F_{460}^a S_{460} \alpha(\rho) \\ &= I_{460}^{a+b} / \Omega(1 - \phi_1) I_0 F_{460}^b S_{460} \alpha(\rho)\end{aligned}$$

Elimination of  $I_{460}^{a+b}$ ,  $I_{680}^{a+b}$ ,  $I_{460}^{b+a}$ , and  $I_{680}^{b+a}$ , cancellation of the common factors  $\Omega$ ,  $I_0$ , and  $\alpha(\rho)$ , and rearrangement of the remainder gives eq 1. In effect, the subtractive terms in eq 1 correct for the mutual overlap of chlorophyll a and b fluorescences.

- (6) C. S. French, J. S. Brown, and M. C. Lawrence, *Plant Physiol.*, **49**, 421 (1972).
- (7) G. R. Seely, *J. Theor. Biol.*, **40**, 173 (1973).
- (8) T. M. Cotton, A. D. Trifunac, K. Ballschmitter, and J. J. Katz, *Biochim. Biophys. Acta*, **368**, 181 (1974).
- (9) C. E. Strouse, *Proc. Nat. Acad. Sci. U.S.A.*, **71**, 325 (1973).
- (10) G. R. Seely and R. G. Jensen, *Spectrochim. Acta*, **21**, 1835 (1965).
- (11) G. R. Seely, *Spectrochim. Acta*, **21**, 1847 (1965).

## On the Annihilation Lifetimes of Positrons Bound in Positronium Complexes<sup>1</sup>

William J. Madia and Hans J. Ache\*

Department of Chemistry, Virginia Polytechnic Institute and State University, Blacksburg, Virginia 24061 (Received July 29, 1975)

An experimental approach is described to determine the annihilation lifetimes,  $\tau_c$ , of positrons in Ps complexes of *p*-dinitrobenzene and *p*-benzoquinone in organic solvents. It is based on the dependence of  $I_2$ , the intensity of the long-lived component in the positron lifetime spectra, on the chemical reaction rates of the Ps atoms with the substrate molecules, which in turn vary as a function of temperature. From the experiments an average value for  $\tau_c = 0.36 \pm 0.10$  ns has been obtained.

### Introduction

A positron may combine with an electron to form a electron-positron bound state, the positronium atom (Ps). This species has a lifetime of about  $10^{-7}$  to  $10^{-9}$  s which is too short for its reactions to be followed by conventional product analysis. The chemical reactions of positronium can be studied by observing changes in its average lifetime and decay modes which are dependent on the chemical reactivity and physical composition of its environment.<sup>2</sup>

By using these methods Madia, Nichols, and Ache<sup>3</sup> have been able to show that Ps undergoes reversible molecular complex formation in solutions with compounds which are known in conventional chemistry as strong complex formers, such as nitrobenzene, benzoquinone, etc. Temperature studies were carried out which resulted in an assessment of the kinetics and the activation parameters of these processes.

Very little, however, is known about the exact nature of the Ps complex,<sup>4</sup> especially about the annihilation lifetime of the positron in the Ps complex. At the present time only a few quantum mechanical calculations have been published, which would predict lifetimes of about 0.31 ns for  $\text{PsLi}^+$ ,<sup>5,6</sup> 0.33 ns for  $\text{PsNa}^+$ ,<sup>5,6</sup> 5 ns for  $\text{PsCl}$ ,<sup>7,8</sup> and 0.45 ns for  $\text{PsH}$ .<sup>9</sup>

Thus in the following we wish to report the results of a preliminary experimental study from which an estimate of the positron annihilation lifetimes in Ps complexes of com-

pounds such as dinitrobenzene and *p*-benzoquinone may be derived.

### Experimental Section

The experimental procedures were essentially the same as previously described.<sup>3,10</sup>

(a) *Positron Lifetime Measurements.* Positron lifetime measurements were carried out by the usual delayed coincidence method.<sup>2</sup> The resolution of the system as measured by the prompt time distribution of <sup>60</sup>Co source and without changing the 1.27- and 0.511-MeV bias was found to be less than 0.4 ns

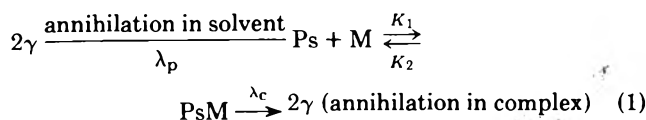
(b) *Purity and Source of Reagents.* All solvents were of highest available purity. They were dried by means of a molecular sieve and redistilled. The other compounds used in these investigations were purified by suitable methods, distillation, recrystallization, and preparative gas chromatography, until subsequent tests showed a purity of better than 99.5%.

(c) *Preparation of Sample.* Specially designed sample vials (cylindrical glass tubes 100 mm long and 10 mm i.d.) were filled with about 1 ml of solution. The positron sources were 3–5  $\mu\text{Ci}$  <sup>22</sup>Na prepared by evaporating carrier free neutral solutions of either <sup>22</sup>NaHCO<sub>3</sub> or <sup>22</sup>NaCl (obtained from ICN) onto a thin aluminum foil. The radioactive foils were suspended in the solutions and all solutions were carefully degassed by freeze-thaw techniques to re-

move oxygen. The vials were subsequently sealed off and immersed in a specially designed thermostat which allowed control of the temperature within  $\pm 1.0^\circ\text{C}$ . Special care has been taken to evaluate the potential effects of heat and irradiation (by the  $^{22}\text{Na}$  source) on the sample. Thus data points were first obtained at increasing temperatures, then the cycle was reversed and data were obtained at decreasing temperatures. The data were found to be reproducible throughout the full cycle which clearly indicated that no significant changes had occurred in the samples.

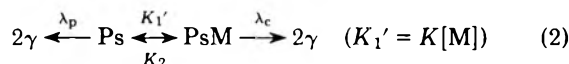
## Results and Discussion

As discussed in our previous paper<sup>3</sup> the experimental results obtained in solutions of diamagnetic organic compounds, such as nitrobenzene derivatives and *p*-benzoquinone, provide strong evidence that thermal Ps atoms react with these molecules via a mechanism which involves the reversible formation of a Ps complex. It can be formulated as follows:



According to the above reaction scheme the following reactions have been considered: (1) reaction of Ps with substrate M to form a Ps complex PsM (rate constant  $K_1$ ); (2) decomposition of PsM (rate constant  $K_2$ ); (3) positron annihilation in complex (decay constant  $\lambda_c$ ); (4) annihilation of Ps in bulk solvent with rate  $\lambda_p$ .

Since the concentration of M, the substrate, remains essentially constant throughout the experiment the mechanism can be simplified to



Appropriate kinetic equations have been set up<sup>3</sup> which led to a correlation between  $\lambda_2 = 1/\tau_2$ , where  $\tau_2$  is the lifetime of the long-lived component in the positron lifetime spectra, and  $\lambda_p$ ,  $\lambda_c$ , and the rate constants  $K_1$ ,  $K_2$ :

$$\lambda_2 = \lambda_p + \frac{K_1\lambda_c}{K_2 + \lambda_c} [M] \quad (3)$$

$$\frac{K_1\lambda_c}{K_2 + \lambda_c} \equiv K_{\text{obsd}}$$

Figure 1 shows a plot of  $K_{\text{obsd}}$  vs.  $1/T$  (the reciprocal of the absolute temperature). The Arrhenius behavior of the various systems observed at lower temperature suggested that in this region  $K_2 \ll \lambda_c$ , so that  $K_{\text{obsd}}$  becomes equal to  $K_1$ ,<sup>3</sup> which in turn indicates that under these conditions most Ps atoms which have formed the Ps molecule complex will annihilate from the bound state (Ps complex) before the Ps complex decomposes. Thus in this region the Ps reaction can be adequately described as follows:



The appropriate rate equations for this reaction were solved in a similar fashion as described elsewhere.<sup>2,3,10-13</sup> One obtains for  $\lambda_2$ :

$$\lambda_2 = \lambda_p + K_1[M]$$

and for the number of positrons,  $I_2$ , decaying with the rate  $\lambda_2$ :

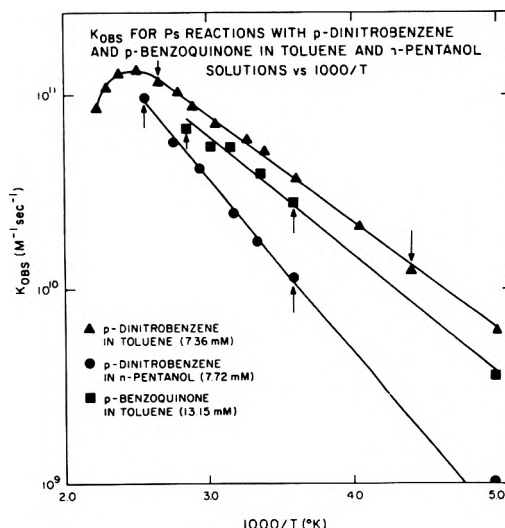


Figure 1.  $K_{\text{obsd}}$  for Ps reactions with *p*-dinitrobenzene and *p*-benzoquinone in different solvents vs.  $1000/T$ . (Arrows indicate region used for computation of  $\lambda_c$ .)

TABLE I: Temperature Dependence of  $K_1$ ,  $\lambda_2$ , and  $I_2$  for the Reaction of Orthopositronium with *p*-Dinitrobenzene and *p*-Benzoquinone in Solution

Solute	$T, ^\circ\text{C}$	$\lambda_2, \mu\text{s}^{-1}$ ( $\pm 0.005$ )	$I_2, \%$ ( $\pm 0.5$ )	$K_1, \text{M}^{-1}$ $\text{ns}^{-1}$
7.36 mM				
<i>p</i> -dinitrobenzene (solvent toluene)	-45	0.459	32.4	12.7
	-26	0.507	32.4	20.8
	5	0.595	32.4	35.6
	21	0.700	34.9	51.3
	35	0.752	35.3	59.5
	54	0.819	35.0	70.4
	70	0.927	36.5	86.5
	85	1.043	40.0	103.6
105	1.125	40.9	116.5	
13.15 mM				
<i>p</i> -benzoquinone (solvent toluene)	5	0.725	33.7	29.8
	23	0.846	37.3	39.9
	41	1.035	43.1	55.2
	58	1.014	38.7	54.4
	78	1.193	48.5	69.0
7.72 mM				
<i>p</i> -dinitrobenzene (solvent 1-pentanol)	5	0.414	19.9	11.6
	22	0.462	19.6	17.8
	40	0.516	20.6	24.9
	65	0.657	24.2	43.1
	88	0.758	27.3	56.9
	113	0.924	34.3	99.2

$$I_2 = N_{T^0} \left( 1 + \frac{K_1[M]}{\lambda_c - \lambda_2} \right) \quad (5)$$

( $N_{T^0}$  is the formation probability of (thermalized) *o*-Ps). Equation 5 can be rearranged to

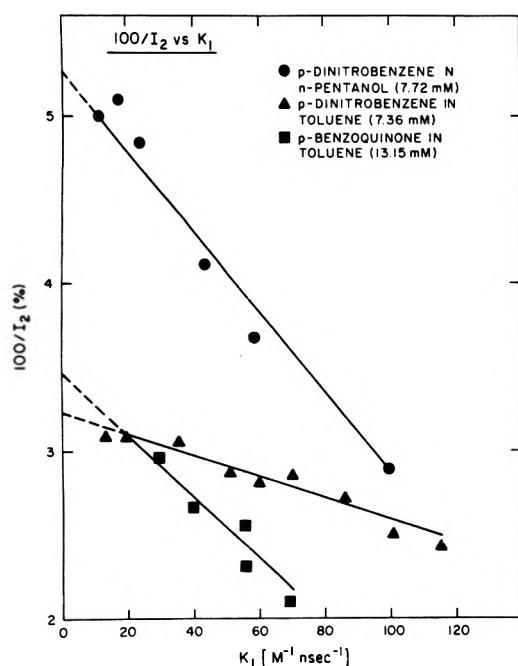
$$1/I_2 = 1/N_{T^0} - K_1[M]/(\lambda_c - \lambda_2)N_{T^0} \quad (6)$$

The  $I_2$  and  $\lambda_2$  values observed by varying the temperature in systems, such as *p*-dinitrobenzene in pentanol and toluene, and *p*-benzoquinone in toluene, are listed in Table I. Only those data points or temperature ranges have been considered, where (a) Arrhenius behavior, i.e.,  $K_1 = K_{\text{obsd}}$  (vide supra) can be safely assumed and (b) where the  $I_2$  values for the pure solvents (listed in Table II) show no significant changes, i.e., for *p*-dinitrobenzene in pentanol 5–113  $^\circ\text{C}$ ; *p*-dinitrobenzene in toluene -45 to 123  $^\circ\text{C}$ , and



TABLE II: Temperature Dependence of  $\lambda_2$  and  $I_2$  in Toluene and 1-Pentanol

Compound	$T, ^\circ\text{C}$	$\lambda_2, \text{ns}^{-1}$ ( $\pm 0.005$ )	$I_2, \%$ ( $\pm 0.5$ )
Toluene	-75	0.381	37.3
	-57	0.373	36.4
	-27	0.355	36.4
	3	0.333	37.3
	21	0.319	36.8
	37	0.312	36.5
	53	0.303	36.2
	72	0.294	37.1
	91	0.277	37.8
	110	0.260	38.1
1-Pentanol	22	0.324	22.2
	22	0.326	22.8
	36	0.326	22.7
	65	0.325	22.9
	88	0.319	22.8
	108	0.315	23.1

Figure 2.  $1/I_2$  vs.  $K_1$  for solutions of *p*-dinitrobenzene and *p*-benzoquinone in toluene and 1-pentanol.

for *p*-benzoquinone in toluene 5 to 78  $^\circ\text{C}$ . According to eq 6  $1/I_2$  should be under these experimental conditions a linear function of  $K_1[M]$ .

The result is indeed a straight line, as shown in Figure 2 where  $1/I_2$  is plotted vs.  $K_1$ , with an intercept of  $1/N_{T^0}$  and

TABLE III: Orthopositronium Formation Probabilities ( $N_{T^0}$ ) and Annihilation Lifetimes of Positrons ( $\tau_c$ ) in Ps Complexes of *p*-Dinitrobenzene and *p*-Benzoquinone in Toluene and 1-Pentanol Solutions

Solute	Solvent	$\lambda_p,^a \text{ns}^{-1}$	$\tau_c, \text{ns}$	$N_{T^0}, \%$
<i>p</i> -Dinitrobenzene (7.36 mM)	Toluene	0.315	0.25	30.8
<i>p</i> -Benzoquinone (13.15 mM)	Toluene	0.315	0.36	28.7
<i>p</i> -Dinitrobenzene (7.72 mM)	1-Pentanol	0.326	0.48	19.0

<sup>a</sup>  $\lambda_p = \lambda_2$  of pure solvent at 21-37  $^\circ\text{C}$  as listed in Table II.

a slope  $[M]/(\lambda_c - \lambda_p)/N_{T^0}$ . The ratio of the latter two yields  $[M](\lambda_c - \lambda_p)$ . From the pick-off annihilation rate in the pure solvent, taken from Table II, and the known solute concentration  $[M]$ ,  $\lambda_c \equiv 1/\tau_c$  can be obtained.

The results are shown in Table III. The positron annihilation lifetimes  $\tau_c$  in these Ps complexes (in solution) range from 0.25 to 0.48 ns with an average value of 0.36 ns. These numbers agree quite well with those which have been more recently reported for the many electron-positron systems.<sup>5-6,8,9</sup> The relatively large experimental error involved in these measurements does not allow, however, any conclusion at the present time as to the dependence of the lifetime on the nature of the molecule or the solvent used.

## References and Notes

- (1) Work supported by the U.S. Atomic Energy Commission.
- (2) For general references, see (a) J. Green and J. Lee, "Positronium Chemistry", Academic Press, New York, N.Y., 1964; (b) V. I. Goldanskii, *At. Energy Rev.*, **6**, 3 (1968); (c) J. D. McGervey in "Positron Annihilation", A. T. Stewart and L. O. Roellig, Ed., Academic Press, New York, N.Y., 1967, p 143; (d) J. A. Merrigan, S. J. Tao, and J. H. Green, "Physical Methods of Chemistry", Vol. I, Part III D, A. Weissberger and B. W. Rossiter, Ed., Wiley, New York, N.Y., 1972; (e) H. J. Ache, *Angew. Chem., Int. Edit. Engl.*, **11**, 179 (1972); (f) J. H. Green, *MTP Int. Rev. Sci., Inorg. Chem., Ser. One*, **8**, 251 (1972); (g) V. I. Goldanskii and V. G. Virsov, *Ann. Rev. Phys. Chem.*, **22**, 209 (1971).
- (3) W. J. Madia, A. L. Nichols, and H. J. Ache, *J. Am. Chem. Soc.*, **97**, 5041 (1975).
- (4) See, e.g., W. J. Madia, J. C. Schug, A. L. Nichols, and H. J. Ache, *J. Phys. Chem.*, **78**, 2682 (1974).
- (5) Din Van Hoang, *Zh. Eksp. Teor. Fiz.*, **49**, 630 (1965); *Teor. Eksp. Khim.*, **2**, 260 (1966).
- (6) R. Bell and M. Jorgenson, *Can. J. Phys.*, **38**, 652 (1960).
- (7) L. Simons, *Phys. Rev.*, **90**, 165 (1953).
- (8) R. A. Ferrell, *Phys. Rev.*, **103**, 1266 (1956).
- (9) P. Navin, D. M. Schrader, and C. F. Lebeda, *Appl. Phys.*, **3**, 159 (1974); *Phys. Rev. A*, **8**, 2248 (1974).
- (10) T. L. Williams and H. J. Ache, *J. Chem. Phys.*, **50**, 4493 (1969).
- (11) H. Horstmann, *J. Inorg. Nucl. Chem.*, **27**, 1191 (1965).
- (12) S. J. Tao and J. H. Green, *J. Chem. Soc. A*, 408 (1968).
- (13) P. Jansen, M. Eldrup, B. Skyttejensen, and O. E. Mogensen, *Chem. Phys.*, **10**, 303 (1975).

## Adenosine-Sensitized Photolysis of Carboxylic Acids in Frozen Aqueous Solutions

I. Rosenthal,\* R. Poupko, K. A. Muszkat, and Sh. Sharafi-Ozeri

Department of Organic Chemistry, Isotope Department, and Department of Structural Chemistry, The Weizmann Institute of Science, Rehovot, Israel (Received April 18, 1975; Revised Manuscript Received October 6, 1975)

The interaction of electronically excited adenine or adenosine with carboxylic acids yields free radicals generated by the homolytic cleavage of the carboxyl group. When an amino acid serves as substrate, the loss of the amino group is the predominant process.

### Introduction

Photochemical reactions of purines may serve as model systems for the study of radiation damage to nucleic acids in living organisms. Electronically excited purines have been reported to react with alcohols,<sup>1</sup> amines,<sup>2,3</sup> and aliphatic  $\alpha$ -amino acids<sup>4</sup> to give the corresponding substituted purines. In several cases the functional group of the substrate did not appear in the final product. This observation suggests that the substrate was cleaved by interaction with the excited purine.

The present study aims at the investigation of photoinduced reactions of purines with carboxylic acids, primarily the identification of the reactive species generated. Thus, the light-induced reactions of adenine and adenosine with a number of aliphatic carboxylic acids and amino acids have been performed and the transient species generated have been characterized by ESR.

### Experimental Section

The organic compounds were from commercial sources and were purified before use. The protected amino acids and peptides used in this work were prepared by standard procedures and were chromatographically pure. The electron spin resonance spectra were recorded with a Varian E 12 ESR spectrometer equipped with a Varian E 257 variable temperature unit. The excitation in the microwave cavity was accomplished by ultraviolet irradiations with a dc operated Osram 200-W high-pressure mercury lamp housed in a Wild reflector. A cutoff Corning filter 7910 (2 mm) placed in front of the lamp removed light of wavelength shorter than 220 nm. The experimental procedure consisted of ultraviolet irradiation at  $-180^\circ\text{C}$  of an aqueous solution of adenine ( $5 \times 10^{-4}$  M) or adenosine ( $5 \times 10^{-3}$  M) and organic acid (0.1 M) titrated with NaOH to pH 7. The solutions were thoroughly flushed with helium before freezing. The ESR spectra obtained were symmetrical and the hyperfine coupling constants could be measured to an accuracy of  $\pm 1$  G.

### Results and Discussion

Adenine or adenosine sensitized photolysis of carboxylic and amino acids in frozen aqueous solution yields alkyl free radicals which could be detected and subsequently characterized by ESR spectroscopy. These species are produced by the homolytic cleavage of a carboxyl or amino group from the substrate. The results are summarized in Table I.

Thus, the formation of methyl free radical from acetic acid, ethyl radical from propionic acid, and cyclopentyl

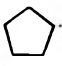
radical from cyclopentanecarboxylic acid have been observed by irradiation of the parent acids in the presence of adenosine at liquid nitrogen temperature. For purposes of comparison, we produced the identical radicals by the photooxidative decarboxylation of the same carboxylic acid with  $\text{K}_3\text{Fe}(\text{CN})_6$  as photosensitizer.<sup>5</sup> The formation of the more stable tertiary radical from isobutyric acid results from abstraction of a hydrogen atom probably by the radical initially formed by decarboxylation.

When amino acids served as substrates, loss of the amino group occurred instead of the decarboxylation process. This conclusion is supported by the splitting pattern obtained, as well as by deuterium exchange experiments. Thus, when photolyses of the amino acids were carried out in  $\text{D}_2\text{O}$ , the spectra were unchanged, indicating the absence of exchangeable amino protons adjacent to the odd electron. When present, such as in the  $^+\text{NH}_3\text{-CH}_2$  radical, the amino protons are equivalent to the rest of hydrogen atoms and can be easily detected.<sup>5</sup> Additional support in the favor of this assignment was provided by experiments with partially protected amino acids. While a weak poorly resolved signal was generated from *N*-acetylalanine, the alanylamide gave the same radical as free alanine. These results confirm a previous report<sup>6</sup> that the interaction of photoactivated adenosine with glycine leads to the fragmentation of the latter through the loss of the amino group. The relative deamination rates of the free amino acids were established to be  $\alpha$ -aminoisobutyric > Ala > Gly. This order corresponds to the stability of the generated radical. Furthermore, the same reaction pattern was observed for several alanine peptides. Thus AlaGly, AlaAla, AlaVal, AlaSer, (Ala)<sub>3</sub>, and (Ala)<sub>4</sub> displayed a five-line spectrum characteristic of the residual alanine  $\text{CH}_3\text{CH-}$  entity formed by deamination.

In frozen aqueous solutions, aggregates of purine molecules are formed<sup>7,8</sup> and this complex formation could play some role in the photochemical reaction. Since these aggregates can be broken by the addition of salts to the aqueous solution before freezing, we performed parallel experiments under the same conditions, in the presence and absence of NaCl (0.5 M). Since the ESR signal intensities in these experiments were virtually unchanged it follows that either the aggregates do not play a significant role in this photochemical reaction or that they were already destroyed by the substrate, i.e., the acid at the concentrations employed (0.1 M).

The question of the nature of the primary photochemical process is particularly intriguing. The present reaction takes place by initial excitation of the purine chromophore in its 260-nm absorption band. Blanks, composed of solu-

TABLE I

Compound	Radical	Hfsc
Acetic acid	$\dot{\text{C}}\text{H}_3$	( $a^{\text{H}} = 22.5 \text{ G}$ )
Propionic acid	$\dot{\text{C}}_2\text{H}_5$	( $a_{\alpha}^{\text{H}} = 22 \text{ G}$ , $a_{\beta}^{\text{H}} = 26.5 \text{ G}$ )
Isobutyric acid	$(\text{CH}_3)_2\dot{\text{C}}\text{COO}^-$	( $a^{\text{H}} = 22 \text{ G}$ )
Cyclopentane-carboxylic acid		( $a_{\alpha}^{\text{H}} = a_{\beta}^{\text{H}} = 24 \text{ G}$ )
Glycine	$\dot{\text{C}}\text{H}_2\text{COO}^-$	( $a^{\text{H}} = 20 \text{ G}$ )
Alanine	$\text{CH}_2\dot{\text{C}}\text{HCOO}^-$	( $a_{\alpha}^{\text{H}} = a_{\beta}^{\text{H}} = 24 \text{ G}$ )
$\alpha$ -Aminoisobutyric acid	$(\text{CH}_3)_2\dot{\text{C}}\text{COO}^-$	( $a^{\text{H}} = 22 \text{ G}$ )
Alanylamine	$\text{CH}_2\dot{\text{C}}\text{HCONH}_2$	( $a_{\alpha}^{\text{H}} = a_{\beta}^{\text{H}} = 24 \text{ G}$ )
AlaGly, AlaAla, AlaVal, AlaSer, (Ala) <sub>3</sub> , (Ala) <sub>4</sub>	$\text{CH}_2\dot{\text{C}}\text{H}-\text{CONHR}$	( $a_{\alpha}^{\text{H}} = a_{\beta}^{\text{H}} = 24 \text{ G}$ )

tions of acids in the absence of purine base verified that direct photolysis of substrate was insignificant.

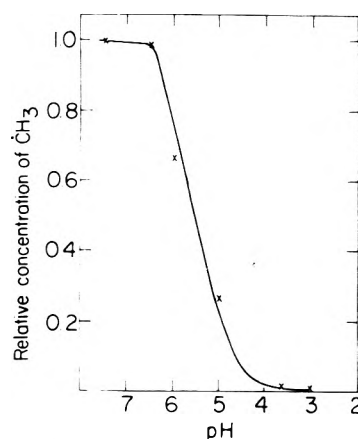
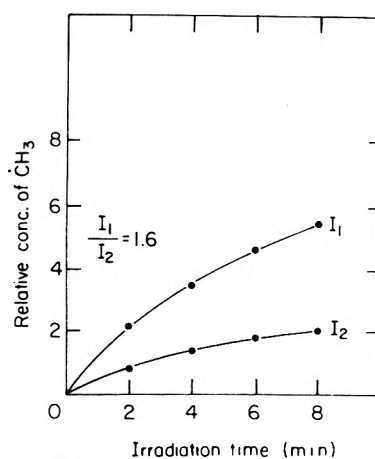
Helene et al.<sup>9</sup> have shown that the initial step in the ultraviolet irradiation of an aqueous solution of adenosine is photoionization via a two-photon mechanism with a triplet state as intermediate. It has also been suggested that the subsequent chemical transformations in the adenosine-sensitized photoreactions are due to the interaction between the photoejected electron and substrate.<sup>6,9</sup>

In the present case, our reasons for postulating biphotonic ionization process involving the triplet state are as follows.

(1) We have found that the reaction is entirely suppressed by paramagnetic ions  $\text{Co}^{2+}$  and  $\text{Cu}^{2+}$  ( $5 \times 10^{-4} \text{ M}$ ). At the adenine:quencher (10:1) ratio employed, the fraction of light absorbed by the transition metal salts ( $\text{CoCl}_2$  or  $\text{CuSO}_4$ ) is negligible at the 260-nm absorption maximum of adenine. Therefore, the inhibition observed is most probably due to quenching of triplet adenine.<sup>10</sup>

(2) A study of the relative concentrations of paramagnetic species generated from acetic acid as a function of pH (Figure 1) shows that the radical generation is severely inhibited at low pH. Since adenosine has been shown to have its phosphorescence quenched by protonation at the  $\text{N}_1$  position<sup>11</sup> ( $\text{p}K_a \sim 4$ ) the failure to observe radicals at low pH values suggests that the presence of the adenosine triplet is vital in this process. Two observations point against the other alternative, that the acid inhibition is due to scavenging of the photoejected electrons by acid protons. (a) Despite efforts no ESR evidence for hydrogen atoms could be obtained at  $-196^\circ\text{C}$ . (b) Radiolyses of acetic acid in aqueous solution at  $-196^\circ\text{C}$  yield methyl radicals.<sup>12</sup> Thus decarboxylation of carboxylic acids by reaction with electrons still takes place in an acid medium. Similarly the reaction between electrons photoejected from aromatic amino acids and divalent cations, although affected, still occurs to a considerable extent even in the presence of a mineral acid.<sup>13</sup>

(3) Finally we measured the dependence of the rate of formation of free radicals on the intensity of photolyzing light. The intensity of the light source was varied by means of a calibrated metal screen. For a given light intensity we recorded the initial increase in the ESR resonance signal with the time of irradiation. It was found that the rate of radical formation thus determined was proportional to the square of the light intensity which suggests a biphotonic absorption as the rate-determining step (Figure 2). The re-

Figure 1. Relative  $\dot{\text{C}}\text{H}_3$  concentration as a function of pH.Figure 2. Relative  $\dot{\text{C}}\text{H}_3$  concentration as a function of irradiation time at two different light intensities.

producibility of these measurements was in the limits of 10% error. The experimental conditions were chosen as to ensure a linear dependence of the concentration of the triplet excited adenosine molecules on the light intensity. This correlation was separately established by recording the phosphorescence emission of the adenosine solution at different light intensities.

(4) Despite the crucial role played by the adenosine triplet, the reaction could not be sensitized with acetone in acid medium, although the lowest lying triplet state of protonated adenosine is reached using acetone as a triplet donor.<sup>14</sup>

(5) In order to further characterize the intermediate transients, electron scavenging experiments with  $\text{N}_2\text{O}$ , an efficient electron scavenger,<sup>15</sup> were performed. Thus the concentration ratio of radicals generated under identical irradiation conditions in solutions saturated respectively with helium or  $\text{N}_2\text{O}$  before freezing was  $2.1 \pm 0.2$ . This quenching effect identifies the free electron resulting from the photoionization of adenosine as a reactant, while an additional route such as energy transfer from the higher triplet state of adenosine reached by the biphotonic absorption to the acid could also be involved.

We have analyzed theoretically the two suggested routes for the photodecarboxylation of an aliphatic acid. The discussion is based on the bonding properties of extended Huckel (EH) wave functions<sup>16</sup> of acetic acid, chosen as a

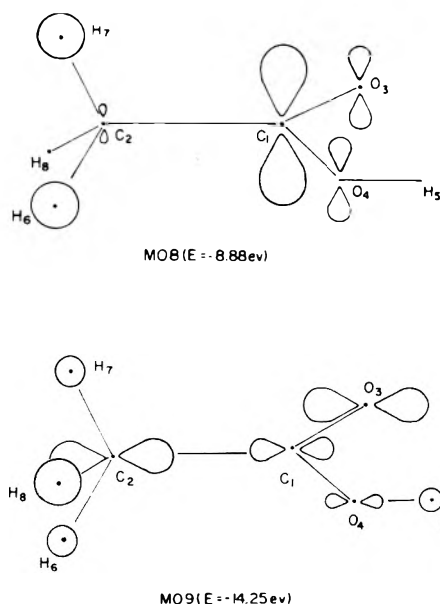


Figure 3. EH molecular orbitals of  $\text{CH}_3\text{COOH}$ . MO 9 and MO 8 are respectively the highest occupied and the lowest unoccupied molecular orbitals.

model molecule. Mulliken electronic overlap populations<sup>17</sup> between bonded or nonbonded centers serve as a semi-quantitative measure of electronic interaction, of bond strength, and of reactivity.<sup>18-20</sup> This approach has thus far given good results in analyses of electronic state sequences in the photoelectron spectra of diazabicyclo[2.2.2]octane<sup>18</sup> and of pyrazine<sup>19</sup> and in the analysis of photocyclization reactivity of 1,2-diarylethylenes.<sup>20</sup>

MO 9 and MO 8, respectively the highest occupied and the lowest unoccupied molecular orbitals of  $\text{CH}_3\text{COOH}$ , are illustrated in Figure 3. MO 9 is a  $p\sigma$  orbital strongly bonding between  $\text{C}_1$  and  $\text{C}_2$  and also between  $\text{H}_6$ ,  $\text{H}_7$ , and  $\text{H}_8$  and  $\text{C}_1$ . MO 8 is the highest energy  $p\pi$  orbital of the COOH fragment, antibonding between  $\text{C}_1$  and both  $\text{O}_3$  and  $\text{O}_4$ . In the region of interest this MO is weakly antibonding between  $\text{C}_1$  and  $\text{C}_2$  but bonding between  $\text{C}_1$  and both  $\text{H}_6$  and  $\text{H}_7$ . The two most likely reactive transients are either the molecular anion radical ( $\text{M}^-$ )  $\text{CH}_3\text{COOH}^-$  or the molecular first excited triplet state ( $\text{M}^*$ ). The electronic configuration of  $\text{M}^-$  is  $10^2 9^2 8^1$  while that of the neutral molecule  $\text{M}$  is  $10^2 9^2 8^0$ . The most important configuration of  $\text{M}^*$  is assumed to be  $10^2 9^1 8^1$ . Considering the bonding properties of MO 9 and MO 8 it is obvious that the configuration of  $\text{M}^*$  is susceptible to decarboxylation, since there is only one electron in the  $\text{C}_1$ - $\text{C}_2$  bonding MO 9 of  $\text{M}^*$ .

The electronic overlap populations for atom pairs  $k$  and  $l$ ,  $n(k,l)$ , for the three configurations  $\text{M}$ ,  $\text{M}^-$ , and  $\text{M}^*$  and the differences relative to  $\text{M}$ , e.g.,  $\Delta n(k,l)_{\text{M}^*} = n(k,l)_{\text{M}^*} - n(k,l)_{\text{M}}$  are listed in Table II. The process  $\text{M} \rightarrow \text{M}^-$  results in an antibonding change in  $n(1,2)$ ,  $\Delta n = -0.013$ ; at the same time the interactions between  $\text{C}_1$  and  $\text{H}_6$  and  $\text{H}_7$  acquire a stronger antibonding character,  $\Delta n(1,6) + \Delta n(1,7) = -0.038$ . Thus in  $\text{M}^-$  the  $\text{C}_1$ - $\text{C}_2$  bond is weaker than in  $\text{M}$  due to a decrease in  $n(1,2)$  and to more negative  $n(1,6)$  and  $n(1,7)$  values. The change in  $n(1,2)$  for the  $\text{M}^*$  configuration  $\Delta n(1,2) = -0.216$  is even larger than in the previous case. The total change in the  $\text{C}_1$ -H ( $\text{H}_6$ ,  $\text{H}_7$ , or  $\text{H}_8$ ) interactions is very small (0.005) and the total change in the  $\text{C}_2$ -O interactions is 0.056. Though the change in the  $\text{C}_2$ -O inter-

TABLE II:  $n(k,l)$ , Electronic Overlap Populations and  $\Delta n(k,l)$ , Differences Relative to  $\text{M}$

	$n(1-2)$	$n(1-6)$	$n(1-7)$	$n(1-8)$	$n(2-3)$	$n(2-4)$
	$n(k,l)$					
$\text{M}$	0.805	-0.032	-0.032	-0.044	-0.068	-0.050
$\text{M}^-$	0.792	-0.051	-0.051	-0.044	-0.068	-0.050
$\text{M}^*$	0.589	-0.039	-0.039	-0.025	-0.031	-0.031
	$\Delta n(k,l)$					
$\text{M}^-$	-0.013	-0.019	-0.019	0	0	0
$\text{M}^*$	-0.216	-0.007	-0.007	0.019	0.037	0.019

actions is positive its effect cannot possibly modify the primary weakening due to the decrease in the  $\text{C}_1$ - $\text{C}_2$  interaction for this configuration.

Thus, considerations based on MO calculations indicate that both the anion  $\text{M}^-$  and the excited state  $\text{M}^*$  would show a weakening of the  $\text{C}_1$ - $\text{C}_2$  bond which facilitates the decarboxylation.

Unfortunately this model does not enable a similar analysis for amino acids. However, in this case<sup>21-23</sup> the substantial experimental evidence leaves little doubt that the interaction between electrons and amino acids ends in deamination.

As described above the adenosine-sensitized cleavage may proceed through either electron photoejection or energy transfer. Though both paths require a two-photon absorption process this does not necessarily weaken the role that this chemical reaction might play in biological systems. At room temperature, in the fluid media, the solvation energies of the electron and radical ions can supply the energy deficit for one-photon ionization,<sup>24</sup> thus providing by a chemical reaction similar to that described a route for photochemical nucleic acid-protein interaction. The caffeine-sensitized photocleavage of amino acids at room temperature<sup>4</sup> supports such a possibility.

## References and Notes

- H. Steinmaus, I. Rosenthal, and D. Elad, *J. Org. Chem.*, **36**, 3594 (1971).
- A. Stankunas, I. Rosenthal, and J. N. Pitts, Jr., *Tetrahedron Lett.*, 4779 (1971).
- J. Salomon and D. Elad, *Photochem. Photobiol.*, **19**, 21 (1974).
- D. Elad and I. Rosenthal, *Chem. Commun.*, 905 (1969).
- R. Poupkov, I. Rosenthal, and D. Elad, *Photochem. Photobiol.*, **17**, 395 (1973).
- R. Santus, C. Helene, and M. Ptak, *C.R. Acad. Sci. Paris, Ser. D*, **262**, 2077 (1966).
- C. Helene, *Biochem. Biophys. Res. Commun.*, **22**, 237 (1966).
- C. Helene, R. Santus, and M. Ptak, *C.R. Acad. Sci. Paris, Ser. C*, **262**, 1349 (1966).
- C. Helene, R. Santus, and P. Douzou, *Photochem. Photobiol.*, **5**, 127 (1966).
- C. Helene, M. Ptak, and R. Santus, *J. Chim. Phys.*, **65**, 160 (1968).
- R. O. Rahn, J. W. Longworth, J. Eisinger, and R. G. Shulman, *Proc. Natl. Acad. Sci. U.S.A.*, **51**, 1299 (1964).
- P. B. Ayscough, K. Mach, J. P. Oversby, and A. K. Roy, *Trans. Faraday Soc.*, **67**, 360 (1973).
- R. Santus, A. Helene, C. Helene, and M. Ptak, *J. Phys. Chem.*, **74**, 550 (1970).
- A. A. Lamola, M. Gueron, T. Yamane, J. Eisinger, and R. G. Shulman, *J. Chem. Phys.*, **47**, 2210 (1967).
- S. Gordon, E. J. Hart, M. S. Matheson, J. Rabani, and J. K. Thomas, *Discuss. Faraday Soc.*, **36**, 193 (1963).
- R. Hoffmann, *J. Chem. Phys.*, **39**, 1397 (1963).
- R. S. Mulliken, *J. Chem. Phys.*, **23**, 1833, 1841 (1955).
- E. Heilbronner and K. A. Muszkat, *J. Am. Chem. Soc.*, **92**, 3819 (1970).
- K. A. Muszkat and J. Schaublin, *Chem. Phys. Lett.*, **13**, 301 (1972).
- K. A. Muszkat and S. Sharafi-Ozeri, *Chem. Phys. Lett.*, **20**, 397 (1973); K. A. Muszkat, G. Seger, and S. Sharafi-Ozeri, *J. Chem. Soc., Faraday Trans. 2*, **71**, 1529 (1975).
- P. Neta, M. Simic, and D. Hayon, *J. Phys. Chem.*, **74**, 1214 (1970).
- M. D. Sevilla, *J. Phys. Chem.*, **74**, 2096 (1970).
- R. Braams, *Radiat. Res.*, **27**, 319 (1966).
- H. I. Joschek and L. I. Grossweiner, *J. Am. Chem. Soc.*, **88**, 3261 (1966).

## Solvation of Electrons in Alcohol Glasses from $10^{-6}$ to $10^2$ s after Pulse Radiolysis at 77 K

J. R. Miller,\* B. E. Clift, J. J. Hines, R. F. Runowski, and K. W. Johnson

Chemistry Division, Argonne National Laboratory, Argonne, Illinois 60439 (Received March 17, 1975; Revised Manuscript Received November 14, 1975)

Publication costs assisted by Argonne National Laboratory

Spectral changes associated with solvation of electrons in glassy (77 K) methanol, ethanol, and 1- and 2-propanol have been studied from  $10^{-6}$  to  $10^2$  s after a short pulse of ionizing radiation. Continuous changes are observed over this wide time range, except for the case of methanol, in which electron solvation appears to be nearly complete before  $10^{-7}$  s. The data indicate a very wide range of relaxation times for electron solvation in frozen alcohols. Techniques for data collection over a wide time range are described in the supplementary material.

This paper describes observation of electron solvation in frozen alcohols from  $10^{-6}$  to  $10^2$  s after a pulse of ionizing radiation. The subject was studied earlier, on a much narrower time range.<sup>1,2</sup> Very recently Klassen and co-workers studied ethanol out to  $10^{-1}$  s.<sup>3</sup> The present results show that the solvation processes in MeOH, EtOH, and the propanols are complex, with important rate components, which vary over at least eight orders of magnitude in some areas.

### Experimental Section

Reagent grade alcohols or alcohol solutions were degassed and sealed in quartz cells as described previously. The sample cell was immersed in liquid nitrogen during the experiment also as described before.<sup>4</sup> Clear, crack-free glasses were formed. The samples were placed in liquid nitrogen at least 5 min before starting an experiment, because tests with a thermocouple in the samples showed that it took about 4 min for the center of the sample to reach 77 K.

The Argonne Linac produced 4–40-nsec pulses of  $13 \pm 2$  MeV electrons, which entered the reaction cell in a direction perpendicular to that of the analyzing light.

The optical system was carefully designed to minimize optical bleaching by the analyzing light, while maintaining time resolution. Details are given in the Appendix (available as supplementary material, see paragraph at end of text regarding supplementary material). The effect of the analyzing light on absorbance changes in ethanol at 77 K was checked. With the analyzing light intensity reduced a factor of 4.5 the growth of absorbance at 550 nm and the decay at 800 nm were unchanged within experimental uncertainty, which was 5% of the observed absorption changes at these wavelengths.

One of the purposes of this paper is to describe methods for recording spectrophotometric data over eight orders of magnitude change in time after a radiation pulse. Two methods have been used. One method used pulsed unblanking of an oscilloscope at a number of trigger delays spaced logarithmically in time after the radiation pulse. The oscilloscope photograph obtained consists of a series of dots rather than a continuous line.

In the second method the data are digitized by a Biomation 8100 transient recorder under active control of the

Chemistry Division's Sigma 5 computer. Both of these methods are described, with illustrations of raw data, in the supplementary material. Other general information about experimental techniques is also given there.

### Results

*Ethanol.* The absorbance as a function of time at several wavelengths in EtOH at 77 K is shown in Figure 1. The spectral changes occur over a very wide range of relaxation times extending from at least  $10^{-7}$  to  $10^2$  s. The initial absorption spectrum increases toward the infrared and is similar to initial spectra reported by Richards and Thomas<sup>1</sup> and by Kevan,<sup>2</sup> and to the spectrum observed after  $\gamma$  radiolysis at 4 K.<sup>5-7</sup> The absorbance increases with time at short wavelengths, and decreases at long wavelengths. At intermediate wavelengths (650 and 750 nm) the absorbance first increases and then decreases.

Recently Klassen and co-workers have made similar measurements in EtOH. Their use of an InAs detector allowed observation of the maximum of the initial ( $10^{-7}$  s) spectrum near 1300 nm. The present results are in complete accord with those of Klassen and co-workers, including the observation that spectrum develops much more slowly than indicated in ref 1 and 2.

*Methanol.* The absorption spectrum in MeOH (containing 5% ethylene glycol to prevent crystallization) is almost fully developed at the time of our earliest observations ( $10^{-7}$  to  $10^{-6}$  s). Observations using standard pulse radiolysis equipment showed that the absorption at 550 nm was almost full developed at 10 ns.<sup>8</sup> Electrons are solvated at very short times in glassy MeOH. This correlates with the observation that spectrum of trapped electrons in  $\gamma$ -irradiated methanol at 4 K is similar to the spectrum at 77 K.<sup>5</sup> Figure 2 is plotted to show the similarity of absorption changes in MeOH from  $10^{-7}$  to  $10^{-4}$  s to those in EtOH from  $10^{-2}$  to  $10^2$  s. This comparison suggests that electron solvation in MeOH is similar to that in EtOH, but  $10^5$  times faster. While this comparison should not be taken too seriously, the spectral changes observed for EtOH in the microsecond region may be similar to those for MeOH in the picosecond region.

*1- and 2-Propanol.* Figures 3 and 4 show the changes of absorption observed in 1-propanol and 2-propanol. The changes in 2-propanol are somewhat similar to those in

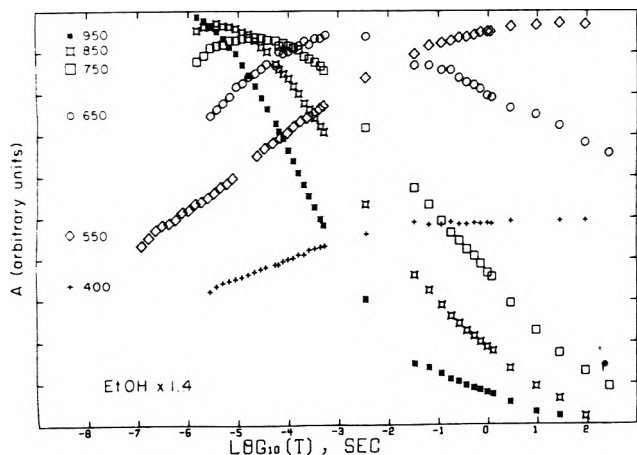


**Figure 1.** Absorbance of trapped electrons as a function of time following pulse radiolysis in ethanol glass at 77 K. The several wavelengths are indicated in nanometers. Because the absorbances are smaller in ethanol, the absorbance scale here is expanded 1.4 times relative to that for methanol (Figure 2). The origin in represents zero absorbance in all of the figures.

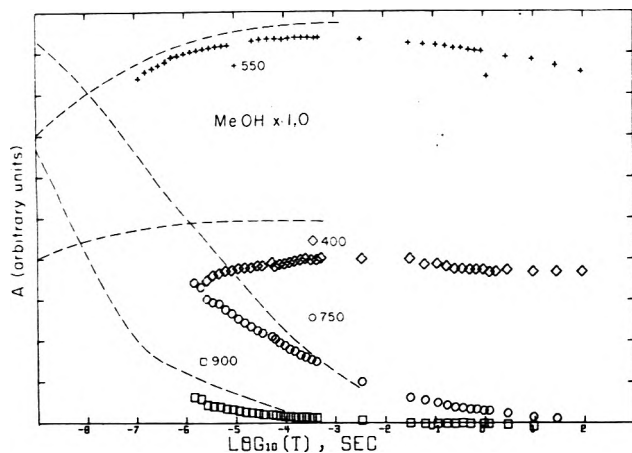


**Figure 2.** Absorbance as a function of time in methanol glass (+5% ethylene glycol to prevent crystallization) at 77 K at 400, 550, 750, and 900 nm. The dashed lines show absorbance changes in ethanol glass (400, 550, 750, and 950 nm) shifted a factor  $10^{-5}$  in time. Comparison is suggestive that the absorbance changes in MeOH glass are similar to those in EtOH glass, but  $10^5$  times faster.

EtOH, but are spread over a greater range of time and shifted to longer times. The absorption at 550 nm appears, on the logarithmic time scale, to start slowly and to speed up its growth in the millisecond time region.

In 1-propanol the behavior is different. The initial ( $10^{-6}$  s) absorption at short wavelengths is greater for 1-propanol than for 2-propanol, but there is little growth of the absorption at any wavelength. This seems difficult to understand in comparison to 2-propanol, because while 1-propanol shows less growth at short wavelengths (400–600 nm), it shows more decay at long wavelengths (750–950 nm).

## Discussion

The experimental findings reported here may be summarized as follows. (1) Electron solvation proceeds logarithmically with time over several orders of magnitude change in time in ethanol and propanol glasses at 77 K. (2) The solvation process is so fast in MeOH glass that it is nearly complete in  $10^{-6}$  s. The kinetics after  $10^{-6}$  s are very similar to

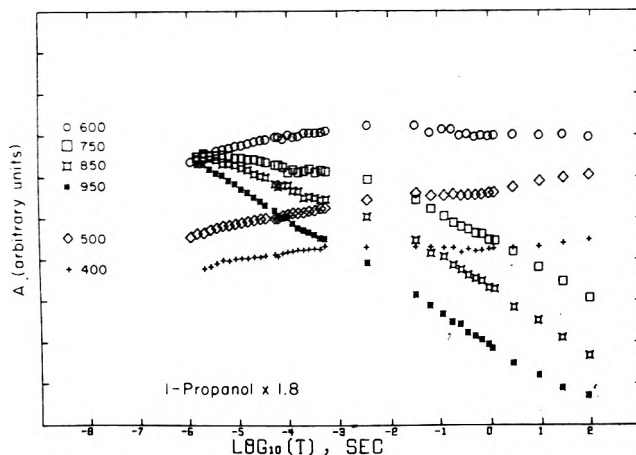


**Figure 3.** Absorbance as a function of time following pulse radiolysis of 1-propanol glass at 77 K. The absorbance scale is expanded 1.8 times relative to that for methanol (Figure 2).

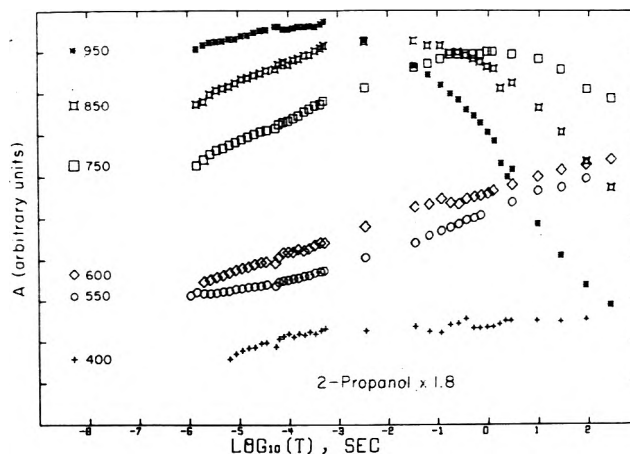


**Figure 4.** Absorbance as a function of time in 2-propanol glass at 77 K. The absorbance scale is expanded 1.8 times relative to that for methanol (Figure 2).

those in EtOH after  $10^{-1}$  s. (3) The absorbance first increases and then decreases at intermediate wavelengths (650–850 nm) in ethanol and 2-propanol.

The presently available experimental data are not sufficient to specify the mechanism of the spectral shift. The data are consistent with the conclusion of Kevan<sup>2</sup> that the spectral shifts result from deepening of traps by gradual reorientation of solvent molecules around the trapped electrons, rather than by migration of electrons from shallow to deeper preexisting traps. The slower spectral changes in matrices composed of larger molecules are consistent with the molecular reorientation mechanism. Richards and Thomas<sup>1</sup> suggested that reorientation of the solvent molecules is probably driven by the strong electric field near the electron. The large range of relaxation times observed here may be due, in part, to different field strengths seen by solvent molecules at different distances from the electron. This would imply that each electron is solvated in stages, which is consistent with the rise and fall of absorption at intermediate wavelengths.

The increase and decrease cannot be accounted for by assuming that there are only two configurations for each electron, for this would predict the absorbance at each

wavelength would be monotonically increasing or decreasing. Thus the spectra at intermediate times might be more accurately described as belonging to metastable intermediate configurations rather than to weighted sums of spectra from two extremes of shallow and deep traps. These intermediate configurations appear to be absent or very short lived in liquid ethanol near the freezing point. Baxendale and Wardman<sup>9</sup> observed an "end of pulse" (ca. 5 ns) spectrum in ethanol at 160 K which showed a minimum at about 1000 nm. Such a minimum is not indicated in ethanol glass at 77 K either in the work of Klassen<sup>3</sup> or in the present work.

*Supplementary Material Available:* an Appendix of ex-

perimental details (8 pages). Ordering information is given on any current masthead page.

### References and Notes

- (1) J. T. Richards and J. K. Thomas, *J. Chem. Phys.*, **53**, 218 (1970).
- (2) (a) L. Kevan, *Chem. Phys. Lett.*, **11**, 140 (1971); (b) *J. Chem. Phys.*, **56**, 838 (1972).
- (3) N. V. Klassen, H. A. Gillis, G. G. Teather, and L. Kevan, *J. Chem. Phys.*, **62**, 2474 (1975).
- (4) J. R. Miller, *J. Phys. Chem.*, **79**, 1070 (1975).
- (5) H. Hase, M. Noda, and T. Higashimura, *J. Chem. Phys.*, **54**, 2975 (1971).
- (6) H. Hase, T. Wishimura, M. Noda, A. Namiki, and T. Higashimura, *J. Chem. Phys.*, **57**, 1039 (1972).
- (7) T. Shida, S. Iwata, and T. Watanabe, *J. Phys. Chem.*, **76**, 3683 (1972).
- (8) J. Miller, unpublished.
- (9) J. H. Baxendale and P. Wordman, *J. Chem. Soc., Faraday Trans. 1*, **69**, 584 (1973).

## Semiconductor Electrodes. IV. Electrochemical Behavior of n- and p-Type Silicon Electrodes in Acetonitrile Solutions

Daniel Laser and Allen J. Bard\*

*Department of Chemistry, The University of Texas at Austin, Austin, Texas 78712 (Received August 27, 1975)*

*Publication costs assisted by the National Science Foundation*

The behavior of n- and p-Si as electrodes for the reduction and oxidation of several redox systems (e.g., benzonitrile, 9,10-diphenylanthracene, anthraquinone, benzoquinone) in acetonitrile solutions in the dark and under illumination was investigated. The results were correlated with the relative energy levels of the valence and conduction bands of the semiconductor and those of the redox couples in solution, estimated by determination of the flat-band potential of the semiconductor-solution system by photopotential methods. The electrode behavior of Si strongly depended upon the electrode pretreatment and the absence of ideal semiconductor electrode behavior for this relatively small band gap material suggests the importance of surface states and breakdown phenomena for these electrodes. A unique electrogenerated chemiluminescence (ECL) experiment with a p-Si electrode is described.

### Introduction

Although nonaqueous solutions offer many advantages in carrying out and understanding simple electrochemical processes (for example, an extended range of available potentials, the availability of numerous reversible one-electron transfer reactions without kinetic complications, and fewer difficulties with surface phenomena) only a few studies have been made with semiconductor electrodes in these media. Krotova and Pleskov<sup>1</sup> determined the capacitance of a Ge electrode in *N,N*-dimethylformamide (DMF), while Mark and Pons<sup>2</sup> qualitatively performed a reductive electrolysis at a Ge internal reflection plate. Acetonitrile (ACN) solutions were employed by Osa and Kuwana<sup>3</sup> with highly doped SnO<sub>2</sub> transparent electrodes and by Landsberg and coworkers<sup>4</sup> with n-type GaP. A previous paper in this series<sup>5</sup> dealt with the behavior of n-type TiO<sub>2</sub>, a wide band gap semiconductor (sc), in ACN. This paper is concerned with the electrochemical properties of Si, a small band gap (1.1 eV) sc, and a comparison of the behavior of several redox systems at Pt, n-, and p-Si in ACN solutions, in the dark and under illumination.

General and detailed treatments of sc electrochemistry have been given by Myamlin and Pleskov<sup>6</sup> and Gerischer,<sup>7,8</sup> as well as in numerous papers on the properties of specific sc materials.<sup>9-16</sup> The picture which emerges for faradaic processes shows three main differences between metal and sc electrodes. These differences occur because for sc electrodes:

(a) The heterogeneous reaction rate (i.e., the exchange current) depends upon the relative energy (or redox potential) of the redox reaction and the energy levels of the sc bands. If a redox couple is represented by some Gaussian energy distribution function of electron acceptor levels (oxidized forms) and donor levels (reduced forms) in solution, equi-energetic charge transfer between the sc band at the surface and levels in solution requires a favorable overlap between these levels.<sup>17</sup> The exchange current depends upon this overall overlap, and thus on the relative position of the levels, the number of sc free carriers available for exchange, and the concentration of electroactive species in solution at the redox couple's equilibrium potential (thermodynamically independent of electrode material). For a

small band gap sc, there may be overlap of a redox couple with both the conduction and valence bands so that there may be contributions to the exchange current from both bands.<sup>7</sup> Experimentally a low exchange current will mean that even when the electrode potential is shifted from equilibrium the charge transfer reaction will still be slow and irreversible.

(b) The total applied overvoltage may not be effective in changing the potential drop between sc surface and solution. The kinetic stimulation of the electrochemical reaction by changing the activation energy of the preelectrode state in solution will be prevented, if the change in the applied potential does not change the value of the potential drop in the Helmholtz layer at the sc-electrolyte interface. In the case of a sc, unlike a metal, most of the applied overvoltage contributes to changes in the potential barrier in the space charge region and in the population of free carriers in it, so that the influence of the potential on electrode kinetics can be attributed to this effect. This is the usual situation at a sc unless a high density of surface states exists or a condition of high degeneracy prevails.<sup>7</sup>

(c) The current may be limited by the supply of free carriers. In contrast to metal electrodes, whenever minority carriers participate in the electrochemical process, the reaction rate may be limited by their rate of supply to the electrode-electrolyte interface. Minority carriers which are consumed may be resupplied to the surface by diffusion from the bulk through the quasineutral region,<sup>6</sup> generated in the space charge region<sup>18</sup> or at the surface,<sup>19</sup> usually leading, in a moderately doped sc, to very small currents. When mass transfer in solution is not a constraining factor, minority carrier participation in the electrochemical reaction will be characterized by a limiting current.

Other mechanisms of carrier production and transfer, such as intraband tunneling,<sup>20</sup> space charge region ionization,<sup>21</sup> and photogeneration must be considered as well. The organic systems employed allowed us to subject the Si electrodes to various conditions which are unacceptable in water so that its behavior could be interpreted according to the considerations discussed above. Electrode reactions involving the electrode material itself (i.e., anodic dissolution) were avoided, however.

### Experimental Section

Si single crystals were mounted in a glass tube using silicone rubber adhesive (General Electric) which was found to be resistant to ACN and which insulated all electrode parts except the area exposed to solution. Electrodeposited nickel provided ohmic contact to the n-material and thermally deposited gold (Hanovia Liquid Gold, Engelhard, N.Y.) was used for the p-type. Two samples of each type were used: 5 ohm cm (211 plane exposed to solution) and 1 ohm cm (100) for the n-type and 0.05 ohm cm (211) and  $\approx$  5 to 10 ohm cm (111) for the p-type. The doping levels were all in the range of about  $10^{15}$ – $10^{18}$  cm<sup>-3</sup>; the dopants were boron and phosphorous. Although the electrode surfaces were visually different, there was no difference between the sample of each type in the electrochemical behavior within the usual experimental reproducibility unless otherwise specified. The low resistance materials (n, 1 ohm cm; p, 0.05 ohm cm) (kindly donated by Texas Instruments, Dallas, Tx.) were received polished to a high mirror finish and were not wet by water. The other two samples had a hazy gray appearance, even after mechanical polishing. The usual pretreatment for the electrodes involved etching

them in an HF-HNO<sub>3</sub> mixture followed by drying in an oven prior to use. The n-type visually seemed to be little affected by a 2 min etching, while the p-type 5 ohm cm surface became somewhat duller and the 0.05 ohm cm p-type sample dissolved vigorously with black patches of amorphous Si<sup>22</sup> peeling off. Mechanical polishing with 0.3- $\mu$  alumina which was not followed by etching, although resulting in a visually smoother surface always led to a more active electrode. The behavior in this case resembled that of a metal electrode, especially when the sc was first used. Whenever changes in electrode behavior were observed during this work, the results obtained immediately after etching were taken to represent the electrode behavior, since these results were the most reproducible.

An Ag wire immersed in 0.01 M AgNO<sub>3</sub> in ACN, separated from the main solution by a porous Vycor (Corning) plug served as a reference electrode and all of the potentials are reported with respect to this reference. Its value vs. an aqueous SCE in ACN is about +0.3 V. This electrode was found to be very stable and reliable. No leakage of Ag<sup>+</sup> into the main solution was detected. A coiled platinum wire in a separate compartment was used as the auxiliary electrode.

All reagents and ACN were purified according to known procedures.<sup>23</sup> A vacuum-tight Pyrex cell equipped with a flat window facing the electrode surface contained the solution and electrode assembly. Solutions were prepared and the cell filled in a Vacuum Atmospheres Corporation dry-box (Hawthorne, Calif.) under a helium atmosphere.

All measurements utilized the three-electrode potentiostatic mode, employing a Princeton Applied Research (PAR) Model 173 potentiostat, a PAR Model 175 programmer and a Model 2000 X-Y recorder (Houston Instrument Company, Austin, Tex.). To overcome the electrode bulk resistance and solution resistance, positive feedback resistance compensation was employed. In order not to overcompensate (e.g., because of the formation of a depletion layer, see Results) the amount of maximum compensation was determined either under a condition which led to sc degeneracy or when the electrode was illuminated, i.e., under conditions when the resistive element of the space charge region was minimized. Impedance measurements were performed by superimposing a 10-mV sine wave on a potential scan of 0.5 V/s. The in- and out-of-phase components of the current were separated by a PAR Model HR-8 lock-in amplifier. The instantaneous photopotential was measured with 0.5-ms strobe light pulses used for illumination.

The working electrode was biased against the auxiliary one with a power supply and its potential change vs. the reference electrode was displayed on an oscilloscope. A 500-W tungsten lamp equipped with an Esco 4811-0 3-mm red glass filter was used as the light source. For eel measurements a photomultiplier detector was used, with its input filtered by an Esco-3-mm blue glass filter, so that the blue light could be detected in the presence of the red background illumination.

### Results and Discussion

*Useful Working Range.* Figure 1 depicts most of the useful working range of the Si electrodes in ACN–0.1 M TBAP compared to the range of the same samples in aqueous (20% HF) solutions. This range in ACN extends over an interval twice as wide as the Si band gap; the flat band potential of the n-Si, as will be shown later, lies at about the mid-



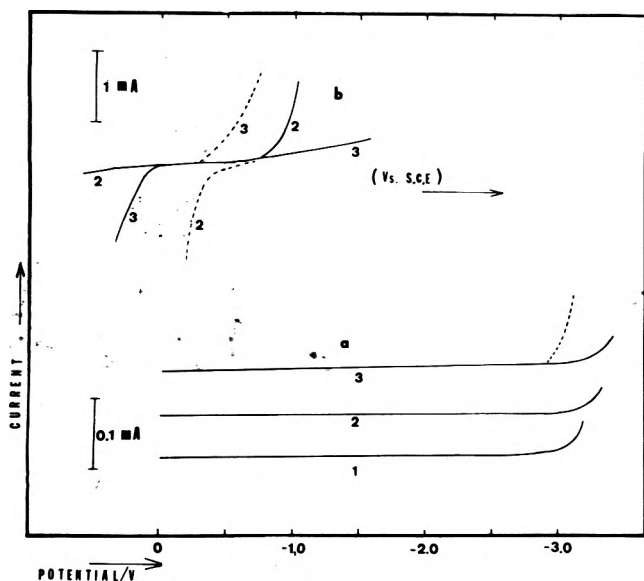


**Figure 1.** Background current. (a) ACN, 0.1 M TBAP (cathodic limit only); (b) aqueous, 20% HF. (1) Pt electrode; (2) n-Si, 5 ohm cm; (3) p-Si, 10 ohm cm. Dashed line shows effect of illumination.

dle of this range. Potentials positive of 0 V were avoided so as not to subject the electrodes to electrochemical conditions which might drastically change their surface properties (dissolution, passivation, etc.). Little difference was found between the n- and p-type samples and between both of them and Pt for the cathodic background reduction process (in the dark) compared to the clear difference seen in water. Under irradiation, the background current on p-Si was shifted to potentials positive of where background reduction occurs at a Pt electrode. The n-type electrode is unaffected by illumination in this potential region.

**Flat Band Potential.** The importance of this variable has been discussed elsewhere.<sup>24</sup> For an extrinsic sc the flat band potential,  $V_{fb}$ , closely represents the location of the majority carrier energy band in the bulk sc if the potential drop in the Helmholtz layer can be neglected.  $V_{fb}$  is needed so that the position of the sc bands and the energy levels in solution can be located with respect to one another on a common relative scale (e.g., with respect to a given reference electrode). Knowledge of the relative energy positions allows one to estimate the exchange current and to have an idea about which band will be involved in the charge transfer. Moreover, by knowing  $V_{fb}$  the "electrical state" of the sc (i.e., the carrier and potential distributions in the space charge region) at some other applied electrode potentials can be predicted.

Thus for an intrinsic sc the nature of its electrical states is symmetric with respect to  $V_{fb}$ , and for a small amount of band bending and in the absence of surface states, changes of applied potential hardly affect the potential drop in the Helmholtz layer. For a moderately doped sc (e.g., n-type) the electrical behavior is asymmetric with respect to  $V_{fb}$ . Degeneracy will occur following formation of a slight accumulation layer (e.g., upon negative polarization) when the concentration of majority carriers (e.g., electrons) in the space charge region approaches the effective density of states of the corresponding band (e.g., conduction band). On the other hand inversion and depletion layers<sup>25</sup> form over a much wider range of applied potentials (e.g., upon positive polarization). Hence a knowledge of  $V_{fb}$  is neces-

sary for an understanding of the effect of the imposed overpotential on electrode kinetics.

The flat band potentials were estimated by observing photoeffects caused by electrode illumination on electrode potentials and on electrode impedance. In the first method, the instantaneous perturbation in the equilibrium potential of the electrode due to illumination is minimized at the flat band position<sup>26</sup> (in the absence of fast surface states). The second method is based on the detection of the electrode potential at which a depletion layer begins to form when the sc bias (electrode potential) is increased in the appropriate direction from  $V_{fb}$ . Let us consider this second method in more detail. The sc impedance can be represented by a complex network of idealized passive elements.<sup>27</sup> The  $V_{fb}$  value can often be determined by measurement of the  $C_{sc}$ , the space charge capacitance as a function of potential (Shottky-Mott plot).<sup>6</sup> However our measurements of the dark in- and out-of-phase current components resulting from a 10-mV sine wave superimposed on a 0.5 V/s dc scan, could not be interpreted in a unique and meaningful way so as to obtain  $V_{fb}$ . However, we noticed that the resistive component of the impedance monotonically increases from a certain potential in the dark and is decreased to a constant level under electrode illumination (Figure 2). No faradaic current is detected at these potentials (even under electrode illumination), thus no shunting of the sc resistive elements is provided by the light. The capacitive component changes in a more complex way with electrode illumination but the relative magnitude of this change is much smaller. Although no arbitrary separation between the components is possible, we feel that the following interpretation of this effect allows estimation of  $V_{fb}$ . The monotonic increase of the resistive component with potential in the dark mainly reflects the formation of a depletion layer consisting of immobile charge in the space charge region. Electrode illumination, by forming free mobile carriers, eliminates this resistance. Thus the position of  $V_{fb}$  can be taken as the point where the dark resistive component deviates from that under illumination. Because all of the samples were fairly thick (1–2 mm), light effects that could arise at the ohmic metal-sc contact were avoided.

Since the resistive component varies approximately with the square root of potential in the dark, as expected from the variation of depletion layer width with potential,<sup>28</sup> and p- and n-type samples show symmetric behavior and yield an estimated band gap near the known value for Si, the above treatment is at least approximately correct. Moreover the n-type Si  $V_{fb}$  value coincides with that obtained by the photovoltage method. A related method which could provide similar information about the resistance variation under illumination involves surface conductivity measurements. Within the reproducibility of the measurement and the nature of the assumptions we place  $V_{fb}$  for n-type Si at  $-1.20 \pm 0.15$  V and that for p-type Si at  $-0.10 \pm 0.15$  V, independent of the doping level.

**Relative sc-Solution Energy Levels.** The energy levels in solution for a certain redox couple are identified closely with its standard electrode potential<sup>17</sup> and were determined by using cyclic voltammetry at a Pt electrode, where all couples showed reversible, one-electron waves. The midpoint between the cathodic ( $E_{pc}$ ) and anodic ( $E_{pa}$ ) peak potentials was taken as the standard potential of the system.<sup>29</sup> Figure 3 is a schematic representation of the relative energy positions of the sc bands and the systems employed,

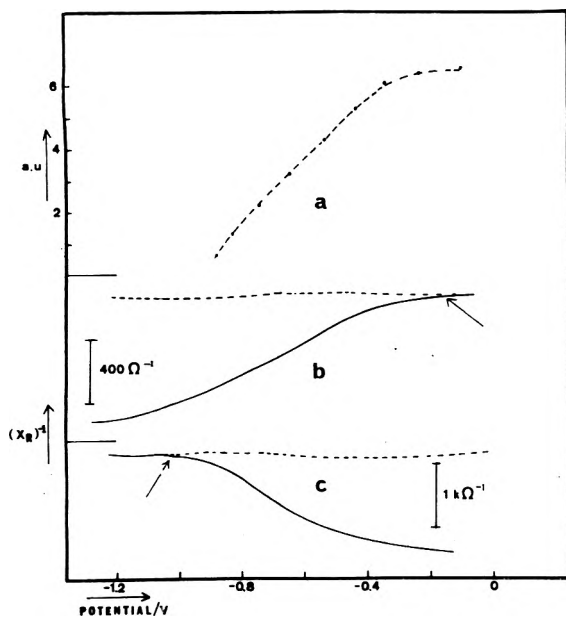


**Figure 2.** (a) Instantaneous photopotential at n-Si, 5 ohm cm; (b) resistive component of electrode impedance, p-Si 10 ohm cm; (c) resistive component of electrode impedance, n-Si, 5 ohm cm. For b and c dashed line, with electrode illumination; 4000 Hz, 10 mV sine wave; lock-in amplifier time constant, 1 ms. Arrows show estimated flat band potentials.

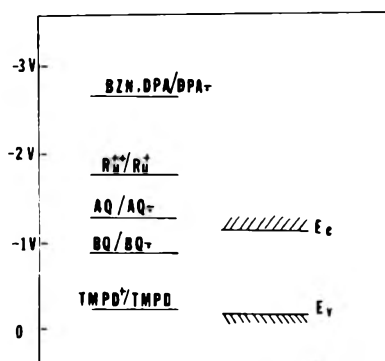


**Figure 3.** Schematic energy relation between Si bands and redox couples in ACN-0.1 M TBAP solution: TMPD, *N,N,N',N'*-tetramethyl-*p*-phenylenediamine; BQ, *p*-benzoquinone; AQ, 9,10-antraquinone,  $\text{Ru}^{2+}$ ,  $\text{Ru}(\text{bpy})_3(\text{ClO}_4)_2$ ; BZN, benzonitrile; DPA, 9,10-diphenylanthracene.

based on the measurements to be described. The acceptor (oxidized form) levels are supposed to have a Gaussian distribution of width  $\lambda$  which equals the difference in the oxidized and reduced form solvation energy, positioned  $\lambda/2$  eV above the horizontal line representing the level, while the donor levels of the same shape are positioned  $\lambda/2$  eV below.<sup>17</sup> Since  $\lambda$ , which is at least 0.5 to 1 eV, is comparable to the band gap of Si (1.1 eV), a fair amount of overlap is expected between the sc bands and levels in solution even for levels positioned in the gap region. Under these conditions contribution of both sc bands to the exchange current can occur.

*n*-Type Si. The system with the most negative standard potential,  $E_s$ , investigated was benzonitrile (BZN), which undergoes a reversible reduction at a Pt electrode in ACN. During the reduction of such a system, with an  $E_s$  so negative of  $V_{fb}$  that it is located well within the conduction band (cb), the sc properties of the *n*-type electrode are sup-

pressed. Degeneracy prevails and the Helmholtz potential drop at the sc-solution interface may be modulated so that metallic behavior is expected with only a small degree of irreversibility (Figure 4). Very similar behavior is exhibited by another negative system,  $\text{DPA}|\text{DPA}^-$  (where DPA is 9,10-diphenylanthracene). For systems with somewhat more positive  $E_s$  values but those still negative of the n-Si  $V_{fb}$  one expects that both reduction and reoxidation of the reduced species will occur through the cb. The reduction will be stimulated by the applied overpotential either through electrons accumulating in the cb, yielding an apparent transfer coefficient of 1,<sup>30</sup> or, as before, through modulation of the Helmholtz potential because of degeneracy. For the concentrations (1–10 mM) employed here mass transfer in solution governs the reaction rate. The reoxidation, however, should be influenced less by a positive overvoltage, if the potential and population in the space charge region are modulated, because the number of free vacancies in the cb which accept electrons in the reoxidation process are nearly independent of potential. The three successive reductions and reoxidations of the chelate  $\text{Ru}(\text{bpy})_3(\text{ClO}_4)_2$  (bpy = bipyridyl)<sup>31</sup> are an example of this case (Figure 5). The reason for the broadening of the third wave is unclear. The reoxidation of the +1 to the +2 species is sluggish and fails to produce a definite current peak. The cyclic voltammetry of anthraquinone (AQ) at Pt and n-Si is shown in Figure 6. The reduction to the radical anion,  $\text{AQ}^-$ , occurs at Pt at -1.3 V, a potential just slightly negative of  $V_{fb}$  of n-Si. Thus while the cb is almost certainly involved in the reduction process, there is also the possibility of some overlap between solution levels and the valence band (vb). The reduction of AQ at n-Si occurs with an  $E_{pc}$  0.1–0.2 V more negative than that at Pt, suggesting that a slight accumulation layer must be formed in the space charge region before reduction occurs. Both cb and vb are candidates for the oxidation of  $\text{AQ}^-$  but participation by the vb requires hole injection into solution and a rough calculation of the maximum supply of minority carriers based on estimated diffusion and hole generation rates predicts that this dark vb oxidation route is negligible. A small, but definite, oxidation current for  $\text{AQ}^-$  is observed with some anodic overpotential compared to Pt; this anodic current increases significantly when the electrode is illuminated. Thus, in addition to an inefficient route for  $\text{AQ}^-$  oxidation involving the cb or surface states near it, photosensitized oxidation via the vb is possible. In this case a sufficiently high electric field has to be formed in the space charge region (i.e., depletion layer formation) for the separation of the photogenerated carriers to occur, thus preventing electron-hole recombination. To observe the photoeffect the electrode potential must be sufficiently positive; thus the oxidation, even under illumination, occurs with some anodic overpotential.

*p*-Benzoquinone (BQ) shows similar behavior. The redox potential of this system at Pt is -0.85 V, positive of the n-Si  $V_{fb}$ . For this system a very pronounced negative overpotential is found compared to Pt, so that the reduction of BQ and AQ ( $\approx 0.4$  V more negative on Pt) nearly coincide at n-Si. Indeed, the BQ reduction, if carried out via the cb, will not occur as long as the sc space charge region is in a depletion situation; only at an electrode potential where accumulation of electrons in the space charge region takes place, will BQ be reduced, and thermodynamically these potentials allow the reduction of AQ as well. As concerns the oxidation of  $\text{BQ}^-$ , again a photoeffect was found, thus

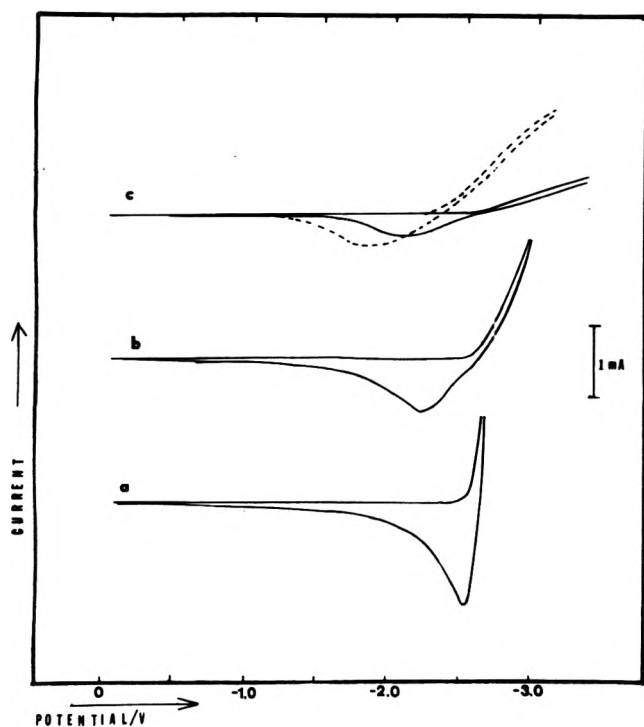


Figure 4. Current-voltage curve of 50 mM BZN in ACN-0.1 M TBAP: (a) Pt electrode; (b) n-Si, 5 ohm cm; (c) p-Si, 10 ohm cm. Dashed line, with electrode illumination. Potential scan rate, 50 mV/s.

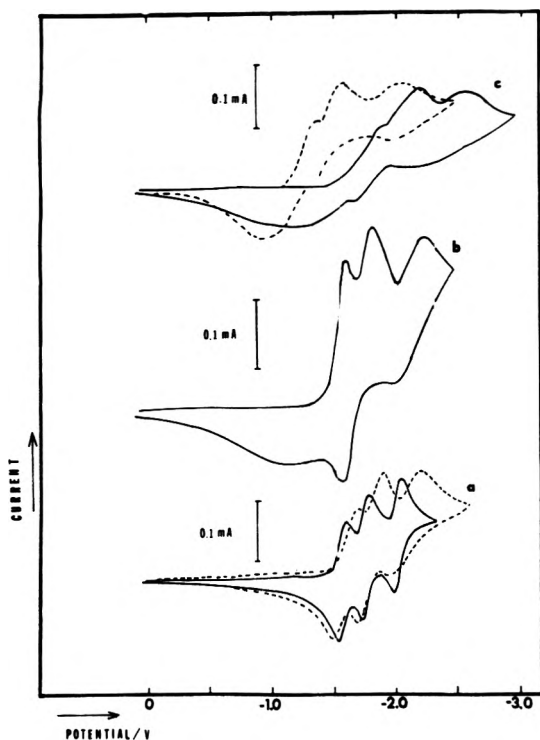


Figure 5. Cyclic voltammetry of 5 mM of  $\text{Ru}(\text{bpy})_3^{2+}$  in ACN-0.1 M TBAP: (a) Pt electrode; dashed line, "activated" p-Si 0.05 ohm cm (see text); (b) n-Si, 1 ohm cm; (c) p-Si, 10 ohm cm dashed line, with electrode illumination. Potential scan rate, 50 mV/s.

demonstrating participation of the vb. In the dark, irreproducible behavior was found which was dependent on the electrode pretreatment. Sometimes no perceptible anodic current was observed and sometimes a small but definite

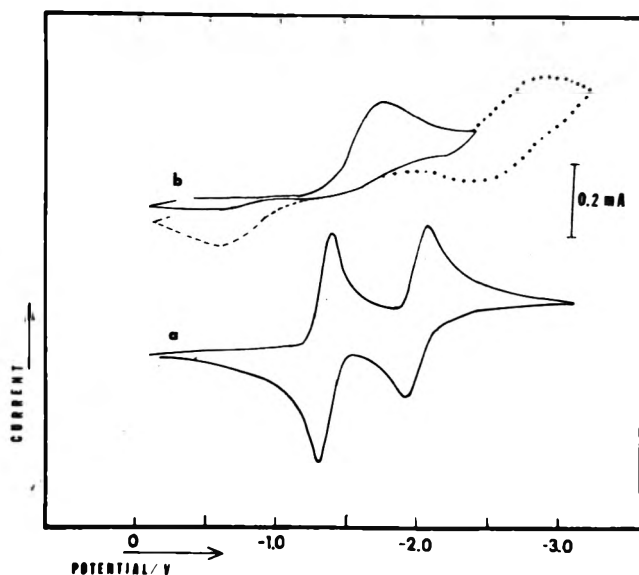
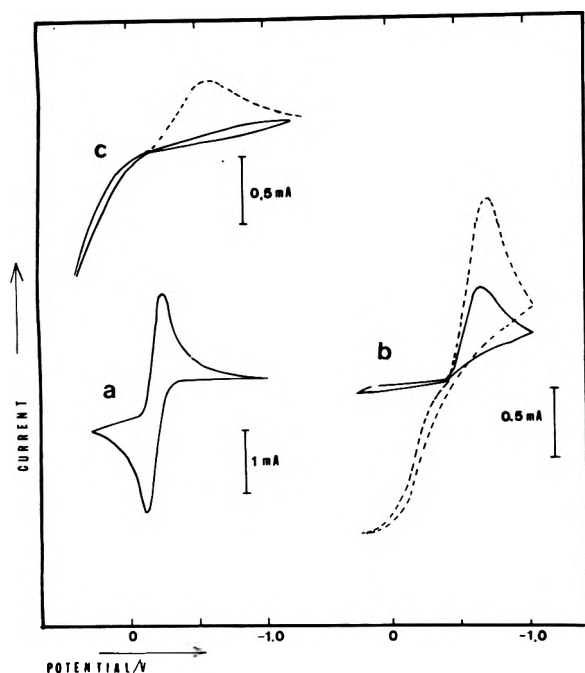


Figure 6. Cyclic voltammetry of 20 mM AQ in ACN-0.1 M TBAP: (a) Pt electrode; (b) n-Si, 5 ohm cm. Dotted line, scan continuation to more cathodic potentials; dashed line, with electrode illumination. Potential scan rate, 50 mV/s.

current, as for  $\text{AQ}^{\cdot-}$  oxidation, appeared. The energy distribution for  $\text{BQ}^{\cdot-}$  is less favorable for overlap with the cb, thus direct electron transfer to cb, as for  $\text{AQ}^{\cdot-}$ , will probably be very ineffective. However, an indirect route for transferring an electron to the cb in the bulk via surface states (which will be positioned at this high surface band bending above the energy of the conduction band in bulk and hence will be capable of bringing trapped electrons from solution to the conduction band) may still be operative. The sensitivity of the electrode behavior to surface pretreatment implies such an involvement of surface states.

The most positive system investigated was  $\text{TMPD}^{\cdot+}/\text{TMPD}$  (where TMPD is  $N,N,N',N'$ -tetramethyl-*p*-phenylenediamine). A solution containing TMPD and  $\text{TMPD}^{\cdot+}$  in equimolar amounts was prepared by bulk coulometric oxidation of TMPD at a Pt electrode. From its redox potential at a Pt electrode (Figure 7a) of  $-0.25$  V compared with  $V_{\text{fb}}$  of n-Si, this system is expected to interact mainly with the vb, i.e., the solution energy level distribution of TMPD mostly overlaps with the vb while that of  $\text{TMPD}^{\cdot+}$  also overlaps the lower part of the band gap. Reduction of  $\text{TMPD}^{\cdot+}$  at n-Si (Figure 7b) occurs with  $E_{\text{pc}}$  of  $-0.7$  V and shows only a very small associated anodic current on reversal. When the electrode is illuminated, however, a limiting anodic photocurrent, proportional to light intensity, is observed on scan reversal corresponding to TMPD oxidation, and the cathodic current is increased on the next scan because of the higher concentration of  $\text{TMPD}^{\cdot+}$  now in the vicinity of the electrode. A discussion of the mechanism of these redox reactions on n-Si will be given after the behavior of p-Si is described.

*p-Type Si.* Since the relative location of the energy levels in solution and for the p-Si should be essentially the same as for n-Si (as implied in Figure 3), all reductions which proceed primarily via the cb for n-Si (i.e., all compounds other than  $\text{TMPD}^{\cdot+}$ ) would be expected to occur also via the cb in p-Si and hence be limited by the minority carrier supply at the electrode surface. Under these circumstances very small cathodic currents might be expected. In



**Figure 7.** Cyclic voltammetry of  $\text{TMPD}^+|\text{TMPD}$  mixture (ca. 1:1) in  $\text{ACN}-0.1 \text{ M TBAP}$ : (a) Pt electrode; (b) n-Si, 5 ohm cm; dashed line, with electrode illumination; (c) p-type, 10 ohm cm; dashed line, with electrode illumination. Potential scan rate, 50 mV/s.

fact, however, all of the couples showed significant cathodic currents at p-Si with the  $i-E$  curves shifted toward negative potentials compared to the behavior on n-Si (Figures 1, 4, and 5). At electronic equilibrium the surface concentration of electrons in the p-Si should be the same as that for n-Si at the same electrode potential (e.g.,  $E_s$  of  $\text{Ru}(\text{bpy})_3^{2+}$ ). Thus the exchange current for the reduction process, which depends upon surface concentrations of electrons and oxidized species, should be the same on both n- and p-type material.<sup>8</sup> However whereas for n-Si the electrons are the majority carrier and can be supplied by the usual conduction process in the sc, for p-Si the supply of electrons, the minority carriers, will be limited by their rate of supply to the surface. Neither diffusion of electrons through the quasineutral region<sup>6</sup> nor pair generation in the space charge region<sup>18</sup> seems to be sufficiently rapid to provide electrons at the milliamp current level. For these compounds the origin of electrons consumed in the reduction at the p-type electrode is the vb and we feel that the mechanism by which they arrive at the surface is related to the extreme band bending which occurs at this electrode under the reduction conditions. Consider, for example, the first reduction of  $\text{Ru}(\text{bpy})_3^{2+}$  observed at about  $-1.65 \text{ V}$  (at Pt). When the electrode is subjected to this electrode potential, which is more than the band gap energy beyond the p-Si  $V_{fb}$  in the depletion direction, enormous band bending at the surface will take place. It is possible under these conditions that the band gap region, or even the edge of the cb, at the surface will be at the same or even below the energy of the vb in the bulk sc. Then, especially for the highly doped Si, where the potential barrier is narrow, direct transfer of electrons across the space charge region from the vb to a surface level in the gap or to the edge of the cb may be possible. Different mechanisms for a related phenomenon, the supply of holes (minority carriers) to the surface of an n-type sc, have been considered.<sup>21</sup> The intraband electron exchange on highly doped n-ZnO has also recently

been described.<sup>32</sup> Two experimental findings support this mechanism. (a) Reduction of these compounds at p-Si occurred at potentials very negative of  $V_{fb}$  so that large band bending and high potential barriers were established. BQ reduction on p-Si occurs at about the same potentials as at the n-type (ca.  $-1.4 \text{ V}$ ), quite negative of the potential at Pt ( $-0.85 \text{ V}$ ). For n-Si this overpotential probably arises from the necessity of forming an accumulation layer, in the space charge region, while for p-Si this overpotential represents the amount of band bending and surface field needed for this effect to occur. (b) After vigorous etching the 0.05 ohm cm p-type electrode sometimes behaved like an "activated electrode" whose surface consisted mainly of black patches of amorphous silicon<sup>22</sup> and whose behavior resembled that of a metal electrode for reductions much more than any of the n-type electrodes employed (Figure 5a). Indeed, tunneling and related phenomena are expected to be most pronounced for a heavily-doped electrode, because the depletion layer width, and hence the barrier width for tunneling, are inversely proportional to the square root of the majority carrier concentration in the bulk. In all cases the reductions are promoted by illumination of the p-Si electrode (Figures 1, 4, 5, 7). These photoeffects will be discussed in the next section. Oxidations of the reduced forms at p-Si show similar behavior to that found with n-Si for those compounds showing electron transfer mainly with the cb ( $\text{BZN}$ ,  $\text{Ru}(\text{bpy})_3^{2+}$ ). For AQ and BQ oxidation can also occur in the dark at p-Si, since majority carrier (hole) injection is involved.

For the  $\text{TMPD}^+|\text{TMPD}$  system, as discussed for n-Si, overlap is apparently mainly with the vb. For p-Si, where holes are available, oxidation of TMPD observed in the dark is enhanced by the applied potential either by hole accumulation in the space charge region or by changes in the Helmholtz potential drop in solution (Figure 7d). A small cathodic current is observed at p-Si for  $\text{TMPD}^+$  reduction in the dark, which is greatly enhanced under illumination. A reduction occurring via the vb should be relatively independent of potential if the potential drop in the Helmholtz layer remains unchanged. This behavior is found with p-Si (Figure 7d) but not with n-Si (Figure 7b). For the p-Si the reduction is occurring near its  $V_{fb}$ , while for n-Si the potential is quite positive of its  $V_{fb}$  so that large band bending occurs and perhaps results in a change in the potential drop in the Helmholtz layer. The reduction current peak obtained for the n-Si can also result from reduction via surface states. Such surface states, which have been shown to exist in the Si band gap,<sup>15,33,34</sup> are vacant at extreme anodic electrode potentials, but are gradually populated during a potential scan in a negative direction. These states may then transfer electrons to the reducible form. In this case, the potential dependence of the current will reflect the occupation statistics of these states. Such an effect was found for  $\text{TiO}_2$ ,<sup>5</sup> a wide bandgap n-type sc for the reduction of systems located within the band gap region. A reduction of BQ limited by diffusion in solution and occurring with participation of the vb was also observed for the small band gap electrode, n-type Ge.<sup>9</sup>

**Photoeffects at the p-Si Electrode.** Illumination of p-Si with light of energy greater than that of the band gap (e.g., red light) excites electrons to the cb and promotes direct reduction through this band. Only some particular nuances of this well-known photoeffect,<sup>35</sup> i.e., those characteristic to this system, will be discussed here. The photoeffect was observed for all reducible couples employed. Even when the

reduction occurs via the vb (i.e., for  $\text{TMPD}^+$ ) light provides more efficient reduction, although in this case the electrode is subjected to potentials only slightly negative of  $V_{fb}$ , so that a strong depletion layer has not formed and the "electrical state" of the sc is not very favorable for the observation of a photoeffect. The impossibility of an isoenergetic electron transfer directly from the cb to the  $\text{TMPD}^+$  may require the existence of some energy states (e.g., surface states) within the gap which are filled by transfer from the cb before the transfer. Another possibility is that now, as in the dark,  $\text{TMPD}^+$  reduction occurs exclusively via the vb, but that modulation of the Helmholtz potential drop in solution takes place at an illuminated sc electrode, because the extent of the sc surface band bending diminishes under illumination, as is observed in the usual photopotential effect,<sup>35</sup> and this enhances the reduction rate. The photoreduction occurs with an "underpotential" (Figures 1, 4, 5c), i.e., the reduction process takes place at the illuminated p-type Si electrode at less negative potentials than at a Pt electrode where its reduction is nerstian. This phenomenon has been observed at other sc electrodes<sup>36-38</sup> and very generally may be useful for utilizing light energy for driving an electrochemical reaction with a smaller (or no) electrical energy input. Under certain conditions the photoreduction appears to be selective, i.e., the potential sequence in which some of the consecutive photoreductions occur follows their order at a Pt electrode, although all are shifted in a positive direction (Table I). This is a special feature of the photoeffect at low band gap sc electrodes (whenever the background allows differentiation) in contrast to the nonselective photooxidations frequently observed at large band gap electrodes.<sup>37</sup>

Any oxidized form that at a certain electrode potential will be located at an energy position higher (more negative) than the sc cb in the bulk, where this relative energy location can be controlled by the applied potential in the same way as for a metal electrode, will not be reduced by a photogenerated electron in the cb. At a large band gap (e.g., 3 eV) sc, wherever the electrode potential enables the photoprocess to occur, more systems will be located within the bulk energy interval of the sc bandgap and they will all undergo photosensitized charge transfer at about the same potential, that where a sufficient depletion layer is established. Usually no limiting current proportional to light intensity is found. The reason for this seems to be that the reduction also proceeds in the dark via the breakdown mechanism discussed before. Thus a limiting current resulting from the rate of photogeneration of electrons will be partially masked by this dark background current. Moreover even if the breakdown phenomenon is greatly suppressed by light, because the establishment of high surface band bending is prevented in the presence of light, the concentration range employed (1–10 mM) is such that mass transfer limitation in solution occurs and indeed when a high concentration of BZN was used, a limiting photocurrent was found.

**ECL at Si Electrodes.** The medium employed in this work suggested the possibility of carrying out ECL<sup>39,40</sup> (electrogenerated chemiluminescence) at Si electrodes. Briefly, ECL is based on the mutual annihilation of appropriate electrogenerated radical cations with radical anions to give an excited state which emits light when decaying to the ground state. Especially interesting is the possibility of "up-conversion" of red light utilizing ECL at p-Si. Here one uses the features of photosensitized reduction at p-Si,

TABLE I: Photosensitized Potentials for Reductions at a p-Si Electrode Compared to a Pt Electrode for Several Compounds in ACN

Compound <sup>a</sup> reduced	Peak potential Pt, V	Peak potential <sup>b</sup> illuminated p-Si, V
$\text{TMPD}^+$	-0.25	-0.6
BQ	-0.85	-1.3 to -1.4
AQ	-1.30	-1.3
$\text{Ru}(\text{bpy})_3^{2+}$	-1.70	-1.4
DPA	-2.30	-1.95
BZN	-2.60 <sup>b</sup>	-2.25 <sup>c</sup>

<sup>a</sup> Concentration range, 1–10 mM. <sup>b</sup> This potential is not related to thermodynamic properties (e.g., the standard redox potential) as at Pt and is somewhat dependent upon the concentration employed. <sup>c</sup> No peak obtained, foot of the wave.

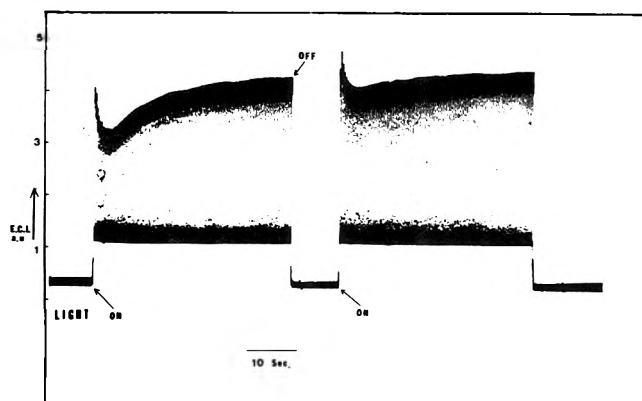


Figure 8. Pulsed ECL at a p-Si electrode with and without electrode illumination. Pulsing mode, -2.3 to -1.3 at 5 Hz; illumination,  $\lambda > 650$  nm, ECL emission at 450 nm. The solution contained 1 mM  $\text{DPACl}_2$  and 0.1 M TBAP in ACN.

including the negative overpotential effect to carry out a photoinduced ECL process.  $\text{DPACl}_2$  (9,10-dichloro-9,10-dihydro-9,10-diphenylanthracene) is an especially useful compound for this experiment, since it produces blue ECL upon reduction.<sup>41,42</sup> By illuminating the p-Si with red light we initiated  $\text{DPACl}_2$  reduction and obtained blue (420–450 nm) emission.<sup>43</sup> The conditions of the experiment were such that neither the electrical input alone (even at a Pt electrode) nor the illumination alone (i.e., a fluorescence experiment) were capable of producing the emission from this system, thus demonstrating the coupling of low photon energy with electrical energy to yield a more energetic photon. Figure 8 demonstrates this principle. Further details have been given elsewhere.<sup>43</sup> The p-Si electrode was subjected to pulses between -1.3 and -2.3 V at a frequency of 5 Hz. Blue ECL emission was observed whenever the p-Si was illuminated with red light, with the emission spatially limited to the area where the red light was impinging and ceasing when the illumination was stopped. Similar behavior has been observed in preliminary experiments with the small band gap sc electrodes p-GaAs and p-InP.

**Acknowledgments.** This research was supported by the U.S. Army Research Office-Durham and the National Science Foundation. We appreciate the gift of the p-type Si material from Dr. Isaac Trachtenberg, Texas Instruments.

## References and Notes

- (1) M. D. Krotova and Yu. V. Pleskov, *Solid State Phys.*, **3**, 2119 (1963).
- (2) H. B. Mark, Jr., and B. S. Pons, *Anal. Chem.*, **40**, 110 (1966).
- (3) T. Osa and T. Kuwana, *J. Electroanal. Chem.*, **22**, 389 (1969).
- (4) R. Landsberg, P. Janietz, and R. Dehmlow, *Z. Chem.*, **15**, 38 (1975).
- (5) S. N. Frank and A. J. Bard, *J. Am. Chem. Soc.*, in press.
- (6) V. A. Myamlin and Yu. V. Pleskov, "Electrochemistry of Semiconductors", Plenum Press, New York, N.Y., 1967.
- (7) H. Gerischer in "Advances in Electrochemistry and Electrochemical Engineering", Vol. I, P. Delahay and C. W. Tobias, Ed., Interscience, New York, N.Y., 1961.
- (8) H. Gerischer in "Physical Chemistry", Vol. IX A, H. Eyring, D. Henderson, and W. Yost, Ed., Academic Press, New York, N.Y., 1970.
- (9) R. Memming and F. Moller, *Ber. Bunsenges. Phys. Chem.*, **76**, 609 (1972).
- (10) R. Memming and F. Moller, *Ber. Bunsenges. Phys. Chem.*, **76**, 469 (1972).
- (11) R. A. L. Vanden Berghe, V. P. Gomes, and F. Cardon, *Ber. Bunsenges. Phys. Chem.*, **77**, 289 (1973).
- (12) B. Pettinger, H.-R. Schöppel, and H. Gerischer, *Ber. Bunsenges. Phys. Chem.*, **78**, 450 (1974).
- (13) T. Ambridge, C. R. Elliot, and M. M. Faktor, *J. Appl. Electrochem.*, **3**, 1 (1973).
- (14) R. Memming and G. Schwandt, *Electrochim. Acta*, **13**, 1299 (1968).
- (15) R. Memming and G. Schwandt, *Surface Sci.*, **5**, 97 (1966).
- (16) P. J. Boddy, *J. Electrochem. Soc.*, **115**, 199 (1968).
- (17) H. Gerischer, *Photochem. Photobiol.*, **16**, 243 (1972).
- (18) J. B. Flynn, *J. Electrochem. Soc.*, **105**, 715 (1958).
- (19) Reference 6, pp 181, 182.
- (20) A. Many, *J. Phys. Chem. Solids*, **26**, 587 (1965).
- (21) R. L. Meek, *Surface Sci.*, **25**, 526 (1971).
- (22) D. R. Turner in "The Surface Chemistry of Metals and Semiconductors", H. C. Gatos, Ed., Wiley, New York, N.Y., 1959.
- (23) C. P. Keszthelyi and A. J. Bard, *J. Electrochem. Soc.*, **120**, 241 (1973).
- (24) W. P. Gomes and F. Cardon, *Z. Physik. Chem. (Frankfurt am Main)*, **86**, 330 (1973).
- (25) H. V. Harten, *Electrochim. Acta*, **13**, 1255 (1968).
- (26) C. G. B. Garrett and W. H. Brattain, *Phys. Rev.*, **99**, 376 (1955).
- (27) K. Lehovek and A. Slobodsky, *Solid State Electron.*, **7**, 59 (1964).
- (28) W. W. Gärtner, *Phys. Rev.*, **116**, 84 (1959).
- (29) R. S. Nicholson and I. Shain, *Anal. Chem.*, **36**, 706 (1964).
- (30) Reference 6, p 164.
- (31) N. E. Tokel-Takvoryan, R. E. Hemingway, and A. J. Bard, *J. Am. Chem. Soc.*, **95**, 6582 (1973).
- (32) B. Pettinger, H.-R. Schöppel, T. Yokoyama, and H. Gerischer, *Ber. Bunsenges. Phys. Chem.*, **78**, 1024 (1974).
- (33) B. F. Lewis and T. E. Fischer, *Surface Sci.*, **41**, 371 (1974).
- (34) J. F. Dewald in "The Surface Chemistry of Metals and Semiconductors", H. C. Gatos, Ed., Wiley, New York, N.Y., 1959.
- (35) H. Gerischer, *J. Electrochem. Soc.*, **113**, 1175 (1966).
- (36) A. Fujishima and K. Honda, *Nature (London)*, **238**, 37 (1972).
- (37) A. Fujishima and K. Honda, *J. Chem. Soc. Jpn.*, **74**, 355 (1971).
- (38) M. D. Archer, *J. Appl. Electrochem.*, **5**, 17 (1975).
- (39) A. J. Bard and L. R. Faulkner in "Electroanalytical Chemistry", A. J. Bard, Ed., Marcel Dekker, New York, N.Y., 1976.
- (40) D. M. Hercules in "Physical Methods of Organic Chemistry", 4th ed, Part II, A. Weissberger and B. Rossitor, Ed., Academic Press, New York, N.Y., 1971.
- (41) T. M. Siegal and H. B. Mark, Jr., *J. Am. Chem. Soc.*, **93**, 6281 (1971).
- (42) K. Boto and A. J. Bard, *J. Electroanal. Chem.*, in press.
- (43) D. Laser and A. J. Bard, *Chem. Phys. Lett.*, **34**, 605 (1975).

## Aqueous Solutions of Azoniaspiroalkane Halides. II. Apparent Molal Volumes and Apparent Molal Heat Capacities

Wen-Yang Wen,\* Antonio LoSurdo,

Jeppson Laboratory, Chemistry Department, Clark University, Worcester, Massachusetts 01610

Carmel Jolicoeur, and Jeanine Boileau

Department de Chimie, Université de Sherbrooke, Sherbrooke, Quebec, Canada (Received July 14, 1975)

Publication costs assisted by the National Science Foundation and the National Research Council of Canada

Densities and heat capacities of aqueous solution of azoniaspiroalkane bromides,  $(\text{CH}_2)_n\text{N}^+(\text{CH}_2)_n\text{Br}^-$  where  $n = 4, 5$ , and  $6$ , have been measured at  $25^\circ\text{C}$  using a flow densimeter and a flow microcalorimeter, respectively. Apparent molal volumes and apparent molal heat capacities obtained for these salts are compared with those of the corresponding tetraalkylammonium bromides. These comparisons show that the apparent molal volumes of the spiro ions are smaller, and the heat capacity of the water surrounding these ions is substantially reduced. Some indications are found for the flexibility of alkyl chains in the tetraalkylammonium ions when volume data for the two types of ions are compared. Forming closed rings from the alkyl chains in tetraalkylammonium ions seems to alter their solution properties greatly and weaken their hydrophobic character considerably.

### Introduction

Earlier studies on the comparative solution properties of hydrophobic ions containing either linear or cyclic alkyl groups have shown some important differences among the properties of these two types of solutes.<sup>1-3</sup> The broad current interest toward the tetraalkylammonium ions as typical hydrophobic species<sup>4</sup> has prompted us to study the solution behavior of their counterpart azoniaspiroalkane ions. The latter should provide information on the role of geometrical and dynamic configurational effects in the ther-

modynamic properties of alkyl-substituted quaternary ammonium ions.

In the first paper of this series (hereafter cited as paper I)<sup>1</sup> enthalpies of solution of azoniaspiroalkane halides,  $(\text{CH}_2)_n\text{N}^+(\text{CH}_2)_n\text{X}^-$ , in  $\text{H}_2\text{O}$  and  $\text{D}_2\text{O}$  have been reported. Apparent molal heat contents and enthalpies of transfer from  $\text{H}_2\text{O}$  to  $\text{D}_2\text{O}$  obtained were compared with those of the corresponding tetraalkylammonium halides. The results showed that forming closed rings from the alkyl chains in tetraalkylammonium ions alter their enthalpic

characteristics and weaken their hydrophobic interactions with water considerably.

In this second communication, we are reporting the results of our measurements on the apparent molal volumes and heat capacities of three azoniaspiroalkane bromides in water at 25 °C. The data obtained are again compared with those of the corresponding tetraalkylammonium halides. Some indications are found which point to the flexibility of the alkyl chains of tetraalkylammonium ions in aqueous solution.

## Experimental Section

1. *Materials.* Azoniaspiroalkane halides were synthesized by a method adapted from Blicke and Hotelling<sup>5</sup> and from Thomas and his co-workers.<sup>6,7</sup> The detailed procedures used for the purification and analysis of each product have been described in paper I. The IUPAC names as well as our abbreviated names of the three compounds are as follows: (i) (CH<sub>2</sub>)<sub>4</sub>N<sup>+</sup>(CH<sub>2</sub>)<sub>4</sub>Br<sup>-</sup>, 5-azoniaspiro[4.4]nonane bromide, "4.4 Br"; (ii) (CH<sub>2</sub>)<sub>5</sub>N<sup>+</sup>(CH<sub>2</sub>)<sub>5</sub>Br<sup>-</sup>, 6-azoniaspiro[5.5]undecane bromide, "5.5 Br"; (iii) (CH<sub>2</sub>)<sub>6</sub>N<sup>+</sup>(CH<sub>2</sub>)<sub>6</sub>Br<sup>-</sup>, 7-azoniaspiro[6.6]tridecane bromide, "6.6 Br".

2. *Flow Densimeter.* The density measurements have been carried out using a "vibrating tube" flow densimeter described by Picker, Tremblay, and Jolicœur.<sup>8</sup> In this technique, the solutions are circulated at constant flow rate through the oscillating tube, the natural vibration period of which is read on a digital frequency meter. The density increment  $\Delta d$  of a solution relative to the solvent is simply given as

$$\Delta d = d - d_0 = B(\tau^2 - \tau_0^2)$$

where  $\tau$  and  $\tau_0$  are the vibration period measured with the solution and the solvent, respectively;  $B$  is a constant determined by calibration using distilled water and nitrogen gas. The reproducibility of relative densities was usually within 3 ppm.

3. *Flow Microcalorimeter.* The specific heat measurements were performed on a flow microcalorimeter designed by Picker et al.<sup>9,10</sup> The instrument consists essentially of two identical flow cells in which the solvent and the solution are circulated with equal flow rates. Heating elements provided symmetrical heating of the flowing liquids so that differences in the volumetric specific heats between these liquids were directly recorded. Under the flow rates (ca. 1 ml/min) and heating power (ca. 110 mW) used, the temperature rise during the measurement was 1.80 °C.

In actual running of the experiments, each solution under study was passed first through the flow densimeter and then the flow calorimeter in succession yielding data of density and specific heat of that solution in one operation. Since the same closed-loop thermostat served to regulate the temperature of both instruments at 25.00 ± 0.02 °C, the specific heat data were actually obtained at the mean temperature of 25.90 °C. However, this is of no significant consequence on either the specific heat ratios defined below or the calculated apparent molal heat capacities.

## Results

The apparent molal volumes  $\phi_v$  were calculated from the solution densities  $d$  using the following equation:

$$\phi_v = \frac{M}{d} + \frac{1000(d_0 - d)}{m d d_0} \quad (1)$$

where  $d_0$  is the density of water at 25 °C (0.997047 g/ml),<sup>11</sup>  $M$ , the formula weight of the salt, and  $m$ , its concentration in mole per kilogram of water. The molal concentrations ( $m$ ) were converted into molarities ( $c$ ) as required.

The apparent molal heat capacities  $\phi_{cp}$  were computed from the measured volumetric specific heat  $\sigma$  (cal K<sup>-1</sup> ml<sup>-1</sup>) of the solutions and the equation

$$\phi_{cp} = M c_p + \frac{1000}{m} (c_p - c_p^0) \quad (2)$$

with

$$c_p/c_p^0 = (d_0/d)(\sigma - \sigma_0)/\sigma_0 \quad (3)$$

In these equations,  $c_p$  is the weight specific heat (cal K<sup>-1</sup> g<sup>-1</sup>) and the zero subscript or superscript refers to pure water;  $c_p^0$  was taken as 0.998877 cal K<sup>-1</sup> g<sup>-1</sup>,<sup>12</sup> where 1 cal = 4.1840 J. The experimental results of  $\phi_v$  and  $\phi_{cp}$  for the aqueous azoniaspiroalkane bromides are given in Table I. The uncertainty in  $\phi_v$  is about ±0.1 ml mol<sup>-1</sup> for concentration range 0.10–1 M; uncertainty in  $\phi_{cp}$  is ±0.5 cal K<sup>-1</sup> mol<sup>-1</sup> for the concentration range 0.10–1 M.

The quantities  $\phi_v$  and  $\phi_{cp}$  were fitted by least-squares methods to the following equations:

$$\phi_v = \phi_v^0 + 1.868c^{1/2} + B_v c \quad (4)$$

$$\phi_{cp} = \phi_{cp}^0 + 6.929c^{1/2} + B_{cp} c \quad (5)$$

The coefficients in  $c^{1/2}$  represent the term given by the Debye-Hückel limiting law and the other coefficients  $\phi^0$  and  $B$  for the salts investigated are given in Tables II and IV. Values of  $(\phi - A c^{1/2})$  are plotted against  $c$  for the salts in Figures 1 and 2.

## Discussion

A. *Apparent Molal Volumes.* As in previous work,<sup>1</sup> it will be of interest to compare the properties of aqueous azoniaspiroalkane halides with those of the tetraalkylammonium halides. It is readily seen from Table II that  $\phi_v^0$  values of azoniaspiroalkane bromides are smaller, and the values of  $B_v$  are less negative than those of the corresponding tetraalkylammonium bromides. With the assignment of 30.21 ml mol<sup>-1</sup> for  $\phi_v^0(\text{Br}^-)$ ,<sup>13</sup>  $\phi_v^0$  values of the 4.4 ion and 6.6 ion are found to be 85.1% of the Et<sub>4</sub>N<sup>+</sup> ion and 84.8% of the Pr<sub>4</sub>N<sup>+</sup> ion, respectively. The smaller volume of azoniaspiroalkane ions are to be expected due to the absence of terminal methyl groups in these ions.

The values of  $\phi_v^0$  are plotted against the number of carbon atoms in Figure 3 for four different types of salts: azoniaspiroalkane bromides, tetraalkylammonium bromides,<sup>14</sup> alkylamine hydrobromides,<sup>15</sup> and cycloalkylamine hydrobromides.<sup>2</sup> Data points appear to fall on four separate straight lines, one line for each type of salts. The slope of the line corresponds to the average volume increment per CH<sub>2</sub> group. The lines seem to be nearly parallel but not exactly so on closer examinations. The lines for R<sub>4</sub>NBr and RNH<sub>3</sub>Br are close together and lie distinctly above the other two and also slightly but definitely steeper. The line for our salts is the lowest of the four but rather close to that of cycloalkylamine hydrobromides. Lowe and Rendall<sup>16</sup> studied aqueous solution of small dialkylpyrrolidinium iodides and dialkylpiperidinium iodides and reported the slope of the straight line obtained by plotting  $\phi_v^0$  vs. number of carbon atoms to be 14.6 ± 0.3 ml mol<sup>-1</sup>. This value is less than that of R<sub>4</sub>N<sup>+</sup> ions but greater than the corresponding value for the azoniaspiroalkane ions.

In this connection it will be of interest to note the fol-

TABLE I: Apparent Molal Volumes and Apparent Molal Heat Capacities of Azoniaspiroalkane Bromides in Water at 25 °C

$(\text{CH}_2)_4\text{N}^+(\text{CH}_2)_4\text{Br}^-$			$(\text{CH}_2)_5\text{N}^+(\text{CH}_2)_5\text{Br}^-$			$(\text{CH}_2)_6\text{N}^+(\text{CH}_2)_6\text{Br}^-$		
$c, \text{M}$	$\phi_v, \text{ml mol}^{-1}$	$\phi_{cp}, \text{cal K}^{-1} \text{mol}^{-1}$	$c, \text{M}$	$\phi_v, \text{ml mol}^{-1}$	$\phi_{cp}, \text{cal K}^{-1} \text{mol}^{-1}$	$c, \text{M}$	$\phi_v, \text{ml mol}^{-1}$	$\phi_{cp}, \text{cal K}^{-1} \text{mol}^{-1}$
0.020085	152.8	64.0	0.010364	180.0	91.4	0.010333	207.5	135.6
0.023604	152.8	64.6	0.023848	180.2	93.2	0.030523	207.7	135.0
0.041455	152.93	64.39	0.030842	180.1	93.2	0.050778	207.71	135.54
0.050085	152.88	64.56	0.044544	180.30	92.97	0.070568	207.79	135.87
0.051728	152.91	64.89	0.051192	180.13	92.18	0.10071	207.62	135.65
0.064037	152.92	65.70	0.067190	180.35	92.90	0.28862	206.92	135.31
0.068943	152.98	64.91	0.070711	180.29	92.69	0.46575	205.99	135.58
0.082597	152.94	65.54	0.084986	180.37	93.59	0.63036	205.24	132.27
0.098583	153.08	65.46	0.10096	180.17	93.12	0.99007	204.05	130.38
0.10151	152.98	65.32	0.10390	180.34	93.04			
0.20444	152.95	66.13	0.19840	180.19	93.69			
0.28822	152.98	66.75	0.29863	179.92	94.38			
0.46418	152.75	66.99	0.47868	179.49	94.29			
			0.64905	179.05	94.14			
			1.04037	177.97	93.12			

TABLE II: Comparison of Apparent Molal Volumes of Azoniaspiroalkane Bromides with Those of Tetraalkylammonium Bromides in Water at 25 °C

	$\phi_v^0,^a$ $\text{ml mol}^{-1}$	$\Delta\phi_v^0$ per $\text{CH}_2$	$B_v$		$\phi_v^0,^b$ $\text{ml mol}^{-1}$	$\Delta\phi_v^0$ per $\text{CH}_2$	$B_v^b$
4.4 Br	152.6		-2.36	$\text{Me}_4\text{NBr}$	114.35		-1.01
		13.8				14.85	
5.5 Br	180.0		-3.75	$\text{Et}_4\text{NBr}$	173.74		-4.12
		13.8				16.41	
6.6 Br	207.5		-5.60	$\text{Pr}_4\text{NBr}$	239.36		-8.77
						15.31	
				$\text{Bu}_4\text{NBr}$	300.59		-11.85

<sup>a</sup> Errors of  $\phi_v^0$  are about  $\pm 0.1 \text{ ml mol}^{-1}$ . <sup>b</sup> G. Perron and J. E. Desnoyers, *J. Chem. Eng. Data*, 17, 136 (1972).

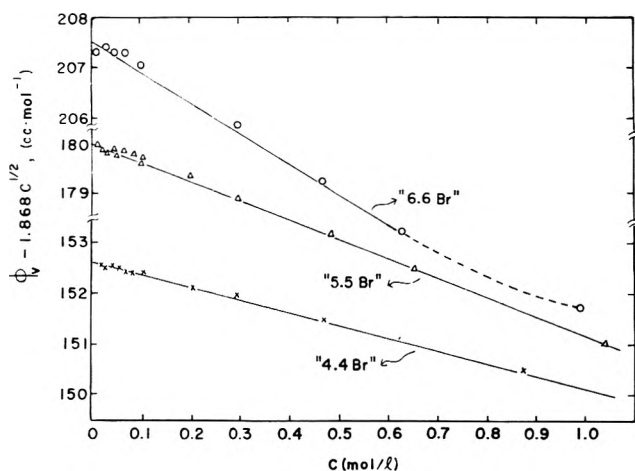


Figure 1. Plot of  $(\phi_v - 1.868c^{1/2})$  vs.  $c$  for the three azoniaspiroalkane bromides in water at 25 °C, where  $\phi_v$  is the apparent molal volume ( $\text{ml mol}^{-1}$ ) and  $c$ , the salt concentration in M. [For the 5.5 and 6.6 salts the ordinate shows only scale and intercept; the data do not span (cross over) the breaks shown on ordinate axis.]

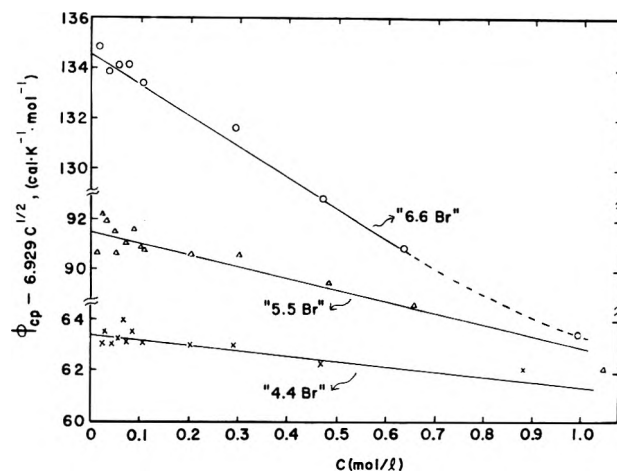


Figure 2. Plot of  $(\phi_{cp} - 6.929c^{1/2})$  vs.  $c$  for the three azoniaspiroalkane bromides in water at 25 °C, where  $\phi_{cp}$  is the apparent molal heat capacity ( $\text{cal K}^{-1} \text{mol}^{-1}$ ) and  $c$ , the salt concentration in M. [For the 5.5 and 6.6 salts the ordinate shows only scale and intercept; the data do not span (cross over) the breaks shown on ordinate axis.]

lowing volume change on step by step cyclization of alkyl chains. The  $\phi_v^0$  value for diethylpyrrolidinium iodide is reported as  $174.9 \text{ ml mol}^{-1}$ ,<sup>16</sup> from which one may assign the cation value of  $132.2 \text{ ml mol}^{-1}$  for the  $\phi_v^0$  of  $(\text{CH}_2)_4\text{N}^+(\text{C}_2\text{H}_5)_2$ . Starting from an ion with four ethyl groups, namely,  $(\text{C}_2\text{H}_5)_4\text{N}^+$ , a  $10.3 \text{ ml mol}^{-1}$  decrease in  $\phi_v^0$  takes place with the formation of one loop to become  $(\text{CH}_2)_4\text{N}^+(\text{C}_2\text{H}_5)_2$ , and a further decrease of  $10.0 \text{ ml mol}^{-1}$  occurs with the formation of the second loop to become  $(\text{CH}_2)_4\text{N}^+(\text{CH}_2)_4$ .

In order to see subtler differences beyond the simple presence or absence of terminal methyl groups, we shall compare the difference of the differences in  $\phi_v^0$  values. The difference in  $\phi_v^0$  between the  $\text{Pr}_4\text{N}^+$  ion and the 6.6 ion is about  $10.5 \text{ ml mol}^{-1}$  greater than the corresponding difference between the  $\text{Et}_4\text{N}^+$  ion and the 4.4 ion. It seems reasonable to attribute this additional  $10.5 \text{ ml mol}^{-1}$  to the combined effect of the following three factors: (a) flexibility of alkyl chains in the larger tetraalkylammonium ion, (b)



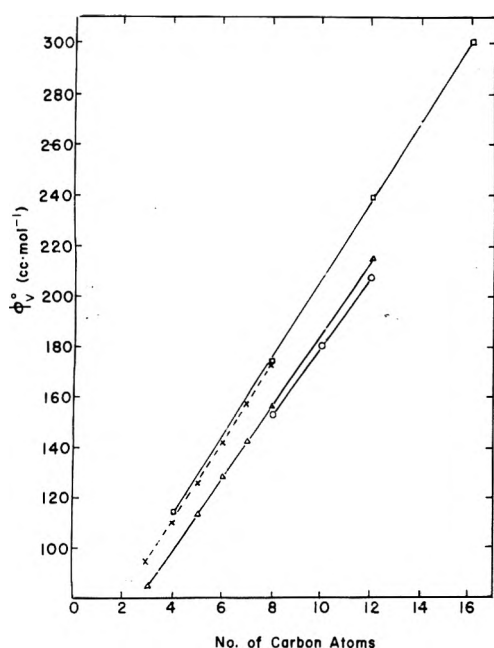


Figure 3. Plot of apparent molal volume at infinite dilution against the number of carbon atoms for different types of salts: tetraalkylammonium bromides ( $\square$ ), alkylamine hydrobromides ( $\times$ ), cycloalkylamine hydrobromides ( $\Delta$ ), and azoniaspiroalkane bromides ( $\circ$ ).

different ways in which water molecules are packed around each organic ion of different size and shape, and (c) difference in hydrophobic effect (solvent structural effect). Clearly, accurate quantitative separation of these factors will be impossible on the basis of thermodynamic data only. Still, it is of interest to consider some relevant points in detail.

First, one may question whether the azoniaspiroalkane ions are really inflexible, though their flexibility is definitely much less than the corresponding tetraalkylammonium ions. We will assume that the volume changes due to the ring flexibility are indeed negligible for our case. Second,  $\phi_v^0$  per  $\text{CH}_2$  group in the 4.4 ion may be different from that in the 6.6 ion due to the different size of these ions around which water molecules have to pack. From our data, we obtain  $\phi_v^0$  to be  $13.8 \text{ ml mol}^{-1}$  of  $\text{CH}_2$  group in going from the 4.4 ion to the 5.5 ion as well as in going from the 5.5 ion to the 6.6 ion. Cabani et al.<sup>3</sup> investigated homologous series of imines and their hydrochlorides in water and reported values of  $13.7$  to  $15.1 \text{ ml mol}^{-1}$  of  $\text{CH}_2$  for two to seven carbon atoms. In the studies of cycloalkylamine hydrobromides in water, Jolicoeur et al.<sup>2</sup> found that the methylene group contribution to  $\phi_v^0$  depended markedly on the ring size. Seven- or eight-membered rings show a minimum value of  $\phi_v^0(\text{CH}_2)$  whereas a five-membered ring gives a maximum value, the difference between extremes as large as  $1.6 \text{ ml mol}^{-1}$ . The latter results indicate that the geometrical aspects of the solvation involve both the structure in the solvent and the shape of the hydrophobic solute.

For the clarity of the subject matter to be discussed below, we must choose one of the following viewpoints: (i) the slopes of the " $\phi_v^0$  vs. number of carbon atoms" lines (Figure 3) observed with salts having loops of methylene groups are "normal" or "regular" and the larger slopes found with the corresponding salts with  $n$ -alkyl chains are ascribed to the flexibility of the linear chains; or (ii) the slopes of the salt homologs with alkyl chains are considered "regular" and the smaller slopes found with salts with

TABLE III: Comparison of Observed Apparent Molal Ionic Volumes of Tetraalkylammonium Ions with Volumes Estimated from Addition of Group Values

	$\phi_v^0(\text{obsd})^a$ $\text{ml mol}^{-1}$	$\phi_v^0(\text{calcd})^b$	
		$\phi_v^0(\text{N}^+) + n\phi_v^0(\text{CH}_2) + 4\phi_v^0(\text{CH}_3)$	$\phi_v^0(\text{obsd}) - \phi_v^0(\text{calcd})$
$\text{Me}_4\text{N}^+$	84.14	(84.14)	(0)
$\text{Et}_4\text{N}^+$	143.53	139.34	4.19
$\text{Pr}_4\text{N}^+$	209.15	194.54	14.61
$\text{Bu}_4\text{N}^+$	270.38	249.74	20.64
$\text{Pe}_4\text{N}^+$	333.69	304.94	28.75

<sup>a</sup> These values are obtained from ref 14 with an assumption of  $\phi_v^0(\text{Br}^-) = 30.21 \text{ ml mol}^{-1}$ . <sup>b</sup> These numbers are obtained on the assumption of the following group values:  $\phi_v^0(\text{CH}_2) = 13.8$ ,  $\phi_v^0(\text{N}^+) = 11.7$ , and  $\phi_v^0(\text{CH}_3) = 18.11 \text{ ml mol}^{-1}$ . Note: The value of  $\phi_v^0(\text{CH}_2)$  is taken from the azoniaspiroalkane ions given in Table II; the value of  $\phi_v^0(\text{N}^+)$  is obtained from the 4.4, 5.5, and 6.6 ions using the additivity assumption; the value of  $\phi_v^0(\text{CH}_3)$  is obtained from the observed value of  $\phi_v^0$  for the  $\text{Me}_4\text{N}^+$  ion and the value of  $\phi_v^0(\text{N}^+)$ .

loops are ascribed to the loss of hydrophobic hydration and/or packing effects.

Since all three effects discussed above may contribute to the differences between the properties of linear and cyclic compounds, there is little ground for deciding upon a particular reference point. At present, it seems that the simplest approach is to consider that the rigid, bulky azoniaspiroalkane ions will exhibit more "regular solution" behavior than ions containing  $n$ -alkyl groups and which readily form clathrates.<sup>4</sup> The enthalpy of dilution data reported in paper I is in favor of this approach. With this viewpoint, and under some further assumptions given below, one can obtain some quantitative estimate of the effect of alkyl chain flexibility in the homologous  $n$ - $\text{R}_4\text{N}^+$  ions.

The data in Table III designated as  $\phi_v(\text{calcd})$  are obtained with the assumptions of  $\phi_v^0(\text{CH}_2) = 13.8$ ,  $\phi_v^0(\text{N}^+) = 11.7$ , and  $\phi_v^0(\text{CH}_3) = 18.11 \text{ ml mol}^{-1}$ . (See footnote in Table III for how these values were obtained.) Thus, the values of  $\phi_v^0(\text{calcd})$  are sums of respective group values based on  $84.14 \text{ ml mol}^{-1}$  of  $\text{Me}_4\text{N}^+$  ion.<sup>14</sup> The quantity,  $\phi_v(\text{obsd}) - \phi_v(\text{calcd})$ , listed as the last column in Table III, will reflect, at least in part, the effect of alkyl chain flexibility in the  $n$ - $\text{R}_4\text{N}^+$  ions as compared to the bicyclic ions. This quantity is seen to increase with alkyl chain length as would be expected if chain configurational effects are involved.

B. *Apparent Molal Heat Capacities.* The values of  $\phi_{cp}^0$  are plotted against the number of carbon atoms in Figure 4 for four different types of salts: azoniaspiroalkane bromides, tetraalkylammonium bromides,<sup>10</sup> alkylamine hydrobromides,<sup>15</sup> and cycloalkylamine hydrobromides.<sup>2</sup> Data points fall on four lines, some of them distinctly curved. The line for cycloalkylamine hydrobromides crosses the curve of  $\text{R}_4\text{NBr}$  at  $\text{C}_{10}$  (ion with ten carbon atoms), while the curve for azoniaspiroalkane bromides remains to be the lowest of the four without crossing others. The low values of  $\phi_{cp}^0$  for azoniaspiroalkane ions with two rings are clearly seen from the plots. As shown in Table IV, the values of  $\phi_{cp}^0$  per  $\text{CH}_2$  group is smaller for the spiro ions than for the corresponding  $\text{R}_4\text{N}^+$  ions. The difference of  $\phi_{cp}^0$  between the  $\text{Pr}_4\text{N}^+$  ion and the 6.6 ion is about  $24.2 \text{ cal K}^{-1} \text{ mol}^{-1}$  greater than the corresponding difference between the  $\text{Et}_4\text{N}^+$  ion and the 4.4 ion. This difference can be partly ascribed to the extra large heat capacity of water around the

TABLE IV: Comparison of Apparent Molal Heat Capacities of Azoniaspiroalkane Bromides with Those of Tetraalkylammonium Bromides in Water at 25 °C

	$\phi_{cp}^0,^a$ cal K <sup>-1</sup> mol <sup>-1</sup>	$\Delta\phi_{cp}^0$ per CH <sub>2</sub>	$B_{cp}$		$\phi_{cp}^0,^b$ cal K <sup>-1</sup> mol <sup>-1</sup>	$\Delta\phi_{cp}^0$ per CH <sub>2</sub>	$B_{cp}^b$
4.4 Br	63.4		-1.99	Me <sub>4</sub> NBr	26.05		4.71
		14.1				16.67	
5.5 Br	91.5		-4.78	Et <sub>4</sub> NBr	92.73		-3.01
		21.6				23.99	
6.6 Br	134.6		-11.6	Pr <sub>4</sub> NBr	188.67		-7.39
				Bu <sub>4</sub> NBr	289.10	25.11	-10.52

<sup>a</sup> Errors of  $\phi_{cp}^0$  are about  $\pm 0.5$  cal K<sup>-1</sup> mol<sup>-1</sup>. <sup>b</sup> P. R. Philip and J. E. Desnoyers, *J. Solution Chem.*, **1**, 353 (1972).

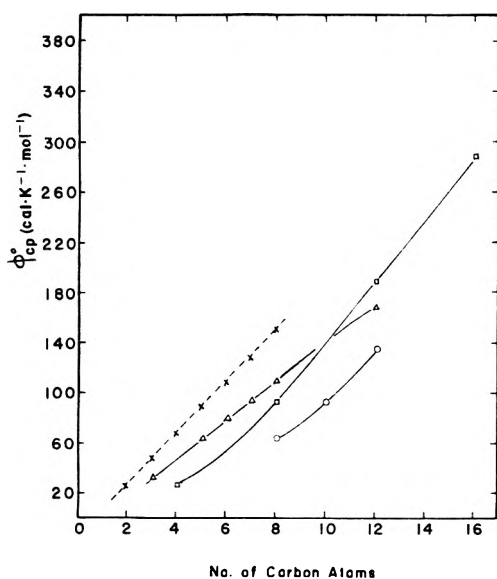


Figure 4. Plot of apparent molal heat capacity at infinite dilution against the number of carbon atoms for different types of salts: tetraalkylammonium bromides (□), alkylamine hydrobromides (×), cycloalkylamine hydrobromides (Δ), and azoniaspiroalkane bromides (○).

terminal methyl groups of the Pr<sub>4</sub>N<sup>+</sup> ion when compared to that of water around the terminal methyl groups of the Et<sub>4</sub>N<sup>+</sup> ion.

In their studies Jolicoeur et al.<sup>2</sup> found that the values of  $\phi_{cp}^0(\text{CH}_2)$  for the homologous series of cycloalkylamine hydrobromides (C<sub>3</sub> to C<sub>12</sub>) fall in a range of 13.5–17.3 cal K<sup>-1</sup> mol<sup>-1</sup>. In contrast,  $\phi_{cp}^0(\text{CH}_2)$  for R<sub>4</sub>N<sup>+</sup> ions (C<sub>4</sub> to C<sub>16</sub>) are 16.7–25.1 cal K<sup>-1</sup> mol<sup>-1</sup>. Our values of  $\phi_{cp}^0(\text{CH}_2)$  are 14.8 and 21.1 cal K<sup>-1</sup> mol<sup>-1</sup> in going from 4.4 Br to 5.5 Br, and from 5.5 Br to 6.6 Br, respectively. Inasmuch as the intrinsic heat capacity of the CH<sub>2</sub> group is about 6–8 cal K<sup>-1</sup> mol<sup>-1</sup>,<sup>17</sup> the data show that the heat capacity of water around the 6.6 ion is considerably less than that around the Pr<sub>4</sub>N<sup>+</sup> ion, but noticeably greater than that around the 4.4 and 5.5 ions.

We have also made some measurements of the apparent molal heat capacities of 5.5 Br and 6.6 Br in D<sub>2</sub>O at 25 °C. Though the number of measurements are few and the results less accurate than those in H<sub>2</sub>O, they are probably good enough to indicate the sign of the heat capacity of transfer. The quantity,  $\phi_{cp}^0(\text{D}_2\text{O}) - \phi_{cp}^0(\text{H}_2\text{O})$ , is about -1 cal K<sup>-1</sup> mol<sup>-1</sup> for 5.5 Br and +1 cal K<sup>-1</sup> mol<sup>-1</sup> for 6.6 Br. The corresponding values are -1.91 cal K<sup>-1</sup> mol<sup>-1</sup> for Et<sub>4</sub>NBr and +6.36 cal K<sup>-1</sup> mol<sup>-1</sup> for Pr<sub>4</sub>NBr. If we use the sign of the above quantity as a criterion for classifying the the water-structure effect, 5.5 Br will be a weak structure

breaker, while 6.6 Br will be a weak structure promoter. As discussed in paper I, this criterion may not be always reliable and requires further investigations.<sup>18,19</sup>

In paper I a comparison of the enthalpies of transfer,  $\Delta\bar{H}_{tr}$ , from H<sub>2</sub>O to D<sub>2</sub>O for various bromides was made. The values of  $\Delta\bar{H}_{tr}$  for the three azoniaspiroalkane bromides were found to fall between those of Me<sub>4</sub>NBr and Et<sub>4</sub>NBr rather than those between Et<sub>4</sub>NBr and Pr<sub>4</sub>NBr. Thus, the heat capacities of transfer and the enthalpies of transfer for the azoniaspiroalkane salts and for the tetraalkylammonium salts exhibit the same general trends though with some differences in their relative numerical values.

In conclusion, forming closed loops from the alkyl chains in tetraalkylammonium ions has a great effect upon the thermodynamic properties, particularly those which have been regarded as characteristic of aqueous tetraalkylammonium salts. The effects usually associated with the hydration of hydrophobic solutes is considerably reduced for the spiro ions, presumably due to their "wrong shape", absence of terminal methyl groups, and lack of flexible alkyl chains.

*Acknowledgments.* It is the pleasure of W.W. and A.L. to acknowledge the financial support of the National Science Foundation. C.J. and J.B. wish to thank the National Research Council of Canada for financial assistance and for the award of a fellowship to J.B.

## References and Notes

- (1) D. P. Wilson and W.-Y. Wen, *J. Phys. Chem.*, **79**, 1527 (1975).
- (2) C. Jolicoeur, J. Boileau, S. Bazinet, and P. Picker, *Can. J. Chem.*, **53**, 716 (1975).
- (3) S. Cabani, G. Conti, and L. Lepori, *J. Phys. Chem.*, **76**, 1338, 1343 (1972); **78** 1030 (1974).
- (4) W.-Y. Wen, "Aqueous Solutions of Symmetrical Tetraalkylammonium Salts", in "Water and Aqueous Solutions", R. A. Horne, Ed., Wiley, New York, N.Y., 1972, Chapter 15, pp 613–661.
- (5) E. F. Blicke and E. B. Hotelling, *J. Am. Chem. Soc.*, **76**, 5099 (1954).
- (6) J. Thomas, *J. Med. Pharm. Chem.*, **3**, 45 (1961).
- (7) B. D. Roufogalis and J. Thomas, *J. Pharm. Pharmacol.*, **20**, 153 (1968).
- (8) P. Picker, E. Tremblay, and C. Jolicoeur, *J. Solution Chem.*, **3**, 377 (1974).
- (9) P. Picker, P. A. Leduc, P. R. Philip, and J. E. Desnoyers, *J. Chem. Thermodyn.*, **3**, 631 (1971).
- (10) P. R. Philip and J. E. Desnoyers, *J. Solution Chem.*, **1**, 353 (1972).
- (11) G. S. Kell, *J. Chem. Eng. Data*, **12**, 66 (1967).
- (12) A. Eucken and M. Eigen, *Z. Elektrochem.*, **55**, 343 (1951).
- (13) This value is based on the conventional partial molal volumes of 24.71 cc mol<sup>-1</sup> for Br<sup>-</sup> [L. A. Dunn, *Trans. Faraday Soc.*, **64**, 2951 (1968)] and the ionic partial molal volume of -5.5 cc mol<sup>-1</sup> for H<sup>+</sup> reported by R. Zana and E. Yeager, *J. Phys. Chem.*, **70**, 954 (1966); **71**, 4241 (1967).
- (14) G. Perron and J. E. Desnoyers, *J. Chem. Eng. Data*, **17**, 136 (1972).
- (15) P. A. Leduc, J. L. Fortier, and J. E. Desnoyers, *J. Phys. Chem.*, **78**, 1217 (1974).
- (16) B. M. Lowe and H. M. Rendall, *Trans. Faraday Soc.*, **67**, 2318 (1971).
- (17) The estimate is made on the basis of data in "Addendum" of ref 2, in which the authors reported the heat capacities of pure cycloalkanes: c-pentane, c-hexane, c-heptane, and c-octane.
- (18) J. A. Burns and R. E. Verrill, *J. Solution Chem.*, **2**, 489 (1973).
- (19) P. R. Philip and C. Jolicoeur, *J. Solution Chem.*, **4**, 105 (1975).

## Infrared Spectra of Ammonia Adsorbed on Zinc Oxide

Tetsuo Morimoto,\* Hiromi Yanai, and Mahiko Nagao

Department of Chemistry, Faculty of Science, Okayama University, Okayama 700, Japan (Received September 5, 1975)

Infrared spectroscopic measurements were carried out on  $\text{NH}_3$  and  $\text{ND}_3$  molecules adsorbed on dehydroxylated and hydroxylated surfaces of ZnO in order to investigate the adsorbed state of ammonia molecules. It has been found that ammonia molecules are chemisorbed on dehydroxylated surfaces of ZnO in two ways, i.e., through dissociative adsorption and coordinately bonded molecules. Hydrogen bonding is also formed between ammonia molecules and surface hydroxyl groups, while on fully hydroxylated surfaces on ZnO the formation of ammonium ions was confirmed. Furthermore, the exchange reaction of chemisorbed  $\text{NH}_3$  with water vapor occurs on the ammoniated surface of ZnO to form ammonia vapor and surface hydroxyl groups.

### Introduction

The adsorption of  $\text{NH}_3$  on metal oxides is important in connection with the acid properties of solid surfaces. The differences between the infrared adsorption spectrum of coordinated  $\text{NH}_3$  molecules and that of ammonium ions has often been employed to differentiate Lewis acid sites from Brønsted acid sites on acid catalysts and related compounds such as silica, alumina, and silica-alumina.<sup>1-10</sup>

It has been found that  $\text{NH}_3$  can be physisorbed and chemisorbed on metal oxides through the coordination of the lone pair electrons in nitrogen atoms to surface metal atoms, the dissociative adsorption of  $\text{NH}_3$  molecules to form an equal number of hydroxyl groups and amide ions,<sup>6,8,10</sup> the formation of ammonium ions, and hydrogen bonding with surface hydroxyl groups. According to Blyholder et al.,<sup>11</sup> chemisorbed  $\text{NH}_3$  does not behave as the sites for physisorption of  $\text{NH}_3$  molecules.

According to the papers cited above, on surfaces treated at elevated temperatures  $\text{NH}_3$  molecules form coordination compounds with surface metal atoms, while on surfaces treated at relatively lower temperatures they undergo hydrogen bonding or bond to ammonium ions because of the presence of surface hydroxyl groups of physisorbed  $\text{H}_2\text{O}$ . It will therefore be interesting to investigate the adsorption of ammonia in relation with that of water.

In the present work, an attempt was made to measure the infrared spectra of ammonia adsorbed on ZnO surfaces on which the amount of chemisorbed  $\text{H}_2\text{O}$  was controlled, and to investigate the adsorbed state of ammonia on ZnO surfaces.

### Experimental Section

**Materials.** The ZnO sample used in this work was Kadox 15, prepared by the New Jersey Zinc Co. The specific surface area of the sample treated at 450 °C, which was obtained by the BET method using nitrogen adsorption, was found to be 8.40 m<sup>2</sup>/g. For measurements of infrared spectra, a self-supporting disk of the ZnO sample of about 100 mg and 20 mm in diameter was prepared by compressing under a pressure of 400 kg/cm<sup>2</sup>.

Two kinds of water vapor,  $\text{H}_2\text{O}$  and  $\text{D}_2\text{O}$ , used as adsorbates were purified by repeated bulb-to-bulb distillation in vacuo.  $\text{NH}_3$  vapor was supplied by evaporation from liquid  $\text{NH}_3$  (99.99%) into vacuum, and purified by repeating the vaporization into vacuum and condensation in a trap

cooled at dry ice-ethanol temperature. Another kind of ammonia,  $\text{ND}_3$ , made by Merck Co., was evaporated from 20% solution in  $\text{D}_2\text{O}$  into vacuum, from which the  $\text{D}_2\text{O}$  vapor was removed by repeated evaporation-condensation cycles in the same way as stated above.

**Apparatus.** An in situ cell equipped with sodium chloride windows, which withstands heat treatment at elevated temperatures in vacuo, was used for the measurement of spectra, as described in the previous paper.<sup>12</sup> An infrared spectrophotometer, Type IR-G, manufactured by Nippon Bunko Co., was used for the present work.

**Pretreatment of Sample.** A sample disk was degassed in the in situ cell at 450 °C for 2 h under a vacuum of 10<sup>-5</sup> Torr. After this treatment, the color of the sample disk changed to gray, and the transmittance for infrared beam decreased remarkably. However, this could be overcome by treating the sample in an oxygen atmosphere:<sup>13-15</sup> after degassing the sample at 450 °C dried oxygen of 50 Torr was introduced in the system and kept for 30 min at the same temperature. The system was then evacuated and a second introduction of oxygen was performed in order to ensure complete oxidation. The system was cooled to room temperature, and evacuated for 2 h at the same temperature, which produced a white sample having the original transmittance of the infrared beam.

### Results and Discussion

**Adsorption of  $\text{H}_2\text{O}$  and  $\text{D}_2\text{O}$  on the ZnO Surface.** The ZnO sample degassed at 450 °C was exposed to  $\text{H}_2\text{O}$  or  $\text{D}_2\text{O}$  vapor of 20 Torr at 30 °C for 14 h, then it was degassed at various temperatures, and the desorbability of adsorbed water was observed by infrared spectroscopy. The results obtained are shown in Figures 1 and 2. Just after adsorption of  $\text{H}_2\text{O}$ , the absorption bands appear at 3640, 3575, 3530, and 3440 cm<sup>-1</sup>, which can be assigned to the OH stretching vibration; the intensity of the latter two peaks decreases with heat treatment at increasingly elevated temperatures, and they disappear after the treatment at 300 °C, whereas the former two remain even after the treatment at 450 °C in vacuo. In the case of adsorption of  $\text{D}_2\text{O}$  (Figure 2), four bands are observed at 2675, 2616, 2580, and 2530 cm<sup>-1</sup>, which have a factor approximate to  $1/\sqrt{2}$  compared to the wavenumbers of the corresponding bands due to the OH stretching, being identified as OD stretching vibrations. The variation of these bands due to heat treatment is quite similar to that of OH bands. The 450 °C

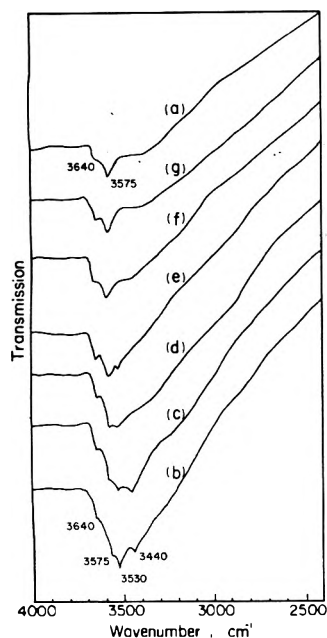


**Figure 1.** Infrared spectra of  $\text{H}_2\text{O}$  adsorbed on ZnO: (a) background spectrum obtained after pretreatment at  $450^\circ\text{C}$ ; (b) after  $\text{H}_2\text{O}$  adsorption at 20 Torr for 14 h; spectra were recorded successively after degassing at (c) 30, (d) 100, (e) 200, (f) 300, and (g)  $400^\circ\text{C}$ .

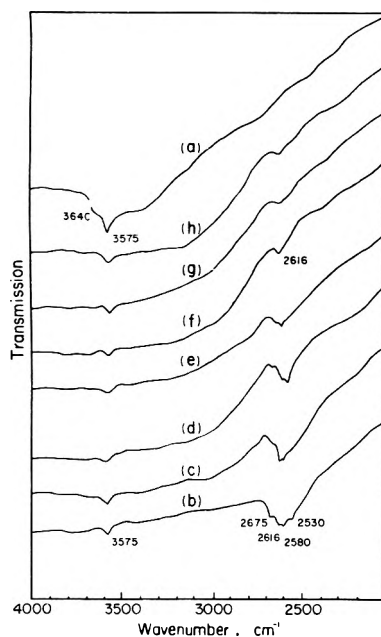


**Figure 2.** Infrared spectra of  $\text{D}_2\text{O}$  adsorbed on ZnO: (a) background spectrum obtained after pretreatment at  $450^\circ\text{C}$ ; (b) after  $\text{D}_2\text{O}$  adsorption at 20 Torr for 14 h; spectra were recorded successively after degassing at (c) 30, (d) 100, (e) 200, (f) 300, (g) 400, and (h)  $450^\circ\text{C}$ .

treatment of the deuterioxyated ZnO in vacuo leaves the band at  $2616\text{ cm}^{-1}$ , suggesting the presence of strongly chemisorbed water. The bending vibration of adsorbed  $\text{H}_2\text{O}$  gives rise to a band at  $1650\text{ cm}^{-1}$ , but it disappears after evacuation at  $30^\circ\text{C}$ , in agreement with the results previously obtained on the desorbability of physisorbed water,<sup>16-18</sup> while the physisorption of  $\text{D}_2\text{O}$  on ZnO does not display the bending mode in the infrared spectra, because the wavenumber overlaps the bulk vibration of ZnO.

In studies of infrared spectroscopy of surface hydroxyls on ZnO surfaces, Atherton et al.<sup>14</sup> discovered five bands in the OH stretching region, Dent and Kokes<sup>19</sup> reported three bands, and Tsyganenko and Filimonov<sup>20</sup> described two bands at  $3675$  and  $3622\text{ cm}^{-1}$ . The present results are almost the same as those of Atherton et al., except for the fact that the band at  $3670\text{ cm}^{-1}$  has not been found in the present work. Absorption bands at  $3640$  and  $3575\text{ cm}^{-1}$  which survive after evacuation of the sample at  $450^\circ\text{C}$  (Figure 1) are probably due to isolated hydroxyls. Of the two, the band at  $3575\text{ cm}^{-1}$  becomes smaller but sharper with increasing treatment temperature, remaining unexchanged in small amount even after the exchange procedure with  $\text{D}_2\text{O}$ , which suggests that a small amount of hydroxyls may exist in the ZnO crystal. The corresponding OD band at  $2616\text{ cm}^{-1}$  also behaves similarly (Figure 2). Atherton et al.<sup>14</sup> have found an absorption band at  $3620\text{ cm}^{-1}$  persisting after treatment at elevated temperatures, which is slightly higher in wavenumber than  $3575\text{ cm}^{-1}$  band in the present work. From crystallographic considerations it is reasonable to infer that the isolated OH groups are able to exist on the (0001) and (000 $\bar{1}$ ) planes of ZnO crystals. On the other hand, relatively broad peaks of lower wavenumbers,  $3530$  and  $3440\text{ cm}^{-1}$ , which are extinguished by degassing at  $300^\circ\text{C}$  may be due to surface hydroxyls which are able to hydrogen bond to each other on the (10 $\bar{1}$ 0) planes, as discussed in the preceding paper.<sup>21</sup>

*Adsorption of  $\text{NH}_3$  and  $\text{ND}_3$  on the Dehydroxylated ZnO Surface.* The ZnO sample treated at  $450^\circ\text{C}$  in vacuo was kept in  $\text{NH}_3$  or  $\text{ND}_3$  for a given interval of time at  $30^\circ\text{C}$ , and infrared spectra were measured at  $30^\circ\text{C}$  after degassing at elevated temperatures. The results obtained are illustrated in Figures 3 and 4. In every measurement, absorption bands at  $3640$  and  $3575\text{ cm}^{-1}$  due to the tenaciously bound hydroxyls are observed to be similar to the cases of Figures 1 and 2.

The normal vibrations of gaseous  $\text{NH}_3$  are known to be  $3414$  ( $\nu_3$ ),  $3338$ ,  $3336$  ( $\nu_1$ ),  $1628$  ( $\nu_4$ ), and  $968$ ,  $932$  ( $\nu_2$ ).<sup>22</sup> A number of works have been devoted to the assignment of the absorption bands of  $\text{NH}_3$  adsorbed on metal oxides.<sup>1-10</sup> It has been thus far confirmed that the adsorption bands of  $\text{NH}_3$  molecules coordinated to metal atoms on solid surfaces appear in two ranges,  $3330$ – $3380\text{ cm}^{-1}$  due to asymmetric stretching vibration and  $3260$ – $3280\text{ cm}^{-1}$  due to symmetric. On the other hand, the  $\text{NH}_3$  hydrogen bonded to surface hydroxyls gives absorption peaks near  $3400$  and  $3320\text{ cm}^{-1}$  due to NH stretching vibrations. When ammonium ions are formed on the surfaces of metal oxides, the absorption band due to the NH stretching appears near  $3200\text{ cm}^{-1}$ , and the one due to the asymmetric bending vibration  $\nu_4$  near  $1400$ – $1470\text{ cm}^{-1}$ , but that due to symmetric  $\nu_2$  is usually not observed because of the overlapping with the absorption of the solid samples themselves. In addition, it has been also described that the simultaneous formation of amide ions and hydroxyls takes place by the dissociative adsorption of  $\text{NH}_3$ ,<sup>6,8,10</sup> and that  $\text{NH}_3$  hydrogen bonded to surface oxide ions gives a broad absorption peak near  $3100\text{ cm}^{-1}$ .<sup>23</sup>

As is seen in Figure 3, the infrared spectra of  $\text{NH}_3$  adsorbed on the ZnO surface represent two pairs of bands at  $3400$  and  $3320\text{ cm}^{-1}$  as well as at  $3350$  and  $3275\text{ cm}^{-1}$ . According to the authors cited above, the former pair can be assigned to the stretching NH vibration of  $\text{NH}_3$  hydrogen bonded to surface hydroxyls remaining on the  $450^\circ\text{C}$  treated sample. The following facts will also substantiate this

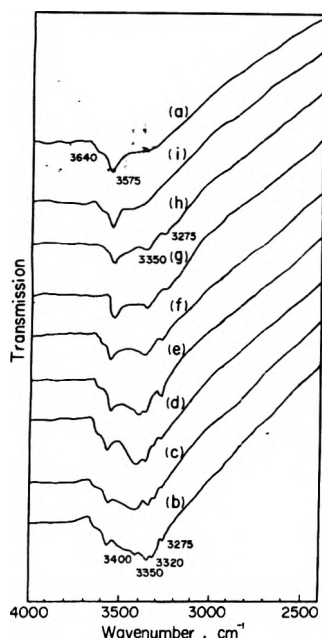


**Figure 3.** Infrared spectra of  $\text{NH}_3$  adsorbed on ZnO: (a) background spectrum obtained after pretreatment at  $450^\circ\text{C}$ ; (b) after  $\text{NH}_3$  adsorption at 20 Torr for 8 h; spectra were recorded successively after degassing at (c) 30, (d) 70, (e) 100, (f) 150, (g) 200, (h) 250, and (i)  $300^\circ\text{C}$ .

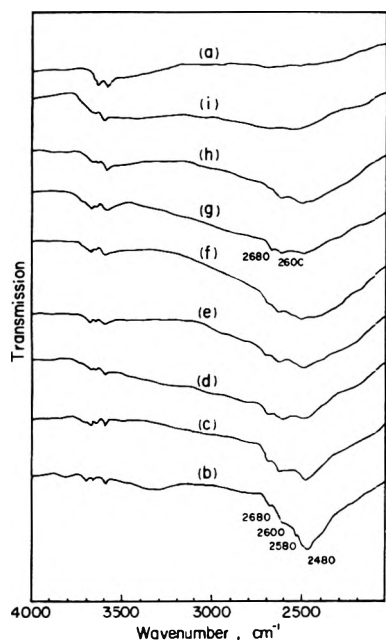


**Figure 4.** Infrared spectra of  $\text{ND}_3$  adsorbed on ZnO: (a) background spectrum obtained after pretreatment at  $600^\circ\text{C}$ ; (b) after  $\text{ND}_3$  adsorption at 20 Torr for 8 h; spectra were recorded successively after degassing at (c) 30, (d) 70, (e) 100, (f) 150, (g) 200, (h) 250, and (i)  $300^\circ\text{C}$ .

conclusion. On adsorption of  $\text{NH}_3$  the intensity of absorption bands at  $3640$  and  $3575\text{ cm}^{-1}$  decreases and at the same time the peaks at  $3400$  and  $3320\text{ cm}^{-1}$  appear, while on degassing the system at higher temperatures absorption bands due to the OH stretching vibration recover the original intensity (Figure 3). On the other hand, the latter pair of absorption bands,  $3350$  and  $3275\text{ cm}^{-1}$ , can be assigned to the asymmetric and symmetric NH stretching vibrations

in  $\text{NH}_3$  coordinated to surface metal atoms,<sup>1,2,5,8-10</sup> being accompanied by the bending vibration at  $1580\text{ cm}^{-1}$ . This set of absorption bands vanishes perfectly by evacuation at  $300^\circ\text{C}$ . The results obtained in Figures 1-3 show that the desorption of chemisorbed  $\text{NH}_3$  is accomplished at a lower temperature than that of chemisorbed  $\text{H}_2\text{O}$ , which indicates that  $\text{H}_2\text{O}$  molecules can be chemisorbed more strongly than  $\text{NH}_3$  molecules.

Here, it is interesting to consider whether the dissociative adsorption of ammonia can take place on the ZnO surfaces or not, since Peri,<sup>6</sup> Low et al.,<sup>8</sup> and Blomfield and Little<sup>10</sup> reported the dissociative adsorption of  $\text{NH}_3$  on metal oxides such as  $\gamma\text{-Al}_2\text{O}_3$  and porous glass. As stated above, a small part of surface hydroxyls remain even after the treatment of ZnO at  $450^\circ\text{C}$  (Figures 1-3), and the dissociative adsorption of one molecule of  $\text{NH}_3$  on the surface of metal oxides will produce a pair of hydroxyl and amide groups. In order to distinguish the newly formed hydroxyls by dissociation of  $\text{NH}_3$  from the original hydroxyls remaining on the surfaces, the adsorption of  $\text{ND}_3$  was carried out. The results obtained are given in Figure 4. In this experiment, the pretreatment temperature of the sample was raised to  $600^\circ\text{C}$ , which resulted in a remarkable decrease in the amount of the remaining surface hydroxyls and accordingly in the intensity of the absorption bands in the region  $3660\text{--}3575\text{ cm}^{-1}$ . In Figure 4, the absorption bands at  $2680$ ,  $2600$ ,  $2580$ , and  $2480\text{ cm}^{-1}$  are clearly observed; the former three can be assigned to the stretching OD bands in light of the results in Figure 2. The last one at  $2480\text{ cm}^{-1}$  agrees well with the absorption band assigned to the ND stretching vibration by Tench.<sup>24</sup> However, there are two possibilities that this ND stretching vibration may come from  $\text{ND}_3$  molecules coordinated to surface metal ions or from amide  $\text{ND}_2$  groups formed by the dissociative adsorption of  $\text{ND}_3$ . Since infrared absorption data on the ND stretching vibration in amide  $\text{ND}_2$  groups are very few, we have estimated their wavenumber by the following way. The ratios of wavenumbers of the normal vibrations  $\nu_3$ ,  $\nu_1$ , and  $\nu_4$  in gaseous  $\text{NH}_3$  to the corresponding ones in  $\text{ND}_3$  give an almost equal value 0.735 on the average. Assuming that this ratio is also valid to the vibrations in amide groups, we can calculate the wavenumbers of the ND stretching vibration in amide ( $\text{ND}_2$ ) to be  $2573$  and  $2499\text{ cm}^{-1}$  for  $\nu_3$  and  $\nu_1$ , respectively, by combining the experimental data on the wavenumbers  $3500$  and  $3400\text{ cm}^{-1}$  of the NH stretching vibration in free amide ( $\text{NH}_2$ ) and the above ratio.

On the other hand, it is known that the band of the NH stretching vibration in the  $\text{NH}_3$  molecules coordinately bonded to a solid surface usually shifts to a lower wavenumber by  $40\text{--}80\text{ cm}^{-1}$  from the normal vibration of gaseous  $\text{NH}_3$ , and appears in the ranges of  $3330\text{--}3380$  ( $\nu_3$ ) and  $3260\text{--}3280\text{ cm}^{-1}$  ( $\nu_1$ ).<sup>1-10</sup> Therefore, it may be reasonable to expect that the same tendency holds also in the case of the ND stretching vibration in coordinated  $\text{ND}_3$  molecules, giving the calculated wavenumbers of  $2470\text{--}2520$  and  $2345\text{--}2370\text{ cm}^{-1}$  for  $\nu_3$  and  $\nu_1$ , respectively.

The absorption peak at  $2480\text{ cm}^{-1}$  observed in Figure 4, therefore, may come from coordinated  $\text{ND}_3$  molecules and/or amide groups bonded to the surface. However, it is seen from Figure 4 that the degassing the  $\text{ND}_3$ -adsorbed sample at increasingly elevated temperatures results in the simultaneous decrease of the strength of the OD and ND stretching vibrations. Thus, simultaneous appearance and decrease of both OD and ND stretching vibrations make it possible to infer that the dissociative reaction of  $\text{ND}_3$  mole-

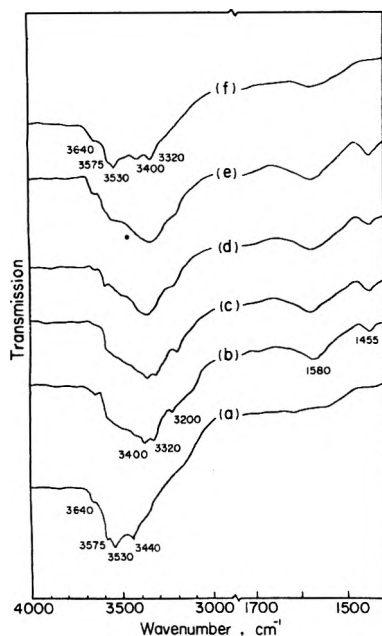


**Figure 5.** Infrared spectra of  $\text{NH}_3$  adsorbed on hydroxylated surface of ZnO: (a) spectrum of hydroxylated ZnO; spectra were recorded successively on exposing to  $\text{NH}_3$  at 20 Torr for (b) 1, (c) 2, (d) 4, (e) 10 h; then (f) after degassing at 30 °C for 4 h.

cules with surface oxide ions takes place to form OD and  $\text{ND}_2$  groups at the same time.

**Adsorption of  $\text{NH}_3$  on the Hydroxylated Surface of ZnO.** Figure 5 shows the infrared spectra of  $\text{NH}_3$  molecules adsorbed on the hydroxylated surface of ZnO. It is seen from Figure 5 that the bands observed between 3440 and 3640  $\text{cm}^{-1}$  on the fully hydroxylated surface of ZnO shift to 3300–3400  $\text{cm}^{-1}$  after the adsorption of  $\text{NH}_3$ , and at the same time the sharp peaks appear at 3200, 1580, and 1455  $\text{cm}^{-1}$ . The broad band at 3300–3400  $\text{cm}^{-1}$  will involve both the OH stretching vibration of surface hydroxyls bonded to  $\text{NH}_3$  molecules through hydrogen bonding and the NH stretching vibration of the adsorbed  $\text{NH}_3$  molecules. The absorption band at 1580  $\text{cm}^{-1}$  may be considered to be due to the bending vibration of  $\text{NH}_3$  molecules, because it is identical with that found in the coordinately bonded  $\text{NH}_3$  molecules. The intensity of this absorption band, however, decreases in parallel with the decrease of the broad band at 3300–3400  $\text{cm}^{-1}$  by degassing at room temperature and finally disappears after evacuation for 4 h, which suggests that the bending vibration is of the weakly adsorbed  $\text{NH}_3$  molecules.

The appearance of absorption bands at 3200 and 1455  $\text{cm}^{-1}$  implies the formation of  $\text{NH}_4^+$  ions on ZnO surfaces,<sup>1,3,7,9</sup> though they disappear after degassing at room temperature. The situation resembles the case of the adsorption of  $\text{NH}_3$  on the  $\alpha\text{-Fe}_2\text{O}_3$  surface, where  $\text{NH}_4^+$  ions are formed by the interaction of  $\text{NH}_3$  molecules with physisorbed  $\text{H}_2\text{O}$  on  $\alpha\text{-Fe}_2\text{O}_3$ .<sup>11</sup> The formation of  $\text{NH}_4^+$  ions has not been observed on the surface of the hydroxylated  $\text{MgO}$ ,<sup>24</sup> on which  $\text{NH}_3$  molecules could be adsorbed just through hydrogen bonding. On the contrary, the formation of  $\text{NH}_4^+$  ions has been well known on the surfaces of silica-alumina, which have Brønsted acid sites.<sup>1,3,7,9</sup> Our preliminary tests showed that the formation of  $\text{NH}_4^+$  ions was scarcely observed on ZnO surfaces on which the surface OH density was about one-half of that on fully hydroxylated surfaces.

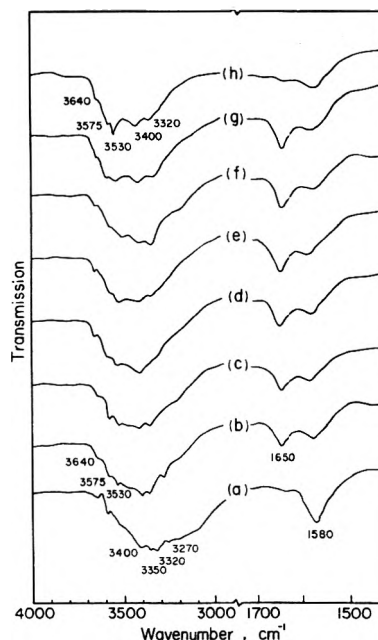


**Figure 6.** Infrared spectra of ammoniated surface of ZnO in the presence of  $\text{H}_2\text{O}$  vapor: (a) spectrum of ammoniated ZnO; spectra were recorded successively on exposing to  $\text{H}_2\text{O}$  at 20 Torr for (b) 1, (c) 2, (d) 3, (e) 4, (f) 5, (g) 14 h; then (h) after degassing at 30 °C for 4 h.

Quantitative studies on the physisorption of  $\text{NH}_3$  on ZnO have revealed that the amount of weakly adsorbed  $\text{NH}_3$  in the forms of  $\text{NH}_4^+$  ions and of hydrogen bonding is great.<sup>25</sup>

**Adsorption of  $\text{H}_2\text{O}$  on the Ammoniated Surface of ZnO.** On the ZnO sample treated at 450 °C in vacuo,  $\text{NH}_3$  was preadsorbed at 30 °C under a pressure of 20 Torr for 8 h, and then the sample was degassed at 30 °C, which left the strongly adsorbed  $\text{NH}_3$  on the surface. The sample thus treated was equilibrated with  $\text{H}_2\text{O}$  vapor, followed by the infrared spectroscopic investigation. The results obtained are illustrated in Figure 6. It is seen from Figure 6 that on exposing the surface to  $\text{H}_2\text{O}$  vapor of 20 Torr at 30 °C the intensity of absorption bands of 3400, 3350, 3320, and 3270  $\text{cm}^{-1}$ , which are assigned to the vibration modes of adsorbed  $\text{NH}_3$ , decreases with time, and at the same time the absorption bands at 3530–3640 and 1650  $\text{cm}^{-1}$  due to the OH stretching and bending vibrations of  $\text{H}_2\text{O}$  appear and gradually increase. Degassing the sample after exposing to  $\text{H}_2\text{O}$  vapor for 14 h results in a remarkable decrease in the intensity of the absorption bands, 3350 and 3270  $\text{cm}^{-1}$ , which originated in the chemisorption of  $\text{NH}_3$ , and instead the intensity of the absorption bands due to the OH stretching increases. The analysis of the equilibrated gas showed the presence of a quantity of  $\text{NH}_3$ .

These facts positively give the evidence that the exchange reaction occurred between  $\text{H}_2\text{O}$  vapor and ammoniated surfaces of ZnO to form  $\text{NH}_3$  vapor and hydroxylated surfaces. A more distinct result was obtained by the same experiment carried out with  $\text{D}_2\text{O}$  vapor and ammoniated surfaces of ZnO, because of the clear detection of OD stretching vibrations which appear at the range of wavenumbers apart from that of the  $\text{NH}_3$  stretching vibrations.

Similar dual adsorption experiments with  $\text{NH}_3$  and  $\text{H}_2\text{O}$  have been projected on  $\alpha\text{-Fe}_2\text{O}_3$ <sup>11</sup> and silica-alumina,<sup>9</sup> but the possibility of exchange reaction has not been detected.

Very recently, the exchange reaction between H<sub>2</sub>O vapor and chemisorbed CO<sub>2</sub> on ZnO has been reported.<sup>26,27</sup> Those and present results give clear evidence that the chemisorption energy of H<sub>2</sub>O is larger than that of CO<sub>2</sub> or NH<sub>3</sub>.

*Acknowledgment.* The authors wish to thank Mr. Munehiko Goto for his assistance in a part of the experiments.

### References and Notes

- (1) J. E. Mapes and R. P. Eischens, *J. Phys. Chem.*, **58**, 1059 (1954).
- (2) L. M. Roev, V. N. Fillimonov, and A. N. Terenin, *Opt. Spektrosk.*, **4**, 328 (1958).
- (3) D. E. Nicholson, *Nature (London)*, **186**, 630 (1960).
- (4) J. B. Peri and R. B. Hannan, *J. Phys. Chem.*, **64**, 1526 (1960).
- (5) N. W. Cant and L. H. Little, *Can. J. Chem.*, **42**, 802 (1964).
- (6) J. B. Peri, *J. Phys. Chem.*, **69**, 231 (1965).
- (7) J. J. Fripiat, A. Leonard, and J. B. Uytterhoeven, *J. Phys. Chem.*, **69**, 3274 (1965).
- (8) M. J. D. Low, N. Ramasubramanian, and V. V. Subba Rao, *J. Phys. Chem.*, **71**, 1726 (1967).
- (9) M. R. Basila and T. R. Kantner, *J. Phys. Chem.*, **71**, 467 (1967).
- (10) G. A. Blomfield and L. H. Little, *J. Catal.*, **21**, 149 (1971).
- (11) G. Blyholder and E. A. Richardson, *J. Phys. Chem.*, **66**, 2597 (1962).
- (12) T. Morimoto, J. Imai, and M. Nagao, *J. Phys. Chem.*, **78**, 704 (1974).
- (13) J. H. Taylor and C. H. Amberg, *Can. J. Chem.*, **39**, 535 (1961).
- (14) K. Atherton, G. Newbold, and J. A. Hockey, *Discuss. Faraday Soc.*, **52**, 33 (1971).
- (15) C. C. Chang, L. T. Dixon, and R. J. Kokes, *J. Phys. Chem.*, **77**, 2634 (1973).
- (16) T. Morimoto, M. Nagao, and F. Tokuda, *Bull. Chem. Soc. Jpn.*, **41**, 1533 (1968).
- (17) T. Morimoto and M. Nagao, *Bull. Chem. Soc. Jpn.*, **43**, 3746 (1970).
- (18) M. Nagao, *J. Phys. Chem.*, **75**, 3822 (1971).
- (19) A. L. Dent and R. J. Kokes, *J. Phys. Chem.*, **73**, 3781 (1969).
- (20) A. A. Tsyganenko and V. N. Filimonov, *Spectrosc. Lett.*, **5**, 477 (1972).
- (21) T. Morimoto and M. Nagao, *J. Phys. Chem.*, **78**, 1116 (1974).
- (22) K. Nakamoto, "Infrared Spectra of Inorganic and Coordinate Compounds", 2nd ed, Wiley-Interscience, New York, N.Y., 1970.
- (23) A. J. Tench and D. Giles, *J. Chem. Soc., Faraday Trans. 1*, **68**, 193 (1972).
- (24) A. J. Tench, *J. Chem. Soc., Faraday Trans. 1*, **68**, 197 (1972).
- (25) To be submitted for publication.
- (26) T. Morimoto and K. Morishige, *Bull. Chem. Soc. Jpn.*, **47**, 92 (1974).
- (27) T. Morimoto and K. Morishige, *J. Phys. Chem.*, **79**, 1573 (1975).

## Resonance Raman Spectra of Monolayers Adsorbed at the Interface between Carbon Tetrachloride and an Aqueous Solution of a Surfactant and a Dye

Tohru Takenaka\* and Taisuke Nakanaga

*Institute for Chemical Research, Kyoto University, Uji, Kyoto-Fu, 611, Japan (Received September 5, 1975)*

*Publication costs assisted by Kyoto University*

Resonance Raman spectra have been recorded of a monolayer adsorbed at the interface between carbon tetrachloride and an aqueous solution of cetyltrimethylammonium bromide (CTAB, a cationic surfactant) and methyl orange (MO, an anionic azo dye) by using a new method of total reflection of the exciting light at the interface. The adsorbed monolayer consisted of an interaction product of CTAB with MO, and the latter served as an absorber of the exciting light of an Ar<sup>+</sup> laser to give rise to the resonance Raman effect. The band frequencies of MO in the monolayer were slightly shifted from those in bulk aqueous solution toward those of solid MO, indicating that the MO molecules in the monolayer were in an environment similar to a crystal field. Theoretical consideration of the Raman scattering activity due to an evanescent wave in the total reflection has been made of uniaxially oriented molecules. From polarization measurements of the resonance Raman spectra, it was found that the long axes of the MO molecules were tilted in the monolayer with a large angle of 50–60° with the axis normal to the interface.

### Introduction

Oriented monolayers of surface-active agents adsorbed from solution at the interface between two phases, i.e., liquid-gas, liquid-liquid, or liquid-solid, are the basic concept in surface and colloid chemistry, and spectroscopic study of the adsorbed monolayers in situ has been a subject of much interest in this field. However, previous studies have been very limited in number. Tweet<sup>1,2</sup> has designed the *monolayer spectrometer* and obtained visible absorption spectra of monolayers at the air-water interface by means of the multiple reflection of a beam between two parallel mirrors through the interface. It is generally agreed, however, that visible and ultraviolet spectra are too simple in most cases to afford sufficient information on the complex structure of monolayers. The infrared spectrum may be informative, but it is very difficult to apply to studies of monolayers on

liquid substrates, because of an extremely small number of molecules in monolayers and of strong absorption of the substrates. These difficulties are expected to be overcome by the recently developed technique of resonance Raman spectra, in which enormous enhancement of Raman intensity is observed. In addition, there is the advantage of Raman spectroscopy with laser excitation that suitable methods are possible for irradiation of the exciting light upon monolayers at interfaces and for collection of the scattered Raman radiation.

In the present work, we succeeded in recording the resonance Raman spectra of monolayers adsorbed at the interface between carbon tetrachloride and an aqueous solution of cetyltrimethylammonium bromide (CTAB, a cationic surfactant) and methyl orange (MO, an anionic azo dye) using a new method of total reflection of the exciting light

at the interface. The reasons for the choice of CTAB and MO are as follows. First, a dilute aqueous solution of MO ( $2 \times 10^{-4}$  M) and CTAB ( $1 \times 10^{-5}$  M) has a strong electronic absorption band around 460 nm,<sup>3</sup> and gives rise to the resonance Raman effect for the exciting wavelengths of 488.0 and 514.5 nm of an Ar<sup>+</sup> laser.<sup>4</sup> The corresponding absorption band of *trans*-azobenzene has been assigned by Jaffé et al.<sup>5,6</sup> to the lowest  $\pi$ - $\pi^*$  transition with the transition moment parallel to the long axis of the molecule. Second, the interaction between long-chain alkyltrimethylammonium bromide and MO in dilute aqueous solutions has been studied by Hiskey and Downey,<sup>3</sup> who have pointed out the formation of a 1:1 interaction product due to two factors. One is a Coulombic interaction between the negatively charged sulfonic group on MO and the positive charge on the cationic surfactant, and the other is a van der Waals-London type of interaction between the hydrocarbon portions of these two molecules. Finally, it is found in the present work that the interaction product of CTAB with MO is adsorbed at the interface between carbon tetrachloride and the aqueous solution forming a monolayer.

It is noted also that the Raman radiation scattered from a monolayer by this total reflection method is due to an evanescent, nonpropagating wave and not due to a propagating wave as in the usual method. Theoretical consideration of the Raman scattering activity due to the evanescent wave has been made of uniaxially oriented molecules by reference to results about principal values of the derived polarizability obtained from measurements of the depolarization ratios of a bulk aqueous solution. From polarization measurements of resonance Raman spectra, the orientation of the MO molecules in the adsorbed monolayer was discussed.

## Experimental Section

**Materials.** A sample of MO was obtained from a commercial source and was recrystallized several times from water. That of CTAB was the guaranteed reagent and was used without further purification. Pure water was prepared by redistillation of distilled water which had been passed through an ion-exchange resin column.

**Measurements of Interfacial Tension.** The interfacial tension between carbon tetrachloride and an aqueous solution was measured by the Wilhelmy plate method using a Shimadzu Model ST-1 surface tensometer and a Teflon plate. Prior to the measurements, the interface was allowed to stand overnight, so that the adsorption equilibrium was established.

**Measurements of the Resonance Raman Spectra of Adsorbed Monolayers.** After some examinations, the total reflection method illustrated in Figure 1 was used. Carbon tetrachloride and a dilute aqueous solution of CTAB and MO were successively poured into a truncated pyramidal Raman cell (placed upsidedown) which was made of glass or acrylic acid resin. A horizontally propagating laser beam was incident upon the lower part of the cell, inside of which carbon tetrachloride was placed. After the refraction at an inclined optical window of the cell, the laser beam approached the interface between carbon tetrachloride and the aqueous solution through the former with a large incidence angle. Since the refractive index of carbon tetrachloride (1.46) is higher than that of the aqueous solution (1.34), the beam was totally reflected at the interface and followed by the refraction at the exit window of the cell. The beam thus emerging from the cell was reflected by a

concave mirror (a laser booster) back through the identical pass with the forward propagation. This was useful to increase the energy of the sample excitation. Both the forward and backward beams were focused upon the interface. The scattered Raman radiation due to the evanescent wave in the total reflection was collected by a condenser lens in a direction perpendicular to the plane of incidence of the exciting light and was led to the monochromator. Another concave mirror (a Raman booster) was provided behind the cell to enable the revival of the Raman radiation scattered backward. This total reflection method has advantages that the optical system is quite simple, and that the polarization measurements of Raman spectra are possible as shown later. We now define the space-fixed axes  $X$ ,  $Y$ , and  $Z$  as shown in Figure 1.

Apparently, the angle of incidence of the exciting light at the interface is determined by the angle of inclination of the cell window, and it was designed to form the angle of incidence  $84^\circ$ , while the critical angle is  $66.6^\circ$ . In this case, the penetration depth of the evanescent wave in the aqueous solution was calculated to be  $1390 \text{ \AA}$  for the exciting 488.0-nm light of the Ar<sup>+</sup> laser.<sup>7</sup>

The Raman spectra were recorded on a Japan Electron Optics Laboratory Model JRS-S1 laser Raman spectrophotometer with a Spectra-Physics Model 164 Ar<sup>+</sup> laser (4 W). The spectral slitwidth was 12 and  $14 \text{ cm}^{-1}$  for the 514.5- and 488.0-nm excitations, respectively. The output power of the exciting light was kept to be less than 100 mW to protect the interface from thermal agitation.

The resonance Raman spectra of a bulk solution were obtained using a 1-mm capillary tube.

## Results and Discussion

**Formation of a Monolayer at the Interface.** In Figure 2, the interfacial tension between carbon tetrachloride and aqueous solutions of CTAB and MO is plotted as a function of the logarithm of the concentration of MO in a  $1 \times 10^{-5}$  M CTAB solution. It shows a typical interfacial tension-logarithm concentration curve of surfactants, suggesting that the interaction product has surface activity and is adsorbed at the interface. By the use of the Gibbs adsorption isotherm, the surface excess of the interaction product is calculated to be  $1.9 \times 10^{-10} \text{ mol/cm}^2$  from the descending slope of the linear part of the curve. This means that one interaction product occupies a surface area of  $89 \text{ \AA}^2$ . The same experiments for interfaces between carbon tetrachloride and aqueous solutions of CTAB alone yielded a value of  $43 \text{ \AA}^2$  as the corresponding area for the CTAB molecule, indicating that the contribution of the MO molecule to the surface area occupied by one interaction product is  $46 \text{ \AA}^2$ . Since this value is reasonable as the area of the MO molecule, it may be concluded that the adsorbed interaction products form the monolayer at the interface between carbon tetrachloride and the aqueous solution.

**Resonance Raman Spectra of MO in Bulk Solution and in a Monolayer.** Resonance Raman spectra of the bulk aqueous solution of MO ( $2 \times 10^{-4}$  M) and CTAB ( $1 \times 10^{-5}$  M) are shown in Figure 3A, where  $I_{\parallel}$  and  $I_{\perp}$  denote the intensities of Raman radiations with the electric vectors parallel and perpendicular to that of the exciting light, respectively. The Raman bands of MO in aqueous solutions have been studied by Hacker,<sup>8</sup> Carey et al.,<sup>9</sup> and Machida et al.,<sup>10</sup> and the frequencies are summarized in Table I together with their assignments. It is found from Figure 3A that all of the observed bands give approximately the same



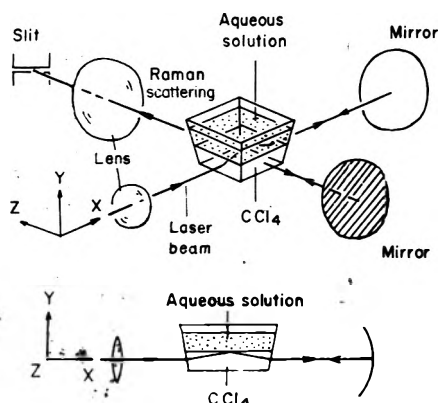


Figure 1. Total reflection method for Raman measurements of monolayers adsorbed at the interface between carbon tetrachloride and aqueous solutions.

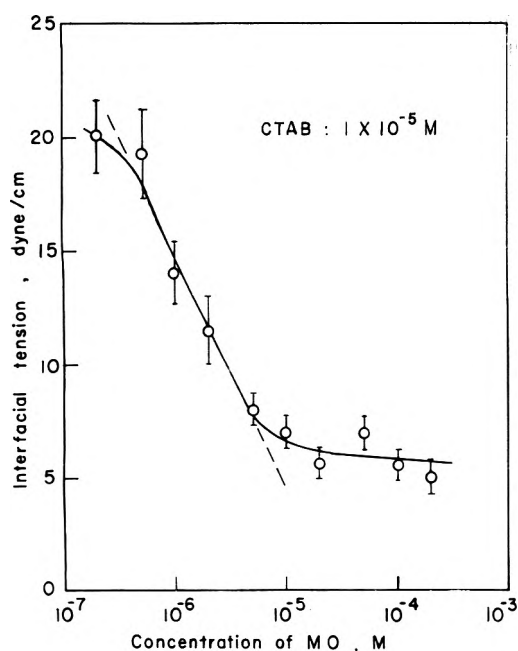


Figure 2. Interfacial tension between carbon tetrachloride and aqueous solutions of MO and CTAB as a function of the logarithm of the concentration of MO. The concentration of CTAB is fixed at  $1 \times 10^{-5}$  M.

values around 0.36 of the depolarization ratio ( $\rho_I = I_{\perp}/I_{\parallel}$ ) irrespective of the excitation wavelength of the Ar<sup>+</sup> laser. Taking account of the experimental error, this value is considered to agree with 0.33, which will be theoretically obtained under the assumptions that the Raman band belongs to the totally symmetric species, and that, of all nonvanishing elements of the derived polarizability tensor, only one diagonal element has an exceptionally large value.<sup>11</sup>

Figure 3B represents a resonance Raman spectrum of MO in the monolayer adsorbed at the interface between carbon tetrachloride and the aqueous solution mentioned above. The spectrum was recorded using the total reflection method of Figure 1, and in this case, a polarizer for the Raman radiation was removed so that  $I_{\parallel} + I_{\perp}$  can be obtained. Although the scattered Raman radiation is so weak that the S/N value is very low, the Raman spectrum which resembles that in the bulk solution can apparently be observed on the background due to carbon tetrachloride. In

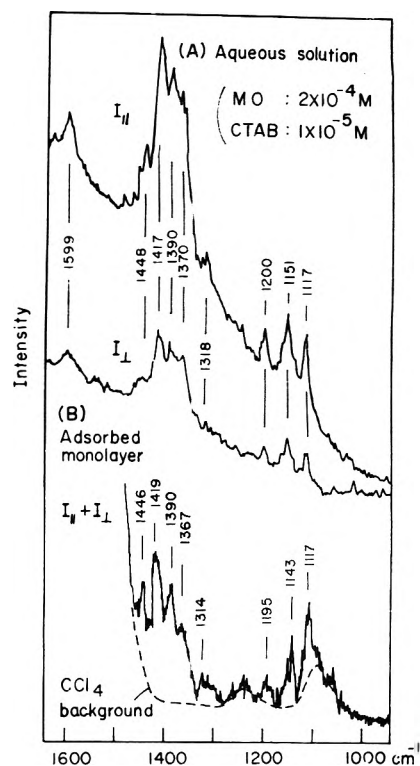


Figure 3. Resonance Raman spectra of MO: (A) aqueous solution of MO ( $2 \times 10^{-4}$  M) and CTAB ( $1 \times 10^{-5}$  M); (B) monolayers adsorbed at the interface between carbon tetrachloride and the aqueous solution.  $I_{\parallel}$  and  $I_{\perp}$  are intensities of Raman radiations with the electric vectors parallel and perpendicular to that of the exciting light, respectively.

Table I, the Raman frequencies of MO in the monolayer are compared with those in bulk solutions and of solid MO. Evidently, the frequencies in the monolayer are slightly shifted from those in bulk solution toward those of solid MO, suggesting that the MO molecules in the monolayer are in an environment similar to the crystal field.

Besides the fact that there is the monolayer at the interface as shown above, additional confirmations of the statement that the Raman spectrum in Figure 3B arises from the monolayer are accomplished by the following examinations. (1) No Raman radiation due to MO can be detected for the interface between carbon tetrachloride and an aqueous solution of MO alone ( $2 \times 10^{-4}$  M), where the adsorption cannot be expected as MO is surface inactive. This may indicate that the evanescent wave penetrated into the aqueous solution does not give rise to detectable Raman radiation whenever the adsorbed monolayer is not formed at the interface.<sup>12</sup> (2) The frequencies of the Raman bands in Figure 3B are different from those in the spectra of the bulk solution (Figure 3A), as mentioned above. Differences are also found in the polarization properties of the Raman bands between the bulk solution and the monolayer as will be seen in the later part of this paper.

In the next section, we discuss the orientation of the MO molecules in the adsorbed monolayer with the aid of polarization measurements of their resonance Raman spectra.

*Molecular Orientation of MO in the Monolayer.* We now consider a three-phase plane-bounded system shown in Figure 4. Phase 1 is the semiinfinite incident phase of carbon tetrachloride, phase 2 the adsorbed monolayer, and phase 3 the semiinfinite final phase of the aqueous solution. Since the adsorbed monolayer is much thinner than

TABLE I: Raman Spectra of MO in Various States

Aqueous solution			Adsorbed monolayer	Solid <sup>a</sup>	Assignment <sup>b</sup>
Ref 9	Ref 10	Present work			
1597	1600	1599	—	1592	Benzene ring
1449	1450	1448	1446	1443	Benzene ring
1423	1420	1417	1419	1419	N=N stretching
1415				1412	
1393	1395	1390	1390	1391	
1373		1370	1367	1368	
1318	1320	1318	1314	1313	Benzene ring
1294				1292	
1201	1200	1200	1195	1197	Benzene ring
1151	1155	1151	1143	1145	Ph-N stretching
1118		1117	1117	1118	

<sup>a</sup> Reference 9. <sup>b</sup> Reference 10.

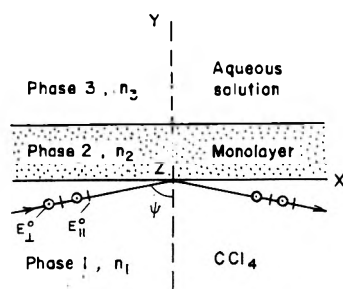


Figure 4. Geometry of total reflection method for Raman measurements of a monolayer at the interface between carbon tetrachloride and an aqueous solution.

the penetration depth, the electric field of the evanescent wave in the total reflection can be assumed constant over the monolayer thickness. For the incident polarized lights with electric vectors parallel and perpendicular to the plane of incidence, the electric field amplitudes<sup>7</sup> in the monolayer are given by

$$E_X = \frac{2(\sin^2 \psi - n_{31}^2)^{1/2} \cos \psi}{(1 - n_{31}^2)^{1/2} (1 + n_{31}^2) \sin^2 \psi - n_{31}^2} E_{\parallel}^0 \quad (1)$$

$$E_Y = \frac{2n_{32}^2 \sin \psi \cos \psi}{(1 - n_{31}^2)^{1/2} (1 + n_{31}^2) \sin^2 \psi - n_{31}^2} E_{\parallel}^0 \quad (2)$$

and

$$E_Z = \frac{2 \cos \psi}{(1 - n_{31}^2)^{1/2}} E_{\perp}^0 \quad (3)$$

where  $n_{ij} = n_i/n_j$  is the ratio of the refractive index of phase  $i$  to that of phase  $j$ ,  $\psi$  the angle of incidence, and  $E_{\parallel}^0$  and  $E_{\perp}^0$  the incoming amplitudes for the parallel and perpendicular polarizations, respectively.  $E_Z$  represents the electric field amplitude for perpendicular polarization  $E_{\perp}$ , and that for parallel polarization  $E_{\parallel}$  is expressed by

$$E_{\parallel} = (|E_X|^2 + |E_Y|^2)^{1/2} \quad (4)$$

When the Raman radiation due to the evanescent wave is observed along the  $Z$  axis, four geometries of polarization measurements are available as a consequence of a combination of two polarization directions of the excitation (parallel and perpendicular to the plane of incidence) and two polarization directions of the Raman radiation (parallel to the  $X$  and  $Y$  axes). The Raman intensities<sup>13</sup> obtained by these polarization geometries will be proportional to

$$I_{\perp X} = \alpha_{ZX}^2 |E_Z|^2 \quad (5)$$

$$I_{\perp Y} = \alpha_{ZY}^2 |E_Z|^2 \quad (6)$$

$$I_{\parallel X} = \alpha_{XX}^2 |E_X|^2 + \alpha_{YX}^2 |E_Y|^2 \quad (7)$$

and

$$I_{\parallel Y} = \alpha_{XY}^2 |E_X|^2 + \alpha_{YY}^2 |E_Y|^2 \quad (8)$$

where the first subscript of  $I$  refers to the excitation polarization and the second to that of Raman radiation, and  $\alpha_{XY}$  etc. are elements of the derived polarizability tensor which is based on the space-fixed axes.

Using proper values,  $n_1 = 1.46$  for carbon tetrachloride,  $n_3 = 1.34$  for dilute aqueous solution, and  $\psi = 84^\circ$ , and making the assumption that  $n_2 = 1.43$  for the adsorbed monolayer, from eq 1-3 we have

$$|E_X|^2 = 0.0415 |E_{\parallel}^0|^2 \quad (9)$$

$$|E_Y|^2 = 0.216 |E_{\parallel}^0|^2 \quad (10)$$

and

$$|E_Z|^2 = 0.277 |E_{\perp}^0|^2 \quad (11)$$

The next task is to express the elements  $\alpha_{XY}$  etc. in terms of elements  $\alpha_{xy}$  etc. which are based on the principal polarizability axes of the molecule.<sup>13,14</sup> To do this, it is convenient to assume a type of orientation of the MO molecule and to use the transformation matrix  $\Phi$  relating the coordinate system  $X, Y, Z$  (designated  $F$ ), and the system  $x, y, z$  (designated  $g$ ) under the assumed type of orientation. Using the elements  $\Phi_{Fg}$ , we may write

$$\alpha_{FF'} = \sum_{gg'} \Phi_{Fg} \Phi_{F'g'} \alpha_{gg'} \quad (12)$$

Here, it is reasonable to assume that the MO molecules in the monolayer are uniaxially oriented with respect to the  $Y$  axis which is normal to the interface, the  $XZ$  plane. This is indicated in Figure 5, where the long axis of the molecule (the  $z$  axis) is rotated around the  $Y$  axis with an angle  $\theta$ , and the molecular  $x$  and  $y$  axes are free to rotate around the  $z$  axis. Under the present assumption of uniaxial orientation,  $\Phi_{Fg}$  may be given by the direction cosines between the  $F$  axes and  $g$  axes as functions of Eulerian angles.<sup>15</sup> The required terms are obtained by averaging over two Eulerian angles other than  $\theta$ ; one refers to the rotation of the MO molecule around the  $z$  axis, and the other to the rotation of the  $z$  axis around the  $Y$  axis.

$$\alpha_{FF'}^2 = \left( \sum_{gg'} \Phi_{Fg} \Phi_{F'g'} \alpha_{gg'} \right)^2 \quad (13)$$

Since for the MO molecule it has already been known from the measurements of the depolarization ratio of the bulk

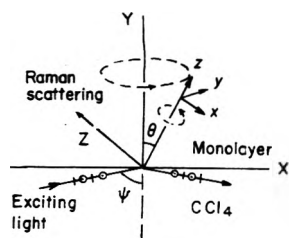


Figure 5. Uniaxial orientation of the  $z$  axis of MO in monolayers with respect to the  $Y$  axis.

aqueous solution that only one diagonal element  $\alpha_{gg}$  has an exceptionally large value as compared with other elements, eq 13 becomes very simple. For two cases in which  $\alpha_{zz}$  is largest (case 1), and where either  $\alpha_{xx}$  or  $\alpha_{yy}$  is largest (case 2), the results are summarized in Table II where expressions of six  $\alpha_{FF}^2$ 's in eq 5–8 are given as coefficients of  $\alpha_{gg}^2$ . In Figure 6, they are shown as a function of  $\theta$ .

Snyder<sup>14</sup> has derived the Raman activities for two special cases ( $\theta = 0$  and  $90^\circ$ ) of uniaxially orientated molecules without any restriction of the values of  $\alpha_{gg}$ 's. Our results coincide with Snyder's, when ours are applied to these special cases of  $\theta$  and at the same time, Snyder's are applied to cases 1 and 2.

Since the transition moment of the electronic absorption band of MO at 460 nm is assumed to be parallel to the long axis (the  $z$  axis) of the molecule,<sup>6</sup> all  $\alpha_{gg}$ 's except  $\alpha_{zz}$  may vanish, that is, case 1 may be true in this case.<sup>11</sup> Thus we have

$$I_{\perp X} = 0.0346 \sin^4 \theta |E_{\perp}|^2 \alpha_{zz}^2 \quad (14)$$

$$I_{\perp Y} = 0.139 \sin^2 \theta \cos^2 \theta |E_{\perp}|^2 \alpha_{zz}^2 \quad (15)$$

$$I_{\parallel X} = (0.0156 \sin^2 \theta + 0.108 \cos^2 \theta) \sin^2 \theta |E_{\parallel}|^2 \alpha_{zz}^2 \quad (16)$$

and

$$I_{\parallel Y} = (0.0208 \sin^2 \theta + 0.216 \cos^2 \theta) \cos^2 \theta |E_{\parallel}|^2 \alpha_{zz}^2 \quad (17)$$

From eq 14–17 and Figure 6, the following polarization pattern is expected: (1) when  $\theta = 0^\circ$ , only  $\alpha_{YY}^2$  has nonzero value and therefore only  $I_{\parallel Y}$  is observable with relatively large intensity. (2) When  $\theta = 90^\circ$ , on the other hand,  $\alpha_{XX}^2$  and  $\alpha_{ZX}^2$  have nonzero values and therefore  $I_{\parallel X}$  and  $I_{\perp X}$  are observable, although these intensities are as small as  $1/4$  and  $1/6$  of  $I_{\parallel Y}$  at  $\theta = 0^\circ$ , respectively, if  $E_{\parallel}^0 = E_{\perp}^0$ . (3) When  $\theta$  is an intermediate value between 0 and  $90^\circ$ , all of the six  $\alpha_{FF}^2$ 's have certain values and therefore the Raman spectra can be observed for all of the four polarization geometries. In this case, from eq 14–17, we have the ratios

$$\frac{I_{\perp X}}{I_{\perp Y}} = \frac{1}{4} \tan^2 \theta \quad (18)$$

and

$$\frac{I_{\parallel X}}{I_{\parallel Y}} = \frac{3 \tan^2 \theta + 20.8}{4 \tan^2 \theta + 41.5} \tan^2 \theta \quad (19)$$

Experimentally, each ratio is obtained by measuring the intensities of the Raman bands recorded by changing the polarization of the Raman radiation in turn from the  $X$  to  $Y$  directions at a fixed polarization direction of the exciting light (either perpendicular or parallel to the plane of incidence).

Figure 7 represents the polarized Raman spectra of MO in the adsorbed monolayer obtained for the four polarization geometries. For the all geometries, the Raman spectra of MO can apparently be observed on the background due

TABLE II: Raman Scattering Activities ( $\alpha_{FF}^2$ ) of Uniaxially Oriented Molecules Expressed as Coefficients of  $\alpha_{gg}^2$

Direction of electric field	Polarization direction of Raman radiation	
	$X$	$Y$
Case 1 ( $\alpha_{zz} \gg$ other elements)		
$X$	$(3/8) \sin^4 \theta$	$(1/2) \sin^2 \theta \cos^2 \theta$
$Y$	$(1/2) \sin^2 \theta \cos^2 \theta$	$\cos^4 \theta$
$Z$	$(1/8) \sin^4 \theta$	$(1/2) \sin^2 \theta \cos^2 \theta$
Case 2 ( $\alpha_{xx}$ or $\alpha_{yy} \gg$ other elements)		
$X$	$(3/64) (3 \cos^4 \theta + 2 \cos^2 \theta + 3)$	$(1/16) \sin^2 \theta (3 \cos^2 \theta + 1)$
$Y$	$(1/16) \sin^2 \theta (3 \cos^2 \theta + 1)$	$(3/8) \sin^4 \theta$
$Z$	$(1/64) (3 \cos^4 \theta + 2 \cos^2 \theta + 3)$	$(1/16) \sin^2 \theta (3 \cos^2 \theta + 1)$

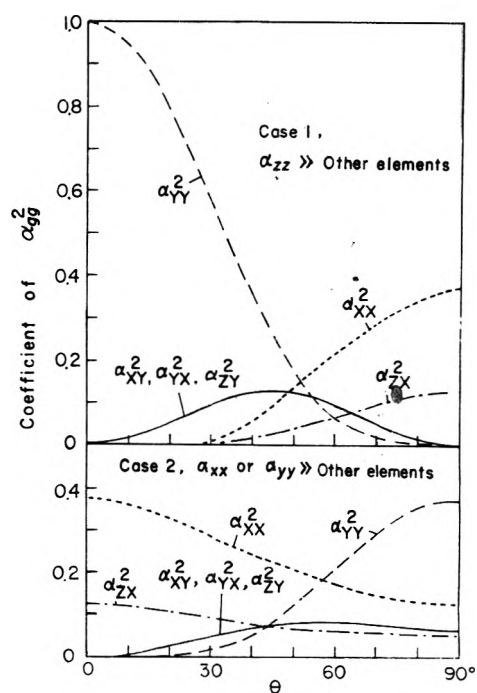


Figure 6. Raman scattering activities ( $\alpha_{FF}^2$ ) of uniaxially oriented molecules as a function of  $\theta$ : case 1,  $\alpha_{zz} \gg$  other elements; case 2,  $\alpha_{xx}$  or  $\alpha_{yy} \gg$  other elements (see text).

to carbon tetrachloride.<sup>16</sup> This fact suggests that  $\theta$  is neither 0 nor  $90^\circ$  and is an intermediate value. Since, unfortunately, the accuracy of the Raman intensity measurements is not so good owing to the very low S/N value, after more than ten measurements of intensities, the mean values of the ratios  $I_{\perp X}/I_{\perp Y}$  and  $I_{\parallel X}/I_{\parallel Y}$  were obtained to be 0.80 and 0.77, respectively, for the phenyl-N stretching band at  $1143 \text{ cm}^{-1}$ . A correction for the polarization character of the monochromator was applied to these values. Substitution of these values into eq 18 and 19 gives the  $\theta$  values of  $60.8$  and  $50.3^\circ$ , respectively. Although it was unable to get one  $\theta$  value which simultaneously satisfied both of eq 18 and 19, the magnitude of this discrepancy may be allowed at present, taking account of the low accuracy of the Raman intensity measurements as mentioned above. Thus it may be concluded that the long axes of the MO molecules are tilted in the adsorbed monolayer with a large angle of  $50$ – $60^\circ$  with the  $Y$  axis. An attempt to improve the

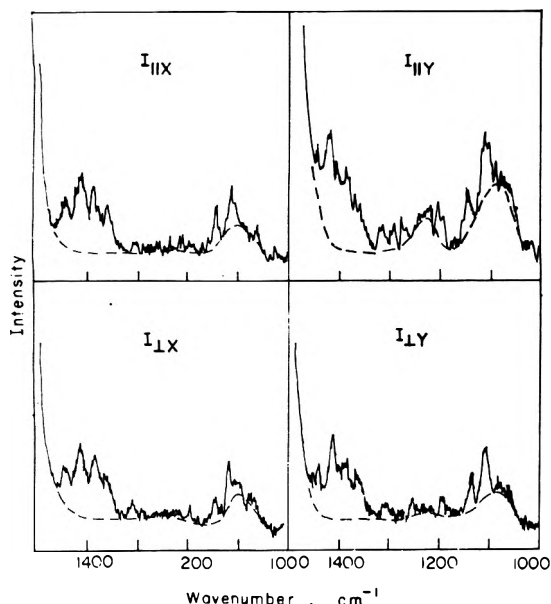


Figure 7. Resonance Raman spectra of MO in the adsorbed monolayer obtained with four polarization geometries.

S/N value is now being made by means of the time averaging using a computer in real time. Unipoint multiple reflection techniques<sup>17</sup> may also compensate for weakness of scattered Raman radiation.

It should be noted here that we measured the resonance Raman spectra of the MO dye and could discuss only about the orientation of these dye molecules. No information

could be obtained about the CTAB surfactant, which may play an important role in the adsorption and formation of the monolayer at the interface. From this point of view, a succeeding study is in progress by using surface-active dyes which give rise to the resonance Raman effect for the exciting lights of Ar<sup>+</sup> laser.

The total reflection method described in this paper may be applied to studies of thin layers not only at liquid-liquid interfaces but also at liquid-gas and liquid-solid interfaces.

## References and Notes

- (1) A. G. Tweet, *Rev. Sci. Instrum.*, **34**, 1412 (1963).
- (2) A. G. Tweet, G. L. Gaines, Jr., and W. D. Bellamy, *J. Chem. Phys.*, **40**, 2596 (1964).
- (3) C. F. Hiskey and T. A. Downey, *J. Phys. Chem.*, **58**, 835 (1954).
- (4) B. Kim, A. Kagayama, Y. Saito, K. Machida, and T. Uno, *Bull. Chem. Soc. Jpn.*, **48**, 1394 (1975).
- (5) H. H. Jaffé, S. J. Yeh, and R. W. Gardner, *J. Mol. Spectrosc.*, **2**, 120 (1958).
- (6) D. L. Beveridge and H. H. Jaffé, *J.-Am. Chem. Soc.*, **88**, 1948 (1966).
- (7) N. J. Harrick, "Internal Reflection Spectroscopy", Interscience, New York, N.Y., 1967, Chapter II.
- (8) H. Hacker, *Spectrochim. Acta*, **21**, 1989 (1965).
- (9) P. R. Carey, H. Schneider, and H. J. Bernstein, *Biochem. Biophys. Res. Commun.*, **47**, 588 (1972).
- (10) K. Machida, B. Kim, Y. Saito, K. Igarashi, and T. Uno, *Bull. Chem. Soc. Jpn.*, **47**, 78 (1974).
- (11) J. Behringer, "Observed Resonance Raman Spectra", in "Raman Spectroscopy", H. A. Szymanski, Ed., Plenum Press, New York, N.Y., 1967, Chapter 6.
- (12) In the monolayer, the number of the MO molecules in a unit volume is as large as a factor of  $10^4$  times that in the bulk aqueous solution.
- (13) E. B. Wilson, Jr., J. C. Decius, and P. C. Cross, "Molecular Vibrations", McGraw-Hill, New York, N.Y., 1955, Section 3-6.
- (14) R. G. Snyder, *J. Mol. Spectrosc.*, **37**, 353 (1971).
- (15) Reference 13, Appendix I.
- (16) The intensity of the background due to carbon tetrachloride depends upon the polarization geometry because of polarization characteristics of the Raman bands of carbon tetrachloride.
- (17) N. J. Harrick, *Appl. Opt.*, **5**, 1236 (1966).

## Raman Spectra of Rhombic Sulfur Dissolved in Secondary Amines

Francis P. Daly and Chris W. Brown\*

Department of Chemistry, University of Rhode Island, Kingston, Rhode Island 02881 (Received June 30, 1975)

Raman spectra of rhombic sulfur dissolved in di-*n*-butylamine, di-*n*-propylamine, and dimethylamine have been measured for the first time. Bands due to S<sub>4</sub><sup>2-</sup> and S<sub>8</sub><sup>n-</sup> were observed in the spectra of the di-*n*-butylamine and di-*n*-propylamine solutions, whereas only bands due to S<sub>8</sub><sup>n-</sup> appeared in the spectrum of the dimethylamine solution. Comparison of the results on secondary amine solutions with our previous results on primary amines indicates that the ability of secondary amines to form small ionic sulfur species is less than that of primary amines.

The Raman spectra of rhombic sulfur dissolved in ethylenediamine, *n*-propylamine, and monomethylamine have been reported previously.<sup>1,2</sup> New bands observed in the 100-600-cm<sup>-1</sup> region were attributed to the open chain polysulfides S<sub>8</sub><sup>n-</sup>, S<sub>4</sub><sup>2-</sup>, and S<sub>3</sub><sup>-</sup>. In this note we report the

Raman spectra of rhombic sulfur dissolved in the following secondary amines: di-*n*-butylamine, di-*n*-propylamine, di-*n*-propylamine, and dimethylamine.

Raman spectra were measured using a Spex Industries Model 1401 double monochromator with photon counting

TABLE I: Vibrational Frequencies ( $\text{cm}^{-1}$ ) and Relative Intensities of Bands Assigned to Open Chain Polysulfides in the Raman Spectra of Rhombic Sulfur Dissolved in Primary and Secondary Amines

$S_8$ in EDA	$S_8$ in $C_3H_7NH_2$	$S_8$ in $CH_3NH_2$	$S_8$ in $(C_4H_9)_2NH$	$S_8$ in $(C_3H_7)_2NH$	$S_8$ in $(CH_3)_2NH$	Assignment
195 vw	193 vw					$S_4^{2-}$
243 vw	242 vw		234 vw		227 w ( $\rho = 0.81$ )	$S_8^{n-}$
297 w			250 w			$S_4^{2-}$
396 vs	397 vs	399 vs	285 w	282 w	272 w ( $\rho = 0.63$ )	$S_8^{n-}$
434 s	438 s	437 s	396 vs	398 vs	402 vs ( $\rho = 0.38$ )	$S_4^{2-}$ and $S_4^{n-}$
502 m	505 m	502 m	439 s	439 s		$S_4^{2-}$
533 s	534 w	535 s	500 m	500 m		$S_4^{2-}$
						$S_3^-$

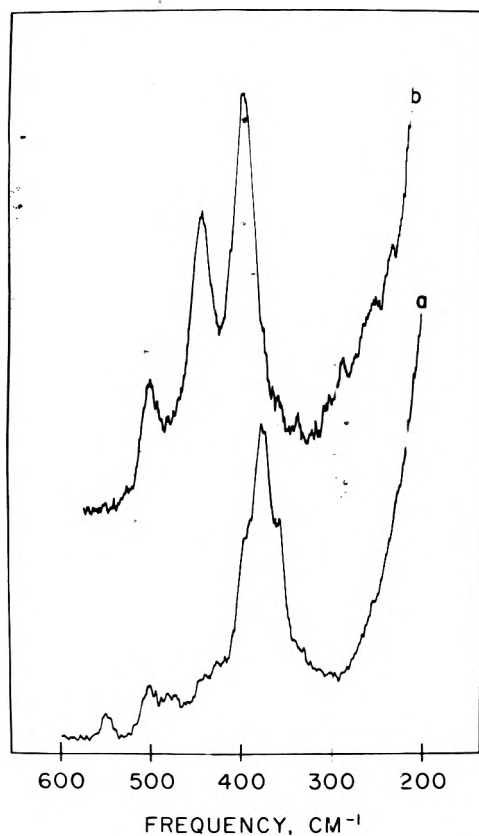


Figure 1. Raman spectra of (a) di-*n*-butylamine and (b)  $\sim 10^{-1}$  M sulfur in di-*n*-butylamine.

detection and a C.R.L. Model 52-A argon ion laser emitting at 4880 Å ( $\leq 150$  mW power at the sample). All spectra were measured with a spectral slit width  $< 8$   $\text{cm}^{-1}$ . Di-*n*-butylamine and di-*n*-propylamine were contained at  $24 \pm 1$  °C in sealed Pyrex capillary tubes with an inner diameter greater than 1.2 mm. Dimethylamine was liquified under vacuum at  $-70$  °C in a Raman cell designed for low-temperature liquids.<sup>3</sup>

The Raman spectrum of a  $10^{-1}$  M solution of sulfur dissolved in di-*n*-butylamine is compared to the spectrum of the solvent in Figure 1. New bands are observed at 234, 250, 285, 396, 439, and 500  $\text{cm}^{-1}$ . The Raman spectrum of a  $10^{-1}$  M solution of rhombic sulfur in di-*n*-propylamine shown in Figure 2 is similar to that of  $S_8$  in di-*n*-butylamine with new bands at 282, 398, 439, and 500  $\text{cm}^{-1}$ . Bands below 270  $\text{cm}^{-1}$  were obscured by Rayleigh scattering.

Dimethylamine was chosen as the third amine for this study because it does not have bands in the spectral region

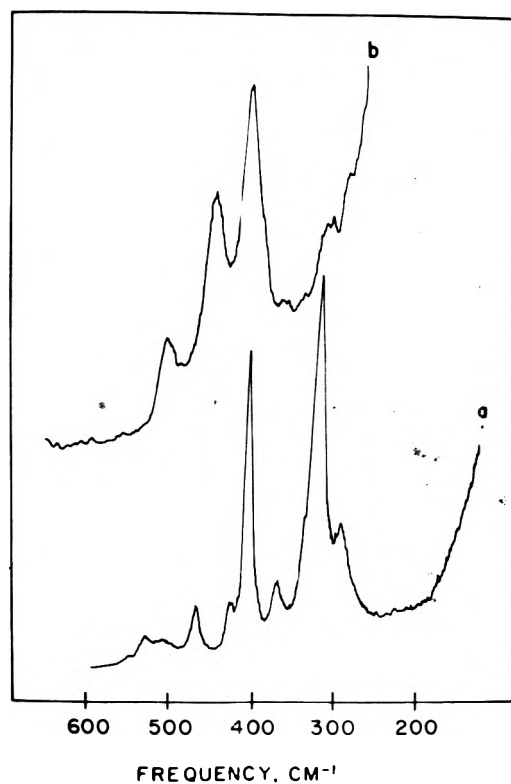
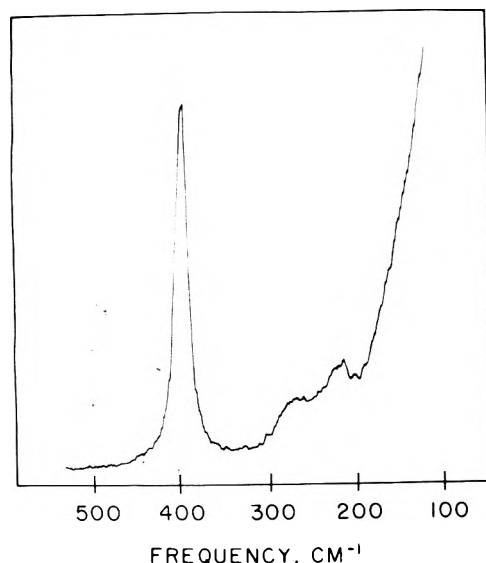


Figure 2. Raman spectra of (a) di-*n*-propylamine and (b)  $\sim 10^{-1}$  M sulfur in di-*n*-propylamine.

of interest. The spectrum of sulfur dissolved in dimethylamine is shown in Figure 3. This spectrum is unlike those of sulfur in all of the other primary and secondary amines, since only three new bands are observed at 227, 278, and 402  $\text{cm}^{-1}$ .

The frequencies and assignments of the bands in the Raman spectra of sulfur dissolved in the six primary and secondary amines are summarized in Table I. In all three primary amines a band assigned to  $S_3^-$  is observed at  $\sim 535$   $\text{cm}^{-1}$ ; however, this band is absent in the spectra of sulfur in the secondary amines. Bands assigned to  $S_4^{2-}$  and  $S_8^{n-}$  in the spectra of sulfur dissolved in primary amines are also observed in the spectra of sulfur in di-*n*-butyl- and di-*n*-propylamine; however, the bands assigned purely to  $S_4^{2-}$  (e.g., 439 and 500  $\text{cm}^{-1}$ ) are not as intense relative to the  $S_8^{n-}$  band ( $\sim 400$   $\text{cm}^{-1}$ ) in the spectra of the secondary amine solutions. In the spectrum of sulfur dissolved in dimethylamine only bands assigned to  $S_8^{n-}$  are observed.

The present results indicate that the ability of secondary amines to form small ionic species from sulfur is less than that of primary amines. This does not mean that  $S_3^-$ , for



**Figure 3.** Raman spectrum of  $\sim 10^{-1}$  M sulfur in dimethylamine measured at  $-70$  °C; dimethylamine does not have bands in the region of interest.

example, is not formed in the secondary amines, but rather that the rate of formation is much slower. Our previous results<sup>1,2</sup> showed that in primary amines the amounts of  $S_3^-$  and  $S_4^{2-}$  increased with time. In the secondary amines  $S_3^-$

cannot be detected and  $S_4^{2-}$  is observed only in the room temperature solutions, i.e., it is not found in the spectrum of sulfur in dimethylamine which was measured at  $-70$  °C. These results are in agreement with those of Davis and Nakshbendi,<sup>4</sup> who observed that the first-order rate constants for color changes of sulfur in amines decreased in the order of primary > secondary > tertiary.

In our previous reports<sup>1,2</sup> the existence of  $S_3^-$  and  $S_4^{2-}$  in amine solutions was supported by similar bands for these species in spectra of other systems. However, due to the presence of these species and overlapping bands, we could only suggest the presence of a third species ( $S_8^{n-}$ ): The present spectrum of sulfur in dimethylamine, in which bands due to  $S_3^-$  and  $S_4^{2-}$  are absent, confirms the suggestion that the strong band at  $400\text{ cm}^{-1}$  is also due to the  $S_8^{n-}$  open chain polysulfide.

*Acknowledgment.* We wish to express our appreciation to the National Science Foundation for a matching grant which made possible the purchase of the Raman instrumentation.

#### References and Notes

- (1) F. P. Daly and C. W. Brown, *J. Phys. Chem.*, **77**, 1859 (1973).
- (2) F. P. Daly and C. W. Brown, *J. Phys. Chem.*, **79**, 350 (1975).
- (3) A. G. Hopkins, F. P. Daly, and C. W. Brown, *Appl. Spectrosc.*, **28**, 194 (1974).
- (4) R. E. Davis and H. F. Nakshbendi, *J. Am. Chem. Soc.*, **84**, 2085 (1962).

## Temperature Dependence of a Process Competing with $S_2$ - $S_1$ Internal Conversion in Indole and Phenol in Aqueous Solutions

Harald B. Steen,

Norsk Hydro's Institute for Cancer Research, Biophysics Department, Montebello, Oslo 3, Norway

Michael K. Bowman, and Larry Kevan\*

Department of Chemistry, Wayne State University, Detroit, Michigan 48202 (Received August 11, 1975)

The drop in  $\phi_f$  with decreasing excitation wavelength, previously attributed to ionization from the  $S_2$  state, increases substantially with increasing temperature for both indole and phenol in aqueous solution. Addition of 2-propanol to the solvent reduces the drop in  $\phi_f$  but not its activation energy which on the other hand depends significantly on the solute.  $\phi_{\text{eq}}$ —measured upon excitation of the  $S_2$  state of indole in  $H_2O$  increases from 0.09 at 25 °C to 0.17 at 65 °C. The results are interpreted in terms of an intermediate charge transfer to solvent state (CTTS) populated from  $S_2$ . In the 2-propanol–water solvent the formation of this CTTS state appears to be governed primarily by interaction of the excited solute with water molecules.

### Introduction

As reported previously, the fluorescence quantum yield  $\phi_f$  of indole and of the aromatic amino acids tryptophan, tyrosine, and phenylalanine is not independent of the excitation wavelength  $\lambda_x$ , but shows a considerable drop with decreasing  $\lambda_x$  between 250 and 220 nm.<sup>1,2</sup> Outside this region  $\phi_f$  is constant. Similar data have been reported for phenol.<sup>3</sup> As a convenient measure of the drop in  $\phi_f$  we use

$$\Delta\phi_f = [\phi_f(>250\text{ nm})/\phi_f(<220\text{ nm})] - 1 \quad (1)$$

The wavelength at which the drop in  $\phi_f$  occurs coincides approximately with the onset of the absorption associated with the second excited state  $S_2$  of the solute, indicating that it is caused by a process that competes efficiently with internal conversion from  $S_2$  to the fluorescent  $S_1$  state. For the case of tryptophan, which is the amino acid derivative of indole, it was found that the drop in  $\phi_f$  is accompanied

by a sharp rise in the quantum yield of photoionization,  $\phi_{\text{e}_{\text{aq}}^-}$ , showing that this may be the process that competes with internal conversion from S<sub>2</sub>.<sup>2,4</sup> To distinguish possible photoionization mechanisms, the effect of solvent polarity, as measured by the static dielectric constant, on  $\Delta\phi_f$  has been studied<sup>4</sup> and indicates that the ionization occurs via an intermediate state, i.e., a charge transfer to solvent (CTTS) state. In the present work we have tried to further elucidate this mechanism by studying the temperature dependence of  $\Delta\phi_f$ .

### Experimental Section

A monochromatic light beam, produced by a D<sub>2</sub> lamp fitted to a grating monochromator, fell on the sample solution in a 1 × 1 cm<sup>2</sup> quartz cell. The solute concentration of 5 × 10<sup>-3</sup> M for indole and 1 × 10<sup>-2</sup> M for phenol is sufficient for total absorption at all excitation wavelengths ( $\lambda_x$ ) less than 280 nm. (For phenol this condition is not fulfilled between 225 and 245 nm.) The fluorescence was detected at a 10° angle to the excitation beam by a second monochromator with a photomultiplier tube at the exit slit. The excitation and emission light beams were collimated to minimize effects of scattered light. Details of the apparatus are given elsewhere.<sup>2</sup>

With the emission monochromator set at the fluorescence maximum, the excitation monochromator scanned the spectrum from 190 to 300 nm. The wavelength dependence of  $\phi_f$  was obtained by comparing the output signal,  $i_f(\lambda_x)$ , for indole or phenol with the signal,  $i_R(\lambda_x)$ , obtained when the sample was replaced by a 3 g/l. solution of rhodamine B in ethylene glycol, the fluorescence quantum yield  $\phi_f^0$  of which is independent of  $\lambda_x$ , and which therefore served as a quantum counter. Thus the fluorescence quantum yield of indole or phenol is

$$\phi_f(\lambda_x) \propto (i_f(\lambda_x)/i_R(\lambda_x))\phi_f^0$$

In the present experiments the sample cell was enclosed in an insulated metal housing which has slits for the excitation and emission light and which can be heated by a heating element in its base or cooled by the N<sub>2</sub> boil-off from a Dewar containing liquid N<sub>2</sub> and a heating element fed through a Variac. The temperature was measured by a thermocouple which was immersed in the solution.

The quantum yield of e<sub>aq</sub><sup>-</sup> from indole was measured by the oxidation of ferrous ion in 0.1 M sulfuric acid as described elsewhere.<sup>4</sup> In order to correct for the autooxidation of Fe<sup>2+</sup> that may occur at high temperatures, the yield of Fe<sup>3+</sup> was also measured for a  $\lambda_x$  of 310 nm which is just outside the absorption spectrum of indole. At room temperature this yield was found to be negligible, whereas at 66 °C it amounted to about 10% of that obtained for  $\lambda_x$  220 nm.

Rhodamine B and phenol were Merck analytical grade, indole was from BDH, ethylene glycol was "Chromatquality" from Matheson Coleman and Bell, 2-propanol was from A/S Vinmonopolet, and water was redistilled from alkaline KMnO<sub>4</sub>. All solutions were saturated with air.

### Results

In Figure 1 are depicted typical recorder traces as observed upon scanning the excitation spectrum of rhodamine B and of indole in H<sub>2</sub>O at two different temperatures as well as the resulting wavelength dependence of  $\phi_f$  for indole. It can be seen that the drop in  $\phi_f$  between 250 and 220 nm is significantly larger at the higher temperature. On the

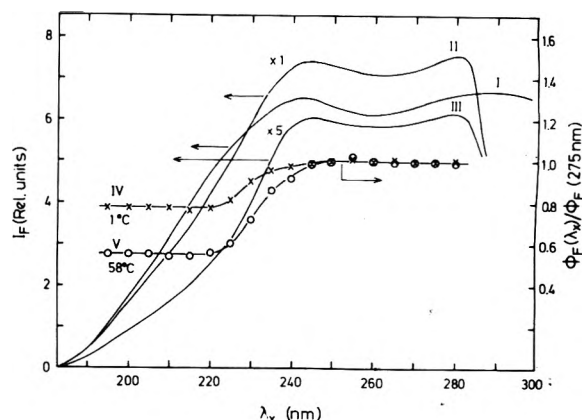


Figure 1. The intensity at the fluorescence maximum as recorded by scanning the excitation wavelength  $\lambda_x$  for 3 g/l. of rhodamine B in ethylene glycol (I) and for 5 × 10<sup>-3</sup> M indole in H<sub>2</sub>O at 1 °C (II) and at 58 °C (III). Curves IV and V are the resulting dependence of  $\phi_f$  on  $\lambda_x$  for the indole solutions, as calculated with the assumption that  $\phi_f$  for the rhodamine B solution is independent of  $\lambda_x$ .

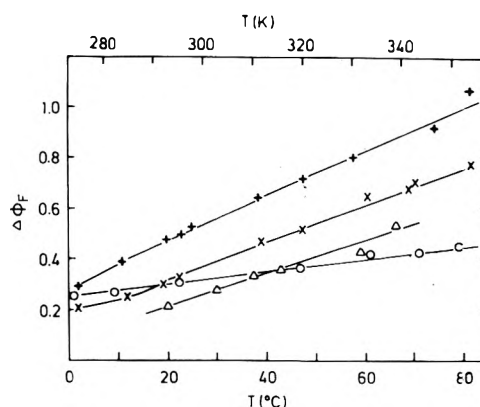


Figure 2. The temperature dependence of the drop in  $\Delta\phi_f$  that occurs between  $\lambda_x$  250 and 220 nm: (+) indole in H<sub>2</sub>O; (x) indole in D<sub>2</sub>O; ( $\Delta$ ) indole in 2-propanol-H<sub>2</sub>O (2:7 by volume); and (O) phenol in H<sub>2</sub>O.

other hand, the wavelength at which this drop occurs is independent of temperature. This wavelength is the same also in various alcohol-water solvents and is independent of the static dielectric constant  $\epsilon_s$  of the solvent.<sup>5</sup> For all samples the fluorescence spectra obtained with  $\lambda_x$  of 215 and 275 nm are identical at both high and low temperatures. Placing the sample between crossed or uncrossed polarizers also had no effect on fluorescence spectra. The value of  $\Delta\phi_f$  is independent of the concentration of indole over the region studied, i.e., between 1 × 10<sup>-3</sup> and 1 × 10<sup>-2</sup> M, and is not affected by ionic strength as observed by addition of 1 M NaCl.

Figure 2 shows the temperature dependence of  $\Delta\phi_f$  for the various solutions studied. It can be seen that  $\Delta\phi_f$  for indole is considerably smaller in the 2-propanol-water mixture than in aqueous solutions. As described previously,<sup>5</sup> this difference can be correlated with the lower value of  $\epsilon_s$  in the former solvent. In various alcohol-water mixtures  $\Delta\phi_f$  has been found to decrease with  $\epsilon_s$  and to reach zero for  $\epsilon_s \sim 40$ ,<sup>5</sup> the decrease being independent of which alcohol was used, indicating that  $\Delta\phi_f$  depends on  $\epsilon_s$  rather than on the chemical composition of the solvent. On the other hand, it can be seen from Figure 2 that  $\Delta\phi_f$  is noticeably smaller in D<sub>2</sub>O than in H<sub>2</sub>O although  $\epsilon_s$  for these solvents is the same within close limits.<sup>6</sup> Also, the temperature depen-

TABLE I: Activation Energies  $\Delta E$  of  $\Delta\phi_f$  and  $\Delta\phi_f^{\text{cor}}$  and Temperature Dependence of  $\phi_{e_{\text{aq}}^-}$  for Various Solute-Solvent Systems

Solute	Solvent	$\Delta E(\Delta\phi_f),^a$ kcal/mol	$\Delta E(\Delta\phi_f^{\text{cor}}),^a$ kcal/mol	$\phi_{e_{\text{aq}}^-}(-25^\circ\text{C})$	$\phi_{e_{\text{aq}}^-}(-65^\circ\text{C})$
Indole	H <sub>2</sub> O	4.0(<15 °C) 2.2(>60 °C)	8.8	0.09 <sup>b</sup>	0.17 <sup>b</sup>
Indole	D <sub>2</sub> O	4.2(<15 °C) 2.2(>60 °C)	8.8		
Indole	2-Propanol- H <sub>2</sub> O (2:7 by vol)	4.2(<15 °C) 2.3(>60 °C)	8.1		
Phenol	H <sub>2</sub> O	1.5			

<sup>a</sup>  $\pm 0.5$  kcal mol<sup>-1</sup>. <sup>b</sup>  $\pm 10\%$ .

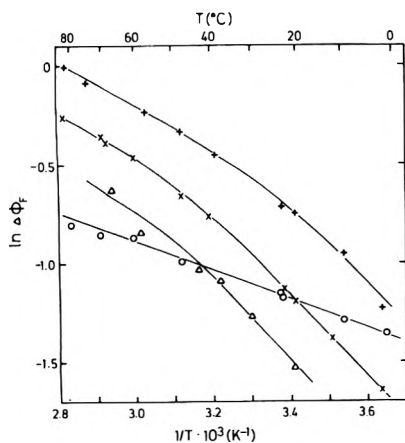


Figure 3. Arrhenius plots of  $\Delta\phi_f$ . For identification of the curves see Figure 2.

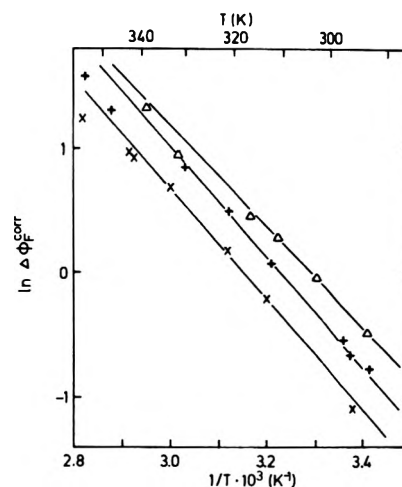


Figure 4. Arrhenius plots of values of  $\Delta\phi_f$  that have been corrected for the dependence of  $\epsilon_s$  on temperature. For identification of the curves, see Figure 2.

dence of  $\Delta\phi_f$  of phenol in H<sub>2</sub>O is different from that of indole in H<sub>2</sub>O.

Arrhenius plots of  $\Delta\phi_f$ , i.e., plots of  $\ln(\Delta\phi_f)$  vs.  $1/T$ , deviate significantly from straight lines for all of the indole solutions as demonstrated in Figure 3. For these solutions the tangents to the Arrhenius plots above 60 °C and below 15 °C correspond to activation energies of 2.2 and 4.0 kcal/mol, respectively (Table I). For the phenol solution, on the other hand, the results are consistent with an activation energy of 1.5 kcal/mol over the entire temperature region.

Since  $\Delta\phi_f$  is a function of  $\epsilon_s$ , which decreases considerably with increasing temperature, the temperature dependence of  $\Delta\phi_f$  is likely to be a composite effect. This assumption is supported by the curved Arrhenius plots for the indole solutions (Figure 3). Consequently we have corrected the observed values of  $\Delta\phi_f$  for the temperature dependence of  $\epsilon_s$  according to

$$\Delta\phi_f^{\text{cor}} \equiv \Delta\phi_f(\epsilon_s^\circ, T) = \frac{\Delta\phi_f(\epsilon_s, T)\Delta\phi_f(\epsilon_s^\circ, T^\circ)}{\Delta\phi_f(\epsilon_s, T^\circ)} \quad (2)$$

where  $\epsilon_s^\circ$  is  $\epsilon_s$  at some reference temperature  $T^\circ$ , e.g. 296 K. Data on the temperature dependence of  $\epsilon_s$  were taken from the literature<sup>6,7</sup> and for the  $\epsilon_s$  dependence of  $\Delta\phi_f$  we have used our previous data for indole in methanol-water mixtures.<sup>5</sup> These data cover only the region  $\epsilon_s < 80$ , which limits the temperature region for which the correction could be carried out in water to  $T > 293$  K. For phenol the  $\epsilon_s$  dependence of  $\Delta\phi_f$  is not known so a similar correction cannot be performed for this solute.

As shown in Figure 4 Arrhenius plots of  $\Delta\phi_f^{\text{cor}}$  yield approximately straight lines, although at high temperatures the data deviate noticeably from this trend. The activation

energies  $\Delta E$  that have been calculated from Figure 4 are given in Table I. It can be seen that  $\Delta E$  is the same for H<sub>2</sub>O and D<sub>2</sub>O and that it does not seem to be affected by the presence of 2-propanol.

The value of  $\phi_{e_{\text{aq}}^-}(220 \text{ nm})$  for indole in H<sub>2</sub>O has been determined at two different temperatures. The results, given in Table I, show that  $\phi_{e_{\text{aq}}^-}$  increases by almost a factor of 2 in going from 25 to 65 °C. In comparison  $G(e_{\text{aq}}^- + \text{H})$  in the radiolysis of aqueous solutions increases only by about 4% over the same temperature region.<sup>8</sup> In a previous study,<sup>4</sup> it was found that the number of  $e_{\text{aq}}^-$  scavenged by  $\text{H}_{\text{aq}}^+$  was the same at pH 1 and 3, indicating that all  $e_{\text{aq}}^-$  produced are included in the measured values of  $\phi_{e_{\text{aq}}^-}$ , i.e., that cation-electron recombination is not significant. We note that our quantum yields at 220 nm ( $S_2$  excitation) are less than those at 265 nm ( $S_1$  excitation) recently reported by Bent and Hayon.<sup>9</sup> Since we have also found that the  $S_1$  ionization yield is only about 10% of the  $S_2$  ionization yield<sup>4</sup> there seems to be a considerable discrepancy which we do not understand. It is possible that biphotonic ionization may have been important in Bent and Hayon's experiments.

Arrhenius plots for the decrease of fluorescence intensity at 280 nm vs. temperature for indole and phenol solutions are shown in Figure 5. The activation energy at high temperatures for this fluorescence quenching of indole in H<sub>2</sub>O, D<sub>2</sub>O, and the 2-propanol-water solvents is  $\Delta E = 10.7$  kcal/mol and for phenol in H<sub>2</sub>O is  $\Delta E = 3.6$  kcal/mol. The results for indole are in good agreement with those of Kirby and Steiner.<sup>10</sup>



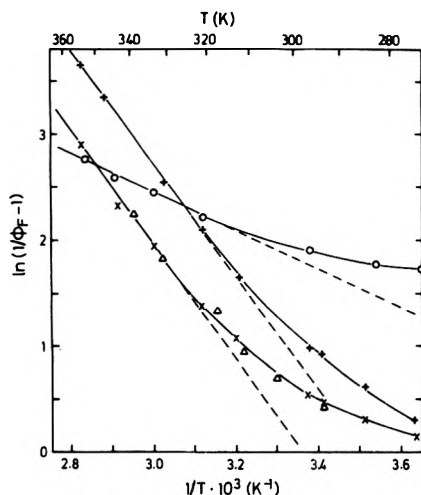


Figure 5. Arrhenius plots of the fluorescence quantum yield of indole and phenol solutions. For identification of the curves see Figure 2.

### Discussion

The present results substantiate our previous conclusion<sup>2,4,5</sup> that ionization from higher excited states of indoles may compete favorably with internal conversion. At elevated temperatures  $\phi_{e_{aq}^-}(220 \text{ nm})$  may exceed 0.2. Hence, the formation of  $e_{aq}^-$ , or at least the first step in this process, takes place within a few picoseconds which is probably the lifetime of the higher excited states. The drop in  $\phi_f$ , which accompanies the photoionization from the higher excited states of indoles, has been observed also for the aromatic amino acids<sup>1</sup> and phenol (Figures 2 and 3). Hence, it appears that ionization from higher excited states takes place with significant yield in a wide variety of molecules.

Other workers<sup>11</sup> have reported that ionization competes effectively with vibrational relaxation to the lowest vibrational level of the S<sub>1</sub> state in  $\beta$ -naphthols. Efficient ionization from higher excited states is also known to occur in  $\text{Mo}(\text{CN})_6^{4-}$  and  $\text{Fe}(\text{CN})_6^{4-}$ .<sup>12,13</sup> However, the photoionization of  $\text{Fe}(\text{CN})_6^{4-}$  is believed to occur at least in part from CTTS states which are formed directly by the absorption of light. This does not seem to be the case for indole. In comparing the absorption spectrum of indole in H<sub>2</sub>O with the spectra observed in various alcohol-water mixtures, where  $\Delta\phi_f$  and hence the yield of photoionization is negligible, we have found that there are no features indicative of direct excitation of a CTTS state in this molecule. The same conclusion was reached for the  $\beta$ -naphthols.<sup>11</sup>

The excitation energy of the S<sub>2</sub> state of indole, from which the ionization occurs, is about 5.3 eV. This is about 2.5 eV below the gas phase ionization potential,<sup>14</sup> and probably at least 1.5 eV below the conduction band in H<sub>2</sub>O.<sup>15</sup> Hence, the electron must be transferred to the solvent without the intermediacy of a quasifree state or a conduction band. The time needed for this transition from aromatic molecules is not known. However, Rentzepis et al.<sup>16</sup> observed that the absorption spectrum of  $e_{aq}^-$ , produced by photoionization of  $\text{Fe}(\text{CN})_6^{4-}$ , is fully developed in about 4 psec.

From our previous studies we came to the conclusion that the formation of  $e_{aq}^-$  from S<sub>2</sub> probably occurs via an intermediate state, i.e., a CTTS state, rather than directly from the S<sub>2</sub> state. A similar mechanism has been suggested for the ionization from the S<sub>1</sub> state of other aromatics.<sup>17,18</sup>

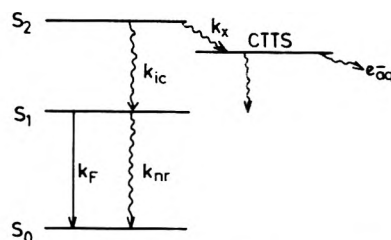


Figure 6. Tentative model for the photoionization from higher excited states of indole in aqueous solution.

The present results seem to support such a mechanism as depicted schematically in Figure 6. Using the designations in this figure,  $\Delta\phi_f$  as defined by eq 1 is

$$\Delta\phi_f = k_x/k_{ic} \quad (3)$$

and also

$$\phi_{e_{aq}^-}(220 \text{ nm}) = p k_x / (k_x + k_{ic}) \quad (4)$$

where  $p$  is the fraction of CTTS states that leads to an observable yield of  $e_{aq}^-$ . If  $p$  is less than unity, ionization must occur via an intermediate state in competition with some relaxation process that does not lead to the fluorescent S<sub>1</sub> state. Alternatively, a value of  $p$  less than unity might be explained by cation-electron recombination, i.e., that not all  $e_{aq}^-$  is detected by the present actinometer. However, since  $\phi_{e_{aq}^-}$  is the same at pH 1 and 3 as noted above, electron-cation recombination appears to be insignificant. The factor  $p$  is given by

$$p = \phi_{e_{aq}^-}(220 \text{ nm})(1 + 1/\Delta\phi_f) \quad (5)$$

The values calculated from the present data on indole in H<sub>2</sub>O (Figure 2 and Table I) are  $p = 0.27$  at  $T = 25^\circ\text{C}$  and  $p = 0.37$  at  $65^\circ\text{C}$ . These values are perhaps 10% too large since the measured values of  $\phi_{e_{aq}^-}(220 \text{ nm})$  also include a small yield of  $e_{aq}^-$  from the S<sub>1</sub> state. In tryptophan, the yield of  $e_{aq}^-$  from S<sub>1</sub> is about 10% of the  $e_{aq}^-$  yield from S<sub>2</sub> at room temperature.<sup>4</sup> Hence, we find that  $p$  is definitely smaller than unity, supporting the involvement of an intermediate state in the ionization process.

The activation energy,  $\Delta E$ , of  $\Delta\phi_f$  is positive indicating that the temperature dependence of  $k_x$  is greater than that of  $k_{ic}$  (see Figure 6). The temperature dependence of the formation of the CTTS state can have several origins. Essentially it should be related to the changes in solvation of the excited solute compared to its ground state. This can involve the static dielectric constant, i.e., the polarizability of the solvent, its dielectric relaxation time, and specific solute-solvent interactions. We have shown previously that  $\phi_f$  depends on the static dielectric constant  $\epsilon_s$ ,<sup>5</sup> but, as shown here, the temperature dependence of  $\epsilon_s$  cannot account for all of the variation of  $\Delta\phi_f$ . We are left with the temperature dependence of  $\Delta\phi_f^{\text{cor}}$  which follows Arrhenius behavior. The dielectric relaxation time  $\tau_r$  of the solvent, H<sub>2</sub>O, does not follow Arrhenius behavior.<sup>19,20</sup> Thus,  $\Delta E$  for  $\tau_r$  varies from 4.2 kcal/mol at  $10^\circ\text{C}$  to  $\Delta E = 3.0$  kcal/mol around  $70^\circ\text{C}$ .<sup>20</sup> These values compare well with those obtained for  $\Delta E$  of  $\phi_f$  of the indole solutions (4.0 and 2.2 kcal/mol), but not with the constant value ( $\Delta E = 1.5$  kcal/mol) found for phenol. Thus, we feel that neither the dielectric constant nor the dielectric relaxation time are the sole factors that are responsible for the temperature dependence of  $\Delta\phi_f$ . It should be kept in mind, however, that both these factors are macroscopic parameters whereas the phenomena-

na we study here depend on the microscopic properties of the medium.

The activation energies for  $\Delta\phi_f$  can also be compared to those for fluorescence quenching of indole derivatives which has been attributed to electron ejection from  $S_1$  by Kirby and Steiner.<sup>10</sup> As seen from Table I, however, the activation energies for fluorescence quenching and for photoionization from  $S_2$  are clearly unrelated, supporting the previous conclusion<sup>2,4</sup> that these processes occur by different mechanisms.

The difference in activation energy of  $\Delta\phi_f$  between indole and phenol in  $H_2O$  suggests the intimate involvement of solute in the temperature dependence of  $\Delta\phi_f$ . Thus, specific solute-solvent interactions are obviously implicated. Within experimental limits there is no difference in the activation energy of  $\Delta\phi_f$  between  $H_2O$  and the  $H_2O$ -2-propanol mixture. This result may suggest that the interaction between the excited solute and water molecules dominates in the formation of the CTTS state, whereas the alcohol largely diminishes the number of  $H_2O$  molecules surrounding the solute and thereby effects the observed reduction of  $\Delta\phi_f$ .

### Conclusions

This work and previous work indicate that for indole and a number of aromatic molecules, excitation by light into  $S_2$  can result in the production of solvated electrons with high efficiency in solutions of high dielectric constant. These solvated electrons appear to be formed from a CTTS state which can be populated from  $S_2$  at a rate competitive with internal conversion to  $S_1$ . The activation energy for population of the CTTS level appears to depend on the solute;

while the formation of the CTTS state is dependent on the dielectric constant. These results have interesting implications for the photochemistry, and possibly also for the radiolysis of proteins and related compounds.

*Acknowledgment.* This work was supported by NATO research Grant No. 683 and by the U.S. Energy Research and Development Agency under Contract No. E(11-1)-2086.

### References and Notes

- (1) I. Tatischeff and R. Klein, Proceedings of the International Conference on Excited States of Biological Molecules, Lisbon, 1974, in press.
- (2) H. B. Steen, *J. Chem. Phys.*, **61**, 3997 (1974).
- (3) K. Kohler and N. Getoff, *Chem. Phys. Lett.*, **26**, 525 (1974).
- (4) H. B. Steen and M. Kongshaug, Proceedings of the International Conference on Excited States of Biological Molecules, Lisbon, 1974, in press.
- (5) L. Kevan and H. B. Steen, *Chem. Phys. Lett.*, **34**, 184 (1975).
- (6) "Handbook of Chemistry and Physics", 45 ed, The Chemical Rubber Co., Cleveland, Ohio, 1964.
- (7) G. Akerlöf, *J. Am. Chem. Soc.*, **54**, 4125 (1932).
- (8) C. J. Hochanadel and J. A. Ghormley, *Radiat. Res.*, **16**, 653 (1962).
- (9) D. V. Bent and E. Hayon, *J. Am. Chem. Soc.*, **97**, 2612 (1975).
- (10) E. P. Kirby and R. F. Steiner, *J. Phys. Chem.*, **74**, 4480 (1970).
- (11) U. K. Klänig, Ch. R. Goldschmidt, M. Ottolenghi, and G. Stein, *J. Chem. Phys.*, **59**, 1973 (1973).
- (12) G. Stein, *Adv. Chem. Ser.*, **No. 50**, 230 (1965).
- (13) M. Shirom and G. Stein, *J. Chem. Phys.*, **55**, 3372 (1971); M. Shirom and Y. Siderer, *ibid.*, **58**, 1250 (1973).
- (14) I. Fischer-Hjalmars and M. Sundbom, *Acta Chem. Scand.*, **22**, 607 (1968).
- (15) A. Henglein, *Ber. Bunsenges. Phys. Chem.*, **78**, 1078 (1974).
- (16) P. M. Rentzepis, R. P. Jones, and J. Jortner, *J. Chem. Phys.*, **59**, 766 (1973).
- (17) L. I. Grossweiner and H. Joschek, *Adv. Chem. Ser.*, **No. 50**, 279 (1965).
- (18) M. Ottolenghi, *Chem. Phys. Lett.*, **12**, 339 (1971).
- (19) D. Eisenberg and W. Kauzmann, "The Structure and Properties of Water", Oxford University Press, New York, N.Y., 1969.
- (20) J. B. Hasted, *Water: Compr. Treatise*, 1972, **1**, 255-305 (1972).

## Fluorescence Quenching of Indole and Model Micelle Systems<sup>1</sup>

M. R. Eftink and C. A. Ghiron\*

Biochemistry Department, University of Missouri, Columbia, Missouri 65201 (Received July 16, 1975)

Acrylamide quenching of indole fluorescence proceeds via both a dynamic and a static process. The rate constant for the dynamic process has a diffusion limited value of about  $7 \times 10^9 \text{ M}^{-1} \text{ s}^{-1}$ . The static quenching component can be described by the expression  $\exp(V[Q])$  with  $V$  values being about  $2.0 \text{ M}^{-1}$ . The possible physical interpretations of the static parameter,  $V$ , are discussed, particularly as they relate to the local distribution of quencher molecules in ordered systems. To demonstrate the potential utility of acrylamide, along with other quenchers, in providing topographical information about ordered systems, quenching studies are presented for an indole-micelle complex, a crude model for a protein. Both the collisional and static quenching components furnish insight as to the positioning of the indole ring in the micelles. Whereas the action of ionic and hydrophobic quenchers is exaggerated in the micelle study, acrylamide appears to be a perfectly neutral quenching probe.

### Introduction

Fluorescence quenching reactions<sup>2-8</sup> have been recently applied to studies with highly ordered biological macromolecules, such as proteins.<sup>9-13</sup> An important class of fluorophores in proteins are the tryptophan residues, which have indole as their side chain. The position assumed by an in-

dole ring in a globular protein will determine the ease with which its excited state will be deactivated by the bombardment of quencher molecules from the solvent. For this reason, the quenching rate constant should provide a kinetic measurement of the residue's exposure to the solution.

This experimental strategy would hold if the exposure of

a residue were determined solely by the amount of steric shielding provided by the protein. However, any specific interaction between the quencher and the protein will jeopardize this interpretation. For example, if the quencher used in this type of study carries a charge, which is almost always the case,<sup>11,12</sup> electrostatic effects may have a dominating influence on the rate of quenching.<sup>14</sup> It is obvious that in order to obtain an unambiguous evaluation of the exposure of a tryptophan in a protein, an uncharged quencher, which has no tendency to bind to the protein in any particular fashion, must be used.

In our laboratory, we have found acrylamide to be a very useful quenching probe for topological studies with proteins.<sup>9,13</sup> In this communication, we will examine the fundamental aspects of the acrylamide quenching reaction in order to lay a foundation for its use as a probing technique. Some physicochemical studies of the reaction will be presented, along with a discussion of the manner in which the data may be analyzed, emphasizing the more practical interpretations of the kinetic process. The attributes of some other quenching agents will be considered for comparison with acrylamide. Finally, an example of the type of structural information that can be gained by quenching experiments involving acrylamide, as well as other quenchers, will be exhibited by studies with a model micelle system.

### Experimental Section

**Materials.** The following commercially obtained chemicals were recrystallized in the solvents mentioned in parentheses before use: acrylamide (ethyl acetate), indole (hexane, twice), 5-methoxyindole (cyclohexane), pyrene (ethanol, twice), naphthalene (ethanol), sodium dodecyl sulfate (ethanol), and cetyltrimethylammonium bromide (ethanol). 1-Methylindole, which along with 5-methoxyindole, was a generous gift from Dr. R. Lumry, was purified by vacuum distillation. Optical grade CsCl was obtained from Schwarz Bioresearch Inc., and  $\text{EuCl}_3$  from Apache Chemicals Inc. The solvents, glycerol and dioxane, were spectroquality from Matheson Coleman and Bell, and the ethanol was absolute. Ultrapure urea and guanidine-HCl (GuHCl) were Schwartz-Mann products. All other chromophores, quenchers, and salts were obtained commercially and used without further purification. Water was distilled.

**Methods.** Fluorescence intensity measurements at ambient temperatures were made on a Farrand Mark I spectrofluorometer, equipped with a magnetic stabilizer for the xenon arc light source. Bandwidths of 5 nm were routinely used. For temperature-dependence studies, a Perkin-Elmer MPS-3 spectrofluorometer, equipped with temperature controls, was used. A YSI Tele-thermometer was employed to measure the temperature in the cuvettes immediately after fluorescence measurements. For both of these instruments, the lamp intensity was found to be extremely stable over the time course of the quenching experiments. In every study reported involving an indole derivative, the shape and position of the emission spectrum were not noticeably altered by the addition of quencher. The intensity at the emission maxima was, therefore, monitored in the quenching studies.

The quenching experiments were performed by using a couple of different routines, both giving the same results. In one, the fluorescence of a series of samples, containing a constant amount of fluorescent compound and a graduated amount of quencher, was measured. However, it was found more convenient to simply add small aliquots (i.e., 1–10  $\mu\text{l}$ )

of a very concentrated quencher solution to about 2.5 ml of a single sample solution in a fluorimetric cuvet, having an optical density of 0.1 or less at the excitation wavelength. After each addition, the solution was gently agitated by inversion and the fluorescence intensity measured. With this procedure, which permits an experiment to be performed in about 15 min, a high degree of precision may be obtained. Errors due to serial sample preparation, transferring of solutions, and instrumental drift can be minimized. Corrections for the dilution of the fluorescent material were made when necessary. The concentrated quencher solutions were, for example, 8 M acrylamide, 5 M NaI (containing  $\sim 10^{-4}$  M  $\text{Na}_2\text{S}_2\text{O}_3$  to prevent  $\text{I}_3^-$  formation) or 10.4 M trichloroethanol (pure liquid). With ionic quenchers, the Job method<sup>15</sup> was often used in order to maintain a constant ionic strength with NaCl.

Certain of the quenchers, acrylamide and  $\text{EuCl}_3$ , absorb light at the excitation wavelength, and a correction factor,  $\text{antilog } \Delta\text{OD}/2$ , was applied for the attenuation of the incident light<sup>16</sup> (where  $\Delta\text{OD}$  is the incremental increase in the optical density at the excitation wavelength as quencher is added, and 0.5 cm is the effective path length of the cell).

In water, acrylamide has a molar extinction coefficient of about 0.23 at 295 nm, the  $\lambda$  chosen to excite the indole derivatives, and is transparent at longer  $\lambda$  where the emission is observed. In this study the correction factor required for acrylamide was at most about 10% and normally much less. Acrylamide quenching studies with tryptophan performed at an excitation  $\lambda$  of 280 nm, where the screening factor is a factor of 10 greater, agree with those at 295 nm, indicating that the screening factor is a minor complication that is adequately dealt with. However, in nonpolar solvents, such as dioxane, the absorption by acrylamide at 295 nm is much greater, and the correction factors become very weighty, thus limiting the studies in these solvents. For  $\text{Eu}^{3+}$ , the screening factor is about the same magnitude as that for acrylamide.

Fluorescence lifetime measurements were performed as described previously<sup>13</sup> on an instrument resembling the Model 9200 nanosecond fluorescence spectrometer (ORTEC) constructed by S. Stevens and J. W. Longworth. The lifetime measurements were well described by a single exponential decay, even when quencher was present.

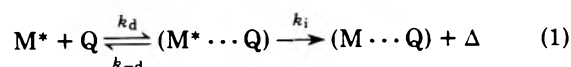
For those indole derivatives for which lifetimes were not directly measured, they were either taken from the literature, or estimated based on the proportionality between the fluorescence yield and lifetime<sup>17</sup> (using the yield data of Kirby and Steiner<sup>18</sup> when possible).

The micelle complexes were prepared by stirring and warming a 0.05 M sodium dodecyl sulfate or 0.02 M cetyltrimethylammonium bromide solution with about  $5 \times 10^{-5}$  M of the appropriate indole derivative for about 1 h. These detergent concentrations are well above the critical micelle concentrations.<sup>19</sup> Approximately one out of every ten micelles would have an associated derivative. Also, the viscosity of the micelle solutions was not significantly different from that of water.

Solution viscosities were measured using an Ostwald viscometer and a water bath. Optical densities were measured on a Gilford 240 spectrometer.

### Interpretation of Data

**Stern-Volmer Relationship.** In the quenching reaction between an excited state of a chromophore,  $M^*$ , and a quencher, Q



the encounter complex,  $(M^* \cdots Q)$ , that is formed with a diffusion-controlled rate constant,  $k_d$ , reacts to dissipate the electronic energy by some internal mechanism<sup>6</sup> with rate constant,  $k_i$ . Stern and Volmer derived the following relationship to describe collisional quenching under steady-state conditions:<sup>2,3,20</sup>

$$\Phi_0/\Phi = 1 + K_{sv}[Q] = \tau_0/\tau \quad (2)$$

where  $\Phi_0$  and  $\Phi$ ,  $\tau_0$  and  $\tau$  are the yield and lifetime in the absence and presence of  $Q$ , respectively.  $K_{sv}$  is the collisional quenching constant which is equal to  $k_q\tau_0$ .  $k_q$  is the apparent rate constant for the collisional quenching process given by eq 1, and is equal to  $k_d$  when the efficiency of the quenching reaction,  $\gamma$ , approaches unity (i.e.,  $k_q = \gamma k_d$ ).<sup>2</sup> In cases where the efficiency of the reaction is less than one, every encounter between  $Q$  and  $M^*$  does not result in quenching and  $k_q$  is approximately equal to  $k_d k_i / k_{-d}$ .<sup>21</sup>

**Positive Deviations-Static Quenching.** The data presented in Figures 1, 2, 4, and 6 are Stern-Volmer plots obtained for a variety of systems by fluorescence intensity ( $F$ ) measurements. As can be seen, the plots are often curved upwards in a fashion similar to those found in many other detailed quenching studies.<sup>4,22-26</sup> This type of deviation from the expected linear plot can be explained by the fact that only a certain fraction of the excited states is actually quenched by the collisional mechanism as described by Stern and Volmer.<sup>3</sup> Some of the excited states are deactivated almost instantaneously after being formed because a quencher molecule happens to be randomly positioned in their proximity at the time they are excited. A number of models can be employed to describe this instantaneous, or static, quenching process, all leading to the following modified form of the Stern-Volmer equation:

$$\frac{F_0}{F e^{V[Q]}} = 1 + K_{sv}[Q] = \frac{\tau_0}{\tau} \quad (3)$$

where  $V$  is the static quenching constant. Three models, and the significance of  $V$  in each, will be briefly presented.

**Transient Effects Model.** The complete Smoluchowski equation for diffusion-controlled reactions contains an often neglected transient term<sup>27</sup>

$$k_d = 4\pi N'RD + 4R^2(\pi D)^{1/2}t^{-1/2} \quad (4)$$

= (steady state rate parameter) + (transient term)

where  $N'$  is Avogadro's number per millimole,  $R$  is the encounter distance between the reactants,  $D$  is the sum of the individual diffusion coefficients of the reactants, and  $t$  is time. Retention of the latter term leads to an additional factor in the Stern-Volmer equation, which, according to Weller<sup>3</sup> is approximately equal to  $\exp(V[Q])$ .

**Sphere of Action.** Frank and Vavilov<sup>28</sup> have suggested that instantaneous quenching results at those instances in a randomly distributed system that a quencher molecule happens to reside within a "sphere of action" of volume  $V/N' (= 4\pi r^3/3)$  and radius  $r$  surrounding a fluorophor at the time of excitation.

**Dark Complex Model.** In the model of Boaz and Rollefson,<sup>22</sup> instantaneous quenching follows the excitation of the ground state encounter complex,  $(M \cdots Q_n)$ .<sup>29</sup> The nature of this complex is defined such that no specific physical contact is required; the quencher(s) need only be close

to (but not necessarily in contact with) the potential fluorophor. The association constant for such a weak complex is  $V$  ( $\approx k_d/k_{-d}$  if the quencher is uncharged).

The transient effects model is undoubtedly the more rigorous treatment for explaining this type of anomalous quenching, which is often referred to as being "static" (that is, viscosity independent, no lifetime drop<sup>30</sup>). Strictly speaking, if the quenching is truly a manifestation of the time dependent term in the Smoluchowski equation, it is actually a dynamic, rather than a static process. However, the work of Nemzek and Ware<sup>24</sup> indicates that the positive deviations in the Stern-Volmer plots cannot be completely described by the transient effects model, and that true static quenching, due to the existence of dark contact pairs of reactants, must also be occurring. On the other hand, a more qualitative treatment of the data in terms of the latter two models should still remain successful. The active volume and dark complex models are so loosely defined that instantaneous quenching resulting from both transient and contact phenomena are included by the expression  $\exp(V[Q])$ . These models also offer conceptual advantages by assigning a molecular significance to the static parameter,  $V$ . The experiments presented later in this paper with micelle complexes are designed to illustrate the ways in which  $V$  can provide information concerning the local distribution of quencher molecules around a fluorophor.

## Results and Discussion

**Acrylamide Quenching of Indole Derivatives.** Presented in Figure 1 are the results, plotted in Stern-Volmer fashion (eq 2), of acrylamide quenching studies of indole and *N*-acetyltryptophanamide (NATA) in water. The amount of fluorescence observed in the presence of quencher was not time dependent, indicating that permanent photochemistry is not involved, to any great extent, in the quenching process. No fluorescence from an indole-acrylamide excited state complex was observed. Also, no evidence for a ground state complex was found from the absorption spectrum.

It is apparent, in Figure 1, that the ratio of  $F_0/F$  gives an upward curving plot. By treating the data according to eq 3, by plotting  $F_0/F \exp(V[Q])$  vs.  $[Q]$  for varying  $V$  until a linear plot is obtained, the static and collisional quenching modes can be dissected. For acrylamide quenching of indole and NATA we find, respectively,  $K_{sv} = 30.5 \text{ M}^{-1}$ ,  $V = 2.5 \text{ M}^{-1}$ , and  $K_{sv} = 17.5 \text{ M}^{-1}$ ,  $V = 2.0 \text{ M}^{-1}$ .<sup>32</sup> In similar fashion, the quenching parameters for other indole derivatives are listed in Table I. The estimated limits of error for the assigned values of  $V$  are  $\pm 25\%$ ; this leads to a variability in the resulting  $K_{sv}$  of only about  $\pm 10\%$ . Whereas the  $V$  values are all about the same for the series ( $1.5\text{--}3.0 \text{ M}^{-1}$ ), the  $K_{sv}$  values show a large variation and are proportional to the fluorescence lifetime of the derivative. The collisional rate constant for quenching, which is  $K_{sv}/\tau_0$ , is approximately  $6\text{--}7 \times 10^9 \text{ M}^{-1} \text{ s}^{-1}$ , being slightly larger for the unsubstituted indole ring and decreasing as the side chain becomes larger and more hydrated.

To demonstrate that the data can be correctly dissected into its collisional and static components by treatment according to eq 3 coincidence of the  $\tau_0/\tau$  and  $F_0/F \exp(V[Q])$  plots for the acrylamide quenching of NATA in 55% glycerol is noted (see Figure 2). In this solvent mixture, the prevalence of the collisional quenching process is diminished due to the increased viscosity. Our analysis yields a  $V$  of  $1.5 \text{ M}^{-1}$  and  $K_{sv}$  of  $5.4 \text{ M}^{-1}$ . Since the  $\tau_0/\tau$  plot reflects only

TABLE I: Acrylamide Quenching of Indole Derivatives in Water at Room Temperature<sup>a</sup>

	$K_{SV}$ , M <sup>-1</sup>	$V$ , M <sup>-1</sup>	$\tau_0$ , ns	$k_q$ , $\times 10^{-9}$ M <sup>-1</sup> s <sup>-1</sup>
Indole	30.5	2.5	4.3	7.1
1-Methylindole	55.5	3.0	8.5 <sup>b</sup>	6.5
2-Methylindole	12.8	2.0	2.0 <sup>b</sup>	6.4
5-Methoxyindole	30.0	3.0	4.0 <sup>c</sup>	7.5
Acetyltryptophanamide	17.5	2.0	2.8	6.3
Acetyltryptophan	26.6	1.5	(4.2) <sup>d</sup>	6.3
Tryptamine	33.0	2.0	(5.5) <sup>d</sup>	6.0
Tryptophan	14.8	1.5	(2.5) <sup>d</sup>	5.9
Tryptophane <sup>e</sup>	14.5	1.5	(2.5) <sup>d</sup>	5.8

<sup>a</sup> Excitation wavelength, 295 nm; emission monitored at fluorescence maxima of sample, which was about 355 nm, except for indole (345 nm) and 5-methoxyindole (333 nm); all  $\tau_0$  are at 25 °C. <sup>b</sup> Lifetimes from ref 31. <sup>c</sup> Lifetime from ref 36. <sup>d</sup> Lifetimes estimated by assuming proportionality to the yield. <sup>e</sup> Excited at 280 nm.

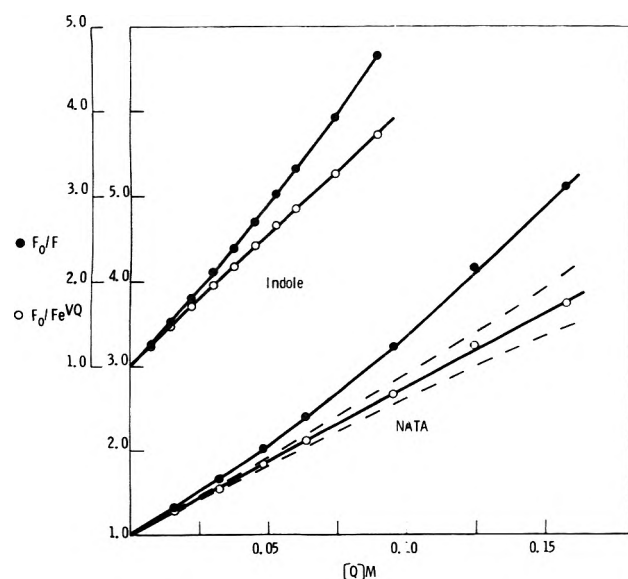


Figure 1. Acrylamide quenching of indole and NATA in water. For NATA the dashed lines are for  $V$  values that are  $\pm 25\%$  of  $2.0 \text{ M}^{-1}$ .

collisional quenching, the agreement between the two plots indicates that  $F_0/F \exp(1.5[Q])$  also truly represents the dynamically quenched fluorescence.

Acrylamide quenching of NATA was also investigated as a function of the solvent composition to determine what factors, if any, influenced the quenching reaction. The effects of ionic strength, the addition of structure "making" and "breaking" solutes,<sup>35</sup> and the addition of common denaturants on the rate constant for quenching,  $k_q$ , as presented in Table II, were found to be easily explained by simply noting the macroscopic viscosity of the solutions. In solvents which are less polar than water, such as dioxane, the quenching reaction seemed to still be quite efficient. This result, along with the fact that the nonexplexed fluorescence of 5-methoxyindole<sup>36</sup> in water is also effectively quenched, indicates that neither the electronic character of the excited state nor the dielectric constant of the medium are dominant factors in the quenching reaction.

In all the studies  $V$  is found to vary only slightly from  $2.0 \text{ M}^{-1}$ . According to the models for static quenching de-

TABLE II: Acrylamide Quenching of NATA in Various Solutions<sup>a</sup>

	$K_{SV}$ , M <sup>-1</sup>	$V$ , M <sup>-1</sup>	$\tau_0$ , ns	$\eta$ , <sup>b</sup> cP	$k_q$ , <sup>c</sup> $\times 10^{-9}$ M <sup>-1</sup> s <sup>-1</sup>
Dioxane <sup>c</sup>	41.0	3.0	4.5 <sup>d</sup>	1.1	9.1
Ethanol <sup>c</sup>	23.5	2.0	3.8 <sup>d</sup>	1.0	6.2
1 M NaCl	16.5	2.0	(2.8) <sup>e</sup>	1.0	5.9
2 M KCl	22.0	2.2	(3.2) <sup>e</sup>	0.85	6.9
2 M MgSO <sub>4</sub>	12.8	2.0	(2.9) <sup>e</sup>	2.5	4.4
7.7 M Urea	14.8	2.0	(4.0) <sup>e</sup>	1.45	3.7
6.7 M GuHCl	9.5	1.75	(2.8) <sup>e</sup>	1.6	3.4
55% Glycerol	5.4	1.5	3.8	5.3	1.4

<sup>a</sup> Excitation wavelength, 295 nm; emission monitored at fluorescence maxima. Quenching measurements made at room temperature,  $\sim 25$  °C. <sup>b</sup> Viscosities measured with an Ostwald viscometer at 25 °C. <sup>c</sup> Fluorophor was indole rather than NATA. <sup>d</sup> Taken from ref 6. <sup>e</sup> Lifetimes estimated by assuming a proportionality to the yield.

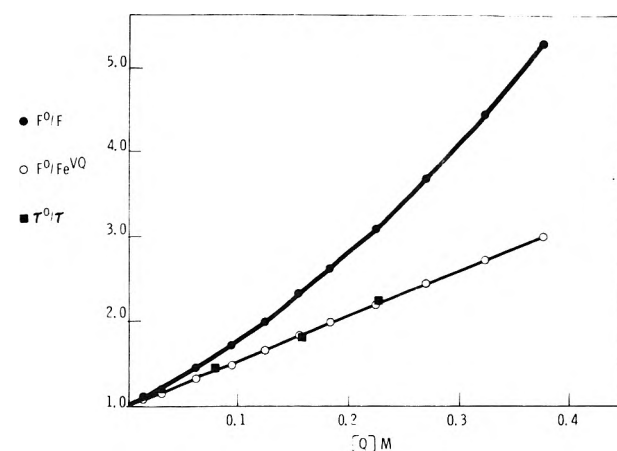


Figure 2. Acrylamide quenching of NATA in 55% glycerol.

scribed,  $V$  can be thought of as an association constant (if so, a very weak one) or as a surrounding volume element having a radius  $r$ . As can be seen in Tables I and II, the magnitude of  $V$  does not depend greatly on whether or not the enamine nitrogen is substituted, or on the dielectric constant, ionic strength, temperature,<sup>33</sup> or composition of the solution. For these reasons, it seems most reasonable in the case of the indole derivatives to discuss the static quenching phenomena in terms of the sphere of action, rather than the dark complex model. From the  $V$  of  $2.5 \text{ M}^{-1}$  for indole we calculate the radius of the active volume to be  $\sim 10 \text{ \AA}$ . This radius is larger than the value of  $6\text{--}7 \text{ \AA}$  which can be estimated for the sum of the molecular radii of the indole ring and acrylamide molecule. This suggests that static quenching can occur even if the quencher is not in physical contact with the fluorophor at the exact moment that it becomes excited. This is apparently due to the fact that the quencher can diffuse those extra  $3\text{--}4 \text{ \AA}$  so rapidly after the excitation of a neighboring indole ring, that the quenching still appears instantaneous. That static quenching may occur even if the quencher is separated from the indole ring by a solvent layer at the time of excitation points to the slight dynamic character predicted by the transient effects model.<sup>24</sup>

For the derivatives possessing side chains, the active volume element,  $V/N'$ , is smaller. (Compare the  $V$ 's for indole

and tryptophan.) This can be attributed to the occupation of the active volume by the side chains, thereby sterically limiting the occasions in which a quencher might randomly exist within the sphere of radius 10 Å. In other words, the size of the active volume is no smaller than that for indole, but the effective concentration of neighboring quenchers is sterically reduced.

**Quenching Efficiency.** A quenching rate constant of  $7.1 \times 10^9 \text{ M}^{-1} \text{ s}^{-1}$  (for indole) agrees favorably with the diffusion limited value of  $7.4 \times 10^9$  that is predicted by the steady-state portion of the Smoluchowski equation (eq 4), when the parameters  $R$  and  $D$  are assigned the reasonable values of 6.5 Å and  $1.5 \times 10^{-5} \text{ cm}^2/\text{s}$  based on the molecular volumes and the Stokes-Einstein relationship. This suggests that the efficiency of the quenching reaction is unity. It is desirable that this be the case, so that the magnitude of  $k_q$  can be interpreted as the frequency of collisional encounter between the two reactants. If  $\gamma$  happens to be less than unity, the expression for  $k_q$  becomes more complicated; in particular, the magnitude of  $k_{-d}$ , which may vary widely for ordered systems, becomes significant.

To further prove that acrylamide is an efficient quencher, studies were performed to show that  $k_q$  behaves as a diffusion-limited rate constant,  $k_d$ . As shown in Figure 3,  $k_q$  has an inverse dependence on  $T/\eta$  of the solution, as expected for a diffusion-controlled reaction.<sup>37</sup> In a temperature dependence study<sup>33</sup> (see Figure 4), the activation energy for  $k_q$  was found to be 3.7 kcal/mol, suggesting that the rate of the reaction is limited only by the diffusion of the reactants through the aqueous solution.<sup>39</sup> Since  $k_q$  behaves as  $k_d$  in these experiments, the argument can be made that the efficiency of the quenching reaction between acrylamide and the fluorescent state of the indole derivatives must approach unity.

**Quenching by Other Agents.** When other agents are employed for the quenching of indole, such as  $\text{I}^-$ ,  $\text{Eu}^{3+}$ , or trichloroethanol (TCE, a water soluble analog of carbon tetrachloride) the Stern-Volmer plots obtained, as in Figure 5, again show positive deviations similar to that for acrylamide. (The data for  $\text{I}^-$  falls almost exactly on the curve for TCE.) Regardless of what the internal mechanism for the respective quenching reactions might be in these cases, a collisional and static process must be operative. With  $\text{H}^+$  as a quencher, the plot obtained shows only a slight amount of static quenching. Similarly, the acrylamide quenching of long-lived fluorescent molecules, such as naphthalene, exhibits no noticeable positive deviations. In actuality, static quenching probably does occur in these situations, but the collisional component is so overwhelming (large  $K_{sv}$ ) that the plots simply appear to be linear. When the viscosity of an indole-containing solution is increased by the addition of glycerol, thus reducing the collisional component, static quenching by  $\text{H}^+$  becomes more obvious. The static constants found to describe the action of all of the above quenchers fall in the range of 1–3  $\text{M}^{-1}$ . Although we have not performed detailed investigations of these quenchers, other workers have proposed that  $\text{I}^-$  and  $\text{Eu}^{3+}$  are efficient indole quenchers,<sup>11,40,41</sup> and by comparison of the Stern-Volmer plots in Figure 5, it seems that TCE is as well.

In contrast to the above cases, for a number of other fluorophore-quencher pairs investigated, upward curving Stern-Volmer plots were not observed. Plots which were linear within experimental error were found for the  $\text{Cs}^+$  or  $\text{Br}^-$  quenching of indole (see Figure 5), TCE quenching of

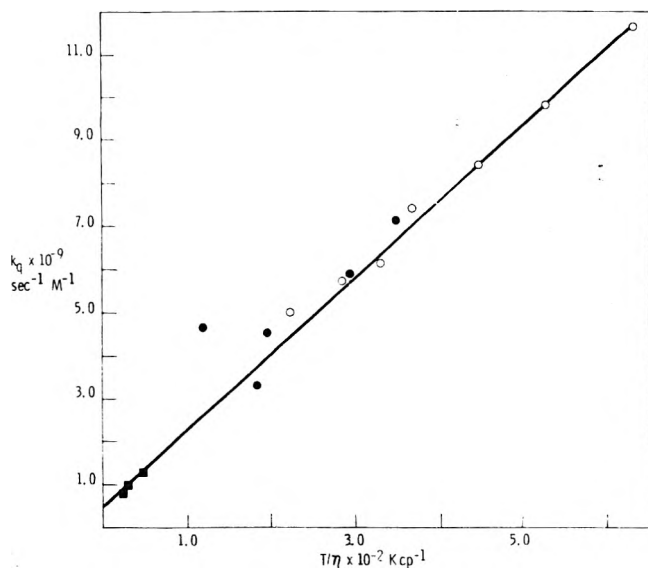


**Figure 3.** Dependence of the rate constant for collisional quenching of NATA on  $T/\eta$ . The data are taken largely from Table II. Aqueous solutions at various temperatures (O); various salt solutions (●); 55% glycerol solutions at various temperatures (■).

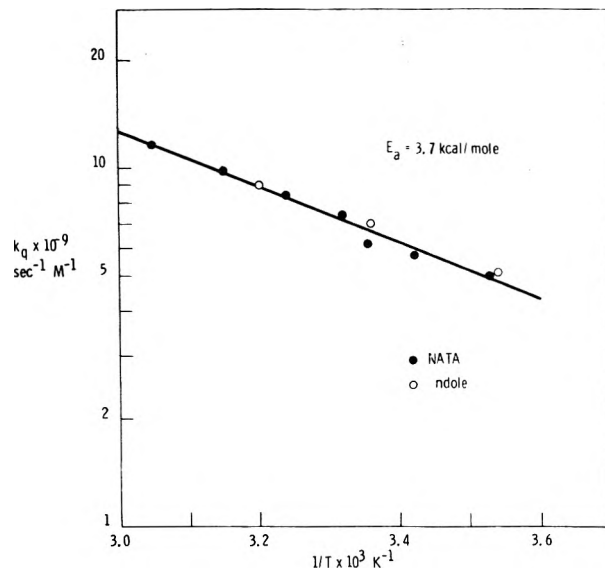


**Figure 4.** Arrhenius plot for the acrylamide quenching of NATA and indole in water.

naphthalene, and acrylamide quenching of pyrene. The positive deviation due to static quenching that is commonly observed in other systems is either absent or masked by an opposing negative deviation in the collisional component. The quenching rate constants found in these systems are much lower than the diffusion-limited value, indicating that the quenching process is inefficient ( $\gamma < 1$ ). Quenching by such agents was found not to be responsive to changes in  $T/\eta$  of the solution. The  $k_q$  for  $\text{Br}^-$  quenching of NATA decreased only from  $2.3 \times 10^8$  to  $2.1 \times 10^8 \text{ M}^{-1} \text{ s}^{-1}$  upon a fivefold increase in viscosity, emphasizing the complexities involved in dealing with inefficient quenchers.<sup>21,38</sup>

**Topographical Studies.** Having laid this foundation for the acrylamide quenching reaction, we intend to utilize it as a probe for studying more complicated systems, such as proteins, as was alluded to in the Introduction. To demonstrate the manner in which quenching studies can be used

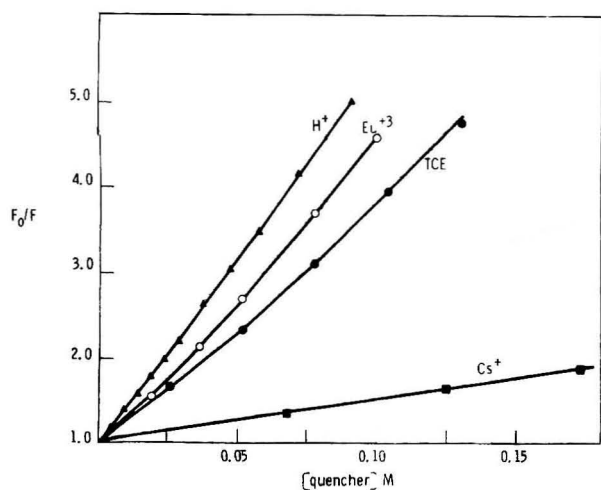


Figure 5. Quenching in indole fluorescence by other agents.

to investigate the arrangement of an ordered system, the indole-micelle work is presented.

Certain indole derivatives will interact with detergent micelles. For example, tryptamine (TAM), a positively charged indole derivative, will interact with the negatively charged micelles formed by sodium dodecyl sulfate (SDS) in aqueous solution.<sup>42</sup> In doing so, the emission maximum of TAM blue shifts from about 355 to 338 nm, and the fluorescence yield drops by approximately 50%. These alterations in the fluorescence of TAM occur approximately at the critical micelle concentration of SDS,<sup>19</sup> suggesting that the interaction is a strong one, as would be expected for the oppositely charged species. (When indole is added to a SDS solution, a blue shift is observed only at a much higher concentration of SDS.) A similar complex is formed between the negatively charged *N*-acetyltryptophan (NAT) and the positively charged detergent cetyltrimethylammonium bromide (CTAB), resulting in a 10-nm blue shift and about a 50% exaltation of the yield.

The micelles formed by these detergents in water are thought to be very loosely defined spheres, having a diameter of about 30 Å, with the charged head groups facing the aqueous solution and the alkyl chains forming an oily, hydrophobic core. The micelle complexes, such as the one between SDS and TAM, are, in many ways, excellent models for proteins. They possess a hydrophobic interior, polar periphery, and a fluorescing "tryptophan residue". However, the positioning, or "exposure" of the fluorophor in these ordered systems is unknown. As shown in Figure 6, the ring may be buried to some extent in the hydrophobic core, or it may be merely jutting out into the aqueous medium. The uncertainty about the topography of the complex makes it an interesting model with which to test the quenchers.

Four different quenchers, including acrylamide, were used with these systems; the results are presented in Figure 7. The experiments with the ionic quenchers,  $I^-$  and  $Cs^+$ , were clearly dominated by electrostatic effects. A TAM molecule associated with a negatively charged SDS micelle is greatly protected from collision with  $I^-$ .<sup>43</sup> On the other hand, association with the micelle "catalyzes"<sup>19,44</sup> the ability of the oppositely charged  $Cs^+$  ion to quench the fluorescence of TAM.

$K_{sv}$  for acrylamide quenching of TAM drops from 33.0  $M^{-1}$  in water to 10.5  $M^{-1}$  in the TAM-SDS complex, with  $V$  remaining approximately the same.<sup>45</sup> This drop reflects a

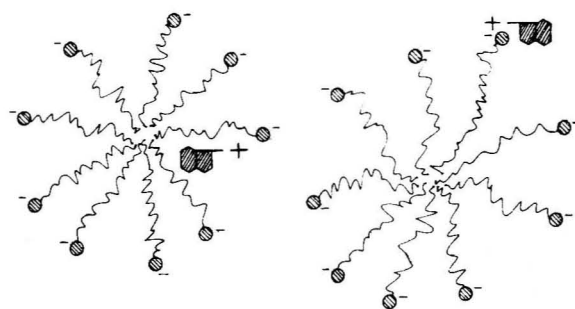


Figure 6. Possible portrayals of the TAM-SDS micelle complex.

~40% decrease in  $k_q$  from about  $6.0 \times 10^9$  to about  $3.7 \times 10^9 M^{-1} s^{-1}$ . A reduction of  $k_q$  of this order would be expected, according to the steady-state portion of the Smoluchowski equation (eq 4), if the fluorophor were anchored to a slowly diffusing structure, such as a micelle. The absence of any further reduction in  $k_q$  indicates that the micelle offers no significant barrier to the diffusion of acrylamide toward the fluorophor. Also, the fact that the static component does not change to any extent, argues that acrylamide has the same opportunity to be a neighbor of TAM in the micelle as it does in pure water.

TCE exhibits a remarkable enhancement in its ability to quench the fluorophor when it is complexed with the micelle. The Stern-Volmer plot is positively curved, and for the TAM-SDS complex our analysis yields  $K_{sv} = 42 M^{-1}$  and  $V = 20 M^{-1}$ .<sup>45</sup> Both of these quenching constants are abnormally high. Due to the peculiarity of these results, an experiment was performed to independently characterize the kinetic nature of TCE quenching of the micelle complexes. This was explored by performing what we have termed a "double quenching" experiment,<sup>46</sup> which confirmed the assignment of the quenching constants made above.

The obvious interpretation for the exalted degree of quenching by TCE lies in the fact that TCE is a hydrophobic molecule and will become partitioned into the relatively apolar core of the micelle. The indole ring in the complexes apparently also samples the micellar interior in such a manner that it sees a very large local concentration of TCE. As a result, the frequency of encounter between the reactants is increased, accounting for the apparent large collisional quenching component.

However, much of the quenching by TCE appears static; in fact, a  $V$  that is a factor of 10 larger than that in water is found. In ordered systems the magnitude of  $V$  can be related to the local distribution of quencher molecules, in terms of the models for static quenching presented earlier. To illustrate the possible ways in which the quencher might be distributed around an indole ring, the models in Figure 8 are presented. The dashed circles represent the active volume for static quenching. In case a the quencher is randomly distributed, just as it would be in an aqueous solution. For this type of situation, we commonly find a static quenching constant of about 2.0  $M^{-1}$  for studies with acrylamide and TCE, corresponding to an active volume of radius 9–10 Å.

When the effective concentration of quencher surrounding the indole is greater than the bulk concentration, as in case b, the static constant,  $V$ , will appear much larger than 2.0  $M^{-1}$ . An example of such a nonrandom distribution is given by the TCE-micelle system. Here the large amount of static quenching is facilitated by the mutual solubiliza-

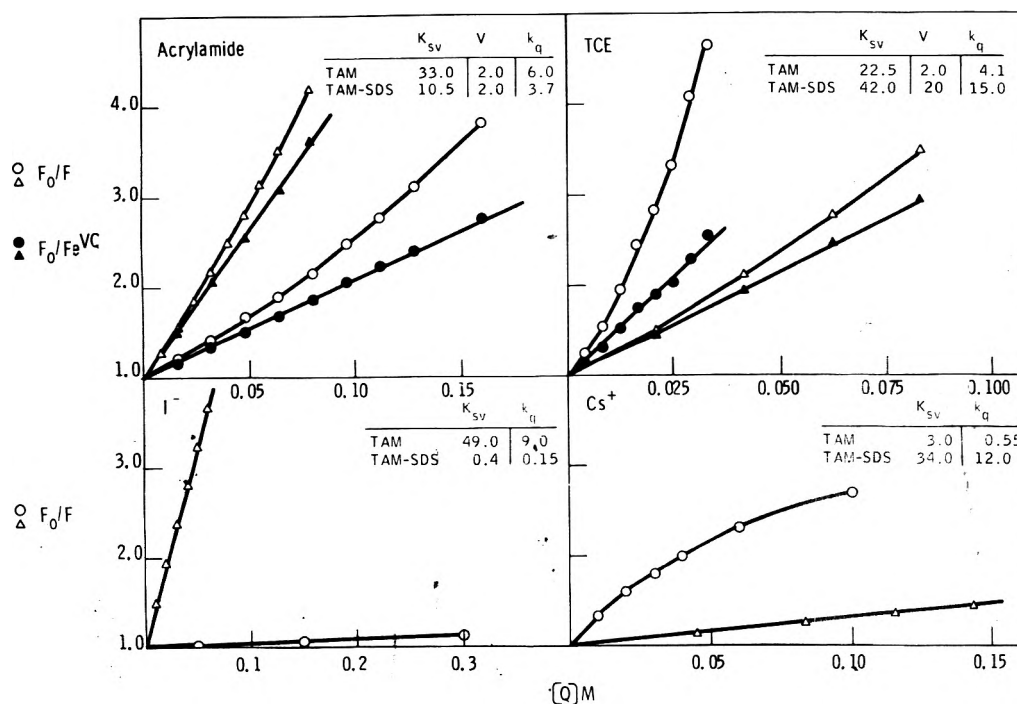


**Figure 7.** Quenching of TAM ( $\Delta$ ,  $\blacktriangle$ ) and TAM-SDS micelle complexes ( $O$ ,  $\bullet$ ). Open symbols represent the normal Stern-Volmer plots; closed symbols, the modified form, eq 3. The lifetime of the TAM-SDS complex was estimated to be about 2.8 ns by considering its relative yield compared to free TAM.  $K_{sv}$  and  $V$  values are  $M^{-1}$ ,  $k_q$ 's are  $\times 10^{-9} M^{-1} s^{-1}$ . For certain of the  $Cs^+$  and  $I^-$  data, the  $K_{sv}$  reported is the initial slope of the plots. For the ionic quenchers, the ionic strength was not held constant.

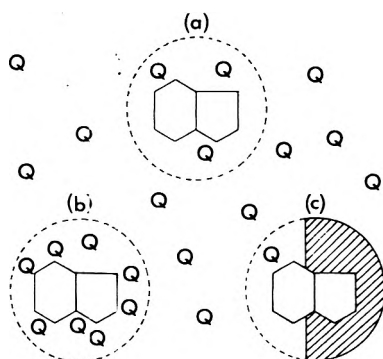


**Figure 8.** Possible distributions of quencher, Q, around an indole ring. The relative concentrations are exaggerated.

tion of TCE and the indole derivative into the micelle. Since the apparent  $V$  found is about  $20 M^{-1}$ , the local concentration of TCE must be about a factor of 10 times that of the bulk. Those TCE molecules within 9–10 Å of the ring would quench it statically, and those located in remote regions of the micelle would quench it collisionally. In situations such as this, where  $V$  is large, it is most convenient to regard it as an association constant (or a partition coefficient) à la the dark complex model.

When part of the active volume is occupied, as in case c, by some groups that are intimately in contact with the indole ring, the effective local concentration of quencher will be reduced. Therefore, we would expect to see a decreased degree of static quenching. As previously pointed out, this might be the case with indole derivatives having bulky side chains. Also we might add that in previous studies on the acrylamide quenching of the single tryptophan in ribonuclease  $T_1$ , we were not able to detect any significant amount of static quenching.<sup>13</sup> This could be an extreme ex-

ample of case c in which the steady-state concentration of quencher within the active volume is very low, presumably because the tryptophan is embedded in the interior of the protein.

A model for the location of the indole derivative in these micelles, which is consistent with the data for all four quenchers, is that the charged moiety of the derivative interacts with the charged Stern layer of the micelle, allowing the ring to penetrate slightly into the hydrophobic core. While the other quenchers clearly point to this model, the experiment with acrylamide provides further insight as to the environment of the indole ring. Acrylamide, unlike TCE, is very insoluble in hydrocarbon solutions, and would not be expected to be accumulated into a micelle. The fact that it quenches the fluorescence of the complexes with a rate constant that is approximately diffusion controlled, and that the amount of static quenching is not sterically reduced argues that the micelles are very loosely ordered near the surface where the indole ring is proposed to lie. Many other recent studies<sup>44,47</sup> have indicated that the interior of a detergent micelle is not nearly as apolar as had once been assumed. Their structures are very weakly defined, and polar molecules, such as acrylamide or water, may readily penetrate them.

## Conclusion

Acrylamide is an efficient, easily handled quencher of indole fluorescence, which operates by both a collisional and static mechanism. According to the models presented, static quenching can be interpreted in a meaningful way in terms of either an active volume element surrounding the fluorophore, or a dark complex between the reactants. The collisional quenching process is diffusion limited, with an activation enthalpy of 3.7 kcal/mol in water.

A model system involving the complex between an indole



derivative and a micelle has been used to test the properties of acrylamide, as well as other agents, as quenching probes for ordered systems. This comparative study highlights the distinguishing characteristics and limitations of each that would need to be considered in studies with systems such as proteins, and it emphasizes the unbiased nature of acrylamide. The action of charged quenchers is greatly influenced by the local charge distribution about the fluorescing group. A hydrophobe, such as TCE and possibly molecular oxygen,<sup>10,44</sup> will have a tendency to be accumulated into apolar regions of a protein or supramolecular structure, and to quench buried fluorophores by a process that may be static, collisional, or a combination of both. Ionic and hydrophobic quenchers may be able to report detailed information about the microenvironment of a fluorophore in an ordered system, but the factors governing their action must be appreciated.

Acrylamide seems to be an ideal type of quencher which is both polar and uncharged. Thus, its ability to collisionally quench fluorescing groups should depend solely on the ease with which it is able to diffuse to meet the excited molecule. Of the quenchers investigated, acrylamide will undoubtedly prove to be the most straightforward and valuable for the study of proteins. However, a cautious use of the others in conjunction with acrylamide would appear to be very promising.

**Acknowledgments.** We wish to express our thanks to Dr. J. W. Longworth, Oak Ridge National Laboratory, Oak Ridge, Tenn., not only for the use of his fluorescence lifetime instrument, but for the help that he and S. Stevens, Oak Ridge National Laboratory, provided in analyzing our lifetime data. We thank Dr. M. Vorbeck and Dr. J. Franz, both of the Department of Biochemistry, University of Missouri, for the use of their spectrofluorometers.

This work was supported by Research Council Grant URC-NSF-1241 from the University of Missouri, Oak Ridge Associated Universities Agreement No. S-1381, and by the Department of Biochemistry and School of Medicine, University of Missouri.

## References and Notes

- (1) This work is presented by M.R.E. in partial fulfillment of the requirements for the Doctor of Philosophy degree at the University of Missouri, Columbia, Mo.
- (2) A. H. Alwattar, M. D. Lumb, and J. B. Birks, "Organic Molecular Photo-physics", Vol. 1, J. B. Birks, Ed., Wiley, New York, N.Y., 1973, pp 403-454.
- (3) A. Weller, *Prog. React. Kinet.*, **1**, 187 (1961).
- (4) W. R. Ware and J. S. Novos, *J. Phys. Chem.*, **70**, 3246 (1966).
- (5) N. Mataga and T. Kubota, "Molecular Interactions and Electronic Spectra", Marcel Dekker, New York, N.Y., 1970, pp 458-484.
- (6) R. F. Steiner and E. P. Kirby, *J. Phys. Chem.*, **73**, 4130 (1969).
- (7) W. R. Ware, D. Watt, and J. D. Holmes, *J. Am. Chem. Soc.*, **96**, 7853 (1974).
- (8) K. H. Grellman, A. F. Watkins, and A. Weller, *J. Phys. Chem.*, **76**, 469 (1972).
- (9) D. Sellers and C. A. Ghiron, *Photochem. Photobiol.*, **18**, 393 (1973).
- (10) J. Lakowicz and G. Weber, *Biochemistry*, **12**, 4171 (1973).
- (11) S. S. Lehrer, *Biochemistry*, **10**, 3254 (1971).
- (12) E. A. Burstein, N. S. Vedenkina, and M. N. Ivkova, *Photochem. Photobiol.*, **18**, 263 (1973).
- (13) M. R. Eftink and C. A. Ghiron, *Proc. Natl. Acad. Sci. U.S.A.*, **72**, 3290 (1975).
- (14) H. J. Pownall and L. C. Smith, *Biochemistry*, **13**, 2594 (1974).
- (15) J. W. Longworth and R. O. Rahn, *Biochim. Biophys. Acta*, **147**, 526 (1967).
- (16) C. A. Parker, "Phosphorescence of Solutions", Elsevier, New York, N.Y., 1968, pp 220-222.
- (17) (a) R. A. Badley and F. W. J. Teale, *J. Mol. Biol.*, **44**, 71 (1969); (b) I. Weinryb and R. F. Steiner, *Biochemistry*, **7**, 2488 (1968); (c) R. W. Ricci, *Photochem. Photobiol.*, **12**, 67 (1970).
- (18) E. P. Kirby and R. F. Steiner, *J. Phys. Chem.*, **74**, 4480 (1970).
- (19) E. J. Fendler and J. H. Fendler, "Advances in Physical Organic Chemistry", Vol. 8, V. Gold, Ed., Academic Press, New York, N.Y., 1970, pp 271-406.
- (20) O. Stern and M. Volmer, *Phys. Z.*, **20**, 183 (1919).
- (21) J. B. Birks, "Photophysics" J. B. Birks, Ed., Wiley-Interscience, New York, N.Y., 1970, pp 433-447.
- (22) H. Boaz and G. K. Rollefson, *J. Am. Chem. Soc.*, **72**, 3435 (1950).
- (23) E. J. Bowen and W. S. Metcalf, *Proc. R. Soc. London, Ser. A*, **206**, 437 (1951).
- (24) T. L. Nemzek, and W. R. Ware, *J. Chem. Phys.*, **62**, 477 (1975).
- (25) E. A. Burstein, *Biofizika*, **13**, 433 (1968).
- (26) C. R. Mullin, M. A. Dillon, and M. Burton, *J. Chem. Phys.*, **40**, 3053 (1964).
- (27) M. V. Smoluchowski, *Z. Phys. Chem.*, **92**, 129 (1917).
- (28) I. M. Frank and S. I. Vavilov, *Z. Phys.*, **69**, 100 (1931).
- (29) Others have simplified this model by assuming that the dark complex has a one to one stoichiometry. See, for example, A. Y. Moon, D. C. Poland, and H. A. Scheraga, *J. Phys. Chem.*, **69**, 2960 (1965); W. M. Vaughn and G. Weber, *Biochemistry*, **9**, 464 (1970). This assumption introduces the factor  $(1 + V[Q])$  into eq 2. This expression is approximately equal to  $\exp(V[Q])$  at small  $V[Q]$ , and will adequately treat most of our data. However, in systems where  $V[Q]$  becomes large, such as is the case for acrylamide quenching of NATA in 55% glycerol,  $(1 + V[Q])$  fails to handle the data (yielding imaginary numbers); the full expression,  $\exp(V[Q])$ , is successful, as seen in Figure 2.
- (30) A. J. Pesce, C. Rosen, and T. L. Pasby, "Fluorescence Spectroscopy", Marcel Dekker, New York, N.Y., 1971, pp 37-63.
- (31) M. S. Walker, T. W. Bednar, and R. Lumry, "Molecular Luminescence", E. C. Lim, Ed., W. A. Benjamin, New York, N.Y., 1969, pp 135-152.
- (32) E. A. Burstein has recently informed us that he has independently determined very similar values for  $k_q$ ,  $V$ , and the activation energy for acrylamide quenching of indole. His work is to be published in *Stud. Biophys.*
- (33) The temperature dependence of the reaction was studied by measuring  $K_{sv}(T)$ ;  $V$  was found to be practically temperature independent. Due to the proportionality of  $\tau_0$  and the yield, knowledge of  $\tau_0$  at one temperature allows one to independently determine  $\tau_0(T)$  by a simple measurement of the temperature dependence of the relative yield.<sup>34</sup> Having  $\tau_0(T)$ ,  $k_q(T)$  may then be solved for.
- (34) (a) M. S. Walker, T. W. Bednar, R. Lumry, and F. Humphries, *Photochem. Photobiol.*, **14**, 147 (1971); (b) J. Eisinger and G. Navon, *J. Chem. Phys.*, **50**, 2069 (1969).
- (35) S. N. Vinogradov and R. H. Linnell, "Hydrogen Bonding", Van Nostrand-Reinhold, New York, N.Y., 1971, pp 198-222.
- (36) M. V. Hershberger and R. W. Lumry, results to be published in *Photochem. Photobiol.*
- (37) In the acrylamide studies, the fact that  $k_q$  at low  $T/\eta$  does not go exactly to zero is most likely another example of the failure of the Stokes-Einstein equation to precisely describe the diffusion of small molecules. See ref 2, 23, and A. Biancneria and G. Kegeles, *J. Am. Chem. Soc.*, **79**, 5908 (1957). When  $k_q T/\eta$  is plotted vs.  $\eta$ , a curve is found that is similar to those compiled by Birks (ref 2) for a variety of diffusional processes.
- (38) W. H. Melhuish and W. S. Metcalf, *J. Chem. Soc.*, 976 (1954).
- (39) R. Fenichel and S. B. Horowitz, *Ann. N. Y. Acad. Sci.*, **125**, 290 (1965).
- (40) R. W. Ricci and K. B. Kilichowski, *J. Phys. Chem.*, **78**, 1953 (1974).
- (41) J. Eisinger and A. A. Lamola, *Biochim. Biophys. Acta*, **240**, 299 (1971).
- (42) D. Namaa, M. A. Katibnikov, and S. U. Konev, *Vestsi Akad. Navuk B. SSR, Ser. Fiz.-Mat. Navuk*, **4**, 93 (1974).
- (43) The  $\Gamma^-$  experiment also provides strong evidence that the TAM molecules are strongly associated with the micelles, since no turnover due to the rapid quenching of a free fraction of fluorophores was detected. See R. A. Badley, *Biochim. Biophys. Acta*, **379**, 517 (1975).
- (44) R. R. Hautala, N. E. Schore and N. J. Turro, *J. Am. Chem. Soc.*, **95**, 5508 (1973).
- (45) Acrylamide and TCE quenching studies with the NAT-CTAB complex were qualitatively similar. However, slightly lower parameters for acrylamide quenching ( $k_q \approx 2.5 \times 10^9 \text{ M}^{-1} \text{ s}^{-1}$ ,  $V \approx 1.0 \text{ M}^{-1}$ ) and an even greater quenching action by TCE were noticed, possibly reflecting some difference in the order of this micelle complex.
- (46) The procedure involves using a secondary collisional quencher (acrylamide in this case) to determine whether or not a primary quencher (TCE) has decreased the lifetime of the remaining fluorescence (that is, if it has quenched statically or collisionally). For a TAM-SDS micelle that had been quenched 65% by  $[TCE] = 0.021 \text{ M}$ , we found only a 48% reduction in the acrylamide  $K_{sv}$ . This is consistent with the quenching constants given above, which predict that at this  $[TCE]$ , 47% of the fluorescence would be collisionally quenched, and the rest statically.
- (47) (a) A. S. Waggoner, O. H. Griffith, and C. R. Christensen, *Proc. Natl. Acad. Sci. U.S.A.*, **57**, 1198 (1967); (b) N. Muller and R. H. Birkhahn, *J. Phys. Chem.*, **71**, 957 (1967); (c) N. Muller and T. W. Johnson, *ibid.*, **73**, 2042 (1969).

## Photodissociation of Electron Acceptor Complexes of Perylene

Peter Hentzschel and A. R. Watkins\*<sup>1</sup>

Max-Planck-Institut für Biophysikalische Chemie, 3400 Göttingen-Nikolausberg, West Germany (Received June 27, 1974)

Publication costs assisted by the Max-Planck-Institut für Biophysikalische Chemie

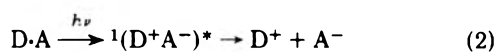
The formation of charge transfer complexes between organic molecules and suitable donor or acceptor molecules in solution is a well-known phenomenon. This paper reports a flash-photolysis study of the photodissociation of such complexes formed between the aromatic hydrocarbon perylene and two strong electron acceptors. Irradiation of these complexes leads to dissociation into the component radical ions; one aim of this work was to determine the quantum yield of this process for the two complexes. Since the complexes exist in equilibrium with the free hydrocarbon and acceptor molecules, the radical ions can also be produced by excitation of a free perylene molecule followed by electron transfer to a free acceptor molecule. The quantum efficiency of this second process was also measured. The results show that the quantum yields for a particular pathway for ion formation change unexpectedly little on going from one complex to the other; the reasons for this are briefly discussed.

### Introduction

It is well known that many organic molecules in the presence of suitable electron donor or acceptor molecules can form weakly bound complexes, usually known as EDA or charge transfer complexes.<sup>2</sup> Such a complex will exist in equilibrium with its component molecules:

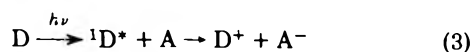


(where D denotes a molecule having electron donor properties and A an electron acceptor molecule) and is characterized by a spectrum commonly having a long-wavelength band not present in the component molecules. This band corresponds to a transition from the ground state of the complex D·A to the highly polar charge transfer state  ${}^1(D^+A^-)^*$ .<sup>2</sup> We were interested in the fact that the state  ${}^1(D^+A^-)^*$ , in a suitable solvent, is able to dissociate into its component radical ions:<sup>3</sup>



This process will occur in competition with other processes leading to the disappearance of this state, chief of which are internal conversion to the ground state and intersystem crossing to the triplet state. Our investigations were aimed at measuring the relative efficiencies of dissociation into ions and internal conversion to the ground state in complexes where no formation of the triplet states of D or A could take place.

A complication in such measurements arises due to the presence of the uncomplexed molecules D and A. Thus, when such a system is irradiated, in addition to ions being formed by dissociation of  ${}^1(D^+A^-)^*$  as described above, excitation of, e.g., a free D molecule to its (fluorescing) first excited singlet state, followed by the appropriate electron transfer reaction with an unexcited A molecule, can also lead to production of radical ions.<sup>4-6</sup>



(The production of triplet states of D and A by this process

can be ruled out by suitable choice of D and A.<sup>7,8</sup>) It was therefore necessary in this work not only to have some measure of the overall efficiency of ion production in such systems, but also to be able to distinguish between those radical ions that are produced by excitation of the charge transfer complex (reaction 2) and those that are produced by excitation of one of the free component molecules (reaction 3).

It would in principle be possible to make such a distinction by measuring the kinetics of the individual steps involved in reactions 2 and 3; the difficulty with this approach is that these steps occur on a time scale which is very fast compared to the time resolution of our flash photolysis apparatus. The free ions themselves, however, have lifetimes ( $\sim 10^{-4}$  s) which are long enough for them to be detected conveniently in a flash photolysis experiment. It is thus feasible to measure the amounts of radical ions formed, and hence their quantum yields of formation, which are ultimately related to the rate constants of the steps involved in the formation process. The contributions to the observed ion yields from complex excitation and excitation of the free molecules can be separated by using the combined results of light intensity dependence and concentration dependence experiments; the details of this procedure are given below.

The complexes chosen for this investigation were those formed between the aromatic hydrocarbon perylene (which functioned as an electron donor) and two strong electron acceptors: pyromellitic dianhydride (PMDA) and tetracyanoethylene (TCNE). (In much of the subsequent discussion the symbols D and A have been used; these can be understood to refer to perylene and PMDA or TCNE, respectively.) PMDA and TCNE have reduction potentials of  $-0.66$  and  $+0.24$  V vs. SCE, respectively; this means that the pairs of ions produced by either reaction 2 or reaction 3 will have energies differing by about 0.9 eV. These energies will, incidentally, be low enough to ensure that no triplet states of D or A are formed. This large difference in energy might be expected to profoundly affect the mechanism by which the ions are formed; the work to be reported here was thus also directed at investigating this aspect of the photodissociation process.

## Experimental Section

**Principle of the Method.** The technique used in this work was flash photolysis with an optical absorption detection system, which has proven to be ideally suited to the study of reactions with relatively long-lived transient species (radical ions, triplet states) as products.<sup>4,6</sup> The experiments described here were performed with cut-off filters to ensure that no free acceptor molecules were excited by the incident flash light. The methods to be described also assume that the complex, in the spectral region in which the flash light was absorbed by the sample, had, to a good approximation, the same absorption spectrum as perylene. This assumption is discussed in more detail below.

As mentioned above, two types of experiment proved to be necessary: one where the overall quantum yield of ion production at a particular acceptor concentration could be measured, and one which gave an estimate of the ratio of the quantum yields from reactions 2 and 3. Measuring the overall quantum yield involved a series of experiments in which the yield of a transient species (triplet state or ion) was studied as a function of the exciting flash intensity, while the measurement of the quantum yield ratio depended on following the variation of ion yield with acceptor concentration. The basic principles of these two types of experiment are as follows.

(a) **Dependence on Flash Intensity.** This method of measuring the overall quantum yield depends on using formation of the triplet state of the aromatic hydrocarbon as an internal actinometer. In other words, if the triplet yield of perylene before adding the electron acceptor is measured, and then subsequently (under the same experimental conditions) the yield of either the perylene radical cation or the acceptor radical anion after the acceptor has been added is determined, the ratio of measured yields can be set equal to the ratio of the quantum yields, making it possible to derive the quantum yield of ion formation from a knowledge of the quantum yield of triplet formation.<sup>6</sup> This presupposes a linear relationship between the measured yield and the quantum yield; this, however, will not be the case unless conditions are chosen such that the transient being measured decays by a first-order process<sup>9</sup>:

$$c = c_0 e^{-k_1 t} \quad (4)$$

where  $c$  is the observed transient concentration at a time  $t$ , and  $k_1$  is the first-order rate constant of the decay process.  $c_0$  is a hypothetical starting concentration, and, in addition to depending linearly on the quantum yield of the process forming the transient, will also depend on the incident light intensity in a linear way for the mechanisms considered here.<sup>9</sup>

The procedure for making such measurements consisted of carrying out pairs of experiments in which perylene was flashed at different incident light intensities, first in the absence of any acceptor molecule and then with acceptor present. In this way two plots of  $c_0$  vs. flash intensity were obtained, one for the perylene triplet and one for the radical ions. The ratio of the slopes of these plots will, if the experimental conditions (including the absorption characteristics of the sample) remain the same, be equal to the ratio of the total quantum yields for transient formation in these two cases. It should be noted that, at high exciting light intensities, the observed dependence of  $c_0$  on flash intensity is no longer linear (see below). The reason for this is that decay by a second-order process (triplet-triplet annihilation

in the case where the transient is the perylene triplet, cation-anion recombination where the transient is an ion) will become increasingly important as the flash intensity, and hence the transient yield, is made larger. In this case the simple proportionality between  $c_0$  and quantum yield no longer holds.<sup>9</sup> The linearity of the dependence of  $c_0$  on incident flash intensity is thus an important criterion of whether the experiments are taking place in a region where transient decay is by purely first-order processes.

(b) **Dependence on Acceptor Concentration.** This type of experiment serves to separate the individual contributions from reactions 2 and 3 to the overall quantum yield of ion formation. It is based on the fact that, since the complex is in equilibrium with its components, a change in acceptor concentration will shift the position of this equilibrium and hence change the relative magnitudes of the ion yield due to excitation of the complex and of free perylene.

To derive an expression for the variation of overall ion yield with acceptor concentration, we define  $P_1$  and  $P_2$  as the efficiency with which the primarily excited species ( $^1D^*$  in (3) and  $^1(D^+A^-)^*$  in (2)) are produced. Thus  $P_1$  corresponds to the number of moles of  $^1D^*$  produced by the flash per mole of D in reaction scheme 3; the quantity  $P_2$  has an analogous meaning for reaction 2. The concentration of free ions produced by subsequent reaction of these primarily excited species will be

$$[D^+]_1 = [A^-]_1 = P_1 \phi_1 [D] \quad (5)$$

for excitation of free perylene, and

$$[D^+]_2 = [A^-]_2 = P_2 \phi_2 [D \cdot A] \quad (6)$$

for excitation of the complex (D·A). Here  $\phi_1$  and  $\phi_2$  are the probabilities of the states  $^1D^*$  and  $^1(D^+A^-)^*$  reacting to give the ions  $D^+$  and  $A^-$ ; the magnitudes of  $\phi_1$  and  $\phi_2$  are naturally dependent on the efficiencies of the individual steps involved in going from the primarily excited species to the ions.

We now make use of the fact that an equilibrium exists, as shown in reaction 1, between the complex and its free components. Assuming that the acceptor concentration  $[A]$  is very much larger than the bulk perylene concentration  $[D]_0$  (the case in all the experiments to be reported here), we obtain

$$\frac{[D^+](1 + K[A])}{[D]_0} = P_1 \phi_1 + P_2 \phi_2 K [A] \quad (7)$$

It is clear that an analogous equation can be derived for  $[A^-]$ .

The derivation to this point has assumed that fluorescence quenching is complete. In fact, this is not the case for the acceptor concentrations used in this work, and a factor  $B$ , equal to the fractional fluorescence quenching, must be introduced into eq 7 to take account of this.  $B$  has values lying, in this investigation, between 0.85 and 1.0; details of the way in which  $B$  is calculated are given below. Equation 7 will be further modified by the fact that optical densities  $E_{D^+}$  are measured instead of concentrations  $[D^+]$ . The result of these changes is

$$\frac{E_{D^+}(1 + K[A])}{B[D]_0} = \epsilon_{D^+} P_1 \phi_1 + \epsilon_{D^+} P_2 \phi_2 K \frac{[A]}{B} \quad (8)$$

Plotting the left-hand side of eq 8 against  $[A]/B$  should give a straight line for which the following relation holds:

$$R = \frac{\phi_1}{\phi_2} = \frac{P_2}{P_1} \frac{\text{intercept}}{\text{slope}} K \quad (9)$$

enabling the ratio  $\phi_1/\phi_2$  to be calculated from a knowledge of  $P_2/P_1$ . The way in which  $P_2/P_1$  is estimated is described below.

This result can be combined with the overall quantum yield (denoted by  $\phi$ ) derived from the dependence of the ion yield on incident flash intensity.  $\phi$  is, of course, the quantum yield of formation of ions from complex excitation and excitation of free perylene, and at a particular acceptor concentration will be given by

$$\phi = (1 - \alpha)\phi_1 + \alpha\phi_2 \quad (10)$$

where  $\alpha$  is the degree of association of the complex. From eq 9 and 10 the following relations for the individual quantum yields can be derived:

$$\phi_1 = \frac{R\phi}{R(1 - \alpha) + \alpha} \quad (11)$$

$$\phi_2 = \frac{\phi}{R(1 - \alpha) + \alpha} \quad (12)$$

**Experimental.** Perylene and acetonitrile were purified as described previously.<sup>6</sup> PMDA was purified by recrystallization from dioxane followed by drying and sublimation in vacuo; TCNE was purified by recrystallizing several times from chlorobenzene and vacuum subliming. All experiments were carried out in acetonitrile at room temperature.

Absorption spectra were measured on a Cary 17 spectrophotometer, and fluorescence spectra on a Hitachi-Perkin-Elmer fluorescence spectrophotometer MPF2A. Fluorescence quenching experiments were carried out in the absence of air either in an all-glass degassed apparatus described previously,<sup>10</sup> or by passing oxygen-free nitrogen through the system during the experiment.

The flash apparatus used in this work has been described previously.<sup>11</sup> The cells used in these experiments had a rectangular cross section  $1 \times 10$  mm;<sup>12</sup> kinetic decay curves were digitalized and fitted (in a computer) by a least-squares procedure to eq 4. All experiments with perylene-acceptor systems were carried out by inserting cut-off filters (Schott GG395) between the flash lamps and the sample in order to prevent direct excitation of the acceptor molecule.

The experimental procedure followed in determining the total quantum yield of radical ion formation was to flash a solution of perylene without acceptor at a number of different flash intensities; this could be achieved by attenuating the incident flash light with wire mesh filters of known transmission. The resulting decay curves for the perylene triplet were fitted to eq 4 and values of  $c_0$ , the hypothetical starting concentration at time zero, were plotted against filter transmission. The experiment was then repeated by admitting a perylene solution of the same concentration containing the appropriate acceptor through a break-seal in the flash cell, after which the radical ion absorption was monitored as a function of flash intensity under identical experimental conditions (same sample geometry, filters, etc.) and analyzed in the same way as for the perylene triplet. This technique has already been applied to other systems.<sup>13</sup>

The concentration dependence experiments were carried out in a cuvet of special design.<sup>14</sup> The experimental procedure used was identical with that used for measuring the flash intensity dependence, except that acceptor concentration and not filter transmission was varied during the course of the experiment. Individual points used in analyzing the data from the flash intensity dependence and con-

centration dependence experiments represent an average of three experimental flash curves at the particular acceptor concentration or wire mesh filter used; the accuracy is generally  $\pm 5\%$ .

## Results and Discussion

(a) **Complex Formation.** Equilibrium constants and extinction coefficients for the two complexes (Pe-PMDA and Pe-TCNE), determined by the Benesi-Hildebrand method,<sup>15</sup> are listed in Table I. The wavelengths at which these determinations were made lie in the region of the charge-transfer absorption bands of these complexes. These bands are not included in Figure 1, which shows the absorption spectra of the two complexes, together with that of uncomplexed perylene. These spectra were obtained by recording the spectrum of an acetonitrile solution of known concentrations of perylene and acceptor, and subtracting the absorption due to the uncomplexed perylene. The extinction coefficient  $\epsilon$  of each complex was then calculated as a function of wavelength using the previously determined value of the equilibrium constant  $K$ .

(b) **Fluorescence Quenching.** The rate of the reaction between uncomplexed perylene, excited to its first excited singlet state, and acceptor, could be obtained by measuring the quenching of perylene fluorescence on addition of acceptor. This measurement is complicated in the present case by the fact that a (nonfluorescent) complex is formed between perylene and the added acceptor. Under these conditions the variation of relative fluorescence intensity  $I/I_0$  with acceptor concentration is given by<sup>16</sup>

$$I_0/I = (1 + K[A])(1 + K_L[A]) \quad (13)$$

where  $K_L$  is the quenching constant, and  $K$  is the equilibrium constant defined in reaction 1.  $K_L$  is related to the overall rate constant  $k$  of the process by

$$K_L = k\tau_0 \quad (14)$$

where  $\tau_0$  is the fluorescence lifetime of perylene in the absence of any quencher. The experiments to be discussed here were carried out at acceptor concentrations such that complex formation did not exceed 10%; in this case eq 13 becomes

$$I_0/I \approx 1 + (K + K_L)[A] \quad (15)$$

The reciprocal relative fluorescence intensity  $I_0/I$  should thus show a linear dependence on acceptor concentration, from which the quantity  $(K + K_L)$  can be obtained. This, together with the values of  $K$  determined as above, allows  $K_L$  to be calculated for each acceptor molecule; these values can be found in Table I.

The values of  $K_L$  obtained here are, when the fluorescence lifetime of perylene is taken into account, suggestive of a diffusion-controlled reaction, as would be expected for these two electron acceptors.<sup>17</sup> The kinetics of such reactions are generally made up of two contributions: one,  $K_L^a$ , from a "nonstationary state" term where a certain proportion of excited molecules find themselves in the immediate vicinity of an acceptor molecule directly after excitation, and the other contribution,  $K_L^s$ , from a "stationary state" term where quencher molecules must diffuse to within an interaction distance  $a$  before quenching can take place.<sup>16</sup> If both effects are allowed for, the variation of fluorescence intensity with acceptor concentration will be given by<sup>16</sup>

$$\frac{I}{I_0} = \frac{e^{-k[A]}}{1 + K_L[A]} \quad (16)$$

TABLE I: Experimentally Determined Parameters for Complex Formation and Fluorescence Quenching (See Text)

	Perylene-PMDA	Perylene-TCNE
$K, M^{-1}$	$30 \pm 16\%$	$43 \pm 12\%$
$\epsilon, cm^{-1} M^{-1}$	900 (490 nm)	800 (480 nm)
$K_L, M^{-1}$	$215 \pm 5\%$	$135 \pm 7\%$
$a, \text{\AA}$	8.2	5.8
$K_L^a, M^{-1}$	27	12
$K_L^s, M^{-1}$	186	123
$k_q, M^{-1} s^{-1}$	$3.1 \times 10^{10}$	$2.1 \times 10^{10}$

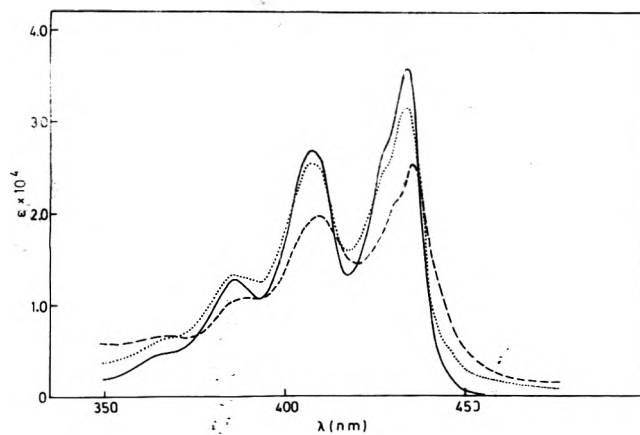


Figure 1. Absorption spectra of perylene and complexes in acetonitrile: (—) perylene; (.....) Pe-TCNE; (- - -) Pe-PMDA. The spectra do not include the charge-transfer transitions to longer wavelengths.

where

$$k' = 4\pi N' a^2 \sqrt{D'\tau} \quad (17)$$

In these equations  $D'$  is the sum of the diffusion coefficients of the two reacting molecules,  $\tau$  is the fluorescence lifetime at the particular acceptor concentration  $[A]$ , and  $N'$  has the value  $6.023 \times 10^{20}$ . At low acceptor concentrations eq 16 can be rearranged to give

$$2a = (D'\tau_0 + K_L/(\tau N' \sqrt{D'\tau}))^{1/2} - \sqrt{D'\tau_0} \quad (18)$$

where  $\tau$  has been replaced by  $\tau_0$  (taken as  $6.0 \text{ ns}^{18}$ ), the fluorescence lifetime in the absence of acceptor. The interaction distance  $a$  can thus be calculated from the measured value of  $K_L$  together with values for  $D'$  and  $\tau_0$ . Unfortunately no direct measurements of the diffusion coefficients in acetonitrile of the molecules used in this work have been made. We have instead relied on the results of Miller et al.<sup>19</sup> for the diffusion coefficients of aromatic hydrocarbons in acetonitrile; on this basis we have set  $D'$  equal to  $5.0 \times 10^{-5} \text{ cm}^2 \text{ s}^{-1}$  for both systems. The values of  $a$  so obtained, together with  $K_L^a$ ,  $K_L^s$ , and  $k_q$ , the rate constant for stationary-state quenching, are shown in Table I.

The  $a$  values of Table I are in the order expected from the molecular sizes of PMDA and TCNE; their absolute values, however, are made somewhat uncertain by the uncertainty in the values of  $D'$  used in eq 18. From these  $a$  values, together with fluorescence lifetimes calculated from

$$\tau = \tau_0/(1 + K_L[A]) \quad (19)$$

values of  $B$  can be calculated from eq 16; these are in turn necessary for the application of eq 8 to the experimental results. The uncertainties in  $a$  will have no very significant effect on the quantity  $B$ . It can also be noted that the

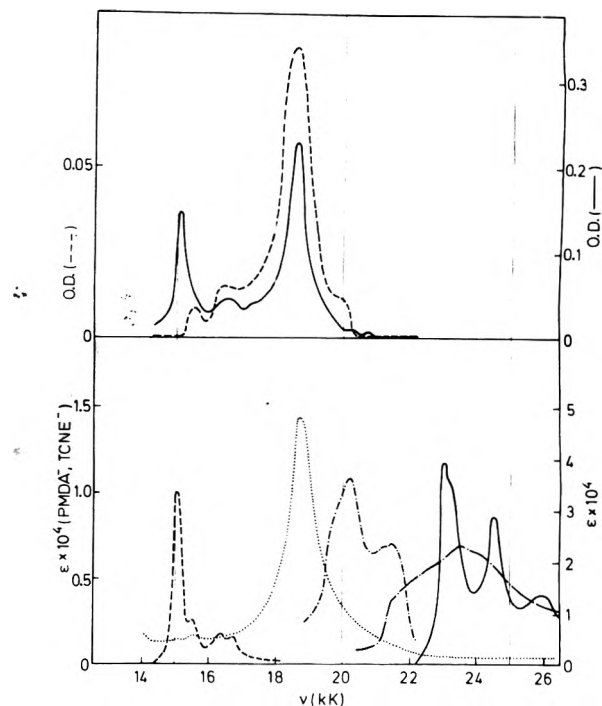


Figure 2. Transient spectra obtained on flashing perylene-acceptor systems in acetonitrile. Upper half: (—) perylene-PMDA; (- - -) perylene-TCNE. Lower half: reference spectra, taken from the literature (—) perylene ground state absorption (ref 20); (- · - ·) TCNE radical anion (ref 33); (.....) perylene triplet (ref 34); (.....) perylene radical cation (ref 20); (- - - -) PMDA radical anion (ref 35).

values of  $k_q$  in Table I are typical for diffusion-controlled reactions in acetonitrile.<sup>17</sup>

(c) *Flash Experiments.* The upper half of Figure 2 shows the transient spectra obtained on flashing the systems perylene-PMDA and perylene-TCNE in acetonitrile. With the aid of the literature spectra contained in the bottom half of this figure it can be seen that the perylene radical cation (peak at 18.6 kK) is formed on flashing both systems. Another characteristic of both systems is that no triplet states, either of perylene or of the acceptor molecules, are present; as has already been mentioned, this is to be expected for systems of this type.<sup>8</sup> The radical anion of PMDA (peak at 15.1 kK) is present in the flash spectrum of perylene-PMDA; the TCNE radical anion cannot be seen in the spectrum of perylene-TCNE, since its weak absorption is masked by the ground state absorption of perylene.

A slowly decaying ( $\sim 5 \text{ s}$ ) structureless absorption (not shown in Figure 2), which could not be further identified, was observed on flashing the system Pe-PMDA. Since this absorption appeared only some milliseconds after the exciting flash, rising to no more than 10% of the absorption due to the initially formed radical ions, it was disregarded in the measurements described below, which were all carried out within the first few hundred microseconds. No effect of this sort was observed on flashing the system Pe-TCNE.

Figures 3 and 4 show the results of the flash light intensity dependence experiments for the two systems studied here. In these figures the triplet and ion yields have been plotted against the percentage transmission of the neutral filters used to attenuate the incident flash light. As expected from the discussion above, the absorption  $E$  rises linearly with increasing filter transmission (increasing flash in-

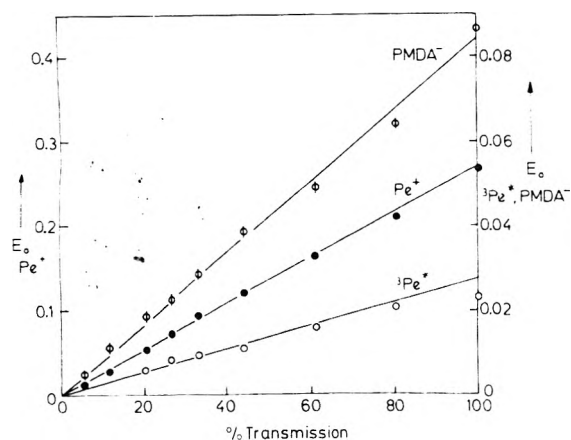


Figure 3. Dependence of triplet and radical ion yields on flash intensity for the system perylene-PMDA.

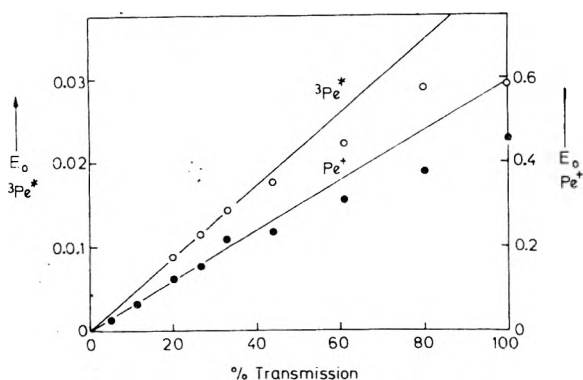


Figure 4. Dependence of triplet and perylene radical cation yields on flash intensity for the system perylene-TCNE.

tensity) until, at relatively high values of filter transmission, departures from linearity become evident for  ${}^3\text{Pe}^*$  in Figure 3 and for  $\text{Pe}^+$  and  ${}^3\text{Pe}^*$  in Figure 4; the slopes of the linear portions will be proportional to the quantum yields. If we designate the slope, extinction coefficient of the transient formed, and its quantum yield of formation as  $S_T$ ,  $\epsilon_T$ ,  $\phi_T$  and  $S$ ,  $\epsilon$ , and  $\phi$ , for the experiments without and with added acceptor, respectively (the subscript T referring to the perylene triplet; no subscript refers to the radical ions), we have

$$\phi = \frac{\epsilon_T S}{\epsilon S_T} \phi_T \quad (20)$$

Unfortunately, no measurements of extinction coefficients and quantum yields for the species in acetonitrile considered here appear to have been made. We have taken  $\epsilon(\text{Pe}^+) = 4.8 \times 10^4 \text{ M}^{-1} \text{ cm}^{-1}$ ,<sup>20</sup>  $\epsilon_T = 1.43 \times 10^4 \text{ M}^{-1} \text{ cm}^{-1}$ ,<sup>21</sup> and  $\phi_T = 0.015$ .<sup>22</sup> The values of  $\phi$  calculated using these values, together with the values of  $\alpha$  for the acceptor concentrations used, are given in Table II.

If it is assumed, for the system  $\text{Pe-PMDA}$ , that equal amounts of  $\text{Pe}^+$  and  $\text{PMDA}^-$  are formed, a value of  $\epsilon$  for  $\text{PMDA}^-$  can be calculated from the appropriate straight line in Figure 3. The value of  $\epsilon$  at 15.1 kK so obtained is  $1.6 \times 10^4 \text{ M}^{-1} \text{ cm}^{-1}$ .

The concentration dependence experiments were carried out as shown above; the application of eq 8 to these results is shown in Figures 5 and 6 for the systems  $\text{Pe-PMDA}$  and  $\text{Pe-TCNE}$ , respectively. In both cases the points follow,

TABLE II: Experimentally Determined Quantum Yields and Rate Constants for Ion Production (See Text)

	Perylene-PMDA	Perylene-TCNE
$\phi$	0.044	0.062
$\alpha$	0.47	0.56
$R$	$4.8 \pm 40\%$	$4.6 \pm 40\%$
$\phi_1$	0.070	0.110
$\phi_2$	0.015	0.024
$k_g$	$5.3 \times 10^{10}$	$3.2 \times 10^{10}$
$\phi_2$	0.21	0.22

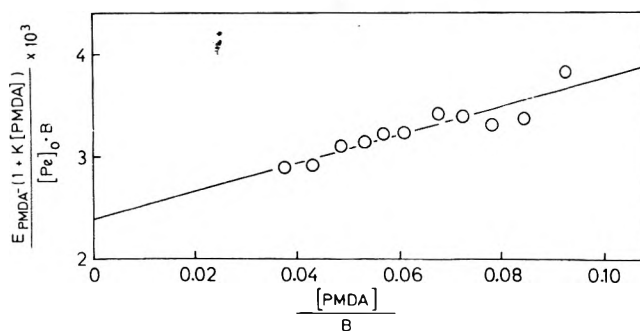


Figure 5. Application of eq 14 (see text) to the variation of PMDA radical anion yield with PMDA concentration for the system perylene-PMDA.

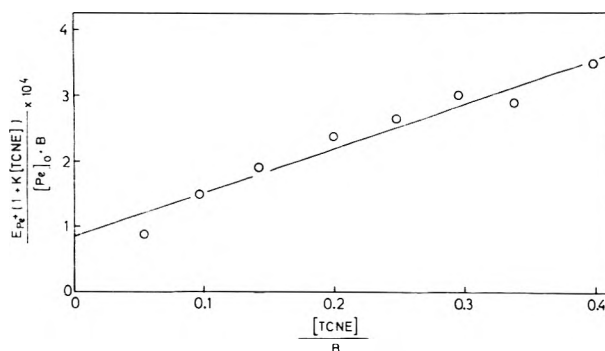


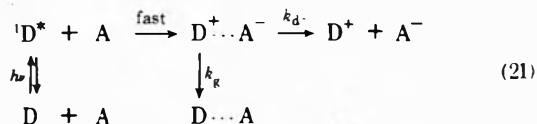
Figure 6. Application of eq 14 (see text) to the variation of perylene radical cation yield with TCNE concentration for the system perylene-TCNE.

within experimental error, a straight line, from which, using eq 9, the quantity  $R$  can be calculated.

In order to do this, it is necessary to be able to measure the ratio  $P_2/P_1$ . Since the flash intensity and other experimental parameters remain constant during the experiment,  $P_2/P_1$  will be equal to the ratio of the integrated absorption spectrum of uncomplexed perylene to that of the charge transfer complex in the wavelength interval used for excitation. This ratio can be estimated from the spectra of Figure 1; since the long-wavelength ( $>460 \text{ nm}$ ) absorption of the charge-transfer complex is 30–40 times weaker than in the region to shorter wavelengths, it has been neglected in this calculation. An implicit assumption in this method is that the spectra corresponding to  $P_1$  and  $P_2$  are similar; that this is justified is seen from Figure 1. From Figure 1 values of  $P_2/P_1$  of 1.00 and 0.91 are obtained for the systems  $\text{Pe-TCNE}$  and  $\text{Pe-PMDA}$ , respectively. The resulting values of  $R$ , and the values of  $\phi_1$  and  $\phi_2$  subsequently calculated from eq 11 and 12, are given in Table II.

It is perhaps simpler, in discussing the quantum yields measured in these experiments, to begin by considering the production of ions by interaction of an excited perylene

molecule with an acceptor molecule in its ground state. This is shown in a simplified way in reaction 3. It is known that this process in fact proceeds, after the initial collision between  ${}^1D^*$  and A, via an ion pair; this ion pair can either dissociate into free ions or return directly to the ground state by a reverse electron transfer.<sup>8</sup> We can therefore rewrite reaction 3 as



All steps in this process occur very quickly; only the free ions  $D^+$  and  $A^-$  can be observed experimentally.

Due to the method used in deriving eq 8 (in particular the inclusion of the factor  $B$  to allow for incomplete quenching of the excited perylene by the added acceptor) the quantum yields  $\phi_1$  refer to the case where each excited perylene molecule is converted to an ion pair with unit efficiency. The measured value of  $\phi_1$  will then be determined by the relative magnitudes of  $k_d$  and  $k_r$ , and we write

$$k_r = k_d(1 - \phi_1)/\phi_1 \quad (22)$$

Knibbe, Rehm, and Weller<sup>5</sup> have estimated  $k_d$  to be  $4 \times 10^9 \text{ s}^{-1}$ ; using this value of  $k_d$ , values of  $k_r$  can be calculated. These are shown in Table II.

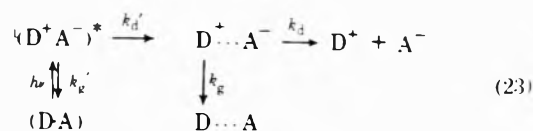
The values of  $\phi_1$  shown in Table II indicate that the ion-pair state which is initially formed disappears with about 90% probability to the ground state in both cases. These results are considerably higher than for other analogous systems in acetonitrile.<sup>8</sup> The fact that the reverse electron transfer step occurs with a rate constant of some  $10^{10} \text{ s}^{-1}$  seems to indicate that the ion pair, although basically a loose associate bound by Coulombic forces, nevertheless has enough overlap of the electron orbitals of the component ions to make electron interchange a very fast process.

It is perhaps useful, in discussing the photodissociation of the charge transfer complexes, to start by considering their spectral properties, since these will determine which electronic states are populated by the initial absorption of light. The part of the complex absorption spectrum that is of interest in the present work is that falling in the wavelength range of the flash; this consists of a perylene-like part (shown in Figure 1) and, to longer wavelengths, a weak, structureless absorption (not shown in Figure 1). The effect of an electric field on the absorption intensity of this long-wavelength band,<sup>24</sup> together with measurements of the dipole moments<sup>25</sup> and absorption spectra<sup>26</sup> of the state reached in this transition, shows that the long-wavelength band of such complexes corresponds to a transition to the charge-transfer state  ${}^1(D^+A^-)^*$ . The perylene-like part corresponds to a transition to a locally excited state  ${}^1(D^*A)$ , which can be regarded as an excited state of perylene perturbed by the presence of the other component of the complex.<sup>23</sup>

It is clear that, although both of these states will be excited under the conditions used in these experiments, ionization can occur only through the state  ${}^1(D^+A^-)^*$ . If we can assume that all initially excited  ${}^1(D^*A)$  decay to the state  ${}^1(D^+A^-)^*$  with unit efficiency, then the quantum yield of ion production will depend on the properties of this state and the route it follows in dissociating to the free ions. This corresponds to the simple sequence of steps shown in reaction 2. It is clear that, in addition to dissociating into ions, the  ${}^1(D^+A^-)^*$  states can return directly to the

ground state; the relative importance of these two pathways for the disappearance of  ${}^1(D^+A^-)^*$  will be one factor determining the observed quantum yield. It is possible, however, that the state  ${}^1(D^+A^-)^*$  dissociates through one or more intermediates; the properties of such intermediates would, in the same way, have an additional effect on the measured ion quantum yield.

A guide to the possible existence of such intermediates is provided by the results of emission measurements on complexes. In nonpolar solvents some charge transfer complexes emit fluorescence; studies of this emission have shown that the state from which fluorescence is emitted is *not* the same as the state initially reached by optical absorption (the charge transfer state  ${}^1(D^+A^-)^*$ ), this latter state appearing to undergo a temperature- and solvent-dependent relaxation before emission takes place.<sup>28</sup> The solvent dependence takes the form of an increase in the Stokes shift of the fluorescence with increase in solvent polarity,<sup>27</sup> indicating that the relaxation process leads to states of lower energy as the dielectric constant of the solvent increases. This suggests that the emitting state is formed from the initially excited state by solvent rearrangement and mutual reorientation of D and A, the latter perhaps including an increase in the mean D-A distance. Both of these effects seem to increase as solvent polarity increases. Although no fluorescence from charge transfer complexes can be observed in solvents as polar as acetonitrile,<sup>29</sup> it might be expected that the same process of relaxation of the initially excited state  ${}^1(D^+A^-)^*$  to a state of lower energy occurs. We can regard this as a relaxation to an ion pair which is the same ion pair as in (21), since this is, from above, an intermediate in the formation of the free ions  $D^+$  and  $A^-$ . We can thus re-formulate the reaction scheme 2 for the photodissociation of these complexes as



The experimentally determined quantum yields  $\phi_2$  for ion formation on irradiation of the complex are given in Table II. From these figures it appears that between 97 and 99% of the initially excited complex molecules return to the ground state before reaching the stage at which the free ions are present. This may be compared with the 90% probability of return to the ground state found for the system tetracyanobenzene-benzene in acetonitrile,<sup>29</sup> where excitation was exclusively to the charge transfer state.

The experimentally measured overall quantum yield for ion production  $\phi_2$  is equal to the product of the probabilities of the steps  ${}^1(D^+A^-)^* \rightarrow D^+ \cdots A^-$  and  $D^+ \cdots A^- \rightarrow D^+ + A^-$ . The second of these quantities has already been measured; it is the  $\phi_1$  of eq 5. If we designate the probability of the first of these two steps as  $\phi_2'$ , then

$$\phi_2' = \phi_2/\phi_1 \quad (24)$$

Values of  $\phi_2'$  calculated in this way are given in Table II.

It would in principle be possible to estimate  $k_r'$  from the values of  $\phi_2'$  obtained here. However, this is more difficult than for the case where uncomplexed excited perylene reacts with an acceptor, since there is no satisfactory way of estimating  $k_d'$ . All that can be said with any certainty about these systems is that  $k_r'$  is larger than  $k_d'$ , by factors of 3.76 and 3.55 for the systems Pe-PMDA and Pe-TCNE,

respectively. There have been suggestions that ionization of charge-transfer complexes proceeds by way of a triplet state<sup>31</sup> or from a Franck-Condon state of the excited complex.<sup>32</sup> Since the evidence for these intermediates is inconclusive, we have depicted ionization as proceeding through the relaxed singlet state  ${}^1(D^+A^-)^*$ . The above conclusions will not be affected in any essential way should one or more other states function as intermediates in the ion formation.

Two assumptions have been made in calculating  $\phi_2'$ . The first is that any higher excited states of the complex decay to the state  ${}^1(D^+A^-)^*$  with unit efficiency, i.e., states such as  ${}^1(D^*A)$  will decay to the ground state only via the charge transfer state  ${}^1(D^+A^-)^*$ . This could be checked by examining the wavelength dependence of  $\phi_2$ . We were not able to do this; however, the similarity between our results and those of other authors<sup>29</sup> who have irradiated exclusively in the charge transfer band suggests that this assumption might be justified. The second assumption postulates that interaction of an excited uncomplexed perylene molecule with an acceptor molecule leads exclusively to the ion pair  $D^+ \cdots A^-$ . There does not appear to be any way of checking this experimentally; it can, however, be justified on the general grounds that dissipation of large amounts of electronic energy without any intermediate stage being involved is an improbable process.<sup>16</sup>

Examination of Table II shows that  $\phi_1$ , which measures the efficiency of the dissociation of  $D^+ \cdots A^-$  in reactions 21 and 23, increases by about 60% on going from perylene-PMDA to perylene-TCNE; the energies of the corresponding ion pairs change from 1.47 to 0.57 eV. The changes in  $\phi_1$  are mirrored in the corresponding decrease in  $k_g$ , the rate at which the reverse electron transfer to give the neutral molecules D and A takes place. The dependence of the rate of electron transfer reactions on the free energy change of the reaction is given approximately by the expression

$$k = Z e^{-(\Delta F^*/RT)} \quad (25)$$

where

$$\Delta F^* \approx \frac{w^p + w}{2} + \frac{\lambda}{4} + \frac{\Delta F^0}{2}$$

and  $Z$  and  $\Delta F^0$  are respectively the frequency factor and free energy change of the electron transfer reaction. The constants  $w^p$ ,  $w$ , and  $\lambda$  are defined in the original paper.<sup>30</sup> While there is insufficient information to be able to calculate absolute values of  $k$ , it is possible to obtain an estimate of the change in  $k$  on going from one system to the other if we assume that  $w^p$ ,  $w$ , and  $\lambda$  are roughly the same for both systems. On this basis we would expect  $k_g$  in reactions 21 and 23 to decrease by a factor of about  $3 \times 10^7$  on going from perylene-PMDA to perylene-TCNE. In fact the experimentally observed decrease (see Table II) is less than a factor of 2, suggesting that the discrepancy between the observed and calculated results is not simply a result of the approximations made in deriving eq 25, but that the model on which this expression is based may not be appropriate to these systems. There appear to be no results in the literature with which these results could be directly compared, and there is an obvious need for more data (in particular

energies and entropies of activation) on such reactions before it will be possible to understand the factors governing the behavior of such electron transfer processes in ion pairs. With regard to the state  ${}^1(D^+A^-)^*$  we can conclude that the near identity of the  $\phi_2'$  values for both systems must mean that  $k_d'$  and  $k_g'$  change by a constant factor or not at all on going from one system to the other. Without additional information it is not possible to obtain absolute values of  $k_d'$  and  $k_g'$ . It is clear, however, that these methods are in principle capable of providing a good deal of new information about the dynamic behavior of the state  ${}^1(D^+A^-)^*$ .

*Acknowledgments.* Thanks are due to Miss U. Heine and Mrs. S. Watkins for assistance with the experimental work, and to Dr. W. Kühnle for purifying the solvent.

## References and Notes

- (1) Address correspondence to this author at the Research School of Chemistry, Australian National University, Canberra, A.C.T. 2600, Australia.
- (2) R. Foster, "Organic Charge-Transfer Complexes", Academic Press, London, 1969.
- (3) Reference 2, p 326.
- (4) H. Leonhardt and A. Weller, *Z. Phys. Chem. (Frankfurt am Main)*, **29**, 227 (1961).
- (5) H. Knibbe, D. Rehm, and A. Weller, *Ber. Bunsenges. Phys. Chem.*, **72**, 257 (1968).
- (6) K. H. Grellmann, A. R. Watkins, and A. Weller, *J. Phys. Chem.*, **76**, 469 (1972).
- (7) M. Ottolenghi, *Acc. Chem. Res.*, **6**, 153 (1973).
- (8) K. H. Grellmann, A. R. Watkins, and A. Weller, *J. Phys. Chem.*, **76**, 3132 (1972).
- (9) A. R. Watkins, *Z. Phys. Chem. (Frankfurt am Main)*, **96**, 125 (1975).
- (10) A. R. Watkins, *J. Phys. Chem.*, **78**, 2555 (1974).
- (11) K. H. Grellmann, A. R. Watkins, and A. Weller, *J. Luminescence*, **1**, 2, 678 (1970).
- (12) K. H. Grellmann and A. R. Watkins, *Chem. Phys. Lett.*, **9**, 439 (1971).
- (13) A. R. Watkins, *J. Phys. Chem.*, **78**, 1885 (1974).
- (14) A. R. Watkins, *Mol. Photochem.*, **6**, 325 (1974).
- (15) H. A. Benesi and J. H. Hildebrand, *J. Am. Chem. Soc.*, **71**, 2703 (1949).
- (16) Th. Förster, "Fluoreszenz Organischer Verbindungen", Vandenhoeck and Ruprecht, Göttingen, 1951, Chapter 10.
- (17) D. Rehm and A. Weller, *Isr. J. Chem.*, **8**, 259 (1970).
- (18) W. R. Ware, *J. Phys. Chem.*, **66**, 455 (1962).
- (19) T. A. Miller, B. Prater, J. K. Lee, and R. N. Adams, *J. Am. Chem. Soc.*, **87**, 121 (1965).
- (20) "UV Atlas of Organic Compounds", Butterworths, London, 1966.
- (21) R. Bensasson and E. J. Land, *Trans. Faraday Soc.*, **67**, 1911 (1971).
- (22) C. A. Parker and T. A. Joyce, *Chem. Commun.*, 108 (1966).
- (23) R. S. Mulliken and W. B. Person, "Molecular Complexes", Wiley-Interscience, New York, N.Y. 1969.
- (24) C. A. G. O. Varma and L. J. Oosterhoff, *Chem. Phys. Lett.*, **9**, 406 (1971); C. J. Eckhardt, *J. Chem. Phys.*, **56**, 3947 (1972).
- (25) J. Czekalla and K. O. Meyer, *Z. Phys. Chem. (Frankfurt am Main)*, **27**, 185 (1961).
- (26) R. Potashnik and M. Ottolenghi, *Chem. Phys. Lett.*, **6**, 525 (1970); H. Masuhara and N. Mataga, *Z. Phys. Chem. (Frankfurt am Main)*, **80**, 113 (1972); N. Tsujino, H. Masuhara, and N. Mataga, *Chem. Phys. Lett.*, **21**, 301 (1973).
- (27) J. Prochorow and R. Siegoczyński, *Chem. Phys. Lett.*, **3**, 635 (1969).
- (28) T. Kobayashi, K. Yoshihara, and S. Nagakura, *Bull. Chem. Soc. Jpn.*, **44**, 2603 (1971); K. Egawa, N. Nakashima, N. Mataga, and C. Yamanka, *ibid.*, **44**, 3287 (1971); *Chem. Phys. Lett.*, **8**, 108 (1971).
- (29) H. Masuhara, M. Shimada, N. Tsujino, and N. Mataga, *Bull. Chem. Soc. Jpn.*, **44**, 3310 (1971).
- (30) R. A. Marcus, *J. Phys. Chem.*, **67**, 853 (1963).
- (31) D. F. Ilten and M. Calvin, *J. Chem. Phys.*, **42**, 3760 (1965); M. Irie, S. Tomimoto, and K. Hayashi, *J. Phys. Chem.*, **76**, 1419 (1972); Y. Achiba, S. Katsumata, and K. Kimura, *Chem. Phys. Lett.*, **13**, 213 (1972).
- (32) M. Shimada, H. Masuhara, and N. Mataga, *Chem. Phys. Lett.*, **15**, 364 (1972).
- (33) W. Liptay, G. Briegleb, and K. Schindler, *Z. Elektrochem.*, **66**, 331 (1961).
- (34) H. Staerk, private communication.
- (35) R. Potashnik and M. Ottolenghi, *Chem. Phys. Lett.*, **6**, 525 (1970).



## Structure of Aqueous Solutions. Relative Intensity Studies of the Infrared Librational Band in Nitrate Solutions

Richard F. Armishaw and David W. James\*

Chemistry Department, University of Queensland, St. Lucia, Queensland 4067, Australia

(Received January 27, 1975; Revised Manuscript Received October 24, 1975)

A method for measuring the relative intensity of water bands in the infrared is described and techniques of allowing for reflection losses are described. The infrared librational bands for solutions of  $\text{LiNO}_3$ ,  $\text{NaNO}_3$ ,  $\text{KNO}_3$ , and  $\text{NH}_4\text{NO}_3$  are reported and variations both with concentration and temperature are examined. The spectra are analyzed to show that the probable hydration number for  $\text{LiNO}_3$ ,  $\text{NaNO}_3$ , and  $\text{KNO}_3$  is 5 while for  $\text{NH}_4\text{NO}_3$  it is 4. There is a noticeable cation dependence for both band energy and band intensity. The intense infrared-active  $\nu_3$  band of the nitrate ion is also examined and the variations noted with concentration and cation change are similar to those observed in the Raman spectrum.

Use of infrared absorption to study the interactions between water and dissolved species has been in the main limited to studies of molecular modes of water and dissolved species or to the overtones of these vibrations. In studying the librational region of the spectrum it is necessary to use very thin path lengths because the absorption is very high. In addition the spectral feature is a very broad band which extends down to the far-infrared region. These features make it difficult to obtain good reproducibility and render physical interpretation more difficult.

This paper reports a thin-film technique for measuring the librational band with excellent reproducibility. The corrections necessary for reflection losses are described, and the results obtained in a systematic study of nitrate salts are discussed.

The librational region is expected to be particularly useful in the description of interactions in solution because the measurements involve cooperative rocking motions of water molecules under the constraint of the surrounding medium. Changes in the water-water or water-solute interactions are therefore expected to be mirrored in changes in the characteristics of the librational bands. A systematic study was undertaken by Raman spectroscopy some years ago,<sup>1</sup> a survey of the effect of electrolytes on the infrared band in  $\text{D}_2\text{O}$  has been reported,<sup>2</sup> and the present results complement these earlier studies.

### Technique of Band Measurement

Following the method developed by Yasumi<sup>3</sup> the real transmittance,  $T_{\text{real}}$ , and real absorbance,  $A_{\text{real}}$ , for an observed transmittance,  $T_{\text{obsd}}$ , are given by

$$T_{\text{real}} = T_{\text{obsd}}/T_{\text{base}}R \quad (1)$$

$$A_{\text{real}} = \log R + \log T_{\text{base}} - \log T_{\text{obsd}} \quad (2)$$

where  $R$  is the correction for reflection losses and  $T_{\text{base}}$  is the baseline transmission of the cell. (An abbreviated derivation of this expression is given as supplementary material.) These expressions were tested using an empty cell with results shown in Figure 1. The transmittance of a single cell window corresponds to  $T_{\text{base}}$ , while the transmittance curve for the empty cell may be used to calculate the cell thickness. Application of expression 1 gave a corrected curve which did not follow the expected  $T_{\text{base}}$  curve. The reflection losses are apparently overcompensated. If the re-

flexion loss correction was reduced from  $R$  to  $\sqrt{R}$ , the corrected curve closely followed the  $T_{\text{base}}$  curve between 1200 and 400  $\text{cm}^{-1}$  as shown in Figure 1. The modified expression was tested using  $n$ -pentane which has no absorption below 1400  $\text{cm}^{-1}$  and again the corrected curve coincided with  $T_{\text{base}}$ . We have therefore used the modified correction expression

$$A_{\text{real}} = \frac{1}{2} \log R - \log (T_{\text{obsd}}) + \log (T_{\text{base}}) \quad (3)$$

in the present study. The failure of expression 1 to describe the spectra obtained could be due to variation in flatness and parallelism of the cell windows and other small changes in the geometry of the cell.

The thin-film cell was constructed using an RIIC cell holder (FH01) fitted with KRS-5 windows. KRS-5 is a suitable window material for the study of aqueous solutions as it has a very low solubility and is transparent down to 200  $\text{cm}^{-1}$ . The plates were polished to an optical flatness of about 3 fringes/cm for visible light. A Teflon spacer ( $\sim 7 \mu$ ) was used to provide the required cell cavity. The inlet and outlet tubes were fitted with Luer ports to allow the cell to be filled from a syringe. The cell was mounted in a thermostatically controlled water jacket and temperature was measured by a fine thermocouple situated within 1 mm of the sample.

Throughout this study the librational band, 1200–250  $\text{cm}^{-1}$ , was recorded on the Perkin-Elmer 457 spectrophotometer. The  $\nu_3(\text{E}')$  nitrate band was recorded on the Perkin-Elmer 225 as this instrument enabled the spectra to be recorded with an expanded wavenumber scale and hence more accurate transmission readings could be taken at 5- $\text{cm}^{-1}$  intervals.

### Determination of the Absorption Spectra of Water and Aqueous Solutions

The reproducibilities of the cell and spectrometer were tested by examining the spectrum of pure water. After temperature equilibration of the cell for 30 min the spectrum of water from 4000 to 250  $\text{cm}^{-1}$  was run a number of times. A new sample of water was introduced for each run. The spectra were found to be reproducible to within 0.2% of the 0–100% transmittance scale. This constancy of the transmittance over a considerable period of time reflects the stability of the cell dimensions, which is essential if quantita-

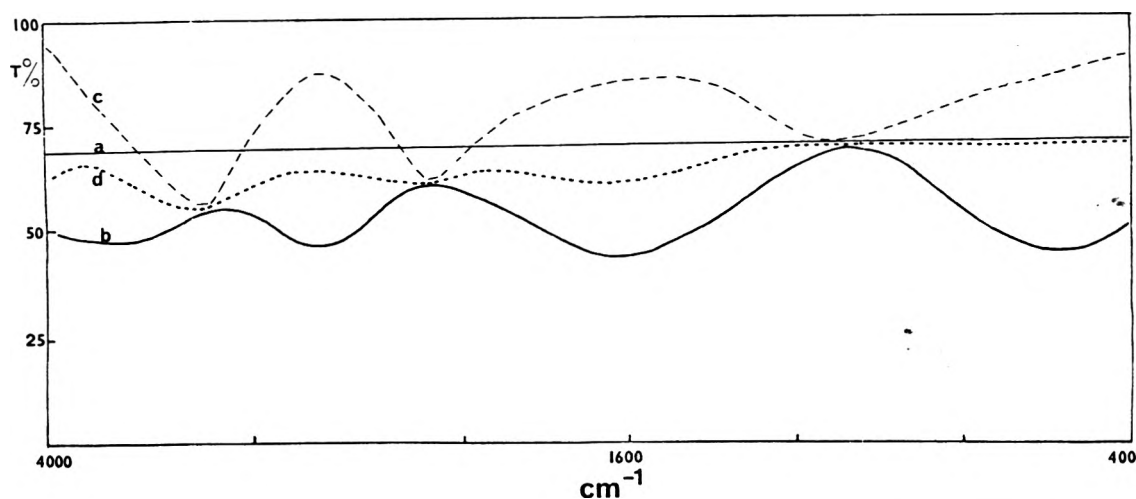


Figure 1. Reflection loss correction tests: (a) transmittance of cell window,  $T_{\text{base}}$ ; (b) transmittance of empty cell,  $T_{\text{obsd}}$ ; (c) transmittance of cell corrected for reflection loss,  $T_{\text{obsd}}/R$ ; (d) transmittance of cell corrected for reflection loss,  $T_{\text{obsd}}/\sqrt{R}$ .

tive measurements are to be made. Representative spectra of water and 6 M sodium nitrate are shown in Figure 2.

During the course of this study, because of the need to dismantle and reassemble the cell, the cell thickness varied up to 10%. The water librational band was adopted as a reference standard which enabled the intensities of spectra obtained from cells of different thicknesses to be compared, quantitatively. Hence all librational band intensities were calculated as a ratio relative to the librational band intensity of pure water. A check was also made during a run on the constancy of the cell thickness, by running a water spectrum after every two or three samples. If the standard water band did not remain constant while all the solutions of one salt were run, the spectra were repeated. The spectra of aqueous solutions were obtained by using a procedure identical with that described for water. Approximately  $\frac{1}{4}$  ml of sample was required to flush the previous sample from the cell, ensuring that the new solution was not contaminated by the old.

All spectra in this study were run with the reference beam attenuated by approximately 10%. This lowered the spectral baseline, effectively expanding the transmittance scale of the recorded spectrum enabling more accurate measurements of transmittance to be made. Such a small attenuation was not considered to reduce the sensitivity significantly at higher absorbance as the band maxima are broad and flat. Because the spectra of solutions were referred to the spectrum of pure water taken under the same conditions, it is not significant that the absolute absorbances are not correct.

The spectra of approximately 30 samples were run before clouding of the plates occurred because of the slight solubility of KRS-5. The cell was dismantled and the plates repolished. The cell thickness was redetermined after each dismantling operation.<sup>4</sup>

#### Refractive Indexes of $\text{H}_2\text{O}$ , $\text{NaNO}_3$ , and $\text{NaClO}_4$ Solutions

The "reflection loss factor",  $R$ , which compensates for the boundary reflections in a thin film can only be determined if the ir refractive indexes of the solution are known. As these refractive indexes are not available in the literature, they were calculated by means of the Kramers-Kronig transform.<sup>5</sup> (This is described in the supplementary material.)

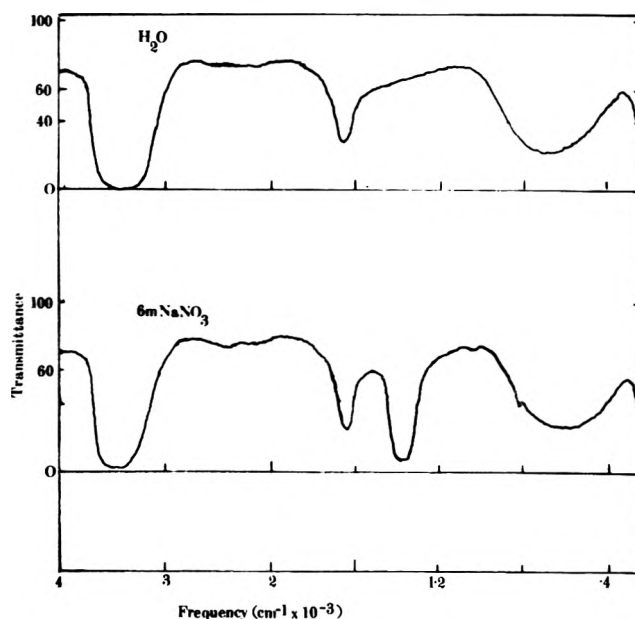


Figure 2. Spectra of water and 6 M  $\text{NaNO}_3$ .

#### Experimental Section and Results

For the spectra of sodium, lithium, potassium, and ammonium nitrate solutions each curve was visually smoothed to compensate for random noise. The two weak nitrate bands  $\nu_1(A_1')$  at  $1048 \text{ cm}^{-1}$  and  $\nu_2(A_2'')$  at  $831 \text{ cm}^{-1}$ , which are superimposed upon the librational band, were very sharp and were readily removed by extrapolation of the librational band. The relative absorbance curves ( $A_{\text{rel}}$ ) for each concentration were calculated. These were then converted to equivalent absorbances (related to the same water concentrations) by the relation  $A_{\text{eq}} = A_{\text{rel}}(55.5/[\text{H}_2\text{O}])$  where  $[\text{H}_2\text{O}]$  is the molar concentration of water. From the area under the  $A_{\text{eq}}$  curves the relative molar intensity,  $I_R$ , the ratio of the solution librational band intensity relative to the water band intensity, was determined. The range of values of  $R$ , the reflection loss factor, is approximately 0.900–0.970 and this causes the relative absorbance and observed absorbance to differ by 3–6%. The ir librational bands at  $30^\circ\text{C}$  of  $\text{H}_2\text{O}$ ,  $\text{NH}_4\text{NO}_3$ , and  $\text{NaNO}_3$  are shown in Figure 3, with the equivalent absorbance plotted against wavenumber.

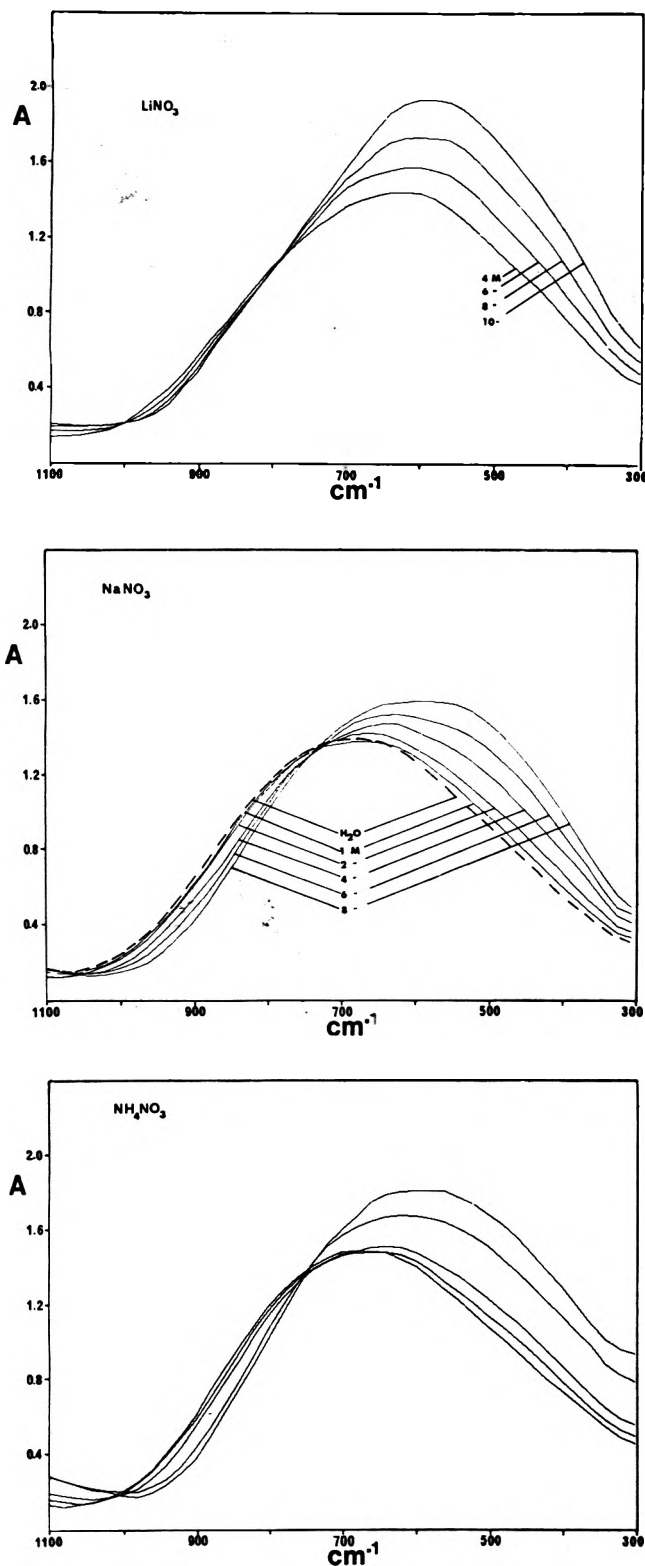


Figure 3. Infrared librational bands at 30°C for H<sub>2</sub>O and solutions of NaNO<sub>3</sub>, LiNO<sub>3</sub>, and NH<sub>4</sub>NO<sub>3</sub>.

The shape and symmetry of each band were investigated by determining the "symmetry axis" of the band which was the line joining the midpoints of isoabsorbance chords of the band. The point at which the symmetry axis cuts the half-height isoabsorbance chord was defined as the band center,  $\nu_C$ . The point at which the symmetry axis cuts the band is taken as the peak maximum frequency,  $\nu_M$ . The

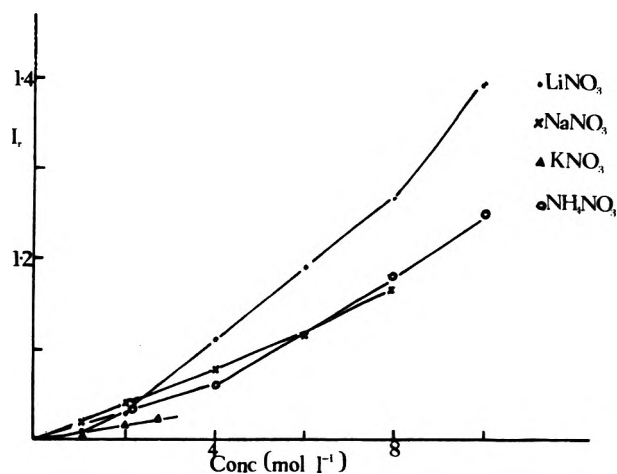


Figure 4. Variation of the relative intensity of the librational band with concentration change.

asymmetry index was then defined as  $\nu_{AS} = \nu_C - \nu_M$ . The greater the asymmetry of the band the greater the magnitude of  $\nu_{AS}$ . The relative molar intensity,  $I_R$ , the peak maximum frequency,  $\nu_M$ , the bandwidth at half-height, and the asymmetry index,  $\nu_{AS}$ , of each band are listed in Table I. The several relative intensities for each solution were averaged and the mean value of  $I_R$  for each sodium, lithium, potassium, and ammonium nitrate solution is plotted against the nitrate concentration in Figure 4.

The effect of adding alkali metal nitrates to water is to shift the bands to lower frequency and to increase the overall intensity. The shifts for NaNO<sub>3</sub> and LiNO<sub>3</sub> are the same within experimental error. An increase in the electrolyte concentration from 0 to 8 M causes an increase in intensity of 27%, 16.5%, and 18% for LiNO<sub>3</sub>, NaNO<sub>3</sub>, and NH<sub>4</sub>NO<sub>3</sub>, respectively. The asymmetry indexes indicate that the bands for NaNO<sub>3</sub> and LiNO<sub>3</sub> solutions become more symmetrical as the concentration is increased. The constant asymmetry indexes of the NH<sub>4</sub>NO<sub>3</sub> librational bands show that almost no change in symmetry occurs as the concentration increases. The plots of the relative intensity against nitrate concentration (Figure 4) are not linear but slightly curved. The intensity is cation dependent with the larger cation producing bands of lower intensity,  $\text{Li}^+ > \text{Na}^+ > \text{NH}_4^+ > \text{K}^+$ . The asymmetric shape of the pure water librational band, (Figure 3) is as observed previously.<sup>1,6</sup> The band frequency  $\nu_M$  agrees closely with the value published by Draeger et al.<sup>6</sup> The band is quite smooth without any sign of unresolved components.

Comparison of figures in Table I, for different runs, shows that the bands determined in this study can be quantitatively compared. The intensities of librational bands determined in this study are reproducible to within  $\pm 2\%$ . Variation of peak frequencies and half-widths which was normally less than  $\pm 10 \text{ cm}^{-1}$  confirms the reproducibility of the techniques.

The librational bands for NaNO<sub>3</sub>, LiNO<sub>3</sub>, and NH<sub>4</sub>NO<sub>3</sub> solutions in Figure 3 show a distinct isosbestic point. This suggests an equilibrium between two or more discrete species each making a distinct contribution to the absorption band.<sup>7</sup> The water involved in direct ion-water interactions, primary hydration (designated type A), is considered to give rise to absorptions which are distinct from those of all other waters including secondary hydration. The water molecules not involved in the primary hydration of an ion

TABLE I: Relative Intensity ( $I_R$ ), Mean Intensity, Peak Maximum Frequency ( $\nu_M$ ), Half-Width, and Asymmetry Index ( $\nu_{as}$ ) of the Librational Bands of  $\text{LiNO}_3$ ,  $\text{NaNO}_3$ ,  $\text{KNO}_3$ , and  $\text{NH}_4\text{NO}_3$  Solutions

Sample	Concn, M	$I_R$	$I_R$ (mean)	$\nu_M$ , $\text{cm}^{-1}$	Half-width, $\text{cm}^{-1}$	$\nu_{as}$ , $\text{cm}^{-1}$
$\text{LiNO}_3$	10	1.392	$1.392 \pm 2\%$	$580 \pm 10$	$453 \pm 10$	+8
	8	1.285		603	462	0
			1.266			
	8	1.246		606	446	-3
	6	1.192	1.192	616	475	0
	4	1.105		635	483	-7
			1.110			
	4	1.115		650	465	-15
	2	1.025	1.025	680	463	-30
	1	1.005	1.005	687	460	-27
$\text{NaNO}_3$	8	1.176	$1.164 \pm 2\%$	595	474	-3
	8	1.152		595	472	-2
	6	1.114	1.114	610	478	-3
	4	1.089		645	488	-30
			1.076			
	4	1.072		640	481	-24
	2	1.040	1.037	662	475	-30
			1.035			
	2	1.035		670	479	-30
1	1.026	1.015	675	470	-35	
		1.015				
$\text{KNO}_3$	1	1.005		695	468	-45
	2.7	1.022	1.022	670	493	-37
	2	1.015	1.015	690	489	-40
	1	0.996	0.996	690	480	-40
$\text{NH}_4\text{NO}_3$	10	1.249	1.249	595	512	-33
	8	1.180	1.180	620	517	-42
	4	1.058	1.058	653	501	-37
	2	1.030	1.030	670	493	-40
	1	1.015	1.015	680	486	-40

are assumed to be spectroscopically identical with water in the pure liquid and this is designated type B. The observed absorption bands are therefore the sum of contributions from "A" and "B" water librations.

Using the technique described elsewhere<sup>4,8</sup> (see supplementary material), the band was separated into components due to type A and type B water; also, the probable hydration numbers were determined. The variation of the relative intensity of the type A bands for nitrate solutions is shown in Figure 5. Up to concentrations of 8 M the relative intensities show a linear variation with a distinct cation-dependence evident. The smaller cations produce the greatest intensity. The "best fit" hydration numbers are 5 for the alkali metal nitrates and 4 for ammonium nitrate.

#### Temperature Effect on Librational Bands

The librational bands of water,  $\text{NaNO}_3$ ,  $\text{LiNO}_3$ ,  $\text{NH}_4\text{NO}_3$ , and  $\text{KNO}_3$  were run at 10, 30, and 50°C. Determination of the cell thickness, at each of the three temperatures, showed that no change had occurred. The quantitative comparison of spectra obtained at different temperatures was thus simplified. The relative integrated intensity of each band was determined as a ratio relative to the water intensity at 10°C ( $I_R^{10}$ ), 30°C ( $I_R^{30}$ ), or 50°C ( $I_R^{50}$ ). The relative intensities, peak frequencies,  $\nu_M$ , and the band half-widths for each temperature are listed in Table II. The librational bands of pure water,  $\text{KNO}_3$ , and  $\text{NaNO}_3$  at 10, 30, and 50°C are plotted in Figure 6.

It is evident that temperature change produces smaller changes in the librational band than the addition of electrolytes. A 40°C temperature increase shifts the bands, at most, 60  $\text{cm}^{-1}$  to lower frequency and produces an increase in  $I_R^{10}$  of as little as 5%. The magnitude of the temperature

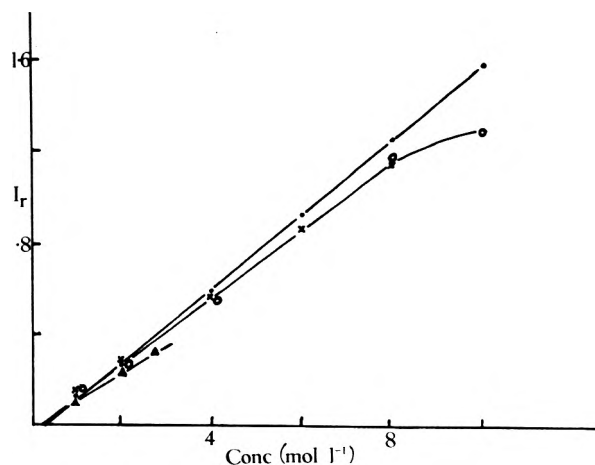


Figure 5. Variation with concentration of the relative intensity of the primary hydration librational band of  $\text{LiNO}_3$ ,  $\text{NaNO}_3$ ,  $\text{KNO}_3$ , and  $\text{NH}_4\text{NO}_3$  (legend as for Figure 4).

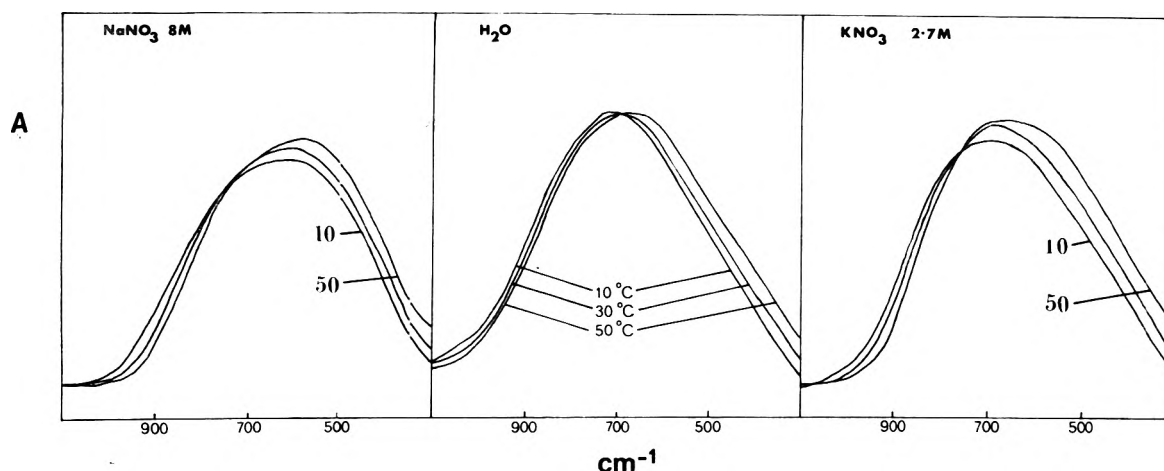
shift appears to be cation dependent with the order of change  $\text{NH}_4^+ > \text{H}_2\text{O} > \text{Na}^+ > \text{Li}^+$ . The band half-width increases slightly for water, 8 M  $\text{NH}_4\text{NO}_3$ , and 2.75 M  $\text{KNO}_3$ , remains unchanged for 8 M  $\text{LiNO}_3$ , and decreases for 8 M  $\text{NaNO}_3$ . Comparison of  $I_R^{10}$ ,  $I_R^{30}$ , and  $I_R^{50}$  shows that they are equal within experimental uncertainty. The water band frequency shift with temperature is approximately  $-0.75 \text{ cm}^{-1}/\text{deg}$  which compares favorably with the value of  $-0.7 \text{ cm}^{-1}/\text{deg}$  determined by Draeger et al.<sup>6</sup>

#### Nitrate Bands

The spectra of  $\text{NaNO}_3$ ,  $\text{LiNO}_3$ , and  $\text{KNO}_3$  solutions were examined. Quantitative spectra were not obtained for

TABLE II: Librational Band Characteristics for Solutions at 10, 30, and 50°C

Sample	Conc, M	10°C			30°C				50°C			
		$I_R^{10}$	$\nu_M$ , $\text{cm}^{-1}$	Half-width, $\text{cm}^{-1}$	$I_R^{10}$	$I_R^{30}$	$\nu_M$ , $\text{cm}^{-1}$	Half-width, $\text{cm}^{-1}$	$I_R^{10}$	$I_R^{50}$	$\nu_M$ , $\text{cm}^{-1}$	Half-width, $\text{cm}^{-1}$
H <sub>2</sub> O		1.000	700	465	1.025		685	470	1.049		660	490
NH <sub>4</sub> NO <sub>3</sub>	1	1.000			1.045	1.020						
	2	0.988			1.045	1.020						
	4	1.050			1.062	1.036						
	8	1.101	640	490	1.144	1.116	610	501	1.140	1.090	580	525
NaNO <sub>3</sub>	1	1.020			1.032	1.008						
	2	1.012			1.033	1.008						
	4	1.066			1.075	1.049						
	8	1.121	590	490	1.170	1.142	585	475	1.176	1.121	560	450
LiNO <sub>3</sub>	1	1.032			1.049	1.024						
	2	1.040			1.064	1.038						
	4	1.105			1.130	1.101						
	8	1.285	600	430	1.302	1.273	600	430	1.392	1.267	585	430
KNO <sub>3</sub>	1	1.000			1.019	0.995						
	2	1.031			1.043	1.018						
	2.75	1.032	675	490	1.053	1.027	670	490	1.102	1.032	654	505

Figure 6. Variation with temperature of the librational band of H<sub>2</sub>O, NaNO<sub>3</sub> (8 M), and KNO<sub>3</sub> (2.7 M).

NH<sub>4</sub>NO<sub>3</sub> solutions because of the interference of the  $\nu_4(\text{F}_2)$  band of NH<sub>4</sub><sup>+</sup>, at 1410  $\text{cm}^{-1}$ . The transmittance from each spectrum was measured at 5- $\text{cm}^{-1}$  intervals. The refractive indexes of NaNO<sub>3</sub> were used for LiNO<sub>3</sub> and KNO<sub>3</sub> solutions as the  $\nu_3(\text{E}')$  bands were similar in shape, half-width, and intensity. It was considered that no significant error was caused by this approximation. The relative absorbance,  $A_{\text{rel}}$ , was determined by a procedure identical with that described for the librational band. This was the sum of contributions from a background water absorbance with the nitrate absorbance superimposed. The nitrate band baseline was found by extrapolating the water absorbance under the band. The residual water absorbance was subtracted from  $A_{\text{rel}}$  leaving the absorbance due to the nitrate ion.

The integrated intensity of the  $\nu_3(\text{E}')$  band was determined as a ratio relative to the intensity of the band for the 4 M NaNO<sub>3</sub> solution. The resulting band profiles are shown in Figure 7 while band characteristics are collected in Table III.

The  $\nu_3(\text{E}')$  nitrate band in each case is obviously not a single band. This can probably be attributed to the lifting of the degeneracy. However, the NaNO<sub>3</sub> band appears to become more symmetric while the LiNO<sub>3</sub> band becomes more widely split with increasing concentration. The posi-

tion of the low-frequency component (1350  $\text{cm}^{-1}$ ) was determined with ease, but the higher frequency component appears as a shoulder with no distinct maximum, making accurate frequency determinations impossible. The peak frequencies for NaNO<sub>3</sub>, KNO<sub>3</sub>, and LiNO<sub>3</sub> are concentration dependent while the frequency of the NH<sub>4</sub>NO<sub>3</sub> band appears unaffected by concentration change. The shift of NaNO<sub>3</sub> and KNO<sub>3</sub> to higher frequency is greater than for LiNO<sub>3</sub>. The LiNO<sub>3</sub> band is shifted 10  $\text{cm}^{-1}$  by a concentration change from 1 to 8 M while the NaNO<sub>3</sub> band is shifted 20  $\text{cm}^{-1}$ . The band half-widths also demonstrate marked cation effects with LiNO<sub>3</sub> again showing distinct behavior from that of NaNO<sub>3</sub> and KNO<sub>3</sub>.

The molar integrated intensity,  $I_M$ , of the total contour (Figure 8) decreases rapidly at concentrations <2 M but tends toward constant value at higher concentrations.  $I_M$  does not appear to be significantly cation dependent.

The shift of the ir  $\nu_3(\text{E}')$  band of NaNO<sub>3</sub> solutions, as concentration increases, to higher frequencies with an accompanied decrease in half-width and visually increased symmetry suggests a decrease in the splitting of the degenerate band. This conclusion is confirmed by the Raman studies of this band which showed<sup>9</sup> that the band could be analyzed into two components and that a small decrease in the band splitting did occur. A shift was observed of the

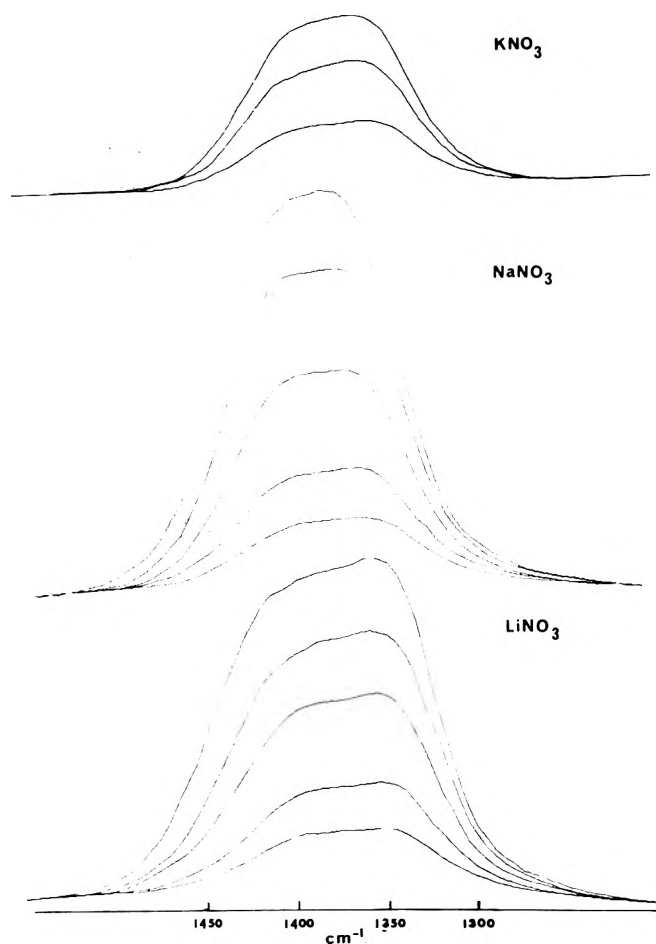


Figure 7. Variation with concentration of  $\nu_3(E')$  of nitrate ion for solutions of  $\text{LiNO}_3$  (1, 2, 4, 6, 8 M),  $\text{NaNO}_3$  (1, 2, 4, 6, 8 M), and  $\text{KNO}_3$  (1, 2, 2.7 M).

low-frequency component from 1348 to 1362  $\text{cm}^{-1}$  which compares closely with the shift of the ir band from 1355 to 1375  $\text{cm}^{-1}$ . For  $\text{LiNO}_3$  solutions the findings are again similar to Raman measurements<sup>9</sup> which show that considerable increase in the band splitting does occur. At 10 M the splitting is 71  $\text{cm}^{-1}$  which approaches the melt value of 110  $\text{cm}^{-1}$ . The shift in the ir band, 1350 to 1360  $\text{cm}^{-1}$ , compared closely with that observed in the low-frequency Raman component, 1348 to 1356  $\text{cm}^{-1}$ . Hence the greater shift of  $\nu_3(E')$  band in  $\text{NaNO}_3$  than in  $\text{LiNO}_3$  is shown in both the Raman and ir studies. However, the Raman data do show that at high concentration a sharp increase occurs in the  $\text{LiNO}_3$  shift bringing it approximately equal to the maximum  $\text{NaNO}_3$  shift.

The  $\nu_1(A_1')$  and the  $\nu_2(A_2'')$  bands were run under conditions of low resolution and were very weak. Hence the frequency values cited in Table III are subject to an uncertainty of at least  $\pm 5 \text{ cm}^{-1}$  and any small shifts that may have occurred with concentration increase are not able to be detected. The ir frequency for the  $\nu_1(A_1')$  band shows cation dependence and is 1049  $\text{cm}^{-1}$  for  $\text{NaNO}_3$  and  $\text{LiNO}_3$  solutions and 1043  $\text{cm}^{-1}$  for  $\text{NH}_4\text{NO}_3$ . Raman studies of the  $\nu_1(A_1')$  band<sup>9,10</sup> showed that its frequency was concentration and cation dependent. The frequency shifts were small, approximately 3  $\text{cm}^{-1}$  for  $\text{NaNO}_3$  and  $\text{LiNO}_3$ , but the cation dependence was the same as for the 1350- $\text{cm}^{-1}$ ,  $\nu_3(E')$ , band where the  $\text{Na}^+$  frequency was greater than that for  $\text{Li}^+$ . The  $\nu_1(A_1')$  band for  $\text{NH}_4\text{NO}_3$  solutions was not shifted by concentration increase.

TABLE III: Nitrate  $\nu_3(E')$  Bands of Alkali Metal and Ammonium Nitrate Solutions

Sample	Concn, M	$I_R^a$	$I_M^b$	$\nu_M, \text{cm}^{-1}$	Half-width, $\text{cm}^{-1}$
$\text{NaNO}_3$	8	1.810	0.226	1375	105
	6	1.455	0.243	1370	104
	4	1.000	0.250	1365	105
	2	0.585	0.292	1360	109
$\text{KNO}_3$	1	0.360	0.360	1355	110
	2.7	0.772	0.280	1360	101
	2	0.595	0.297	1358	103
$\text{LiNO}_3$	1	0.364	0.364	1355	106
	8	1.840	0.230	1360	130
	6	1.390	0.232	1358	124
	4	1.035	0.259	1355	119
$\text{NH}_4\text{NO}_3$	2	0.585	0.292	1353	115
	1	0.372	0.372	1350	116
	10			1350	
	8			1350	
	4			1350	
	2			1355	

Sample	$\nu_2(A_2'')$	$\nu_1(A_1')$	Sample	$\nu_2(A_2'')$	$\nu_1(A_1')$
$\text{LiNO}_3$	830	1049	$\text{KNO}_3$	832	1050
$\text{NaNO}_3$	831	1048	$\text{NH}_4\text{NO}_3$	831	1050

<sup>a</sup> $I_R$  is the intensity relative to that of the band for 4 M sodium nitrate. <sup>b</sup> $I_M$  is the molar relative intensity  $I_R/[\text{NO}_3^-]$ .

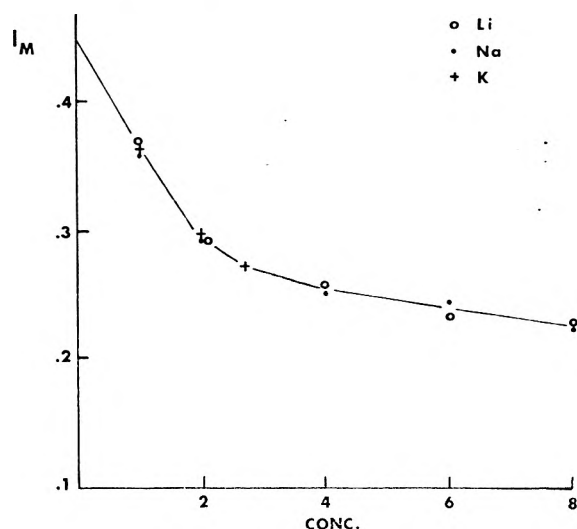


Figure 8. Variation of molar relative intensity of  $\nu_3$  with nitrate ion concentration for  $\text{LiNO}_3$ ,  $\text{NaNO}_3$ , and  $\text{KNO}_3$  solutions.

#### Nature of Hydration of Solute Salts

Information on ion hydration comes from the extraction of an "A" band having a concentration-independent shape and position but having a band intensity increasing linearly with concentration. These observations are consistent with the bands arising from discrete stable water-electrolyte species  $\text{M}^+(\text{H}_2\text{O})_n\text{X}^-$  which increase in concentration linearly with the concentration of electrolyte MX. It is not possible from these measurements to determine whether the water in these species is associated with the cation, with the anion, or with the ion pair. Other studies have shown that for electrolytes of the type  $\text{MX}_2$  the hydration number is the same as for MY whereas for electrolytes of the type  $\text{M}_2\text{Z}$  the hydration number is approximately doubled (M remains the same throughout). This indicates that the relaxation time of the measurement is short enough

that anion hydration, in which water-exchange time is short, is not defined but that the hydration number refers to water bound to the cation.

The band maximum and band intensity of the librational "A" bands show the influence of both cation and anion on the spectrum as shown in Table IV and Figure 5. The simple cation-water interaction, although it yields a hydration number, is evidently insufficient to explain completely the spectral changes. The anion influence could be through the formation of hydrated ion pairs as previously proposed<sup>9,10,12,13</sup> from studies of the nitrate ion in aqueous solutions and in crystals. The further elucidation of the anionic influence requires the study of a wider range of electrolyte species.

### Intensity of Librational Bands

The intensity of a librational mode may not be dependent simply on the magnitude of the water molecule dipole moment. All electrolytes produce an increase in intensity accompanied by a decrease in the frequency of the librational band which indicates a direct relationship between intensity and frequency. It is possible that a low librational frequency indicates that the intermolecular forces which restrict rotation are weak, allowing the less rotationally hindered water molecule to librate with greater amplitude. Increased amplitude involves a larger dipole change relative to the rotational axes and would lead to a more intense ir librational band. If this view is correct, then the librational intensity enhancement caused by electrolytes results from both the increased dipole moment and the increased librational amplitude. The intensity of the "A" bands shows the cation dependence,  $\text{Li} > \text{Na} > \text{NH}_4$ . The frequencies of  $\text{LiNO}_3$  and  $\text{NaNO}_3$  "A" bands are identical; hence, the intensity difference results from the more polarizing  $\text{Li}^+$  ion inducing a larger dipole in the hydration water molecules by polarizing the nonbonding electrons on the oxygen atom.

At concentrations greater than 8 M the band characteristics of the  $\text{LiNO}_3$  "A" bands change. The band frequency, constant from 1 to 8 M, shifts to lower frequency, the half-width decreases, and the asymmetry index increases. At 8 M, the "B" water concentration approaches zero and the hydrated ion pairs will be adjacent. At higher concentrations the number of water molecules hydrating each ion pair must decrease and the water molecules become increasingly influenced by other neighboring cations and anions. Almost all water-water interactions will be disrupted. A more highly ionic environment can be expected to lead to the observed lowering of the librational frequency in 10 M  $\text{LiNO}_3$ . The decrease in the band half-width suggests that the water is becoming increasingly ordered.<sup>14,15</sup>

The "A" bands for  $\text{NH}_4\text{NO}_3$  solution, unlike the symmetrical "A" bands of  $\text{LiNO}_3$  and  $\text{NaNO}_3$ , are similar in shape to the librational band of pure water. Unlike the other ions,  $\text{NH}_4^+$  is capable of H bonding tetrahedrally.<sup>16</sup> Hence it is considered that the ammonium ion in the species  $\text{NH}_4^+(\text{H}_2\text{O})_4\text{NO}_3^-$  may be tetrahedrally H bonded to the primary hydration molecules which may not be significantly disoriented from their normal tetrahedral environment. The hydration water would then give rise to a libration band similar in shape to the pure water band. Disruption and weakening of the primary hydration by interaction with the nitrate ion would broaden and shift this band to a lower frequency than the pure water band.

Our results give support to the generally held view that

TABLE IV: Librational "A" Band Characteristics for 4 M Electrolyte Solutions

Salt	$I_R$	$\nu_M, \text{cm}^{-1}$	Salt	$I_R$	$\nu_M, \text{cm}^{-1}$
$\text{NaNO}_3$	0.56	595	$\text{NaBr}$	0.68	530
$\text{NaClO}_4$	0.69	570	$\text{NaI}$	0.60	500
$\text{NaCl}$	0.56	545			

$\text{NH}_4^+$ , with its four H-bonding protons, fits well into the structure of liquid water. The  $B$  viscosity coefficient for  $\text{NH}_4^+$  is close to zero,<sup>17</sup>  $\text{NH}_4\text{Cl}$  barely affects the proton resonance of water,<sup>18</sup> and the partial molar volumes of  $\text{NH}_4^+$  and water are identical.<sup>19</sup> Vollmar<sup>10</sup> considered that  $\text{NH}_4^+$  and  $\text{H}_2\text{O}$  formed H bonds of similar strength. He observed that  $\text{NH}_4\text{NO}_3$ , unlike numerous other nitrates, produced no change in the intensity frequency and half-width of the  $\nu_1(\text{A}_1')$  nitrate band, even at high concentrations when cation-anion contact was inevitable. It was concluded that there was similar hydrogen bonding between  $\text{NO}_3^-$  and either  $\text{NH}_4^+$  or  $\text{H}_2\text{O}$ .

The relatively small frequency shifts and intensity changes in the ir librational bands of water and aqueous solutions suggests that temperature change weakens the intermolecular structure by only a small degree. Weakening and distortion of water-water and  $\text{NH}_4^+$ -water H bonding leads to the shift to lower frequency and the increased half-width in water and 8 M  $\text{NH}_4\text{NO}_3$  solution. The strong Coulombic cation-water interactions which would predominate in 8 M  $\text{LiNO}_3$  appear less influenced by temperature as evidenced by the smaller frequency shift and constant half-width.

Small intensity increase of the ir librational band of pure water with temperature is in contrast to the large decrease in the corresponding Raman band.<sup>20</sup> It seems that the polarizability of the water molecule is much more sensitive to small changes in the intermolecular H bonding than the water molecule dipole moment. This view is further supported by the observation that electrolytes produce large increases in the Raman librational intensity while the ir intensity increase is relatively small.

*Acknowledgments.* The Australian Research Grants Committee is thanked for a grant enabling purchase of the Perkin-Elmer 225 spectrometer. R.F.A. acknowledges receipt of a Rural Credits Development Fund award during the tenure of which this work was carried out.

*Supplementary Material Available:* derivation of eq 2, determination of refractive indexes, separation of the librational band into A and B components, and determination of hydration number (6 pages). Ordering information is given on any current masthead page.

### References and Notes

- G. E. Walrafen, *J. Chem. Phys.*, **36**, 1035 (1962).
- D. A. Draegert and D. Williams, *J. Chem. Phys.*, **48**, 401 (1968).
- M. Yasumi, *Bull. Chem. Soc. Jpn.*, **24**, 54 (1951); **28**, 489 (1955).
- For more details of this method, see R. F. Armishaw, Ph.D. Thesis, University of Queensland, St. Lucia, Australia, 1972.
- G. R. Wilkinson in "Infrared Spectroscopy and Molecular Structure", M. Davies, Ed., Elsevier, Amsterdam, 1963.
- D. A. Draegert, N. W. B. Stone, B. Curnutte, and D. Williams, *J. Opt. Soc. Am.*, **56**, 64 (1966).
- J. R. Morrey, *J. Phys. Chem.*, **66**, 2169 (1962).
- D. W. James and R. F. Armishaw, *Aust. J. Chem.*, **28**, 1179 (1975).
- D. E. Irish and A. R. Davis, *Can. J. Chem.*, **46**, 943, (1968); J. D. Riddell, D. J. Lockwood, and D. E. Irish, *ibid.*, **50**, 2951 (1972).
- P. M. Vollmar, *J. Chem. Phys.*, **39**, 2236 (1963).
- D. W. James, R. F. Armishaw, and R. L. Frost, unpublished data.

- (12) H. Lee and J. K. Wilfurst, *Aust. J. Chem.*, **17**, 943 (1964).  
 (13) S. C. Wait, Jr., A. T. Ward, and G. J. Janz, *J. Chem. Phys.*, **45**, 133 (1966).  
 (14) W. J. Jones in "Infrared Spectroscopy and Molecular Structure", M. Davies, Ed., Elsevier, London, 1963, p 160.  
 (15) A. C. Jones and D. D. Tunnicliff, *Anal. Chem.*, **34**, 261R (1962).  
 (16) L. Pauling, "The Nature of the Chemical Bond", 3rd ed, Cornell University Press, Ithaca, N.Y., 1960.  
 (17) M. Kaminsky, *Discuss. Faraday Soc.*, **24**, 171 (1957).  
 (18) J. C. Hindman, *J. Chem. Phys.*, **36**, 1000 (1962).  
 (19) K. Fajans and O. Johnson, *J. Am. Chem. Soc.*, **64**, 668 (1942).  
 (20) G. E. Walrafen, *J. Chem. Phys.*, **44**, 1546 (1966).

## Internal Heavy Atom Studies on the Triplet State of Dimethyl- and Dihaloxanthenes

Henry J. Pownall\*<sup>1</sup>

Department of Medicine, Baylor College of Medicine, Houston, Texas 77025

and Itshak Granoth

Israel Institute for Biological Research, Ness-Ziona, Israel (Received January 13, 1975; Revised Manuscript Received November 3, 1975)

Publication costs assisted by the National Institutes of Health

The lowest triplet of these xanthenes has been studied by phosphorescence spectroscopy. In 1:1 ether:ethanol, xanthone and its dimethyl derivatives have lowest triplets which contain considerable  $^3(\pi, \pi^*)$  character with some  $^3(n, \pi^*)$  character as assessed from phosphorescence lifetimes. The spectral positions and phosphorescence lifetimes are determined in part by both positional and inductive effects of the substituent. The phosphorescence of the dihaloxanthenes exhibits additional spectral changes which can be attributed to an internal "heavy atom" effect which we attribute to a greater participation of the  $^3(\pi, \pi^*)$  component of a "mixed" triplet state.

### Introduction

The xanthone (abbreviated XAN) system (cf. Figure 1) has been the subject of numerous studies on its phosphorescence properties in various media.<sup>2-9</sup> Although the anomalous nonexponential phosphorescence decay of these xanthenes<sup>2,3</sup> might be a complex study in itself, we have focused on the more obvious changes which methyl or halogen substituents produce in the phosphorescence of this aromatic carbonyl compound. Xanthone is well-suited for this type of study since earlier work has established the polarization of several of its major absorption bands.<sup>2</sup> The advantage of full  $C_{2v}$  symmetry which was exploited in that study is still applicable in this study since minor nonconjugative substituents should not greatly perturb the  $C_{2v}$  symmetry of the xanthone system. Thus, by a judicious choice of methyl and halo substituents on the xanthone nucleus, one can separate the substituent positional effects from those of "heavy atoms" in determining the spectral position and oscillator strength of the various excited triplet states of xanthone. It is known that an internal heavy atom in aromatic hydrocarbons can greatly enhance both radiative and nonradiative processes occurring from the lowest triplet.<sup>10</sup> In aromatic carbonyl compounds one must consider the occurrence of a similar phenomenon an open question if only for the lack of but a small number of definitive studies. In the simple halogen-substituted benzophenones, all of which have a lowest  $^3(n, \pi^*)$  state, no significant changes in the phosphorescence are observed.<sup>11</sup> The phosphorescence of the halogen substituted flavones (3-phenylbenzo-1,4-pyranone, an aromatic ketone) is highly sensitive to the introduction of a "heavy atom", and has led

to the assignment of its lowest triplet as  $^3(\pi, \pi^*)$ .<sup>12</sup> In the xanthenes, however, the problem is complicated by "dual phosphorescence" and the interchange of  $^3(n, \pi^*)$  and  $^3(\pi, \pi^*)$  states which can be effected by substituents or a change in solvent polarity.

The dual emission and sensitivity of the phosphorescence of aromatic carbonyl compounds to various solvents and substituents has been explained by several mechanisms, some of which have been reviewed by Long et al.<sup>13</sup> One of the more widely accepted mechanisms invokes vibronic coupling between energetically similar  $^3(n, \pi^*)$  and  $^3(\pi, \pi^*)$  states.<sup>13-16</sup> In a previous study,<sup>7</sup> the lowest triplet state of xanthone in 3-MP (3-methylpentane) between 2 and 45 K and in EPA (ethanol:diethyl ether:isopentane, 5:5:2) at all temperatures has been assigned to a vibronically "mixed"  $^3(n, \pi^*)$  and  $^3(\pi, \pi^*)$  state. The purpose of this study is to examine the effects of internal "heavy atom" substituents on the phosphorescence of the xanthone system in polar aprotic solvents where one would expect a lowest triplet state having a "mixed" configuration.

### Experimental Section

**Phosphorescence Spectra and Lifetimes.** Phosphorescence spectra were measured on an Aminco-Bowman spectrofluorimeter calibrated with a low-pressure mercury lamp as previously described.<sup>12</sup> No provision was made to correct for the spectral sensitivity of the analyzing system. All spectra were run in E:E (ethanol + diethyl ether, 1:1) at a concentration of  $\leq 5 \times 10^{-5}$  M in 2-mm cylindrical quartz cuvetts. E:E was selected since all of these xanthenes are very soluble in this solvent mixture which forms a clear



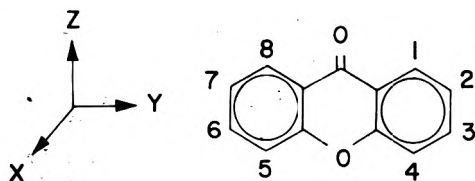


Figure 1. Structure and coordinate system of xanthone.

rigid glass at 77 K. Initial attempts to measure the phosphorescence of the xanthenes in various hydrocarbon glasses were frustrated by solute aggregation which occurred on cooling. This produced "cloudy" glasses which had a much lower optical density than the sample had at ambient temperatures. The absorption spectra of these samples consisted of broadened absorption bands rather than the sharper bands expected upon cooling. The xanthenes were prepared and purified as described previously.<sup>17</sup>

Typically, an excitation wavelength of  $\sim 340 \pm 5$  nm was employed with 2-mm excitation slits. The analyzing portion of the unit had 0.5-mm entrance and exit slits which focused on an RCA 1P28 photomultiplier tube.

Phosphorescence lifetimes were recorded without degassing by interrupting the excitation light source with a shutter (risetime  $\sim 0.5$  ms) and displaying the output on either an X-Y recorder or an oscilloscope. The lifetimes were determined by a graphical procedure. Because these compounds frequently exhibit complex decay patterns, only the initial slopes were recorded for a better comparison. The average deviations of these lifetimes are less than 10% of the given value.

## Results

The phosphorescence spectra and lifetimes of the xanthenes have been recorded in E:E at 77 K. The phosphorescence spectrum of each of the xanthenes is reproduced in Figure 2. The salient features of these spectra are as follows. (1) No clearly defined 0-0 band is observed in any of these xanthenes except perhaps 2,7-dibromo-, 2,7-diiodo-, 2-bromo-7-fluoro-, and 2-bromo-7-chloroxanthone, each of which contains at least one atom in the 2 or 7 position with an atomic weight equal to or greater than that of bromine. (2) The spectra of XAN and the dimethylxanthenes are similar in shape whereas the series of dihaloxanthenes from difluoro- to diiodoxanthone shows a reduction of the 430- and 460-nm bands and a growth in the band  $\sim 420$  nm. (3) The phosphorescence lifetimes (cf. Table I) of these xanthenes are highly variable depending upon the substituent and position involved; substitution of a methyl group in the 2,7 position extends  $\tau_p$  whereas 3,6-dimethylxanthone has a phosphorescence lifetime less than that of XAN. 2,6-Dimethylxanthone has a  $\tau_p$  between that of the latter two dimethylxanthenes. (4) In the series, 2,7-difluoro-, 2,7-dichloro-, 2,7-dibromo-, and 2,7-diiodoxanthone, one observes, with increasing atomic weight of the substituents, a decrease in  $\tau_p$  which extends over three orders of magnitude. (5) Among the mixed dihalo compounds, one observes a slightly longer lifetime for 2-fluoro-6-bromo- or 2-chloro-6-bromoxanthone relative to the corresponding 2,7-dihalo derivatives. Furthermore, among these last four xanthenes,  $\tau_p$  for the chloro derivative is less than that of the analogous fluoro compound. (6) A broadening of the 420-nm band appears when Br is moved from position 6 to 7. (7) No fluorescence was detected in any of the xanthenes in E:E at either ambient or low temperatures.

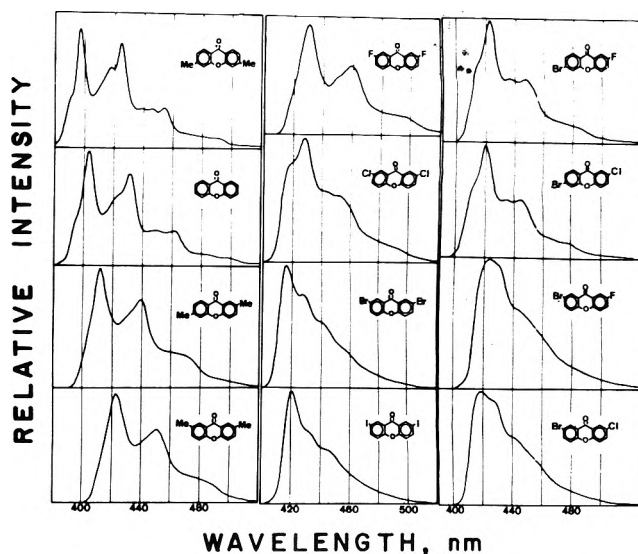


Figure 2. Phosphorescence of the xanthenes in ethanol:ether (1:1) at 77 K.

TABLE I: Phosphorescence Properties of Substituted Xanthenes in E:E at 77 K

	$E(0-0)^a$ , kK	$E_{\max}$ , kK	$\tau_p$ , ms <sup>b</sup>
Xanthone	25.6	24.8	145
3,6-Dimethylxanthone	26.0	25.2	90
2,6-Dimethylxanthone	25.2	24.3	275
2,7-Dimethylxanthone	24.5	23.6	475
2,7-Difluoroxanthone	24.2	23.3	500
2,7-Dichloroxanthone	24.5	23.4	170
2,7-Dibromoxanthone	24.6	24.0	5
2,7-Diiodoxanthone	24.4	23.8	$\leq 0.5$
2-Bromo-7-fluoroxanthone	24.4	23.6	13
2-Bromo-7-chloroxanthone	24.6	23.9	11
2-Fluoro-6-bromoxanthone	25.0	24.0	40
2-Chloro-6-bromoxanthone	25.2	24.1	25

<sup>a</sup> 0-0 band is determined from the spectral position at the onset of phosphorescence where 10% of full emission intensity is recorded. <sup>b</sup> Values are  $\pm 10\%$  for initial slope through 1 decade.

## Discussion

The five para-substituted benzophenones have lowest triplet energies within 0.20 kK of the mean (24.4 kK),  $\tau_p$  which are 6-11 ms with the average  $\tau_p = 9$  ms and a similar spectral shape containing the C=O stretch frequency as a prominent vibration.<sup>11</sup> The xanthenes, however, have highly variable phosphorescence lifetimes and energies and only exhibit the carbonyl frequency in their phosphorescence spectra if the samples are measured in hydrocarbon solvent. These distinctions suggest that the xanthone and benzophenone triplet levels, i.e.,  $^3(n,\pi^*)$  and  $^3(\pi,\pi^*)$ , should not necessarily be correlated and that the mechanism whereby the xanthenes obtain their phosphorescence intensity may be different. Polarization data are not useful for the assignment of the lowest triplet in the xanthenes since most of these compounds have no well-defined phosphorescence 0-0 band in E:E.<sup>18</sup> Lifetime data alone are not useful since a short lifetime may be due to a  $^3(n,\pi^*)$  state which is intrinsically short-lived and unaffected by heavy atoms or, alternatively, due to a heavy atom perturbation of a  $\pi$ -electronic system having an emitting  $^3(\pi,\pi^*)$  state.

A correlation between the singlet-triplet transition prob-

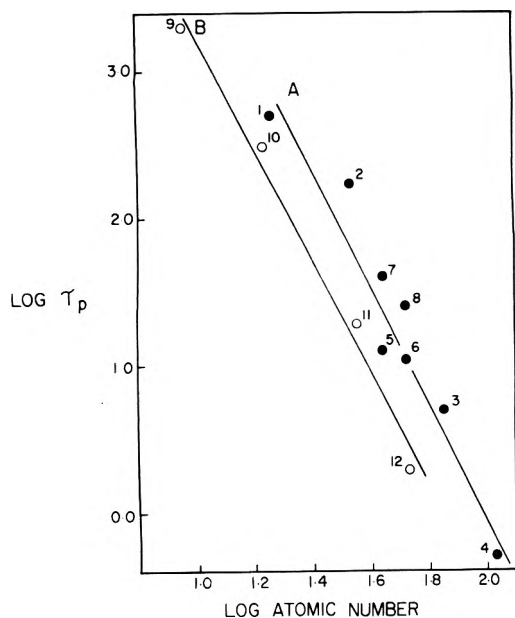


**Figure 3.** Plot of  $\log \tau_p$  vs.  $\log$  atomic number of the halogen substituted xanthenes: (1) 2,7-difluoro-; (2) 2,7-dichloro-; (3) 2,7-dibromo-; (4) 2,7-diiodo-; (5) 2-bromo-7-fluoro-; (6) 2-bromo-7-chloro-; (7) 2-fluoro-6-bromo-; (8) 2-chloro-6-bromo-; (9) 1-fluoronaphthalene; (10) 1-chloronaphthalene; (11) 1-bromonaphthalene; (12) 1-iodonaphthalene. Curve A and the filled circles represent the dihaloxanthenes; curve B and the open circles refer to the values for the 1-haloxanthenes and are based on the data of McGlynn et al.<sup>22</sup> Atomic numbers are taken as the total halogen weight in each of these compounds.

ability and the heavy atom substituents, haloxanthone, can be obtained from a plot of  $\log \tau_p$  vs.  $\log$  (atomic number) where the atomic number is taken as the sum of the two substituents if they are different.<sup>19</sup> In Figure 3, the dihaloxanthenes (filled circles) show a fairly good linear fit to this relationship. A similar plot of the phosphorescence lifetimes of the 1-haloxanthenes is also linear and is nearly parallel to that of the xanthenes. The lifetimes of the 1-haloxanthenes, however, are not as short as those of the dihaloxanthenes which suggests that the lowest triplet state of the xanthenes may not be adequately described by a  $^3(\pi, \pi^*)$  assignment. Similarly, the linear relationship between  $\log k_p$  and  $\log \sum_k \zeta_k^2$  where  $\zeta_k$  represents the spin-orbit coupling factor of the  $k$ th substituent shown in Figure 4 for the haloxanthenes is comparable to that reported for the halogenated anthracenes<sup>20-22</sup> which have a lowest  $^3(\pi, \pi^*)$  state and a skeletal structure similar to that of XAN. Although these similarities indicate that the lowest triplet states of the dihaloxanthenes are  $^3(\pi, \pi^*)$  and that the variation in phosphorescence is only a consequence of the presence of heavy atom substituents, the tremendous differences in spectral shape among the dihaloxanthenes suggests that we are not dealing with "pure"  $^3(\pi, \pi^*)$  states; e.g., in comparing the 2,7-dihaloxanthenes, one observes a gradual modification of the spectrum in going from 2,7-difluoro- to 2,7-diiodoxanthone.<sup>23</sup> From this, one might conclude that there is a change in the electronic configuration of the lowest triplet state of xanthone through this series of substitutions but the data of Figure 4 suggest that the lowest triplet state is  $^3(\pi, \pi^*)$  in all of the dihaloxanthenes. These two observations are not inconsistent in a simple model in which the lowest triplet state of xanthone has a "mixed" configuration in which both  $^3(n, \pi^*)$  and  $^3(\pi, \pi^*)$  contributions are important. Therefore, the phosphores-

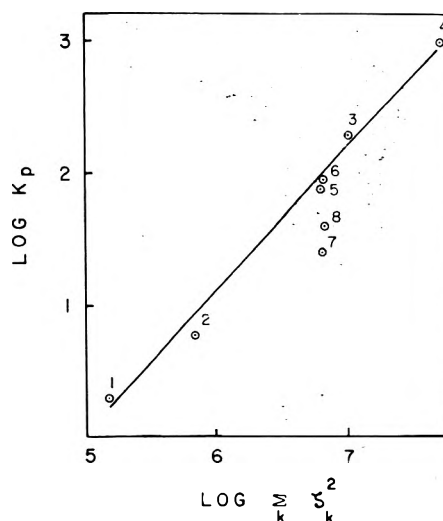


**Figure 4.**  $\log k_p$  vs.  $\log \sum_k \zeta_k^2$  for the dihaloxanthenes: (1) 2,7-difluoro-; (2) 2,7-dichloro-; (3) 2,7-dibromo-; (4) 2,7-diiodo-; (5) 2-bromo-7-fluoro-; (6) 2-bromo-7-chloro-; (7) 2-fluoro-6-bromo-; (8) 2-chloro-6-bromo-.

cence lifetimes of XAN, the dimethylxanthenes and 2,7-difluoroxanthone are not as short as that of benzophenone since  $^3(\pi, \pi^*)$  character is "mixed" into its lowest triplet state. Similarly, from its phosphorescence lifetime, spectral shape, and energy, we suggest that 3,6-dimethylxanthone and XAN contain more  $^3(n, \pi^*)$  character than the other ten xanthenes. The 2,7-dibromo- and 2,7-diiodoxanthenes contain largely  $^3(\pi, \pi^*)$  character since (1) their lifetimes are much shorter than those of benzophenone or xanthone due to a heavy atom effect on  $^3(\pi, \pi^*)$  states, (2) the spectral shape of these two xanthenes lacks any progressions which usually characterize  $^3(n, \pi^*)$  states, and (3) the absorption spectra of these two xanthenes indicate lowest  $^1(\pi, \pi^*)$  state whereas the other xanthenes have lowest  $^1(n, \pi^*)$  states (unpublished results). It appears that the heavy atoms in the 2 or 7 position are more effective in mixing singlet character into the triplet state but the mechanism for this is not clear. Although the relative contribution of the  $^3(\pi, \pi^*)$  configuration to the wave function may be small, the introduction of increasingly heavy atoms appears to mix more singlet character into the lowest triplet state by virtue of only the  $^3(\pi, \pi^*)$  component of that state. We have divided the xanthenes into three cases according to their triplet lifetimes, energies, and spectral shapes. Case a corresponds to a lowest  $^3(n, \pi^*)$  state and is similar to what one would predict for an aromatic carbonyl compound which has a relatively "pure lowest  $^3(n, \pi^*)$  state. This case is best exemplified by benzophenone which has a phosphorescence lifetime of 8.3 ms.<sup>11</sup> Case b corresponds to aromatic carbonyl compounds having a lowest  $^3(\pi, \pi^*)$  state, e.g., 2-acetonaphthone which has  $\tau_p = 97$  ms<sup>24</sup> or flavone with  $\tau_p = 675$  ms.<sup>12</sup> Case c corresponds in varying degrees to the substituted xanthenes in E:E studied here which have phosphorescence lifetimes which are between those of cases a and b except in the bromo or iodo derivatives which are assigned as having largely  $^3(\pi, \pi^*)$  character in spite of the short  $\tau_p$  (vide infra). The xanthenes in E:E have a small amount of  $^3(n, \pi^*)$  character and the introduction of the heavier atom permits greater expression of the lowest triplet as a  $^3(\pi, \pi^*)$  when the magnitude of the mixing of singlet character into the triplet state via a heavy atom mechanism exceeds that obtained by  $^3(n, \pi^*)$  spin-

orbit coupled with a  $^1(\pi, \pi^*)$  state; i.e., the transition probability for phosphorescence would be given by the second-order spin-orbit coupling scheme

$$\langle ^1\phi_p | H_{sd} | ^3\phi(\pi, \pi^*) \rangle \langle ^3\phi(\pi, \pi^*) | H_{EV} | ^3\phi(n, \pi^*) \rangle$$

where  $^1\phi_p$  is the perturbing singlet,  $H_{so}$  is the spin-orbit coupling operator, and  $H_{EV}$  is the operator for vibration-electronic coupling of the lowest zero-order triplet with an intermediate zero-order triplet state. Depending upon the system this scheme may involve a different perturbing singlet state and a different  $H_{so}$ . This description has neglected the possible differences due to the oscillator strengths of the perturbing singlets and the energy gaps between the states. The series XAN  $\sim$  3,6-dimethylxanthone  $<$  2,7-dibromoxanthone  $<$  2,7-diiodoxanthone represents the order of increased participation of the  $^3(\pi, \pi^*)$  state in determining the phosphorescence lifetime of a vibronically perturbed triplet state which has been described by  $^{15} ^3\phi(n, \pi^*) + b^3\phi(\pi, \pi^*)$  and illustrates the dominating influence of  $^3(\pi, \pi^*)$  states in aromatic carbonyl compounds containing heavy atoms.

*Acknowledgment.* We thank Drs. Robert E. Connors and Richard Clark of Boston University for assistance in some of the measurements and for the use of their laboratory facilities.

## References and Notes

- (1) Author to whom reprint requests and correspondence should be sent.
- (2) H. J. Pownall, R. E. Connors, and J. R. Huber, *Chem. Phys. Lett.*, **22**, 403 (1973).
- (3) H. J. Pownall and J. R. Huber, *J. Am. Chem. Soc.*, **93**, 6429 (1971).
- (4) R. N. Nurmukhametov, L. A. Meleshina, and D. N. Shigorin, *Opt. Spektrosk.*, **22**, 404 (1967).
- (5) J. F. Ireland and P. A. H. Wyatt, *J. Chem. Soc., Faraday Trans. 1*, **68**, 1053 (1972).
- (6) J. F. Ireland and P. A. H. Wyatt, *J. Chem. Soc., Faraday Trans. 1*, **69**, 161 (1973).
- (7) T. F. Hunter, *Trans. Faraday Soc.*, **66**, 300 (1970).
- (8) H. J. Pownall and W. W. Mantulin, *Mol. Phys.*, in press.
- (9) H. J. Pownall, *Mol. Photochem.*, **6**, 425 (1975).
- (10) V. Ermolaev and K. Svitashv, *Opt. Spectrosc.*, **7**, 399 (1959).
- (11) B. F. Borkman and D. R. Kearns, *J. Chem. Phys.*, **46**, 2333 (1967).
- (12) H. J. Pownall, *Spectrochim. Acta, Part A*, **30**, 953 (1974).
- (13) M. E. Long, Y. H. Li, and E. C. Lim, *Mol. Photochem.*, **3**, 221 (1971).
- (14) R. M. Hochstrasser and C. A. Marzocco, "Molecular Luminescence", E. C. Lim, Ed., W. A. Benjamin, New York, N.Y., 1969, p 631.
- (15) L. Goodman and M. Koyanagi, *Mol. Photochem.*, **4**, 369 (1972).
- (16) N. Hirota, *Chem. Phys. Lett.*, **4**, 305 (1969).
- (17) I. Granoth and H. J. Pownall, *J. Org. Chem.*, **40**, 2088 (1975).
- (18) The arguments given herein apply to the E:E solvent system; in a hydrocarbon solvent an entirely different picture might emerge.
- (19) R. M. Hochstrasser, "Behavior of Electrons in Atoms", W. A. Benjamin, New York, N.Y., 1964.
- (20) J. W. Hilpern, G. Porter, and L. J. Stief, *Proc. R. Soc. London, Ser. A*, **277**, 437 (1964).
- (21) M. F. Hoffman and G. Porter, *Proc. R. Soc. London, Ser. A*, **268**, 46 (1962).
- (22) S. P. McGlynn, T. Azumi, and M. Konoshita, "Molecular Spectroscopy of the Triplet State", Prentice-Hall, Englewood Cliffs, N.J., 1969, p 265.
- (23) Though it appears that the phosphorescence of 2,7-dichloroxanthone could be represented by a superposition of the phosphorescence spectra of difluoro- and dibromoxanthone, variation of the chopper speed failed to resolve the spectrum into two components.
- (24) V. Ermolaev and A. Terenin, *Sov. Phys. Usp. (Engl. Transl.)*, **3**, 423 (1960).

## Conductivity and Dielectric Dispersions of Hydrated and Partially Hydrated Synthetic Faujasites

Robert A. Schoonheydt,\* Willy De Wilde, and Firmin Velghe

Katholieke Universiteit Leuven, Centrum voor Oppervlakteschelkunde en Colloidale Scheikunde, De Croyleaan 42, B-3030 Heverlee, Belgium (Received April 28, 1975; Revised Manuscript Received November 3, 1975)

Publication costs assisted by the Katholieke Universiteit Leuven

Conduction in hydrated zeolites is due to the movement of the supercage cations, while dielectric dispersions in the kilohertz region are ascribed to the cations in the sodalite units. The activation energies and entropies for conduction vary in the range 100–30 kJ mol<sup>-1</sup> and -69 to 226 J mol<sup>-1</sup> K<sup>-1</sup>, respectively, according to the type of cation and the cation-water ratio. The activation energies for cationic relaxation range from 100 to 58 kJ mol<sup>-1</sup>. A combination of these two techniques allows a study of the cationic distribution in mixed cationic zeolites. The stepwise dehydration down to 90 H<sub>2</sub>O/unit cell does not affect the cationic distribution at low cation-water ratios but does to a limited extent at high cation-water ratios. Below that hydration level the zeolites undergo the change from hydrated to dehydrated cationic distribution. Water molecules are highly polarized by the cations and no freezing in the sense of a sharp phase transition occurs upon cooling down to 200 K.

### Introduction

The interpretation of dielectric dispersion data obtained on hydrated and partially hydrated zeolites X and Y is a matter of controversy. In the kilohertz region two relaxa-

tions were observed, which were attributed to the cations, to water molecules, or to Maxwell-Wagner effects but no uniform interpretation could be extracted from the literature.

As long as the zeolite contained x-ray unlocalizable cations, Lohse et al.<sup>1,2</sup> found no water relaxation but a Maxwell-Wagner effect at low frequencies and a cationic relaxation at high frequencies. In the other cases high-frequency water relaxations were reported and, at high water contents, Maxwell-Wagner effects in the low-frequency range. The first case was confirmed by Jansen and Schoonheydt<sup>3</sup> for partially hydrated Na<sup>+</sup>- and K<sup>+</sup>-zeolites X and Y. However, for the hydrated samples in the range 200–300 K these authors<sup>3</sup> attributed the low-frequency (LF) relaxation to the interstitial cations on sites III' in the supercages. The high-frequency (HF) relaxation was attributed to water molecules on the basis of the similarity between the dielectric and proton magnetic relaxation times.<sup>4</sup> LF water and HF cationic relaxations were also reported by Morris<sup>5</sup> on partially hydrated A-type zeolites even in cases where the dehydrated zeolite contained unlocalizable cations, in contradiction with Lohse's interpretation.<sup>1,2</sup> Matron et al.<sup>6</sup> attributed the two relaxations in the kilohertz region to cations on different sites in the structure, whereas Chapoton et al.<sup>7</sup> interpreted them as a Maxwell-Wagner effect (LF) and a cationic relaxation (HF). The latter explicitly showed that water relaxations occurred in the region 100 MHz–10 GHz at room temperature.

Besides these different assignments of the relaxational spectra in the kilohertz region, there is no agreement on the mechanism of cationic relaxation and the cations involved, i.e., their location in the structure.

In view of these results it was interesting to investigate a series of faujasite type zeolites, fully and partially hydrated, to see how water influences the cationic relaxations in an effort to reconcile the conflicting interpretations of dielectric relaxations in the kilohertz region. These relaxation studies were supplemented by conductivity data on the hydrated samples at low temperatures. They are compared with available tracer diffusion studies.<sup>8–12</sup>

### Experimental Section

**Samples.** The Na<sup>+</sup> forms of the zeolites were obtained by exchange of the commercial sieves (obtained from Union Carbide, Linde Division) with 1 N NaCl at room temperature for 24 h. No analysis was done but in view of this Na<sup>+</sup> concentration and the large solid/liquid ratios (20 g/l.) no large cation deficiency was expected.<sup>13</sup> The ideal dehydrated unit cell formulae are: Na<sub>86.5</sub>(AlO<sub>2</sub>)<sub>86.5</sub>(SiO<sub>2</sub>)<sub>105.5</sub>, Na<sub>69.8</sub>(AlO<sub>2</sub>)<sub>69.8</sub>(SiO<sub>2</sub>)<sub>122.2</sub>, Na<sub>54.7</sub>(AlO<sub>2</sub>)<sub>54.7</sub>(SiO<sub>2</sub>)<sub>137.3</sub>, and Na<sub>48.2</sub>(AlO<sub>2</sub>)<sub>48.2</sub>(SiO<sub>2</sub>)<sub>143.8</sub>. These zeolites and those derived from them by ion exchange are denoted in this paper by the symbol F preceded by the main exchangeable ion and followed by the silica-to-alumina ratio. This gives for the Na<sup>+</sup>-saturated zeolites respectively NaF2.5, NaF3.4, NaF5.0, and NaF5.8. The Ca<sup>2+</sup> and Cu<sup>2+</sup> forms prepared from the Na<sup>+</sup>-zeolites are listed in Table I together with their exchangeable cation content, determined by atomic absorption after HF dissolution of the samples. The Ca<sup>2+</sup> forms symbolized by the number 1 between brackets were prepared by room temperature exchange in 0.1 N CaCl<sub>2</sub> for 24 h. CaF2.5(2) and CaF5.0(2) were prepared by exchange in 0.1 N CaCl<sub>2</sub> at 90 °C for 14 days and 3 months, respectively, with regular renewal of the exchange solution. The CuF5.0(1) and CuF5.0(2) were prepared by room temperature ion exchange with solutions containing the appropriate Cu<sup>2+</sup>/Na<sup>+</sup> ratio to obtain the desired exchange level at a total normality of 0.1 during 24 h. CuF5.0(3) was obtained after exchange at room tempera-

TABLE I: Cation Content of the Synthetic Faujasites

Samples	Cations/unit cell		
	Na <sup>+</sup>	Ca <sup>2+</sup>	Cu <sup>2+</sup>
CaF2.5(1)	16.1	36.2	
CaF2.5(2)	2.0	42.2	
CaF3.4(1)	13.2	28.3	
CaF5.0(1)	14.7	20.1	
CaF5.0(2)	3.4	26.8	
CaF5.8(1)	14.1	17.0	
CuF5.0(1)	47.3		3.4
CuF5.0(2)	35.5		8.8
CuF5.0(3)	19.4		21.0

ture in 0.1 N CuCl<sub>2</sub> solution at room temperature during 24 h. Before use the samples were air dried at 50 °C and stored in a desiccator over a saturated NH<sub>4</sub>Cl solution.

**Electrical Measurements.** A detailed picture of the conductivity cell has been published.<sup>14</sup> Essentially, it consists of a stainless steel three electrode system. The diameters of the lower and upper electrodes are respectively  $1.55 \times 10^{-2}$  and  $1 \times 10^{-2}$  m. The guard ring electrode, lying around the upper electrode, has an inner diameter of  $1.1 \times 10^{-2}$  m. It is connected to the neutral line of the Wayne Kerr B221 MkIII bridge-detector for measurements in the frequency range 200– $2 \times 10^4$  Hz or of the Wayne Kerr B602 bridge for the  $10^5$ – $10^7$ -Hz frequency range. The sinusoidal signal generators for these two bridges are respectively the Wayne Kerr S121 and Wayne Kerr SR268. The latter is a source-detector. The signal generated by the S121 can be chosen in the range 0–30 V. The amplitude of the signal generated by the SR268 is 2 V rms. Pellets of  $\sim 1.2 \times 10^{-3}$  m thickness and  $1.5 \times 10^{-2}$  m diameter and a density of 63–75% of the real crystal density are obtained by pressing 300 mg of zeolite powder in a stainless steel die. A gold layer ( $\geq 1 \times 10^{-6}$  m) is evaporated on upper and lower sides of each pellet to ensure good electrical contacts. A ring was scratched in the gold layer around the upper electrode to separate it from the guard ring electrode electrically. With this set-up the conduction  $G$  ( $\text{ohm}^{-1}$ ) and capacity  $C$  (F) are measured in the frequency range 200– $3 \times 10^6$  Hz for different hydration levels and temperatures. At each point the applied signal is chosen for  $G$  and  $C$  to be independent of the amplitude. Usually the range 0.3–30 V is sufficient to cover the experiments.  $G$  and  $C$  are converted to the conductivity  $\sigma = G(l/s)$  and the electrical permittivity  $\epsilon' = C/C_0$  where  $l$  is the sample thickness and  $s$  the surface area of the sample under the upper electrode.  $C_0 = \epsilon_0(l/s)$  is the capacity of the system under vacuum ( $\epsilon_0 = 8.85419 \times 10^{-12}$  F m<sup>-1</sup>). One obtains the dielectric loss  $\epsilon'' = \sigma/\omega$ , where  $\omega = 2\pi\nu$  and  $\nu$  is the frequency. Finally the loss tangent  $tg\delta = \epsilon''/\epsilon'$  and the real and imaginary parts of the electrical modulus are calculated respectively from

$$M' = \frac{\epsilon'}{(\epsilon')^2 + (\epsilon'')^2}$$

and

$$M'' = \frac{\epsilon''}{(\epsilon')^2 + (\epsilon'')^2}$$

The calculations were performed on an IBM 370 computer. The data were stored on magnetic tape from which they are plotted by a Calcomp plotter.

The advantage of using the  $tg\delta$  and  $M''$  notation besides  $\epsilon''$  is that for a given relaxation with a distribution of times the average relaxation time deduced from the experimental

plots varies in the order  $\langle \tau_{\epsilon''} \rangle > \langle \tau_{tg\delta} \rangle > \langle \tau_{M''} \rangle$ . Thus, a relaxation whose maximum intensity falls outside the experimental frequency range on the low-frequency side in the  $\epsilon''$  representation can be clearly seen in the  $tg\delta$  or  $M''$  representation and vice versa for the high-frequency side. Moreover, the lowest intensity relaxation in the  $\epsilon''$  or  $tg\delta$  representations has the highest intensity in the  $M''$  representation. This allows in some cases easy detection of relaxation phenomena which are obscured in the conduction tail of  $\epsilon''$  or  $tg\delta$  curves or by overlap with a more intense relaxation.

**Measurements on Partially Hydrated Zeolites.** Isotherms of the electric permittivity and the conductivity vs. water content were obtained at four different temperatures between 258 and 300 K and, for each temperature, at 15 different frequencies in the range  $200\text{--}3 \times 10^6$  Hz. The isotherms were scanned by desorption of controlled amounts of water. The amount of water desorbed at each point of the isotherm was calculated from the weight change of an identical pellet in a Mac Bain balance, connected in series with the conductivity cell to the same vacuum system. It was assumed that the water loss of the pellet in the conductivity cell was identical with that of the pellet in the Mac Bain balance, both submitted at the same time to the same treatment. The desorption was continued until the conductivity became immeasurably low. Controlled amounts of water were allowed to adsorb simultaneously on the pellets in the Mac Bain balance and in the conductivity cell in order to check the reversibility. The temperature was kept constant with a Haake Kältebad to within 0.5 K. At each point of the isotherm care was taken to measure equilibrium values of conduction and capacity. Usually, at least 24 h was needed after each desorption step before the system was electrically in equilibrium. At room temperature  $\sim 75\%$  of the water content could be desorbed by simply pumping under vacuum. More water was desorbed by heating at increasingly higher temperatures under vacuum. However, in no case was the temperature increased above  $\sim 473$  K in order to avoid structural changes.

**Measurements on Hydrated Zeolites.** Measurements on fully hydrated samples were performed in the range 200 K–room temperature, after equilibration of the pellets in air. The low temperatures were obtained by evaporation of liquid air in a vessel and by conduction of the cold air vapor in a jacket around the conductivity cell. The amount of air vapor, and thus the temperature, were controlled by application of a variable voltage on a resistance in the liquid air of the vessel.

Independently, low temperature thermogravimetric experiments indicated that no appreciable water loss or gain occurred during cooling of the pellets.

Water diffusion studies indicate that above 80% saturation water molecules adsorbed on the external surfaces dominate the diffusion process above 263 K.<sup>15,16</sup> On compression into pellets these external water films, which may contain some dissolved cations, contact each other and provide the pellet with easy passages for the electric current. As the temperature lowers, this water freezes<sup>17</sup> around 268 K and the intracrystalline properties become apparent below that temperature. Such phenomena are common to materials with high intra- to intercrystalline surface ratio. When this ratio becomes small no distinction between internal and external surface properties is possible.<sup>18</sup> Our conduction measurements on hydrated zeolites are therefore significant only below  $\sim 260$  K.

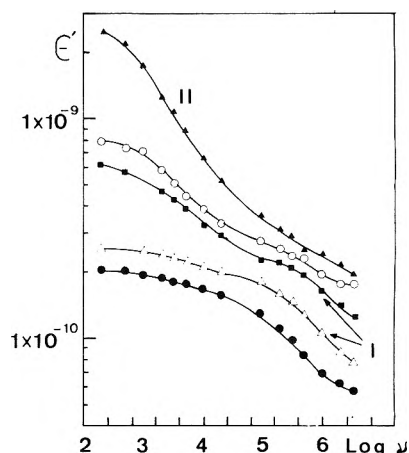


**Figure 1.**  $\epsilon''$  ( $\text{F m}^{-1}$ ) as a function of the logarithm of the frequency at 298 K for NaF2.5: ( $\blacktriangle$ ) 276  $\text{H}_2\text{O}/\text{unit cell}$ ; ( $\circ$ ) 177  $\text{H}_2\text{O}/\text{unit cell}$ ; ( $\blacksquare$ ) 85  $\text{H}_2\text{O}/\text{unit cell}$ ; ( $\triangle$ ) 45  $\text{H}_2\text{O}/\text{unit cell}$ ; ( $\bullet$ ) 19  $\text{H}_2\text{O}/\text{unit cell}$ .

## Results

**Partially Hydrated Zeolites.** Figure 1 shows the behavior at room temperature of  $\epsilon''$  as a function of the logarithm of the frequency at different hydration levels for NaF2.5. Two relaxations (I at high frequencies and II at low frequencies) are evidenced. As the water content decreases, relaxation II diminishes drastically in intensity to attain nearly zero intensity at 19  $\text{H}_2\text{O}/\text{unit cell}$ . This makes relaxation I apparent at the high frequency side of II. Its critical frequency decreases regularly with diminishing water content, but because of the overlap with relaxation I it is hard to decide from Figure 1 if its intensity changes with water content. NaF5.0 has qualitatively the same behavior, except for the appearance of a third low-frequency relaxation at the highest water contents. Figure 2 shows the dependence of the critical frequencies of the three relaxations for NaF5.0, read from the  $tg\delta$  plots, on the water content. Relaxation I of NaF2.5 is also shown. Its critical frequency is 1 to 2 orders of magnitude larger than that of relaxation I for NaF5.0 at the same water content. Moreover, relaxation I of NaF2.5 persists down to 0  $\text{H}_2\text{O}/\text{unit cell}$ . For NaF5.0 relaxation I becomes apparent at  $\sim 140$   $\text{H}_2\text{O}/\text{unit cell}$  with the same intensity as relaxation I of NaF2.5 at 0–20  $\text{H}_2\text{O}/\text{unit cell}$ . A decrease of the water content creates a sudden drop of intensity at  $\sim 60$   $\text{H}_2\text{O}/\text{unit cell}$  and at zero water content and room temperature no relaxation is observed in the experimental frequency range. More detailed information about the intensity variations with water content are found in Table II (available as supplementary material). The intensity is arbitrarily taken as the  $tg\delta$  value at the critical frequency.

Partially  $\text{Ca}^{2+}$ -exchanged zeolites exhibit also two relaxations. By analogy with the corresponding  $\text{Na}^+$  forms, we denote the high-frequency relaxation as I and the low-frequency relaxation as II. An example is shown in Figure 3. This figure shows that II is only apparent at the highest water levels and that I can already be seen from  $\sim 220$   $\text{H}_2\text{O}/\text{unit cell}$ . Figure 4 gives the dependence of the critical frequencies of I, taken from the  $tg\delta$  plots, on the water content. At the same water level they are lower in  $\text{Ca}^{2+}$  samples than in  $\text{Na}^+$ -zeolites and above 120  $\text{H}_2\text{O}/\text{unit cell}$ , the critical frequency is inversely proportional to the  $\text{Ca}^{2+}$  ion content. In the range 90–120  $\text{H}_2\text{O}/\text{unit cell}$  a discontinuity in the critical frequency plots of CaF2.5(1), CaF3.4(1), and CaF5.0(1) is observed in the form of a sudden increase of

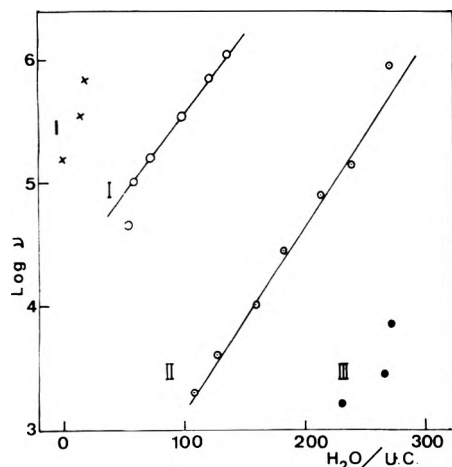


Figure 2. The critical frequencies of the three relaxations in NaF5.0 against the water content: (X) relaxation I for NaF2.5.

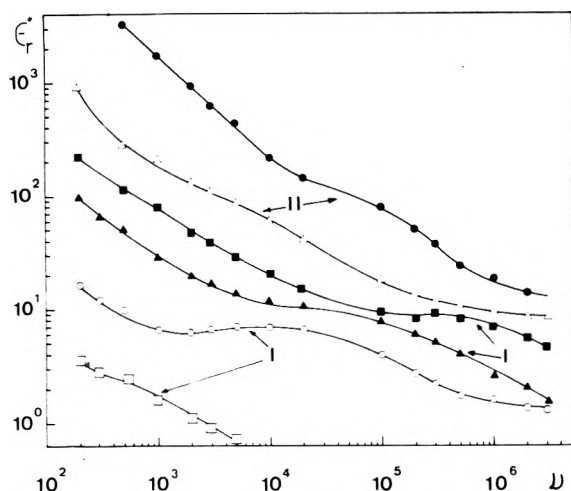


Figure 3. Double logarithmic plot of  $\epsilon_r''$  as a function of the frequency for CaF5.0(1) at room temperature: (●) 251 H<sub>2</sub>O/unit cell; (Δ) 223 H<sub>2</sub>O/unit cell; (■) 187 H<sub>2</sub>O/unit cell; (▲) 137 H<sub>2</sub>O/unit cell; (○) 72 H<sub>2</sub>O/unit cell; (□) 32 H<sub>2</sub>O/unit cell.

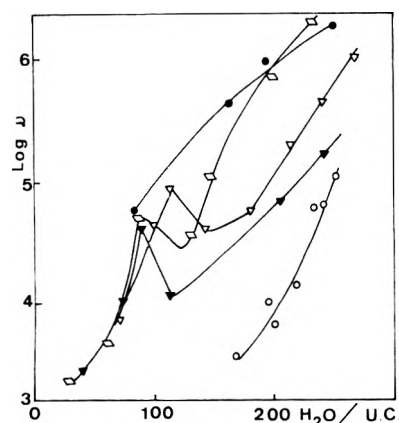


Figure 4. The variation of the critical frequency of relaxation I with water content: (●) CaF5.8(1); (◊) CaF5.0(1); (▼) CaF3.4(1); (○) CaF2.5(1); (○) CaF2.5(2).

the critical frequency. Below 90 H<sub>2</sub>O/unit cell the critical frequency drops out of our experimental range on the low-frequency side and the intensities fall rapidly to zero (Table II). This evolution is valid for the four temperatures

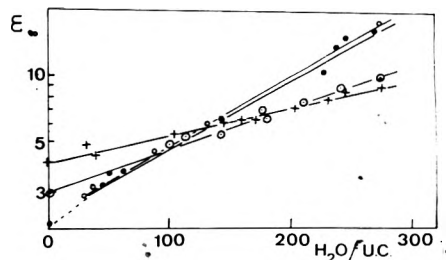


Figure 5.  $\epsilon_\infty$  as a function of water content: (○) CaF5.8(1); (●) CaF5.0(1); (◊) CaF3.4(1); (+) CaF2.5(1).

studied in the range 257–300 K. The activation energies for the Ca<sup>2+</sup>-zeolites given in Table II are independent of the water and the Ca<sup>2+</sup> contents in the range 90–200 H<sub>2</sub>O/unit cell. The average value is 58 kJ mol<sup>-1</sup>.

Isotherms of the electrical permittivity as a function of water content are not easy to determine because the relaxations extend outside the experimental frequency range in many cases (see Figures 1–4). If  $\epsilon_\infty$  is defined as the high-frequency limit of relaxation I, no  $\epsilon_\infty$  isotherms can be determined for the Na<sup>+</sup> forms. Those for the Ca<sup>2+</sup>-zeolites are shown in Figure 5.  $\epsilon_\infty$  decreases linearly with decreasing water content and the slope is steeper for CaF5.0(1) and CaF5.8(1) than for CaF3.4(1) and CaF2.5(1). The  $\epsilon_\infty$  values for the dehydrated samples were determined in our earlier work.<sup>19</sup> The extrapolation to the first experimental points at ~50 H<sub>2</sub>O/unit cell is taken arbitrarily to be linear.  $\epsilon_s$ , defined as the low-frequency limit of relaxation II, is plotted against water content in Figure 6. The isotherms are characterized by a steep decrease from hydrated samples down to ~220 H<sub>2</sub>O/unit cell, followed by a leveling off and another drastic decrease below ~90 H<sub>2</sub>O/unit cell. All the phenomena described so far are not reversible. Adsorption of controlled amounts of water invariably gave the same shape of the curves but at identical water content the value of  $\epsilon_\infty$ , and critical frequencies were lower.

**Hydrated Zeolites.** At every temperature between 190 and 300 K the conductivity is frequency dependent. Extrapolation to zero frequency to obtain dc conductivity values is only possible when no low-frequency relaxation occurs. Overall plots of  $\sigma$  and  $\epsilon_r''$  as a function of the logarithm of the frequency at different temperatures for NaF2.5 are shown in Figure 7 (microfilm). They illustrate the influence of the presence or absence of low-frequency relaxations on the behavior of the conductivity in the low-frequency range.

**Conduction.** Arrhenius plots of the dc conductivities are shown in Figures 8–10 (microfilm). Rather large scatter of experimental points is observed in some cases, due to the inaccuracy of the graphical extrapolation of the conductivities to 0 frequency. In any case, only one conduction mechanism is present. The conductivity of NaF5.0 exceeded that of NaF2.5 contrary to their behavior in the dehydrated state.<sup>14</sup> The introduction of divalent cations decreases the conductivity with respect to the corresponding Na<sup>+</sup> forms. This is especially evident for the Cu<sup>2+</sup>-zeolites. For the Ca<sup>2+</sup>-zeolites the conductivity follows the order CaF5.8(1) > CaF5.0(1) > CaF3.4(1) > CaF2.5(1) and this is the same as for the dehydrated case.<sup>19</sup>

The thermodynamic characteristics for the conduction process are summarized in Table III in terms of the activation energy and activation entropy. The activation energy and entropy of NaF2.5 are considerably higher than those

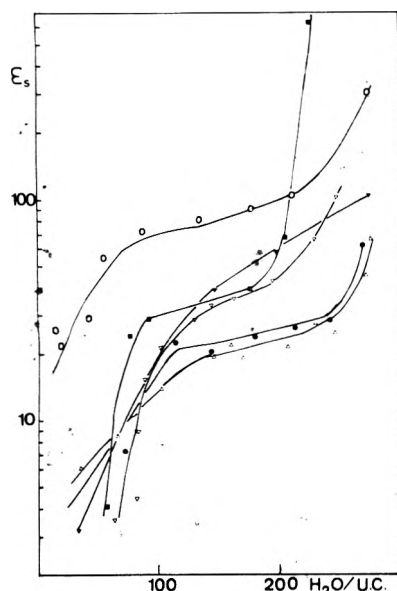


Figure 6.  $\epsilon_s$  as a function of water content: (O) NaF2.5; (■) NaF5.0; (▽) CaF5.8(1); (▼) CaF5.0(1); (●) CaF5.4(1); (Δ) CaF2.5(1).

TABLE III: Activation Energies and Entropies for Conduction in Hydrated Zeolites

Sample	H <sub>2</sub> O/supercage cation	$E$ , kJ mol <sup>-1</sup> (±10)	$\Delta S$ , J mol <sup>-1</sup> K <sup>-1</sup> (±20)
NaF2.5	3.7 (15 m) <sup>a</sup>	100	226
NaF5.0	7.2 (7.7 m)	59	98
CaF2.5(1)	8.2 (7 m)	46	-42
CaF3.4(1)	10.3 (5.4 m)	56	3
CaF5.0(1)	13.6 (4.1 m)	46	-21
CaF5.0(2)	20.8 (2.7 m)	36	-69
CaF5.8(1)	14.7 (3.8 m)	64	68
CuF5.0(1)	7.3 (7.6 m)	72	111
CuF5.0(2)	8.5 (6.5 m)	54	16
CuF5.0(3)	14.6 (3.8 m)	44	-46

<sup>a</sup> The numbers in parentheses are the molarities of cationic solutions with the same concentration.

for NaF5.0. The introduction of divalent cations decreases both values significantly and  $\Delta S$  becomes negative.

**Relaxations.** In the experimental frequency and temperature ranges two relaxations were observed. This is illustrated in Figures 11–13 (microfilm). Again we denote the low-frequency relaxation by II, the high-frequency relaxation by I. The activation energies for relaxation I are summarized in Tables IV and V. They are equal to those for conduction in NaF5.0 and NaF2.5 but for the Ca<sup>2+</sup>- and Cu<sup>2+</sup>-zeolites they are significantly higher. The shapes of the experimental curves in Figures 11–13 are indicative for large distributions of relaxation times. This is a common characteristic for the zeolites, whether hydrated, or dehydrated.<sup>14,19</sup> The distribution of relaxation times is especially large for hydrated Cu<sup>2+</sup>-zeolites (Figure 12). Because of this, the incompleteness of the relaxations, the superposition with a low-frequency relaxation, and a conduction phenomenon a more detailed analysis could not be performed with reasonable accuracy. The intensities of relaxation I, taken as  $tg\delta$  at the critical frequency are temperature dependent. For Ca<sup>2+</sup>-zeolites relaxation I starts to appear around 220 K, increases steeply in intensity to reach a maximum value which is inversely proportional to the Ca<sup>2+</sup>

TABLE IV: Maximum Values of  $tg\delta$  and Activation Energies for the High-Frequency Relaxation of Hydrated Zeolites

Sample	$tg\delta$ (±0.05)	$E$ , kJ mol <sup>-1</sup> (±10)	No. of cations/ unit cell in dense cages	
			Na <sup>+</sup>	Ca <sup>2+</sup>
NaF2.5	0.57 (243K)	102	17	
NaF5.0	0.59	59	20	
CaF2.5(1)	0.20	77	16.1	6
CaF3.4(1)		73		
CaF5.0(1)	0.38	77	14.7	4.7
CaF5.0(2)	0.32	70	3.4	11.0
CaF5.8(1)	0.42	84	14.1	4.7
CuF5.0(1)	0.48 (248K)			
CuF5.0(2)	0.40	64		
CuF5.0(3)	0.30	86		

TABLE V: Temperature Dependence of Maximum Values of  $tg\delta$  for NaF2.5

$T$ , K	$tg\delta$ (±0.05)	$T$ , K	$tg\delta$ (±0.05)
218	0.45	234	0.62
221	0.50	243	0.57
231	0.65	244	0.55

content. This behavior is illustrated in Figure 14. The same temperature dependence was observed for the Cu<sup>2+</sup>-zeolites. The maximum  $tg\delta$  values are given in Table IV. For CuF5.0(1) this value is temperature dependent:  $tg\delta = 0.64$  at 228 K but 0.48 at 240 K. The intensity of relaxation I of NaF2.5 reaches a maximum of 0.65 at 231 K and decreases at higher temperatures (Table V). For NaF5.0 relaxation I could only be seen below 220 K, but its intensity remained constant at 0.59 in the 190–220 K range.

## Discussion

As the partially hydrated zeolites were studied during dehydration we start with the discussion of the data of hydrated zeolites, proceed to the partially hydrated forms, and attempt to link the data to those obtained on dehydrated zeolites.<sup>14,19</sup>

**Hydrated Zeolites. Conduction.** The decrease of the conductivity with divalent cation content and the dependence of the thermodynamic parameters of conduction on the number and kind of exchangeable cations translate the fact that conduction in hydrated zeolites is ionic, the exchangeable cations being responsible for the conduction. The nature of a conduction experiment is such that diffusion of the fastest cations is measured, i.e., the supercage cations. The activation energy of 100 kJ mol<sup>-1</sup> for Na<sup>+</sup> diffusion in hydrated NaF2.5 is much higher than the activation energy for diffusion in dilute ionic solution<sup>20</sup> but remarkably agrees with that of Li<sup>+</sup> in concentrated (8–12 m) LiCl solutions.<sup>21</sup> From this comparison with ionic solutions the 59 kJ mol<sup>-1</sup> for NaF5.0 can be explained by the difference in cationic concentration of the supercages of NaF5.0 and NaF2.5. There are 3.7 water molecules per Na<sup>+</sup> in NaF2.5, not enough to fulfill the coordination requirements of Na<sup>+</sup>. In order to achieve their coordination the Na<sup>+</sup> ions are preferentially located near sites II: Olson<sup>22</sup> reports 24 Na<sup>+</sup> on II in NaF2.5 and Costenoble<sup>23</sup> only 5.3 in NaF5.0. As a consequence too the cationic population of sites I and the cubooctahedra is completely different for the two zeolites: Olson<sup>22</sup> finds 9 Na<sup>+</sup> on I and 8 Na<sup>+</sup> on I' in NaF2.5; Coste-

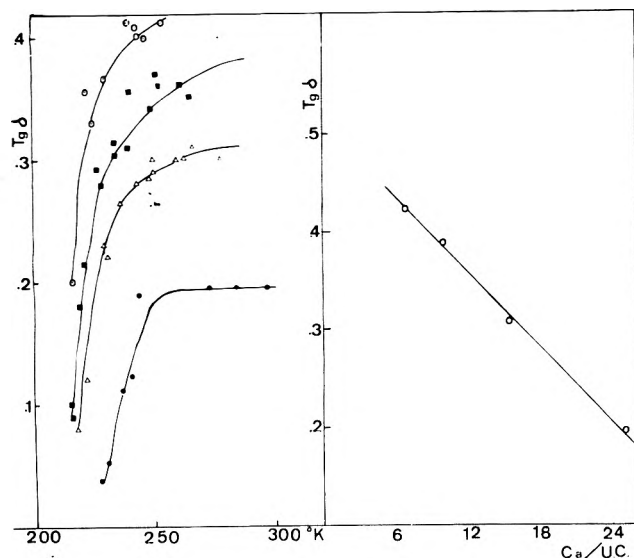


**Figure 14.** Left:  $tg\delta$  at the critical frequency against the temperature: (O) CaF5.8(1); (■) CaF5.0(1); (Δ) CaF5.0(2); (●) CaF2.5(1). Right: maximum values of  $tg\delta$  plotted against the  $Ca^{2+}$  content of the zeolites.

noble<sup>23</sup> finds no  $Na^+$  on I, 14.1  $Na^+$  on I', and 5.8 on II' in NaF5.0. Thus, as in the dehydrated state<sup>19</sup> the cationic occupancies of the sites are not independent of each other. Our activation energy for  $Na^+$  diffusion in NaF2.5 (100  $kJ\ mol^{-1}$ ) contrasts with the value of 40.5  $kJ\ mol^{-1}$  reported by Brown and Sherry<sup>12</sup> from isotopic diffusion studies in the temperature range 276–299 K and the 36.8  $kJ\ mol^{-1}$  found by Jansen and Schoonheydt<sup>3</sup> at  $10^3$  Hz. The latter was obtained from nonequilibrium measurements. This, and the fact that no real dc conductivities were shown, makes comparison with the present results difficult. In any case the discrepancy with the isotopic diffusion studies remains and it may be that two diffusion mechanisms are present, depending on the temperature range.

The decrease of the conductivity, activation energy, and activation entropy (Table III, Figure 9 and 10) upon introduction of divalent cations parallels the behavior of the  $Na^+$  conductivity in the corresponding dehydrated forms.<sup>19</sup>

Although no detailed cation distributions for the present samples are available<sup>24,25</sup> the ion exchange data<sup>26–28</sup> indicate that the majority of charge carriers in the supercages are the divalent cations, except for CuF5.0(1) and CuF5.0(2). The variations among the activation energies and activation entropies may not so much reflect changes in the cationic composition of the supercages than variations in concentration of the supercage solution with varying divalent cation content. It is interesting to compare the present data to those obtained from radiochemical diffusion studies.<sup>8–11</sup> For  $Ba^{2+}$ ,  $Ca^{2+}$ , and  $Sr^{2+}$  in the supercages two activation energies were reported. Below 273 K it was  $\sim 83\ kJ\ mol^{-1}$ , above 273 K it was  $\sim 40\ kJ\ mol^{-1}$ .<sup>8–10</sup> Thus, the activation energies of the present study ( $T < 273\ K$ ) agree with those obtained above 273 K with the radiochemical technique. Why this is so cannot be answered yet. Recently, Dyer and Townsend<sup>11</sup> ascribed the high-temperature diffusion of  $Zn^{2+}$  in synthetic zeolites X and Y to migration of  $Zn^{2+}$  in the cubooctahedra and the low-temperature diffusion mechanism to  $Zn^{2+}$  in the supercages. The latter assignment is in agreement with our interpretation.

As the available sites and the exchangeable cations con-

stitute a sublattice with a large number of vacancies, cationic motion is a cooperative process, complicated by the presence of water.

We note with Calvet<sup>29</sup> that at high cation–water ratios, the cations cannot hydrate themselves in the activated state because every water molecule is already in interaction with a cation. They only provoke a local disorder in the system upon diffusion and the activation entropy is positive. If “free” water molecules are present, i.e., at low cation–water ratios, the cations can hydrate themselves in the activated state and  $\Delta S$  is negative. However, whether the cations are hydrated in the sense that the hydrated cation behaves as a well-defined unit is unlikely. In solution the hydration number of the cations tend to zero above 1.67 M for  $Na^+$  and 0.95 M for  $Ca^{2+}$ .<sup>30</sup> These concentrations are much lower than those in the supercages of the zeolites. Probably the cations in the zeolites are not hydrated or only partially but are mainly surrounded by coordination water, the terms hydration and coordination being defined as Bockris and Saluja did.<sup>30</sup>

**Relaxations.** As the hydrated zeolites exhibit ionic conductivity we expect a Maxwell–Wagner effect in the kilohertz region and assign the low-frequency relaxation to it. The intensities and the activation energies of the high-frequency relaxation are cation dependent. This is a cationic relaxation, i.e., an ionic relaxation due to the restricted motion of exchangeable cations. In the dehydrated state two cationic relaxations were revealed: one around room temperature and ascribed to the cations on sites III' and one at high temperatures, due to the migration of cations within the sodalite cages.<sup>14,19</sup> The intensity of these processes is a function of the cationic occupancy of these sites and especially for the cations in the cubooctahedra, it can be shown that the maximum intensity of the relaxational process occurs at approximately two cations per cubooctahedron.<sup>31</sup> We believe that it is this relaxational process of cations in the cubooctahedra which is measured on the hydrated zeolites. Indeed, the maximum intensities for the  $Ca^{2+}$ - and  $Cu^{2+}$ -zeolites are inversely proportional to the  $Ca^{2+}$  and  $Cu^{2+}$  contents, a fact which cannot be explained on the basis of the cationic content of the supercages (mainly  $M^{2+}$  ions) nor on the basis of the number of residual  $Na^+$  ions. The latter are nearly in equal number for the samples CaF2.5(1), CaF3.4(1), CaF5.0(1), and CaF5.8(1) although the relaxational intensities differ by a factor 2 (Tables IV and V). Moreover the activation energies for the ionic relaxation in divalent zeolites are significantly higher than those for the conduction process in the supercages, suggesting that cations in other parts of the zeolitic structure are active. It can then only be a cationic migration within the cubooctahedra. The activation energy difference between migration in supercages and migration in cubooctahedra reflects (i) the different cation–water ratios; (ii) the different cationic compositions of the cubooctahedra. This picture of the ionic relaxation process, together with the published cation occupancies of the sodalite cages for NaF2.5 and NaF5.0<sup>22,23</sup> allows the construction of Figure 15 with the aid of the  $tg\delta$  values of Tables IV and V. Interpolation of the  $tg\delta$  values for the  $Ca^{2+}$ - and  $Cu^{2+}$ -zeolites allows a calculation of the number of charges per sodalite cage for the different zeolites. This number is higher than the total  $Na^+$  content for the  $Ca^{2+}$ -zeolites, CuF5.0(2) and CuF5.0(3). Thus, the sodalite cages are at least partially occupied by  $Ca^{2+}$  and  $Cu^{2+}$  ions. For CaF5.0 zeolites Costenoble<sup>23</sup> recently showed that sites I were empty and all the



residual  $\text{Na}^+$  ions were in the cubooctahedra. On this basis the cationic occupancy of the cubooctahedra of  $\text{CaF5.0(1)}$ ,  $\text{CaF5.0(2)}$ , and  $\text{CaF5.8(1)}$  was calculated from Figure 15 and reported in Table IVA to be in excellent agreement with the x-ray data.<sup>23</sup> If in  $\text{CaF2.5(1)}$  all the  $\text{Na}^+$  ions are also supposed in the sodalite cages, 6  $\text{Ca}^{2+}$  must be put there too to fulfill Figure 15. The agreement with the x-ray data may be considered as another a posteriori proof of our assignment of the cationic relaxation to the cations in the cubooctahedra. The occupancies of the small cages by divalent ions in partially exchanged zeolites may be due to the drying process at 323 K after exchange followed by storage in the excicator. It may also be due to direct exchange with  $\text{Na}^+$  in the small cavities as suggested by Maes and Cremers for transition metal ions.<sup>28</sup> The fact that a relaxational process, due to cationic motion within the sodalite cages, is measured does not mean that these cations do not move out into the supercages. Indeed, maximum intensities are observed at characteristic temperatures for each cation suggesting that above these temperatures exchange is established between cations in cubooctahedra and in supercages as explained by Brown and Sherry.<sup>12</sup> Below these temperatures cationic motion is restricted mainly inside the cubooctahedra and this idea has been proposed by Hoinkis and Levi.<sup>8</sup> Thus, on the basis of the present results we conclude that the interpretations of the isotopic diffusion data by Brown and Sherry<sup>12</sup> and Hoinkis and Levi<sup>8</sup> are both valid for zeolites. However, they predominate in different temperature ranges.

*Partially Hydrated Zeolites.* The desorption of water leads to a discontinuous decrease of  $\epsilon_s$  and the conductivity, while  $\epsilon_\infty$  decreases linearly. The steep decrease of  $\epsilon_s$  near saturation is clearly due to intercrystalline water which provides the pellets with easy passages for electrical current. The remaining asymptotic behavior reflects the variation of the cationic mobility with decreasing water content. It shows that below 80–100  $\text{H}_2\text{O}/\text{unit cell}$  the cations are immobilized very fast. This water content corresponds to that below which the critical frequency of relaxation I and its intensity fall to zero too. This correspondence suggests that relaxation I is a cationic relaxation. This conclusion follows also from the fact that for  $\text{NaF2.5}$  relaxation I goes over in the cationic relaxation of the dehydrated sample.<sup>14</sup> Relaxation II is then the Maxwell-Wagner effect, while relaxation III is an electrode polarization phenomenon. The latter two are spurious effects, introduced by the heterogeneity of the systems under discussion and are disregarded in the following.

The experimental data gathered in Table II can be divided in two groups. The samples  $\text{CaF5.0(1)}$  and  $\text{CaF5.8(1)}$  with low cation-water ratios have constant relaxational intensities down to  $\sim 90 \text{ H}_2\text{O}$ . The samples  $\text{CaF3.4(1)}$  and  $\text{CaF2.5(1)}$  with higher cation-water ratios show an increase of the relaxational intensity with water content down to  $\sim 90 \text{ H}_2\text{O}/\text{unit cell}$ . Not enough water levels could be investigated for the  $\text{Na}^+$  forms to substantiate this point. These results means that at low cation-water ratios dehydration down to 90  $\text{H}_2\text{O}/\text{unit cell}$  does not affect the cationic distribution, a conclusion confirmed by unpublished x-ray results on  $\text{CaF5.0(2)}$ .<sup>23</sup> When this cation-water ratio increases water molecules directly coordinated to the cations are affected by the dehydration and, as a result, cations rearrange themselves and affect the relaxational intensity. However, the main redistribution occurs below 90  $\text{H}_2\text{O}/\text{unit cell}$  as shown by the sudden decrease of both the relax-

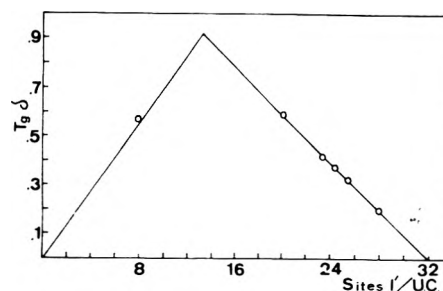


Figure 15.  $Tg\delta$  vs. the occupancy of sites I' in the sodalite cages.

ational intensity and the critical frequency. The discontinuities at 90–120  $\text{H}_2\text{O}/\text{unit cell}$  in the plots of Figure 4 may indicate an enhanced cationic mobility due to the start of this rearrangement.

For  $\text{NaF2.5}$  the cationic relaxation goes over into that of the dehydrated state and is therefore also ascribed to site III' cations moving between two occupied sites II.<sup>14,19</sup> For the other samples the data do not allow a clear distinction between a relaxation due to migration of cations on III' or due to cationic jumping inside the cubooctahedra. Indeed, as dehydration affects mainly the water content of the supercages, and thus, decreases the cationic mobility therein, it may well be that relaxation I is due to interstitial cations in the supercages, becoming immobilized upon gradual dehydration. The sudden drop of intensity below 90  $\text{H}_2\text{O}/\text{unit cell}$  reflects then the redistribution of the cations from a "hydrated" to a "dehydrated" distribution, leaving no or nearly no cations on sites III'.<sup>19</sup> The difficulty with this interpretation is that it does not offer an explanation for the tremendous difference in critical frequency between the samples (Figures 2 and 4). If, on the other hand, relaxation I of the partially exchanged zeolites is ascribed to jumping of cations inside the cubooctahedra, it must be assumed that, as the very beginning of the dehydration decreases their mobility (Figures 2 and 4), this initial dehydration affects the water content of the cubooctahedra. It is not clear then why the activation energies are independent of the water content, and, in any case, lower than for the same relaxation on the hydrated forms but at lower temperatures. Also, because the intensities do not conform with those of the hydrated forms the cationic occupancy of the sodalite cages should be dependent on the temperature and the water content, especially for the samples with high cation/water ratios,  $\text{NaF2.5}$ ,  $\text{NaF5.0}$ ,  $\text{CuF5.0(1)}$ ,  $\text{CaF2.5(1)}$ , and  $\text{CaF3.4(1)}$ . It should be interesting to verify this by x-ray diffraction studies of hydrated and partially hydrated zeolites at different temperatures below room temperature.

In these interpretations of the relaxational behavior of hydrated and partially hydrated zeolites in the kilohertz region there is no room for a water relaxational process. We agree with Lebrun and coworkers<sup>7</sup> that these phenomena take place in the frequency range 100 MHz–10 GHz. The consequence is that the variations of  $\epsilon_\infty$ , the high-frequency limit of the cationic relaxations, reflect the properties of the adsorbed water molecules at different hydration levels.

An exact procedure to extract the electrical permittivity of adsorbed water does not exist but some approximations have been discussed by Mc Intosh.<sup>32</sup> The results from the Fiat-Folman-Garbatski treatment<sup>33</sup> and the extended Böttcher equation are summarized in Table VI. Although the absolute values may be of little use for further quantitative work they clearly express that zeolitic water is highly

TABLE VI: Electrical Permittivity of Adsorbed Water

H <sub>2</sub> O/ unit cell	CaF5.0(1)		CaF2.5(1)	
	Fiat et al.	Böttcher (extended)	Fiat et al.	Böttcher (extended)
50	3.41	3.07	2.90	2.72
100	8.09	6.42	5.04	4.49
150	13.84	11.37	7.54	6.55
200	23.07	18.45	10.56	9.07
250	35.62	28.80	13.75	11.75

polarized under influence of the surface and the exchangeable cations. The higher the cation content the lower the electrical permittivity of adsorbed water. The electrical permittivity of a 4 M solution is 46.4,<sup>34</sup> as compared to 35.62 found for hydrated CaF5.0(1) with the same cationic concentration in the supercages. The influence of the surface may account for the difference. For CaF2.5(1)  $\epsilon$  (H<sub>2</sub>O) is lower than usually reported for concentrated ionic solutions.<sup>34</sup> Such low electrical permittivities are indicative of the fact that freezing of water in the supercages of the zeolites is impossible in the sense of a real phase transition. Of course, as the temperature lowers cations and water molecules are immobilized gradually as evidenced by our experiments. It should be interesting to see if at very low temperatures this results in an ordering of the water molecules, which may be called a glass transition.<sup>35</sup>

**Acknowledgment.** Acknowledgment is made to the Belgian Government (Programmatie van het Wetenschapsbeleid) for financial support. R. Schoonheydt is indebted to the N.F.W.O. for a grant as "Aangesteld Navorsers". W. De Wilde acknowledges an I.W.O.N.L. research fellowship. The authors are grateful to L. Leplat for technical assistance. Calculations were performed at the computer center of the Katholieke Universiteit Leuven. The authors thank Professor J. B. Uytterhoeven for his vivid interest.

**Supplementary Material Available:** Table II and Figures 7–13 (12 pages). Ordering information is given on any current masthead page.

## References and Notes

- (1) U. Lohse, H. Stach, M. Hollnagel, and W. Schirmer, *Monatsber. Dtsch. Akad. Wiss. Berlin*, **12**, 828 (1970); *Z. Phys. Chem.*, **246**, 91 (1971); **247**, 65 (1971).
- (2) U. Lohse, H. Stach, and W. Schirmer, *Z. Phys. Chem.*, **254**, 59 (1973).
- (3) F. J. Jansen and R. A. Schoonheydt, *Adv. Chem. Ser.*, No. **121**, 96 (1973).
- (4) H. A. Resing and J. K. Thompson, *Adv. Chem. Ser.*, No. **101**, 473 (1971); H. A. Resing, *Adv. Mol. Relaxation Processes*, **1**, 109, 189 (1968).
- (5) B. Morris, *J. Phys. Chem. Solids*, **30**, 73, 103 (1969).
- (6) W. Matron, G. Ebert, and F. H. Müller, *Kolloid-Z. Z. Polym.*, **248**, 986 (1971).
- (7) J. M. Wacrenier, J. Fontaine, A. Chapoton, and A. Lebrun, *Rev. Gen. Electr.*, **76**, 719 (1967); A. Chapoton, B. Vandorpe, and J. M. Wacrenier, *C. R. Acad. Sci. Paris*, **268**, 1729 (1969); A. Chapoton, A. Lebrun, and G. Ravalitera, *ibid.*, **271**, 525 (1970); A. Chapoton, B. Vandorpe, and M. Choquet, *ibid.*, **272**, 1261 (1971); A. Chapoton, G. Ravalitera, B. Vandorpe, M. Choquet, and A. Lebrun, *J. Chim. Phys.*, **1191** (1972).
- (8) E. Hoinkis and H. W. Levi, *Z. Naturforsch. A*, **23**, 813 (1968); **24**, 1511, 1672, 1784 (1969); "Ion Exchange in the Process Industries", The Society of Chemical Industries, London, 1970, p 339.
- (9) A. Dyer and J. M. Fawcett, *J. Inorg. Nucl. Chem.*, **28**, 615 (1966).
- (10) A. Dyer, R. B. Gettins, and J. G. Brown, *J. Inorg. Nucl. Chem.*, **32**, 2389, 2395, 2401 (1970).
- (11) A. Dyer and R. P. Townsend, *J. Inorg. Nucl. Chem.*, **35**, 3001 (1973).
- (12) L. H. Brown and H. S. Sherry, *J. Phys. Chem.*, **75**, 3855 (1971).
- (13) A. Maes and A. Cremers, *Adv. Chem. Ser.*, No. **121**, 230 (1973).
- (14) F. J. Jansen and R. A. Schoonheydt, *J. Chem. Soc., Faraday Trans. 1*, **69**, 1338 (1973).
- (15) J. Kärger, *Z. Phys. Chem., Leipzig*, **248**, 27 (1971); J. Kärger, H. Pfeifer, E. Riedel, and H. Winkler, *J. Colloid Interface Sci.*, **44**, 187 (1973).
- (16) E. Riedel, J. Kärger, and H. Winkler, *Z. Phys. Chem., Leipzig*, **252**, 161 (1973).
- (17) A. R. Haly, *J. Phys. Chem. Solids*, **33**, 129 (1972).
- (18) J. Mamy and J. P. Gauthier, *Bull. Groupe Fr. Argiles*, **25**, 43 (1973).
- (19) R. A. Schoonheydt and W. De Wilde, *J. Chem. Soc., Faraday Trans. 1*, **70**, 2132 (1974); R. A. Schoonheydt and F. Velghe, *ibid.*, accepted for publication.
- (20) A. Cremers, "Ionic Movement in a Colloidal Environment", N. V. De Vlaamse Drukkerij, Leuven, Belgium, 1968, p 113.
- (21) C. T. Moynihan, R. D. Bressel, and C. A. Angell, *J. Chem. Phys.*, **55**, 4414 (1971).
- (22) D. H. Olson, *J. Phys. Chem.*, **74**, 2758 (1970).
- (23) M. Costenoble, preliminary results.
- (24) J. V. Smith, *Adv. Chem. Ser.*, No. **101**, 171 (1971).
- (25) P. Gallezot and B. Imelik, *J. Catal.*, **26**, 295 (1972).
- (26) H. S. Sherry, *J. Phys. Chem.*, **72**, 4086 (1968).
- (27) E. Gallei, D. Eisenbach, and A. Ahmed, *J. Catal.*, **33**, 62 (1974).
- (28) A. Maes and A. Cremers, *J. Chem. Soc., Faraday Trans. 1*, **71**, 265 (1975).
- (29) R. Calvet, *Ann. Agron.*, **24**, 77, 135 (1973).
- (30) J. O'M Bockris and P. P. S. Saluja, *J. Phys. Chem.*, **76**, 2140 (1972).
- (31) R. A. Schoonheydt, Aggregaatsthesis, K. U. Leuven, 1975.
- (32) R. L. Mc Intosh, "Dielectric Behavior of Physically Adsorbed Gases", Marcel Dekker, New York, N.Y., 1966, Chapter 2.
- (33) D. Fiat, M. Folman, and U. Garbatski, *Proc. R. Soc. London, Ser. A*, **260**, 409 (1961).
- (34) J. B. Hasted, "Dielectric and Related Molecular Processes", Vol. 1, M. Davies, Ed., The Chemical Society, London, 1972, Chapter 5.
- (35) W. D. Basler and H. Lechert, *Ber. Bunsenges. Phys. Chem.*, **76**, 1234 (1972).

# Substituent Effects on Nitroaromatic Radical Anions in Aqueous Solution<sup>1</sup>

P. Neta and Dan Melsel\*

Radiation Research Laboratories and Department of Chemistry, Mellon Institute of Science, Carnegie-Mellon University, Pittsburgh, Pennsylvania 15213 (Received October 6, 1975)

Publication costs assisted by Carnegie-Mellon University and the U.S. Energy Research and Development Administration

The effect of substituents on the ESR parameters of nitroaromatic radical anions in aqueous solutions has been studied by observing the spectra of some 20 such radicals using the in situ radiolysis steady-state ESR technique. The results focus on the effect of substitution and disubstitution at positions ortho to the nitro group. Higher nitrogen splittings were found to result in lower hyperfine constants for both para and ortho protons (or methyl groups), while meta hydrogens are affected to a much smaller extent. An inverse linear correlation is in fact found between  $a_{\text{NO}_2}^{\text{N}}$  and  $a_{\text{para}}^{\text{H}}$ . When  $a_{\text{NO}_2}^{\text{N}}$  increases to values greater than  $\sim 20$  G the meta proton splittings become higher than those for the para and ortho protons. The effect of an ortho OH group is relatively small but the effect of its basic form ( $\text{O}^-$ ) is comparable to that of a methyl group. A strong synergistic effect of the second substituent in ortho disubstituted nitroaromatics is observed. It is also found that the rate of electron-transfer reaction from  $(\text{CH}_3)_2\dot{\text{C}}\text{OH}$  to the parent compounds can be correlated with the spin density on the ring of the resultant radical anion as indicated by the inverse correlation with  $a_{\text{NO}_2}^{\text{N}}$ .

The effect of substituents on the geometry and the electronic structure of nitroaromatic molecules and their radical anions have been studied in detail. Several techniques, including uv and NMR spectroscopy and dipole moment measurements, have been utilized in elucidating these effects in the parent molecules.<sup>2</sup> The same effects in the radical anions have been studied using ESR spectroscopy,<sup>3-7</sup> while polarographic<sup>6-9</sup> and kinetic studies<sup>2</sup> yield information concerning the effects of substituents on the energetics of the transformation from the molecule to its radical anion and the activated complex involved. Recently we have been able to correlate the one electron reduction potentials of several nitro aromatic compounds in aqueous solutions with the nitrogen hyperfine constants ( $a_{\text{NO}_2}^{\text{N}}$ ) for the radicals.<sup>10</sup>

The effect of electron-withdrawing groups in decreasing  $a_{\text{NO}_2}^{\text{N}}$  and of electron-donating groups in increasing  $a_{\text{NO}_2}^{\text{N}}$  was correlated with Hammett's constants.<sup>3</sup> The relevance of such a correlation was intensified by the comparison of the effect of the same substituents in different conjugated systems.<sup>3</sup> These correlations were, however, confined mainly to substitution at positions para and meta to the nitro group. On the other hand, the most striking effect of substitution or disubstitution occurs at the ortho position. The work of Geske et al.<sup>7</sup> clearly establishes that the effect of such a substitution exceeds by far any mesomeric effect and has to be attributed to spacial twisting of the nitro group out of the plane of the benzene ring. Recent INDO MO calculations corroborates these conclusions.<sup>11</sup> The calculated twist angles in the radicals resemble those estimated for the molecules.<sup>7</sup>

The only substituents studied thus far from this point of view are the bulky methyl and *tert*-butyl groups in nitrobenzenes and nitroanilines in organic solvents. We have undertaken the present study with the hope of gaining further insight into the effect of polar charged and uncharged ortho substituents in nitrobenzene radical anions in aqueous solutions. Some specific effects due to the water are to be expected and  $a_{\text{NO}_2}^{\text{N}}$  is usually found to be higher in this solvent than in aprotic solvents.<sup>12</sup> Indeed, it was found that

hydrogen bonding between the nitro and the hydroxyl group in *o*-nitrophenol radical anion results in a pronounced increase in the  $\text{p}K_{\text{a}}$  of this proton.<sup>13</sup> Two techniques were used in this study. One was the in situ radiolysis steady-state ESR technique and the other was kinetic spectrophotometric pulse radiolysis which enables us to measure the absolute rate constants for electron transfer from the 2-propanol radical to the nitro compound.

## Experimental Section

Deoxygenated aqueous solutions containing  $10^{-4}$  to  $10^{-3}$  M of the nitroaromatic compound, 0.1 M isopropyl alcohol, and  $5 \times 10^{-3}$  M phosphate buffer at pH 7 (unless otherwise stated) were irradiated by 2.8-MeV electrons from a Van de Graaff accelerator. Radiation produced  $e_{\text{aq}}^-$  reacts with  $\text{ArNO}_2$  at diffusion-controlled rates, while H and OH react with the alcohol to produce  $(\text{CH}_3)_2\dot{\text{C}}\text{OH}$  which also reduces  $\text{ArNO}_2$  efficiently. The nitroaromatic radical anions thus produced were studied by the steady-state in situ radiolysis ESR technique.<sup>13</sup>

Rate constants for the reduction of  $\text{ArNO}_2$  by  $(\text{CH}_3)_2\dot{\text{C}}\text{OH}$  were determined by kinetic spectrophotometric pulse radiolysis using  $\text{N}_2\text{O}$  saturated solutions. Experimental conditions were adjusted such that  $e_{\text{aq}}^-$  is quantitatively converted into OH by reaction with  $\text{N}_2\text{O}$  and then all OH and H react with isopropyl alcohol. The absolute rate constant for the reaction of  $(\text{CH}_3)_2\dot{\text{C}}\text{OH}$  with  $\text{ArNO}_2$  was determined by following the kinetics of formation of the  $\text{ArNO}_2^-$  optical absorption, usually at 300–350 nm. The total radical concentration produced by the pulse was kept at 1–3  $\mu\text{M}$  to minimize second-order decay. Details of the computer-controlled pulse radiolysis system have been given previously.<sup>14</sup>

## Results

The ESR spectra recorded with irradiated aqueous solutions of the nitroaromatic compounds were usually of high line intensities because of the relatively long lifetime of the radical anions observed. In a few cases, the spectra were quite complex and despite the reasonable line intensities

**TABLE I: ESR Parameters of Nitroaromatic Radical Anions<sup>a</sup> and Rate of Reduction of Their Parent Compounds by (CH<sub>3</sub>)<sub>2</sub>COH**

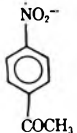
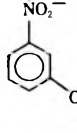
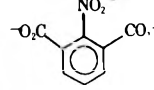
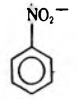
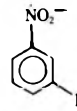
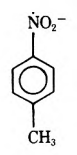
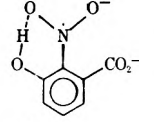
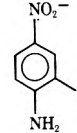
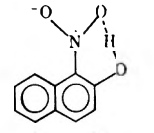
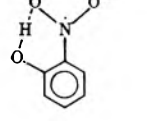
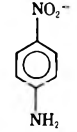
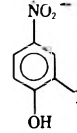
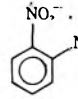
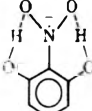
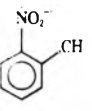
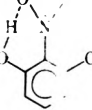
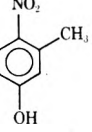
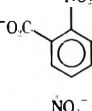
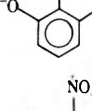
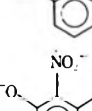
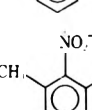
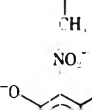
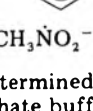
Radical	pH	<i>g</i>	<i>a</i> <sub>NO<sub>2</sub></sub> <sup>N</sup>	<i>a</i> <sub>O</sub> <sup>H</sup>	<i>a</i> <sub>m</sub> <sup>H</sup>	<i>a</i> <sub>p</sub> <sup>H</sup>	<i>a</i> (others)	<i>k</i> <sub>1</sub> , M <sup>-1</sup> s <sup>-1</sup>
	7	2.00470 <sup>b</sup>	11.57	3.24(2)	1.08(2)		<i>a</i> <sub>CH<sub>3</sub></sub> <sup>H</sup> = 0.43	3.8 × 10 <sup>9</sup> <sup>c</sup>
	7	2.00448 <sup>b</sup>	13.66	3.38(2)	1.12	3.60	<i>a</i> <sub>CH<sub>3</sub></sub> <sup>H</sup> < 0.1	
	7,14	2.00459	13.68		1.17(2)	3.36		1.5 × 10 <sup>8</sup>
	6,12	2.00448 <sup>d</sup>	14.20	3.38(2)	1.15(2)	3.65		1.6 × 10 <sup>9</sup> <sup>e</sup>
	7	2.00451	14.20	3.30(2)	1.10	3.53	<i>a</i> <sub>NH<sub>2</sub></sub> <sup>H</sup> = 0.43 <i>a</i> <sub>NH<sub>2</sub></sub> <sup>N</sup> = 0.22	1.5 × 10 <sup>9</sup>
	7	2.00442	14.45	3.39(2)	1.13(2)	3.82(CH <sub>3</sub> )		
	7	2.00458	14.64		1.01; 0.91	3.45	<i>a</i> <sub>OH</sub> <sup>H</sup> = 0.28	3.3 × 10 <sup>8</sup>
	7	2.00468	14.68	<i>f</i>				
	7	2.00467	14.82	<i>f</i>				
	7,14	2.00451 <sup>d</sup>	14.85	3.39	1.04; 0.91	3.60	<i>a</i> <sub>OH</sub> <sup>H</sup> = 0.38	
	7	2.00441	14.90	3.35(2)	1.05(2)		<i>a</i> <sub>NH<sub>2</sub></sub> <sup>H</sup> = 1.05 <i>a</i> <sub>NH<sub>2</sub></sub> <sup>N</sup> = 1.05	7.2 × 10 <sup>8</sup>
	7	2.00448	14.94	3.62; 3.18	1.08		<i>a</i> <sub>NH<sub>2</sub></sub> <sup>H</sup> = 0.43 <i>a</i> <sub>NH<sub>2</sub></sub> <sup>N</sup> = 0.43	
	7	2.00457	15.22	<i>f</i>				9.2 × 10 <sup>8</sup>

TABLE I (Continued)

Radical	pH	<i>g</i>	$a_{\text{NO}_2}^{\text{N}}$	$a_{\text{O}}^{\text{H}}$	$a_{\text{m}}^{\text{H}}$	$a_{\text{p}}^{\text{H}}$	$a(\text{others})$	$k_1, \text{M}^{-1} \text{s}^{-1}$
	7	2.00463	15.60		0.99(2)	3.41	$a_{\text{OH}}^{\text{H}} = 0.34(2)$	$6.8 \times 10^6$
	7	2.00474	16.69	2.73; 2.22(CH <sub>3</sub> )	1.23; 0.95	2.73		$4.8 \times 10^6$
	7	2.00477	17.37	1.94(CH <sub>3</sub> )	0.92(2)	2.48		$2.9 \times 10^6$
	7	2.00474	17.67	2.71; 2.02(CH <sub>3</sub> )	1.14; 0.88			
	7	2.00501	19.18	0.98(CH <sub>3</sub> )	0.98(2)	1.43		$1.9 \times 10^6$
	1 M KOH	2.00489	19.64		0.89; 0.73	1.24		
	7	2.00502	21.65	0.32(CH <sub>3</sub> )	0.93; 0.75	0.41		$2.3 \times 10^6$
	1 M KOH 4 M KOH	2.00499	21.68 21.84		0.82(2) 0.82(2)	0.37 0.30		
	7	2.00501	21.95 <sup>g</sup>	0.30(2CH <sub>3</sub> )	0.89(2)	0.30(CH <sub>3</sub> )		
	1 M KOH	2.00497	22.12	0.24(CH <sub>3</sub> )	0.92(2)	<0.2		
$\text{CH}_3\text{NO}_2^-$	7	2.00495 <sup>h</sup>	25.96				$a_{\text{CH}_3}^{\text{H}} = 12.12$	

<sup>a</sup> Determined in irradiated aqueous solutions containing  $1-5 \times 10^{-4}$  M of the nitro compounds, 0.1 M 2-propanol, 2 mM phosphate buffer at pH 7 or KOH, and deoxygenated by bubbling with pure nitrogen. The hyperfine constants *a* are given in gauss and are accurate to  $\pm 0.03$  G. The *g* factors were determined relative to the signal from the silica cell<sup>13</sup> and are accurate to  $\pm 0.00005$ . Second-order corrections have been made. <sup>b</sup> ESR parameters from ref 10. <sup>c</sup> From ref 25. <sup>d</sup> ESR parameters from ref 13. <sup>e</sup> From ref 27. <sup>f</sup> The pattern of the smaller splittings could not be resolved sufficiently to allow analysis. <sup>g</sup> ESR parameters from ref 10, assignments of the small splittings has been changed as discussed in text. <sup>h</sup> ESR parameters from ref 26.

small splittings could not be resolved sufficiently to allow complete analysis. However, determination of the nitro group nitrogen hyperfine constant was always straightforward because the three groups of lines were fully separated. The experimental results are summarized in Table I where the radicals are arranged in order of increasing  $a_{\text{NO}_2}^{\text{N}}$ .

Assignment of the ortho, meta, and para proton splittings in the first half of Table I could be easily made following previous assignments where  $a_{\text{p}}^{\text{H}} \geq a_{\text{o}}^{\text{H}} > a_{\text{m}}^{\text{H}}$ . This order, however, fails to describe the observed spectra when

$a_{\text{NO}_2}^{\text{N}}$  becomes large and  $a_{\text{p}}^{\text{H}}$  small. It appears that an increase in  $a_{\text{NO}_2}^{\text{N}}$ , i.e., shift of spin density from the ring toward the nitro group, results in a decrease in  $a_{\text{o}}^{\text{H}}$  and  $a_{\text{p}}^{\text{H}}$  but has only a small effect on  $a_{\text{m}}^{\text{H}}$ . At high  $a_{\text{NO}_2}^{\text{N}}$  the para proton splitting becomes even smaller than that for the meta. The most conclusive evidence for this change in the relative magnitude of para vs. meta hyperfine constants is obtained from the results for 2-nitroresorcinol and 3-methyl-2-nitrophenol at high pH (21 and 23 in Table I and spectra in Figure 1). In the first case the splitting by the

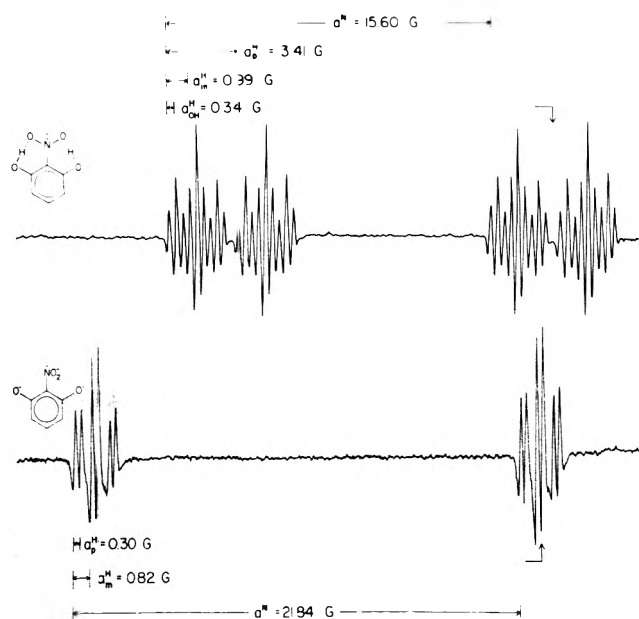
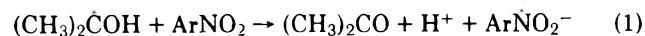


**Figure 1.** ESR spectra of the 2-nitroresorcinol radical anion: upper spectrum at pH 7, lower spectrum in 4 M KOH solution. In both cases the irradiated solutions contained 1 mM 2-nitroresorcinol and 0.1 M 2-propanol and were deoxygenated by bubbling with nitrogen. The arrows indicate the center of the spectra and the third group of lines is omitted. Note  $a_p^H$  vs.  $a_m^H$  in both cases.

single para proton is less than half that by the two equivalent meta protons. In the case of the 3-methyl-2-nitrophenol the splitting by the para proton was too small to be resolved, i.e.,  $<0.2$  G, as compared with 0.92 G observed for two approximately equivalent meta protons. It should be noted that for these two compounds the spectra at 1 M KOH were somewhat distorted, probably because of incomplete dissociation of the OH group, but at 4 M KOH symmetric spectra are again observed. This observation is in agreement with previous findings that the  $pK_a$  for the radical anion of *o*-nitrophenol is above 14.<sup>13</sup>

In the other radicals with  $a_{NO_2}^H$  larger than 20 G (2-nitro-mesitylene and 3-methyl-2-nitroanisole) the assignments are less certain and were made on the basis of best fit with the line in Figure 3 (see below). This approach causes us to change our previous assignment<sup>10</sup> of the proton splittings in nitro-mesitylene radical anion.

The rate constants measured for the electron transfer from  $(CH_3)_2COH$  to the nitro compounds



are also summarized in Table I. These rate constants were determined by pulse radiolysis of  $N_2O$  saturated solutions under pseudo-first-order conditions ( $[ArNO_2] \gg [(CH_3)_2\dot{C}OH]$ ) at various concentrations of the nitro compound. From the linear plots of the observed rate constant vs. the concentration of the nitro compound, the second-order rate constants were calculated, as exemplified in Figure 2.

## Discussion

The results for the radical anions 1–12 in Table I exhibit the effect of electron-withdrawing and electron-donating substituents on  $a_{NO_2}^H$ . As expected, substitution at the para position causes a greater change in  $a_{NO_2}^H$  than substitution at the meta position. Along with the change in the nitrogen

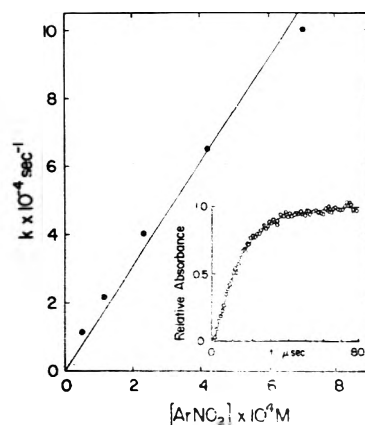


**Figure 2.** Characteristic experimental results for the determination of  $k_1$  for  $ArNO_2 = 2$ -nitroisophthalic acid. Insert shows the computer-processed oscillogram for  $[ArNO_2] = 2.34 \times 10^{-4}$  M at  $\lambda = 310$  nm. All solutions contain 0.1 M 2-propanol, 5 mM phosphate buffer (pH 7), and were saturated with  $N_2O$ .

splitting small changes in the ring proton splittings are also observed. The present data are not sufficient to show the trend of such changes but previous work has shown that electron-withdrawing substituents cause decrease of both the nitrogen and the ring proton splittings (see, e.g., ref 6).

Methyl substitution at the ortho position has an effect much greater than that at the para position. This ortho effect must result from sources other than mesomeric effects and is usually attributed to the twisting of the nitro group out of the plane of the ring.<sup>7,11</sup> As a result of this twist, spin delocalization becomes less favorable and  $a_{NO_2}^H$  increases while ring proton splittings decrease. This correlation is shown in Figure 3 where  $a_p^H$  (or  $0.9 a_{p-CH_3}^H$ )<sup>15</sup> for ortho substituted nitrobenzene radical anions is found to decrease considerably with the increase in  $a_{NO_2}^H$ . The linear correlation of  $a_p^H$  with  $a_{NO_2}^H$  strongly suggests that the increase in  $a_{NO_2}^H$  is due to an increased spin localization on the nitro group at the expense of the spin density in the ring  $\pi$  system rather than spin redistribution among the components of the nitro group itself. This effect is far greater than the effect of electron donation by the substituent, the latter being represented by the small changes shown by radicals 4–12 (Table I and Figure 3).

The decrease in  $a_o^H$  upon increasing  $a_{NO_2}^H$  appears to be similar in magnitude to that in  $a_p^H$ . However,  $a_m^H$  is affected to a much smaller extent as shown by the dashed line in Figure 3. Increasing  $a_{NO_2}^H$  from 14 to 22 G causes only  $\sim 20\%$  decrease in  $a_m^H$  while both  $a_o^H$  and  $a_p^H$  decrease by more than 90%. The INDO calculations indeed predict that the effect of the change in twist angle of the nitro group on  $a_m^H$  should be smaller than that on  $a_o^H$  and  $a_p^H$ .<sup>11</sup> Previous results for methyl-substituted nitroaromatics in acetonitrile showed similar trends<sup>7</sup> but due to the solvent effect higher values of  $a_{NO_2}^H$  are obtained in the present study along with lower values of  $a_o^H$  and  $a_p^H$  so that the latter actually drop to values lower than  $a_m^H$ . Based on their INDO MO calculations Gilbert and Trenwith<sup>11</sup> predicted that  $a_m^H$  should become higher than  $a_p^H$  and  $a_o^H$ . However, no experimental data were available to verify this prediction.

The effect of the solvent on the hyperfine constants has been studied experimentally and theoretically.<sup>12,16–21</sup> Assuming the approach of Pannell<sup>19</sup> the correlation between the nitro group nitrogen hyperfine constants in two solvents A and B ( $a_A^N$  and  $a_B^N$ , respectively) is given by

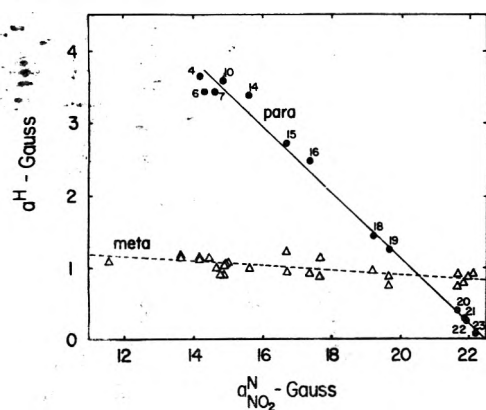


Figure 3. Correlation of  $a^H$  with  $a_{NO_2}^N$ : ● (solid line),  $a_p^H$ , Δ (dashed line),  $a_m^H$ . Numbers refer to the compounds in Table I.

$$a_B^N = ma_A^N + 2Q_{ON}(\rho_{OA} - m\rho_{OB}) + Q_{CN}(\rho_{CA} - m\rho_{CB}) \quad (2)$$

where  $m = \rho_{NA}/\rho_{NB}$  and  $Q$  and  $\rho$  have the usual meaning of the Karplus-Fraenkel relation<sup>22</sup> with the A and B subscripts indicating the different solvents. According to eq 2, for a series of closely related radicals, a linear relation should exist between the hyperfine constants in the two solvents, provided that  $m$  is constant and that the  $Q$  coefficients and the spin distribution among the nitrogen neighbors remains constant along the series in both solvents. This is shown to be the case for the unhindered radicals (Figure 4). However, with those radicals for which the nitro group is thought to be twisted, the effect of water solvation and hydrogen bonding is seen to be much higher. Obviously there seems to be some synergistic effect of the water on  $a_{NO_2}^N$  and once the nitro group is taken out of the ring plane its vulnerability to further solvation and/or hydrogen bonding increases. It is noted that from the solid line in Figure 4 one gets  $a_{NO_2(H_2O)}^N = a_{NO_2(CH_3CN)}^N$  at 25.5 G which coincides with the value for nitroalkanes. Indeed, no solvent effect was found for these compounds.<sup>12</sup> The solid line, i.e., the correlation for the unhindered radicals, is the appropriate one to lead to this conclusion since no synergistic effect is expected for nitroalkanes. Similar synergistic effect is observed for most of the ortho disubstituted compounds studied. Once the first ortho substitution twists the nitro group out of plane, the second substitution, which by itself may have negligible effect, increases the extent of this twist. This is demonstrated by the cases of 2-nitrotoluene (15, Table I) compared to 2,6-dimethylnitrobenzene<sup>7</sup> or 2,4,6-trimethylnitrobenzene (22, Table I). Similarly the effect on  $a_{NO_2}^N$  of an ortho methoxyl group in nitrobenzene is very small<sup>19</sup> while that of a similar substitution in 2-nitrotoluene is very pronounced (compare 15 and 20, Table I). The effect of ortho carboxylate substitution<sup>23</sup> and disubstitution is even more striking. For 2-nitroisophthalate (3, Table I)  $a_{NO_2}^N$  is about 0.5 G smaller than that for nitrobenzene while for 3-methyl-2-nitrobenzoate (18)  $a_{NO_2}^N$  is 2.5 G higher than that for *o*-nitrotoluene. Obviously, in the case of the nitroisophthalate radical, the gain in resonance energy obtained when the nitro anion group is locked in the ring plane is sufficient to overcome any energy gain from the orientation of the carboxylate groups in this plane. The van der Waals radii, however, demand that the carboxylate groups be twisted out of plane in order for the nitro group to remain in plane. For 3-methyl-2-nitrobenzoate such a situation is impossible and the carboxylate group causes

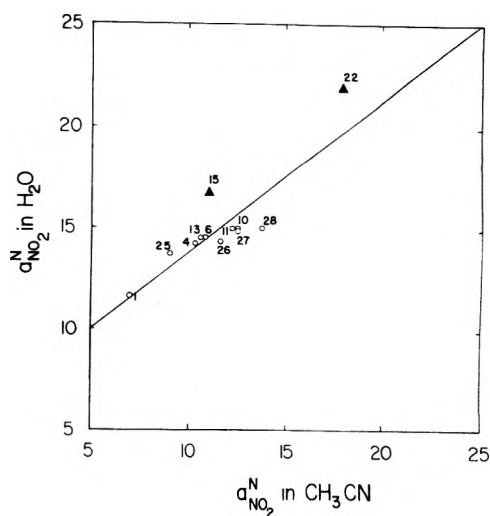


Figure 4. Correlation of  $a_{NO_2}^N$  in water with that in acetonitrile. Numbers refer to compounds in Table I and added are: 25, *o*-nitroacetophenone; 26, *p*-nitroanisole; 27, *m*-nitrophenol; 28, *p*-nitrophenol. Sources for these compounds are in ref 24.

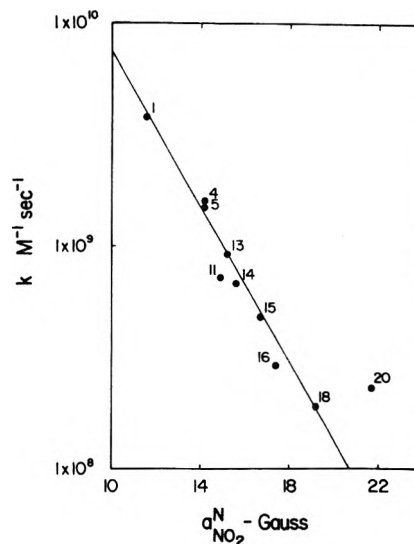


Figure 5. Correlation of the rate constant for reaction 1 with  $a_{NO_2}^N$ . Numbers refer to compounds in Table I.

further twisting of the nitro group. The same situation occurs with 3-hydroxy-2-nitrobenzoate at high pH (19).

The effect of a hydroxyl group at the position ortho to the nitro group is surprising. As long as the hydroxyl group retains its proton the net effect of this group is rather small (7, 10, 14, Table I). Probably the small steric effect of the OH group is overcome by hydrogen bonds which hold the nitro group close to the plane (see structure 14 in Table I). When the proton is lost the gain in the resonance energy for  $O^-$  and possibly also the electrostatic repulsion are sufficient to decouple the nitro group from the plane of the  $\pi$  system (19, 21, 23, Table I). This effect of the  $O^-$  group is comparable in magnitude to that of methyl.

The correlation between the rate of electron transfer from  $(CH_3)_2\dot{C}OH$  radicals to the nitro compound (reaction 1) with the nitrogen hyperfine constant is shown in Figure 5. The rate constant drops with an increase in  $a_{NO_2}^N$ , i.e., with the decrease in the spin density on the ring of the resultant radical anion. This effect is in line with our previ-

ous finding<sup>10</sup> that the one electron reduction potential of nitro aromatic compounds is more negative when  $a_{\text{NO}_2}^{\text{N}}$  for its radical is higher. These findings indicate that the transfer of electron to the nitro compound occurs via the nitro group, but the efficiency of transfer as reflected by its rate constant and reduction potential is determined by its ability to delocalize the additional electron over the rest of the molecule. The lower stability of the twisted radical is thus reflected in the higher activation energy for its formation. The relatively low value of  $k_1$  for 2-nitroisophthalate may be rationalized if it is assumed that the nitro group in the parent molecule is twisted out of the plane more than in the radical ion.

In conclusion, the present study clearly demonstrates that substitution ortho to the nitro group, even by relatively small groups such as  $\text{O}^-$  or carboxylate, may result in a strong decoupling of the nitro group from the ring  $\pi$  system of the radical anion. The linear inverse correlation between the nitro group nitrogen hyperfine constant and that of the para hydrogen (or methyl) suggests that this decoupling results in the localization of the spin density on the nitro group at the expense of the spin density on the ring. This localization, and decreased stability, is also manifest in the lower rate constants for electron transfer to the parent molecule.

## References and Notes

(1) Supported in part by the U.S. Energy Research and Development Administration.

- (2) B. M. Wepster, in "Progress in Stereochemistry", W. Klyne and P. B. D. de la Mare, Ed., Academic Press, New York, N.Y., 1958, p 99.
- (3) E. G. Janzen, *Acc. Chem. Res.*, **2**, 279 (1969).
- (4) K. W. Bowers in "Radical Ions", E. T. Kaiser and L. Kevan, Ed., Wiley, New York, N.Y., 1968, p 211.
- (5) P. B. Asycough, F. P. Sargent, and R. Wilson, *J. Chem. Soc.*, 5418 (1963).
- (6) A. H. Maki and D. H. Geske, *J. Am. Chem. Soc.*, **83**, 1852 (1961).
- (7) D. H. Geske, J. L. Ragle, M. A. Bambenek, and A. L. Balch, *J. Am. Chem. Soc.*, **86**, 987 (1964).
- (8) M. Fields, C. Valler, and M. Kane, *J. Am. Chem. Soc.*, **71**, 421 (1949).
- (9) O. H. Wheeler, *Can. J. Chem.*, **41**, 192 (1963).
- (10) D. Meisel and P. Neta, *J. Am. Chem. Soc.*, **97**, 5198 (1975).
- (11) B. C. Gilbert and M. Trenwith, *J. Chem. Soc. Perkin Trans. 2*, 2010 (1973).
- (12) L. H. Piette, P. Ludwig, and R. N. Adams, *J. Am. Chem. Soc.*, **84**, 4212 (1962).
- (13) K. Eiben and R. W. Fessenden, *J. Phys. Chem.*, **75**, 1155 (1971).
- (14) L. K. Patterson and J. Lilie, *Int. J. Radiat. Phys. Chem.*, **5**, 109 (1974).
- (15) The ratio between the  $\alpha$  and  $\beta$  proton hyperfine constants of the isopropyl radical, R. W. Fessenden and R. H. Schuler, *J. Chem. Phys.*, **39**, 2147 (1963).
- (16) J. Gendell, J. H. Freed, and G. K. Fraenkel, *J. Chem. Phys.*, **37**, 2832 (1962).
- (17) P. H. Rieger and G. K. Fraenkel, *J. Chem. Phys.*, **39**, 803 (1963).
- (18) P. Ludwig, T. Layloff, and R. N. Adams, *J. Am. Chem. Soc.*, **86**, 4568 (1964).
- (19) J. Pannell, *Mol. Phys.*, **7**, 317, 599 (1964).
- (20) C. Corraja and G. Giacometti, *J. Am. Chem. Soc.*, **86**, 1750 (1964).
- (21) J. O. Chambers and R. N. Adams, *Mol. Phys.*, **9**, 411 (1965).
- (22) M. Karplus and G. K. Fraenkel, *J. Chem. Phys.*, **35**, 1012 (1961).
- (23) For *o*-nitrobenzoate  $a_{\text{NO}_2}^{\text{N}} = 13.85$  G was determined in this laboratory.
- (24)  $a_{\text{NO}_2}^{\text{N}}$  in acetonitrile were taken from: H. Fischer, in *Landolt-Bornstein Numerical and Functional Relationships, Group II, Vol. 1*, K. H. Hellwege and A. M. Helwete, Ed., 1965.  $a_{\text{NO}_2}^{\text{N}}$  in water for all compounds are results obtained in this laboratory using the same in situ radiolysis setup.
- (25) G. E. Adams and R. L. Willson, *J. Chem. Soc., Faraday Trans. 1*, **69**, 719 (1973).
- (26) D. Behar and R. W. Fessenden, *J. Phys. Chem.*, **76**, 1710 (1972).
- (27) K.-D. Asmus, A. Wigger, and A. Henglein, *Ber. Bunsenges. Phys. Chem.*, **70**, 862 (1966).

## Mass Spectrometric Observation of Large Sulfur Molecules from Condensed Sulfur

D. L. Cocke, G. Abend, and J. H. Block\*

Fritz-Haber-Institut der Max-Planck-Gesellschaft, Berlin-Dahlem, Germany (Received August 8, 1975)

Publication costs assisted by Fritz-Haber-Institut

Sulfur molecules  $\text{S}_x$  with from 2 to 22 sulfur atoms have been desorbed from a condensed sulfur layer on a tungsten field emitter of a field ionization time-of-flight mass spectrometer. The condensed sulfur layer has been found to be in a highly mobile liquidlike steady state. The observation of these large sulfur molecules is important to the current models of liquid sulfur.

### Introduction

The molecular composition of pure liquid sulfur, being one of the most complex and difficult to study problems in sulfur chemistry, has prompted the recent call<sup>1</sup> for more sophisticated physical and chemical investigations. In the present investigation, the field ionization time-of-flight mass spectrometric technique has yielded data which bear directly upon this problem.

Many models of the composition of liquid sulfur have been proposed, none of which agrees fully with experimental results.<sup>2,3</sup> These proposed models differ substantially in terms of the amounts and kinds of  $\text{S}_x$  species assumed to

be present, even though little if any experimental data exist as to the presence of the possible species. A recently proposed model by Harris<sup>3</sup> gives more or less satisfactory agreement with existing experimental results. It involves the assumption that liquid sulfur is a complex mixture of ring species, a predominant amount of  $\text{S}_8$ , and higher linear polymers. A large amount of the experimental data used to check these models comes from experiments involving quenched sulfur. These quenching techniques are severely hindered by the thermodynamic instability of the molecular species  $\text{S}_x$  (linear or ring structures) with respect to  $\text{S}_8$ . Quenching a sulfur melt is not sufficiently fast to preserve the molecular composition. However, the separation of cy-



clododecasulfur  $S_{12}$  from the sulfur melt<sup>4</sup> supports the models involving large ring species (i.e.,  $S_x$ ;  $x > 8$ ).

Davis et al.,<sup>5</sup> using a field ionization quadrupole mass spectrometer, recently examined the field ionization and field desorption of sulfur from a tungsten field emitter. Under conditions of steady electric fields and continuous supply of  $S_2$  gas molecules, they observed the molecular ions  $S_5^+$ ,  $S_6^+$ ,  $S_7^+$ , and  $S_8^+$ . The precursors of these ions were found to result from the reactions which are occurring in a weakly adsorbed layer ( $\beta$ ) on top of a tightly bound chemisorbed layer ( $\alpha$ ). The characteristics of these two adsorbed layers of sulfur on tungsten have been examined by field electron microscopy (FEM). At room temperature, the  $\alpha$  layer was shown to be immobile while the  $\beta$  layer exhibited a high degree of surface mobility.<sup>6</sup>

In the present investigation, this weakly adsorbed  $\beta$  layer has been further examined with a high sensitivity mass spectrometer capable of single particle detection and found to be in a liquidlike steady state. The results from these experiments give evidence for the presence of a large number of sulfur species hitherto not directly considered in the models of liquid sulfur.

### Experimental Section

The field ionization time-of-flight mass spectrometer which was used in these experiments consisted of a Bendix 2-m flight tube and ion detector fitted with a custom-built field ionization source and accompanying electronics for producing high voltage pulses. In the pulsed field mode of operation, ions were desorbed from the surface of the field emitter by repeating high voltage pulses. The surface layer was analyzed during the time the pulse was on. At the highest field pulses, the surface layer was completely removed while at the lowest field pulses, only a small portion was desorbed. During the time the pulse was off (adjustable as small as  $10^{-5}$  s), chemical reactions which rebuild the surface structure could occur. The leading edge of the pulse defined the start time of the desorbed ions. The ion energy used was 8.6 keV with typical flight times of 20  $\mu$ s and an uncertainty in the start times of about 500 ns. The resolution, due to the width of the applied high voltage pulse, was as low as  $\delta M/M \approx 1/35$  which would have been sufficient to distinguish between  $S_{40}$  and  $S_{41}$ , had they been observed. A more detailed elaboration of the operation of the instrument has been reported previously.<sup>7</sup>

A rather blunt tungsten field emitter of several thousand angstroms radius was intentionally used to give an increased monitored area.

A molecular beam of  $S_2$  molecules produced from an electrochemical Knudsen cell<sup>5,8</sup> was directed at the tungsten tip of the field ion source. The electrochemical Knudsen cell was operated at temperatures between 230 and 250 °C, a cell current of 100  $\mu$ A, and a cell potential of 165 mV. From published equilibrium data,<sup>8,6</sup> the composition of the molecular beam should consist of more than 99%  $S_2$  molecules. The beam density was estimated to be  $2 \times 10^{15}$   $S_2$   $cm^{-2}$   $s^{-1}$ , from the known amount of S atoms being electrolytically produced in the Knudsen cell. This is in accordance with a calibration of the source with krypton, which showed that about 20 surface sites in an area of the tip surface of about 30 Å diameter were contributing to the ion current.

Most of the experiments were performed with the field emitter at room temperature. Temperature variation experiments were carried out by cooling the tip assembly via

copper wires attached to a cool finger or by heating the tip with a resistance loop.

For comparison, experiments were also performed with Knudsen cell conditions ( $T = 473$  K, emf = 198 mV) such that the molecular beam consisted of equal amounts of  $S_6$  and  $S_2$  along with 20% of a mixture of  $S_5$ ,  $S_7$ , and  $S_8$  molecules.

In a typical experiment, the tungsten field emitter which had been initially cleaned at 2500 K was flashed to 2000 K in the  $S_2$  beam and the coverage of the cleaned tip with sulfur was immediately monitored visually with a field emission picture. When coverage was complete, the desorption pulses were applied and the mass spectra were recorded.

Alignment and focusing of the mass spectrometer for maximum ion counts were performed with a continuous high voltage field applied to the emitter. In this mode of operation, no mass resolution was possible, and only total ion counts could be taken. It was the results from this type of measurements which supplied the initiative for further investigation.

### Results

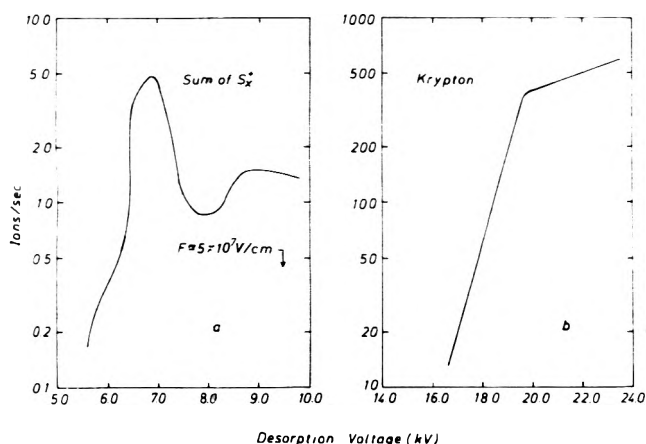
The variation of the ion count with dc desorption field is shown in Figure 1 for the  $S_x$  species and krypton. Krypton shows the expected dependence of ion intensity of a rare gas on field strength. That is, a rapid increase of ion current at the onset field where a strong increase of the ionization probability ( $P$ ) occurs and a decreased rise as  $P$  approaches unity. The increase of the ion current with field strength at the higher fields is due to increased particle supply due to polarization effects.

The  $S_x^+$  ion intensity shows a large maximum at the lower fields. This is a similar result as obtained by Davis et al.<sup>5</sup> if their data are replotted in terms of total ion intensity. The variation of the individual  $S_x$  ion intensities with 10-kHz pulsed field strength is shown in Figure 2. In agreement with reported results,<sup>5</sup> the  $S_7^+$  and  $S_8^+$  ions with smaller intensities of  $S_5^+$  and  $S_6^+$  ions are the species contributing most to the high maximum in the low-field range. These ions are formed from the corresponding  $S_x$  molecules which are the products of surface reactions.

The total ion count of the low-field maximum in Figure 2 is directly proportional to the frequency of the field pulses. Figure 2b shows that the ionization probability ( $P$ ) for all  $S_x$  species decreases below a desorption voltage of about 8 kV. Because  $P$  is low below 8 kV, not all particles are desorbed with each pulse. The removal of particles by field desorption is no longer the determining factor in establishing the concentration of particles on the tip. The concentration is now maintained by supply and thermal desorption. Under these conditions, the surface concentration of particles becomes independent of the pulse frequency. Now, each pulse has the same low probability of desorbing a particle. Consequently, the ion count is proportional to the pulse frequency (more precisely, duty cycle). The fact that the large low-field maximum occurs even at a much reduced desorption voltage shows that the supply of particles must be strongly increased.

Experiments with the different molecular beam composition (see Experimental Section) gave similar results as with the pure  $S_2$  beam. This indicates that the established steady state on the tip and the diffusion supply is not influenced by composition changes of the impinging beam.

Thorough mass spectrometric examination under the conditions giving the low-field onset of the maximum in



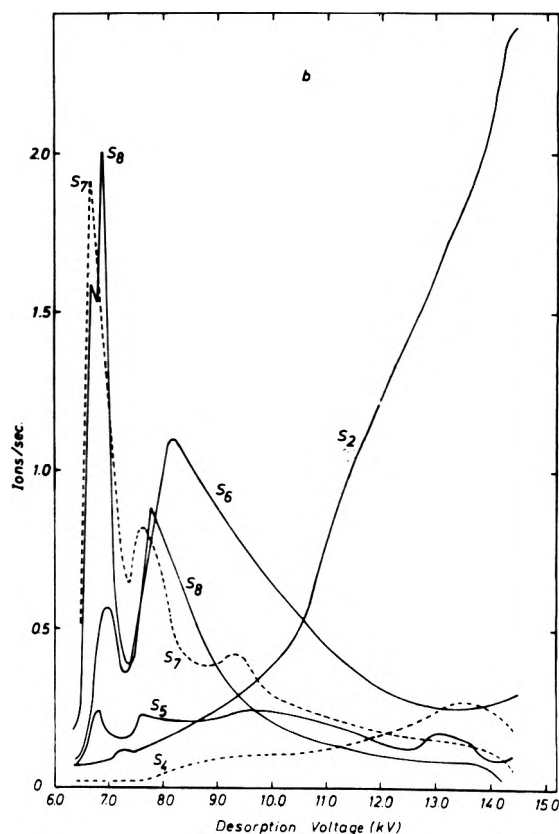
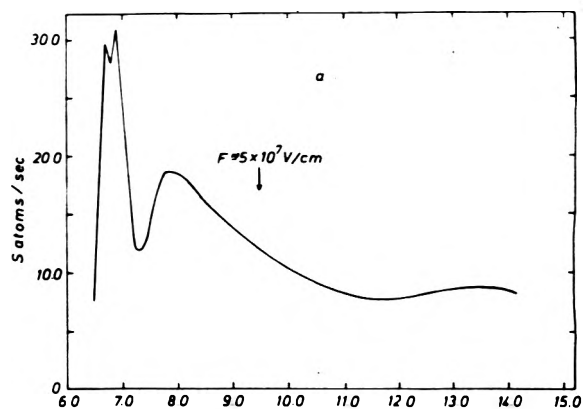
**Figure 1.** Dependence of ion current on dc desorption voltage. (a) Total  $S_x^+$  dc ion current taken at a tip temperature of 300 K. (b) Krypton ion current taken at a tip temperature of 250 K. The approximate desorption voltage corresponding to a field strength of  $5 \times 10^7$  V/cm at the apex of the tip is indicated by the arrow on (a).

Figure 2 yielded the mass spectrum shown in Figure 3. The spectrum was taken at the low-field onset of the maximum (6.5 kV) to ensure that the ionization probability was low and the surface concentration of particles was not affected by the pulses. Figure 3 shows that there is a rich supply of  $S_x$  species on the surface. All sulfur molecules from  $S_2$  to  $S_{22}$  are present in the spectrum. Such a large variety of  $S_x$  molecules (particularly the larger sulfur polymers) was only observed at low-field conditions corresponding to the large maxima in Figures 1 and 2.

The relative ion abundances under these conditions were found to be independent of the pulse rate. From this, one can conclude that the established steady state on the tip was not being disturbed by the high voltage pulses. The relative ion abundances, however, cannot be taken as a quantitative measure of the composition of this steady state, since different ionization probabilities must be taken into account.

At higher fields, species larger than  $S_9$  were not observed because the higher field strength removes the adsorbed surface structure with each pulse. Insufficient time is then available between two pulses to restore the surface structure. Only those species are then observed which can be formed within the time between the pulses where multilayer formation is excluded.

Variation of the tip temperature yielded results which are in agreement with those of Davis et al.<sup>5</sup> These results are explainable in terms of the combined effects of diffusion, thermal desorption, and surface reactions. Heating to 400 K decreased the total ion count. The  $S_2^+$  ion intensity was decreased by the largest amount (a factor of 10). This was followed by  $S_4^+$  (a factor of 5).  $S_6^+$ ,  $S_7^+$ , and  $S_8^+$  were only slightly reduced in intensity.  $S_3^+$ ,  $S_5^+$ , and the higher polymeric ions were decreased by factors of from 2 to 3. Cooling the tip also generally decreased the ion intensities. Reducing the temperature slightly resulted in increased intensities for  $S_2^+$ ,  $S_3^+$ , and  $S_4^+$  and reduced intensities for  $S_6^+$  and  $S_8^+$ , but caused little change in the other  $S_x$  species. Further cooling of the tip to about 250 K resulted in all ion intensities decreasing with  $S_2^+$ ,  $S_3^+$ , and  $S_4^+$  being the least affected. The temperature dependence of the small species  $S_2$ ,  $S_3$ , and  $S_4$  relative to  $S_6$ ,  $S_7$ , and  $S_8$  seems indicative of overriding reaction kinetic influences.



**Figure 2.** Dependence of ion current on pulsed desorption voltage. Tip temperature is 300 K. (a) Field dependence of the sum of S atoms contained in all  $S_x^+$  ions. (b) Field dependence of the individual  $S_x^+$  ions. The approximate desorption voltage corresponding to a field strength of  $5 \times 10^7$  V/cm at the apex of the tip is indicated by the arrow on (a).

It was noted that changing the temperature made irreversible changes in the spectra, but the trends given above were obvious.

The species observed in Figure 3 were reaching the monitored area by diffusion in the  $\beta$  layer. The sequence of the different ions being counted was observed to be completely statistical. This observation is only possible with the time-of-flight mass spectrometer which allows the registration of all masses simultaneously. The diffusing  $S_x$  species were arriving in the monitored area in a random fashion. This indicated that no long-range order existed in the structure of the highly mobile physically adsorbed layer.

The existence of a liquidlike structure is further support-

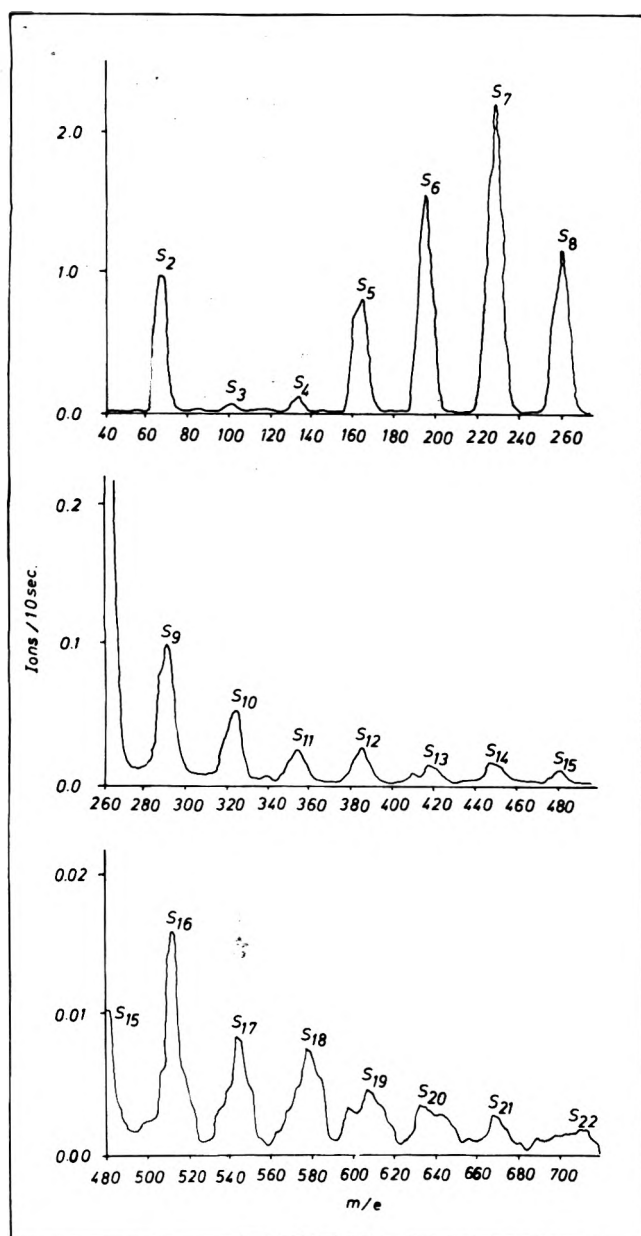


**Figure 3.** Mass spectrum of the field desorbed species from the liquidlike  $\beta$  layer of a sulfur covered tungsten tip. This is a mean value taken over 10 single spectra and represents a total analysis time of 9 h. The tip temperature is 300 K. Pulse repetition rate is 10 kHz. Due to the large pulse width (500 ns), the signals are broadened toward longer flight times, i.e., higher masses.

ed by the fact that the physically adsorbed layer is a strongly reacting system where the continuous impact of a relatively large number of highly reactive  $S_2$  molecules continually hinders the formation of an ordered structure. Long-range order appears unlikely in a reacting, diffusing mixture, especially with such a large variety of  $S_x$  species present.

### Discussion

Recent experimental work<sup>5,6</sup> along with the present results and established principles of field ionization mass spectrometry<sup>10,11</sup> and physical adsorption<sup>12</sup> allow the results to be discussed in terms of a liquidlike sulfur structure on the field emitter at low desorption fields. It has been shown<sup>6</sup> that  $S_2$  molecules striking a cleaned tungsten

surface are chemisorbed in a tightly bound  $\alpha$  state. Continued impact of  $S_2$  molecules after the  $\alpha$  layer is complete results in a physically adsorbed  $\beta$  layer being formed, which is quite mobile.

It has been a long established fact that physically adsorbed layers usually behave like two-dimensional liquids<sup>12</sup> and contemporary theories treat them as such.<sup>13</sup> Additionally, these layers exhibit melting points which are well below the normal melting temperatures of the bulk materials.<sup>12,14</sup> By FEM, Gomer<sup>15,16</sup> has visually observed multi-layer adsorption of various gases on a tungsten field emitter. He has noted that these layers are liquids, for all practical purposes, far below their bulk melting points. In these cases, the substrate lattice structure introduces disturbances into the adsorbate layers and prevents the bulk structure of the adsorbate from forming over large distances, thereby preventing long-range order (ref 11, p 133). The FEM work<sup>6</sup> concerning sulfur on tungsten found no evidence of order in the  $\beta$  layer. It was not unexpected that at room temperature the physically adsorbed layers of sulfur had high mobility and a liquidlike structure far below the bulk melting point of sulfur [mp ( $S_8$ ) = 119 °C].

It is well known<sup>10</sup> that particle supply to the field emitter tip can come from the gas phase as well as from the electrostatically enhanced surface diffusion from the large reservoir of adsorbed particles on the shank. Because of the tip shape, the field strength and, consequently, the ionization probability increases from the shank toward the apex. The concentration of adsorbed particles therefore decreases due to desorption at a certain distance from the apex which depends on the applied voltage. This desorption boundary has been observed mass spectrometrically by angular distribution studies and gives a pronounced maximum in ion currents due to diffusion supply from the shank, particularly for large and polar molecules.<sup>17</sup>

The general form of the dependence of total  $S_x$  ion intensity on desorption field strength (Figure 1) is understandable in terms of an extension of this simple model. At high dc fields, the ionization probability is unity and no  $S_2$  is reaching the part of the surface (about 30 Å diameter) of the tip being monitored by the mass spectrometer because it is being ionized immediately. In addition, at the higher fields, the distance of the desorption boundary from the monitored area on the apex is larger and no  $S_x$  species from the shank are able to diffuse into the monitored area. As the field is decreased, the ionization probability of  $S_2$  is decreased, and more and more  $S_2$  is allowed to reach the tip to participate in surface reactions. As the field strength is decreased further, all ionization probabilities become lower. Consequently, the desorption boundary moves closer to the monitored area and the diffusion of the reaction products begins to also add to the  $S_x$  species being monitored. This, being coupled with the increased  $S_2$  reaching the surface, causes the maxima in Figures 1 and 2.

Additional information is given by Figure 2 where 10-kHz pulses are used and  $S_2$  is reaching the tip between the pulses even in the high-field region. Here, apparently  $S_2$  is being desorbed from the surface before it can participate in the surface reactions because the desorption probability is unity while the pulse is on. However, at lower pulsed field strengths, a similar situation occurs as with the dc conditions in that the desorption probability of  $S_2$  is decreased, allowing more  $S_2$  to participate in the  $S_x$  reactions as well as allowing increased diffusion contributions as the angle of desorption decreases. In Figure 2, one can note two maxima

at lower fields. The smaller of the two on the high-field side is the result of surface reactions from the  $S_2$  molecules reaching the surface and of localized diffusion. The ion intensities decrease toward lower fields because of the reduced field desorption probability. The rapid increase to the maximum at still lower fields is due to the diffusing  $S_x$  molecules from the shank of the emitter actually encroaching into the monitored area giving a large supply of molecules to a few surface sites, i.e., some sites with the highest ionization probabilities. The fact that diffusion is occurring is evident from the plot of total S atoms in Figure 2a. Such a large supply of sulfur at lower fields can only come from surface diffusion.

The situation on the tip under field conditions near the low field onset is one in which a few surface sites are producing ions from a large, very mobile  $S_x$  supply, possibly a multilayer and a steady-state situation exists where the sampling is being taken of a liquidlike surface structure. The steady state is being maintained by diffusion, sulfur radical reactions, a continuous supply of highly reactive  $S_2$  species, and thermal desorption. Thermal desorption plays a significant role in maintaining this steady state in accordance with the following. The vapor pressures of the different  $S_x$  species at room temperature most likely range from  $10^{-3}$  to  $10^{-6}$  Torr with  $S_6$  being more volatile than  $S_8$  and with  $S_4$  possibly being more volatile than  $S_6$ .<sup>18</sup> Allowing for field compression and a higher heat of physical adsorption than heat of liquefaction (at least in the first physically adsorbed monolayer) the rate of thermal desorption is near in value to the rate of  $S_x$  supply from impinging  $S_2$ . Therefore, multilayer formation is also likely.

That only a few surface sites are contributing to the ion current is indicated by the large intensity fluctuations observed. This can be explained by variations in the number and quality of contributing surface sites, and the corresponding large effects on the ionization probability. Temperature variation experiments seem to verify this model by making irreversible changes in the steady-state microstructure of the  $\alpha$  layer. Bechtold et al.<sup>6</sup> observed diffusion within the  $\alpha$  layer at about 400 K. The surface microstructure is thought to be more on the order of a surface roughness of the  $\alpha$  layer than actual whisker formation as was observed for selenium.<sup>19</sup>

Two occurrences which possibly could influence the qualitative interpretation of the spectrum in Figure 3 are field induced fragmentation and ion cluster formation. However, both are unlikely to occur. Fragmentation is not likely since the field desorption process gives little surplus energy to the ions. Ion formation is merely a tunneling process in which case an electron goes from the molecule through the potential barrier into the metal. Additionally, field fragmentation of  $Se_x$  molecules was not observed<sup>20</sup> under similar experimental conditions. Since Se-Se bonds are weaker than S-S bonds,<sup>21</sup> field fragmentation of the  $S_x$  molecules can be ruled out. Ion cluster formation has been found to occur only for polar molecules.<sup>10</sup> It can, in the present case, be disregarded on experimental grounds. Cluster formation should be evidenced in Figure 3 by a periodicity of ion intensities or a maximum of intensities around  $S_{15}$  [ $x$  times the most abundant monomer,  $S_7$ ]. This is seen not to be the case.

Since the Tobolsky and Eisenberg model<sup>22</sup> of the cyclooctasulfur and poly- $S_8$ -chain equilibrium was proposed, it has been much used to describe the properties of liquid sulfur. The case against this oversimplified model has recently been thoroughly discussed by Schmidt and Siebert.<sup>1</sup> However, this equilibrium polymerization model is still being used to delineate the properties of liquid sulfur.<sup>23</sup> In light of this model, it can be seen in Figure 3 that  $S_{16}$  is relatively more abundant than the other high molecular weight  $S_x$  polymers. It should be mentioned, however, that  $S_{24}$  was never observed to be above the background level.

The fact that small reactive sulfur species such as  $S_3$  and  $S_4$  are present in liquid sulfur as well as the implied presence of  $S_5$ ,  $S_6$ , and  $S_7$  means that these species are the participants of reactions occurring in the liquid.<sup>24</sup> The same or similar reactions undoubtedly must be occurring in the liquidlike sulfur multilayer examined in these experiments. Thus, the  $S_x$  ( $x = 2$  to 22) species observed in the spectrum given in Figure 3 are most likely present in liquid sulfur and should be considered in the models of liquid sulfur.

These observations therefore support a model of liquid sulfur with complex molecular composition similar to that as proposed by Harris.<sup>3</sup>

*Acknowledgments.* One of the authors D.L.C. expresses his appreciation to the Max-Planck-Gesellschaft for a fellowship. This work was further financially supported by the Deutsche Forschungsgemeinschaft and by the Senat für Wirtschaft in West Berlin. This support is gratefully acknowledged.

## References and Notes

- (1) M. Schmidt and W. Siebert in "Comprehensive Inorganic Chemistry", Vol. 2, A. F. Trotman-Dickerson, Ed., Pergamon Press, New York, N.Y., 1973, pp 795-933.
- (2) M. Schmidt, *Angew. Chem.*, **85**, 474 (1973).
- (3) R. E. Harris, *J. Phys. Chem.*, **74**, 3102 (1970).
- (4) M. Schmidt and H. D. Block, *Angew. Chem.*, **79**, 944 (1967).
- (5) P. R. Davis, E. Bechtold, and J. H. Block, *Surface Sci.*, **45**, 585 (1974).
- (6) E. Bechtold, L. Wiesberg, and J. H. Block, *Z. Phys. Chem. (Frankfurt am Main)*, **97**, 7 (1975).
- (7) J. H. Block and A. W. Czanderna in "Methods and Phenomena", Vol. 1, A. W. Czanderna, Ed., Elsevier, Oxford, 1975.
- (8) H. Rickert, "Einführung in die Elektrochemie fester Stoffe", Springer-Verlag, Berlin, 1973, pp 184-192.
- (9) D. Detry, J. Drowart, P. Goldfinger, H. Keller, and H. Rickert, *Z. Phys. Chem. (Frankfurt am Main)*, **55**, 314 (1967).
- (10) H. D. Beckey, "Field Ionization Mass Spectrometry", Pergamon Press, New York, N.Y., 1971.
- (11) R. Gomer, "Field Emission and Field Ionization", Harvard University Press, Cambridge, Mass., 1961.
- (12) D. M. Young and A. D. Crowell, "Physical Adsorption of Gases", Butterworths, London, 1962.
- (13) D. S. Newsome, *J. Phys. Chem.*, **78**, 2600 (1974).
- (14) E. Schmidt-Inh and K. G. Weil, *Ber. Bunsenges. Phys. Chem.*, **79**, 982 (1975).
- (15) R. Gomer, R. Wortman, and R. Lundy, *J. Chem. Phys.*, **26**, 1147 (1957).
- (16) R. Gomer, *J. Phys. Chem.*, **63**, 468 (1959).
- (17) H. D. Beckey, J. Dahmen, and H. Knöppel, *Z. Naturforsch. A*, **21**, 141 (1966).
- (18) J. Berkowitz and W. A. Chupka, *J. Chem. Phys.*, **40**, 287 (1964).
- (19) H. Saure and J. Block, *Int. J. Mass Spectrom. Ion Phys.*, **7**, 157 (1971).
- (20) H. Saure and J. Block, *Int. J. Mass Spectrom. Ion Phys.*, **7**, 145 (1971).
- (21) B. Siegel, *Q. Rev., Chem. Soc.*, **19**, 77 (1965).
- (22) A. V. Tobolsky and A. Eisenberg, *J. Am. Chem. Soc.*, **81**, 780 (1959).
- (23) M. E. Baur and D. A. Horsma, *J. Phys. Chem.*, **78**, 1670 (1974).
- (24) B. Meyer, T. V. Oommen, and D. Jensen, *J. Phys. Chem.*, **75**, 912 (1971).

## Stabilization of the Daughter Species Following the Auger Event in Some Cobalt(III) Chelates in Different Matrices

T. S. Srivastava and Amar Nath\*

Department of Chemistry, Drexel University, Philadelphia, Pennsylvania 19104 (Received September 2, 1975)

Publication costs assisted by Drexel University

The emission Mössbauer spectra of  $[^{57}\text{Co}(\text{III})(\text{phen})_3](\text{ClO}_4)_3 \cdot 2\text{H}_2\text{O}$  and  $[^{57}\text{Co}(\text{III})(\text{bpy})_3](\text{ClO}_4)_3 \cdot 3\text{H}_2\text{O}$  dispersed in matrices of sucrose, poly(ethylene oxide), and the corresponding Fe(II) chelates were studied. The ratio of the Fe(II)/Fe(III) species stabilized varies from matrix to matrix. These observations have been interpreted on the basis of electron acceptor and donor centers.

### Introduction

The electron-capture decay of a cobalt-57 atom triggers an Auger event resulting in the loss of several electrons. In solids, the electronic relaxation is rapid and the 14.4-keV Mössbauer emission conveys information regarding the chemical forms in which the daughter iron-57 is stabilized within  $10^{-7}$  s following the electron capture. A considerable effort has gone into the study of the chemical state of iron produced by the decay of divalent cobalt in various ionic compounds.<sup>1-3</sup> Friedt and Adloff<sup>4</sup> examined the role of the water of hydration and found that the ratio of  $\text{Fe}^{3+}/\text{Fe}^{2+}$  increases with increasing degree of hydration in  $\text{CoCl}_2 \cdot n\text{H}_2\text{O}$ ,  $\text{CoSO}_4 \cdot n\text{H}_2\text{O}$ , and  $\text{CoF}_2 \cdot n\text{H}_2\text{O}$ . They suggested that the stabilization of the higher charge state,  $\text{Fe}^{3+}$  in hydrated compounds, is due to the formation of OH· radicals by radiolysis of water molecules caused by low energy Auger electrons. The OH· radicals oxidize the  $\text{Fe}^{2+}$  ions formed after the electronic relaxation following the Auger event to  $\text{Fe}^{3+}$ . Gütlich et al.<sup>5</sup> and Wertheim and Buchanan<sup>6</sup> showed that the  $^{60}\text{Co}$   $\gamma$ -irradiation or high-energy electron bombardment of ferrous ammonium sulfate hexahydrate produces a species whose Mössbauer absorption spectrum is similar to the emission spectrum of the  $^{57}\text{Co}$ -doped compound. It was also shown that the Auger electron ionization in the molecule incorporating the  $^{57}\text{Co}$  atom was sufficient to radiolyze a water molecule in about one-third of the decay events, a result in good agreement with the experimental yield of  $\text{Fe}^{3+}$ . The role of water in stabilizing alternative charge states continues to receive attention from several workers.<sup>7-9</sup> On the basis of these observations, the following mechanism was proposed. The low-energy Auger electrons cause local radiolysis of the lattice surrounding the affected atom forming a nest of radicals.<sup>10</sup> The radicals produced in the lattice may act as electron acceptors (e.g., OH·) or donors (e.g.,  $\text{NH}_2\cdot$ ) and may decide the final stabilization forms of the iron species.

There has been a great deal of interest in the stabilization of  $^{57}\text{Co}^{2+}$  in several oxides with sodium chloride type of structure.<sup>1,3</sup> The ratio of  $\text{Fe}^{3+}/\text{Fe}^{2+}$  observed in  $^{57}\text{Co}$ -doped cobaltous and nickelous oxides seems to depend on the nature of the semiconductivity. It varies as a function of the p-type dopant lithium and the n-type dopants chromium and gallium. When the Li doping is raised sufficiently, it is possible to completely suppress the  $\text{Fe}^{2+}$  species at room temperature. Investigations of a somewhat similar

nature have also been reported on  $^{57}\text{Co}$ -doped  $\text{A}^{\text{III}}\text{B}^{\text{V}}$  semiconductors.<sup>11,12</sup>

In view of the very interesting observations made on ionic systems, we decided to look into the stabilization forms of low spin-labeled cobalt chelates with strong field ligands, namely tris(phenanthroline)cobalt(III) perchlorate, and tris(bipyridyl)cobalt(III) perchlorate. These chelates are highly conjugated and escape fragmentation in most of the Auger events<sup>13,14</sup> and their spectra are easier to computer analyze and interpret unambiguously with the near absence of the fragmented species, viz., ionic  $\text{Fe}^{2+}$  and/or  $\text{Fe}^{3+}$ . In chelates with strong ligand fields, the low-spin Fe(II) formed has a spectrum distinctly different from the ionic  $\text{Fe}^{2+}$  species resulting from fragmentation. On the other hand, the spectrum for coordinated high-spin Fe(II) chelate may not be very different from that for  $\text{Fe}^{2+}$ .

Mössbauer spectra of the following solid dispersions were studied:  $[^{57}\text{Co}(\text{III})(\text{phen})_3](\text{ClO}_4)_3$  and  $[^{57}\text{Co}(\text{III})(\text{bpy})_3](\text{ClO}_4)_3$  dispersed in sucrose, poly(ethylene oxide), and in the corresponding Fe(II) chelates, viz.,  $[\text{Fe}(\text{II})(\text{phen})_3](\text{ClO}_4)_2$  and  $[\text{Fe}(\text{II})(\text{bpy})_3](\text{ClO}_4)_2$ , respectively.

### Experimental Section

A few milligrams of  $[\text{Co}(\text{III})(\text{phen})_3](\text{ClO}_4)_3 \cdot 2\text{H}_2\text{O}$  and  $[\text{Co}(\text{III})(\text{bpy})_3](\text{ClO}_4)_3 \cdot 3\text{H}_2\text{O}$  which were synthesized by conventional methods<sup>15,16</sup> were doped with a couple of millicuries of carrier-free  $^{57}\text{CoCl}_2$  and allowed to undergo solid state isotopic exchange in a humid chamber (~95% relative humidity) at 35 °C for several days. The free  $^{57}\text{Co}^{2+}$  if any, was extracted from aqueous solutions of the labeled chelates by 0.1% 8-hydroxyquinoline in chloroform. This procedure for labeling cobalt chelates through solid state exchange<sup>13</sup> is quite convenient especially when a small quantity of a chelate with relatively high specific activity is desired. The yields in conventional synthetic procedures for milligram quantities tend to be rather low.

Solid dispersions were formed by dissolving about 1 mg of the labeled chelate in a viscous solution containing approximately 100 mg of poly(ethylene oxide) or sucrose. The viscous solutions were chilled in liquid nitrogen with constant swirling and freeze-dried on a vacuum line. The clustering of the chelate molecules during freezing is presumably eliminated or considerably diminished by the relatively high viscosity of the solution. The dispersions in the corresponding Fe(II) chelates were prepared in a similar fashion.

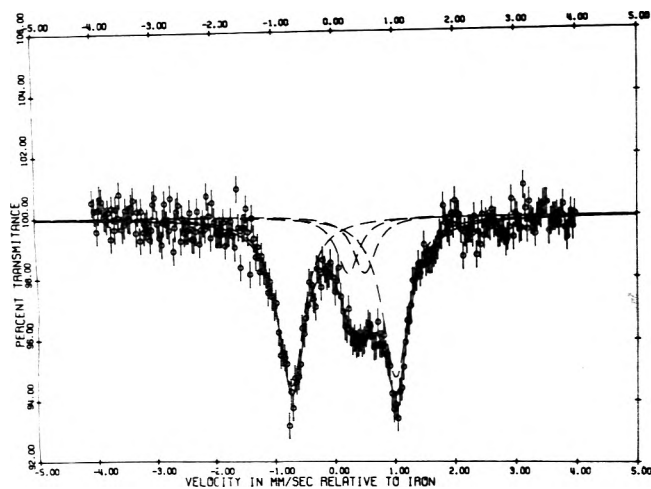


Figure 1. Emission Mössbauer spectra of  $[^{57}\text{Co(III)(phen)}_3](\text{ClO}_4)_3$  dispersed in sucrose at 80 K.

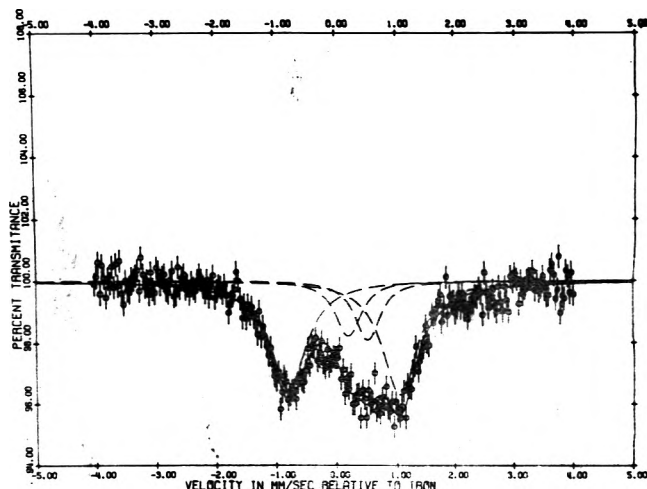


Figure 4. Emission Mössbauer spectra of  $[^{57}\text{Co(III)(bpy)}_3](\text{ClO}_4)_3$  dispersed in sucrose at 80 K.

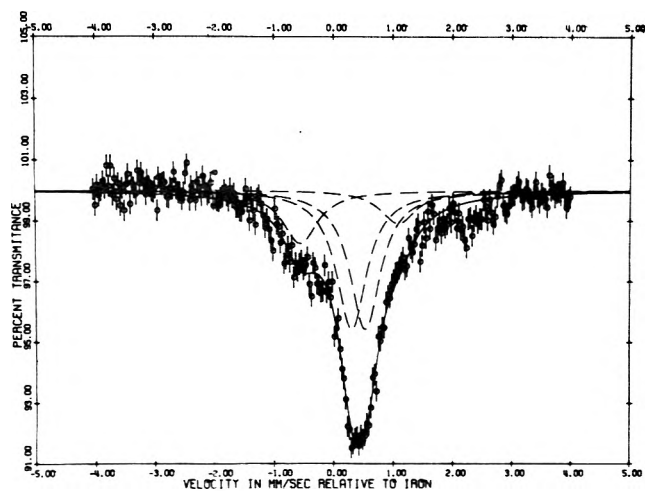


Figure 2. Emission Mössbauer spectra of  $[^{57}\text{Co(III)(phen)}_3](\text{ClO}_4)_3$  dispersed in poly(ethylene oxide) at 80 K.

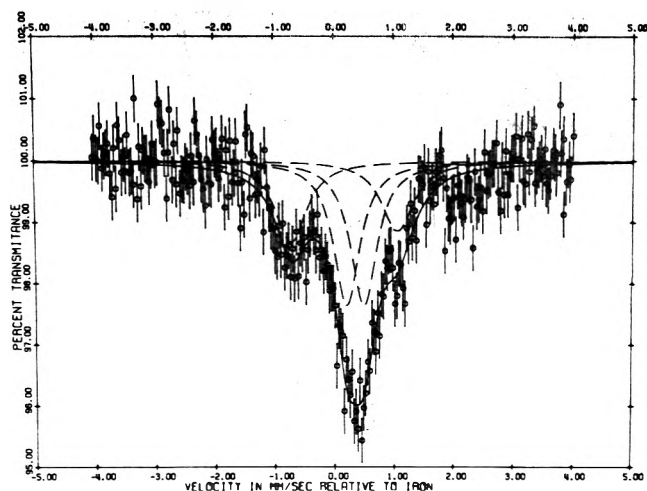


Figure 5. Emission Mössbauer spectra of  $[^{57}\text{Co(III)(bpy)}_3](\text{ClO}_4)_3$  dispersed in poly(ethylene oxide) at 80 K.

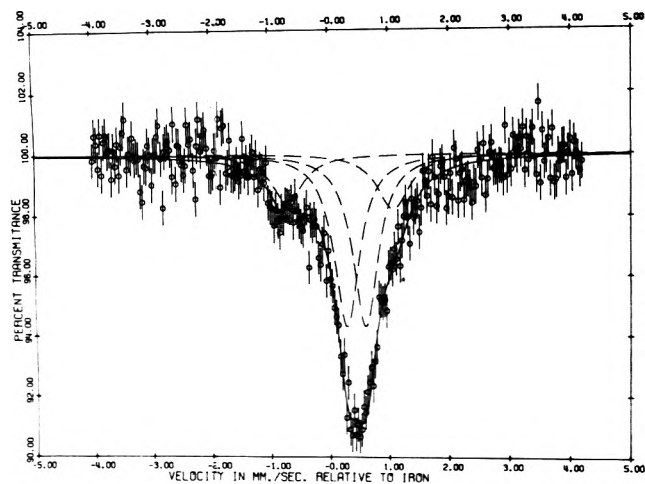


Figure 3. Emission Mössbauer spectra of  $[^{57}\text{Co(III)(phen)}_3](\text{ClO}_4)_3$  dispersed in  $[\text{Fe(II)(phen)}_3](\text{ClO}_4)_2$  at 80 K.

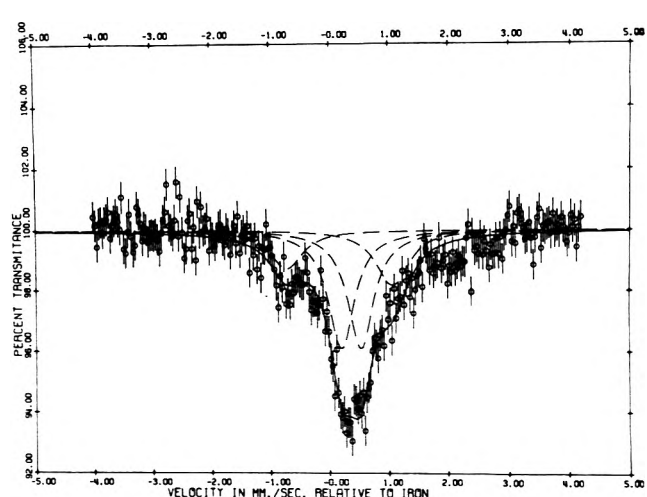


Figure 6. Emission Mössbauer spectra of  $[^{57}\text{Co(III)(bpy)}_3](\text{ClO}_4)_3$  dispersed in  $[\text{Fe(II)(bpy)}_3](\text{ClO}_4)_2$  at 80 K.

The phenanthroline and bipyridyl chelates of iron(II) and iron(III) were synthesized by the methods reported in the literature.<sup>15,16</sup>

The Mössbauer spectra were obtained in Elscint's AME-

30 spectrometer. In emission runs, potassium ferrocyanide (0.25 mg  $^{57}\text{Fe}$  per  $\text{cm}^2$ ) was used as a standard absorber. The standard absorber was maintained at room tempera-

TABLE I: Mössbauer Parameters Observed in Emission Experiments at 80 K

Chelate	Dispersion in sucrose		Dispersion in poly(ethylene oxide)		Dispersion in the corresponding Fe(II) chelate		
	Fe(III)	Fe(II)	Fe(III)	Fe(II)	Fe(III)	Fe(II)	
$[^{57}\text{Co(III)(phen)}_3](\text{ClO}_4)_3$	$\delta$	0.14	0.36	0.22	0.40	0.15	0.40
	$\Delta$	1.74	0.29	1.72	0.25	1.76	0.30
$[^{57}\text{Co(III)(bpy)}_3](\text{ClO}_4)_3$	$\delta$	0.12	0.34	0.16	0.35	0.11	0.34
	$\Delta$	1.86	0.35	1.78	0.33	1.84	0.35

TABLE II: Mössbauer Parameters Observed in Absorber Experiments at 80 K

$[\text{Fe(III)(phen)}_3](\text{ClO}_4)_3$		$[\text{Fe(II)(phen)}_3](\text{ClO}_4)_2$		$[\text{Fe(III)(bpy)}_3](\text{ClO}_4)_3$		$[\text{Fe(II)(bpy)}_3](\text{ClO}_4)_2$	
Present work	Ref 17	Present work	Ref 18	Present work	Ref 17	Present work	Ref 18
$\delta$	0.15	0.10	0.40	0.10	0.06	0.39	0.33
$\Delta$	1.82	1.71	0.31	0.23	1.81	1.80	0.44

TABLE III: Ratio of Fe(II)/Fe(III) Stabilized in Different Matrices at 80 K

Chelate	Neat	Dispersion in sucrose	Dispersion in poly(ethylene oxide)	Dispersion in the corresponding Fe(II) chelate	
				Present work	Ref 18
$[^{57}\text{Co(III)(phen)}_3](\text{ClO}_4)_3$	0.2 <sup>a</sup>	0.3	2.5		3.3
$[^{57}\text{Co(III)(bpy)}_3](\text{ClO}_4)_3$	~0 <sup>b</sup>	0.4	1.4		2.4

<sup>a</sup> Reference 14. <sup>b</sup> Reference 13.

ture while the chelate sample was cooled by liquid nitrogen in a cryotip. In the absorption experiments, the absorber was in the cryotip and the standard  $^{57}\text{Co}(\text{Cu})$  source was maintained at room temperature. A NBS standard iron foil was used to calibrate the velocity scale. The sign of the velocities in the computer plots of the emission runs have been inverted to correspond with that of the absorption experiments. The centroids of the emission spectra and the absorption spectra have been shifted by 0.04 and 0.226 mm/s, respectively, to give the isomer shifts relative to the centroid of metallic iron.

The widths for the two quadrupole split lines of any species were constrained to be equal during the computer analysis of the Mössbauer spectra.

The total counts collected in the emission spectra ranged from 40 000 to 80 000.

### Data and Discussion

Figures 1–6 depict the emission spectra of the labeled cobalt chelates dispersed in sucrose, poly(ethylene oxide), and in the iron(II) chelate matrices. The computer analyzed Mössbauer parameters of the Fe(III) and Fe(II) chelates stabilized after the Auger event are summarized in Table I. The parameters are in fair agreement with that obtained from absorption experiments (cf. Tables I and II). It may be mentioned that one would expect the Mössbauer parameters for any particular compound to show slight variations from one matrix to another and especially from the neat chelate, where the crystal structure could constrain the ligands in a particular configuration.<sup>13</sup>

Now, let us consider the stabilization of the species following the Auger event. The Auger event triggers the loss of several electrons from the molecule incorporating the cobalt-57 nucleus undergoing radioactive decay. In a solid, one would expect fairly rapid neutralization of the charges by transfer of electrons from the neighboring molecules and also by back diffusion of a fraction of the low-energy Auger electrons or diffusion to the site of some of the sec-

ondaries produced by the energetic primaries in the immediate environment. In general, one would expect that Fe(III) be stabilized in a neat Co(III) chelate because Fe(IV) and Fe(II) chelate molecules (if they exist) would constitute shallow acceptors and donors, respectively, in the matrix. Fe(II) is stabilized in fair proportion in the  $[\text{Co(III)(phen)}_3](\text{ClO}_4)_3 \cdot 2\text{H}_2\text{O}$  lattice while practically none of Fe(II) is stabilized in the  $[\text{Co(III)(bpy)}_3](\text{ClO}_4)_3 \cdot 3\text{H}_2\text{O}$  lattice (Table III). It may be mentioned that the ratio of Fe(II)/Fe(III) did not show any significant change for the anhydrate phenanthroline chelate as compared to the hydrate. This is in contrast with the observations made on ionic compounds<sup>4</sup> where the water of hydration tends to stabilize  $\text{Fe}^{3+}$ . The ability of Fe(II) to stabilize in the phenanthroline chelate in contrast to the bipyridyl complex may perhaps be understood in terms of the larger depth of the Fe(II) donor center in the latter. However, this aliovalent species, viz. Fe(II), can be further stabilized by defects, which may convert them into deeper centers. Phenanthroline ligand being bulkier than bipyridyl, may lead to a larger concentration of anionic vacancies in the  $[\text{Co(III)(phen)}_3](\text{ClO}_4)_3$  lattice,<sup>19</sup> which may tend to stabilize the Fe(II) chelate molecule.

When the labeled cobalt(III) chelates of phenanthroline and bipyridine are dispersed in the corresponding Fe(II) chelates, the situation is reversed as expected. Fe(II) is the predominantly stabilized species (Figures 3 and 6 and Table III) while there is only a smaller fraction of Fe(III). The Fe(III) chelate molecules constitute shallow acceptors in the Fe(II) matrix. The possibility of some degree of coalescence of the  $^{57}\text{Co(III)}$  chelate molecules during freezing cannot be ruled out. The coalescence if any will reduce the observed ratio of Fe(II)/Fe(III).

It may be mentioned that one can discern a very small peak at about 2.5 mm/s in all the spectra (Figures 1–6), which belongs to the ionic species,  $\text{Fe}^{2+}$ , the other peak belonging to the quadrupole split pair is expected to be near 0 mm/s. The ionic  $\text{Fe}^{2+}$  is formed as a consequence of frag-

mentation of the chelate molecule in a small fraction of the Auger events. For the sake of convenience, this pair of lines has been disregarded during the computer analyses of the spectra. This is not likely to affect the results of the computer analyses significantly.<sup>20</sup>

The <sup>57</sup>Co(III) chelate dispersals in the matrices of sucrose and poly(ethylene oxide) exhibit very interesting behavior. The poly(ethylene oxide) matrix has a very strong tendency to stabilize the Fe(II) species, while the sucrose matrix also tends to stabilize Fe(II) but to a much lesser extent. One may interpret these observations by assuming that Fe(III) chelate molecules (formed as a result of electronic relaxation following the Auger event) form shallow acceptors in these matrices, especially in poly(ethylene oxide); however, this assumption is not plausible. Alternatively, it seems that the Auger electrons either populate preexisting defects in the immediate neighborhood of the affected molecule (i.e., the molecule incorporating the cobalt-57 undergoing radioactive decay) or the Auger electrons create defects, presumably a radiolytic product. The populated preexisting defects or the ones created by the Auger event may form very shallow donors in the immediate vicinity of the affected molecule. A donor can transfer its electron to the Fe(III) chelate molecule forming Fe(II).

*Acknowledgment.* We are particularly grateful to Dr. Kimio Inoue for his help in computer analyses of some of the spectra.

## References and Notes

- (1) G. K. Wertheim, *Acc. Chem. Res.*, **4**, 373 (1971).
- (2) J. P. Adloff and J. M. Friedt, *Proc. Symp. Mossbauer Spectrosc. Its Appl.*, IAEA, 301 (1972).
- (3) A. G. Maddock, *MTP Int. Rev. Sci., Inorg. Chem., Ser. One*, **8**, 213 (1972).
- (4) J. M. Friedt and J. P. Adloff, *C.R. Acad. Sci. Paris*, **264**, 1356 (1967); **288**, 1342 (1969).
- (5) P. Gütlich, S. Odar, B. W. Fitzsimmons, and N. E. Erickson, *Radiochem. Acta*, **10**, 147 (1968).
- (6) G. K. Wertheim and D. N. E. Buchanan, *Chem. Phys. Lett.*, **3**, 87 (1969).
- (7) E. Baggio-Saitovitch, D. Raj, and J. Danon, *Chem. Phys. Lett.*, **17**, 74 (1972).
- (8) D. Raj and J. Danon, *Radiochem. Radioanal. Lett.*, **13**, 83 (1973).
- (9) J. M. Friedt, G. K. Shenoy, G. Abstreiter, and R. Poinot, *J. Chem. Phys.*, **59**, 3831 (1973).
- (10) P. R. Geissler and J. E. Willard, *J. Phys. Chem.*, **67**, 1675 (1963).
- (11) B. I. Boltaks, A. A. Efimov, P. P. Seregin, and V. T. Shipatov, *Sov. Phys. Solid State*, **12**, 1592 (1971).
- (12) P. P. Seregin, A. K. Kamolov, and A. I. Blashku, *Sov. Phys. Solid State*, **16**, 1311 (1975).
- (13) A. Nath, M. P. Klein, W. Kundig, and D. Lichtenstein, *Radiat. Effects*, **2**, 211 (1970).
- (14) T. S. Srivastava and A. Nath, *Radiochem. Radioanal. Lett.*, **16**, 103 (1974).
- (15) A. A. Schilt and R. C. Taylor, *J. Inorg. Nucl. Chem.*, **9**, 211 (1959).
- (16) F. H. Burstall and R. S. Nyholm, *J. Chem. Soc.*, 3570 (1952).
- (17) R. R. Berrett, B. W. Fitzsimmons, and A. Owusu, *J. Chem. Soc. A*, 1575 (1968).
- (18) R. L. Collins, R. Pettit, and W. A. Baker, Jr., *J. Inorg. Nucl. Chem.*, **28**, 1001 (1966).
- (19) J. Baker, L. M. Engelhardt, B. N. Figgis, and A. H. White, *J. Chem. Soc., Dalton, Trans.*, 530 (1975).
- (20) K. E. Siekierska, J. Fenger, and J. Olsen, *J. Chem. Soc., Dalton Trans.*, 2020 (1972).



# An Investigation of the Fluorescence Properties of Carboxyl Substituted Anthracenes

T. C. Werner,\* Thomas Matthews, and Babs Soller

Department of Chemistry, Union College, Schenectady, New York 12308 (Received August 1, 1975)

Publication costs assisted by the Petroleum Research Fund

The spectral properties of the three monocarboxyl substituted anthracenes have been investigated. Methyl 9-anthroate (9-COOMe), methyl 1-anthroate (1-COOMe), and methyl 2-anthroate (2-COOMe) are the specific compounds used in this study. Their fluorescent lifetimes ( $\tau_f$ ), quantum yields ( $\phi_f$ ), and spectra are shown to be quite dependent on solvent and the position of substitution. The electronic transition responsible for the long wavelength absorption and the fluorescence spectrum of all three esters is primarily the  $^1A_1 \rightarrow ^1L_a$  anthracene transition. No evidence is found for enhancement of the long axis polarized  $^1A_1 \rightarrow ^1L_b$  transition or for a solvent induced inversion of the  $^1L_a$  and  $^1L_b$  states when the carboxyl group is in the 2 position. HMO calculations, molecular models, and electronic spectra suggest that a substantial change in the equilibrium molecular geometry occurs on excitation to the first excited singlet state ( $S_1$ ) for 9-COOMe. By contrast, for 1 and 2 substitution the equilibrium geometry does not change much on excitation. However, a restriction in the number of conformers which can exist about the minimum energy conformation is observed in  $S_1$  relative to the ground state. The variation in  $\phi_f$  for 1- and 2-COOMe from non-polar solvents through solvents of moderate hydrogen bonding properties is consistent with the existence of a thermally assisted intersystem crossing (ISC) pathway to a triplet level near  $S_1$ . This triplet level is thought to be the second anthracene triplet rather than an  $n,\pi^*$  triplet as previously implicated in the ISC process for carbonyl-substituted anthracenes. In strong hydrogen bonding solvents a solvent induced internal conversion pathway replaces ISC as the major nonradiative pathway.

## Introduction

Anthracene has three positions for monosubstitution and the ability of a substituent to electronically interact with the anthracene ring is quite dependent on the position of substitution. In the 9 or meso position, a substituent encounters the most electron-rich position of the ring and it also lies along the polarization axis of the lowest energy anthracene transition ( $^1A_1 \rightarrow ^1L_a$ ). However, complete coplanarity between a substituent at the 9 position and the ring is often prevented by steric hindrance with the peri hydrogens at the 1 and 8 positions. For substitution in the 2 position, which is the least electron-rich position, the substituent axis is more closely aligned with the polarization direction of the second anthracene transition ( $^1A_1 \rightarrow ^1L_b$ ). Steric hindrance to coplanarity from ring hydrogens appears to be insignificant for 2 substitution. The electron density at the 1 position is intermediate between the other two positions. A substituent in the 1 position lies more nearly along the axis of the  $^1A_1 \rightarrow ^1L_a$  transition and encounters considerably less steric hindrance from ring hydrogens than in the 9 position but more than in the 2 position. It is not surprising then that the spectral properties of monosubstituted anthracenes are dependent on the position of substitution.

When the substituent is a carboxyl group, the resulting anthracene derivatives have some unusual excited state behavior. The carboxyl group, by its electron-withdrawing nature, is classified as a fluorescence inhibiting group and benzoic acid is indeed nonfluorescent.<sup>2</sup> Other similar substituents (nitro, carbonyl) produce virtually nonfluorescent anthracene derivatives<sup>3,4</sup> but the anthroic acids and their esters are quite fluorescent in some solvents. The  $\phi_f$  values for all three of the methylanthroates are quite solvent dependent and the nature of this solvent dependency is very much a function of the position of substitution. The lowest excited singlet energies of all three esters are also solvent

dependent showing increasing red shifts as solvent polarity increases. In addition, a comparison of the absorption and fluorescence spectra of methyl 9-anthroate (9-COOMe) reveals a substantial difference in the equilibrium geometry of the ground ( $S_0$ ) and lowest excited singlet state ( $S_1$ ).<sup>5-7</sup> For methyl 1-anthroate (1-COOMe), the spectra are consistent with a smaller difference in the equilibrium geometries of the two states while for methyl 2-anthroate (2-COOMe) the equilibrium geometry of both  $S_0$  and  $S_1$  appears to be quite similar.

We have previously discussed the spectral properties of 9-substituted esters in some detail.<sup>5-7</sup> In this work, we have extended our investigation to the 1- and 2-methyl esters in order to explain the solvent and substituent position dependence observed for the fluorescence behavior of monocarboxyl-substituted anthracenes. A correction is also made in the previous assignment of the emitting state of 2-anthroic acid in polar solvents which we now believe is in error.<sup>8</sup>

## Experimental Section

The ethanol used in the spectral measurements was obtained from U.S. Industrial Chemicals. All other spectral solvents were Matheson Coleman and Bell Spectroquality solvents.

Methyl 9-anthroate was prepared from 9-anthroic acid (Aldrich Chemical Co.) and diazomethane.<sup>9</sup> Methyl 2-anthroate was made by a free acid esterification of 2-anthroic acid (K & K Labs) with methanol with subsequent recrystallization from glacial acetic acid.<sup>10</sup> Methyl 1-anthroate was synthesized in a three step procedure beginning with benzanthrone (Aldrich Chemical Co.). To remove impurities, the benzanthrone was extracted with acetone in a Soxhlet extractor. After removal of the acetone, the benzanthrone was allowed to react to form anthraquinone-1-

carboxylic acid.<sup>10</sup> This acid was then reduced to 1-anthroic acid and then esterified with methanol using the free acid procedure of Coulson.<sup>10</sup> Purification of the final ester product was performed by dissolving the ester in hot glacial acetic acid and inducing crystallization by the addition of hot water. All melting points agreed with literature values.

Absorption measurements were made on either a Cary Model 14 spectrophotometer or a Beckman D.U. spectrophotometer.

Fluorescence emission spectra were recorded on a Perkin-Elmer MPF-2A spectrofluorometer using excitation and emission band passes of 7 and 3 nm, respectively. The spectra were corrected for the response function of the instrument as described earlier.<sup>5a</sup> The response function was obtained by comparison of the fluorescence spectra of methyl 9-anthroate in several solvents taken on our instrument with those on an identical instrument having a corrected spectral attachment. The band passes above were identical with those used on the latter instrument. Fluorescence excitation spectra at 77 K were obtained using the phosphorescence attachment of the MPF-2A with the chopper removed.

Fluorescence quantum yield ( $\phi_f$ ) determinations were obtained using the following equation where  $r$  and  $u$  stand for reference and unknown, respectively:

$$\phi_u = \phi_r \frac{n_u^2 A_r F_u I_r D_u}{n_r^2 A_u F_r I_u D_r}$$

$A$  is the absorbance at the exciting wavelength ( $<0.03$ , 1-cm cells, bandpass  $\leq 3$  nm),  $F$  is the area under the corrected emission spectrum (by cut and weigh),  $n$  is the solvent refractive index,  $I$  is the relative source intensity at the exciting wavelength ( $\lambda_{ex}$ ) determined by the rhodamine B quantum counter method of Chen,<sup>11</sup>  $\phi_r$  is the reference quantum yield (0.18 for methyl 9-anthroate in ethanol determined vs. an anthracene in ethanol standard having  $\phi_f = 0.28$ ),<sup>7</sup> and  $D$  is the deoxygenation factor.  $D$  is used to correct for the quenching of fluorescence by dissolved oxygen. To determine  $D$  for a given sample in a given solvent, the solution is first deoxygenated by at least three freeze-pump-thaw cycles (pressure  $<10^{-4}$  Torr). The cell containing the solution is removed from the vacuum line and the fluorescence spectrum is recorded. Then the cell is opened to the atmosphere and reequilibrated with air. A second fluorescence spectrum is run and the intensity ratio of the first to the second spectrum is equal to  $D$ . The measurement is repeated at least twice and agreement was usually  $<2\%$ . The maximum deviation between measurements was 5% even when data were obtained using different samples on different days. Once the  $D$  values are known, all  $\phi_f$  data can be taken in aerated solution. The  $D$  values for each of the esters in the different solvents are given in Table I along with the  $\lambda_{ex}$ 's used in the  $\phi_f$  determinations.

To determine the  $\phi_f$  of 2-anthroic acid (2-COOH) in acetonitrile it was necessary to add a trace of  $H^+$  to suppress ionization of 2-COOH at the low concentrations used ( $10^{-6}$  M). Addition of 5  $\mu$ l of a  $10^{-2}$  M solution of HCl in acetonitrile to 5 ml of 2-COOH in acetonitrile was found to be sufficient. This gave an  $H^+$  concentration of  $\sim 5 \times 10^{-5}$  M.

Our previously reported fluorescence lifetime ( $\tau_f$ ) measurements for methyl 9-anthroate were made in the laboratory of Dr. Renata Cathou at Tufts University using an Ortec single photon counting system.<sup>5a</sup> The  $\tau_f$  data reported herein for the 1- and 2-methyl esters were taken by Dr. Fred Lytle of Purdue University using a modified TRW

TABLE I:  $D$  Values and Excitation Wavelengths ( $\lambda_{ex}$ ) Used for  $\phi_f$  Determinations

Solvent	9-COOMe		1-COOMe		2-COOMe	
	$\lambda_{ex}$ , nm	$D$	$\lambda_{ex}$ , nm	$D$	$\lambda_{ex}$ , nm	$D$
Hexane					355	1.70
Cyclohexane	362	1.31	365	1.08	355	1.41
Benzene	362	1.29			359	1.52
Dioxane	363	1.20			358	1.20
Acetonitrile	362	1.26	370	1.67	355	2.02
Ethanol	362	1.13	362	1.54	356	1.71
Methanol	362	1			356	1.95
60% Dioxane- 40% water	362	1				
Trifluoroethanol	362	1			355	1.70

instrument.<sup>5b</sup> All samples were dilute ( $A < 0.03$ , 1-cm cells) and deoxygenated by the freeze-pump-thaw method. The  $\tau_f$  of methyl 9-anthroate in cyclohexane was also determined on this latter instrument.

The bimolecular rate constant for the quenching of 2-COOMe fluorescence by ethyl iodide (Aldrich Chemical Co.) in several solvents was determined from the Stern-Volmer equation

$$\frac{F^0}{F} - 1 = K_{sv}[Q] \quad K_{sv} = \tau_f' k_q$$

$F^0$  and  $F$  are the fluorescence intensities of an aerated 2-COOMe solution in the absence and presence of a quencher, respectively,  $[Q]$  is the quencher concentration, and  $K_{sv}$  is the slope of a plot of  $(F^0/F - 1)$  vs.  $[Q]$ .  $K_{sv}$  is equal to the product of the fluorescence lifetime in aerated solution ( $\tau_f'$ ) and the bimolecular quenching constant ( $k_q$ ). The fluorescence lifetime of 2-COOMe in deoxygenated solution ( $\tau_f$ ) was directly measured in three solvents of widely varying polarity (Table II). From this data, it was clear that the following relation holds for two different solvents:

$$(\phi_f)_1/(\phi_f)_2 = (\tau_f)_1/(\tau_f)_2$$

By measuring the  $\phi_f$  in a given solvent, one could use this relation along with the measured  $\tau_f$  and  $\phi_f$  in ethanol to calculate  $\tau_f$  in the solvent of interest.  $\tau_f$ 's were then divided by the solvent deoxygenation factors ( $D$ ) to obtain  $\tau_f'$ 's. Once  $\tau_f'$  is known for a given solvent,  $k_q$  for that solvent can be determined from  $K_{sv}$ . Dilute concentrations ( $A \leq 0.05$  at exciting wavelength) of 2-COOMe were used in all measurements. The concentration of ethyl iodide was varied up to a maximum of 0.05 M when  $k_q$  was large ( $>10^9$  M<sup>-1</sup> s<sup>-1</sup>) and up to 0.5 M when  $k_q$  was small ( $<10^9$  M<sup>-1</sup> s<sup>-1</sup>).

The HMO calculations were performed on a Burroughs 5500 computer using a Fortran IV program written by Dr. Peter Frosch of our department.

## Results

*I. Absorption and Fluorescence Spectra of the Esters.* The absorption and fluorescence spectra of 9-COOMe in cyclohexane are shown in Figure 1. The absorption spectrum is quite anthracene-like having wavelength maxima which show little solvent dependence. Conversely, the fluorescence spectrum becomes more diffuse and the wavelength maximum ( $\lambda_f$ ) red shifts in solvents of increasing polarity.<sup>5</sup>

In Figures 2 and 3, the absorption and fluorescence spectra of 1-COOMe and 2-COOMe in cyclohexane are given. Note that the fluorescence spectrum of both molecules in

TABLE II: Fluorescence Data for the Three Methyl Anthroates<sup>f</sup>

Solvent <sup>a</sup>	9-COOMe			1-COOMe			2-COOMe		
	$\bar{\nu}_m^b$	$\phi_f$	$\tau_f^c$	$\bar{\nu}_m^b$	$\phi_f$	$\tau_f^c$	$\bar{\nu}_m^b$	$\phi_f$	$\tau_f^c$
Hexane (30)							2.37	0.33 ± 0.01	
Cyclohexane (33) <sup>d</sup>	2.20	0.85 ± 0.02	12.5 ± 1	2.29	0.12 ± 0.01	3.0 ± 1	2.36	0.49 ± 0.02	10.3 ± 0.3
Ether (34)	2.19			2.33			2.35		
Benzene (34)		0.75 ± 0.03	14.1 ± 0.5				2.32	0.72 ± 0.02	
Dioxane (36)	2.15	0.70 ± 0.03	14.4 ± 0.5	2.20			2.32	0.78 ± 0.02	
Methyl formate (40)	2.14			2.17			2.31		
Benzonitrile (42)	2.10			2.14			2.27		
Dimethyl- formamide (44)	2.11			2.13			2.27		
Acetonitrile (46)	2.10	0.41 ± 0.03	8.1 ± 0.5	2.15	0.72 ± 0.02	15.0 ± 0.5	2.28	0.97 ± 0.02	21.5 ± 0.5
Ethanol (52)	2.06	0.18 ± 0.01	4.1 ± 1	2.12	0.67 ± 0.02	16.5 ± 0.5	2.24	0.98 ± 0.02	21.8 ± 0.3
Methanol (55.5)		0.11 ± 0.01	1.7 ± 1				2.21	0.92 ± 0.02	
60% Dioxane- 40% water (55.6)	2.02	0.07 ± 0.01		2.03			2.16		
Trifluoroethanol (61.1) <sup>e</sup>		0.02					2.09	0.75 ± 0.05	

<sup>a</sup> Values in parentheses are the solvent  $E_T(30)$  values. <sup>b</sup>  $\times 10^{-4} \text{ cm}^{-1}$ . <sup>c</sup> Nanoseconds. <sup>d</sup> Estimated from  $E_T(30)$  values of hexane and benzene. <sup>e</sup> Estimated by comparison of  $\phi_f$  of 9-COOMe in trifluoroethanol with  $\phi_f$  of 9-COOMe in  $\text{H}_2\text{O}$ -dioxane mixtures of known  $E_T(30)$  values. <sup>f</sup>  $T = 22^\circ \text{C}$ .

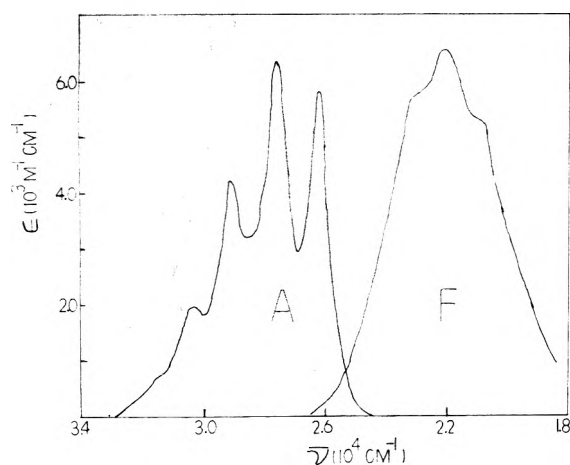


Figure 1. Absorption (A) and fluorescence (F,  $< 10^{-5} \text{ M}$ ) spectra of 9-COOMe in cyclohexane. The two spectra are normalized to the same intensity.

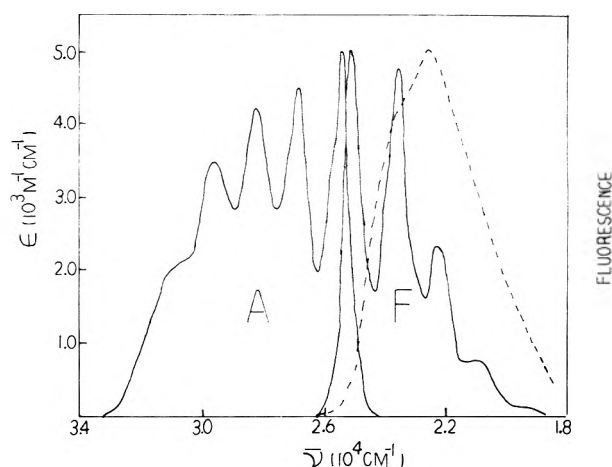


Figure 3. Absorption spectrum (A) of 2-COOMe in cyclohexane and fluorescence spectra (F,  $< 10^{-5} \text{ M}$ ) of 2-COOMe in cyclohexane (—) and in ethanol (---). All spectra are normalized to same intensity.

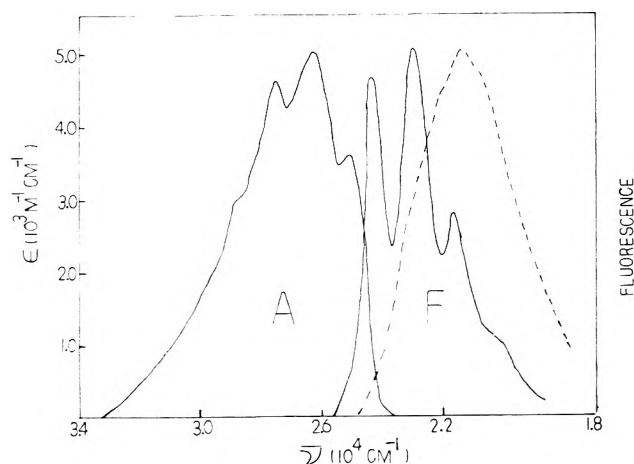


Figure 2. Absorption spectrum (A) of 1-COOMe in cyclohexane and fluorescence spectra (F,  $< 10^{-5} \text{ M}$ ) of 1-COOMe in cyclohexane (—) and in ethanol (---). All spectra are normalized to same intensity.

cyclohexane has a structured, anthracene-like appearance. As with 9-COOMe, only the fluorescence spectra of 1-COOMe and 2-COOMe show significant solvent depen-

dence. With increasing solvent polarity the fluorescence maximum red shifts and a severe loss of vibrational structure is observed. The fluorescence spectra of 1-COOMe and 2-COOMe in ethanol shown in Figures 2 and 3 illustrate these points.

The fluorescence excitation spectra of anthracene at 77 K and of 2-COOMe at room temperature and at 77 K in ethanol-methanol (4:1) are given in Figure 4. These spectra are uncorrected for the wavelength response of the source-excitation monochromator system. It can be seen that the excitation spectrum of 2-COOMe at 77 K is considerably more structured and anthracene-like in appearance than is the room temperature spectrum. The 77 K fluorescence excitation spectrum of 1-COOMe in Figure 5 is also more structured than its room temperature counterpart but less structured than the 77 K spectrum of 2-COOMe in Figure 4.

II. Solvent Dependence of Ester Spectral Properties. The solvent dependence of the lowest excited singlet ( $S_1$ ) energy, the fluorescence quantum yield ( $\phi_f$ ), and the fluorescence lifetime ( $\tau_f$ ) for all three esters are shown by the data in Table II. The solvents are listed in order of increasing solvent polarity as measured by the empirical  $E_T(30)$

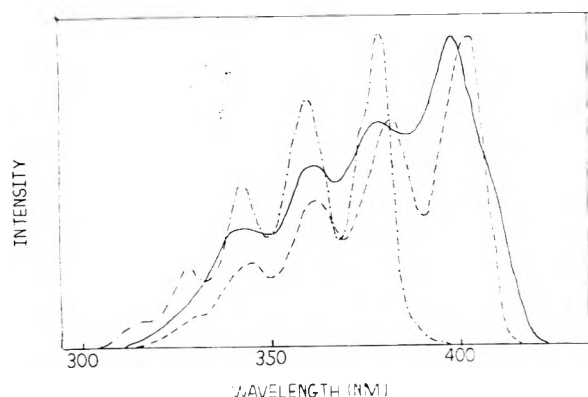


Figure 4. Fluorescence excitation spectra of 2-COOMe at room temperature (—) and at 77 K (---) and of anthracene at 77 K (-·-·-). All concentrations  $<10^{-5}$  M. Excitation bandpass = 7 nm, emission bandpass = 3 nm.

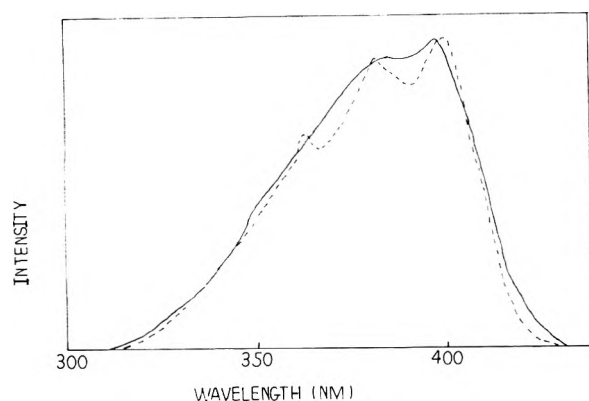


Figure 5. Fluorescence excitation spectra of 1-COOMe at room temperature (—) and at 77 K (---); concentration  $<10^{-5}$  M. Excitation bandpass = 7 nm, emission bandpass = 3 nm.

polarity scale.<sup>12</sup> As a measure of the  $S_1$  energy, the mean wavenumber of fluorescence ( $\bar{\nu}_m$ ) has been calculated in each solvent from the following relation:<sup>13</sup>

$$\int_{\bar{\nu}_1}^{\bar{\nu}_m} F(\bar{\nu}) d\bar{\nu} = \frac{1}{2} \int_{\bar{\nu}_1}^{\bar{\nu}_2} F(\bar{\nu}) d\bar{\nu} \quad (I)$$

where  $\bar{\nu}_1$  and  $\bar{\nu}_2$  are the minimum and maximum wavenumbers at which measurable fluorescence occurs, respectively, and  $F(\bar{\nu})$  is the corrected fluorescence intensity at a given wavenumber. To determine  $\bar{\nu}_m$ , the corrected fluorescence spectrum in wavelength is first converted to a wavenumber scale. The  $\bar{\nu}_m$  value is then obtained by comparing the areas under the curve (by cut and weigh) from  $\bar{\nu}_1$  to  $\bar{\nu}_m$  with the total area under the spectrum. By the use of  $\bar{\nu}_m$  values, excited state energies taken from spectra of differing shape and structure can be compared with validity.

Generally, the energy of  $S_1$  is observed to decrease as solvent polarity increases for all three esters. In a given solvent, the  $S_1$  energy always decreases in the following order:  $S_1(2\text{-COOMe}) > S_1(1\text{-COOMe}) > S_1(9\text{-COOMe})$ .

The  $\phi_f$  of 9-COOMe generally decreases as solvent polarity increases especially in solvents which are hydrogen bond donors.<sup>5</sup>  $\phi_f$  values in Table II for 9-COOMe in cyclohexane, benzene, and acetonitrile are higher than reported previously<sup>5</sup> due to more efficient deoxygenation procedures presently employed. The observed trend for 2-COOMe is, however, quite different than that of 9-COOMe. In the very nonpolar solvent hexane, the  $\phi_f$  of 2-COOMe is at a mini-

TABLE III: Natural Excited-State Lifetimes for the Methyl Anthroates<sup>c</sup>

Compound	Solvent	$\tau_{r1}$ , ns <sup>a</sup>	$\tau_{r2}$ , ns <sup>b</sup>
2-COOMe	Cyclohexane	21 ± 1	19
2-COOMe	Acetonitrile	22 ± 1	23
2-COOMe	Ethanol	22 ± 1	22
1-COOMe	Cyclohexane	25 ± 9	18
1-COOMe	Ethanol	25 ± 1	28
9-COOMe	Cyclohexane	15 ± 2	
9-COOMe	Acetonitrile	20 ± 3	
9-COOMe	Ethanol	23 ± 6	

<sup>a</sup> From  $\tau_f/\phi_f$ . <sup>b</sup> From Strickler-Berg equation, ref 13. <sup>c</sup>  $T = 22^\circ\text{C}$ .

TABLE IV:  $\pi$  Bond Order for the Ring-Carboxyl Bond in  $S_0$  and  $S_1$  for the Anthroate Esters

Compound	$P_{rs}(S_0)$	$P_{rs}(S_1)$
9-COOMe	0.6884	0.7415
1-COOMe	0.4561	0.5165
2-COOMe	0.4320	0.4819

mum (0.33). As solvent polarity begins to increase,  $\phi_f$  begins to rise rapidly until it reaches a value near unity in both acetonitrile and ethanol. The  $\phi_f$  begins to decrease again in the better hydrogen bond donor solvents methanol and trifluoroethanol. From the limited  $\phi_f$  data in Table II, it appears that the  $\phi_f$  of 1-COOMe shows a similar solvent dependence as the  $\phi_f$  of 2-COOMe.

The  $\tau_f$ 's for the three esters follow the same solvent trends as do the  $\phi_f$ 's for the respective esters. The  $\tau_f$  of 9-COOMe in cyclohexane was measured on both the Ortec and TRW instruments (see Experimental Section) and found to agree within 1 ns. An average value of the two determinations is reported in Table II.

II. Natural Excited-State Lifetime of the Esters. The natural excited state lifetime ( $\tau_f$ ) of the esters was calculated by two methods. First, from the fluorescence properties of the ester via

$$\tau_{r1} = \tau_f/\phi_f \quad (II)$$

and second from the Strickler-Berg equation

$$1/\tau_{r2} = (2.88 \times 10^{-9})n^2(\bar{\nu}^{-3})^{-1} \int (\epsilon/\bar{\nu}) d\bar{\nu} \quad (III)$$

which depends on an integration over the absorption spectrum, where  $n$  is the index of refraction,  $\epsilon$  is the molar extinction coefficient, and  $(\bar{\nu}^{-3})^{-1} = \int f(\bar{\nu}) d\bar{\nu} / \int \bar{\nu}^{-3} f(\bar{\nu}) d\bar{\nu}$ .<sup>14</sup> The  $f(\bar{\nu})$  term is the corrected fluorescence intensity as a function of frequency. Results of these calculations are given in Table III. Strickler-Berg calculations were not carried out for 9-COOMe because there is some question as to the validity of this calculation when significant geometry changes accompany excitation.<sup>14</sup>

IV. HMO Calculations of  $\pi$  Bond Order for the Substituent Bond. Simple HMO calculations were performed on the three esters to determine the  $\pi$  bond order ( $P_{rs}$ ) of the ring to carboxyl group bond in the ground ( $S_0$ ) and in first excited singlet ( $S_1$ ) state. The heteroatom parameters suggested by Streitwieser<sup>15</sup> were used for the carboxyl oxygens and the geometry of both  $S_0$  and  $S_1$  was assumed to be planar for the calculation. Comment on this latter assumption will be made in the Discussion. The results of these calculations are given in Table IV. Note that for all three esters the  $\pi$  bond order is larger in  $S_1$  than in  $S_0$ . Also,  $\pi$  bond

TABLE V: Heavy Atom Quenching of 2-COOMe Fluorescence as a Function of Solvent

Solvent	$E_T(30)$	$K_{sv}$	$\tau_f', \text{ nsc}$	$10^9 k_{q1}, \text{ M}^{-1} \text{ s}^{-1}$	$\phi_f$
Hexane	30.9	15.3	4.3	3.6	0.33
Cyclohexane	33 <sup>a</sup>	14.8	7.3	2.0	0.49
Dioxane	36	4.7	14.3	0.33	0.78
Acetonitrile	46	3.0	10.6	0.28	0.97
Ethanol	51.9	1.6	12.7	0.13	0.98
Methanol	55.5	1.3	10.5	0.12	0.92
Trifluoroethanol	61.1 <sup>b</sup>	0.42	9.8	0.043	0.75

<sup>a</sup> Estimated from  $E_T(30)$  values of hexane and benzene.

<sup>b</sup> Estimated by comparison of  $\phi_f$  of 9-COOme in trifluoroethanol with  $\phi_f$  of 9-COOme in H<sub>2</sub>O-dioxane mixtures of known  $E_T(30)$  values. <sup>c</sup> In aerated solution.

order increases in the sequence  $P_{rs}(9\text{-COOme}) > P_{rs}(1\text{-COOme}) > P_{rs}(2\text{-COOme})$  in both states.

V. *Heavy Atom Quenching of 2-COOme Fluorescence.* The quenching of 2-COOme fluorescence by ethyl iodide in several solvents was investigated. Typical Stern-Volmer plots were obtained in each solvent when  $(F^0/F - 1)$  was plotted against quencher concentration. The slope of the straight line plot ( $K_{sv}$ ) is equal to  $k_q\tau_f'$  where  $k_q$  is the rate constant for bimolecular quenching and  $\tau_f'$  is the lifetime of 2-COOme in aerated solvent. Values for  $K_{sv}$ ,  $\tau_f'$ , are  $k_q$  are given in Table V for the solvents studies. Also included in Table V are the  $\phi_f$  of 2-COOme in each solvent and the solvent  $E_T(30)$  values.

## Discussion

Most of this section will be confined to a discussion of the 1- and 2-COOme spectral properties. The spectral behavior of 9-COOme has already been discussed<sup>5a,7</sup> and the results of that work will be mentioned here for a comparison with the 1- and 2-COOme excited state behavior.

I. *Nature of the Electronic Transitions Involved in the Long Wavelength Absorption and Fluorescence.* The long wavelength absorption spectrum of anthracene is thought to contain two overlapping transitions which are classified by Platt as  $^1A_1 \rightarrow ^1L_a$  or  $^1L_a$  and  $^1A_1 \rightarrow ^1L_b$  or  $^1L_b$ .<sup>16</sup> The allowed  $^1L_a$  transition is short axis polarized and considerably more intense than the long axis polarized and forbidden  $^1L_b$  transition.<sup>16</sup> Indeed, the difference in intensity of the two transitions has made the detection of the weaker  $^1L_b$  transition subject to considerable uncertainty. PPP-SCF calculations place the  $^1L_a$  and  $^1L_b$  excited states at about 28 000 and 29 000  $\text{cm}^{-1}$ , respectively.<sup>17</sup> Experimentally, the origin of the  $^1L_b$  transition has been placed anywhere from 25 000 to about 30 000  $\text{cm}^{-1}$ .<sup>17-20</sup> The best agreement with the calculated value comes from two photon and polarized spectral work which position the  $^1L_b$  transition onset near 30 000  $\text{cm}^{-1}$ .<sup>17,18</sup>

When a substituent is attached to the anthracene ring, its ability to affect a given electronic transition will depend on the position of substitution. For naphthalene, where the  $^1L_a$  and  $^1L_b$  transitions can be nearly resolved, the former transition is more red shifted than the latter by substitution in the 1 position while the opposite is true for 2 substitution.<sup>21</sup> Thus the transition which is more affected by substitution is the one polarized along the direction of substitution. By analogy to naphthalene, substitution in the 9 and 1 positions of anthracene should have a greater effect on the  $^1L_a$  transition while 2 substitution is expected to have a greater effect on the  $^1L_b$  transition. One of the main goals of this work was to see whether methyl ester substitu-

tion in the 2 position would lead to a greater expression of the  $^1L_b$  transition in either absorption or fluorescence. Previously, we reported that the  $^1L_b$  level become the emitting state for 2-anthroic acid in polar solvents.<sup>8</sup>

The absorption and fluorescence spectra of 2-COOme in cyclohexane shown in Figure 3 seem to suggest enhancement of the  $^1L_b$  transition in absorption. The lack of mirror image symmetry between the two spectra is consistent with overlapping absorption transitions with only the lower energy transition responsible for the fluorescence. However, the natural lifetime data in Table III are not in agreement with this suggestion.  $\tau_{r2}$  values for 1- and 2-COOme are quite similar indicating that the transition responsible for the long wavelength absorption of both esters is essentially the allowed  $^1L_a$  transition. In addition, the excellent agreement between  $\tau_{r1}$  and  $\tau_{r2}$  for 1- and 2-COOme is further evidence that the long wavelength absorption is comprised of one major electronic transition. A significant contribution from a second transition would result in  $\tau_{r1} > \tau_{r2}$ .<sup>22</sup> Apparently, intensification of the  $^1L_b$  transition for 2-COOme is not great enough for this transition to make significant contribution to the overall absorption intensity. A second consideration which follows from the agreement of  $\tau_{r1}$  and  $\tau_{r2}$  is that the fluorescence transition for both esters must be the reverse of the absorption, i.e.,  $^1L_a \rightarrow ^1A_1$ . Support for this assignment is evident in the fluorescence spectra of 1- and 2-COOme in cyclohexane (Figures 2 and 3). These spectra closely resemble that of anthracene fluorescence ( $^1L_a \rightarrow ^1A_1$ ) and possess similar vibrational spacing ( $\sim 1400 \text{ cm}^{-1}$ ) as found in the anthracene spectrum. Clearly, the invariance of  $\tau_{r1}$  as a function of solvent for 2-COOme argues against an excited state inversion in polar solvents and substantiates that the  $^1L_a$  state is the emitting state in solvents of widely varying polarity. Carboxyl substitution will undoubtedly introduce some degree of charge transfer (CT) character into the  $^1L_a$  state resulting in a more polar excited state than that of anthracene.<sup>5a</sup> The CT character of  $S_1$  is confirmed by the following observations; the carboxyl group becomes more basic on excitation to the  $^1L_a$  state,<sup>23</sup> the energy of  $S_1$  red shifts in more polar solvents (Table II), and the fluorescence spectra of the esters in ethanol (Figures 2 and 3) show the expected polar solvent-induced spectral smearing.

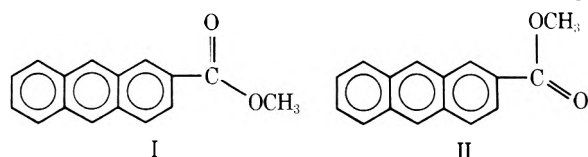
Our present findings for 2-COOme raise doubts about the previously reported results concerning fluorescence from the  $^1L_b$  level of 2-anthroic acid (2-COOH) in polar solvents.<sup>8</sup> These results were based on  $\phi_f$  and  $\tau_f$  data for 2-COOH in cyclohexane and acetonitrile. We have repeated these measurements. In the three solvents mentioned in Table III, the  $\tau_{r1}$ 's for 2-COOH range from 24 to 26 ns which is in substantial agreement with the 2-COOme values. Thus we conclude that our prior assignment of the  $^1L_b$  state as the emitting state for 2-COOH in polar solvents is in error. Our earlier  $\phi_f$  and  $\tau_f$  values for 2-COOH were lower than our present values especially in acetonitrile. One reason for this is that the earlier data were obtained with a less efficient deoxygenation system than we presently use. The moderately long  $\tau_f$ 's for these compounds make their fluorescence relatively sensitive to oxygen quenching. A second reason for the discrepancy involves ground state ionization of the 2-COOH in acetonitrile. At the low concentrations used for  $\phi_f$  and  $\tau_f$  determinations in the previous work ( $\sim 2 \times 10^{-6} \text{ M}$ ), substantial formation of the 2-anthroate anion occurs in acetonitrile. We have avoided this complication in our present work by adding a trace of  $\text{H}^+$  ( $\sim 5 \times 10^{-5} \text{ M}$ ) to suppress ionization

in polar solvents. On addition of this  $H^+$  the fluorescence intensity increased but underwent no further change on a second addition of  $H^+$ . Thus we believe that this  $H^+$  addition ensures that all of the 2-COOH is in the molecular form in  $S_0$  and that  $H^+$  at this concentration does not quench 2-COOH fluorescence.

It is concluded, then, that carboxyl substitution in the 2 position of anthracene does not cause an inversion of the anthracene  $^1L_a$  and  $^1L_b$  levels in any solvent. Nor does carboxyl substitution provide sufficient intensification of the  $^1L_b$  transition to be detectable by a comparison of  $\tau_r$ 's. Several workers have reported a greater expression of the  $^1L_b$  transition in some side substituted anthracenes. Albrecht et al., using polarized absorption and fluorescence measurements, have presented evidence for the spectral detection of the  $^1L_b$  transition in 2-methoxy- and 2,3-dimethoxyanthracene.<sup>17</sup> The predicted and observed polarization of the  $^1L_b$  transition for the 2-methoxy derivative is along the short axis of anthracene indicating significant state mixing with the  $^1L_a$  wave function.<sup>17</sup> It is worth noting that even for the 2,3-dimethoxy derivative the  $^1L_a$  state appears to be the lowest energy excited state.<sup>17</sup> Suzuki and Baba, using solvent perturbation and vibrational analysis, have observed the  $^1L_b$  transition in 2-hydroxyanthracene.<sup>24</sup> They propose that the  $^1L_b$  state is actually below the  $^1L_a$  level and thus fluorescence originates from the  $^1L_b$  state in this molecule. McKelvey and King have also presented evidence for the detection of the  $^1L_b$  transition in 2-hydroxyanthracene based on oscillator strengths.<sup>25</sup> However, they suggest that the lowest energy, fluorescing state remains the  $^1L_a$  level.

**II. Ground and Excited State Geometries of the Anthroate Esters.** Previously it has been shown that the spectral properties of 9-COOme reflect significant differences in the equilibrium geometries of the ground ( $S_0$ ) and first excited singlet states ( $S_1$ ).<sup>7</sup> The anthracene-like appearance of the 9-COOme absorption spectrum in Figure 1 is in agreement with the near perpendicularity of the ring and carboxyl group planes in  $S_0$ .<sup>26</sup> Electronically, a planar  $S_0$  is favored but steric hindrance with the peri hydrogens results in the more perpendicular conformation.<sup>26</sup> The calculated  $\pi$  bond order ( $P_{rs}$ ) for 9-COOme in  $S_0$  is a considerable overestimation of the true  $P_{rs}$  value since it is based on a planar  $S_0$ . More likely,  $P_{rs}$  approaches zero in  $S_0$ . On excitation, a significant increase in  $P_{rs}$  occurs resulting in an  $S_1$  geometry approaching coplanarity. Accompanying this geometry change in  $S_1$  is a degree of charge transfer (CT) toward the carboxyl group.<sup>5</sup> The resulting diffuse fluorescence shown in Figure 1 is attributed to the geometry difference between  $S_0$  and  $S_1$  and to the CT character of the  $S_1$  state.<sup>5a</sup>

The situation with 2-COOme is in considerable contrast with that of 9-COOme. Molecular models indicate no steric hindrance to coplanarity for either of the two conformers (I and II). Thus it is likely that the 2-COOme molecule is pla-



nar in both  $S_0$  and  $S_1$ . McGlynn and Lui have presented spectral evidence which shows that methyl and ethyl esters of 2-naphthoic acid are planar in both states.<sup>27</sup> However, as Table IV demonstrates, there is a substantial increase in

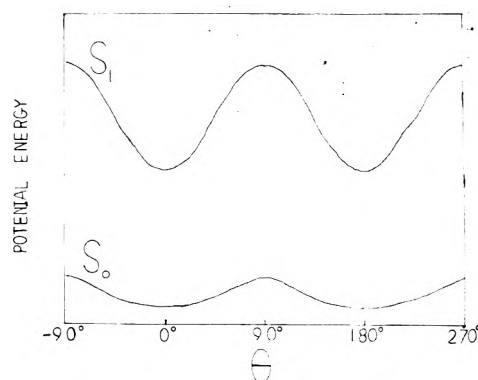
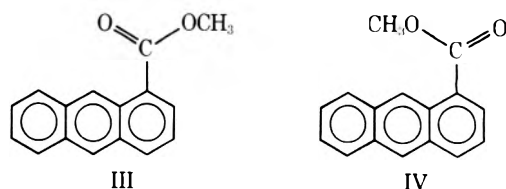


Figure 6. Potential energy as a function of  $\theta$  for the ground ( $S_0$ ) and first excited singlet state ( $S_1$ ) of 2-COOme.

$P_{rs}$  in  $S_1$  for 2-COOme. The significance of this fact with respect to the spectral behavior of 2-COOme is evident from the curves in Figure 6. These curves represent the relative potential energy of 2-COOme as a function of molecular conformation in  $S_0$  and  $S_1$ . The angle  $\theta$  is the angle between the planes of the ring and the carboxyl group. Molecular models show no steric hindrance to coplanarity for either of the two coplanar conformers (I and II,  $\theta = 0$  and  $180^\circ$ ) and therefore, we assume that the energies of I and II are quite similar in both states. Since  $P_{rs}$  is greater in  $S_1$ , the potential function for this state should rise more steeply than the  $S_0$  function as the molecule is rotated away from the potential minima. Thus while the equilibrium angles for both states are the same, the distribution of conformers about the equilibrium angle is different in the two states. At a given temperature, a greater number of conformations will exist in the  $S_0$  level. The electronic transition energy of a given conformer will differ slightly from that of other conformers thereby resulting in a greater range of transition energies for the state with the greater distribution of conformers. It follows, then, that one would expect a more diffuse absorption spectrum than fluorescence spectrum for 2-COOme. This is confirmed by the spectra in cyclohexane shown in Figure 3. By lowering the temperature to 77 K, the distribution of conformers in  $S_0$  will decrease until only those associated with the energy minima remain. Therefore at 77 K, a more "anthracene-like" absorption spectrum is expected for 2-COOme and this is indeed observed in Figure 4. The significance of this observation is that the lack of a mirror image relationship, as in Figure 3, does not necessarily mean that  $S_0$  and  $S_1$  have different equilibrium geometries. Rather, it may signify a different distribution of conformers about the equilibrium geometry in the two states.

A molecular model of 1-COOme demonstrates that neither of the conformers (III and IV) can achieve complete



coplanarity in  $S_0$ . X ray analysis of 1-naphthoic acid places the angle  $\theta$  at  $11^\circ$  in  $S_0$  and we would expect a similar  $S_0$  geometry for 1-COOme.<sup>28</sup> The electronic spectra of the methyl ester of 1-naphthoic acid are consistent with a noncoplanar geometry for  $S_0$  and a nearly coplanar geometry for

$S_1$ .<sup>27</sup> From our calculated  $P_{rs}$  values in Table IV, we also predict a more coplanar  $S_1$  for 1-COOMe. Thus, with respect to the relative geometries in  $S_0$  and  $S_1$ , the behavior of 1-COOMe is between 9-COOMe and 2-COOMe although closer to the latter. That is, a change in the equilibrium geometry does occur subsequent to excitation for 1-COOMe but the change in  $\theta$  is considerably smaller than for 9-COOMe.

The  $S_0$  potential function for 1-COOMe will also contain two minima as a function of  $\theta$ . However these minima should differ from those for 2-COOMe in two ways. First, the minima for 1-COOMe will be obtained at  $\theta > 0^\circ$  and  $\theta < 180^\circ$ . Second, it is likely that the energies at these two minima will not be the same since models suggest that structure III can become more planar than structure IV. Also, for a given  $\theta$ , carboxyl substitution in the 1 position should have a greater effect on the  ${}^1L_a$  transition than 2 substitution since the 1 position is more electron rich and lies more nearly along the polarization axis. The diffuse room temperature absorption spectrum of 1-COOMe in Figure 2 is consistent with a distribution of conformers about the two  $S_0$  potential minima. Note, however, that the excitation spectrum of 1-COOMe in Figure 5 is still considerably more diffuse than the 77 K excitation spectrum of 2-COOMe in Figure 4. Two reasons for this could obtain. It is possible that even at 77 K a significant population of conformers exists in the higher energy minima. These conformers would have slightly differing excitation energies than those associated with the lower minima the result being overlapping absorption. A second possibility involves the relative shapes of the  $S_1$  and  $S_0$  potential functions. The  $S_1$  function will have minima at  $\theta \sim 0^\circ$  and  $\sim 180^\circ$  and rise more steeply than the  $S_0$  function because of the increases in  $P_{rs}$  on excitation. Because of the difference in equilibrium  $\theta$ , absorption from  $S_0$  may terminate in the steeply rising portion of the  $S_1$  function. This would tend to accentuate the difference in excitation energy for the distribution of conformers which can exist at 77 K in  $S_0$ .

It seems likely from models that structure III could accommodate the coplanar geometry of  $S_1$  with less steric repulsion than structure IV. As a result, the energy difference between the two potential minima is expected to be greater in  $S_1$  than in  $S_0$ . In the equilibrium excited state, virtually all of the molecules may now exist about the lower energy minima. The steeper  $S_1$  function will again result in a more restricted range of conformers about this minimum than in  $S_0$  and this in turn would produce a more structured fluorescence spectrum. This suggestion is in agreement with the anthracene-like fluorescence spectrum of 1-COOMe in cyclohexane shown in Figure 2.

III.  $\phi_f$  as a Function of Solvent for the Anthroate Esters. The solvent dependence of the  $\phi_f$  for 9-COOMe has been discussed previously.<sup>5a</sup> As seen in Table II, the  $\phi_f$  of 9-COOMe in nonpolar solvents is relatively high but decreases markedly in polar protic solvents. The high  $\phi_f$  value in nonpolar solvents is thought to be a result of the relative energies of  $S_1$  and the two lowest triplets ( $T_1$  and  $T_2$ ). In anthracene,  $T_2$  is slightly below  $S_1$  and the small  $\Delta E_{S_1-T_2}$  leads to efficient intersystem crossing (ISC).<sup>29</sup> It is usually assumed that triplet levels of anthracene are less sensitive to substitution and solvent than is  $S_1$ .<sup>30</sup> Thus the  $T_1$  and  $T_2$  energies of all three esters are probably quite similar to those of anthracene. However, the ester  $S_1$  energies are all lower than that of anthracene particularly for 9-COOMe where  $S_1$  is ca.  $3000\text{ cm}^{-1}$  below the anthracene  $S_1$ .<sup>5a</sup>

Therefore in nonpolar solvents the  $S_1$  state of 9-COOMe should be below  $T_2$  by as much as  $2000\text{ cm}^{-1}$  but above  $T_1$  by as much as  $7000\text{ cm}^{-1}$ .<sup>5a</sup> ISC becomes much less efficient than for anthracene which explains the threefold larger  $\phi_f$  observed for 9-COOMe. The decrease in the  $\phi_f$  for 9-COOMe in polar protic solvents is due to an increase in one or both of the nonradiative rate constants ( $k_{isc} + k_{ic}$ ) rather than a decrease in the radiative rate constant ( $k_f$ ).<sup>5a</sup> Although  $\Delta E_{S_1-T_1}$  is expected to decrease in protic solvents, the magnitude of  $\Delta E_{S_1-T_1}$  in these solvents would seem to be too large to account for the reduced  $\phi_f$  in terms of an increase in  $k_{isc}$ . Instead, it has been suggested that a solvent induced enhancement of  $k_{ic}$  occurs in protic solvents.<sup>5a</sup>

The solvent dependence of the  $\phi_f$  for 2-COOMe appears to be quite different from that of 9-COOMe (Table II). Nonetheless, the solvent trends for the 2-substituted ester can be rationalized using the same excited state scheme as above. The key difference between the 9- and 2-substituted esters is the energy of  $S_1$  which is always higher for the latter ester. For example, in cyclohexane the  $S_1$  energy for 2-COOMe is higher by  $1600\text{ cm}^{-1}$  which would place the  $S_1$  level of 2-COOMe much closer to the  $T_2$  level than for 9-COOMe. As a result, efficient intersystem crossing is possible leading to a  $\phi_f < 0.5$  in hexane and cyclohexane. It is interesting to note the dramatic increase in  $\phi_f$  which accompanies a relatively small shift in  $S_1$  in these saturated hydrocarbon solvents. This is precisely the behavior one would expect if  $S_1$  lies slightly below  $T_2$  so that intersystem crossing (ISC) must be thermally assisted. We are currently investigating the temperature dependence of the  $\phi_f$  of 2-COOMe to clarify this mechanism. With further increases in solvent polarity, the  $S_1$  energy continues to decrease and therefore  $\Delta E_{S_1-T_2}$  must become larger thereby inhibiting the thermally assisted ISC process. In ethanol and acetonitrile the  $\phi_f$  of 2-COOMe has risen to near unity which is believed to be the highest  $\phi_f$  value ever reported for a side-substituted anthracene.

The  $\phi_f$  of 2-COOMe in ethanol is much greater than that of 9-COOMe in this solvent (0.18). The large difference in  $\phi_f$ 's implies that the protic solvent induced quenching observed for 9-COOMe in ethanol is not significant for 2-COOMe. In stronger hydrogen bond donating solvents such as methanol and trifluoroethanol, the  $\phi_f$  of 2-COOMe is observed to decrease. An explanation for the reduced  $\phi_f$  in these solvents is ISC to  $T_1$ . However, although the magnitude of  $E_{S_1-T_1}$  should decrease in these solvents, it should remain too large for significant  $S_1 \rightarrow T_1$  decay to occur. Solvent induced internal conversion may be the dominant nonradiative pathway in polar protic solvents.

Our mechanism above is based on  $T_2$  lying above  $S_1$  in all the solvents studied. It is possible that  $S_1$  might actually be above  $T_2$  in some of the nonpolar solvents. In this case, the efficiency of ISC could increase or decrease as  $S_1$  approaches  $T_2$  in more polar solvents because small differences in  $\Delta E_{S_1-T_2}$  when the magnitude of  $\Delta E_{S_1-T_2}$  is small can lead to significant variation in the Franck-Condon factor which govern the  $S_1 \rightarrow T_2$  process.<sup>30</sup> We observe only an increase in  $\phi_f$  as solvent polarity increases through ethanol. Therefore we believe that  $S_1$  probably lies below  $T_2$  even in the very nonpolar solvents.

The  $\phi_f$  trend with solvent for 1-COOMe is similar to that for 2-COOMe but two differences stand out. The  $\phi_f$ 's for 1-COOMe are lower than the 2-COOMe values in a given solvent implying a slightly lower  $T_2$  energy for the former ester if ISC is thermally assisted. Also, the  $\phi_f$  of 1-COOMe

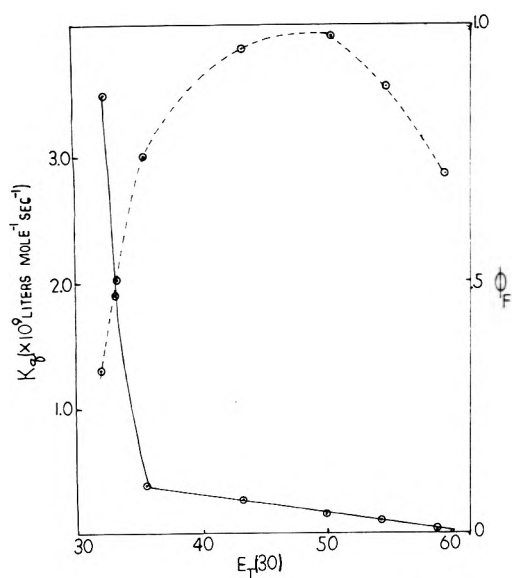


Figure 7. The dependence of the  $\phi_f$  for 2-COOMe and of  $k_q$  for the ethyl iodide quenching of 2-COOMe fluorescence on solvent polarity:  $\phi_f$  (---);  $k_q$  (—).

in the protic solvent ethanol is slightly lower than in acetonitrile. Apparently some protic solvent induced quenching is already being observed in ethanol for 1-COOMe.

It is clear from the above discussion that experimental location of the ester triplet levels is necessary to substantiate the decay mechanisms. Unfortunately, all attempts to locate these triplets by phosphorescence or triplet-triplet absorption have thus far been unsuccessful.<sup>31</sup> The explanation presented above for the solvent dependent  $\phi_f$  of 1- and 2-COOMe implies that ISC is controlled by a small, solvent dependent  $\Delta E_{S_1-T_2}$  in nonpolar solvents and that ISC is unimportant in polar solvents due to a large  $\Delta E_{S_1-T_1}$ . The presence of a heavy atom, either internally or externally, is known to quench fluorescence by enhancing ISC via spin-orbital coupling. Recently, it has been shown that the efficiency with which a heavy atom quenches fluorescence is inversely related to the energy gap between the fluorophore's  $S_1$  and accepting triplet.<sup>32</sup> As this energy gap increases, heavy atom induced ISC becomes less competitive with fluorescence because the former process requires increasingly larger amounts of electronic energy to be converted into vibrational energy during the transition. Heavy atom quenching is only observed for aromatic molecules when the  $S_1$  to accepting triplet gap is significantly less than  $10^4 \text{ cm}^{-1}$ .<sup>32</sup> We felt that the ability of a heavy atom to quench the fluorescence of 2-COOMe in different solvents might reflect the relative gap between  $S_1$  and the nearest accepting triplet. Ethyl iodide was used as the heavy atom quencher and the bimolecular quenching constant ( $k_q$ ) was used as a measure of quenching efficiency. The  $k_q$  values obtained in the various solvents are presented in Table V along with the  $\phi_f$  of 2-COOMe in each solvent. A rather dramatic inverse relationship is observed between  $k_q$  and  $\phi_f$  as solvent polarity increases from hexane through ethanol. This is graphically illustrated in Figure 7. The variation of  $k_q$  as a function of solvent far exceeds that expected for differences in diffusion rate among these solvents. In hexane, where  $\phi_f$  has its minimum value,  $k_q$  has its maximum value which is near that for diffusion control. This is in complete agreement with the small  $\Delta E_{S_1-T_2}$  proposed for this solvent. As solvent polarity increases through ethanol,

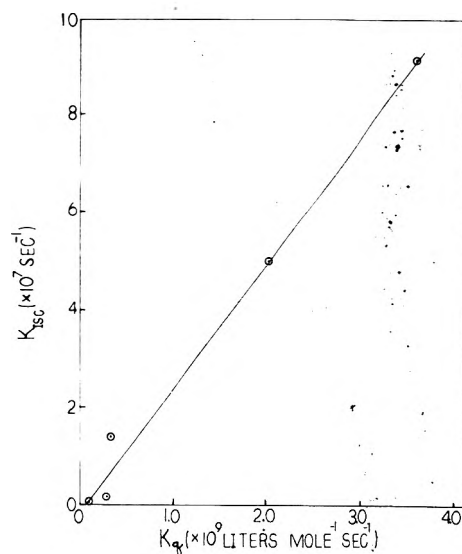


Figure 8. A plot of the calculated rate constant for ISC ( $k_{isc}$ ) vs. the rate constant for heavy atom quenching ( $k_q$ ) in the same solvent.

$k_q$  decreases and  $\phi_f$  increases as expected if  $\Delta E_{S_1-T_2}$  is increasing and  $\Delta E_{S_1-T_1}$  is large. Note that in methanol and trifluoroethanol the  $k_q$  value continues to decrease even though the  $\phi_f$  has now begun to decrease from the value in ethanol. This substantiates our earlier suggestion that the reduction in  $\phi_f$  in these two solvents is due to protic solvent induced internal conversion rather than ISC. If we assume that internal conversion is the only significant nonradiative decay made in these two latter solvents, the calculated values from eq IV for the internal conversion rate constants ( $k_{ic}$ ) are  $3.9 \times 10^6 \text{ s}^{-1}$  (methanol) and  $1.5 \times 10^7 \text{ s}^{-1}$  (trifluoroethanol). By contrast, the  $k_{ic}$  value for 9-COOMe in methanol is  $5.3 \times 10^8 \text{ s}^{-1}$ .<sup>5a</sup>

The variation in the  $\phi_f$  of 2-COOMe from hexane through ethanol is attributed solely to variation in  $k_{isc}$  and, for these solvents,  $k_f, k_{isc} \gg k_{ic}$ . Thus we can calculate  $k_{isc}$  from eq IV for 2-COOMe in these solvents. Figure 8 shows

$$k_i = \frac{k_f}{\phi_f} - k_f \quad k_i = k_{ic} \text{ or } k_{isc} \quad (\text{IV})$$

a plot of these calculated  $k_{isc}$  values vs. the  $k_q$  values from the heavy atom quenching experiments. A relatively good linear relationship exists between the two sets of rate constants. Although no direct linear relationship is predicted on theoretical grounds, there seems little doubt that the plot in Figure 8 confirms the mutual dependence of the two rate constants on the same single-triplet gap.

We have tried to measure  $k_q$  values for the ethyl iodide quenching of 9-substituted ester fluorescence. No quenching could be observed with the procedure used to measure  $k_q$  for 2-COOMe. This is then confirmation of the predicted large  $\Delta E_{S_1-T_1}$  and consequent lack of significant ISC for the 9-substituted esters. One note of caution must be added in interpretation of this data. Electron-withdrawing substituents in the 9 position will considerably reduce the electron-donating power of the ring. The anthracene ring apparently behaves as an electron donor in formation of the complex with ethyl iodide which leads to quenching.<sup>33</sup> Therefore the lack of heavy atom quenching for a 9-substituted ester could be due in part to weak complex formation as well as a large  $\Delta E_{S_1-T_1}$ .

Finally, it is worthwhile to compare our results obtained with carboxyl substituted anthracenes to recent work with



carbonyl substituted anthracenes. These latter compounds are virtually nonfluorescent at room temperature in solvents such as cyclohexane and ethanol.<sup>4</sup> Presumably, very efficient ISC occurs from  $S_1$  to a lower  $T$  ( $n, \pi^*$ ) level of the carbonyl group.<sup>4</sup> It is well known that the  $S_1$  ( $n, \pi^*$ ) energies of aliphatic carboxylic acids and esters are substantially higher than the  $S_1$  ( $n, \pi^*$ ) energies of aliphatic aldehydes and ketones.<sup>34</sup> Assuming the same is true for  $T_1$  ( $n, \pi^*$ ) levels, the  $T_1$  ( $n, \pi^*$ ) state of the carboxyl group should be too high in energy to influence the  $S_1$  decay of the anthroate esters. In conclusion, then, it is ISC to the  $T_2$  level of anthracene rather than to the  $T_1$  ( $n, \pi^*$ ) of the carboxyl group which can compete with anthroate fluorescence in nonpolar solvents.

**Acknowledgment.** Acknowledgment is made to the donors of the Petroleum Research Fund, administered by the American Chemical Society, for support of this work.

The authors also wish to thank Dr. Fred Lytle of Purdue University for the lifetime measurements and Dr. Peter Frosch of Union College for developing the computer program for molecular orbital calculations.

## References and Notes

- (1) Presented in part at the 169th National Meeting of the American Chemical Society, Philadelphia, Pa., April, 1975.
- (2) R. Williams, *J. Roy. Inst. Chem.*, **83**, 611 (1959).
- (3) T. Vember, L. Kizanskaya, and A. S. Cherkasov, *J. Gen. Chem. USSR*, **33**, 2281 (1963).
- (4) T. Matsumoto, M. Sato, and S. Hirayama, *Chem. Phys. Lett.*, **13**, 13 (1972).
- (5) (a) T. C. Werner and R. M. Hoffman, *J. Phys. Chem.*, **77**, 1611 (1973); (b) F. E. Lytle, D. R. Storey, and M. E. Juricich, *Spectrochim. Acta, Part A*, **29**, 1357 (1973).
- (6) T. C. Werner, R. Fisch, and G. Goodman, *Spectrosc. Lett.*, **7**, 385 (1974).
- (7) T. C. Werner and D. M. Hercules, *J. Phys. Chem.*, **73**, 2005 (1969).
- (8) T. C. Werner and D. M. Hercules, *J. Phys. Chem.*, **74**, 1030 (1970).
- (9) J. A. Moore and D. E. Reed, *Org. Syn.*, **41**, 16 (1961).
- (10) C. A. Coulson, *J. Chem. Soc.*, 1932 (1930).
- (11) R. F. Chen, *Anal. Biochem.*, **20**, 339 (1967).
- (12) K. Dimroth, C. Reihert, T. Siermann, and F. Bohlman, *Ann.*, **661**, 1 (1963).
- (13) I. B. Berlman, "Handbook of Fluorescence Spectra of Aromatic Molecules," 2nd ed, Academic Press, New York, N.Y., 1971, Chapter 1.
- (14) S. J. Strickier and R. A. Berg, *J. Chem. Phys.*, **37**, 814 (1962).
- (15) A. Streitwieser, Jr., "Molecular Orbital Theory for Organic Chemists", Wiley, New York, N.Y., 1961.
- (16) J. R. Platt, *J. Chem. Phys.*, **17**, 484 (1949).
- (17) D. M. Friedrich, R. Mathies, and A. C. Albrecht, *J. Mol. Spectrosc.*, **51**, 166 (1974).
- (18) A. Bergman and J. Jortner, *Chem. Phys. Lett.*, **15**, 309 (1972).
- (19) J. G. Foss and M. E. McCarville, *J. Chem. Phys.*, **44**, 4350 (1960).
- (20) J. P. Larkindale and D. J. Simkin, *J. Chem. Phys.*, **55**, 5668 (1971).
- (21) A. E. Lutsikii and L. A. Antropova, *Zh. Fiz. Khim.*, **39**, 1131 (1965).
- (22) Reference 13, Chapter 3.
- (23) T. C. Werner and D. M. Hercules, unpublished studies.
- (24) S. Suzuki and H. Baba, *J. Chem. Phys.*, **38**, 349 (1963).
- (25) J. M. McKelvey and A. D. King, Jr., *J. Chem. Phys.*, **43**, 3178 (1965).
- (26) R. O. C. Norman and P. D. Ralph, *J. Chem. Soc.*, 2221 (1961).
- (27) Y. Lui and S. P. McGlynn, *J. Mol. Spectrosc.*, **49**, 214 (1974).
- (28) J. Trotter, *Acta Crystallogr.*, **13**, 732 (1962).
- (29) R. S. Becker, "Theory and Interpretation of Fluorescence and Phosphorescence", Wiley-Interscience, New York, N.Y., 1969, Chapter 11.
- (30) F. Tanaka and J. Osugi, *Chem. Phys. Lett.*, **27**, 133 (1974).
- (31) We have tried unsuccessfully to measure the phosphorescence of all three esters. Also, Professor D. M. Hercules of the University of Georgia has been unable to detect triplet-triplet absorption for 9-COOme in several solvents.
- (32) H. Dreeskamp, E. Koch, and M. Zander, *Chem. Phys. Lett.*, **31**, 251 (1975).
- (33) T. C. Werner and B. Soller, unpublished studies.
- (34) S. Suzuki, "Electronic Absorption Spectra and Geometry of Organic Molecules", Academic Press, New York, N.Y., 1967, Chapter 21.

## Electron Spin Resonance Line Width Studies of Vanadium(IV) in Acidic and Basic Aqueous Solutions<sup>1</sup>

Melanie M. Iannuzzi, Clifford P. Kubiak, and Philip H. Rieger\*

Metcalf Research Laboratories, Brown University, Providence, Rhode Island 02912 (Received July 23, 1975)

Publication costs assisted by the National Institutes of Health

ESR line widths of vanadium(IV) in acidic and basic media were determined. Analysis of the  $m_I$ -dependent line width contributions gave rotational correlation times which were linear in  $T/\eta$  and resulted in radius estimates of  $0.34 \pm 0.01$  nm for  $\text{VO}(\text{H}_2\text{O})_5^{2+}$  and  $0.27 \pm 0.02$  nm for  $\text{VO}(\text{OH})_3(\text{H}_2\text{O})_2^-$ . Spin-rotation line width contributions were found to be in satisfactory agreement with the theory of Atkins and Kivelson. Comparison of residual line widths obtained in  $\text{H}_2\text{O}$  and  $\text{D}_2\text{O}$  solutions showed that the average contribution of unresolved proton hyperfine structure was about 0.4 G for the aquo vanadyl ion and 6.5 G for the trihydroxo anion. Line shape simulations show the contribution for the aquo ion to be consistent with the proton coupling of 1.1 G determined by NMR methods. A much larger proton coupling is implied for the trihydroxo anion.

### Introduction

Vanadium(IV) has recently been shown to exist in basic aqueous solution as the trihydroxo anion,  $\text{VO}(\text{OH})_3(\text{OH}_2)_2^-$ .<sup>2</sup> This species exhibits an eight-line ESR spectrum qualitatively similar to that of the aquo ion but

distinguished by a smaller isotropic vanadium nuclear hyperfine splitting and a less anisotropic  $g$  tensor.<sup>2</sup> ESR parameters for the trihydroxo anion and the aquo cation are given in Table I. In this paper, we describe the line widths of the basic solution vanadium(IV) species and compare

TABLE I: ESR Parameters for  $\text{VO}(\text{H}_2\text{O})_5^{2+}$  and  $\text{VO}(\text{OH})_3(\text{H}_2\text{O})_2^{-a}$

	$\text{VO}(\text{H}_2\text{O})_5^{2+}$	$\text{VO}(\text{OH})_3(\text{H}_2\text{O})_2^{-}$
$\langle g \rangle$	1.964	1.970
$\langle a \rangle$	116.4 G	96.1 G
$g_{\parallel} - g_{\perp}$	-0.043	-0.020
$a_{\parallel} - a_{\perp}$	-129.5 G	-120.0 G

<sup>a</sup> From ref 2.

the results with a parallel reinvestigation of the aquo vanadyl ion.

The aquo vanadyl ion has been the subject of several ESR line width studies.<sup>3-7</sup> At lower temperatures, the dominant line width contribution is due to motional averaging of the anisotropies in the  $g$  and  $a$  tensors. The effect is well understood through the work of McConnell<sup>8</sup> and Kivelson<sup>9</sup> and leads to the well-known dependence of line width on the nuclear spin quantum number,  $m_I$ . The contribution is proportional to the rotational correlation time and hence should be linear in  $\eta/T$ . A second contribution, due to the interaction of the electron spin magnetic moment with the magnetic moment arising from rotation of the ion, has been treated by Kivelson;<sup>10</sup> all lines are expected to be equally broadened, the contribution to the line widths increasing with  $T/\eta$ . Residual line widths, not explainable by either of the two mechanisms, have been noted and attributed to unresolved hyperfine structure arising from coupling of the equatorial ligand protons to the unpaired electron.<sup>6,7</sup> No attempt has been made, however, to quantitatively determine the size of this contribution. In this work, we examine the "residual" line widths and treat quantitatively the contribution of unresolved proton hyperfine structure.

### Experimental Section

Solutions of vanadium(IV) in 1 M sodium perchlorate or in 1 M sodium hydroxide were prepared as described earlier.<sup>2</sup>

Solutions of vanadyl chloride in  $\text{H}_2\text{O}$  or  $\text{D}_2\text{O}$  were prepared by the reduction of vanadium pentoxide, suspended in 2 M HCl or DCl, by mercury in a system continuously purged by nitrogen. Mercury and mercury(I) chloride were removed by filtration and the solution diluted with water (or  $\text{D}_2\text{O}$ ) to give solutions 5.0 mM in  $\text{VOCl}_2$  and approximately 0.01 M in HCl or DCl. Vanadium pentoxide was prepared by thermal decomposition of ammonium metavanadate in an oxygen stream at 300 °C.

$\text{D}_2\text{O}$  solutions, 5.0 mM in vanadium(IV) and 0.1 M in NaOH, were prepared by dropwise addition of 0.0125 M vanadyl sulfate in  $\text{D}_2\text{O}$  to 0.167 M NaOH in  $\text{D}_2\text{O}$  with vigorous stirring under nitrogen. Both solutions were purged with nitrogen before mixing. Samples were removed from the mixing chamber with a syringe and sealed in sample tubes on a vacuum line. Solutions prepared in this way were stable for a week or more.

Solution viscosities were measured with an Ostwald viscometer using standard procedures.<sup>11</sup> Solutions were filtered through a 10–15- $\mu\text{m}$  sintered glass filter before measurement; calibration was with distilled water. ESR spectra from which line widths were measured were recorded as described in a previous paper.<sup>2</sup>

### Results and Discussion

*Determination of Line Width Parameters.* It is a property of Lorentzian lines that the width of the first deriva-

tive is inversely proportional to the square root of the amplitude. Since amplitudes can be measured with considerably greater precision than widths, we determined line widths by the following procedure. The quantity

$$Z = \frac{1}{8} \sum_i w_i A_i^{1/2} \quad (1)$$

proportional to the square root of the integrated intensity, was first computed from the measured widths (between derivative extrema),  $w_i$ , and amplitudes,  $A_i$ , of a spectrum. Corrected widths were then computed from the amplitudes

$$w_i^{\text{cor}} = Z A_i^{-1/2} \quad (2)$$

and fitted to the power series expression

$$w_i^{\text{cor}} = \alpha + \beta m_i + \gamma m_i^2 + \delta m_i^3 \quad (3)$$

where  $m_i$  is the vanadium nuclear spin quantum number for the  $i$ th hyperfine line.

The line width parameters,  $\alpha$ ,  $\beta$ ,  $\gamma$ , and  $\delta$ , were determined as a function of temperature for 5 mM vanadium(IV) in 1 M  $\text{NaClO}_4$  at pH 2.0 and in 1 M NaOH and are given in Tables II and III.

*Contribution of Motional Averaging to Line Widths.* The contributions to the line width parameters from motional averaging of anisotropies may be obtained from equations given by Wilson and Kivelson.<sup>9</sup> For a molecule of axial symmetry, the derivative line width contributions are

$$\alpha' = \zeta \tau_R \{ 90(\Delta g/g_0)^2 H_0^2 (4 + 3u) + b^2 I(I+1) [3 + 7u - 5uf(a/H_0)] - 2(\Delta g/g_0) ab I(I+1)(1+u) \} \quad (4a)$$

$$\beta = \zeta \tau_R \{ 4(\Delta g/g_0) b H_0 (4 + 3u) - 4(\Delta g/g_0)^2 a H_0 (4 + 3u + 3uf) - b^2 (a/H_0) I(I+1)(1+u + 7uf) - b^2 (a/H_0) (3 + 2uf) \} \quad (4b)$$

$$\gamma = \zeta \tau_R \{ b^2 [5 - u + 5uf(a/H_0) - 2(\Delta g/g_0) ab (7 + 5u + 12uf)] \} \quad (4c)$$

$$\delta = 2\zeta \tau_R b^2 (a/H_0) (1 + u + uf) \quad (4d)$$

In these equations,  $\tau_R$  is the rotational correlation time,  $g_0 = (2g_{\perp} + g_{\parallel})/3$ ,  $\Delta g = g_{\parallel} - g_{\perp}$ ,  $a = (2g_{\perp} + a_{\parallel})/3$ ,  $b = a_{\parallel} - a_{\perp}$ ,  $H_0 = \hbar \omega_0 / g_0 \beta_0$  is the center field of the spectrum, and  $\zeta = g_0 \beta_0 / 45 \sqrt{3} \hbar$ ;  $I$  is the nuclear spin (in this case 7/2),  $\beta_0$  is the Bohr magneton,  $u = (1 + \omega_0^2 \tau_R^2)^{-1}$ , and  $f = \omega_0^2 \tau_R^2 u$ . With the exception of the rotational correlation time, all parameters are known experimentally.<sup>2</sup>

If we identify the above expressions for  $\beta$ ,  $\gamma$ , and  $\delta$  with the experimental values, any one of them could be used to compute  $\tau_R$ . In practice, however, we have used eq 4c for this purpose since: (i)  $b$  is known experimentally to greater precision than is  $\Delta g$ ;<sup>2</sup> and (ii)  $\gamma$  is found from the least-squares fit to eq 3 with greater precision than is  $\beta$  or  $\delta$  (which are usually coupled by a substantial covariance). Given a value of  $\tau_R$ , obtained from the parameter  $\gamma$ , however, the parameters  $\alpha'$ ,  $\beta$ , and  $\delta$  may be computed and compared with experimental values. These are given in Tables II and III, together with the computed values of  $\tau_R$ .

Examination of the results given in the tables reveals generally satisfactory agreement between the experimental and calculated values of the line width parameters  $\beta$  and  $\delta$ ; the differences are usually within one standard deviation. There is, however, a good correlation between  $(\beta_{\text{expt}} - \beta_{\text{calcd}})$  and  $(\delta_{\text{expt}} - \delta_{\text{calcd}})$  as expected from the covariances found from the least-squares fits.

The rotational correlation time of a solute molecule may be expressed as<sup>12</sup>

TABLE II: Line Width Parameters<sup>a</sup> for Vanadium(IV) in 1.0 M NaClO<sub>4</sub>

t, °C	Exptl				Calcd			
	α	β	γ	δ	τ <sub>R</sub> <sup>b</sup>	α'	β	δ
3.0	19.6 ± 1.2	3.34 ± 0.22	1.45 ± 0.09	-0.043 ± 0.010	7.4	15.6	3.10	-0.021
10.5	17.8 ± 0.9	3.18 ± 0.17	1.22 ± 0.06	-0.038 ± 0.004	6.3	13.7	2.68	-0.019
20.5	15.6 ± 1.0	2.09 ± 0.15	0.84 ± 0.06	-0.021 ± 0.007	4.4	10.7	2.01	-0.014
24.5	15.0 ± 0.9	1.78 ± 0.11	0.70 ± 0.04	-0.016 ± 0.002	3.7	9.7	1.78	-0.013
37.6	14.4 ± 1.0	1.43 ± 0.10	0.54 ± 0.04	-0.007 ± 0.001	2.9	8.7	1.50	-0.011
51.0	14.0 ± 0.9	1.14 ± 0.07	0.39 ± 0.02	-0.004 ± 0.002	2.09	7.5	1.21	-0.009
63.0	13.9 ± 0.5	0.91 ± 0.05	0.28 ± 0.01	-0.003 ± 0.004	1.54	6.5	0.96	-0.007

<sup>a</sup> In units of gauss; uncertainties given are standard deviations. <sup>b</sup> In units of 10<sup>-11</sup> s.

TABLE III: Line Width Parameters<sup>a</sup> for Vanadium(IV) in 1.0 M NaOH

t, °C	Exptl				Calcd			
	α	β	γ	δ	τ <sub>R</sub> <sup>b</sup>	α'	β	δ
-2.5	18.8 ± 0.9	1.49 ± 0.21	0.98 ± 0.06	-0.051 ± 0.020	6.0	11.0	1.22	-0.013
3.0	17.7 ± 1.6	1.32 ± 0.15	0.89 ± 0.08	-0.021 ± 0.010	5.5	10.3	1.14	-0.012
10.5	17.2 ± 1.1	0.97 ± 0.07	0.63 ± 0.04	-0.014 ± 0.004	4.0	8.4	0.90	-0.010
20.1	16.9 ± 0.8	0.71 ± 0.04	0.42 ± 0.02	-0.007 ± 0.003	2.7	7.0	0.70	-0.007
20.5	16.7 ± 0.9	0.65 ± 0.04	0.38 ± 0.02	-0.005 ± 0.005	2.5	6.8	0.67	-0.007
24.5	16.4 ± 0.7	0.60 ± 0.03	0.33 ± 0.01	-0.006 ± 0.007	2.15	6.4	0.60	-0.007
37.6	16.2 ± 0.4	0.48 ± 0.02	0.24 ± 0.01	-0.005 ± 0.002	1.60	5.6	0.49	-0.005
51.0	16.0 ± 0.7	0.36 ± 0.04	0.18 ± 0.01	-0.001 ± 0.003	1.23	4.8	0.39	-0.004
63.0	15.6 ± 0.6	0.30 ± 0.03	0.13 ± 0.01	-0.002 ± 0.003	0.94	4.0	0.30	-0.003

<sup>a</sup> In units of gauss; uncertainties given are standard deviations. <sup>b</sup> In units of 10<sup>-11</sup> s.

$$\tau_R = \frac{4\pi r^3 \kappa \eta}{3kT} \quad (5)$$

where  $r$  is the effective molecular radius,  $k$  is the Boltzmann constant, and  $\kappa$  is the anisotropic interaction parameter, usually having a value between 0.5 and 1.0.<sup>12</sup> Thus we expect the rotational correlation times to be at least approximately linear in  $\eta/T$ , the solution viscosity divided by the absolute temperature. The correlation times of Tables II and III are plotted in Figure 1 against  $\eta/T$ , determined for 1.0 M NaClO<sub>4</sub> and 1.0 M NaOH, respectively. Reasonably good straight lines are indeed found, leading to values of  $r\kappa^{1/3}$  of  $0.34 \pm 0.01$  nm for VO(H<sub>2</sub>O)<sub>5</sub><sup>2+</sup> and  $0.27 \pm 0.02$  for VO(OH)<sub>3</sub>(H<sub>2</sub>O)<sub>2</sub><sup>-</sup>. Although  $\kappa$  is unknown and may be different for the two species, it is reasonable to conclude that the trihydroxo anion is comparable in size to the aquo cation. This result removes any remaining doubts about the monomeric nature of the basic solution vanadium(IV) species.

*Spin-Rotation Contributions to the Line Widths.* Calculated values of  $\alpha'$ , given in Tables II and III, are substantially smaller than the experimental values of the parameter  $\alpha$ . This difference is due, at least in part, to the contribution of the spin-rotation interaction. The contribution of this effect to derivative line widths for an axially symmetric system is, according to Atkins and Kivelson,<sup>10</sup>

$$\alpha'' = (2h/9\sqrt{3}g_0\beta_0)(\Delta g_{\parallel}^2 + 2\Delta g_{\perp}^2)\tau_R^{-1} \quad (6)$$

where  $\Delta g_{\parallel} = g_e - g_{\parallel}$  and  $\Delta g_{\perp} = g_e - g_{\perp}$ ;  $g_e$  is the free electron  $g$  value. The residual line widths,  $\alpha - \alpha'$ , are plotted as functions of  $\tau_R^{-1}$  in Figure 2. A very good correlation is found for the acidic solution data; for the basic solution data, the correlation is less satisfactory, but still within experimental error limits. The least-squares slopes of the lines in Figure 2 are  $(6.6 \pm 0.4) \times 10^{-11}$  and  $(4.4 \pm 0.7) \times 10^{-11}$  G s for the acidic and basic solution data, respective-

ly. These values may be compared with slopes, computed from eq 6 with the experimental values of  $\Delta g_{\parallel}$  and  $\Delta g_{\perp}$ , of  $4.2 \times 10^{-11}$  and  $2.5 \times 10^{-11}$  G s, respectively. The agreement, while not spectacular, is really quite good considering the approximate nature of eq 6 and the errors inherent in the experimental data.<sup>13</sup>

*Contribution of Unresolved Hyperfine Structure to Line Widths for the Aquo Vanadyl Ion.* As the plots of Figure 2 show, inclusion of the spin-rotation interaction leaves substantial temperature-independent line width components:  $3.3 \pm 0.2$  and  $7.6 \pm 0.4$  G for the acidic and basic solution data, respectively. Lewis and Morgan<sup>6</sup> found a residual line width of 3.3 G for the aquo ion in their reinterpretation of the line width data of Rogers and Pake<sup>4</sup> and of McCain and Myers.<sup>5</sup> In a more recent study of vanadyl sulfate in 3 M HCl, Chasteen and Hanna<sup>7</sup> found a residual line width,  $\alpha - \alpha' - \alpha''$ , of 1.85 G, using eq 6 to compute  $\alpha''$ . Both groups attributed the residual line width to unresolved isotropic hyperfine interaction of the unpaired electron on vanadium with the protons of the coordinated water molecules. A proton hyperfine coupling of 2.8 G has been observed in vanadyl-doped zinc Tutton salt,<sup>14</sup> but NMR contact shift measurements lead to the smaller value of 1.1 G in solution.<sup>15</sup>

Lines broadened by unresolved hyperfine structure are intrinsically non-Lorentzian. Thus the contribution from unresolved hyperfine structure is not additive, but is dependent on the width of the hyperfine components. In order to determine the contribution made by unresolved hyperfine structure to line widths in the spectrum of the aquo ion, computer line shape simulations were carried out assuming hyperfine coupling of eight equivalent protons. Some of the results are shown in Figure 3 where the ratio of the observed line width to the component line width is plotted as a function of the observed derivative width for proton hyperfine couplings of 1, 2, and 3 G. The ratio of ob-

TABLE IV: Line Width Parameters<sup>a</sup> for Vanadium(IV) in Various Media

Species	Exptl				Calcd			
	$\alpha$	$\beta$	$\gamma$	$\delta$	$\tau_R^b$	$\alpha'$	$\beta$	$\delta$
$\text{VO}(\text{H}_2\text{O})_5^{2+}$	$12.7 \pm 0.4$	$1.83 \pm 0.11$	$0.74 \pm 0.06$	$-0.010 \pm 0.011$	3.8	10.1	1.86	$-0.013$
$\text{VO}(\text{D}_2\text{O})_5^{2+}$	$13.0 \pm 0.7$	$2.26 \pm 0.21$	$0.90 \pm 0.08$	$-0.026 \pm 0.016$	4.6	11.1	2.10	$-0.015$
$\text{VO}(\text{OD})_3^-$	$9.4 \pm 0.3$	$0.66 \pm 0.15$	$0.35 \pm 0.03$	$-0.021 \pm 0.023$	2.3	6.6	0.63	$-0.007$

<sup>a</sup> In units of gauss; uncertainties given are standard deviations; parameters given are averages of several spectra at ambient temperature. <sup>b</sup> In units of  $10^{-11}$  s.

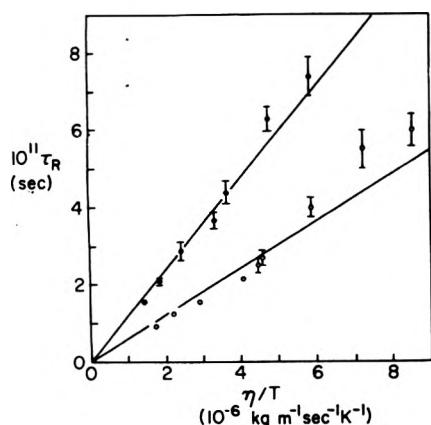


Figure 1. Rotational correlation times for the aquo vanadyl ion (closed circles) and the trihydroxo anion (open circles) as functions of the ratio of solution viscosity to absolute temperature.

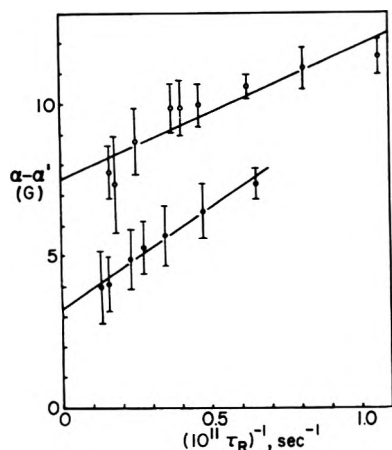


Figure 2. Residual line widths for the aquo vanadyl ion (closed circles) and the trihydroxo anion (open circles) as functions of the inverse of the rotational correlation time.

served derivative amplitude to the sum of the component amplitudes is also plotted in Figure 3.

The line width data collected for  $\text{VO}(\text{H}_2\text{O})_5^{2+}$  in 1.0 M  $\text{NaClO}_4$  were corrected, using Figure 3, for an unresolved 1-G proton hyperfine coupling and reanalyzed; a plot similar to that in Figure 2 was obtained, having a slope corresponding to  $\alpha'' = (6.2 \pm 0.4) \times 10^{-11}/\tau_R$  and an intercept corresponding to a residual line width of 3.0 G. Thus the average contribution of a 1-G hyperfine coupling to the ESR line widths of the aquo vanadyl ion is only 0.3 G.

In order to verify this result, ESR spectra were obtained of  $\text{D}_2\text{O}$  solutions, 5.0 mM in  $\text{VO}^{2+}$  and 0.01 M in  $\text{DCl}$ , and identical solutions in  $\text{H}_2\text{O}$ . The resulting line width parameters are summarized in Table IV. The  $\text{H}_2\text{O}$  results given are averages of three independent spectra while the  $\text{D}_2\text{O}$

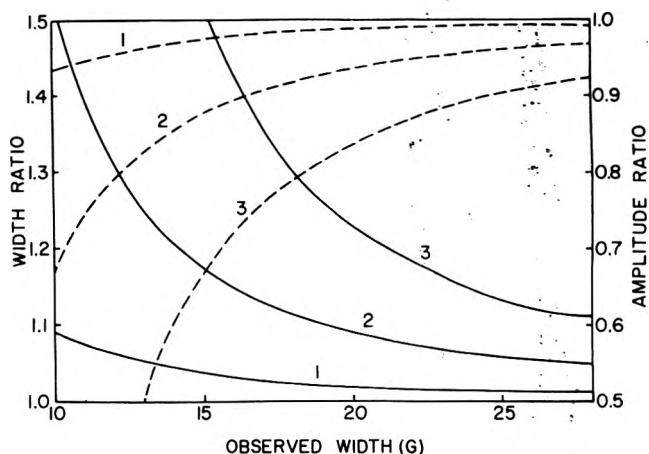


Figure 3. The effect of unresolved hyperfine splitting of eight equivalent protons on line shape parameters for proton splittings of 1, 2, and 3 G: the ratio of observed line width to component line width (solid lines) and the ratio of the observed first-derivative amplitude to the sum of the components amplitudes (dashed lines) as functions of the observed derivative width.

results are averages of 18 spectra. Assuming the spin-rotation contributions to be given by  $\alpha'' = 6.6 \times 10^{-11}/\tau_R$  (the empirical result obtained above), we obtain  $\alpha'' = 1.7$  and 1.4 G for the  $\text{H}_2\text{O}$  and  $\text{D}_2\text{O}$  solutions, respectively. The residual widths then are  $\alpha - \alpha' - \alpha'' = 0.9$  and 0.5 G for the  $\text{H}_2\text{O}$  and  $\text{D}_2\text{O}$ . Thus at ambient temperature, the average contribution of proton hyperfine structure to the line widths is on the order of 0.4 G. Although this value is not precisely determined, it is not strongly affected by uncertainties in the  $g$  tensor components and is entirely consistent with the broadening expected for a proton coupling of 1.1 G.

Interpretation of the remaining unexplained line widths for the aquo vanadyl ion, 3.0 G in 1 M  $\text{NaClO}_4$  and 0.5 G in 0.01 M  $\text{HCl}$  solutions, is not obvious. Other authors<sup>7,10</sup> have considered, and rejected, several line broadening mechanisms. Before searching for another mechanism, however, it is well to remember that, because of the uncertainties in  $\Delta g$  and other possible systematic errors in the data analysis,<sup>13</sup> there may be no effect to explain.

*Unresolved Hyperfine Structure in the Basic Solution Spectrum.* The large residual width found for the basic solution spectra prompted an examination of vanadium(IV) in 0.1 M  $\text{NaOH}$  in  $\text{D}_2\text{O}$ . The ambient temperature results for seven independent spectra are summarized in Table IV. The parameters may be analyzed as before to give  $\alpha'' = 1.9$  G and  $\alpha - \alpha' - \alpha'' = 0.9$  G. This may be compared with the intercept in Figure 2 of 7.6 G. Thus the residual line width is reduced by 6.5 G on eliminating the possibility of unresolved proton hyperfine structure.

In an attempt to estimate the proton coupling constant required to produce an average broadening of 6.5 G, line

shape simulations similar to those described above were carried out, assuming five interacting protons. It was found that an average proton coupling of about 4.5 G is required to produce the observed broadening. The protons must be inequivalent, however; resolution of a 1:5:10:10:5:1 pattern would be expected on the narrower vanadium hyperfine lines for a proton splitting greater than about 4 G.

A large proton hyperfine coupling in  $\text{VO}(\text{OH})_3(\text{H}_2\text{O})_2^-$  may be rationalized by several lines of argument. Because of the overall negative charge of the complex, the  $d_{xy}$  vanadium orbital, which contains the odd electron, is probably somewhat more diffuse than in the aquo ion. This effect would be expected to lead both to a smaller vanadium hyperfine coupling, as is observed, and to a larger coupling of the ligand protons. Furthermore, the equatorial V-O bonds in the trihydroxo anion appear to be somewhat more covalent than the corresponding bonds in the aquo ion;<sup>2</sup> if they are thus slightly shorter, the ligand protons are placed in a region of higher spin density. Finally, there may be a qualitatively different conformation for a hydroxo ligand than for a coordinated water molecule which increases the overlap of the  $d_{xy}$  orbital the hydrogen 1s orbitals.

NMR experiments are now in progress which may give a more direct measure of the magnitude of the hyperfine coupling constant.

*Acknowledgments.* Helpful discussions with R. G. Lawler and T. J. Swift and the experimental assistance of W. C. Copenhafer are gratefully acknowledged. The work was

partially supported by a grant from the National Institute of Environmental Health Sciences.

### References and Notes

- (1) Taken in part from the Ph.D. Thesis of M.M.L. Brown University, 1974; presented in part at the 169th National Meeting of the American Chemical Society, Philadelphia, Pa., April 11, 1975.
- (2) M. M. Iannuzzi and P. H. Rieger, *Inorg. Chem.*, **14**, 2895 (1975).
- (3) G. E. Pake and R. H. Sands, *Phys. Rev.*, **98**, 266 (1955).
- (4) R. N. Rogers and G. E. Pake, *J. Chem. Phys.*, **33**, 1107 (1960).
- (5) D. C. McCain and R. J. Myers, *J. Phys. Chem.*, **71**, 192 (1967).
- (6) W. B. Lewis and L. O. Morgan in "Transition Metal Chemistry", Vol. 4, R. L. Carlin, Ed., Marcel Dekker, New York, N.Y., 1968, p. 52.
- (7) N. D. Chasteen and M. W. Hanna, *J. Phys. Chem.*, **76**, 3951 (1972).
- (8) H. M. McConnell, *J. Chem. Phys.*, **25**, 709 (1956).
- (9) D. Kivelson, *J. Chem. Phys.*, **33**, 1094 (1960); R. Wilson and D. Kivelson, *ibid.*, **44**, 154 (1966).
- (10) P. W. Atkins and D. Kivelson, *J. Chem. Phys.*, **44**, 169 (1966).
- (11) F. Daniels, J. W. Williams, P. Bender, R. A. Alberty, C. D. Cornwell, and J. E. Harriman, "Experimental Physical Chemistry", 7th ed., McGraw-Hill, New York, N.Y., 1970, p. 164.
- (12) J. Hwang, D. Kivelson, and W. Plachy, *J. Chem. Phys.*, **58**, 1753 (1973).
- (13) Small errors in the components of the  $g$  tensor may lead to substantial uncertainties in these results. The  $g$  tensor anisotropies were obtained from line shape fitting of the frozen solution spectra and are accurate (for the frozen solutions) to approximately  $\pm 0.001$ .<sup>2</sup> There is no assurance, however, that  $\Delta g$  is not temperature dependent or perhaps different in liquid solution than in the frozen state. Propagation of an uncertainty in the  $\Delta g$ 's of  $\pm 0.001$  through eq. 4a leads to an uncertainty in the computed values of  $\alpha'$  of about 3% for the aquo ion and 7% for the trihydroxo anion. In the plots of Figure 2, these errors lead further to uncertainties of  $\pm 0.5 \times 10^{-11}$  G s for the slopes and  $\pm 0.6$  and  $\pm 0.8$  G for the intercepts of the acidic and basic solution plots, respectively. The limitations imposed by random error and the possibility of significant systematic error in these results should be kept in mind in assessing the significance of these and other similar experiments.
- (14) R. H. Borcherts and C. Kikuchi, *J. Chem. Phys.*, **40**, 2270 (1964); W. B. Lewis, *Inorg. Chem.*, **6**, 1737 (1967).
- (15) J. Reuben and D. Fiat, *Inorg. Chem.*, **8**, 1821 (1969).

# Very Low-Pressure Pyrolysis of Alkyl Cyanides. III. *tert*-Butyl Cyanide. Effect of the Cyano Group on Bond Dissociation Energies and Reactivity<sup>1</sup>

Keith D. King\* and Richard D. Goddard

Department of Chemical Engineering, The University of Adelaide, Adelaide, South Australia, 5001 (Received November 10, 1975)

The unimolecular decomposition of *tert*-butyl cyanide has been investigated over the temperature range 1023–1254 K using the technique of very low-pressure pyrolysis (VLPP). The reaction proceeds via the competing pathways of C–C bond fission and HCN elimination, with the former accounting for >95% of the overall decomposition. Taking into account the mutual interaction of the two pathways in the falloff region, application of unimolecular reaction rate theory shows that the experimental rate constants are consistent with high-pressure Arrhenius parameters given by  $\log(k_1, \text{s}^{-1}) = (15.9 \pm 0.3) - (74.9 \pm 1.6)/\theta$  for bond fission, and  $\log(k_2, \text{s}^{-1}) = (14.1 \pm 0.3) - (74.1 \pm 1.6)/\theta$  for HCN elimination, where  $\theta = 2.303RT$  kcal/mol. The activation energy for C–C fission leads to  $\text{DH}^\circ[(\text{CH}_3)_2\text{C}(\text{CN})-\text{CH}_3] = 74.7 \pm 1.6$ ,  $\Delta H_f^\circ[(\text{CH}_3)_2\dot{\text{C}}\text{CN}, \text{g}] = 39.8 \pm 2.0$ , and  $\text{DH}^\circ[(\text{CH}_3)_2\text{C}(\text{CN})-\text{H}] = 86.5 \pm 2.0$ , all in kcal/mol at 298 K. The stabilization energy of the  $\alpha$ -cyanoisopropyl radical has been found to be  $5.5 \pm 2.2$  kcal/mol. This is in excellent agreement with values which we have determined previously for the cyanomethyl and  $\alpha$ -cyanoethyl radicals. The results of this work and previous studies are included in a discussion on the effect of the CN group on bond dissociation energies and reactivity. Revised values of the contributions of the  $[\dot{\text{C}}(\text{H})_2(\text{CN})]$ ,  $[\dot{\text{C}}(\text{H})(\text{C})(\text{CN})]$ , and  $[\dot{\text{C}}(\text{C})_2(\text{CN})]$  groups to the heat of formation of free radicals are calculated.

## Introduction

Recently we have shown from very low-pressure pyrolysis (VLPP) experiments that isopropyl cyanide,<sup>2</sup> *n*-propyl cyanide,<sup>3</sup> and isobutyl cyanide<sup>3</sup> decompose mainly (>90%) via C–C bond fission adjacent to the CN group. HCN elimination is a minor process. These observations suggest that *tert*-butyl cyanide (TBCN) should also decompose predominantly via C–C fission but HCN elimination should be more readily observable than in the case of the primary and secondary compounds.

Previous work on the pyrolysis of TBCN has been carried out by Hunt, Kerr, and Trotman-Dickenson<sup>4</sup> (HKT), and Dastoor and Emovon<sup>5</sup> (DE). HKT, using the aniline-carrier technique over the temperature range 875–925 K, obtained results which were indicative of C–C fission. However, the Arrhenius *A* factor is low in comparison with the estimates for other alkyl cyanides<sup>2,3</sup> and the activation energy yields a value of 10.6 kcal/mol<sup>6</sup> for the cyano stabilization energy which is significantly higher than recent determinations.<sup>2,3,7,8</sup> In marked contrast, DE, using a conventional flow system, found that TBCN decomposes via HCN elimination over the temperature range 838–927 K. The reaction appeared to be homogeneous and molecular, and DE suggested that it is a four-center elimination similar to HX elimination from alkyl halides.<sup>9</sup> If this is the case, however, then the reported *A* factor ( $10^{12.2} \text{ s}^{-1}$ ) is much too low for this type of reaction and the activation energies found by DE for the series  $\text{C}_2\text{H}_5\text{CN}$ , *i*- $\text{C}_3\text{H}_7\text{CN}$ , *t*- $\text{C}_4\text{H}_9\text{CN}$ , do not show any trend with  $\alpha$ -methyl substitution. Free radical chain processes could make a significant contribution to the rate of HCN elimination under DE's experimental conditions (cf. isopropyl cyanide<sup>2</sup>).

In this paper we describe an investigation of the VLPP of TBCN as part of our continuing studies of the thermal unimolecular reactions of organic cyanides. A significant advantage of the VLPP technique is that secondary bimolecular reactions can be eliminated.

Our previous studies<sup>2,3</sup> have yielded values for the heats of formation and stabilization energies of the cyanomethyl and  $\alpha$ -cyanoethyl radicals. The results of this work lead to values for these quantities for the  $\alpha$ -cyanoisopropyl radical. Our accumulated kinetic data on primary, secondary, and tertiary alkyl cyanides allow general conclusions to be drawn about the effect of the CN group on bond dissociation energies and reactivity.

## Experimental Section

TBCN (Koch-Light) and methyl vinyl cyanide (Eastman) were degassed and vacuum distilled bulb-to-bulb. Isobutene (Matheson, CP) was degassed, and argon (C.I.G., high-purity dry) was used directly as an internal standard. The gases were used to calibrate the system by determining mass-spectral peak intensity ratios for known mixtures of product and reactant.

The application of the VLPP technique to unimolecular reactions has been discussed previously,<sup>10,11</sup> and the experimental system used in this work has been described in detail.<sup>8</sup>

## Results

The expected reactions are



RRK calculations<sup>12</sup> show that under VLPP conditions all the cyanoisopropyl radicals will decompose via H atom loss to form methyl vinyl cyanide (MVCN).



The product mass spectrum confirmed these expectations.

The disappearance of TBCN was monitored at  $m/e = 42$  amu (fragment peak) using argon ( $m/e = 40$  amu) as an internal standard. C–C fission was followed by monitoring

TABLE I: VLPP Data for TBCN ( $Z = 19\ 550$ , flow rate =  $2.6 \times 10^{14}$  molecules/s)

Temp, K	% decomposition				$k_{\text{uni}}, \text{s}^{-1}$	
	TBCN decay	MVCN formation	<i>i</i> -C <sub>4</sub> H <sub>8</sub> <sup>e</sup> formation			
				MVCN	<i>i</i> -C <sub>4</sub> H <sub>8</sub>	
1023 <sup>a</sup>	10.8	11.9		0.093		
1023	14.6	10.7		0.083		
1024 <sup>b</sup>	12.4	10.9		0.034		
1036 <sup>c</sup>	15.1	15.8		0.133		
1044	21.1	17.8		0.152		
1044 <sup>b</sup>	20.2	17.8		0.150		
1044 <sup>a</sup>	18.5	19.7		0.172		
1056 <sup>c</sup>	24.4	24.7		0.233		
1058	27.6	23.7		0.221		
1062 <sup>a</sup>	28.0	28.1		0.277		
1073 <sup>b</sup>	34.1	31.7		0.33		
1076	36.9	33.2		0.36		
1078 <sup>c</sup>	36.9	36.0		0.41		
1084 <sup>a</sup>	40.8	39.3		0.47		
1095	48.2	43.5		0.56		
1104 <sup>a</sup>	52.6	49.8	2.2	0.73	0.032	
1113 <sup>b</sup>	58.0	55.1	1.5	0.90	0.025	
1114	58.1	55.8	2.2	0.94	0.037	
1123 <sup>a</sup>	64.0	59.8	2.3	1.12	0.043	
1133 <sup>b</sup>	67.9	65.3	1.6	1.41	0.034	
1135	67.8	64.6	2.3	1.40	0.051	
1148	73.1	71.1	2.5	1.93	0.067	
1155	76.2	73.2	2.4	2.17	0.072	
1167	79.7	77.7	2.5	2.82	0.083	
1177	82.5	81.0	2.5	3.5	0.100	
1177 <sup>d</sup>	83.4	81.1	2.5	3.6	0.100	
1188 <sup>d</sup>	85.4	84.1	2.1	4.5	0.113	

<sup>a</sup> Flow rate =  $2.8 \times 10^{15}$  molecules/s. <sup>b</sup> Flow rate =  $8.3 \times 10^{14}$  molecules/s. <sup>c</sup> Flow rate =  $3.8 \times 10^{15}$  molecules/s. <sup>d</sup> Flow rate =  $1.9 \times 10^{15}$  molecules/s. <sup>e</sup> Isobutene formation at temperatures below 1104 K was too small to be of quantitative significance.

MVCN at  $m/e = 67$  amu (parent peak) while HCN elimination was followed by isobutene formation at  $m/e = 56$  amu (parent peak). The results for each reactor aperture setting over the temperature range 1023–1254 K are presented in Tables I–III. The percentages of the decomposition based on reactant disappearance show good agreement with calculations based on the formation of products. Bond fission is clearly the major reaction; the yield of isobutene accounts for only ca. 3% of the overall decomposition.

$k_{\text{uni}}$  does not exhibit a dependence on aperture size or flow rate (in the range where the gas–gas collision frequency is smaller than the gas–wall collision frequency). These observations confirm the unimolecularity of the reactions studied.<sup>8,11</sup>

The VLPP technique yields a low-pressure rate constant  $k_{\text{uni}}$  which can be related to the high-pressure rate constant  $k_{\infty}$  by means of RRK(M) theory.<sup>13</sup> Furthermore, when a reactant decomposes via competing unimolecular paths in the falloff region energized molecules are depleted by all reaction paths and each path feels the effect of the drain on energized molecules of other paths. We take into account this interaction by using the RRK/2 method.<sup>10</sup>

We have outlined previously<sup>2</sup> an appropriate transition-state model for C<sub>2</sub>–C<sub>3</sub> fission in alkyl cyanides and its application to TBCN yields  $A_{\infty}(1100 \text{ K}) = 10^{15.4} \text{ s}^{-1}$  per path or  $10^{15.9} \text{ s}^{-1}$  overall, which is in agreement with the values for other alkyl cyanides.<sup>2,3</sup> A four-center cyclic transition state was assumed for HCN elimination and the  $A$  factor was estimated according to the procedure of O'Neal and

TABLE II: VLPP Data for TBCN ( $Z = 2140$ , flow rate =  $3 \times 10^{15}$  molecules/s)

Temp, K	% decomposition				$k_{\text{uni}}, \text{s}^{-1}$	
	TBCN decay	MVCN formation	<i>i</i> -C <sub>4</sub> H <sub>8</sub> formation			
				MVCN	<i>i</i> -C <sub>4</sub> H <sub>8</sub>	
1095 <sup>a</sup>	9.6	10.3		0.73		
1104	10.1	12.0		0.88		
1106 <sup>a</sup>	12.8	12.4		0.91		
1119 <sup>a</sup>	17.0	16.2		1.25		
1122	17.4	18.6		1.48		
1124	17.9	19.4		1.56		
1135 <sup>a</sup>	23.1	21.4		1.77		
1141	24.8	25.6		2.26		
1145 <sup>b</sup>	24.4	25.5		2.24		
1155 <sup>b</sup>	28.5	29.7		2.80		
1165	36.3	35.6		3.7		
1174 <sup>a</sup>	39.0	37.2	0.9	4.0	0.093	
1175 <sup>b</sup>	37.4	38.4	1.2	4.2	0.126	
1185 <sup>b</sup>	41.8	42.4	1.2	5.0	0.138	
1188	46.7	45.4	1.2	5.7	0.176	
1192 <sup>a</sup>	48.1	45.7	0.9	5.7	0.117	
1197 <sup>b</sup>	48.0	47.7	1.3	6.2	0.167	
1202	52.7	51.7	1.4	7.4	0.228	
1213 <sup>c</sup>	55.7	54.3	1.5	8.2	0.221	
1213 <sup>a</sup>	56.9	55.2	1.1	8.4	0.164	
1213 <sup>d</sup>	58.3	54.7	1.4	8.3	0.214	
1214 <sup>b</sup>	55.2	55.0	1.4	8.4	0.207	
1225	62.5	61.3	1.6	11.2	0.32	
1233 <sup>b</sup>	62.6	62.8	1.5	11.9	0.28	
1246	69.3	68.5	1.8	15.6	0.40	
1253 <sup>b</sup>	69.3	69.7	1.6	16.5	0.38	
1253 <sup>c</sup>	70.3	69.0	1.7	16.0	0.39	

<sup>a</sup> Flow rate =  $9.9 \times 10^{14}$  molecules/s. <sup>b</sup> Flow rate =  $1.5 \times 10^{15}$  molecules/s. <sup>c</sup> Flow rate =  $6.2 \times 10^{15}$  molecules/s. <sup>d</sup> Flow rate =  $1.1 \times 10^{16}$  molecules/s.

TABLE III: VLPP Data for TBCN ( $Z = 246$ , flow rate =  $1-2 \times 10^{15}$  molecules/s)

Temp, K	% decomposition		
	TBCN decay	MVCN formation	$k_{\text{uni}}, \text{s}^{-1}$
1174 <sup>a</sup>	7.6	9.7	4.6
1174 <sup>b</sup>	8.6	10.0	5.0
1186	8.1	12.2	5.5
1194 <sup>a</sup>	12.8	13.8	7.5
1195	14.4	14.4	8.2
1203	12.7	15.6	8.1
1215 <sup>b</sup>	17.3	19.0	10.9
1216	16.5	19.3	10.8
1217 <sup>c</sup>	17.1	18.4	10.8
1217	19.9	19.1	12.0
1217 <sup>a</sup>	18.0	19.8	11.6
1225 <sup>c</sup>	19.5	20.5	12.5
1233	21.5	23.3	14.4
1233 <sup>a</sup>	22.7	23.9	15.1
1241 <sup>b</sup>	24.2	26.4	16.9
1241	28.1	25.9	18.5
1245 <sup>d</sup>	25.8	27.2	18.1
1254 <sup>a,d</sup>	29.1	29.9	21.1

<sup>a</sup> Flow rate =  $5 \times 10^{15}$  molecules/s. <sup>b</sup> Flow rate =  $1.5 \times 10^{16}$  molecules/s. <sup>c</sup> Flow rate =  $4.9 \times 10^{14}$  molecules/s. <sup>d</sup> Isobutene was detected;  $k_{\text{uni}} \approx 0.50 \text{ s}^{-1}$ . <sup>e</sup> Average.

Benson<sup>14,15</sup> to be  $10^{14.1} \text{ s}^{-1}$  at 1100 K or  $10^{13.9} \text{ s}^{-1}$  at 600 K, which is similar to the values for HX elimination from *tert*-butyl halides.<sup>9,15</sup>

Details of the frequency assignments for the molecule and the activated complexes are given in the Appendix.





TABLE IV: Thermochemical Data

Species	$\Delta H_f^\circ$ (298 K), kcal/ mol	$S_{298}^\circ$ , cal K <sup>-1</sup> mol <sup>-1</sup>	$C_p^\circ$ , cal K <sup>-1</sup> mol <sup>-1</sup>			
			300	500	800	1000
<i>t</i> -C <sub>4</sub> H <sub>9</sub> CN <sup>a</sup>	-0.8 <sup>b</sup>	79.6	28.2	40.0	54.0	60.0
CH <sub>3</sub> <sup>c</sup>	34.1	46.4	8.3	10.1	12.6	14.0
(CH <sub>3</sub> ) <sub>2</sub> CCN <sup>c</sup>	<i>d</i>	75.8	21.2	29.1	39.0	43.5
<i>i</i> -C <sub>4</sub> H <sub>9</sub> <sup>e</sup>	-4.0	70.3	21.4	31.2	41.9	46.9
HCN <sup>f</sup>	32.3	48.2	8.6	10.0	11.3	12.2

<sup>a</sup> Reference 18. <sup>b</sup> Reference 19. <sup>c</sup> Reference 20. <sup>d</sup> See Discussion. <sup>e</sup> Reference 21. <sup>f</sup> JANAF Thermochemical Tables, *Natl. Stand. Ref. Data Ser., Natl. Bur. Stand., No. 37* (1970).

ized, however, that these values all refer to the stabilization energy relative to a hydrogen atom, i.e., the activation energy for decomposition of the substituted compound was compared with that for the parent hydrocarbon. It is more appropriate, however, to make the comparison with respect to the corresponding alkyl substituent. Such a comparison is, by definition,<sup>24</sup> already included in the values for the cyanoalkyl radicals. On this basis, the corrected values<sup>27</sup> are 5.0 kcal/mol from the pyrolysis of cyclopropyl cyanide,<sup>7a</sup> 5.1 kcal/mol from the pyrolysis of cyclobutyl cyanide,<sup>8</sup> and 4.7 kcal/mol from the pyrolysis of 1,4-dicyanobicyclo-[2.2.0]hexane.<sup>26</sup> The agreement with the values for the cyanoalkyl radicals is excellent.

In terms of valence bond theory, the stabilization energy is a function of the number of canonical forms of similar energy which can contribute to the hybrid structure. The relative thermodynamic stabilities of *i* and *ii* may be determined from a comparison of the C≡N  $\pi$ -bond energy in the cyanide with the C=C  $\pi$ -bond energy in the keteneimine. Insufficient data are available for the calculation of these energies but we have shown previously<sup>2</sup> that the former should be significantly greater than the latter. Thus the stabilization energies of cyanoalkyl radicals are less than those of the corresponding allylic radicals<sup>25</sup> since the contributing forms of the latter have very similar stabilities.

It has been shown that methyl substitution increases the stabilization energy of the allyl radical by ~3 kcal/mol per group<sup>28</sup> and a similar value has been found for the acetyl radical.<sup>29</sup> It has been suggested that this is due to an inductive effect.<sup>25,29</sup> Our results suggest that  $\alpha$ -methyl substitution does not lead to any significant variation in the cyano stabilization energy. However, any small effect could be masked by the anticipated error limits in the measured stabilization energies.

Our accumulated data on  $\alpha$ -cyanoalkyl radicals show that the effect of replacing a methyl group in an alkyl radical by a cyano group is to increase the heat of formation by ~32 kcal/mol (see Table V). Group additivity methods have been demonstrated to apply to the estimation of thermochemical properties of free radicals and O'Neal and Benson<sup>20</sup> have estimated heat of formation contributions of the groups [C-(H)<sub>2</sub>(CN)], [C-(H)(C)(CN)], and [C-(C)<sub>2</sub>(CN)] based on radical stabilization energies of 10.8–12.6 kcal/mol. These estimates clearly need revision and the values derived from our results are [C-(H)<sub>2</sub>(CN)] = 58.5, [C-(H)(C)(CN)] = 60.2, and [C-(C)<sub>2</sub>(CN)] = 60.0 kcal/mol.

In Table VI are compared C-H and C-C bond dissociation energies for alkanes and alkyl cyanides. Inspection of the results shows that CN substitution decreases the adja-

TABLE V: Effect of CN Substitution on Free Radical Heat of Formation<sup>a</sup>

Radical	R = CH <sub>3</sub> <sup>b</sup>	CN <sup>c</sup>	$\Delta^d$
CH <sub>2</sub> R	25.9 ± 1.3	58.5 ± 2.2	32.6 ± 2.6
CH <sub>3</sub> CHR	18.2 ± 1.5	50.1 ± 2.3	31.9 ± 2.7
(CH <sub>3</sub> ) <sub>2</sub> CR	7.6 ± 1.2	39.8 ± 2.0	32.2 ± 2.3

<sup>a</sup> All values in kcal/mol. <sup>b</sup> Reference 25. <sup>c</sup> This work and ref 2 and 3. <sup>d</sup> Difference.

TABLE VI: Effect of CN Substitution on Bond Dissociation Energies<sup>a</sup>

Bond	R = CH <sub>3</sub> <sup>b</sup>	CN <sup>c</sup>	$\Delta^d$
H-CH <sub>2</sub> R	98 ± 1	~93	~5
CH <sub>3</sub> -CH <sub>2</sub> R	85 ± 1.5	80.3 ± 2.5	4.5 ± 2.9
C <sub>2</sub> H <sub>5</sub> -CH <sub>2</sub> R	82 ± 1.5	76.9 ± 1.7	5.1 ± 2.3
<i>i</i> -C <sub>3</sub> H <sub>7</sub> -CH <sub>2</sub> R	80 ± 1.5	73.5 ± 1.7	6.5 ± 2.3
H-CH(CH <sub>3</sub> )R	95 ± 1	89.9 ± 2.3	5.1 ± 2.5
CH <sub>3</sub> -CH(CH <sub>3</sub> )R	84 ± 1.5	78.8 ± 2.0	5.2 ± 2.5
H-C(CH <sub>3</sub> )R	92 ± 1	86.5 ± 2.0	5.5 ± 2.2
CH <sub>3</sub> -C(CH <sub>3</sub> ) <sub>2</sub> R	80 ± 1.5	74.7 ± 1.6	5.3 ± 2.2

<sup>a</sup> All values in kcal/mol. <sup>b</sup> References 14 and 25. <sup>c</sup> This work and ref 2 and 3. <sup>d</sup> Difference.

cent bond energy consistently by an average of ~5.3 kcal/mol. This is a consequence of the cyano stabilization energy and it confirms the findings of Rogers, Wu, and Kuitu,<sup>24</sup> who have shown that the  $\pi$ -delocalization energy for free radicals is a property of the radical and invariant to changes in the bond being broken.

The heat of formation of the  $\alpha$ -cyanoisopropyl radical may be combined with  $\Delta H_f^\circ(\text{MVCN}) = 34.1$  kcal/mol<sup>30</sup> to yield  $\Delta H_3^\circ = 46.4$  kcal/mol for the enthalpy of its decomposition to MVCN. This latter value may be used to derive  $\text{DH}_\pi^\circ[\text{CH}_2=\text{C}(\text{CH}_3)\text{CN}] = 51.6$  kcal/mol if it is assumed that  $\text{DH}^\circ[\beta\text{C-H}]$  in the radical is equivalent to  $\text{DH}^\circ[(\text{CH}_3)_2\text{CHCH}_2\text{-H}] = 98$  kcal/mol. This  $\pi$ -bond energy is very close to our previous determination<sup>2</sup> of 53 kcal/mol for  $\text{DH}_\pi^\circ(\text{CH}_2=\text{CHCN})$ . The effect of the CN group on  $\text{DH}_\pi^\circ(\text{C}=\text{C})$ <sup>31</sup> is about the same as its effect on C-C and C-H bond energies. These results suggest that the experimental activation energies for the *cis-trans* isomerizations of crotonitrile<sup>32</sup> and  $\beta$ -cyanostyrene<sup>33</sup> are in serious error.

The Arrhenius parameters for HCN elimination may be compared with  $\log(k, \text{s}^{-1}) = 12.2 - 63.69/\theta$  determined by DE. As mentioned previously, DE's *A* factor is clearly too low for a four-center molecular elimination but combination of the reported rate constant at the mid temperature of their study with our predicted *A* factor gives *E* = 72.4 kcal/mol which is reasonably close to our value. Figure 2 shows the comparison between our values and the experimental data of DE. Both our work and that of HKT clearly indicate that HCN elimination cannot compete with C-C bond fission over the temperature range of DE's study. We have suggested and confirmed experimentally that free radical chain processes make a significant contribution to HCN formation in the "high-pressure" pyrolysis of isopropyl cyanide.<sup>2</sup> A chain contribution to the rate of HCN elimination from TBCN under DE's experimental conditions seems very likely. (C-C fission, followed by decomposition of the  $\alpha$ -cyanoisopropyl radical (reaction 3), can lead to H-atom chains.)

The activation energies for HCN elimination may be calculated theoretically by using the Benson-Haugen<sup>34</sup> (BH) semiion pair theory, or its modification developed by

TABLE VII: Comparison of Theoretical and Experimental Activation Energies for HCN Elimination

	$E(298\text{ K}), \text{ kcal/mol}$		
	BH <sup>a</sup>	TMJ <sup>b</sup>	Exptl
C <sub>2</sub> H <sub>5</sub> CN	78.4	79.0	<i>c</i>
<i>n</i> -C <sub>3</sub> H <sub>7</sub> CN	76.0	74.8	≥75.7
<i>i</i> -C <sub>3</sub> H <sub>7</sub> CN	73.1	78.6	75.3
<i>t</i> -C <sub>4</sub> H <sub>9</sub> CN	63.0	73.6	73.6

<sup>a</sup> Semiion pair model of Benson and Haugen.<sup>34</sup> <sup>b</sup> Modified semiion pair model of Tschuikow-Roux, Maltman, and Jung.<sup>35</sup> <sup>c</sup> We have not been able to observe HCN elimination from ethyl cyanide under VLPP conditions at temperatures up to ca. 1150 K. We have estimated  $E \sim 82$  kcal/mol.<sup>3</sup>

Tschuikow-Roux, Maltman, and Jung<sup>35</sup> (TMJ), to evaluate the activation energies for the four-center addition of HCN to olefins, and then adding the endothermicity of the elimination reaction. The results of these calculations (see Appendix) are presented in Table VII. The agreement between theory and experiment is good except in the case of the BH calculation for TBCN. However this model, in which we have treated the HCN molecule as a pseudodiatom with bond length equal to the H-N distance, is very sensitive to the choice of parameters for the transition state.<sup>36</sup> If the H-C bond is considered to be the reacting part of the HCN molecule then the calculated activation energies are  $\sim 13.5$  kcal/mol lower than the values listed in Table VII. Similar difficulties are not encountered with the TMJ model since the only information required for the calculation are the values of the bond energies of the participating bonds, and their single-bond lengths, i.e., ground-state properties of reactants and products. However, it does require known Arrhenius parameters for one or more calibration reactions in any homologous series in order to fix certain constants and in view of the limited experimental data the model may not be as good as the results tend to suggest. The predicted energy difference between Markovnikov and anti-Markovnikov addition of HCN is in the wrong direction.

It is of interest to compare the Arrhenius parameters for HCN elimination with those for HX elimination from alkyl halides (see Table VIII). HCN elimination is considerably slower than dehydrohalogenation and the effect of  $\alpha$ -methyl substitution is very much reduced compared with the halides. Maccoll<sup>37</sup> has suggested that the kinetic data for the alkyl halides points to heterolysis of the carbon-halogen bond as the rate-determining stage and he has shown that the activation energy for dehydrohalogenation correlates with the heterolytic bond dissociation energy,  $D(\text{R}^+\text{X}^-)$ . We estimate<sup>38</sup> that  $D(\text{R}^+\text{CN}^-)$  is about the same as  $D(\text{R}^+\text{F}^-)$  yet the activation energies for elimination differ by ca. 20 kcal/mol. The evidence suggests that the "degree of heterolysis"<sup>39</sup> of the R-CN bond is very small. This is further substantiated by the data in Table IX which compares the Arrhenius parameters for HX elimination from a series of *tert*-butyl compounds. The activation energy for HCN elimination is almost as large as that for the orbital symmetry-forbidden, 1,2-H<sub>2</sub> elimination. The transition state for HCN elimination must be essentially homolytic in character.

There appears to be other evidence in favor of a high-energy barrier to HCN elimination. Maccoll<sup>37</sup> has shown that there is an analogy between the gas-phase dehydrohalogenation of alkyl halides and the reactions of elimination

TABLE VIII: Arrhenius Parameters<sup>a</sup> for HX Elimination from Alkyl Halides<sup>b</sup> and Cyanides

Compound	log $A^c$	$E$				
		I	Br	Cl	Fe	CN <sup>f</sup>
C <sub>2</sub> H <sub>5</sub> X	13.3	50.6	53.5	56.5	59.9	
<i>n</i> -C <sub>3</sub> H <sub>7</sub> X	13.2	48.4 <sup>d</sup>	51.5	54.2	58.3	≥76.5
<i>i</i> -C <sub>3</sub> H <sub>7</sub> X	13.7	45.0	47.8	51.2	53.9	75.7
<i>t</i> -C <sub>4</sub> H <sub>9</sub> X	13.8	38.4	41.8	45.2	51.5	73.8

<sup>a</sup>  $A$  in s<sup>-1</sup> and  $E$  in kcal/mol. <sup>b</sup> Except as otherwise indicated, values are from O'Neal and Benson.<sup>15</sup> <sup>c</sup> These are the  $A$  factors estimated according to the method of O'Neal and Benson.<sup>15</sup> The experimental value for each compound may differ slightly but the deviation is not significant for the purposes of this comparison. <sup>d</sup> Reference 10. <sup>e</sup> P. Cadman, M. Day, and A. F. Trotman-Dickenson, *J. Chem. Soc. A*, 2498 (1970); 248 (1971). <sup>f</sup> VLPP results; values refer to 600 K.

TABLE IX: Arrhenius Parameters for HX Elimination from *tert*-Butyl Compounds<sup>a</sup>

-X	log ( $A, \text{ s}^{-1}$ )	$E, \text{ kcal/mol}$
-H <sup>b</sup>	$\sim 13.5$	≥77
-CN <sup>c</sup>	13.9	73.8
-NH <sub>2</sub>	14.2	67.0
-OH	13.4	61.6
-OCH <sub>3</sub> <sup>d</sup>	13.9	59.0
-SH	13.3	55.0
-F <sup>e</sup>	13.4	51.5
-Cl	13.8	45.2
-Br	13.8	41.8
-NCS <sup>f</sup>	13.0	39.5
-I	13.8	38.4

<sup>a</sup> Except as otherwise indicated, values are from the compilations of O'Neal and Benson.<sup>6,15</sup> <sup>b</sup> Estimates; see Z. B. Alfassi, D. M. Golden, and S. W. Benson, *Int. J. Chem. Kinet.*, 5, 991 (1973). <sup>c</sup> This work. <sup>d</sup> K. Y. Choo, D. M. Golden, and S. W. Benson, *Int. J. Chem. Kinet.*, 6, 631 (1974). <sup>e</sup> P. Cadman, M. Day, and A. F. Trotman-Dickenson, *J. Chem. Soc. A*, 248 (1971). <sup>f</sup> N. Barroeta, A. Maccoll, and A. Fava, *J. Chem. Soc. B*, 347 (1969).

and substitution of the corresponding compounds by the E1 or S<sub>N</sub>1 mechanism in polar solvents. Thus it is noteworthy that in solution CN<sup>-</sup> is a very sluggish leaving group and HCN elimination seems only to occur via the E1cB mechanism from polycyano compounds.<sup>40</sup> Gale and Cherkofsky<sup>41</sup> found that dehydrocyanation occurs in the gas phase but only at moderately high temperatures (ca. 200 °C) and in the presence of solid, granular base. A carbanion mechanism appears to be operative and dehydrochlorination under the same conditions was found to be very much faster.

There is the possibility of a five-membered ring transition-state involving interaction of a  $\beta$  hydrogen with the cyano-nitrogen atom; the charge distribution within the cyano group<sup>42</sup> would facilitate such a process. This would mean a lower  $A$  factor than for a four-center reaction. However, an examination of stereomodels shows that this transition state would require a considerable reduction in the C-C≡N angle from its ground state value of 180°; the energy requirements may be too large. Furthermore, the transition state seems inappropriate when the reaction is viewed from the reverse, addition direction.<sup>43</sup>

*Acknowledgment.* This research was supported by the Australian Research Grants Committee. R.D.G. acknowl-

TABLE X: Molecular Parameters for TBCN Pyrolysis

	Molecule	Complex (C-C)	Complex (-HCN)
Frequencies (cm <sup>-1</sup> ) and degeneracies	2950 (9) 2255 (1) 1440 (9) 1125 (3) 935 (2) 869 (2) 753 (2) 561 (3) 371 (3) 255 (2) 220 (2) 175 (1)	2950 (9) 2255 (1) 1440 (9) 1120 (2) 935 (1) 869 (2) 738 (1) 579 (2) 376 (2) 299 (3) 251 (3) 158 (1) 108 (1)	2950 (8) 2230 (2) 1440 (9) 1300 (1) 1070 (2) 935 (1) 869 (2) 787 (2) 553 (2) 463 (1) 366 (4) 260 (2) 176 (1) 140 (1)
$I_A I_B I_C, (\text{g cm}^2)^3 \times 10^{11/3}$	1.70	3.55	3.77
$I_r, (\text{g cm}^2) \times 10^{10}$		5.42 <sup>a</sup>	
Sigma <sup>b</sup>	3.0	1.0	1.0
Collision diameter, Å	6.3 <sup>c</sup>		
$S_{300}^\circ, \text{cal K}^{-1} \text{mol}^{-1}$	79.6	89.7	82.7

<sup>a</sup> Using internal symmetry = "foldness" of the rotor = 3.  
<sup>b</sup> Sigma =  $\sigma/n$ , where  $\sigma$  is the symmetry number for external rotation and  $n$  is the number of optical isomers. <sup>c</sup> Assumed equal to that for *n*-butyl cyanide: S. C. Chan, J. T. Bryant, L. D. Spicer, and B. S. Rabinovitch, *J. Phys. Chem.*, **74**, 2058 (1970).

edges the receipt of a Commonwealth Post-graduate Research Award. We thank Professor E. Tschuikow-Roux of the University of Calgary for the communication of results prior to publication and for a copy of his computer program for the modified semiion pair theory.

## Appendix

**Molecular and Activated Complex Models.** Frequency assignments for the molecule were based on the results of Westrum and Ribner,<sup>18</sup> and Durig, Craven, and Bragin.<sup>44</sup> The moments of inertia, which were calculated using normal bond lengths and angles, agree with the results of Nugent, Mann, and Lide.<sup>45</sup> The calculated molecular entropy at 300 K is in agreement with that determined by Westrum and Ribner.

The activated complex models were constructed according to the procedure outlined in ref 2.

The frequency assignments and parameters are summarized in Table X.

**Activation Energies for HCN Elimination.** We have outlined previously<sup>2</sup> our application of the BH model to isopropyl cyanide. Values of 68.1 kcal/mol for the energy necessary to polarize the HCN molecule, 21.7 kcal/mol for the equilibrium electrostatic interaction energy of the dipoles, and 16.4 kcal/mol for the ground state polarization energy of HCN were calculated on the basis of a pseudodiatom with bond length equal to the H-N distance in the molecule. These values may be combined with the polarization energy of the olefin double bond<sup>34</sup> to yield an activation energy for the addition reaction. Inclusion of the thermal energy content of the reactants upon activation and the endothermicity<sup>46</sup> of the appropriate reaction results in the activation energies listed in Table VII. If H-C is considered to be the reacting bond in HCN then values of 108.8 kcal/mol for the energy necessary to polarize this bond, 10.8 kcal/mol for the equilibrium electrostatic interaction ener-

gy of the dipoles, and 81.5 kcal/mol for the ground state polarization energy may be calculated.<sup>47</sup> These results lead to HCN elimination activation energies of 64.9, 62.5, 59.6, and 49.9 kcal/mol for ethyl cyanide, *n*-propyl cyanide, isopropyl cyanide, and *tert*-butyl cyanide, respectively.

The TMJ model combines the basic concepts of the BH model with the bond-energy-bond-order concepts of Johnston.<sup>49</sup> The energy contributions to the activation process depend only on ground-state properties of reactants and products. The data required are the dissociation energies of the participating bonds and their single-bond lengths. The bond dissociation energy of HCN (123.8 kcal/mol) and the C-CN bond energies were calculated from thermochemical data,<sup>50</sup> the C-H bond energies were taken from ref 25, and our experimental bond energies were used for the C<sub>2</sub>-C<sub>3</sub> bonds in the alkyl cyanides. Single-bond lengths were taken from standard tables.<sup>48</sup>

We disagree with some of the bond energy data used by TMJ to evaluate the constant  $\beta$  in their equation

$$\delta_x^{ol} = \delta_x^e - \beta(p_x^{ol} - p_x^e)$$

where  $\delta_x^{ol}$  is the partial formal charge separation for the reaction olefin + HX and  $p_x^{ol}$  is the value of the  $p$  factor for the C-C bond in this reaction.  $\delta_x^e$  and  $p_x^e$  are the corresponding values for the reaction ethylene + HX. TMJ determined  $\delta_x^e$  and  $\beta$  by trial and error fitting to experimental data. It is fortunate, however, that for the cyanides  $p_x^e$  and  $p_x^{ol}$  are almost equal and therefore the value of  $\beta$  is of little consequence. Thus since  $\delta_x^{ol} \approx \delta_x^e$  we have used the reaction isobutene + HCN  $\rightarrow$  TBCN as the standard for the evaluation of  $\delta_x$ ; the value obtained is 0.1862. The interior angle,  $\phi_1$ , of the convex quadrilateral representing the geometry of the four-center transition state<sup>35</sup> was found to be 69°.

## References and Notes

- (1) Presented in part at the Royal Australian Chemical Institute Symposium on Molecular Rate Processes, Warburton, Victoria, August, 1975.
- (2) K. D. King and R. D. Goddard, *J. Am. Chem. Soc.*, **97**, 4504 (1975).
- (3) K. D. King and R. D. Goddard, *Int. J. Chem. Kinet.*, **7**, 837 (1975).
- (4) M. Hunt, J. A. Kerr, and A. F. Trotman-Dickenson, *J. Chem. Soc.*, 5074 (1965).
- (5) P. N. Dastoor and E. U. Emovon, *Can. J. Chem.*, **51**, 366 (1973).
- (6) S. W. Benson and H. E. O'Neal, *Natl. Stand. Ref. Data Ser., Natl. Bur. Stand.*, No. 21 (1970).
- (7) (a) D. A. Luckraft and P. J. Robinson, *Int. J. Chem. Kinet.*, **5**, 137 (1973); (b) S. F. Sarnar, D. M. Gale, H. K. Hall, and A. B. Fichmond, *J. Phys. Chem.*, **76**, 2817 (1972).
- (8) K. D. King and R. D. Goddard, *Int. J. Chem. Kinet.*, **7**, 109 (1975).
- (9) A. Maccoll, *Chem. Rev.*, **64**, 33 (1969).
- (10) K. D. King, D. M. Golden, G. N. Spokes, and S. W. Benson, *Int. J. Chem. Kinet.*, **3**, 411 (1971).
- (11) D. M. Golden, G. N. Spokes, and S. W. Benson, *Angew. Chem., Int. Ed. Engl.*, **12**, 534 (1973).
- (12) The Arrhenius parameters were estimated from the values for the *tert*-butyl radical<sup>6</sup> by correcting  $E$  for stabilization by CN ( $\sim 5$  kcal/mol) and  $A$  for reaction path degeneracy; thus  $\log(k_3, \text{s}^{-1}) = 14.4 - 48.1/\theta$ . Use of the tables of the Kassel integral (G. Emanuel, *Int. J. Chem. Kinet.*, **4**, 591 (1972)) then yields  $k_{300} = 767 \text{ s}^{-1}$  at 1200 K compared to the fastest  $k_d(10 \text{ mm}) = 54.2 \text{ s}^{-1}$ .
- (13) P. J. Robinson and K. A. Holbrook, "Unimolecular Reactions", Wiley, London, 1972.
- (14) S. W. Benson, "Thermochemical Kinetics", Wiley, New York, N.Y., 1968.
- (15) H. E. O'Neal and S. W. Benson, *J. Phys. Chem.*, **71**, 2903 (1967).
- (16) It has been shown that RRK (using  $s \equiv C_{vb}(T)/R$ ) and RRKM theory give substantially the same result for fall-off calculations for thermally activated systems (D. M. Golden, R. K. Solly, and S. W. Benson, *J. Phys. Chem.*, **75**, 1333 (1971)).
- (17) Assuming that the activation energy of the reverse radical combination reaction is zero at 298 K, when the rate constant is measured in molar concentration units.
- (18) E. F. Westrum, Jr., and A. Ribner, *J. Phys. Chem.*, **71**, 1216 (1967).
- (19) H. K. Hall and J. H. Baldt, *J. Am. Chem. Soc.*, **93**, 140 (1971).
- (20) H. E. O'Neal and S. W. Benson, *Int. J. Chem. Kinet.*, **1**, 221 (1969).
- (21) S. W. Benson, F. R. Cruickshank, D. M. Golden, G. R. Haugen, H. E.

- O'Neal, A. S. Rodgers, R. Shaw, and R. Walsh, *Chem. Rev.*, **69**, 279 (1969).
- (22) M. Talât-Erben and S. Bywater, *J. Am. Chem. Soc.*, **77**, 3710 (1955); P. Smith and A. M. Rosenberg, *ibid.*, **81**, 2037 (1959); P. Smith and S. Carbone, *ibid.*, **81**, 6174 (1959).
- (23) A. A. Bichutinski, A. I. Prokof'ev, and V. A. Shalbalkin, *Russ. J. Phys. Chem.*, **38**, 534 (1964).
- (24) A. S. Rodgers, M. C. R. Wu, and L. Kuitu, *J. Phys. Chem.*, **76**, 918 (1972).
- (25) D. M. Golden and S. W. Benson, *Chem. Rev.*, **69**, 125 (1969).
- (26) D. Bellus and G. Rist, *Helv. Chim. Acta*, **57**, 194 (1974).
- (27) Using activation energies of 63.0 and 62.1 kcal/mol for methylcyclopropane and methylcyclobutane, respectively (see H. E. O'Neal and S. W. Benson, *J. Phys. Chem.*, **72**, 1866 (1968)), and 31.0 kcal/mol for 1,4-dimethylbicyclo[2.2.0]hexane (R. Srinivasan, *Int. J. Chem. Kinet.*, **1**, 133 (1969)).
- (28) A. S. Rodgers and M. C. R. Wu, *J. Am. Chem. Soc.*, **95**, 6913 (1973).
- (29) R. K. Solly, D. M. Golden, and S. W. Benson, *Int. J. Chem. Kinet.*, **2**, 381 (1970).
- (30) Estimated by assuming  $\Delta H_f^\circ(\text{MVCN}) - \Delta H_f^\circ(i\text{-C}_4\text{H}_8) = \Delta H_f^\circ(\text{C}_2\text{H}_3\text{CN}) - \Delta H_f^\circ(\text{C}_3\text{H}_6)$ . Data taken from ref 19 and 21.
- (31) K. W. Egger and A. T. Cocks, *Helv. Chim. Acta*, **56**, 1516 (1973).
- (32) J. N. Butler and R. D. McAlpine, *Can. J. Chem.*, **41**, 2487 (1963).
- (33) G. B. Kistiakowsky and W. R. Smith, *J. Am. Chem. Soc.*, **58**, 2428 (1936).
- (34) S. W. Benson and G. R. Haugen, *J. Am. Chem. Soc.*, **87**, 4036 (1965); *J. Phys. Chem.*, **70**, 3336 (1966); **74**, 1607 (1970); *Int. J. Chem. Kinet.*, **2**, 235 (1970).
- (35) K. R. Maltman, E. Tschuikow-Roux, and K. H. Jung, *J. Phys. Chem.*, **78**, 1035 (1974); E. Tschuikow-Roux and K. R. Maltman, *Int. J. Chem. Kinet.*, **7**, 363 (1975).
- (36) See previous calculations.<sup>2</sup>
- (37) A. Maccoll in "The Transition State", *Chem. Soc., Spec. Publ.*, **No. 16** (1962).
- (38) Using values for  $\Delta H_f^\circ(\text{RCN})$  from Table IV and ref 19 and 21,  $\Delta H_f^\circ(\text{R}^+)$  from ref 31, and  $\Delta H_f^\circ(\text{CN}^-) = 16$  kcal/mol (J. Berkowitz, W. A. Chupka, and T. A. Walter, *J. Chem. Phys.*, **50**, 1497 (1969)) yields  $D(n\text{-C}_3\text{H}_7^+\text{CN}^-) = 217$ ,  $D(i\text{-C}_3\text{H}_7^+\text{CN}^-) = 202$ , and  $D(t\text{-C}_4\text{H}_9^+\text{CN}^-) = 184$  kcal/mol, compared with values of 214, 200, and 189 kcal/mol for the corresponding fluorides.<sup>31</sup>
- (39) A. Maccoll and P. J. Thomas, *Progr. React. Kinet.*, **4**, 119 (1967).
- (40) See, for example, M. Albeck, S. Hoz, and Z. Rappoport, *J. Chem. Soc., Perkin Trans. 2*, 1248 (1972).
- (41) D. M. Gale and S. C. Cherkofsky, *J. Org. Chem.*, **38**, 475 (1973).
- (42) J. Grundes and P. Klabeo, "The Chemistry of the Cyano Group", Z. Rappoport, Ed., Wiley-Interscience, New York, N.Y., 1970, Chapter 3.
- (43) It is unlikely that HCN will undergo prior isomerization to HNC. The latter has only been positively identified in frozen-inert-gas matrices (D. E. Milligan and M. E. Jacox, *J. Chem. Phys.*, **39**, 712 (1963); **47**, 278 (1967)) and a substantial barrier to isomerization of HCN has been calculated (D. Booth and J. N. Murrell, *Mol. Phys.*, **24**, 1117 (1972); P. K. Pearson, G. L. Blackman, H. F. Schaefer, B. Roos, and U. Wahlgren, *Astrophys. J.*, **184**, L19 (1973)).
- (44) J. R. Durig, S. M. Craven, and J. Bragin, *J. Chem. Phys.*, **53**, 38 (1970).
- (45) L. J. Nugent, D. E. Mann, and D. R. Lide, *J. Chem. Phys.*, **36**, 965 (1962).
- (46) Using thermochemical data from Table IV and ref 19 and 21.
- (47) Using values of 1.066 Å for the H-C bond length,<sup>48</sup> 0.79 Å<sup>3</sup> for the H-C bond polarizability (K. G. Denbigh, *Trans. Faraday Soc.*, **36**, 936 (1940)), and 3.00 D for the dipole moment (B. N. Bhattacharya and W. Gordy, *Phys. Rev.*, **119**, 144 (1960)). A value of 0.82 Å<sup>3</sup> for  $\alpha_{\text{H}}^1(\text{H-C})$ , the effective longitudinal bond polarizability in the transition state, was calculated according to the procedure outlined by Benson and Haugen<sup>34</sup> with the assumption that  $\alpha_{\text{mean}}^1(\text{HCN}) \equiv 4\alpha_{\text{mean}}^1(\text{H-C})$  since in the ground state,  $\alpha_{\text{mean}}^0(\text{CN})/\alpha_{\text{mean}}^0(\text{H-C}) \approx 3$ .
- (48) L. E. Sutton, *Chem. Soc., Spec. Publ.*, **No. 11** (1958); **No. 18** (1965).
- (49) H. S. Johnston, "Gas Phase Reaction Rate Theory", Ronald Press, New York, N.Y., 1966.
- (50) Data taken from ref 19, 21, and 25, and JANAF Thermochemical Tables, *Natl. Stand. Ref. Data Ser., Natl. Bur. Stand.*, **No. 37** (1970).

## Fourier Transform Magnesium-25 Nuclear Magnetic Resonance Study of Aqueous Magnesium(II) Electrolytes

Larry Simeral and Gary E. Maciel\*

Department of Chemistry, Colorado State University, Fort Collins, Colorado 80523 (Received September 19, 1975)

Publication costs assisted by Colorado State University

<sup>25</sup>Mg NMR spectra have been determined by the Fourier transform method as a function of concentration for aqueous solutions of Mg(ClO<sub>4</sub>)<sub>2</sub>, Mg(NO<sub>3</sub>)<sub>2</sub>, MgBr<sub>2</sub>, MgCl<sub>2</sub>, and MgSO<sub>4</sub>. The line width data are discussed in terms of four models for quadrupolar nuclear spin relaxation in these systems. For MgCl<sub>2</sub> and MgSO<sub>4</sub> the line width variations cannot be accounted for in terms of variations of viscosity.

### 1. Introduction

Although Mg<sup>2+</sup> and its complexes play vital roles in a variety of chemical systems, including some of great biological importance, direct physical (e.g., spectroscopic) probes of the environment of Mg(II) in solution have largely been lacking. As with other group 1 or group 2 metal ions in their stable oxidation states, such techniques as visible-uv spectroscopy are generally not very useful, and such techniques as EPR are, of course, not applicable.

For some of the alkali metal ions, the direct observation of the metal nuclide resonance has proved to be useful,<sup>1</sup> especially for <sup>7</sup>Li and <sup>23</sup>Na. Studies of both line widths and chemical shifts of these nuclides have proved fruitful for exploring the detailed nature of the cations in solution, and have not required sophisticated techniques for detection,

because of favorable NMR properties (e.g., high natural abundance). A priori, <sup>25</sup>Mg NMR appears far less promising, because this spin 5/2 nuclide has a natural abundance of only 10% and an intrinsic NMR sensitivity (per nucleus) that is one to two orders of magnitude smaller than those of <sup>23</sup>Na or <sup>7</sup>Li. Nevertheless, because of the genuine need for good Mg(II) probes, <sup>25</sup>Mg appears worth exploring, especially in the light of recent advances in multinuclide Fourier transform NMR techniques.<sup>2-4</sup>

The few previous studies of <sup>25</sup>Mg NMR were largely exploratory and were based upon earlier techniques.<sup>5-8</sup> In general, they suffered from a lack of instrumental sensitivity. Nevertheless, these exploratory studies demonstrated the ability of <sup>25</sup>Mg NMR to sense complexation. The present paper, summarizing the first reported attempt to apply Fourier transform techniques to <sup>25</sup>Mg NMR, reports

our results on  $^{25}\text{Mg}$  NMR studies of aqueous Mg(II) electrolytes. With this technique it was possible to study solutions conveniently at concentrations as low as 0.05 m. Using currently available technology, it should be possible to study samples that are about 0.002 M in natural-abundance  $\text{Mg}^{2+}$  in 12 h experiments. This points to a potential for  $^{25}\text{Mg}$  NMR in studies of biological systems, although proper account must be taken of the effect of complexation with large molecules in making such an assessment.<sup>8</sup>

## 2. Experimental Section

a. *Measurements.*  $^{25}\text{Mg}$  NMR spectra were obtained in natural abundance at 5.51 MHz using the modified Bruker spectrometer and Digilab data system described earlier.<sup>4</sup> Ten-mm spinning sample tubes were used throughout these studies. Field/frequency lock was maintained by locking on the  $^{19}\text{F}$  resonance of perfluorobenzene contained in a 1-mm capillary centered within the 10-mm tubes. Sample temperature in all cases was  $295.5 \pm 0.3$  K. Line widths were measured as the full width at half-height and reported as the average of at least four determinations.

Bulk susceptibility corrections to the chemical shifts were estimated by measuring (on a JEOL MH-100 spectrometer) the apparent shift differences between the methyl- $^1\text{H}$  resonances of 3-(trimethylsilyl)propanesulfonate (sodium salt) dissolved in the sample and the  $^1\text{H}$  resonance of tetramethylsilane contained in a 1-mm capillary centered concentrically within the 5-mm NMR tube used for the measurements.

Viscosities were measured at  $295.5 \pm 0.2$  K in a constant temperature water bath using Ostwald-type viscometers calibrated with distilled water and absolute ethanol. The average of at least four flow times was used to calculate the viscosities.

b. *Materials.* Magnesium nitrate, magnesium chloride, and anhydrous magnesium perchlorate were obtained as Fisher Reagent grade chemicals. Anhydrous magnesium sulfate was Mallinckrodt Reagent grade. Anhydrous magnesium bromide was obtained from Rocky Mountain Research, Inc., and was recrystallized from water prior to use. Samples were prepared from stock solutions which had been standardized by atomic absorption.

## 3. Results and Discussion

Table I presents  $^{25}\text{Mg}$  line width and chemical shift data obtained as a function of the concentration of various magnesium salts in aqueous  $\text{MgSO}_4$ ,  $\text{Mg}(\text{NO}_3)_2$ ,  $\text{Mg}(\text{ClO}_4)_2$ ,  $\text{MgBr}_2$ , and  $\text{MgCl}_2$ . Also included in Table I are the viscosities of the solutions investigated.

The transverse relaxation time and associated line width of a quadrupolar nuclide resonance is generally determined by the interaction of the nuclide's quadrupolar moment with electric field gradients at the nucleus. Nevertheless, it is reasonable that for strongly hydrated ions, such as hydrated  $\text{Mg}^{2+}$ , the electric field gradients at the nucleus may be very small due to a highly symmetrical arrangement of the water molecules around the ion. In such a situation, relaxation mechanisms other than the quadrupolar interaction could contribute appreciably to the relaxation of the ion. The relaxation of  $^7\text{Li}^+$ , a strongly hydrated ion, has been shown to have a large contribution from magnetic dipole-dipole interactions with the protons on the surrounding water molecules.<sup>9</sup> This type of behavior in  $^{25}\text{Mg}^{2+}$  was explored by comparing the line width of a magnesium salt solution in  $\text{H}_2\text{O}$  to that in  $\text{D}_2\text{O}$ , where the magnetic dipole-

TABLE I:  $^{25}\text{Mg}$  Nuclear Magnetic Resonance Data for Aqueous Magnesium Salt Solutions

$C$ , m <sup>a</sup>	$\Delta\nu_{1/2}$ , Hz <sup>b</sup>	$\eta$ , cP	$\delta$ , ppm <sup>c</sup>
<b>MgSO<sub>4</sub></b>			
3.40	$11.2 \pm 0.8$	9.10	0.0
3.00	$9.5 \pm 0.3$	7.65	-0.1
2.30	$6.4 \pm 0.3$	4.84	0.0
1.80	$5.4 \pm 0.3$	3.28	0.0
1.30	$4.4 \pm 0.3$	2.39	0.1
0.80	$3.8 \pm 0.3$	1.68	0.0
0.50	$3.2 \pm 0.3$	1.40	0.0
0.40	$3.0 \pm 0.3$	1.29	0.1
0.05	$2.8 \pm 0.4$	1.04	0.0
<b>MgBr<sub>2</sub></b>			
2.70*	$6.8 \pm 0.3$	2.04	0.4
2.30	$6.1 \pm 0.2$	1.77	0.5
1.97	$5.4 \pm 0.2$	1.57	0.4
1.64*	$5.0 \pm 0.2$	1.43	0.3
0.90	$3.9 \pm 0.2$	1.19	0.1
0.47	$3.6 \pm 0.2$	1.10	0.0
0.10*	$2.7 \pm 0.3$	1.01	0.0
<b>Mg(ClO<sub>4</sub>)<sub>2</sub></b>			
4.00	$8.0 \pm 0.3$	3.20	-0.4
3.00	$5.5 \pm 0.3$	2.30	-0.3
2.20	$4.5 \pm 0.3$	1.82	-0.3
1.64	$3.4 \pm 0.3$	1.56	-0.2
1.10	$3.1 \pm 0.3$	1.35	-0.1
0.69	$2.5 \pm 0.3$	1.22	-0.1
0.32	$2.4 \pm 0.3$	1.10	0.0
0.32 in D <sub>2</sub> O	$3.0 \pm 0.3$	1.35	0.0
<b>Mg(NO<sub>3</sub>)<sub>2</sub></b>			
3.10	$9.4 \pm 0.6$	2.99	0.1
2.50	$6.6 \pm 0.3$	2.34	0.0
2.10	$5.5 \pm 0.2$	2.00	0.0
1.70	$4.8 \pm 0.2$	1.70	0.0
1.40	$4.3 \pm 0.3$	1.49	0.0
1.10	$3.6 \pm 0.3$	1.36	0.0
0.48	$3.3 \pm 0.3$	1.13	0.0
0.23	$2.7 \pm 0.3$	1.06	0.0
<b>MgCl<sub>2</sub></b>			
4.10	$7.2 \pm 0.3$	5.5	0.0
3.60	$5.9 \pm 0.3$	4.45	-0.1
3.20	$5.3 \pm 0.2$	3.72	0.0
2.79	$4.8 \pm 0.2$	3.02	0.0
2.30	$4.3 \pm 0.3$	2.40	0.0
1.30	$3.8 \pm 0.2$	1.65	0.0
0.47	$3.2 \pm 0.2$	1.11	0.0
0.10	$2.7 \pm 0.3$	1.05	0.0

<sup>a</sup> Concentration in molality. <sup>b</sup> Line widths were determined as the full-width at half-height. Tabulated values represent the average of at least three determinations with the error limits the standard deviations of the measurements. <sup>c</sup> Chemical shifts ( $\pm 0.1$  ppm) with respect to the signal for  $\text{Mg}(\text{ClO}_4)_2$ , extrapolated to infinite dilution. More positive values refer to lower shielding. Bulk susceptibility corrections have been made.

dipole interaction would be greatly reduced due to the small magnetic moment of the deuteron. Such a comparison is shown in Table I for 0.5 m  $\text{Mg}(\text{ClO}_4)_2$ . If the relaxation in  $\text{D}_2\text{O}$  were less efficient than in  $\text{H}_2\text{O}$ , the line width in  $\text{D}_2\text{O}$  would be narrower. This is not observed; indeed a small effect of the reverse sign may obtain. As can be seen from the table, the small difference in line width for  $\text{D}_2\text{O}$  and  $\text{H}_2\text{O}$  solutions is proportionately accounted for by the fractional difference in viscosities of the two solutions (see eq 6).

Tests were also made for possible contributions to the  $^{25}\text{Mg}^{2+}$  relaxation through interaction with the unpaired electrons of dissolved oxygen in the solutions. Thorough degassing of a selection of solutions, both dilute and concentrated, by purging with purified  $\text{N}_2$  gas did not affect the observed line widths in any way. Thus, we may reasonably eliminate considerations of magnetic dipole-dipole interactions with water protons or molecular oxygen in discussing the  $^{25}\text{Mg}$  line widths for the aqueous solutions reported here.

Other contributions to the  $^{25}\text{Mg}$  relaxation, such as spin-rotation interactions, chemical shift anisotropy, and chemical exchange, cannot be eliminated unequivocally on the basis of the data available here. Because of the small number of electrons associated with magnesium, and the low degree of covalent character assumed for the interactions present in these systems, the spin-rotation and chemical shift anisotropy mechanisms are not expected to be important. Chemical exchange relaxation mechanisms of the usual type, i.e., modulation of the Zeeman term by chemical exchange between sites of different shielding,<sup>10</sup> can be neglected on the basis of the very small range of  $^{25}\text{Mg}$  chemical shifts observed to date.<sup>5-8</sup> Hence, for the discussion which follows, the quadrupolar relaxation mechanism will be assumed to dominate the  $^{25}\text{Mg}$  relaxation. Line-width contributions due to magnetic field inhomogeneities are neglected in this work, because line widths as low as 0.5 Hz have been observed in  $^{43}\text{Ca}$  NMR resonances in the same field and using the same insert.

The  $^{25}\text{Mg}$  line widths in aqueous magnesium salt solutions, unlike the corresponding chemical shifts, are relatively strongly dependent upon the salt concentration. The line width variations are represented in Figures 1-5. Aqueous magnesium salt solutions of the type employed in this work are acidic due to hydrolysis, with pH varying over a range between 4 and 7. Magnuson and Bothner-By<sup>6</sup> have reported that the  $^{25}\text{Mg}$  line width of a magnesium chloride solution is invariant over a wider range of pH, which is consistent with some similar measurements made in this work. Hence, we have neglected the effect of pH variation in the discussion below. It is conceivable that hydrolysis (as reflected in pH) may play some small role in the line width variations, but it cannot be a dominant effect.

As stated above, the line width of  $^{25}\text{Mg}$  resonance in solutions of magnesium salts is primarily determined by the nuclear quadrupolar interaction, via its motional modulation. The equation for the line width, neglecting broadening due to magnetic field inhomogeneities, is

$$\Delta\nu_{1/2} = \frac{1}{\pi T_2} = \frac{3}{40\pi} \frac{2I+3}{I^2(2I-1)} \left(1 + \frac{\eta^2}{3}\right) \left(\frac{e^2qQ}{h}\right)^2 \tau_c \quad (1)$$

for the extreme narrowing condition.<sup>10</sup> Here,  $\tau_c$  is the time constant that describes the motional modulation of the quadrupolar interaction (i.e., the correlation time for reorientation of the electric field gradient with respect to  $H_0$ ),  $I$  is the spin of the nucleus,  $\eta$  is a parameter describing the asymmetry of the electric field gradient, and  $e^2qQ/h$  is the quadrupole coupling constant.

In ionic solutions of the type involved in this study, the modulation of the quadrupolar interaction may arise from at least the following four mechanisms.

(a) The reorientation of electric dipoles of solvent molecules near an ion will generally cause modulation of the electric field gradient at the nucleus of the ion. For this contribution to relaxation, one can replace eq 1 with a more

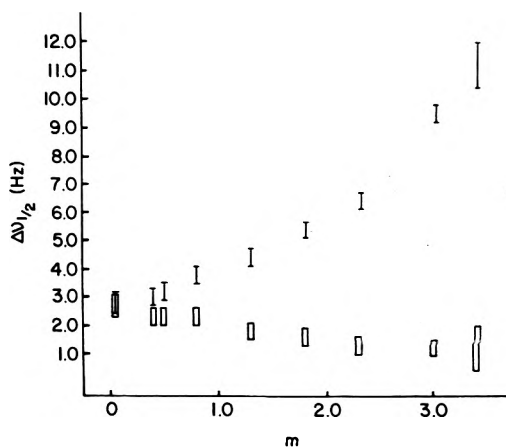


Figure 1. The concentration dependence of the  $^{25}\text{Mg}$  NMR line width for aqueous solutions of  $\text{MgSO}_4$ , verticle bars. The rectangles represent values of  $\Delta\nu_{1/2}/\eta$ .

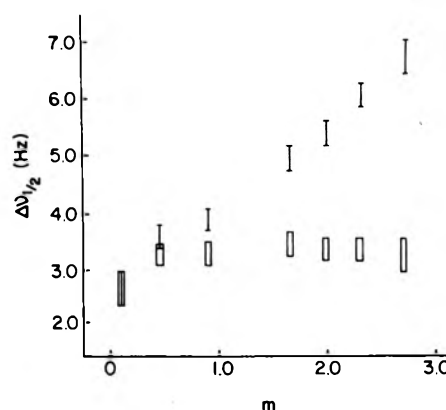


Figure 2. The concentration dependence of the  $^{25}\text{Mg}$  NMR line width for aqueous solutions of  $\text{MgBr}_2$ , verticle bars. The rectangles represent values of  $\Delta\nu_{1/2}/\eta$ .

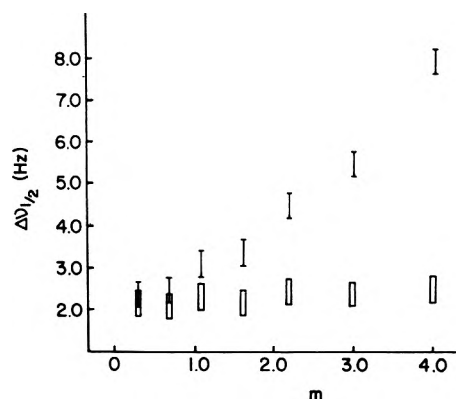


Figure 3. The concentration dependence of the  $^{25}\text{Mg}$  NMR line width for aqueous solutions of  $\text{Mg}(\text{ClO}_4)_2$ , verticle bars. The rectangles represent values of  $\Delta\nu_{1/2}/\eta$ .

specific form, giving<sup>11</sup>

$$\Delta\nu_{1/2} \propto \left(\frac{eQ}{h}\right)^2 \frac{\mu^2}{r^5} N \tau_s \quad (2)$$

In this equation,  $(\mu^2/r^5)N$  is a factor describing the mean electric field gradient due to solvent molecules of dipole moment,  $\mu$ , at a distance,  $r$ , from the nucleus of the ion with a number density,  $N$ , and  $\tau_s$  is a reorientational correlation time.

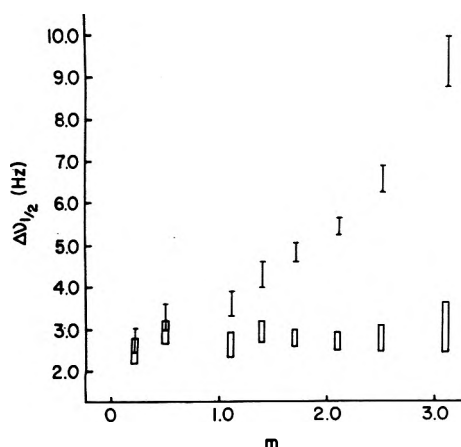


Figure 4. The concentration dependence of the  $^{25}\text{Mg}$  NMR line width for aqueous solutions of  $\text{Mg}(\text{NO}_3)_2$ , verticle bars. The rectangles represent values of  $\Delta\nu_{1/2}/\eta$ .

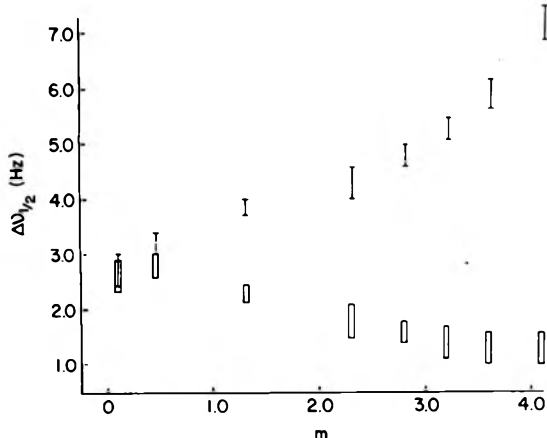


Figure 5. The concentration dependence of the  $^{25}\text{Mg}$  NMR line width for aqueous solutions of  $\text{MgCl}_2$ , verticle bars. The rectangles represent values of  $\Delta\nu_{1/2}/\eta$ .

(b) Electric field gradients at the nucleus of interest arising from electric fields of other ions in solution are modulated by the translational diffusion of these ions. One can again replace eq 1 to describe the specific mechanism, giving<sup>11</sup>

$$\Delta\nu_{1/2} \propto \left(\frac{eQ}{h}\right)^2 \sum_i \frac{Z_i^2 e^2 C_i \tau_i}{3d^3} \quad (3)$$

where  $Z_i e$  is the electric charge of the  $i$ th ion in solution,  $C_i$  is the concentration of the  $i$ th ion,  $d$  is the distance of closest approach of the pertinent ions, and  $\tau_i$  is the correlation time for diffusion of the pertinent ions.

(c) If the ions of interest are involved in complexes of significant lifetime, then interaction of the nuclear quadrupole moment with the net electric field gradient of the complex,  $eq$ , is modulated by the thermal reorientation of the complex. This case, as discussed many times in the literature,<sup>10,11</sup> is given by

$$\Delta\nu_{1/2} \propto \left(\frac{e^2 q Q}{h}\right)^2 \tau_c \quad (4)$$

where  $\tau_c$  is the reorientational correlation time of the complex. If relatively long-lived complexes do form, there will be contributions to the line width from all complexes present; if the mean lifetime,  $\tau_r$ , of a complex is in the range  $\tau_c \ll \tau_r \ll T_2$ , where  $T_2$  is the relaxation time of the

nucleus in the complex, the width of the single observed line will be a population-weighted average of the line widths of all complexes in equilibrium;<sup>12</sup> this average contains a term dependent upon  $\tau_c$ .

(d) The formation of transitory complexes (e.g., ion pairs) from hydrated ions causes a discontinuous modulation of the electric field gradient at the nucleus of interest, changing randomly from a value near zero (symmetrically hydrated  $\text{Mg}^{2+}$ ) to some large value,  $eq_c$ . This mechanism would be expected to follow an equation that includes a term of the form

$$(e^2 q_c Q/h)^2 \tau_r \quad (5)$$

where  $\tau_r$  is the lifetime of the transitory complex. This case differs from case c in that  $\tau_r < \tau_c \ll T_2$ . In the limit as  $\tau_r$  becomes larger than  $\tau_c$ , the complexes become longer lived and mechanism c obtains. As  $\tau_r \rightarrow 0$  the ion-ion encounters become even more transitory in nature and this mechanism gives way to mechanism b.

At the present state of knowledge of this subject it is impossible to predict a priori the relative importance of each of these types of contributions. Furthermore, even if one could, in general the values of various electric field gradient factors in these expressions are not known, so one could not calculate the various correlation times. There is some evidence<sup>13,14</sup> (and it is often assumed) that in solutions of small molecules the molecular reorientational correlation times,  $\tau_c$ , are linearly related to the bulk viscosity of the solution. This idea has its foundation in the Debye theory of dielectric relaxation in polar liquids.<sup>15</sup> In this theory,  $\tau_c$  is related to the viscosity,  $\eta$ , by

$$\tau_c = 4\pi a^3 \eta / 3kT \quad (6)$$

where  $a$  is the hydrodynamic radius,  $k$  is the Boltzmann constant, and  $T$  is the absolute temperature. Within this type of framework, ions have been treated as small molecules, and correlation times,  $\tau_i$ ,  $\tau_c$ , and  $\tau_s$  have been assumed to be linearly related to the viscosity of the solution.<sup>14</sup> Implicit in this approach are the assumptions that (i) for mechanism a the neighboring dipolar molecules undergo motion that is not restricted by any *specific* ion-solvent interactions (i.e., that molecules neighboring the solute of interest still retain the average mobility of bulk solvent molecules); (ii) for mechanism b the ions in solution undergo diffusion that is *not* restricted by any specific ion-ion interactions (i.e., that ion motions are not *specifically* correlated to one another and the ion motions are controlled only by properties related to the viscosity); (iii) for mechanism c the thermal reorientation of the complex is unrestricted by any *specific* solvent-solute interactions.

On the basis of previous work, one does not expect mechanism c to be very important for any of the magnesium salts, except possibly  $\text{MgSO}_4$ , because specific complexation of  $\text{NO}_3^-$ ,  $\text{ClO}_4^-$ ,  $\text{Cl}^-$ , and  $\text{Br}^-$  to  $\text{Mg}^{2+}$  has not been observed.<sup>16,17</sup> Thus, if the above assumptions are valid, the  $^{25}\text{Mg}^{2+}$  line width should be related to the solution viscosity,  $\eta$ , and the solute concentration(s) in the following manner

$$\Delta\nu_{1/2} = F\eta + G\eta + P(C) \quad (7)$$

where  $F$  is a factor associated with solvent properties (see eq 2),  $G$  is a factor associated with properties of the ions in solution (see eq 3), and  $P(C)$  is some function of concentrations related to the kinetic details of the transitory complexes of mechanism d. To the extent that long-lived com-

plexes do exist, mechanism c would also make a contribution, and a term of the form  $R(C)\eta$  would be added to eq 7. A similar expression to the first two terms of eq 7 had been proposed previously for the relaxation of alkali metal ion nuclides and halide ion nuclides.<sup>14</sup>

It is of interest to test the validity of eq 7, and hence, its underlying assumptions, for aqueous solutions of  $^{25}\text{Mg}^{2+}$ . For this purpose, the measured values of the  $^{25}\text{Mg}$  line width and the solution viscosity as functions of magnesium salt concentration were analyzed in terms of the ratio,  $\Delta\nu_{1/2}/\eta$ .

If the first term in eq 7 is dominant, then one would expect the ratio  $\Delta\nu_{1/2}/\eta$  to be independent of the concentration of a magnesium salt. On the other hand,  $\Delta\nu_{1/2}/\eta$  would be linearly related to the concentration if the second term were dominant. In order to explore these possibilities, we have plotted  $\Delta\nu_{1/2}/\eta$  vs. concentration for the magnesium salt solutions investigated here; these plots are shown in Figures 1-5.

For the  $\text{Mg}(\text{ClO}_4)_2$  and  $\text{Mg}(\text{NO}_3)_2$  solutions  $\Delta\nu_{1/2}/\eta$  is nearly constant over the concentration ranges employed.  $\Delta\nu_{1/2}/\eta$  for  $\text{MgBr}_2$  rises at first with increasing concentration (0-0.5 m), and then remains nearly constant as the concentration is increased further. For the  $\text{MgCl}_2$  and  $\text{MgSO}_4$  solutions,  $\Delta\nu_{1/2}/\eta$  is constant at low concentration (0-0.5 m), then decreases as the concentration is further increased. The first term of eq 7 (the one associated with mechanism a) appears to be sufficient to account for the data on  $\text{Mg}(\text{ClO}_4)_2$  and  $\text{Mg}(\text{NO}_3)_2$  solutions, and for the data on  $\text{MgBr}_2$  solutions at concentrations greater than 0.5 m. The first term of eq 7 appears promising for  $\text{MgSO}_4$  and  $\text{MgCl}_2$  solutions only at low concentrations, less than 0.5 m. There is no evidence in any of these plots for important contributions associated with the second term in eq 7, i.e., with mechanism b.

The behavior of  $\text{MgSO}_4$  and  $\text{MgCl}_2$  solutions is rather unusual in that the line width does not increase as rapidly (on a fractional basis) with concentration as the viscosity does. The second term in eq 7 (associated with mechanism b) would require  $\Delta\nu_{1/2}/\eta$  to increase with increasing concentration. If rather specific ion-ion interactions (i.e., ion pairing) were taking place and giving rise to long-lived complexes, then one would expect, based upon previous studies with alkali metal ion<sup>4-8</sup> and our discussion of mechanism c above, an increase in the electric field gradient at the nucleus due to the close proximity of another charged species (ion). One might also expect an increase in the rotational correlation time of the  $\text{Mg}(\text{II})$  species. In such a case, the line width would be expected to increase more rapidly with increasing concentration than the increase in viscosity with increasing concentration. That this behavior is not observed is particularly interesting for  $\text{MgSO}_4$  solutions, where specific ion pairing has been studied by a variety of techniques.<sup>17,18</sup> Previous studies of aqueous  $\text{MgSO}_4$  solutions indicate that appreciable concentrations of magnesium sulfate ion pairs exist over the range of concentrations studied here.

If mechanism d were operative, one could envision a plausible reason for the two cases of substantial decrease in  $\Delta\nu_{1/2}/\eta$  as the concentration increases. That mechanism is associated with the transient formation of complexes, e.g., ion pairs, between  $\text{Mg}^{2+}$  and  $\text{Cl}^-$  and between  $\text{Mg}^{2+}$  and  $\text{SO}_4^{2-}$ . If the lifetimes of these transient species,  $\tau_r$ , even in dilute solutions, are smaller than  $\tau_c$  and if the lifetime decreases with increasing solute concentration, then the ef-

fectiveness of that contribution to relaxation will decrease with increased solute concentration, according to eq 5 (i.e.,  $P(C)$  in eq 7 decreases with increasing  $C$ ). Hence, the line width will not increase with concentration as rapidly as the viscosity increases with concentration. Another plausible explanation for the decrease in  $\Delta\nu_{1/2}$  with increasing  $\text{MgSO}_4$  or  $\text{MgCl}_2$  concentrations, at high concentrations, is the possible effect on  $\text{Mg}(\text{II})$  of changes in water structure as the salt concentration increases. If such changes could bring about a higher symmetry in the time-average hydration of  $\text{Mg}^{2+}$ , then the observed trend would be understandable. The presently available information does not permit a meaningful judgment to be made on this point.

The chemical shifts, when corrected for bulk susceptibility effects, vary over a total range of only about 1 ppm. The largest variations (about 0.4 ppm) occur for  $\text{MgBr}_2$  and  $\text{Mg}(\text{ClO}_4)_2$ . The latter case showed no indication of specific  $\text{Mg}^{2+}\cdots\text{ClO}_4^-$  interactions from line width data. The  $\text{MgCl}_2$  and  $\text{MgSO}_4$  cases, for which the line width data give some indication of transient ion pairs, show almost no chemical shift dependence upon  $\text{Mg}(\text{II})$  salt concentration. Hence, it would appear that these two parameters, the chemical shift and the viscosity-corrected line width, depend upon different types of influences on the  $\text{Mg}^{2+}$  ion.

#### 4. Summary and Conclusions

The  $^{25}\text{Mg}$  NMR line widths of these aqueous solutions of  $\text{Mg}(\text{II})$  salts are seen to be relatively sensitive to variation in concentrations. Using the available models of quadrupolar relaxation in electrolyte systems, it appears as if the dependence of  $\Delta\nu_{1/2}$  upon viscosity is sufficient to explain the data for  $\text{Mg}(\text{ClO}_4)_2$  and  $\text{Mg}(\text{NO}_3)_2$ , and for  $\text{MgBr}_2$  at higher concentrations. For  $\text{MgSO}_4$  and  $\text{MgCl}_2$  at higher concentration, a mechanism involving the formation of transient ion pairs seems attractive, although the possibility exists of explaining the results on the basis of alterations of bulk water structure. The convenience and potential utility of FT  $^{25}\text{Mg}$  NMR for studying the nature of  $\text{Mg}(\text{II})$  solutions is demonstrated.

*Acknowledgment.* The authors are grateful to the National Science Foundation for support of this work under Grants No. GP-33249 and MPS 74-23980, and for grants contributing to the purchase of the spectrometer and data system.

#### References and Notes

- (1) A representative, but not complete list of references: (a) T. L. James and J. H. Noggle, *J. Am. Chem. Soc.*, **91**, 3424 (1969); (b) E. Shchori, J. Jagur-Grodzinski, and M. Shporer, *ibid.*, **95**, 3842 (1973); (c) C. Hall, R. E. Richards, G. N. Schulz, and R. R. Sharp, *Mol. Phys.*, **18**, 529 (1969); (d) M. Eisenstadt and H. L. Friedman, *J. Chem. Phys.*, **46**, 2182 (1967); (e) G. J. Templeman and A. L. VanGeet, *J. Am. Chem. Soc.*, **94**, 5578 (1972); (f) R. E. Richards and B. A. Yorke, *Mol. Phys.*, **6**, 289 (1963); (g) R. H. Erlich and A. I. Popov, *J. Am. Chem. Soc.*, **93**, 5620 (1971); (h) M. S. Greenberg, R. L. Bodner, and A. I. Popov, *J. Phys. Chem.*, **77**, 2449 (1973); (i) E. G. Bloor and R. G. Kidd, *Can. J. Chem.*, **46**, 3425 (1968); (j) R. D. Green and J. S. Martin, *ibid.*, **50**, 3938 (1972); (k) G. E. Maciel, J. K. Hancock, L. F. Lafferty, P. A. Mueller, and W. K. Musker, *Inorg. Chem.*, **5**, 554 (1966).
- (2) D. D. Traficante, J. A. Sims, and M. Mulcahy, *J. Magn. Reson.*, **15**, 484 (1974).
- (3) P. D. Ellis, H. C. Walsh, and C. S. Peters, *J. Magn. Reson.*, **11**, 426 (1973).
- (4) H. C. Dorn, L. Simeral, J. J. Natterstad, and G. E. Maciel, *J. Magn. Reson.*, **18**, 1 (1975).
- (5) M. Ellenberger and M. Villemin, *C. R. Acad. Sci. Paris, Ser. B*, **266**, 1430 (1968).



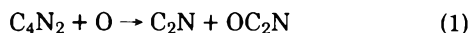
- (6) A. Magnuson and A. A. Bothner-By in "Magnetic Resonance in Biological Research", A. Franconi, Ed., Gordon and Breach, London, 1969, p 365.
- (7) F. Toma, M. Villemin, M. Ellenberger, and L. Brahamet, *Magn. Reson. Relat. Phenom., Proc. Congr. AMPERE, 16th*, 1970, 317 (1971).
- (8) R. G. Bryant, *J. Magn. Reson.*, **6**, 159 (1972).
- (9) D. E. Woessner, B. S. Snowden, Jr., and A. G. Ostroff, *J. Chem. Phys.*, **49**, 371 (1968).
- (10) A. Abragam, "The Principles of Nuclear Magnetism", Clarendon Press, Oxford, 1961, Chapter 8.
- (11) H. G. Hertz, *Z. Elektrochem.*, **65**, 20 (1961).
- (12) T. J. Swift and R. Connick, *J. Chem. Phys.*, **37**, 307 (1962).
- (13) N. Bloembergen, E. M. Purcell, and R. V. Pound, *Phys. Rev.*, **73**, 679 (1948).
- (14) (a) R. E. Richards and B. A. York, *Mol. Phys.*, **6**, 289 (1963); (b) C. Deverell, D. J. Frost, and R. E. Richards, *ibid.*, **9**, 565 (1965); (c) C. Deverell in "Progress in N.M.R. Spectroscopy", Vol. 4, J. W. Emsley, J. Feeney, and L. H. Sutcliffe, Ed., Pergamon Press, London, 1969, Chapter 4.
- (15) P. Debye, "Polar Molecules", Dover Press, New York, N.Y., 1945.
- (16) L. G. Sillen and A. E. Martell, *Chem. Soc., Spec. Publ.*, No. 17 (1964).
- (17) D. R. Kester, Ph.D. Thesis, Oregon State University, Corvallis, Oregon, 1969.
- (18) See, for example, (a) R. M. Chatterjee, W. A. Adams, and A. R. Davis, *J. Phys. Chem.*, **78**, 246 (1974); (b) G. Atkinson and S. Petrucci, *ibid.*, **70**, 3122 (1966); (c) F. H. Fisher, *ibid.*, **66**, 1607 (1962); (d) D. R. Kester and R. M. Pytkowicz, *Geochim. Cosmochim. Acta*, **34**, 1039 (1970).

## COMMUNICATIONS TO THE EDITOR

### Arrhenius Parameters for the Reaction of Oxygen Atoms with Dicyanoacetylene

Publication costs assisted by The University of Alabama

Sir: In a recent publication<sup>1</sup> we discussed the kinetics and mechanism of the reaction between oxygen atoms (ground state) and dicyanoacetylene. By means of measurements in a discharge-flow reactor the rate constant, at room temperature, was found to be  $6.6 \pm 1.8 \times 10^8 \text{ cm}^3 \text{ mol}^{-1} \text{ s}^{-1}$ , with a near-unity stoichiometric ratio of reactant consumption. Several free-radical intermediates were identified, and on the basis of this and other evidence it was proposed that the first step in the overall reaction is



The reaction between oxygen atoms and acetylene has been well studied in recent years<sup>2-6</sup> and should provide a convenient reference for discussions of the reaction rates of substituted acetylenes. The average value of the rate constant for  $\text{C}_2\text{H}_2$ , as found by several different techniques, is  $9.0 \pm 1.2 \times 10^{11} \text{ cm}^3 \text{ mol}^{-1} \text{ s}^{-1}$  at room temperature. Although some earlier work<sup>2</sup> had indicated that the activation energy was close to zero, three more recent studies,<sup>3-5</sup> in very good agreement with one another, yielded the value  $3000 \pm 200 \text{ cal mol}^{-1}$  for the activation energy.

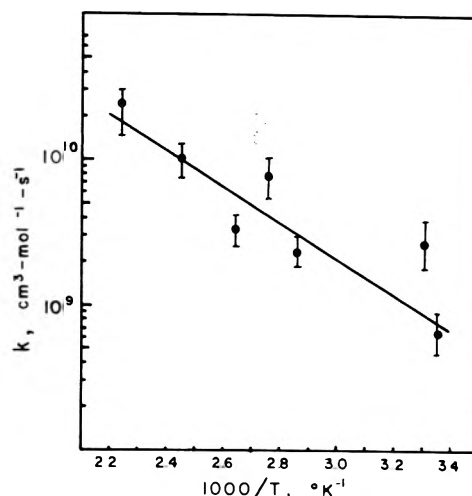


Figure 1. Arrhenius plot of the variation of rate constant with temperature. The point at lowest temperature is taken from ref 1.

Since it is of interest to compare Arrhenius parameters as well as single-temperature rate constants, we have reexamined the reaction between oxygen atoms and dicyanoacetylene; in particular we have measured its rate over the temperature range 300–450 K. The experimental apparatus

TABLE I

$P$ , Torr	$T$ , K	$[\text{O}]$ , atoms $\text{cm}^{-3} \times 10^{-14}$	$[\text{O}]_0/[\text{DCA}]_0$	$t_{\text{max}}$ , s	$V$ , $\text{cm s}^{-1}$	$k_1^a$ , $\text{cm}^3 \text{ mol}^{-1} \text{ s}^{-1}$
0.73	408	1.79	13.9	0.26	178	$16.5 \pm 1.0$
0.77	350	3.20	13.1	0.32	144	$3.92 \pm 0.15$
1.10	378	5.66	13.9	0.33	140	$5.55 \pm 0.16$
1.10	363	1.72	9.0	0.34	134	$12.8 \pm 1.6$
1.00	446	1.44	7.0	0.33	139	$38.9 \pm 2$
1.06	301	1.43	6.2	0.38	122	$4.50 \pm 1.92$
0.7–5 <sup>b</sup>	300					

<sup>a</sup> Indicated errors are standard deviations derived from a least-squares analysis of measurements from at least eight contact times. <sup>b</sup> Average value at room temperature from ref 1.

and procedure was the same as before;<sup>1,7,8</sup> O atoms, produced in a microwave discharge through 90% He-10% O<sub>2</sub>, were mixed with dicyanoacetylene in a cylindrical flow reactor, and the dicyanoacetylene concentration was measured mass spectrometrically as a function of time after mixing. All experiments were done under pseudo-first-order conditions, with O atoms in at least a sixfold excess, and, inasmuch as the earlier study had shown no pressure dependence of the room temperature rate constant over the range 0.7-5.0 Torr, all experiments were done at about 1.0 Torr. Modifications to the apparatus necessary for measurements at elevated temperatures have been described;<sup>7</sup> reactor temperature as measured with a chromel-alumel thermocouple varied less than 5% along the length of the reactor and/or during the course of the measurement.

The results are given in Table I, and shown also in Figure 1 where they are plotted as  $\log k$  vs.  $1000/T$ . Each rate constant was estimated to be accurate to  $\pm 20\%$ , which in our experience is the largest error normally encountered in measurement of oxygen atom concentration. To this 20% was added the standard deviation (shown in Table I) derived from a least-squares treatment of measurements from at least eight reaction times. The resulting error estimate, shown also as error bars in Figure 1, was used in a weighted least-squares treatment which yielded the equation

$$k = 10^{12.9 \pm 0.7} \exp(-5500 \pm 1100/RT) \text{ cm}^3 \text{ mol}^{-1} \text{ s}^{-1}$$

The corresponding equation for the unsubstituted acetylene is

$$k = 10^{13.14 \pm 0.09} \exp(-2980/RT) \text{ cm}^3 \text{ mol}^{-1} \text{ s}^{-1}$$

and thus the preexponential factors are equal within the accuracy of the data.

*Acknowledgment.* We are grateful for the support of the National Science Foundation in the form of an Undergraduate Research Participation Grant, and to The University of Alabama Research Grants Committee. These results were presented in part at the 7th Annual Southeastern Sectional Conference of Undergraduate Student Chemists.

#### References and Notes

- (1) C. W. Hand and R. H. Obenauf, Jr., *J. Phys. Chem.*, **76**, 269 (1972).
- (2) C. A. Arrington, W. Brennen, G. P. Glass, J. V. Michael, and H. Niki, *J. Chem. Phys.*, **43**, 525 (1965).
- (3) A. A. Westenberg and N. de Haas, *J. Phys. Chem.*, **73**, 1181 (1969).
- (4) G. S. James and G. P. Glass, *J. Chem. Phys.*, **50**, 2268 (1969).
- (5) K. Hoyerman, H. G. Wagner, and J. Wolfrum, *Z. Phys. Chem. (Frankfurt am Main)*, **63**, 193 (1969).
- (6) J. T. Herron and R. E. Huie, *J. Phys. Chem. Ref. Data*, **2**, 467 (1973).
- (7) C. W. Hand and R. H. Obenauf, Jr., *J. Phys. Chem.*, **76**, 2643 (1972).
- (8) D. Bogan, Ph.D. Thesis, Carnegie-Mellon University, 1973.

Chemistry Department  
The University of Alabama  
University, Alabama 35486

Clifford W. Hand\*  
Richard M. Myers

Received July 9, 1975; Revised Manuscript Received December 22, 1975

**New concepts  
new techniques  
new interpretations**

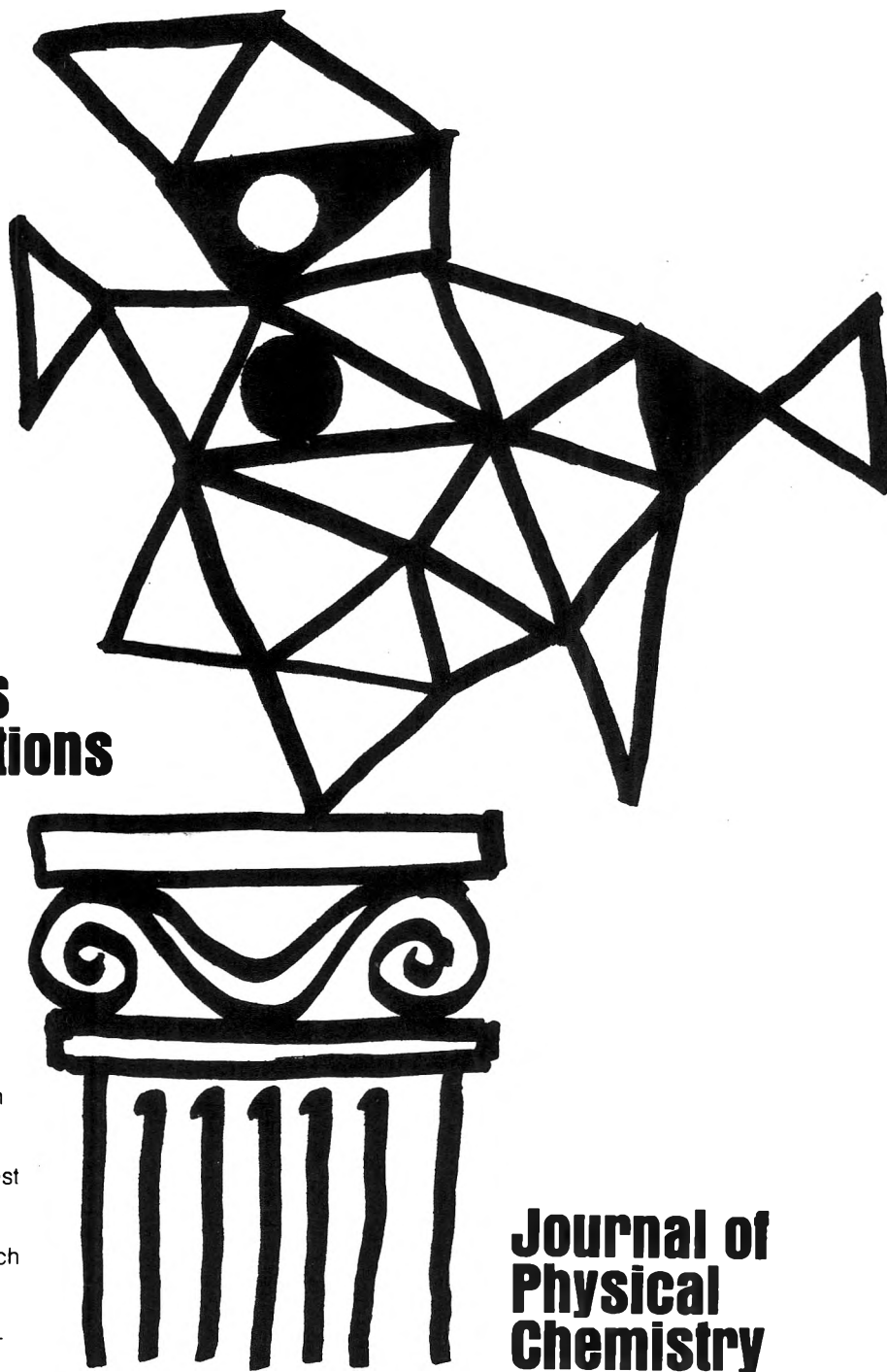
**... together  
with valuable reports  
on classical areas**

They are all waiting for you between the covers of our well-balanced JOURNAL OF PHYSICAL CHEMISTRY. Whatever your particular interest in physical chemistry, you'll find the JOURNAL's broad range of experimental and theoretical research reports are relevant and beneficial to your work. Each biweekly issue brings you an average of 30 authoritative, comprehensive reports on fundamental aspects of atomic and molecular phenomena, as well as timely notes, communications and reports plus the proceedings of selected symposia.

Join your fellow physical chemists who rely on JPC as an excellent biweekly source of data in both new and classical areas. Just complete and return the form to start your own subscription.



... another ACS service



# Journal of Physical Chemistry

**The Journal of Physical Chemistry  
American Chemical Society**

1155 Sixteenth Street, N.W.  
Washington, D.C. 20036

**1976**

Yes, I would like to receive the JOURNAL OF PHYSICAL CHEMISTRY at the one-year rate checked below:

	U.S.	Canada**	Latin America**	Other Nations**
ACS Member One-Year Rate*	<input type="checkbox"/> \$24.00	<input type="checkbox"/> \$30.25	<input type="checkbox"/> \$29.75	<input type="checkbox"/> \$30.25
Nonmember	<input type="checkbox"/> \$96.00	<input type="checkbox"/> \$102.25	<input type="checkbox"/> \$101.75	<input type="checkbox"/> \$102.25

Bill me  Bill company  Payment enclosed

*Air freight rates available on request*

Name \_\_\_\_\_

Street \_\_\_\_\_ Home   
Business

City \_\_\_\_\_ State \_\_\_\_\_ Zip \_\_\_\_\_

**Journal subscriptions start January '76**

\*NOTE: Subscriptions at ACS member rates are for personal use only. \*\*Payment must be made in U.S. currency, by international money order, UNESCO coupons, U.S. bank draft, or order through your book dealer.

# Tape Cassettes From The American Chemical Society Famous Scientists

## ENERGY

- Energy & Industry**  
A Waterland  
**Energy & Environment**  
Dr. S. Maniakin
- Energy on the Shelf**  
Dr. F. Kahhammer  
**H<sub>2</sub> and You**  
Dr. D. Gregory
- Green Thumb Energy**  
Dr. D. Klass  
**Methane from Coalbeds**  
Dr. R. Stefanko
- The Promise of Hydrogen**  
Jack Russell  
**Optical Communications**  
J. Cook, B. DeLoach, A. D. Pearson
- Energy in the Future**  
Dr. Paul Donovan  
**Solar Homes for the Future**  
Coal's New Face  
Dr. Bernard Lee  
**More Power, Less Pollution**  
Dr. Daniel Bernstein
- Cleaning A Dirty Fuel**  
H. Feldman  
**From Wastors to Energy**  
H. Feldman
- Energy: A Critique**  
Dr. Dean Abrahamson  
**Puzzles of Air Pollution**  
Arthur Levy
- Fusion: Prospects & Pitfalls—I**  
Dr. H. Furth & Dr. H. Forsen  
**Fusion: Prospects & Pitfalls—II**  
Dr. H. Furth & Dr. H. Forsen
- Antidote to the Energy Crisis**  
George Long  
**Chemicals In the Environment**  
Dr. Samuel Epstein
- Fusion and Fission: An Appraisal**  
Dr. James L. Turk  
**The Prospects for Energy**  
Dr. M. King Hubert

## ENVIRONMENT

- The Spray Can Threat**  
Dr. F. S. Rowland  
**The Invisible Enemy**  
Dr. R. Stewart
- Cities & Weather—I**  
Dr. R. Brham  
**Cities & Weather—II**  
Dr. R. Brham
- Putting Potatoes in Plastics**  
Dr. Gerald Griffin  
**Lead Poisoning in Children**  
Dan Darow
- New Look in Phosphorus Removal**  
Dr. Gilbert Levin  
**A Solution for Metals**  
Thomas Chapman
- Turning Insects Against Themselves**  
Daniel Lazare  
**Updating Aluminum**  
Dr. Allen Russell
- Energy and Environmental Thrift**  
Dr. S. Berry  
**Tracing the Skeleton's Image**  
Dr. T. Raby
- Seafood From Waste**  
J. Hsuennin  
**Underwater World of Communications**  
Dr. J. Athena
- Water Supply of the Future**  
Dr. I. Kuyperman  
**The Secrets of Salmon**  
Dr. A. Hestler
- Cleaner Water Through Chemistry**  
D. Parker  
**Bromine Chloride: A Better Disinfectant**  
Dr. J. Mills
- The Damaged Air—I**  
**The Damaged Air—II**  
**How Smeets' Shape Up**  
Urban Auto Design  
Dr. John Amooore
- Tough Filaments of Fragile Liquid**  
James Bacon  
**Electricity from Rooftops**  
Dr. Charles Backus
- The Struggle for Clean Water—I**  
**The Struggle for Clean Water—II**  
**The Oil Mystery**  
Harold Bernard  
**The Language of Odors**  
Dr. Stanley Freeman
- The Lonely Atom**  
Dr. Philip Skell  
**How Green The Revolution**  
Lester Brown
- Mercury: Another Look—Part I**  
Dr. John Wood  
**Mercury: Another Look—Part II**  
Dr. John Wood & Dr. G. Langley
- The Troubles with Water**  
Dr. Daniel Okun  
**Pure Oxygen for Polluted Water**  
Dr. Jack McWhirter

- The Lead Issue**  
H. Mayssom & M. H. Hyman  
**Smog: An Environmental Dilemma**  
Dr. James Pitts
- New Weapons Against Insects**  
Dr. G. Staal & Dr. J. Siddall  
**Moths, Drugs, & Pheromones**  
Dr. Wendell Roedelis
- Dr. K. Patel & Dr. L. Kruezer**  
**The Steam Engine: A Modern Approach**  
Dr. W. Doerner & Dr. M. Bechhold

## CANCER RESEARCH

- Cancer & the Cell Membrane**  
Dr. R. Barnett  
**Intercell: From Colds to Cancer**  
Dr. S. Baron
- Cancer & Chemicals—I**  
Dr. Charles Heidelberger  
**Cancer & Chemicals—II**  
Dr. Charles Heidelberger
- Screening for Cancer Agents**  
Dr. Bruce Ames  
**Narcotics & the Brain**  
Dr. Avram Goldstein
- Chemicals Combating Cancer**  
Dr. David Grassetti  
**Chemical Essence of Beer & Ale**  
Dr. Rao Palamand
- Cancer Research I—Perspective & Progress**  
Dr. Frank Rauscher  
**Cancer Research II—Viruses**  
Dr. R. Gallo & Dr. G. Todaro
- Cancer Research III—Chemotherapy**  
Dr. C. Gordon Zubrod  
**Cancer Research IV—Immunology**  
Dr. Paul Levine
- Cancer Research V—Environmental Agents**  
Dr. Umberto Saffroni  
**Cancer Research VI—NCI Roundtable**
- Fighting Fat**  
Dr. J. J. Marshall  
**Tackling Tooth Decay**  
Dr. J. Cassel
- Progress Against Diabetes**  
Dr. D. Steiner  
**The Sticky Cell Problem**  
Dr. R. Jackson
- A New Look at Stroke**  
Dr. R. Wurtman  
**Chemical Look at Mental Illness**  
Dr. S. Key
- Nutrition & the Brain**  
Dr. J. Fernstrom  
**The Forgotten Nutrient**  
Dr. J. Scala
- Remodeling the Body**  
Dr. S. Carr  
**Nuclear Medicine**  
Dr. W. Wolf

## BIO-MEDICAL

- renewing nitrogen legumes**  
Drs. G. Stiles & J. Hobbins  
**Progress in Enzyme Replacement Therapy**  
Dr. Roscoe Brady
- Safety for Premature Infants Help for the Critically Ill**  
Dr. John Morrison  
Dr. Joseph Moylan
- Pinpointing Hepatitis Viruses New Key to Heart Disease**  
Dr. Robert Purcell  
Dr. Antonio Gotto
- Nature's Own Toxicants in Foods Added, Not Intended**  
Dr. J. M. Coon  
Dr. H. Kraybill
- Seventy-Two Per Minute—1**  
Dr. L. Harmon  
**Seventy-Two Per Minute—II**  
Dr. N. Razor
- Two Drugs, More or Less Filling the Molar Gap**  
Dr. K. Hussar  
Dr. J. Cassel
- A Tilt at Genetic Ills**  
V. Agostini  
**Binding the Catalysts of Life**  
Dr. H. Garfinkel
- Early Prenatal Diagnosis of Genetic Disease**  
Dr. M. L. Moss  
**From Mother to Child**  
Dr. M. Honning & Dr. R. Hill
- Insulin & Diabetes—I**  
Dr. George Cahill  
**Insulin & Diabetes—II**  
Dr. George Cahill
- Stalking the Molecules of Memory**  
Dr. Leslie Iverson  
**Immunotherapy**  
Dr. Kenneth Bagshave
- Engineering Enzymes**  
Dr. Victor Edwards  
**On Drugs, Plasticizers, & Mass Spec**  
Dr. G. W. A. Milne
- Birth Control: Problems & Prospects**  
Dr. Carl Dierassi  
**Hormones, Terpenes, & the German Air Force**  
Dr. A. J. Birch
- Prospects for Implants**  
Dr. Donald Lyman  
**New Dimensions for Polymers**  
Dr. Alvin Michaels
- Fabricating Life**  
An Essay Report  
**New Ways to Better Food**  
Dr. R. W. F. Hardy
- Chemistry of the Mind: Schizophrenia**  
Dr. Larry Stein  
**Chemistry of the Mind: Depression**  
Dr. Joel Tikes
- The Molecules of Memory**  
Dr. W. L. Byrne & Dr. A. M. Golub  
**The Matter with Memory**  
Dr. J. McLaughlin
- unsound chemistry**  
Dr. Denham Harman  
**Why We Grow Old**  
Dr. Howard Curtis
- New Materials for Spare Parts Against Individuality**  
Dr. V. Gott & Dr. A. Rubin  
Dr. R. Heisfeld & Dr. B. Kahan
- A Richness of Lipids**  
Dr. Roscoe O. Brady  
**Life: Origins to Quality**  
Dr. Stanley Miller
- The Nitrogen Fixer**  
Dr. Eugene van Tamele  
**Prostaglandins: A Potent Future**  
Dr. E. J. Corey & Dr. S. Bergstrom
- Chemical Evolution**  
Dr. Russell Donlin  
**An Evolving Engine**  
Dr. R. E. Dickerson
- Linus Pauling**  
**The Committed Scientist**  
Dr. Jacob Bronowski  
**Science and Man**
- Glenn Seaborg**  
**The Atomic World of Glenn Seaborg**  
Dr. George Wald  
**Vision, Night Blindness, & Professor Wald**  
Dr. Melvin Calvin  
**The Search for Significance—Parts I & II**
- the view from space**  
Drs. R. Madole & R. Anderson  
**The Attraction of Magnets**  
David Kelland
- Cosmic Ray Astronomy**  
Dr. P. Meyer  
**The Reactor Never Lies**  
T. Raby
- Wire From Native American Grapes—I**  
Dr. A. Rice  
**Wine From Native American Grapes—II**  
Dr. A. Rice
- Community Needs: New Emphasis in Research**  
Dr. H. Gurfurd-Steyer  
**Aspirin vs. Prostaglandins**  
Dr. John Vane
- A Breakdown in Plastics—I**  
Drs. J. Guillet & G. Scott  
**A Breakdown in Plastics—II**  
Drs. J. Guillet & G. Scott
- Protein: The Next Big Production?**  
Dr. Steven Tammentam  
**Clean Energy: A One-Way Dream**  
Dr. J. R. Eaton
- Nitrosamines: A Reappraisal**  
Dr. Phillip Isonberg  
**The Emperor of Ice Cream**  
Dr. Wendell Arducke
- Ethics and Genetics**  
Dr. Robert F. Murray  
**The American Diet: A Critique**  
Dr. Arnold Schaefer
- Probing Creation**  
Dr. Myron A. Cole  
**New Directions in U.S. Science**  
Dr. William McElroy
- Aspirins, Enzymes, & Fragrant Redheads**  
An Essay Report  
**Vitamin D: A New Dimension**  
Dr. Hector DeLuca
- Engineering Microbes**  
Dr. Elmer Galen  
**Liquid Crystals: A Bright Promise**  
Dr. George Hellmeyer
- Lively Ximon**  
Dr. Neil Earhart  
**The Receptor Hunt**  
Dr. Mark Plashine

**SCIENCE**

**NOBEL PRIZE WINNERS**

- Tapping the Oceans**  
Dr. O. Roels  
**Davy Jones' Treasure**  
Dr. S. Gerard
- The Need for Nitrogen**  
Dr. R. Hardy  
**Modifying Milk for Millions**  
A. Rand & J. Hourigan
- The Seas in Motion**  
Dr. Wallace Broecker  
**Humbles in the Earth**  
Dr. Christopher Scholz

**ACS Members \$5.95**      **Nonmembers \$6.95**

**Single cassette \$5.95/cassette**      **Any Eight cassettes \$4.95/cassette**      **\$5.95/cassette**  
**Any 20 or more cassettes to one address \$4.00/cassette**  
**10% Discount if payment accompanies order**

Name \_\_\_\_\_  
 Address \_\_\_\_\_  
 City \_\_\_\_\_ State \_\_\_\_\_ Zip \_\_\_\_\_

Order from: American Chemical Society, Dept. SH  
 1155 16th St., N.W., Wash., D.C. 20036  
 Allow 4 to 6 weeks for delivery

W.A. 251